

THE
American Journal of
ANATOMY

MANAGING EDITOR

DONALD DUNCAN

THE UNIVERSITY OF TEXAS
MEDICAL BRANCH
GALVESTON, TEXAS

ASSOCIATE EDITORS

BURTON L. BAKER
UNIVERSITY OF MICHIGAN

SAM L. CLARK, JR.
WASHINGTON UNIVERSITY

C. P. LEBLOND
MCGILL UNIVERSITY

RICHARD J. BLANDAU
UNIVERSITY OF WASHINGTON

DON W. FAWCETT
HARVARD UNIVERSITY

HARLAND W. MOSSMAN
UNIVERSITY OF WISCONSIN

VOLUME 120

JANUARY, MARCH, MAY 1967

PUBLISHED BY

THE WISTAR INSTITUTE OF ANATOMY AND BIOLOGY
PHILADELPHIA, PA.

CONTENTS

No. 1 JANUARY 1967

RUSSELL T. WOODBURN. Wilfrid Taylor Dempster — A Biographical Sketch	1
WILFRID T. DEMPSTER. Correlation of Types of Cortical Grain Structure with Architectural Features of the Human Skull	7
WILFRID TAYLOR DEMPSTER AND GEORGE R. L. GAUGHRAN. Properties of Body Segments Based on Size and Weight	33
J. K. AVERY, R. A. MEYERS AND L. E. HALE. A Study of Mineral Density Surrounding Resorption Sites in Teeth	55
ALLAN G. BRODIE. The Interrelation of the Digestive and Skeletal Systems as Determinants of Tooth Position	71
F. GAYNOR EVANS AND SEONG BANG. Differences and Relationships Between the Physical Properties and the Microscopic Structure of Human Femoral, Tibial and Fibular Cortical Bone	79
WILLIAM J. L. FELTS AND FRANCIS A. SPURRELL. Microradio-graphic Visualization of Structure in Bones of the Masked Shrew, <i>Sorex cinereus</i>	89
VOIGT R. HODGSON. Tolerance of the Facial Bones to Impact. .	113
DONALD F. HUELKE, LYNN J. BUEGE, AND JAMES H. HARGER. Bone Fractures Produced by High Velocity Impacts	123
ALLAN G. KRAW AND DONALD H. ENLOW. Continuous Attachment of the Periodontal Membrane	133
ALPHONSE R. BURDI AND KATHLEEN FAIST. Morphogenesis of the Palate in Normal Human Embryos with Special Emphasis on the Mechanisms Involved	149
SEONG S. HAN. An Electron Microscopic and Radioautographic Study of the Rat Parotid Gland after Actinomycin D Administration	161

No. 2 MARCH 1967

ALLEN C. ENDERS AND SANDRA SCHLAFKE. A Morphological Analysis of the Early Implantation Stages in the Rat	185
M. H. BURGOS AND R. VITALE-CALPE. The Mechanism of Spermlation in the Toad	227
HAROLD F. PARKS. An Experimental Study of Microscopic and Submicroscopic Lipid Inclusions in Hepatic Cells of the Mouse	253
BENNETT M. STEIN AND MALCOLM B. CARPENTER. Central Projections of Portions of the Vestibular Ganglia Innervating Specific Parts of the Labyrinth in the Rhesus Monkey . . .	281
ADOLPH I. COHEN. An Electron Microscopic Study of the Modification by Monosodium Glutamate of the Retinas of Normal and "Rodless" Mice	319
RAYMOND F. GASSER. The Development of the Facial Muscles in Man	357
NICHOLAS J. LENN. Localization of Uptake of Tritiated Nor-epinephrine by Rat Brain <i>In Vivo</i> and <i>In Vitro</i> Using Electron Microscopic Autoradiography	377

No. 3 MAY 1967

LAURENCE E. WRAGG. Effects of Pinealectomy in the Newborn Female Rat	391
GIUSEPPINA RAVIOLA AND ELIO RAVIOLA. Light and Electron Microscopic Observations on the Inner Plexiform Layer of the Rabbit Retina	403
ELIO RAVIOLA AND GIUSEPPINA RAVIOLA. A Light and Electron Microscopic Study of the Pecten of the Pigeon Eye	427
JOHN A. LONG AND ALBERT L. JONES. The Fine Structure of the Zona Glomerulosa and the Zona Fasciculata of the Adrenal Cortex of the Opossum	463
MILTON B. ENGEL AND EUGENIO ZERLOTTI. Changes in Cells, Matrix and Water of Calcifying Turkey Leg Tendons . . .	489
CAROLYN EYSTER THOMAS. An Electron- and Light-Microscope Study of Sinus Structure in Perfused Rabbit and Dog Spleens	527

CONTENTS

v

LEE VIRN LEAK. The Ultrastructure of Myofibers in a Reptilian Heart: The boa constrictor	553
R. W. GUILLERY. A Light and Electron Microscopical Study of Neurofibrils and Neurofilaments at Neuro-Neuronal Junctions in the Dorsal Lateral Geniculate Nucleus of the Cat	583
ERVIN W. POWELL AND DUANE K. RORIE. Septal Projections to Nuclei Functioning in Oxytocin Release	605
ERNEST N. ALBERT. The Effect of Pregnancy on the Elastic Membranes of Mesometrial Arteries in the Guinea Pig ..	611
JOHN E. PAULY AND LAWRENCE E. SCHEVING. Circadian Rhythms in Blood Glucose and the Effect of Different Lighting Schedules, Hypophysectomy, Adrenal Medullectomy and Starvation	627
INDEX TO VOLUME 120	637



WILFRID TAYLOR DEMPSTER

WILFRID TAYLOR DEMPSTER

1905 - 1965

Wilfrid Taylor Dempster died November 6, 1965, after 36 years of continuous service to the Department of Anatomy, the Medical School, and The University of Michigan. Born November 11, 1905, in Windsor, Ontario, Canada, Dr. Dempster was, at his death, within five days of his sixtieth birthday.

Entering The University of Michigan at the beginning of his sophomore year of college, Dr. Dempster was essentially a product of this University. He received his B.S. degree in 1926, an M.S. in 1927, and an Sc.D. in zoology in 1929. He also studied during summer periods at Woods Hole Marine Biological Station and at Cornell University.

Upon receipt of his Sc.D. degree, Dr. Dempster entered the Department of Anatomy of the Medical School as a junior instructor. He became a regular instructor in 1930, assistant professor in 1945, associate professor in 1949, and professor in 1955. During his entire career he was associated with the teaching of gross anatomy.

In 1947, Professor Dempster assumed full responsibility for teaching gross anatomy to freshman dental students as well as the development and teaching of a special course in head and neck anatomy for junior and postgraduate dental students. He was tireless in his efforts to adapt the work of the courses to the future professional needs of these students. His standards of teaching were high and devoted to the same level of excellence which he maintained in his research efforts. Graduate students and young instructors in the department valued their experience in assisting him for the special knowledge which Dr. Dempster was able to impart in the area of head and neck morphology.

Although teaching in a rather special area, Dr. Dempster was known for his broad scientific interests. His early training ranged from paleontology to marine zoology, and some of his first publications dealt with the general problems of growth. A request by the editors of the Journal of the Michigan State Medical Society led to a long series of articles which appeared between 1933 and 1938. Included in this series were discussions of the historical development and significance of the microscope, biological stain-

ing, hospitals, spectacles, human dissection, the electrocardiograph, percussion and auscultation, anatomical injections, the history of urinalysis, medical photography, and many related subjects down to and including animal experimentation.

Dr. Dempster was an investigator interested in the fundamental problems of his science. Some of the reports which added most to his reputation were precise and detailed studies of fixation of tissues, *mechanics of paraffin sectioning*, distortions produced by technical factors, and rates of penetration of fixing fluids. However, Dr. Dempster's greatest contribution to biological literature probably lay in his numerous studies in the field of body mechanics. Here again he showed his regard for fundamentals, basing his own biological studies on principles of mechanics, engineering, and mathematics. Thus, a number of thorough studies were published on the mechanics of the wrist joint and the relative activity of wrist moving muscles in various functional phases. These were followed by a broader attack on the mechanics and range of movements of the upper limb joints. His work in this area attracted the attention of the Air Force Research and Development Command and Dr. Dempster made a number of studies of an applied nature under the general heading of "Space Requirements of the Seated Operator." While continuing his interest in limb movements, there was an extension in later years to studies of the skull and mandible, the relationship of their trabecular organization and vascular canals, and the bony arrangements for the roots of the teeth within the jaws. At the time of his death, Dr. Dempster had a number of manuscripts on body mechanics in various stages of preparation. There is great loss to science in that some of these cannot be completed for publication.

Dr. Dempster's commitment to biological science is clearly indicated in his sponsorship and high interest in the local science and research societies. He was a focus of strength in the Science Research Club of The University of Michigan as its Secretary-Treasurer in 1936-38, Vice-President, 1938-39, and President, 1939-40. He was an active member of The University of Michigan Research Club. Early in his career, Dr. Dempster was instrumental in organizing a rather select local biological group for discussions in the homes of the membership. This was known informally as the Biological Discussion Group and flourished until recent years with certain temporary lapses during war years. It consisted of biologically interested basic science and clinical people and its roster included many of the most original minds of the

biological portion of the University during its years of activity. Dr. Dempster was a member of Phi Sigma and Omicron Kappa Upsilon, an honorary dental society. On the national scene he was a member of the American Association for the Advancement of Science, American Association of Anatomists, American Association of Physical Anthropology, the History of Science Society, and the Society for Experimental Biology and Medicine.

Dr. Dempster believed in the applications of anatomy and for a ten-year period, 1938-48, he taught an extension course in art anatomy at Cranbrook Art Academy. His talent in sculpture and painting contributed a great deal of pleasure to himself and others and also aided in the design of the simple and dynamic illustrations with which he embellished his scientific articles.

Within the department Dr. Dempster was held in the very highest regard by his colleagues for the level of scholarship which he represented. His approach to all questions was factual, fundamental, and penetrating, and his advice was always based on both pragmatic and historical considerations. In spite of visual limitations of many years duration, Dr. Dempster was a great reader and had a very keen interest in library matters. He was a team player in the best sense, always willing to contribute to the plans which the majority made and always willing to submerge his own opinions in the group decision. He worked not only within the department but for it in every act that he took.

He served the medical school in many ways, especially in those committees to which he could make a real contribution. He was a member and Chairman of the Medical School Library Committee from 1955-61. He was Chairman of the Medical School Accident Trauma Committee from 1955-57. He joined The University of Michigan Gerontology Advisory Committee in 1956 and was Chairman of the Steering Committee of The University of Michigan Coordinating Committee on Automobile Safety Research from 1958 till his death. In 1960, he was made an honorary member of the American Association of Automotive Medicine.

In 1933, Dr. Dempster married Helen Louise Tackabury and their daughters are Allison, born 1940 and Lynn, born 1946. They survive as do Dr. Dempster's brother and mother.

Dr. Dempster's colleagues, locally and nationally, will miss his continuing contribution to biological science but will even more so miss the man. An example in his scientific rectitude, he was also an example of a well-loved colleague. Though physically quite handicapped in later years, he never complained or allowed his

condition to interfere with his scholarly and professional occupations or his contacts with his friends. He was admired for his absolute and uncompromising intellectual honesty and respected for his broad basis of information and opinion in biological matters. A multifaceted man, he encouraged originality and welcomed fresh ideas and new methods. He is especially remembered for his total humility, his tolerance for the frailties of his friends, and his quiet, well-balanced humor.

Ave Atque Vale

RUSSELL T. WOODBURN

Correlation of Types of Cortical Grain Structure with Architectural Features of the Human Skull¹

WILFRID T. DEMPSTER

Department of Anatomy, University of Michigan,
Ann Arbor, Michigan

ABSTRACT Seven grain-form relationships, as indicated by the split-line patterns, are recognized in the cortical bone of the adult human skull: (1) random pattern of braincase, (2) planes and (3) ridges with elongated grain, (4) troughs with transverse grain, (5) concavities with circular grain, (6) edges, and (7) spines. Concavities may show superimposed trough or ridge structure, and troughs may be marked by localized ridges and planes. That is, trough patterns are dominant over concavity patterns, and ridge patterns are dominant over both trough and concavity patterns. Finally, there are a few small cranial areas that are random distributions in some skulls and planes in others; the skull vault proper, however, except for the forehead region and internal sagittal markings, has a random pattern throughout.

The mechanical significance of the various patterns and the areas on which they are found are discussed and explained on the basis of principles of mechanics and architecture. The form-texture relationships are discussed as architectural features of the skull, and their adequacy and limitations are analyzed in terms of their reaction to force systems and their proneness to fracture.

Does the grain structure of cortical bone make the human skull stronger or weaker? An attempt to answer this question brings to light several unrecognized relationships. Distinctive patterns of grain texture are found on the eminences, fossae, processes, and certain other markings of the adult skull, and similar forms all over the skull have similar grain patterns. These form-texture relationships at first sight suggest that some mechanical advantage might accrue from the relationship. This paper, then, (1) examines the several form-texture relationships to clarify the various grain patterns that are repeatedly found, (2) lists nearly 150 skull forms with their characteristic textures to attest to the generality of the finding, and (3) examines the mechanical and architectural features of these form-texture relationships with regard to the weak and strong features of skull architecture and to fracture mechanics. Finally, the current interpretations of force "trajectories" of the skull are criticized.

Forty years ago, Benninghoff ('25) demonstrated an architectural pattern or "grain" in the fibromatrix of the cortex of several flat bones, including those of the skull. Bones were decalcified in acid and punctured with a needle dipped in India

ink; instead of round holes, the punctures usually produced elongate, ink-marked "split-lines" that indicated a grain direction in the organic matrix. They were similar in appearance to Langer's (1861) split-lines of the skin, Hultzkranz's (1898) split-lines in joint cartilage, Benninghoff's ('34) split pattern in mucous membrane, Bühler's ('34) puncture patterns in laryngeal cartilages, and Ilberg's ('35) puncture patterns in nasal cartilages.

Although Tappen ('53) published photographs showing split-line patterns in an adult human skull, Benninghoff's original study, including illustrations of the facial, lateral, and interior basal regions, is the most complete demonstration to date of the grain of the adult skull. Dowgjallo ('32) and Seipel ('48) reported more highly detailed split-line studies of the mandible. (A study of vascular canals in the cortex of the mandible—Dempster and Enlow, '59—by an ink injection-clearing technique, revealed still more elaborate patterns of 11 tracts.) Bruhnke ('29) used the split-line technique on the horse skull, Henckel ('31) on several mammalian skulls, Tappen ('53, '54, '64) on primate skulls, and Ahrens ('36) on

¹This investigation was entirely supported by National Science Foundation grant GB-356.

condition to interfere with his scholarly and professional occupations or his contacts with his friends. He was admired for his absolute and uncompromising intellectual honesty and respected for his broad basis of information and opinion in biological matters. A multifaceted man, he encouraged originality and welcomed fresh ideas and new methods. He is especially remembered for his total humility, his tolerance for the frailties of his friends, and his quiet, well-balanced humor.

Ave Atque Vale

RUSSELL T. WOODBURN

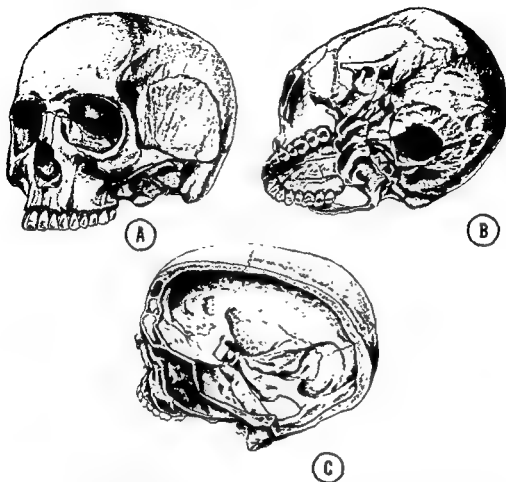


Fig. 1 Three views of the adult skull showing by shading the principal forms, apart from those of the nasal cavity. A, intact skull; B, right zygomatic arch cut away; C, much of left side of cranial vault removed to show interior.

used to designate both the specific forms they describe and the underlying micro-organization of the forms.

B. *Braincase cortex* (fig. 3) shows a dispersed pattern of random lines. This pattern is found on both convex and concave surfaces that have relatively large radii of curvature; for example, in most of the exterior and interior of the skull vault.

P. *Plane surfaces* show either a parallel grain or, in triangular areas, a radiating, fanlike pattern of grain.

R. *Ridges and crests* show the most clearly expressed pattern. They may be plano-convex elevations (like the "barrel arches" of architecture), elliptical eleva-

tions, or saddle-shaped elevations. These forms may lie on either plane or moderately curved surfaces. In each instance, the grain direction shown by split-lines runs parallel to the less convex axis of an elevation; that is, parallel to the crest of the ridge. The grain runs parallel to the ridge whether the top of the ridge is straight, convex, concave, or sigmoid—but the grain is always perpendicular to that cross section of the ridge having the smallest radius of curvature. (This is true even for the occipital condyle, as shown in figs. 2, 5, where the ridge lies obliquely across the length of the condyle.)

various child skulls. None of these studies, however, covers the entire skull or correlates grain with structural features.

The present study reports a more extensive investigation than others have made into the grain patterns of the bones of the whole skull, excluding the mandible. The split-line technique was used on six complete adult skulls (new commercial osteological material) and on miscellaneous parts of some damaged discards. The skulls were soaked overnight in 10% formalin to fix the protein constituents; then the skulls were decalcified for short periods in 5% or 10% HCl. The material in acid was tested with a needle at intervals until the thinnest regions could be easily punctured. If left too long, excessive decalcification resulted in blurring and smudging of the split-lines. A sewing needle, mounted in a jeweler's pin vise and dipped in India Ink, was used to puncture the decalcified bone; after each puncture, excess ink was wiped away with a bit of wet cotton wool to avoid indiscriminate staining. After the thin areas had been treated, the skulls were returned to the acid for further decalcification of the thicker areas; these areas were then punctured as above, with little deterioration of the split-lines in thin areas.

Best results were obtained when the specimens were decalcified in a buffer mixture of formic acid (6N) and sodium formate (1N). Most of the material was stored in 80% alcohol and could be photographed after draining. Other material was allowed to dry slowly and thoroughly to produce hard, and somewhat shrunken, dry specimens. The latter could be handled and demonstrated more easily than the specimens stored in alcohol.

FORMS AND TEXTURE

The three drawings of figure 1 show most of the formations of the skull. Figure 2 shows the same views with a superimposed grain pattern based on the foregoing material. However, before these summary drawings could be made, a number of skull specimens marked with split-lines had to be examined. Although careful study showed that certain form and texture relationships occurred in different regions, no clue to interpretation immedi-

ately suggested itself. This recognition of a few recurring patterns was ineffectual until a fresh approach was used.

Three skulls that had been sawed to show the interior of the braincase were first painted neutral grey. Exterior and interior surface forms were then marked by painting them different colors, each color corresponding to a different shape or form. Initially, the colors were used merely to distinguish planar regions, elevated (convex) areas, and depressed (concave) surfaces. Later, further distinctions were made: elongate ridges were considered apart from domes and saddle-shaped areas; troughs were distinguished from circular basins, and so on. Some of the finer distinctions proved unnecessary when the corresponding grain patterns were compared; others, however, were consistently correlated with differences in grain patterns.

As the split-line skulls were examined, seven patterns of grain, corresponding with seven skull forms, emerged as apparently the most basic. These seven patterns included almost all the surface of the skull. Many of the forms in the seven categories of the new grouping have standard anatomical names, but there are others that have no specific names.

Since the new grouping of seven forms, each with a specific grain pattern, applies to so many forms, both named and unnamed, it will be important to develop a new terminology in which both form and texture are indicated, a terminology that cannot be confused with standard anatomical nomenclature.

The seven form-texture types are diagrammed in figure 3; the illustration also includes an eighth type to be treated separately. Each has a name and a code letter that will identify patterns in the photographic illustrations. In the following discussion of these types, conventional anatomical terms such as "eminence," "crest," and "fossa" are avoided, since they are generalized descriptive terms that apply equally to bones, viscera, and surface anatomy. The present need, rather, is for terms relating specifically to bone structure and denoting both the physical forms and the grain architecture associated with each. Thus, "ridge" and "trough" will be

the foregoing seven forms, grain is related in a rather specific way that is suggestive of some structural significance. Discontinuities, in some instances, are merely a combination of edges and spines, already listed, together with foramina and sharp grooves. Although about 50 discontinuities are listed below, their characteristics can best be considered in a later part of this paper.

A classification of form-textures of the skull

With this introduction to the different categories of form and texture relationships in the skull, a classification of the principal forms of the skull will be given. This will demonstrate how inclusive the relations are. In deriving this catalog of forms, from six to ten specimens (or nearly double these numbers if rights and lefts

are distinguished) were studied. The grain patterns are those of fully adult skulls. Growth patterns with markedly different textures predominate in the fetus, infant, and child (Ahrens, '36); these patterns usually radiate from ossification centers. In time, specializations of form and texture give rise to definitive adult patterns. A certain amount of variability is found: concavities in one specimen may show as troughs in another, or small plane areas of one specimen may show as a random pattern in the next; the pattern common to one area may encroach on an adjacent one; an infantile pattern may persist in a localized region. However, most forms are found consistently, and extreme variations are rare. The following classification arbitrarily lists patterns that appear to be most common, and only a few variants are mentioned. Re-

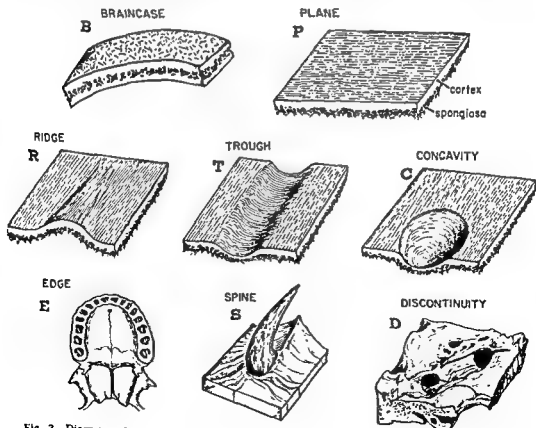


Fig. 3. Diagrams of eight form-textures with their predominant grain direction. All but the last have a characteristic grain pattern. With each sketch is a name and a code letter.

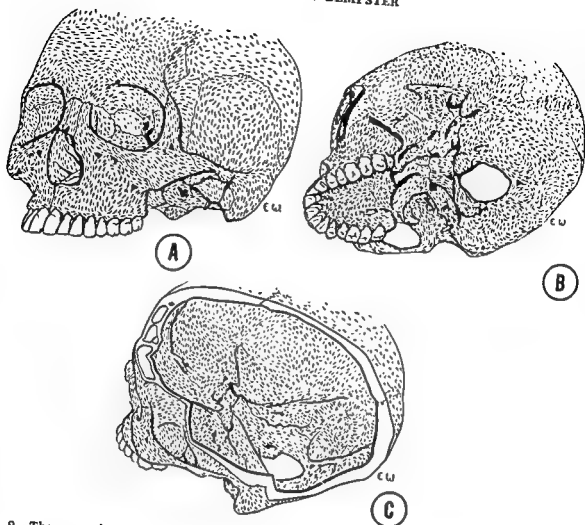


Fig. 2 The same three views of the skull showing the common texture pattern of the cortical bone as revealed by split-lines.

T. *Troughs are elongate, shallow trenches having a transverse grain; their margins, however, often show elongate ridge patterns. Some troughs are elongate plano-concave depressions. Others are doubly concave, and here the radius of curvature is markedly different for the two axes. A minor ridge within a trough will show the characteristic elongate ridge pattern, and the interrupted transverse trough pattern will show on one or both sides of the ridge. This suggests that the ridge pattern is in some sense "dominant" to the trough pattern.*

C. *Concavities are basin-like depressions with an irregular series of concentric circles, whorls, or spirals of grain pattern. If the concavity is elongate, so that its deepest part is like a trough, the base of the concavity will be marked by the*

transverse pattern of split-lines characteristic of troughs: this suggests that the trough pattern is dominant to the concavity pattern. Again, minor ridges running through a concavity show the elongate ridge pattern that seems to be dominant to both the trough and concavity patterns.

E. *Unsupported free edges such as flanges, fins, and margins of thin foramina have a simple pattern of grain that parallels the free edge.*

S. *Spines, hooks, and sharp processes have a grain pattern that follows the shape of the part and converges to an apex.*

A final, eighth category, **D.** *Discontinuities is, to some extent, a convenient catchall for miscellaneous forms, an essential one, however, for a balanced discussion of skull mechanics. In each of*

extending laterally into the temporal fossae; the interior of the skull vault except in the sagittal crests and fossae; also in localized areas of the anterior and middle cranial fossae of the base of the skull (figs. 4 [C], 8 [B], 10 [R]).

P—PLANES and relatively flat surfaces (figs. 3, 4):

I. Exterior of the skull.

1. Supraglabellar plane showing transverse grain (fig. 2A) above and between the superciliary arches; sometimes a random braincase pattern (fig. 4).
2. Frontal process of zygoma, superficial surface (figs. 2A, 2B, 8).
3. Triangular area anterior to superior temporal line, partly superior to lateral orbital margin (figs. 2A, 8 [P]).
4. Maxilla forming floor of the orbit, sometimes random braincase pattern (fig. 2A).
5. Orbital surface of the ethmoid bone (fig. 2A).
6. Orbital surface of the greater wing of the sphenoid bone (fig. 2A).
7. Nasofrontal process and body of maxilla between margins of orbit and piriform aperture (fig. 2A).
8. Posteromedial part of the hard palate, palatine, and maxillary bones (figs. 2B, 9 [P]).
9. Perpendicular plate of vomer (figs. 2A, 2B).
10. Perpendicular plate of ethmoid bone (no fig.).

II. Interior surface of the cranial cavity.

1. Superior surface of the lesser wings of the sphenoid bone; the plane between the two lesser wings (figs. 2C, 10 [P]).
2. Dorsum sellae (fig. 2C).
3. That portion of the petrous part of the temporal bone between its posterior margin and the aqueductus vestibuli (fig. 2C).
4. Localized areas of the sphenoid, temporal, and parietal bones in the lateral part of the skull vault (fig. 2C).

R—RIDGES AND CRESTS (figs. 3, 5):

I. Exterior of the skull.

1. Area across frontal bone between right and left frontal eminences (figs. 2A, 5A [1]).
2. Superciliary arches (figs. 2A, 5A [2]).
3. Superior orbital margin from fronto-sphenoidal process of the zygomatic bone to supraorbital notch; also from the notch to the nasal process of the maxilla (figs. 2A, 5A [3]).
4. Portion of the inferior and lateral margin of the orbit formed by the zygomatic bone (figs. 2A, 5A [4], 8 [R]).
5. Bridge of nose and facial surfaces of nasal bones, extending to adjacent naso-

frontal process of maxillae, usually a saddle-shaped ridge (figs. 2A, 5A [5], 8 [R]).

6. Lacrimal crest and adjacent slopes of the bone (fig. 2A, 5A [6]).
7. The whole alveolar part of the maxilla, below the nasal aperture from the region of the first and second molar teeth on the side across the midline to the opposite side (figs. 2A, 5A [7], 8 [R]).
8. Posterolateral aspect of the body of the maxilla, anterior and parallel to the pterygopalatine fissure (figs. 2B, 5B [8]).
9. Lower part, external face of the body of the zygomatic bone, from the maxillary process to the temporal process (figs. 2A, 5A [9]).
10. Crest of maxilla between lower part of the zygomatic process and first and second molar teeth (figs. 2A, 2B, 5A [10], 8 [R]).
11. Outer surface of zygomatic process of temporal bone (figs. 2A, 5A [11], 8 [R], 11 [R]).
12. Articular tubercle of temporal bone along its whole width—a saddle-shaped ridge (figs. 2B, 9 [R]).
13. Lateral surface of mastoid process—a vertical ridge (figs. 2A, 2B, 2C, 11 [R]).
14. Ridge at lower border of zygomatic root, superior to external acoustic meatus, from postglenoid tubercle to mastoid process (figs. 2B, 11).
15. Transverse ridge—sometimes a plane area—on inferior surface of greater sphenoid wing, anterior to the foramen ovale and between the base of the lateral pterygoid lamina and the articular eminence (figs. 2B, 9).
16. Basal surface of petrous part of the temporal bone anterior to the carotid canal (figs. 2B, 9).
17. Basilar part of occipital and sphenoid bones, between the vomer and the crest of the anterior margin of the foramen magnum (figs. 2B, 9 [R]).
18. Articular surfaces of the occipital condyles; grain runs obliquely across the narrow dimension in a mediolateral direction (figs. 2B, 9 [R]).
19. Anterior margin of foramen magnum and anterior condylar crest (figs. 2B, 9).
20. Lateral postcondylar and posterior margins of foramen magnum (fig. 2B).
21. Superior, inferior, and medial nuchal lines (fig. 2B).
22. Ridge between groove for occipital artery and digastric fossa; juxtamastoid eminence, Taxman, ('63) (no fig.).

II. Interior of the cranial cavity.

1. Frontal crest anterior to the crista galli and foramen cecum; also, continuing ridges at the right and left of the sulcus for the superior sagittal sinus, especially on the frontal and occipital bones (fig. 2C).

presentative illustrations of the texture in different regions will also testify to the fact that anatomical structures in the skull do have a specified form and texture. Following the classification, this paper discusses the associated forms and textural arrangements in terms of their architectural or mechanical implications.

Most features of the skull surface are classified below with regard to both the form and the direction of the grain texture of the cortical bone. Figure 4 illustrates the principal regions of the skull surface that show random braincase structure, planes, and concavities. Figure 5 shows the loca-

tions of ridges and spines, and figure 6 shows where troughs and edges are found. The capital letters at the head of each category are the code letters used in labeling the photographs. The figure numbers in parenthesis after the name of each part refer to figures that illustrate the texture involved. If a structure illustrated in a photograph is labelled with a code letter, that letter in brackets follows the figure number, as: (fig. 7 [C]).

B — BRAINCASE (figs. 2A, 2B, 2C, 3, 4): the random pattern found in most of the skull vault externally between the frontal eminences and the superior nuchal line,

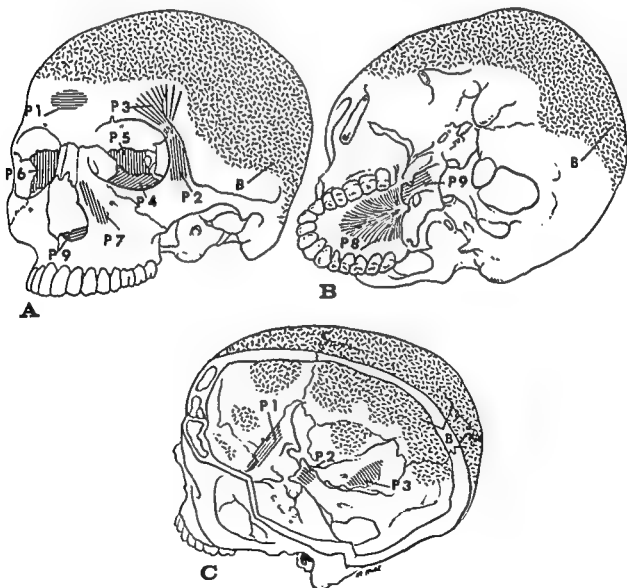


Fig. 4 Areas of the skull surface occupied by braincase texture, B; and by planes, P. The code numbers P1, P2, and so on correspond to the list of planes in the text.

extending laterally into the temporal fossae; the interior of the skull vault except in the sagittal crests and fossae; also in localized areas of the anterior and middle cranial fossae of the base of the skull (figs. 4[C], 8[B], 10[B]).

P—PLANES and relatively flat surfaces (figs. 3, 4):

I. Exterior of the skull.

1. Supraglabellar plane showing transverse grain (fig. 2A) above and between the superciliary arches; sometimes a random braincase pattern (fig. 4).
2. Frontal process of zygoma, superficial surface (figs. 2A, 2B, 8).
3. Triangular area anterior to superior temporal line, partly superior to lateral orbital margin (figs. 2A, 8[P]).
4. Maxilla forming floor of the orbit, sometimes random braincase pattern (fig. 2A).
5. Orbital surface of the ethmoid bone (fig. 2A).
6. Orbital surface of the greater wing of the sphenoid bone (fig. 2A).
7. Nasofrontal process and body of maxilla between margins of orbit and piriform aperture (fig. 2A).
8. Posteromedial part of the hard palate, palatine, and maxillary bones (figs. 2B, 9[P]).
9. Perpendicular plate of vomer (figs. 2A, 2B).
10. Perpendicular plate of ethmoid bone (no fig.).

II. Interior surface of the cranial cavity.

1. Superior surface of the lesser wings of the sphenoid bone; the plane between the two lesser wings (figs. 2C, 10[P]).
2. Dorsum sellae (fig. 2C).
3. That portion of the petrous part of the temporal bone between its posterior margin and the aqueductus vestibuli (fig. 2C).
4. Localized areas of the sphenoid, temporal, and parietal bones in the lateral part of the skull vault (fig. 2C).

R—RIDGES AND CRESTS (figs. 3, 5):

I. Exterior of the skull.

1. Area across frontal bone between right and left frontal eminences (figs. 2A, 5A[1]).
2. Superciliary arches (figs. 2A, 5A[2]).
3. Superior orbital margin from fronto-sphenoidal process of the zygomatic bone to supraorbital notch; also from the notch to the nasal process of the maxilla (figs. 2A, 5A[3]).
4. Portion of the inferior and lateral margin of the orbit formed by the zygomatic bone (figs. 2A, 5A[4], 8[R]).
5. Bridge of nose and facial surfaces of nasal bones, extending to adjacent naso-

frontal process of maxillae, usually a saddle-shaped ridge (figs. 2A, 5A[5], 8[R]).

6. Lacrimal crest and adjacent slopes of the bone (fig. 2A, 5A[6]).
7. The whole alveolar part of the maxilla, below the nasal aperture from the region of the first and second molar teeth on the side across the midline to the opposite side (figs. 2A, 5A[7], 8[R]).
8. Posterolateral aspect of the body of the maxilla, anterior and parallel to the pterygopalatine fissure (figs. 2B, 5B[8]).
9. Lower part, external face of the body of the zygomatic bone, from the maxillary process to the temporal process (figs. 2A, 5A[9]).
10. Crest of maxilla between lower part of the zygomatic process and first and second molar teeth (figs. 2A, 2B, 5A[10], 8[R]).
11. Outer surface of zygomatic process of temporal bone (figs. 2A, 5A[11], 8[R], 11[R]).
12. Articular tubercle of temporal bone along its whole width—a saddle-shaped ridge (figs. 2B, 8[R]).
13. Lateral surface of mastoid process—a vertical ridge (figs. 2A, 2B, 2C, 11[R]).
14. Ridge at lower border of zygomatic root, superior to external acoustic meatus, from postglenoid tubercle to mastoid process (figs. 2B, 11).
15. Transverse ridge—sometimes a plane area—on inferior surface of greater sphenoid wing, anterior to the foramen ovale and between the base of the lateral pterygoid lamina and the articular eminence (figs. 2B, 9).
16. Basal surface of petrous part of the temporal bone anterior to the carotid canal (figs. 2B, 9).
17. Basilar part of occipital and sphenoid bones, between the vomer and the crest of the anterior margin of the foramen magnum (figs. 2B, 9[R]).
18. Articular surfaces of the occipital condyles; grain runs obliquely across the narrow dimension in a mediolateral direction (figs. 2B, 9[R]).
19. Anterior margin of foramen magnum and anterior condylar crest (figs. 2B, 9).
20. Lateral postcondylar and posterior margins of foramen magnum (fig. 2B).
21. Superior, inferior, and medial nuchal lines (fig. 2B).
22. Ridge between groove for occipital artery and digastric fossa; juxtamastoid eminence, Taxman, ('63) (no fig.).

II. Interior of the cranial cavity.

1. Frontal crest anterior to the crista galli and foramen cecum; also, continuing ridges at the right and left of the sulcus for the superior sagittal sinus, especially on the frontal and occipital bones (fig. 2C).

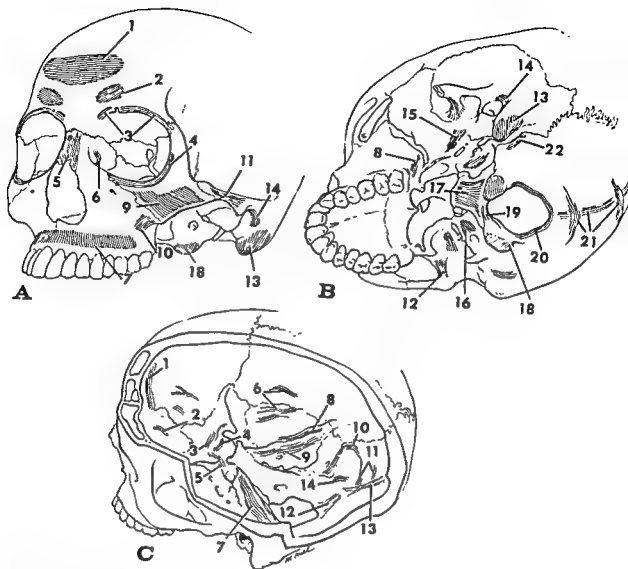


Fig. 5 Areas of the skull surface occupied by ridge form-textures — R. Numbers correspond to the list of ridges in the text.

2. Ridges, usually longitudinal, between the digital fossae of the orbitobasal plate of the frontal bone (figs. 2C, 10 [R]).
3. Transverse ridge anterior to chiasmatic groove, joining anterior clinoid processes (figs. 2C, 10).
4. Tuberculum sellae, transverse pattern between chiasmatic groove and hypophyseal fossa (figs. 2C, 10 [R]).
5. Parasagittal ridges on sphenoid body between the floor of the sella turcica and the carotid grooves (fig. 2C).
6. Ridges between digital fossae of the middle cranial fossa (figs. 2C, 10).
7. Ridges along the length of the anterior surface of the petrous part of the temporal bone, including the arcuate eminence (figs. 2C, 10 [R]).
8. Ridges on the superior margin of the petrous bone, bordering the superior petrosal sinus (figs. 2C, 10).
9. Posterior face of the petrous part of the temporal bone, superior to the aqueductus vestibuli (fig. 2C).
10. Ridge posterior to the sigmoid sulcus (fig. 2C).
11. Ridges above and below the sulcus for the transverse sinus (fig. 2C).
12. Median sagittal crest between right and left cerebellar fossae (fig. 2C).
13. Crest between the right and left posterior cerebral fossae (fig. 2C).
14. Minor ridges in the floor of the cerebellar fossae, inconstant (fig. 2C).

(Commentary: as in Langer's (1861) split-lines in skin, three texture tracts associated with ridges and planes will merge, two by two, to form a triradial pattern with a tiny triangular area or node at the focus. These are shown as black trigones in figure 11 as follows: figure 2A, (1) on the maxilla medial to the infraorbital

foramen, (2) on the anterior face of the zygomatic process of the maxilla, and (3) on the external surface of the zygoma at the junction of the frontal process with the body; figure 2B, the exterior basal aspect of the skull in the mid-sagittal planes: (1) on the basal part of the occipital bone anterior to the foramen magnum, and (2) on the occipital squama posterior to the foramen magnum; figure 2C, on the interior of the skull, on the midline, posterior to the foramen magnum.)

T—TROUPS, grooves, furrow, gutters, or trenches (figs. 3, 6):

I. Exterior of the skull.

1. Walls of the nasolacrimal canal proper, but not the continuous nasolacrimal fossa of the lacrimal bone anterior to the lacrimal crest (no fig.).

2. Posterior surface of the body and frontal process of the zygomatic bone (bounding the temporal fossa); trough pattern, both above and below the level of the infraorbital fissure (figs. 2A, 2B, 2C, 6A [T2], 8 [T]).
3. Groove on the upper surface of the junction of the anterior root of the zygomatic arch with the adjacent squama of the temporal bone — the groove acts as a pulley for the posteriormost fascicles of the temporalis muscle (figs. 2C, 11 [T]).
4. Infratemporal fossa between lateral pterygoid wing and infratemporal crest (figs. 2B, 9 [T]).
5. Gutters on the palate between the palatal and alveolar processes of the maxilla — the anterior and superolateral arches of the palatal vault (figs. 2B, 9 [T]).
6. Roof of the nasal cavity between the vomer bone and the medial pterygoid

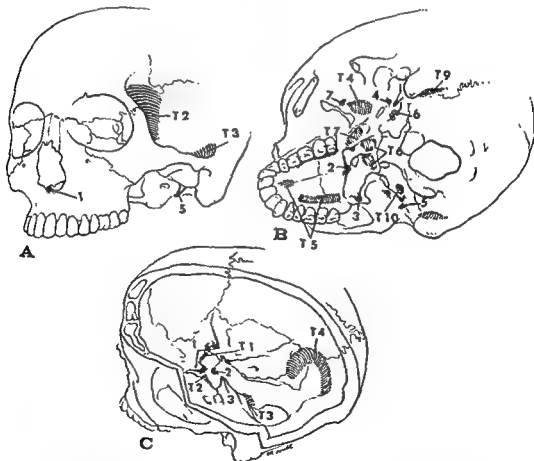


Fig. 3 Areas of the skull surface with the form and textures of troughs—T, and spines—S. The troughs are numbered T1, T2, and so on to correspond to the list of troughs. The other numbers refer to spines as listed.

plate and vertical part of the palatal bone (fig. 2B).

7. Inferior part of pterygoid fossa; transverse grain across fossa (fig. 2B); grain pattern in superior part of the fossa is partly or wholly that of a concavity (C) (figs. 2B, 9 [C]).
8. Inferolateral border of the floor of the nasal cavity (no fig.).
9. Posterior digastric fossa (fig. 2B).
10. Concave wall of the carotid canal (fig. 2B).

II. Interior of the cranial cavity.

1. Hypophyseal fossa (fig. 10 [T]); sometimes the posterior portion or the whole is a concavity (C) (figs. 2C, 9).
2. Wall of carotid canal and of the carotid groove on the body of the sphenoid bone lateral to the sella turcica (figs. 2C, 10).
3. Grain tracts on lowest part of the clivus near the foramen magnum from the medial side of one condyle to the other (figs. 2C, 10); although most of the clivus to the dorsum sellae is concave, ridge tracts from the sides of the foramen magnum above the hypoglossal canals converge to form a dominant ridge-type sagittal pattern of grain. The dorsum sellae proper has a plane structure; its upper margin shows an edge pattern, and the posterior clinoid processes are spines.
4. Transverse and sigmoid sulci, except in the region nearest the jugular foramen (fig. 2C).

C — CONCAVITIES, concave depressions, rounded fossae, bowls, or basins (figs. 2, 7):

I. Exterior of the skull.

1. Lacrimal fossa in the superiorlateral orbital roof (fig. 2A).
2. The facial surface of the maxilla inferior to the infraorbital foramen (figs. 2A, 7A [C2]).
3. Canine fossa, inconstant (no fig.).
4. Variable fossae in the anterior part of the palatal arch between the alveolar process, at the cuspid or bicuspid tooth, and the midline (figs. 2B, 9 [C]).
5. Upper part of the pterygoid fossa (figs. 2B, 9 [C]).
6. Mandibular fossa of temporal bone, sometimes troughlike (fig. 2B).
7. Bilateral areas on the inferior surface of the basilar process of the occipital bone, anterior to the roots of the occipital condyles, inconstant (no fig.).
8. Fossa of the posterior condyloid canal (fig. 2B).
9. Concave anterior wall of jugular fossa (fig. 2B).
10. Fossae on the base of the occipital squama for muscular attachment of suboccipital and semispinalis capitis mm (fig. 2B).

II. Interior of the cranial cavity.

1. The deeper digital fossae at the antero-lateral margins of the anterior cranial fossa (figs. 2C, 10 [C]).
2. Floor of hypophyseal fossa (fig. 2C), sometimes a transverse trough with an anteroposterior grain (fig. 10 [T]).
3. Superior concave surface of the greater wing of the sphenoid bone near the superior orbital fissure — contacts the anterior pole of the temporal lobe (figs. 2C, 10 [C]).
4. Cerebellar fossa of the posterior cranial fossa — often crossed by a trough or ridge (fig. 2C).
5. About 1 cm of the sigmoid sulcus nearest the jugular foramen, below the overhanging rear border of the petrous part of the temporal bone (fig. 2C).

E — EDGES, thin flangelike or finlike plates, or keels with unsupported free edges (figs. 3, 7):

I. Exterior of the skull.

1. Lateral margin of nasal (piriform) aperture on the face bounded by the maxillae, but not including the free ends of the nasal bones (figs. 2A, 2B, 7A [1]).
2. Buccal and lingual alveolar margins — buccal grain tract — thin in the incisor-bicuspid region and wider in the molar region; wider in the lingual than in the buccal region, especially posteriorly; buccal and lingual tracts are continuous behind last molar tooth (figs. 2A, 2B, 7A [2], 7B, 8 [E], 9 [E]).
3. Free margins of medial and lateral pterygoid laminae of sphenoid bone (figs. 2A, 2B, 9).
4. Posterior margin of palatal process of palatine bone (figs. 2B, 9 [E]).
5. Posterior margin of the vertical plate of the vomer bone (fig. 2B).
6. Anterior, superior, and lower margins of infraorbital fissure (figs. 2B, 9 [E]).
7. Anterior border of the bony nasal septum — ethmoid, vomer (fig. 2A).
8. Margins of foramina with thin borders (as foramen ovale); in oblique foramina (as internal acoustic meatus and infraorbital foramen), one side of the foramen has a specialized margin (figs. 2A, 2B, 2C, 9 [E]).
9. Free edge of lateral wall of the nasolacrimal canal (no fig.).
10. Free margins of the nasal conchae (no fig.).

II. Interior of the cranial cavity.

1. Margins of crista galli, ethmoid (fig. 2C).
2. Posterior border of lesser wing of sphenoid, lateral to the anterior clinoid process (figs. 2C, 10 [E]).
3. Lower, outer margin of superior orbital fissure — greater wing of sphenoid (fig. 2C).

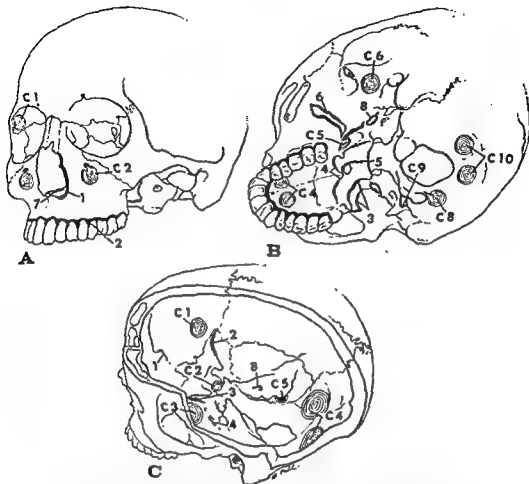


Fig. 7 Areas occupied by edges—E (heavy black lines) and by concavities—C (concentric circles). The edges are designated by numbers corresponding to the list of forms. The concavities are coded C1, C2, and so on.

4. Margins of foramina with thin edges, as foramina ovale, (fig. 2C) and cf. 1-8, above.

S—SPINES, hooks, or sharp processes (figs. 3, 6):

I. Exterior of the skull.

1. Anterior nasal spine, maxillae (figs. 2A, 6A [1]).
2. Posterior nasal spine, palatine bones (figs. 2B, 9 [S]).
3. Pterygoid hamulus (fig. 2B).
4. Spine of angle, sphenoid (fig. 2B).
5. Styloid process, temporal bone (fig. 2B).
6. Spine of vaginal process, tympanic bone (fig. 2B).
7. Spine of infratemporal crest, sphenoid (fig. 2B).

II. Interior of the skull.

1. Anterior clinoid process (figs. 2C, 10 [S]).
2. Posterior clinoid process (fig. 2C).
3. Apex, petrous part of temporal bone (figs. 2C, 10 [S]).

D—DISCONTINUITIES: sharp edges, holes, or foramina; projections; surfaces meeting at sharp angles: the following list in part includes structures of the previous list when sharp breaks in surface continuity or irregular congeries of forms are close together. The discontinuities listed below are not specifically identified in the illustrations (fig. 3):

I. Exterior of the skull.

1. Supraorbital notch or foramen (figs. 1A, 2A).

plate and vertical part of the palatal bone (fig. 2B).

7. Inferior part of pterygoid fossa; transverse grain across fossa (fig. 2B); grain pattern in superior part of the fossa is partly or wholly that of a concavity (C) (figs. 2B, 10 [C]).
8. Inferolateral border of the floor of the nasal cavity (no fig.).
9. Posterior digastric fossa (fig. 2B).
10. Concave wall of the carotid canal (fig. 2B).

II. Interior of the cranial cavity.

1. Hypophyseal fossa (fig. 10 [T]); sometimes the posterior portion or the whole is a concavity (C) (figs. 2C, 9).
2. Wall of carotid canal and of the carotid groove on the body of the sphenoid bone lateral to the sella turcica (figs. 2C, 10).
3. Grain tracts on lowest part of the clivus near the foramen magnum from the medial side of one condyle to the other (figs. 2C, 10); although most of the clivus to the dorsum sellae is concave, ridge tracts from the sides of the foramen magnum above the hypoglossal canals converge to form a dominant ridge-type sagittal pattern of grain. The dorsum sellae proper has a plane structure; its upper margin shows an edge pattern, and the posterior clinoid processes are spines.
4. Transverse and sigmoid sulci, except in the region nearest the jugular foramen (fig. 2C).

C — CONCAVITIES, concave depressions, rounded fossae, bowls, or basins (figs. 2, 7):

I. Exterior of the skull.

1. Lacrimal fossa in the superiorlateral orbital roof (fig. 2A).
2. The facial surface of the maxilla inferior to the infraorbital foramen (figs. 2A, 7A [C2]).
3. Canine fossa, inconstant (no fig.).
4. Variable fossae in the anterior part of the palatal arch between the alveolar process, at the cuspid or bicuspid tooth, and the midline (figs. 2B, 10 [C]).
5. Upper part of the pterygoid fossa (figs. 2B, 10 [C]).
6. Mandibular fossa of temporal bone, sometimes troughlike (fig. 2B).
7. Bilateral areas on the inferior surface of the basilar process of the occipital bone, anterior to the roots of the occipital condyles, inconstant (no fig.).
8. Fossa of the posterior condyloid canal (fig. 2B).
9. Concave anterior wall of jugular fossa (fig. 2B).
10. Fossae on the base of the occipital squama for muscular attachment of suboccipital and semispinalis capitis mm (fig. 2B).

II. Interior of the cranial cavity.

1. The deeper digital fossae at the antero-lateral margins of the anterior cranial fossa (figs. 2C, 10 [C]).
2. Floor of hypophyseal fossa (fig. 2C), sometimes a transverse trough with an anteroposterior grain (fig. 10 [T]).
3. Superior concave surface of the greater wing of the sphenoid bone near the superior orbital fissure — contacts the anterior pole of the temporal lobe (figs. 2C, 10 [C]).
4. Cerebellar fossa of the posterior cranial fossa — often crossed by a trough or ridge (fig. 2C).
5. About 1 cm of the sigmoid sulcus nearest the jugular foramen, below the overhanging rear border of the petrous part of the temporal bone (fig. 2C).

E — EDGES, thin flangelike or finlike plates, or keels with unsupported free edges (figs. 3, 7):

I. Exterior of the skull.

1. Lateral margin of nasal (piriform) aperture on the face bounded by the maxillae, but not including the free ends of the nasal bones (figs. 2A, 2B, 7A [1]).
2. Buccal and lingual alveolar margins — buccal grain tract — thin in the incisor-bicuspid region and wider in the molar region; wider in the lingual than in the buccal region, especially posteriorly; buccal and lingual tracts are continuous behind last molar tooth (figs. 2A, 2B, 7A [2], 7B, 8 [E], 9 [E]).
3. Free margins of medial and lateral pterygoid laminae of sphenoid bone (figs. 2A, 2B, 9).
4. Posterior margin of palatal process of palatine bone (figs. 2B, 10 [E]).
5. Posterior margin of the vertical plate of the vomer bone (fig. 2B).
6. Anterior, superior, and lower margins of infraorbital fissure (figs. 2B, 10 [E]).
7. Anterior border of the bony nasal septum — ethmoid, vomer (fig. 2A).
8. Margins of foramina with thin borders (as foramen ovale); in oblique foramina (as internal acoustic meatus and infraorbital foramen), one side of the foramen has a specialized margin (figs. 2A, 2B, 2C, 9 [E]).
9. Free edge of lateral wall of the nasolacrimal canal (no fig.).
10. Free margins of the nasal conchae (no fig.).

II. Interior of the cranial cavity.

1. Margins of crista galli, ethmoid (fig. 2C).
2. Posterior border of lesser wing of sphenoid, lateral to the anterior clinoid process (figs. 2C, 10 [E]).
3. Lower, outer margin of superior orbital fissure — greater wing of sphenoid (fig. 2C).

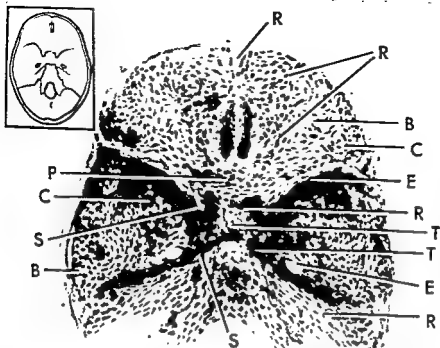


Fig. 10 Photograph of a split-line preparation of anterior portion of interior-basal aspect of the skull. Code: B—braincase, C—concavity, E—edge, P—plane, R—ridge, and T—trough.

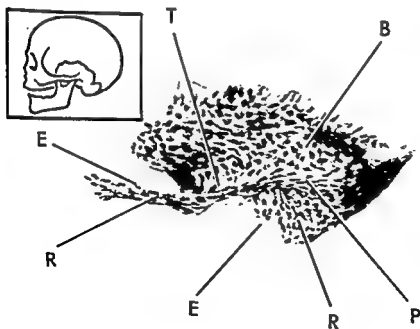


Fig. 11 Photograph of lateral aspect of temporal bone, split-line preparation. Code: B—braincase, E—edge, P—plane, R—ridge, and T—trough.

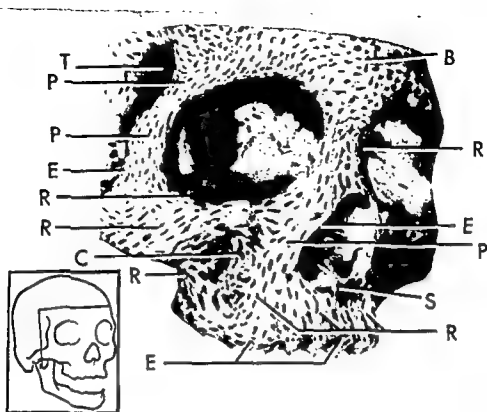


Fig. 8. Photograph of the facial view of a decalcified skull with split-lines. Code: B—braincase, C—concavity, E—edge, P—plane, R—ridge, S—spine, and T—trough.

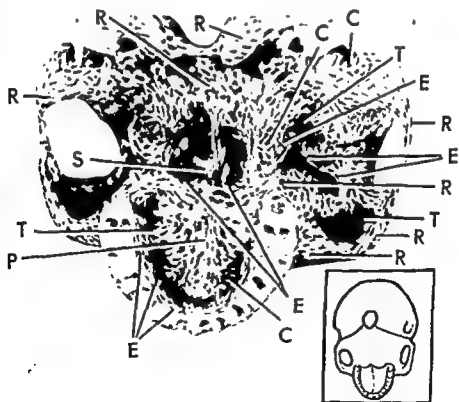


Fig. 9. Photograph of split-line preparation of anterior-basal region of the skull. Code: C—concavity, E—edge, P—plane, R—ridge, S—spine, T—trough.

Cortical grain and bone properties

The tendency of decalcified cortical bone to split in a specific direction when punctured is a distinctive property of the bony matrix; although articular surfaces and minor localized areas of long bones may show round holes rather than splits, this response in the skull—as may be found at the summit of the frontal eminence—is exceptional. This results from the fact that grain patterns are intimately related to the orientation of the microscopic components of the osseous tissue. It was Benninghoff ('25) and Seipel ('48) who first showed that the direction of split-lines correlates closely with the predominant direction of the fibrous tissue of the lamellae of the bone, as in the Haversian systems. A needle penetrating decalcified bone acts like a wedge and splits the matrix a short distance in the direction of least strength. Olivo, Maj, and Tozani ('37) emphasize that although decalcified bone and intact bone have different properties, the predominant direction of split-lines in decalcified bone correlates with the direction of greatest strength in intact bone. Tensile tests of single osteons (Haversian systems), by Ascenzi and Bonucci ('64) show that the strongest osteons are those in which the fibrous bundles of successive lamellae are arranged longitudinally rather than in a strongly oblique (45°) direction, and moreover, that the degree of natural calcification and the action of chemical decalcifying agents are of limited influence on the ultimate tensile strength of osteons.

After testing pieces of femoral and humeral cortex, Dempster and Liddicoat ('52) show that both the ultimate compressive strength and the modulus of elasticity (stiffness) in compression, as in wood, are greater along than across the grain. Dempster and Coleman ('61), using both bending and tensile tests, demonstrate that tibial bone, mandibular bone, and wood are all notably stronger in resisting deformations along rather than across the grain. Evans ('64) shows the mean tensile strength of embalmed wet cortical bone from tibiae is significantly greater than that from femora. Many tests along the grain show that cortical bone is much weaker in tension than

in compression, the ratio of ultimate strengths being roughly three to five.

The foregoing findings imply that a cortical surface with a dominant grain pattern, which might be revealed by split-lines or other techniques (decalcified microscopic sections, ground sections, vascular canal injection, or microradiography), withstands indenting pressures and impacts better lengthwise than crosswise. Grain direction thus becomes a factor—hitherto unrecognized—that influences the initial response of the skull, or other bone, when it fractures.

Skull architectonics

The problem of skull strength in relation to environmental forces depends on several different, though related, considerations: (1) the physical characteristics of bone (including stiffness, yield strength, and ultimate strength in tension, compression, and shear); (2) the force systems that can act on the skull, including magnitude and manner of application; and (3) the architectural features of the skull, including the quantity of bone in different regions, the form of the different parts (with concern for discontinuities), and the direction of grain in each structure. The type of response—for example, safe transmission of forces, puncturing, chipping, shearing, and so on—is entirely dependent on these three considerations.

A number of the general physical properties of bones as a material have been summarized (Evans, '57). Probably most important is the fact that the ultimate compressive strength of human bone is about 25,000 PSI (pounds per square inch) in relation to an ultimate tensile strength of about 15,000 PSI; thus, bone is more likely to be damaged by tensile failure than by compressive failure (Dempster and Liddicoat, '52). Secondly, the tensile strength across the grain is much less the strength along the grain (Dempster and Coleman, '61).

The other two factors affecting strength—force systems and architectural considerations—must be discussed more fully if the overall problem of skull strength is to be understood.

Force systems on the skull. The head and skull are subject to at least three types

2. Lacrimal crest and anterior margin of the lacrimal sulcus (figs. 1A, 2A).
 3. Thin bone of the ethmoid bone; air cells and partitions; ethmoidal foramina (figs. 1A, 2A, 7).
 4. Sharp borders of the infraorbital groove and fissure (figs. 1B, 2B, 7, 8).
 5. Inferior border of supraorbital fissure (figs. 1A, 2A).
 6. Sharp margin, superior and lateral borders of the orbital aditus from the supra-orbital notch laterally to the midlevel of the frontal process of the zygoma (figs. 2A, 7).
 7. Superior margin of the infraorbital foramen (figs. 1A, 2A, 7).
 8. Sharp edge bordering nasal aperture, from nasal bones to anterior nasal spine (figs. 1A, 2A, 7).
 9. Margins of the tooth sockets (fig. 8).
 10. Posterior margin of the incisive foramen (figs. 1B, 2B, 9).
 11. Posterior border of palatine bone from posterior nasal spine to pyramidal process of palatine bone (figs. 1B, 2B, 9).
 12. Posterior border of vomer bone; also articulation with sphenoid bone (figs. 1B, 2B).
 13. Posterior edge of medial pterygoid plate (figs. 1B, 2B, 9).
 14. Inferior and posterior edges of lateral pterygoid lamina; pterygoid spine of Civinini (figs. 1B, 2B, 9).
 15. The crest separating scaphoid from pterygoid fossae (no fig.).
 16. Sharp margins of the spine of the angle of the sphenoid bone (figs. 1B, 2B).
 17. Infratemporal crest and spine (fig. 2B).
 18. Keel at anterior edge of pterygoid process bordering pterygopalatine fossa (no fig.).
 19. Sharp superior border of zygomatic arch; also the continuous acute posterior border of the frontal process of the zygoma, including the angular process and the continuation to the frontal bone as the anterior part of the superior temporal line (figs. 1A, 2A, 7).
 20. Free margin of the tympanic bone at the external acoustic meatus; also continuing sharp edge behind the postglenoid tubercle (figs. 1A, 1B, 2A, 2B).
 21. Miscellaneous irregular edges for tendinous attachment (masseter m.), along the lower border of the zygomatic arch and on the outer border of the mandibular fossa (figs. 1B, 2B).
 22. Lower free edge of tympanic plate including the vaginal process (figs. 1B, 2B).
 23. Inferior edge of the carotid canal (figs. 1B, 2B).
 24. Inferior edge of jugular foramen; also vertical crest on anterior wall of the jugular fossa (figs. 1B, 2B).
 25. Stylomastoid foramen (figs. 1B, 2B).
 26. Anteromedial, anterior, and lateral edges of articular surface of the occipital condyle (figs. 1B, 2B).
 27. Hypoglossal canal (no fig.).
 28. Posterior condyloid foramen (figs. 1B, 2B).
 29. Mastoid foramen, especially anterior border (figs. 1B, 2B).
 30. Foramen ovale (figs. 1B, 2B, 9).
 31. Foramen spinosum (figs. 1B, 2B).
 32. Thin posteriormost portion of foramen magnum (figs. 1B, 2B, 1C, 2C).
 33. Region of anterior palatal foramen; palatal crest (fig. 1B).
 34. Foramen lacerum (figs. 1B, 2B).
 35. Conchae and markings on the lateral wall of the nasal cavity (figs. 1A, 2A).
- II. *Interior of the cranial cavity.*
1. Free edge of crista galli (figs. 1C, 2C).
 2. Foramen cecum (no fig.).
 3. Cribriform plate and olfactory foramina of ethmoid bone (figs. 1C, 2C, 10).
 4. Posterior border of lesser wing of sphenoid (figs. 1C, 2C, 10).
 5. Superior and postero-inferior margin of optic canal (no fig.).
 6. Edges of posterior clinoid process and adjacent edges of dorsum sellae (figs. 1C, 2C, 10).
 7. General region of sphenoid body bounded by superior orbital fissure, foramen rotundum, foramen ovale, foramen spinosum, and intracranial carotid canal (figs. 1C, 2C, 10).
 8. Sharp edges of hiatus of facial canal (figs. 1C, 2C).
 9. Posterior border of internal acoustic meatus (figs. 1C, 2C).
 10. Superior margins of aqueductus vestibuli (no fig.).
 11. Posterior sharp border of petrous part of the temporal bone from apex to lateral terminus in the sigmoid sulcus (figs. 1C, 2C).
 12. Junction with sigmoid sulcus of mastoid foramen and posterior condyloid foramen (figs. 1C, 2C).
 13. The grooves for the middle meningeal artery (no fig.).

Although the foregoing classification covers most of the skull surface, certain regions are not included, such as the labyrinth and tympanic cavity of the temporal bone, the paranasal sinuses, and details of the nasal cavity. The reason in some cases was simply that not enough skulls were examined to permit definitive characterization of the features involved. In other instances, regions of very thin bone, such as the ethmoid bone, after being cleaned and bleached, did not withstand even moderate decalcification. When a few split-lines were produced in very thin bone, they often deteriorated from further decalcification of surrounding thicker bony regions or from storage in alcohol.

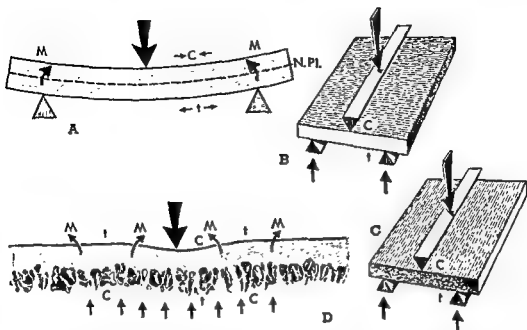


Fig. 12 Force patterns on thin plates with resultant deformations. A: A section through a plate resting on two supports with a deforming load at its middle. N.P.L., the neutral plane with shortened (c—compressed) material on the concave side and elongated (t—tensed) material on the convex side. The curved arrows (M) imply bending moments. B: A plate with a lengthwise grain spanning the supports. C: A cortical plate of bone having grain oriented crosswise to the first is notably weaker to bending loads. D: A thin plate of indeterminate dimensions resting on an elastic substrate, as diploe. A concentrated deforming force, just short of a breaking force, is resisted over a wide area by the substrate. Inward bending moments about the deforming compressive force tend to cause a depressed deformation with a compressed (c) and tensed (t) side. Compensatory outward bending moments with reversed compressed and tensed deformations appear at a distance.

edges; neglecting the weight of the plate in each case, the downward force (wedge and arrow) across the middle is exactly balanced by the sum of the opposite upward forces (arrows). The bending moments, the neutral plane, and the compressive (c) and tensile (t) forces are similar to those of the beam (fig. 12A). In figure 12B, the length of the middle wedge is perpendicular to the grain of the bone; this force system causes bending along (parallel to) the grain. In figure 12C, the wedge is parallel to the grain; this system causes bending across (perpendicular to) the grain. Practical experience with wood suggests that the plate in 12B is less likely to split under a given force than that in 12C, since resistance to bending along the grain (fig. 12B) is greater than resistance to bending across the grain (fig. 12C).

In fact, the experiments of Dempster and Coleman ('61) showed clearly that plates of tibial and mandibular bone (and birchwood) subjected to bending force systems are indeed much stronger in the lengthwise direction of the grain (as in fig. 12B) than in the crosswise direction (as in fig. 12C). In these studies, dry specimens of tibial cortex, mandibular cortex, and birchwood showed ultimate bending strengths crosswise to the grain (as in fig. 12C), that, in whole numbers, were only 17%, 43%, and 8%, respectively of the parallel-to-grain (fig. 12B) strength. The crosswise strength of water-soaked tibial pieces—more like fresh bone—was also 17% of the parallel-to-grain strength shown by wet pieces.

Mechanics of cortical bone in the skull. The skull, of course, is not formed of simple machined plates of cortical bone.

of force systems. First, the skull acts as a container for the brain and other cranial contents, for the eye and orbital contents, for the components of the inner and middle ear, and for the tongue mass. In a static gravitational system, these parts, like a fluid, exert forces against certain containing bony walls. Under the influence of rapid acceleration of centrifugal force acting on the head, or of impacts between the head and other objects, the directions of these container forces will change, and the magnitudes of the forces may exceed the usual gravitational level for short periods. Such container forces are chiefly from the inside out, to be resisted by the containing bony surface.

A second set of forces on the skull is the intrinsic system of tensile and compressive forces associated with muscles, joints, and teeth. Muscle tensions are exerted on the exterior of the skull by the neck muscles to the occipital and temporal bones and by the occlusal group of the masticatory muscles. Other muscles (e.g., buccinator, superior pharyngeal constrictor) exert lesser forces. Equal and opposite compressive forces arise in reaction to the muscle tensions; for example, the action of the atlas bone on the occipital condyles and the forces on the teeth and on the temporomandibular joint.

Other forces, of an extrinsic nature, can impinge on the exterior of the skull. Examples of static loads on the skull and head such as bindings are rather special. Impacts, however, are common. They may be caused, of course, by falls, blows of all sorts, collisions as with the dashboard of a decelerating automobile), bullets and projectiles, and so on. When the head and body form a battering ram, as in football, in bodies ejected to the ground from an automobile, or in diving accidents, the crown of the head makes the impact but the vertebral column may also carry the body inertia into the skull base.

The effect of any force on bone will be to bend the bone, to stretch it, compact it, cause it to shear, or some combination of these types of deformation. The great variety of skull fractures reported in clinical literature suggests that every skull bone can fail if subjected to a force sys-

tem of the proper kind and sufficient magnitude.

A fracture in response to applied forces must start at a particular millisecond of time at some localized area on the surface of the cortical layer of bone and spread from this point to produce a chip, large cleavage, crushed area, or comminuted fracture. In order to evaluate the cortical forms that were classified earlier, it will be necessary to examine some simple models of force systems on beams, plates, and shells.

Mechanics of cortical bone. Figure 12A introduces the basic mechanics of a deforming force (upper arrow) acting on a horizontal beam supported at each end. The total downward force (including the weight of the beam) will be equalled by the sum of the two resisting forces. Part of the middle downward force in relation to the right end force tends to rotate the right half of the beam in a counterclockwise direction; similarly, the middle downward and left end forces tend to rotate the left half in a clockwise direction. Each of these force arrangements is called a *force couple* and the measure of its tendency to bend is its *moment* or *torque*; in the figure, the moments are designated by the letter *M* and the curved arrows. The amount the beam bends downward under the influence of the two force couples depends on its stiffness. These force couples shorten or compress the upper surface of the beam as indicated by the arrows (*c* = compression) and stretches the lower surface (*t* = tension); but the middle plane of the beam (the neutral plane = *N. Pl.*) retains its normal length.

If the beam in figure 12A were a bar of cortical bone under a deforming force system having a magnitude that exceeded the yield strength of the bone, a fracture due to excessive force would be a tension failure, since the ultimate tensile strength of bone is only about 60% of the ultimate compressive strength (Dempster and Coleman, '61; Evans, '57). Thus, a fracture would begin on the convex surface and spread toward the concave side as a deepening split.

Figures 12B and 12C show broad plates of cortical bone instead of a narrow beam, resting on two supports near opposite

downward load act to maintain the form; thus, wedge-shaped pieces (called voussoir and keystone) are firmly pressed together by external pressures. In a bony ridge, the matrix grain is always lengthwise to the arch, so that whatever bony structure is responsible for the grain (lamellar bone, osteons, and so on) must be oriented in a predominantly lengthwise direction. Such elements, like the elements of the arch, would resist external forces efficiently. The elliptical dome or shell at B and the saddle-shaped ridge at C have similar cross sections and comparable fibrous patterns of the bony matrix; again, these patterns of grain represent mechanically advantageous arrangements for resisting external loads and pressures. The sections (mastoid process, frontal boss, and articular eminence) are all cut

transversely to the direction of the ridges and the grain of the ridges; in each instance, the ridge is relatively thick bone—an external pressure would tend to compact the material into a firm arch rather than cause it to collapse.

Troughs, (fig. 3T), such as the sulcus for the sigmoid and transverse sinus, the grooves for the internal carotid artery, and the arched part of the palatal arch, can be visualized as resisting pressure from within the curvature. Troughs are ordinarily much thinner-walled than bony ridges, and their structure is comparable to "membrane" structures in architecture (Nervi, '56; Timoshenko and Woinowsky-Krieger, '59; Salvadori and Heller, '63). A cloth or membrane draped over two supports sags, but it will support weight in its concavity (fig. 13D). The sketches

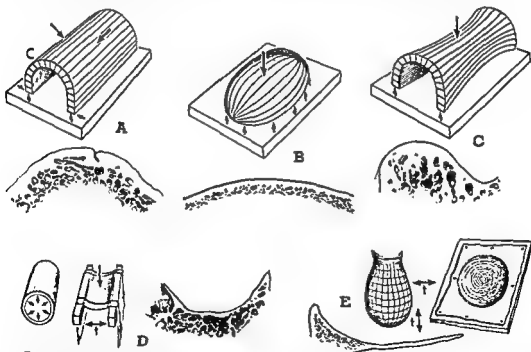


Fig. 13 Mechanical models illustrating certain structural characteristics. A: An arch made of elongate members resists downward external forces. B and C: The same is true for an elongate dome and a saddle-shaped arch. Below each model, the bone sections show (A) a transverse cut through the mastoid process, (B) a vertical cut through the frontal boss, and (C) a sagittal cut through the articular eminence. D: Tubing subjected to internal pressure, a membrane hanging across two supports, pressure against the thin-walled sulcus for the transverse venous sinus—in all these instances, pressure against the concave side of the trough is resisted by transverse, curved tensile fibers. E: A rubber balloon containing fluid, a rubber membrane sagging over a hole, and a section through the thin-walled lacrimal fossa of the orbit; in each instance, pressures are resisted by tensile fibers. In bony concavities, the circular grain predominates.

Most of the cranial and facial parts of the skull have inner and outer cortical bone and a middle layer of spongiosa or diploe. Air sinuses and pneumatic bone are also recognized specializations of the skull. Local areas of the bone in the temporal fossa, in the occipital base, and in the orbital and nasal walls have no spongiosa and consist of cortex alone. It will be convenient first to discuss cortical areas resembling plates or shells.

Many features of the mechanics of plates and shells, presented by Timoshenko and Woinowsky-Krieger ('59) relate to relatively thin, flat and curved engineering structures of sheet metal, concrete and other structural materials. One situation, in particular, applies to much of the inner and outer cortex of the skull: most of the cortex of the face and braincase may be viewed, in effect, as a continuous plate with indefinite limits (i.e., where edges may be ignored), supported by an elastic foundation. The plate may be viewed as having a large area relative to its thickness, and in this sense, it is like the paving of the runways of an airport or a public plaza. In such a system, localized forces cause localized deformations.

This concept (figure 12D) is illustrated by a layer of cortex supported by a foundation of spongiosa. A localized downward deforming force is balanced by equal and opposite forces of the spongiosa. The tendency is to depress the cortex locally (much as a person's foot depresses part of a rubber mat); bending moments (M) cause a downward bending about the downward force, with compressive stresses at the free surface and tensile stress on the spongiosa surface of the cortex. This deformation in turn produces, at a more outward position, compensating bending moments (M) in an opposite direction. The latter moments, in contrast to those near the applied force, produce a tension deformation of the cortex at the free surface and a compressive deformation at the spongiosa. In an isotropic material, a concave, circular depression results, and this is surrounded by a ring of radially tensed material. For a material like bone that is more susceptible in tensile than compressive failure, the initial fracture response would be tangential to the tensile

forces. If the surface being considered has a parallel grain pattern, an elliptical deformation or failure should be produced. This would be true for plane areas (P) of the skull with an oriented grain. A more broadly applied force should be transmitted through the spongiosa to the inner cortex, without localized deformation, and the whole thickness (all layers) of the bone should respond like a uniform plate.

Cranial fractures commonly cross sutures from bone to bone. The interlocking types of suture rarely separate. Doubtless, however, a suitable force applied directly over a simple (harmonic) suture should cause depression, separation, and possibly fracture. A consideration of the effect of force systems on the different types of sutures and synchondroses, however, leads away from the major concern of this paper with the texture and form of skull bone.

Architectural forms of the cortex. More specialized forms in the skull can be compared with common architectural and other structures for an evaluation of their characteristics. The Italian architect, Nervi ('56), and other architects of the past quarter century have pioneered with "form-resistant" structures; these include curved membranelike domes and roofs with a thickness that is small compared to the other dimensions. Unlike more usual framed structures, the strength of these structures, like that of boat hulls and aeroplane wings, is a consequence of the curvature of surfaces. Skull forms of cortical bone are closely related; they differ largely because of the underlying spongiosa. Figure 13 shows five forms that recur in parts of the skull other than the skull vault. At A, B, and C, ridges are shown in representative cross sections of skull bones and in corresponding architectural models. Typically, ridges are caused by undulations of the whole cortical layer and are not mere localized thickenings of cortex. The characteristic grain direction is indicated in the models. Sketch A is a barrel arch; as an architectural form it might exist as a free standing structure, or it could be a viaduct below a roadway or the archway to a building. In such structures, both the weight of the masonry and any superimposed

thin edges are bordered by a region of circular grain texture. In each instance, the part is strengthened by its texture, but it cannot be said whether or not the mechanical advantage due to texture fully compensates for the stress-concentrating effect of the discontinuity. A spine that has an effective texture may show a stress concentrating discontinuity at the angle between its stem and its base. No doubt a force system that is potentially large enough will damage the skull somewhere, and some region of discontinuity is a likely site for fracture initiation.

Massive regional fractures. In addition to the localized fractures discussed above, certain regions of the face or cranium may exhibit extensive fractures. For example, there are greater masses of bone at the level of the palate, at the level of the orbital floor, and at the brow level than in the regions between. As a response to impacts, the teeth and the entire alveolar arch may be sheared across below the palate, separating the region from the rest of the skull. There may be trans-nasal-maxillary sinus shearing fractures or transorbital fractures. These are massive responses to impacts across the face at different levels. The fractures, basically, are at right angles to the cortical grain of the bone.

Architectural and mechanical aspects of the skull vault

The architecture of the skull vault as a gross form may be evaluated profitably in different ways. As indicated previously, braincase cortex is characterized predominantly by a random arrangement of fibrous matrix. Except in responding to a sharp localized force, like a grazing bullet, the whole cranial wall tends to react as a unit. A localized compressive force to the outer surface (fig. 14A) may result in tensile deformation of the underlying inner table, or possibly comminuted fractures of the inner table; but little or no damage may occur to the outer table, because the compressive strength of the bone is much greater than the tensile strength.

A more extensive group of fractures involves the cranium as a whole, irrespective of surfaces. As noted above, the

cranial part of the skull acts as an oval container for the cranial contents. It is bounded, except for part of the basal region, by braincase bone consisting of inner and outer tables of cortex separated by a layer of diploe. The inner and outer cortical plates, except in old age, are generally thicker than facial-bone cortex in parts other than the mandible.

Figure 14B shows a saw-cut cross section of the skull, representing an approximate two-dimensional model that applies, more or less, to most of the skull vault. Under a compressive force system (fig. 14C) the skull section flattens like a ring. The inner cranial surface opposite the applied compressive forces shows tensile deformations; at 90° around the section from the applied force, the deformations are reversed with tension acting on the external table and compression on the internal. Gurdjian and Lissner ('45) have demonstrated this type of skull deformation in experimental impacts. Thus, tensile fractures arising, contracoup, at a distance from an impact site on the skull vault may spread widely. Because they often extend widely from the site of fracture initiation, the fractures may reach into the foramina at the base of the skull or to the middle meningeal artery at the thin bone of the temporal fossa, resulting in hemorrhage or serious soft-tissue damage to cranial nerves. This tendency is increased by the stress-concentrating, bone-weakening effect of discontinuities at the base of the skull.

The cranium should also be viewed as a three-dimensional structure; a barrel provides a satisfactory model (fig. 14D). A barrel may carry a load on its top, forming with the floor a compressive force system. The staves transmit compression while tending to bend outward; the hoops, however, are subjected to tensile forces which oppose the deformation of the staves. Similarly, an uncooked hen's egg may withstand a compressive force of 75 pounds if its ends are suitably padded (fig. 14E). Again, as compressive forces are transmitted from end to end, the sides tend to bulge like the hoop at C, and internal stresses transverse to the length of the egg exerting tension to counteract the bowing outward. The egg, like the barrel,

at D also show rubber tubing subjected to internal pressure; the rubber yields primarily by stretching its circumference. A transverse circular covering, lining, or cordage, will effectively limit this yielding of the rubber and provide greater resisting strength. This is the direction of the grain in bony troughs. Thus, by analogy, the transverse grain pattern found in bony troughs should be suited for the type of strength needed in a trough.

Biconcave depressions (fig. 3C) can also be considered as membranes. Sketch E (fig. 3) shows a rubber balloon containing fluid. The fluid exerts an outward pressure on the surface "membrane" which is under tension in the directions shown; that is, both vertically and transversely along the lines encircling the fluid. As the volume and circumference increase with more fluid, each circular tension line must stretch. Likewise, a thin rubber membrane tacked to a board with a circular hole in it will resist the pressure of fluid through both circular and radial tensions (like those at the lowest part of the drop of fluid). In fact, the circular resistance will be greater than that across the surface, since for every unit that a diameter is increased, the circumference of the corresponding circle on the membrane must increase by π times the diameter. Grain in the floor of bony concavities is generally circular and will thus resist such circumferential stretching, effectively tending to prevent outward deformation of the concavities.

As indicated in the classification, thin, unsupported edges and spines (figs. 3E and S) consistently have an elongate grain pattern that either parallels the edge or runs lengthwise in the spine to converge at the apex. This grain pattern, like the grain of an elongate wooden beam, since it lies in the direction of greatest strength, contributes to the resistance to bending. This is equally true for a cantilever beam, like a spine, and also for an unsupported edge.

Discontinuities as weak regions. Discontinuities require special consideration in the evaluation of the strength of the skull. The force borne by a structure is ordinarily treated in terms of a mean stress — the force per unit area of a cross

section. For engineering or mechanical structures that have uniform cross sections, the average stress to be borne by a particular structure whether tensile, compressive, or shear stress) serves quite suitably as a criterion for evaluating the strength and the margin of safety of the structure. Experience has shown, however, that even small discontinuities in the surface or in the homogeneity of a member will increase the stress in one or more regions, the increase being out of all proportion to the mean stress across the structure. Thus, the part will fail more readily than might be assumed from the average stress values alone.

In this regard, there are two fields of physical science, namely, photoelasticity (Frocht, '41; Heywood, '52; Coker and Filon, '57) and the theory of plates and shells (Timoshenko and Woinowsky-Krieger, '59), that have supplied much evidence that discontinuities such as holes, sharp angles, notches, fillets, sudden changes in thickness, and so on — regardless of the material involved — cause great concentrations of stress. Regions of high stress concentration are regions of weakness and potential failure. Conversely, it has been pointed out (Heywood, '52) that mechanically sound designs avoid discontinuities and the likelihood of dangerous levels of stress.

In bones, discontinuities such as foramina, notches, edges, and sharp angles all concentrate stress much beyond average values, and it is here that fractures may begin to form. Discontinuities of skull bones, such as the mental foramina of the mandible or the cribriform plate of the ethmoid bone, may thus account for the frequency of fractures traversing these structures. Any of the discontinuities in the list above is presumptively a "weak" feature of the skull. Some discontinuities in the skull occur in groups as such complex congeries of edges, spines, and foramina as to defy systematic analysis. The region on each side of the skull bounded by the pterygoid process, the occipital condyle, the mastoid process, and the articular eminence of the temporal bone is such a region.

Spines and edges, as noted, have an elongate grain structure; foramina with

sinus. An eccentric force on the skull vault would result in one pillar or another transmitting much of the load in the base of the skull and vertebral column. The stress distribution through the skull could be much more complex than that of a comparable force system on an egg.

DISCUSSION

Seven grain-form relationships are recognized in the adult skull: (1) a random pattern of braincase cortex, (2) planes and (3) ridges with elongate grain, (4) troughs with transverse grain, (5) concavities with circular patterns, (6) edges, and (7) spines. Concavities may show a superimposed trough or ridge structure, and troughs may be marked by localized ridges and planes. That is, trough patterns are dominant over concavity patterns, and ridge patterns are dominant over both trough and concavity patterns. Finally, there are a few small cranial areas that are random distributions in some skulls and planes in others; the skull vault proper, however, except for the forehead region and internal sagittal markings, has a random pattern throughout.

Bone resists deformation and fracture best in the long direction of its grain texture but is a relatively weak material crosswise. The classification of form-texture relationships presented in this paper includes most of the parts of the adult skull. They are discussed as architectural features of the skull, and their adequacy and limitations are analyzed in terms of their reaction to force systems and their proneness to fracture. All seven form-texture relationships over localized areas show grain directions that are in accord with the best mechanical use of the material of which they are made. Moreover, as shown in figure 5, the various ridges appear to be deployed over the upper- and mid-face and over the skull base, both exterior and interior, so as to provide ribbing and buttressing that should add strength. Plane areas (fig. 4), strong in the direction of the grain and weak crosswise, are typically bounded by ridges, edges, or random braincase bone; the grain direction may be assumed to contribute more to strength than if it were oriented at 90° to the grain actually seen

in the skull. Most random patterned bone (fig. 4) gets its strength from the oval shape of the braincase, from the three layered structure, including diploe, of most of the skull vault, and from the thickness of the cortical tables. The other forms contribute less to total skull strength. Edges (fig. 7) and spines (fig. 6) have a grain pattern that provides localized reinforcement. Troughs (fig. 6) and concavities (fig. 7) are usually localized areas of thin bone; the arrangement of the texture, however, best resists surface pressures.

An eighth relationship — discontinuity — is recognized; this contains regions of potentially high stress concentration and weakness in the skull, even though certain discontinuities such as edges, spines, and thin foramina may show an effective use of texture.

In the mechanics and engineering field known as "strength of materials" homogeneous bars of test materials are subjected to detailed analyses of strains under force systems of different types. For many force situations, as a beam in bending or a column in torsion, the stresses vary from point to point, and maps or diagrams showing the directions of the maximum and minimum, or principal, stresses have been made. Sets of compression and tension lines always cross at right angles; the curves show the direction of stresses only, and the magnitudes of the stresses along the lines vary. For more than a hundred years, these lines of principal stress in homogeneous material have been designated "trajectories."

This term trajectory has now been taken over by some students of bone, and its original and only coherent meaning has been seriously distorted. In particular, since Meyer's demonstration of the trabecular patterns of the spongiosa of the femur and other bones (1867), the trabeculae of the spongiosa have even been regarded as specializations, or as trajectories, for carrying tensile or compressive forces, ignoring completely the weakness of the spongiosa as a material. Koch ('17), however, showed that in the femur, the trabecular pattern parallels the lines of maximum stress as the bone bears loads and transmits forces and thus serves

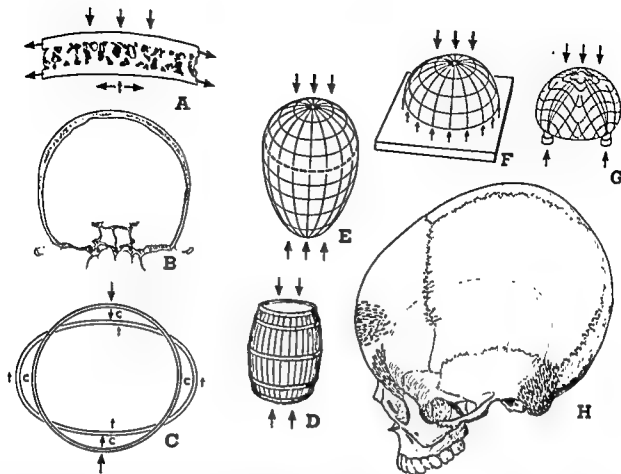


Fig. 14 A: Bone of the skull vault in section; exterior compressive force induces tensile deformation on inner table. B and C: Transverse section of skull under compressive force deforms like circular ring with four regions of high tensile (t) and compressive (c) strains. D and E: In a three-dimensional sense, the skull deforms like the barrel at D and the egg at E. Vertical compression is transmitted from end to end and there are transverse circumferential tensions (suggested by the hoops in the barrel) and a three-dimensional force system analogous to that shown in the section at C. F: A dome on a horizontal support acts like the half of an egg above its equator. G: For a braincase with its random-patterned texture continues the grain pattern shown, both in the base and in several external (and internal) pillars. (Sketches F and G from Salvadori and Heller, '63, with permission.)

exerts both tensile and compressive forces (along lines such as those shown) to resist the external load; yet the egg shell has no grain structure.

Figure 14F is an architectural dome corresponding to the broad end of the egg. Its mode of resisting a vertical force (its own weight, or an external force) is the same as that of the egg. If a dome is supported on pillars (fig. 14G), however, its weight must be counterbalanced at the support points where stress will be concentrated at higher levels.

In the skull the cranial vault is partly supported by ridges of bone with definite grain forming pillars or buttresses (as in

fig. 14G), and is partly continuous with the base of the skull as in fig. 14F). The cortical tables of most of the skull vault have a random pattern of grain, forming a rough equivalent to the grainless structure of the egg. The buttresses (fig. 14H) are: on the external table of the skull vault—the two mastoid processes laterally with a vertical ridge grain; the two zygomatico-frontal buttresses laterally with a vertical fan of plane grain pattern; anteriorly, the frontal boss with a transverse ridge grain. Not shown on the inner table are vertical ridges or crests, with elongate grain, flanking the frontal and occipital parts of the superior sagittal

sinus. An eccentric force on the skull vault would result in one pillar or another transmitting much of the load to the base of the skull and vertebral column. The stress distribution through the skull could be much more complex than that of a comparable force system on an egg.

DISCUSSION

Seven grain-form relationships are recognized in the adult skull: (1) a random pattern of braincase cortex, (2) planes and (3) ridges with elongate grain, (4) troughs with transverse grain, (5) concavities with circular patterns, (6) edges, and (7) spines. Concavities may show a superimposed trough or ridge structure, and troughs may be marked by localized ridges and planes. That is, trough patterns are dominant over concavity patterns, and ridge patterns are dominant over both trough and concavity patterns. Finally, there are a few small cranial areas that are random distributions in some skulls and planes in others; the skull vault proper, however, except for the forehead region and internal sagittal markings, has a random pattern throughout.

Bone resists deformation and fracture best in the long direction of its grain texture but is a relatively weak material crosswise. The classification of form-texture relationships presented in this paper includes most of the parts of the adult skull. They are discussed as architectural features of the skull, and their adequacy and limitations are analyzed in terms of their reaction to force systems and their proneness to fracture. All seven form-texture relationships over localized areas show grain directions that are in accord with the best mechanical use of the material of which they are made. Moreover, as shown in figure 5, the various ridges appear to be deployed over the upper- and mid-face and over the skull base, both exterior and interior, so as to provide ribbing and buttressing that should add strength. Plane areas (fig. 4), strong in the direction of the grain and weak crosswise, are typically bounded by ridges, edges, or random braincase bone; the grain direction may be assumed to contribute more to strength than if it were oriented at 90° to the grain actually seen

in the skull. Most random patterned bone (fig. 4) gets its strength from the oval shape of the braincase, from the three layered structure, including diploe, of most of the skull vault, and from the thickness of the cortical tables. The other forms contribute less to total skull strength. Edges (fig. 7) and spines (fig. 6) have a grain pattern that provides localized reinforcement. Troughs (fig. 6) and concavities (fig. 7) are usually localized areas of thin bone; the arrangement of the texture, however, best resists surface pressures.

An eighth relationship — discontinuity — is recognized; this contains regions of potentially high stress concentration and weakness in the skull, even though certain discontinuities such as edges, spines, and thin foramina may show an effective use of texture.

In the mechanics and engineering field known as "strength of materials" homogeneous bars of test materials are subjected to detailed analyses of strains under force systems of different types. For many force situations, as a beam in bending or a column in torsion, the stresses vary from point to point, and maps or diagrams showing the directions of the maximum and minimum, or principal, stresses have been made. Sets of compression and tension lines always cross at right angles; the curves show the direction of stresses only, and the magnitudes of the stresses along the lines vary. For more than a hundred years, these lines of principal stress in homogeneous material have been designated "trajectories."

This term trajectory has now been taken over by some students of bone, and its original and only coherent meaning has been seriously distorted. In particular, since Meyer's demonstration of the trabecular patterns of the spongiosa of the femur and other bones (1867), the trabeculae of the spongiosa have even been regarded as specializations, or as trajectories, for carrying tensile or compressive forces, ignoring completely the weakness of the spongiosa as a material. Koch ('17), however, showed that in the femur, the trabecular pattern parallels the lines of maximum stress as the bone bears loads and transmits forces and thus serves

in the cross grain direction. The skull vault, like the egg, gains strength through its form and through the use of a structural material that is equally strong in all directions. Strength tests on parietal bone by Evans and Lissner ('57) suggest an intermediate level of tensile strength; the test, however, related to whole thickness bone and not to single tables of cortical bone.

Editor's note

This manuscript was edited from the final rough draft which Dr. W. T. Dempster had written shortly before he died.

F. Gaynor Evans

LITERATURE CITED

- Ahrens, H. J. 1936 Die Entwicklung der Spaltlinienarchitektur des knöchernen menschlichen Schädels. *Morphol. Jahrb.*, 77: 357-371.
- Ascenzi, A., and E. Bonucci 1964 The ultimate tensile strength of single osteons. *Acta Anat.*, 58: 180-183.
- Benninghoff, A. 1925 Spaltlinien am Knochen, eine Methode zur Ermittlung der Architektur platter Knochen. *Verhandl. d. anat. Ges.*, 34th meeting, Vienna, 189-206.
- 1934 Die Architektur der Kiefer und ihrer Weichteilbedeckungen. *Paradentium*, 6: 2-20.
- Bruhne, J. 1929 Ein Beitrag zur Struktur der Knochencompakta bei Quadrupeden. *Morphol. Jahrb.*, 61: 555-588.
- Bühler, E. 1934 Über die funktionelle Architektur der Kehlkopfknorpel des Menschen. *Z. f. Morphol. u. Anthropol.*, 33: 227-260.
- Coker, E. G., and L. N. G. Filon 1957 A Treatise on Photo-elasticity. 2nd. ed. revised by H. T. Jessop. University Press, Cambridge, England, xxiv + 720 pp.
- Dempster, W. T., and R. F. Coleman 1961 Tensile strength of bone along and across the bone. *J. Appl. Physiol.*, 16: 335-360.
- Dempster, W. T., and D. H. Enlow 1959 Patterns of vascular channels in the cortex of the human mandible. *Anat. Rec.*, 135: 189-205.
- Dempster, W. T., and R. T. Liddicoat 1952 Compact bone as a non-isotropic material. *Am. J. Anat.*, 91: 331-362.
- Dowgiallo, N. D. 1932 Die Struktur der Compacta des Unterkiefers bei normalen und reduziertem Alveolarfortsatz. *Z. f. Anat. u. Entw.-gesch.*, Berlin, 97: 55-67.
- Enlow, D., and S. Bang 1965 Growth and remodeling of the human maxilla. *Am. J. Orthodont.*, 51: 446-464.
- Evans, F. G. 1957 Stress and Strain in Bones. Their Relation to Fractures and Osteogenesis. Charles C Thomas, Springfield, Ill., x + 245 pp.
- 1964 Significant differences in the tensile strength of adult human compact bone. *Proc. European Bone and Tooth Symp.* (Oxford, 1963), 1: 319-331.
- Evans, F. G., and H. R. Lissner 1957 Tensile and compressive strength of human parietal bone. *J. Appl. Physiol.*, 10: 493-497.
- Frocht, M. M. 1941 Photoelasticity. 2 vols. J. Wiley and Sons, New York.
- Gurdjian, E. S., and H. R. Lissner 1945 Deformation of the skull in head injury: a study with the "stresscoat" technique. *Surg., Gynec. and Obstet.*, 81: 679-687.
- Henckel, K. O. 1931 Vergleichend-anatomische Untersuchungen über die Struktur der Knochencompakta nach der Spaltlinienmethode. *Morphol. Jahrb.*, 66: 22-45.
- Heywood, R. B. 1952 Designing by Photoelasticity. Chapman and Hall, London, 371 pp.
- Holtkranz, W. 1898 Über die Spaltstrichungen der Gelenkknorpel. *Verhandl. anat. Ges.*, Jena, 12: 248-256.
- Ilberg, A. 1935 Über die funktionelle Architektur der Nasenknorpel und ihrer knöchernen Umgebung beim Menschen. *Z. f. Laryngol., Rhinol., u. Otol.*, 26: 239-257.
- Koch, J. C. 1917 The laws of bone architecture. *Am. J. Anat.*, 21: 177-298.
- Langer, K. 1861 Zur Anatomie und Physiologie der Haut. I. Über die Spaltbarkeit der Cutis. *Sitzungsber. d. Kaiserl. Akad. d. Wiss., Wien. Mathematisch-naturw. Classe*, 44: 19-46.
- Meyer, G. H. 1867 Die Architektur der Spongiosa. *Arch. f. Anat., Physiol., u. Wiss. Med.*, 47: 615-628.
- Nervi, P. L. 1936 Structures. F. W. Dodge, New York, x + 118 pp.
- Olivo, O. M., G. Maj and E. Toajari 1937 Sul significato della minuta struttura del tessuto osseo compatto. *Bull. delle Sci. Med.*, 109: 369-394.
- Salvadori, M., and R. Heller 1963 Structure in Architecture. Prentice-Hall, Inc., Englewood Cliffs, N. J., 370 pp.
- Seipel, C. M. 1948 Trajectories of the jaws. *Acta Odontol. Scand.*, 8: 81-191.
- Tappen, N. C. 1964 An examination of alternative explanations of split-line orientation in compact bone. *Am. J. Phys. Anthrop.*, 22: 423-442.
- 1954 A comparative functional analysis of primate skulls by the split-line technique. *Human Biol.*, 26: 220-238.
- 1953 A functional analysis of the facial skeleton with split-line technique. *Am. J. Phys. Anthrop.*, 11: 503-532.
- Taxman, R. M. 1963 Incidence and size of the juxtamastoid eminence in modern crania. *Am. J. Phys. Anthrop.*, 21: 153-157.
- Timoshenko, S., and S. Woinowsky-Krieger 1959 Theory of Plates and Shells, 2nd ed. McGraw-Hill, New York, 580 pp.
- Weinmann, J. P., and H. Sicher 1947 Bone and Bones, Fundamentals of Bone Biology. C. V. Mosby, St. Louis, 464 pp.

as the most effective distribution of spongiosa. But Koch did not even mention the term trajectory.

In the traditional armchair view of the mechanics of the skull, the masticatory apparatus with its mobile jaw, teeth, and muscles, has been emphasized more than any other system for transmitting stresses. Pressure-carrying specializations in the form of pillars, beam, and buttresses have been postulated from the teeth to the upper skull; these extend vertically between the nose and orbit, through the zygoma, both through the zygomatic arch and the lateral orbital margin, and from the last molar region through the pterygoid process to the skull base. Muscular tensions bridge between the jaw angle and the zygomatic arch, and from the coronoid process to the temporal fossa with the bones transmitting forces to the teeth (Weinmann and Sicher, '47). The pillar idea is based on the general appearance of skull ridges and is not based on any bone measurements showing thick columns of increased cross-sectional area acting to reduce stress values (force per unit area).

When split-line patterns in the skull appeared to parallel the buttresses and pillars, the idea that these tracts served as cortical trajectories, or "cortical pressure lines," was formulated (Benninghoff, '25; Seipel, '48; Tappen, '53). No mechanically coherent interpretation involving force or stress was given to tell what these terms really meant. The implication, however, is that the tracts developed in the individual as response to functional stresses (Wolff's Law). This explanation must be speculative, since we know of no mechanism at the molecular level through which the processes of bone reorganization and growth might form pillars or pressure tracts under the influence of stresses transmitted along the pillars. The so-called masticatory pillars could be genetically determined growth specializations; the orientation of grain along them might or might not be a secondary mechanical adaptation.

The skull of an infant grows and changes its shape and form through childhood and adolescence, eventually acquiring adult architectural characteristics.

That is, the bone is resorbed, redeposited, and reconstructed until the multitude of eminences, processes, and fossae attain the structural forms and textures exhibited by an adult skull. Most of the texture of infantile bone is suppressed by secondary growth changes. This study points out that the grain of bone (as represented by the fibromatrix of the decalcified bone) and the form of bone in adult skulls are closely correlated. The work, however, suggests no clues as to how or why these relations came to be.

An alternate interpretation to the pressure line or trajectory idea of skull texture can be suggested. Since bone is especially weak crosswise to the grain for tension, compression, bending, and torsion, one may assume that crosswise properties, when not specifically arranged to best advantage (because of growth changes and new functional demands), present a weak feature to be modified by osteoblast and osteoclast activity as the bone grows under the stresses of normal functioning. Textures, thus, should reorient from infantile patterns as a response to bone growth influenced by the increasing size of the brain, orbital contents, and tongue, the formation of more cortex, more spongiosa, and more marrow space, the development of diploe, the formation of air sinuses, the adaptation to growing tooth germs, the superimposition of sexual specialization, and so on.

It is reasonable to propose that weak and inefficient bony tissues are replaced during bone reconstruction under the influence of intermittent stresses by bone textures of more effective orientation. Enlow and Bang ('65) have shown that gross form changes and growth of the maxilla involve complex reconstructive changes, periosteal deposition on certain surfaces, periosteal resorption on others, with either endosteal deposition or endosteal resorption on still other surfaces. The adult form-texture relationship presented in this paper should arise in time, as a compensation for mechanically weaker features of a grain oriented initially by embryonic and fetal growth. Such a view further proposes that a randomly oriented braincase texture should be stronger in all directions under tensile and compressive loads than is bone

in the cross grain direction. The skull vault, like the egg, gains strength through its form and through the use of a structural material that is equally strong in all directions. Strength tests on parietal bone by Evans and Lissner ('57) suggest an intermediate level of tensile strength; the test, however, related to whole thickness bone and not to single tables of cortical bone.

Editor's note

This manuscript was edited from the final rough draft which Dr. W. T. Dempster had written shortly before he died.

F. Gaynor Evans

LITERATURE CITED

- Ahrens, H. J. 1936 Die Entwicklung der Spaltlinienarchitektur des knöchernen menschlichen Schädels. *Morphol. Jahrb.*, 77: 357-371.
- Ascenzi, A., and E. Bonucci 1964 The ultimate tensile strength of single osteons. *Acta Anat.*, 58: 160-183.
- Benninghoff, A. 1925 Spaltlinien am Knochen, eine Methode zur Ermittlung der Architektur platter Knochen. *Verhandl. d. anat. Ges.*, 34th meeting, Vienna, 189-206.
- 1934 Die Architektur der Kiefer und ihrer Weichteilbedeckungen. *Paradentium*, 6: 2-20.
- Bruhns, J. 1929 Ein Beitrag zur Struktur der Knochencompakta bei Quadrupen. *Morphol. Jahrb.*, 61: 555-588.
- Bühler, E. 1934 Über die funktionelle Architektur der Kehlkopfknorpel des Menschen. *Z. f. Morphol. u. Anthropol.*, 33: 227-260.
- Coker, E. G., and L. N. G. Filon 1957 A Treatise on Photo-elasticity, 2nd. ed. revised by H. T. Jessop. University Press, Cambridge, England, xxv + 720 pp.
- Dempster, W. T., and R. F. Coleman 1961 Tensile strength of bone along and across the bone. *J. Appl. Physiol.*, 16: 355-360.
- Dempster, W. T., and D. H. Enlow 1959 Patterns of vascular channels in the cortex of the human mandible. *Anat. Rec.*, 135: 189-205.
- Dempster, W. T., and R. T. Liddicoat 1952 Compact bone as a non-isotropic material. *Am. J. Anat.*, 91: 331-362.
- Dowgiallo, N. D. 1932 Die Struktur der Compacta des Unterkiefers bei normalen und reduziertem Alveolarfortsatz. *Z. f. Anat. u. Entw.-gesch.*, Berlin, 97: 55-67.
- Enlow, D., and S. Bang 1965 Growth and remodeling of the human maxilla. *Am. J. Orthodont.*, 51: 446-464.
- Evans, F. C. 1957 Stress and Strain in Bones. Their Relation to Fractures and Osteogenesis. Charles C Thomas, Springfield, Ill., x + 245 pp.
- 1964 Significant differences in the tensile strength of adult human compact bone. *Proc. European Bone and Tooth Symp.* (Oxford, 1963), 1: 319-331.
- Evans, F. C., and H. R. Lissner 1957 Tensile and compressive strength of human parietal bone. *J. Appl. Physiol.*, 10: 493-497.
- Frucht, M. M. 1941 Photoelasticity. 3 vols. J. Wiley and Sons, New York.
- Gurdjian, E. S., and H. R. Lissner 1945 Deformation of the skull in head injury: a study with the "stresscoat" technique. *Surg., Gynec. and Obstet.*, 81: 679-687.
- Henckel, K. O. 1931 Vergleichend-anatomische Untersuchungen über die Struktur der Knochencompakta nach der Spaltlinienmethode. *Morphol. Jahrb.*, 66: 22-45.
- Heywood, R. B. 1952 Designing by Photoelasticity. Chapman and Hall, London, 371 pp.
- Hultzkranz, W. 1898 Über die Spaltstrichtungen der Gelenkknorpel. *Verhandl. anat. Ges.*, Jena, 12: 248-256.
- Uberg, A. 1935 Über die funktionelle Architektur der Nasenknorpel und ihrer knöchernen Umgebung beim Menschen. *Z. f. Laryngol., Rhinol., u. Otol.*, 26: 239-257.
- Koch, J. C. 1917 The laws of bone architecture. *Am. J. Anat.*, 21: 177-298.
- Langer, K. 1861 Zur Anatomie und Physiologie der Haut. I. Über die Spaltbarkeit der Cutis. *Sitzungsber. d. Kaiserl. Akad. d. Wiss., Wien. Mathematisch-naturw. Classe*, 44: 19-46.
- Meyer, G. H. 1867 Die Architektur der Spongiosa. *Arch. f. Anat., Physiol., u. Wiss. Med.*, 47: 615-628.
- Nervi, P. L. 1956 Structures. F. W. Dodge, New York, x + 118 pp.
- Olivio, O. M., G. Maj and E. Tojari 1937 Sul significato della minuta struttura del tessuto osseo compatto. *Bull. delle Sci. Med.*, 109: 369-394.
- Salvadori, M., and R. Heller 1963 Structure in Architecture. Prentice-Hall, Inc., Englewood Cliffs, N. J., 370 pp.
- Seipel, C. M. 1948 Trajectories of the jaws. *Acta Odontol. Scand.*, 6: 81-191.
- Tappen, N. C. 1964 An examination of alternative explanations of split-line orientation in compact bone. *Am. J. Phys. Anthropol.*, 22: 423-442.
- 1954 A comparative functional analysis of primate skulls by the split-line technique. *Human Biol.*, 26: 220-238.
- 1953 A functional analysis of the facial skeleton with split-line technique. *Am. J. Phys. Anthropol.*, 11: 503-532.
- Taxman, R. M. 1963 Incidence and size of the juxtamastoid eminence in modern crania. *Am. J. Phys. Anthropol.*, 21: 153-157.
- Timoshenko, S., and S. Woinowsky-Krieger 1959 Theory of Plates and Shells, 2nd ed. McGraw-Hill, New York, 580 pp.
- Weinmann, J. F., and H. Sicher 1947 Bone and Bones, Fundamentals of Bone Biology. C. V. Mosby, St. Louis, 464 pp.

Properties of Body Segments Based on Size and Weight¹

WILFRID TAYLOR DEMPSTER AND GEORGE H. L. GAUGHRAN

Department of Anatomy, The University of Michigan, Ann Arbor, Michigan
and Department of Anatomy, The Ohio State University, Columbus, Ohio

ABSTRACT Values are presented for body constants based on a study of nine male white cadavers of normal appearance and average build. The limb data are supplemented by a further analysis of 11 upper and 41 lower limbs. Techniques used in the study form standard procedures that can be duplicated by subsequent workers. Each cadaver was measured, weighed, and somatotyped. Joints were placed in the midposition of the movement range and the body was frozen rigid. Joint angles were bisected in a systematic dismemberment procedure to produce unit segments. These segment lengths were weighed, measured for linear link dimensions, and analysed for segment volumes. The segment centers of mass were located relative to link end points as well as in relation to anatomical landmarks. Finally, each segment was dissected into its component parts and these were weighed. The specific gravity of each body part was calculated separately. Data are expressed in mean values together with standard deviations and, where available, are correlated and evaluated with other values in the literature.

Data on the relative bulk of body segments have been scarce. Until recently, the only users of information dealing with the mass and proportion of the human figure have been sculptors and graphic artists. These people usually met their needs through canons of proportions and a trained perception rather than by actual measurement. There are no substitutes though for good empirical data when critical work on body mechanics or accurate analyses of human locomotion are attempted. During the past decade or so, the need for such information has been recognized specifically in designing prosthetic and orthotic devices for the limbs of handicapped persons, for sports analysis, for the construction of test dummies, such as those subjected to vehicular crashes, and for studies on the dynamics of body impacts in crashes and falls. The fundamental nature of data on the mass and dimensions of the body parts cannot be questioned. It is odd that even now there is such a dearth of information.

The research literature up to the present contains usable body segment measurements from only 12 (or possibly 14) un-preserved and dismembered cadavers, all adult white males. A tabulation of data in an Air Force technical report (Dempster, '55a), dealing with seven specimens ca-

daver by cadaver, was the first amplification of the scanty records in more than two generations. The tables on Michigan cadavers were reprinted by Krogman and Johnston ('63) in an abridgment of the original report; Williams and Lisner ('62) presented their own simplifications based on the same study; Barter ('57), Duggar ('62) and Contini, Drillis, and Bluestein ('63) have made tallies of data from the original tabulations along with parts of the older data. None of these studies gave any attention to the procedural distinctions between workers who had procured original data; one even grouped volumes and masses indiscriminately as masses. The Michigan data, however, have not been summarized nor evaluated up to this time. Since the procedures and, especially, the limiting conditions incidental to the gathering of body-segment data, have not been commented on critically since Braune and Fischer (1889), a comprehensive discussion of the entire problem at this point should help further work in this important area.

¹Supported in part by research grants from the Public Health Service National Institutes of Health (GM-07741-06), and from the office of Vocational Rehabilitation (RD-218 60-C), with support a dozen years earlier from a research contract with the Anthropometric Unit of the Wright Air Development Center, Wright Patterson Air Force Base, Dayton, Ohio (AF 15 (600)-43 Project no. 7414).

The present study, therefore, has a four-fold function: (1) to summarize statistically the above mentioned (Michigan) raw data and make minor corrections, (2) to correlate and evaluate these findings with those of others, if appropriate, (3) to present additional information relevant to the segment volumes of cadavers, and (4) to suggest both problems and techniques to future investigators, especially those located where cadavers are more readily available. These objectives require critical and interpretive comment about the earlier studies and about some aspects of our techniques.

Previous studies

Since earlier authors derived body mass data in diverse ways, one must either select the work of one author and ignore the rest, or make an attempt to consolidate and salvage parts of the scanty data. The latter procedure, however, is subject to question when records from different authors are pooled indiscriminately as was done by Barter ('57). In order to correlate old data with more recent work, it is necessary to examine the several procedures for dismemberment in some detail. The order of magnitude of difference in data caused by sawcuts, for example, may be quite significant. One sawcut might remove material from one segment and add it to the adjacent one, whereas another cut might do the reverse. Thus the locations of the center of mass (center of gravity) in a segment may be inconsistent in two groups of data unless allowances are made for the dismemberment procedures used.

The first attempt to obtain comprehensive data on cadaver segments was that of Harless (1857, 1860). Although Harless was a physiologist, his research on body segments related to his lectures and text on art anatomy (1857). Harless dismembered and measured the parts of two male cadavers. The subjects were executed criminals; beheaded, and consequently drained of blood. The mass and center of mass of the head were determined from the severed part, arbitrarily defined as it was by the beheading procedure and the rationale of some other procedures were equally questionable. The soft tissues of

the hip were cut transversely at the joint level and then below this were separated from the lateral face of the pelvis; the joint capsule was encircled by a cut, and the femoral head was simply disarticulated. The shoulder mass was disarticulated after two knife cuts: (1) a vertical cut through the axillary folds and (2) a horizontal cut below the acromial process. The more distal joints of the limbs in extension were sawed through at joint centers at the femoral condyles, at the malleoli, at the humeral condyles, and distal to the ulnar styloid process. Harless described a method of locating joint centers in the living by making triple exposure photographs with the limb in three positions against a dark red background; it is not clear how he located joint centers in the cadavers. Skin flaps at the two ends of a segment were stretched over the cut surface and stitched like amputation stumps to compensate for nonuniform retraction of the soft tissues at the cuts. Harless determined the linear dimensions, the masses, and the centers of mass of the several segments. He also attempted to locate the center of mass of the trunk section by a crude mathematical approximation. The living weight of one subject was obtained before execution; that of the other was taken as the sum of the dismembered parts, corrected by the percentage of loss of blood in the first subject. It is somewhat difficult today to evaluate Harless's measurements in terms of later data. Linear measurements given in hundredths or thousandths of centimeters are technically unrealistic. Harless's research plan was too limited to yield many useful measurements for body mechanics. His simple calculations of trunk mass, for example, involved density correction for the total body rather than for the thoracic and lower trunk sections, and his determinations of centers of mass located them only along the lengths of the segments. Braune and Fischer (1889) criticized Harless's method for obtaining the latter information since it involved suspension of flabby, non-rigid parts. As a subsidiary part of Harless's paper on body segments, he measured the specific gravity (density) of the limb segments of his second speci-

men and those of five other subjects, including females.

During the latter half of the nineteenth century, anatomists and pathologists recorded the mass and specific gravity of numerous body organs, as summarized by Vierordt (1893). More recent tabulations (Spector, '56) show no appreciable increase in this type of data. The first to mention the masses of the head, trunk, and limbs was Krause (1843), and Meyer (1873) used these masses for calculations. By using simple geometrical figures with human dimensions, Meyer estimated the center of mass for the body in various postures. Valentin (1850) tabulated the masses of the head, limbs, and certain viscera for three newborn infants.

In 1884, Meeh (1895) dismembered and measured masses and volumes of the parts of four infants: one premature, two newborn, and one in its second year. (The data were prepared for publication by Voit in 1895). The upper limb segments and the leg and foot were prepared by the same dismemberment procedures used by Harless. The rest of Meeh's technique correlated with procedures that he developed for the measuring of volumes in adult living subjects. In the latter method a subject stood upright in a special tank and water was introduced to predetermined levels, so that horizontal volume levels could be measured by water displacement. To measure the head volume, the subjects immersed their heads below the water surface of the tank to predetermined landmarks. Meeh's dismemberment procedures on infant cadavers were intended to produce parts on which both volume and mass could be determined corresponding to the levels he had defined on adults. Thus, the heads of infant cadavers were severed obliquely by three sawcuts from the external occipital protuberance: (1) to the supraorbital line, (2) to the lips, and (3) to the hyoid bone. Similarly, the trunk and the thighs of the infant cadavers were cut into several transverse zones.

Most of Meeh's attention was given to determining ratios of the volumes (or masses) of the parts to the total body volume (or total body mass), and to comparisons of infant volumes (or masses)

with those of adults. Although Meeh measured masses and volumes on his infant material, it should be noted that he was not concerned with *functional body segments*. He did not calculate specific gravities, and he did not locate centers of mass.

One cannot now read the data of Krause, Valentin, and Meeh out of context; the data do not provide useful information of a mechanico-functional sort. This is true also of numerous measurements of body volumes in boys of different ages by Zook ('32), who in a growth study immersed standing subjects in water to different surface landmarks and measured the weights of water displaced.

If the volumes of body segments are to have any validity for correlations with mass segment data for mechanical analyses, the segments must correspond with the segments that move as a unit in body actions and they must be corrected for segment density — data so far obtained only by Harless and by Dempster. Apparently only Dempster ('55a) has made volume measurements of the segments of 38 living subjects using several specially built tanks and water immersion of limb segments held at approximately midrange postures. Other authors (Meeh, 1895; Contini, Drillis, and Bluestein, '63) who have measured the volumes of limbs held vertically in a standard vertical tank must arbitrarily define segments by the water level; but the proximal ends of the arm and thigh segments cannot be defined meaningfully by a horizontal level at the axilla or groin unless the trunk is bent sharply relative to the limb.

In an initial report by Braune and Fischer (1889), data were taken from three fresh (unpreserved) cadavers that were frozen in the supine posture and dismembered by sawcuts through the joint centers. The dismembered parts remained frozen and rigid throughout all the procedures involved in sawing, measuring dimensions, weighing, and locating the centers of gravity. The cadavers were frozen on boards, supine and extended; Braune and Fischer intended to separate the joints as nearly as possible across "functional" hinge axes.

In accord with the latter intention, Braune and Fischer made their cuts as

follows: (1) shoulder — by a sagittal cut through the armpit toward the center of the humeral head; (2) elbow — through the axis of the humeral condyles; (3) wrist — by a transverse cut through the head of the capitate bone; (4) hip — by an oblique cut along the side of the pelvis as nearly as possible parallel to the inguinal ligament and through the head of the femur;³ (5) knee — by a transverse cut through the axis of the femoral condyles; and (6) ankle — by a transverse cut through the axis of the talocrural joint. The head was sawed by a straight oblique cut from below the chin to the rear of the skull including the upper three or more cervical vertebrae. The remaining torso was handled as a single block without further dismemberment.

Several comments on the methods of Braune and Fischer are appropriate at this point. First, there are ambiguities in their description of the dismemberment procedures used for the upper limbs. Thus, the amount of forearm supination or pronation was not clear from the text and the comment that the fingers were "half-flexed" is vague; both these factors have a relation to the distribution of mass and the location of the center of gravity of the part.

Secondly, a more general criticism applies to the whole of Braune and Fischer's procedure. In determining landmarks for their sawcuts, they moved each joint and estimated the locations of hinge axes, marking these locations before they froze the cadavers. However, this technique is less sophisticated than it appears since functional hinge axes shift position from moment to moment over a vaguely defined region and are not fixed in space like the axis of a door hinge (Dempster, '55a, b). Nominal bending axes, given with reference to well defined anatomical landmarks and relating to mean centers of curvature of the convex joint component, should be used rather than the crude, functionally-established pivot points used by Braune and Fischer. Methods of defining nominal axes for dismemberment procedures will be indicated below.

Braune and Fischer next weighed the rigidly frozen blocks resulting from the operations described above. In order to

determine centers of mass for the segments, each block was suspended from metal pins or rods driven into the mass. Vertical marks in the plane of two plumb lines attached to the pins were made on the skin at appropriate steps in the following procedure: Each frozen segment (1) was suspended crosswise on a pin near the plane of balance, and the first skin marks were made; (2) the segment was then suspended from pins that would establish plumb-line reference planes at about 90° to the first, transverse plane, and these planes were in turn marked in a comparable way. The intersection of the three planes, as indicated by marks on the skin, determined the locus of the center of mass of the part; a transverse sawcut through the intersection point then permitted the location of the center to be defined relative to the anatomy of the section. The segments remained rigidly frozen throughout all these operations.

Braune and Fischer noted that the centers of mass of the limb segments fell on, or near the line connecting the centers of joints at each end of the segments. Then, the authors determined the locations of both the joint centers and centers of mass of one cadaver in terms of Cartesian coordinates. They found that with only slight positional adjustments of the limb segments, all joint centers and all centers of mass (except those of the feet) could be aligned in a single frontal plane. It was found, furthermore, that a man could actually stand with this limb joint posture. By summing the moments of the different centers of mass for this posture in the cadaver, relative to an axis in the plane of reference,³ the center of mass of the whole body could be located as accu-

³ After several trial sawcuts on preserved cadaver material with straightened hip joints, we interpret this section as one that just misses the anterior superior iliac spine, the pubic tubercle, and the ischial tuberosity; such a cut leaves the pelvis with about 1500 g of the limb mass, including parts of the gluteus maximus, gluteus medius, gluteus minimus, and quadratus femoris muscles, and the fatty tissues of the more medial part of the buttock.

³ That is: the sum of the moments of the separate segments with reference to some arbitrary axis in the plane of reference — moments of the segments are their masses times the distances between their centers of gravity and the axis of reference — when divided by the sum of the masses, gives the distance of the whole-body center of gravity from that axis. A similar calculation regarding the moments about another axis at a right angle, gives the location of the center of gravity in the plane of the two axes; a further calculation relative to the third rectangular axis located the center of gravity in space (Braune and Fischer, 1889).

rately as by balancing the body experimentally on a board.

The center of mass of the whole body could also be located by similar calculations in terms of three-dimensional coordinates for various postures in which the limbs were displaced. The data on this one cadaver, in fact, have formed a basis for studies on locomotion by Fischer ('04), Bernstein ('35), and Elftman ('39). It might be noted also that graphical and geometric methods, in addition to the more usual algebraic methods, were developed by Fischer (1892), for locating whole-body and composite centers of gravity if masses and locations of the segmental centers were known. Meyer (1873) had previously attempted this, but in a less sophisticated fashion.

An additional paper by Braune and Fischer (1892) dealt with measurements of the moments of inertia for some of the segments of the limbs of two additional cadavers. Incidental to this work, and without comment, the two authors tabulated the masses and the linear locations of centers of gravity relative to joint-centers of the segments. Presumably, the dismemberment procedures followed their earlier methods. A later publication by Fischer ('06) tabulated data concerning the second body studied in the moment-of-inertia paper (Braune and Fischer, 1892), along with miscellaneous data from their 1889 paper. From a close reading of the tabulated data, it seems clear that Braune and Fischer actually presented data pertinent to statics, but differing in degree of completeness, on five bodies, plus moment of inertia data on two of these. Where appropriate, the scanty data of Braune and Fischer will be grouped with or compared to our own material in the following pages.

Fujikawa ('63) dismembered five adult Japanese bodies including two females; one specimen was unpreserved, the others were embalmed. Centers of mass were located and segmental masses were measured. A sixth head was used in locating the surface landmarks of the center of mass. The applicability of certain tabular data is unclear since the treatment was both brief and complicated by linguistic idiosyncracies.

MATERIAL

The present data were gathered in 1952-1953 and 1962 on seven unpreserved and two embalmed white male cadavers. The two preserved specimens were the first and last bodies utilized in the study; with the first, definitive methods were developed, before any work was done on unpreserved material; the other was used for illustrations and for certain miscellaneous checks performed as the present manuscript was drafted; routine data also were obtained from both. Eleven additional upper and 41 lower limbs were studied concurrently for details. All material was obtained from white, male cadavers of normal appearance. Details relating to the seven unpreserved specimens will be given first.

On receipt at The University of Michigan Anatomy Morgue, each potential specimen was photographed if it seemed tentatively acceptable. Three views were made of the body in a suspended posture; weight and supine stature were measured. Since the Michigan Anatomical Law (prior to 1958) forbade use of cadavers during the first ten days following receipt, the bodies were stored for at least this period in a cold room before they were available for dissection. During this interval, the cadavers were screened as described below, to eliminate abnormal material; meanwhile, some 60 standard caliper, tape and anthropometer measurements were made. These were intended primarily for later use as a check on further measurements of body segments pertaining to joint centers and centers of mass. The three photo views of each body were used for determinations of Sheldon somatotypes; in addition, they were enlarged to about one-seventh life size and some supplementary measurements and checks of the anthropometric measurements were made from the enlargements.

The seven unpreserved white male cadavers ultimately dismembered and summarized in this study consisted of two adults of unknown age and five between 52 and 83 years (avg. 69 years); the average height, measured supine was 67.0 inches with a range of 61.4-73.5 inches (or 169 cm avg., range 155.3-186.6 cm); and the average weight was 134 lbs. with

follows: (1) shoulder — by a sagittal cut through the armpit toward the center of the humeral head; (2) elbow — through the axis of the humeral condyles; (3) wrist — by a transverse cut through the head of the capitate bone; (4) hip — by an oblique cut along the side of the pelvis as nearly as possible parallel to the inguinal ligament and through the head of the femur;¹ (5) knee — by a transverse cut through the axis of the femoral condyles; and (6) ankle — by a transverse cut through the axis of the talocrural joint. The head was sawed by a straight oblique cut from below the chin to the rear of the skull including the upper three or more cervical vertebrae. The remaining torso was handled as a single block without further dismemberment.

Several comments on the methods of Braune and Fischer are appropriate at this point. First, there are ambiguities in their description of the dismemberment procedures used for the upper limbs. Thus, the amount of forearm supination or pronation was not clear from the text and the comment that the fingers were "half-flexed" is vague; both these factors have a relation to the distribution of mass and the location of the center of gravity of the part.

Secondly, a more general criticism applies to the whole of Braune and Fischer's procedure. In determining landmarks for their sawcuts, they moved each joint and estimated the locations of hinge axes, marking these locations before they froze the cadavers. However, this technique is less sophisticated than it appears since functional hinge axes shift position from moment to moment over a vaguely defined region and are not fixed in space like the axis of a door hinge (Dempster, '55a, b). Nominal bending axes, given with reference to well defined anatomical landmarks and relating to mean centers of curvature of the convex joint component, should be used rather than the crude, functionally-established pivot points used by Braune and Fischer. Methods of defining nominal axes for dismemberment procedures will be indicated below.

Braune and Fischer next weighed the rigidly frozen blocks resulting from the operations described above. In order to

determine centers of mass for the segments, each block was suspended from metal pins or rods driven into the mass. Vertical marks in the plane of two plumb lines attached to the pins were made on the skin at appropriate steps in the following procedure: Each frozen segment (1) was suspended crosswise on a pin near the plane of balance, and the first skin marks were made; (2) the segment was then suspended from pins that would establish plumb-line reference planes at about 90° to the first, transverse plane, and these planes were in turn marked in a comparable way. The intersection of the three planes, as indicated by marks on the skin, determined the locus of the center of mass of the part; a transverse sawcut through the intersection point then permitted the location of the center to be defined relative to the anatomy of the section. The segments remained rigidly frozen throughout all these operations.

Braune and Fischer noted that the centers of mass of the limb segments fell on, or near the line connecting the centers of joints at each end of the segments. Then, the authors determined the locations of both the joint centers and centers of mass of one cadaver in terms of Cartesian coordinates. They found that with only slight positional adjustments of the limb segments, all joint centers and all centers of mass (except those of the feet) could be aligned in a single frontal plane. It was found, furthermore, that a man could actually stand with this limb joint posture. By summing the moments of the different centers of mass for this posture in the cadaver, relative to an axis in the plane of reference,² the center of mass of the whole body could be located as accu-

¹ After several trial sawcuts on preserved cadaver material with straightened hip joints, we interpret this section as one that just misses the anterior superior iliac spine, the pubic tubercle, and the ischial tuberosity; such a cut leaves the pelvis with about 1500 g of the limb mass, including parts of the gluteus maximus, gluteus medius, gluteus minimus, and quadratus femoris muscles, and the fatty tissues of the more medial part of the buttock.

² That is: the sum of the moments of the separate segments with reference to some arbitrary axis in the plane of reference — moments of the segments are their masses times the distances between their centers of gravity and the axis of reference — when divided by the sum of the masses, gives the distance of the whole-body center of gravity from that axis. A similar calculation regarding the moments about another axis at a right angle, gives the location of the center of gravity in the plane of the two axes; a further calculation relative to the third rectangular axis located for the center of gravity in space (Braune and Fischer, 1893).

might expect from extrapolations to living subjects of different height, weight, build, or tissue composition.

PROCEDURES

Plan of dismemberment. In this study of cadaver material, the attempt was to obtain the maximum possible amount of data from every specimen. Consequently, each cadaver was subjected to a battery of standardized procedures including: (1) screening, selection, and preliminary measurement; (2) preparation for dismemberment according to a pattern believed to be functionally meaningful; (3) the actual separation and weighing of segments; (4) measurement of the linear dimensions of segments; (5) location of segment centers of mass; (6) determination of segment volumes; and (7) determinations of the specific gravity of tissue. In addition, (8) measurements were made of the frequencies of segments considered as pendulums. The latter data, along with segment lengths and masses, permit determinations of radius of gyration and moment of inertia of segments, factors pertinent to dynamic analyses. (The data dealing with radius of gyration and moment of inertia will be treated in a later paper.) The different phases of the procedure were often handled concurrently with a designated person under supervision assigned to each activity.

The procedures for dismemberment were based on the following rationale. Since segments are in fact continuous, any separation of segments is arbitrary. It is obvious that the soft tissues of such parts as the head, thorax, forearm, foot, and so on, move *en masse* with the more-or-less rigid elements of the body framework, but these units cannot be separated for measurement simply by cutting through the soft tissues and disarticulating joints. A more fundamental understanding of body mechanics is required if the parts measured are to be meaningfully defined.

The links or straight-line distances that span between adjacent joint centers make up the effective core-lines of the body segments. The length of each link is related to the solid structural element or elements in a segment that provide the lever system of the body mechanism. (The link

concept has been developed in detail by Dempster, '55a, b, '61, '65, and Dempster, Sherr and Priest, '64.) Each link in the body is enveloped by such tissues as skin, muscles, and bone, and the composite becomes a mass segment. But the link, like the link in a machine, is the structural unit or functional length of such a unit necessary for any valid consideration of body mechanics. A body segment length is the same as its link, and this length, rather than a length from arbitrary surface landmarks, is needed in locating center of mass or in determining radius of gyration and moment of inertia. Consequently, segments must be separated at joint-centers rather than at joint-surfaces.

Braune and Fischer (1889) separated joints at joint-centers and they described their technique in some detail. In contrast, Harless (1860) dismembered certain limb segments of his specimens by disarticulating the joints but he cut other joints at joint-centers; he spoke, however, of segment lengths as from joint center to joint center. Meeh (1895) also disarticulated joints in his work, following Harless's method.

Braune and Fischer sawed across frozen, straightened limb joints of the supine body at the level of the joint centers. Our basic plan, in contrast, was to freeze joints at the midposition of their movement range, relative to all possible directions of movement, and to bisect the resulting joint-angles by sawcuts through joint centers. Our assumption was that separation across either straightened joints or fully-flexed joints would divide the segments into masses that would not be representative of a large range of joint postures; the bisecting of a joint angle by sawcuts across a midrange position, however, should provide a meaningful compromise for the separation of mean segment masses.

Initial dismemberment techniques. Each cadaver was lashed to a work board, and hip and shoulder joints were bent to their midrange positions (fig. 1A). Thus, the humerus was flexed 60°, abducted 45° and medially rotated 23°; the thigh was flexed 57°, abducted 10° and laterally rotated 3°. A protractor with a movable arm was used to set up these midrange postures based on joint-range measurements of liv-

a range of 109.3–159.5 lbs. (or 61.1 kg avg., range 49.8–72.0 kg).

We avoided cadavers for which the death certificate indicated tuberculosis or wasting diseases; mutilated or deformed bodies were likewise rejected. The cause of death was unknown for one subject; another was a death following surgery for an esophageal carcinoma; the others died of cardiovascular diseases.

The bodies were of average build for their age; Sheldonian somatotypes (Sheldon, Stevens, and Tucker, '40; Sheldon, Dupertuis, and McDermott, '54) were assessed by Prof. C. W. Dupertuis, of Western Reserve University, from the above-mentioned photographs which showed the cadavers suspended by tongs from their acoustic meati. Somatotype was used as a criterion for rejecting specimens that were not of more or less average build. (The first somatotype component in each case, following the classification scheme of Sheldon, was either 3 or 4; the second component was either 2, 3, 4, or 5; and the third was either 2, 3, or 4.)

The work on a given specimen involved a team of 5 or 6 persons, including student help, and usually required a three day session. Consequently, work periods had to be planned for vacations, midyear recesses, or summers. Because of the erratic supply of cadaver material suitable to our purposes, incoming specimens were screened as described above during the 10 to 20 days prior to a feasible work period. Thus, the cadavers were in cold storage prior to dismemberment from ten to as much as 20 days after receipt at the morgue. The interval between death and actual data-taking varied between two and four weeks — including the period of storage in our morgue and a period prior to receipt of the body. The few days of custody by morticians or hospitals immediately after death would normally involve refrigeration.

All measurements and procedures on the two embalmed cadavers were comparable to those described for the unpreserved specimens, although in minor ways the attention to details was different. Because the bodies were preserved, for example, there was no need for freezing of body parts, and the material offered no possible

health hazard for personnel. Since joints were rigid, incisions and minor dissection were sometimes required to locate bony landmarks accurately or to increase joint mobility. The pertinent data for the two preserved bodies are: *Specimen a* (the initial specimen) age, 67 years; supine stature, 66.5 inches (168.9 cm); weight, 113 lbs. (51.24 kg); somatotype 4–5–2½; cause of death, unknown; *Specimen b* (the final specimen) age, 70 years; supine stature, 67.7 inches (172.0 cm); weight, 161 lbs. (73.0 kg); cause of death, coronary insufficiency.

The subjects were of normal build, but elderly and most were below average in stature and weight as compared to present national population statistics. The nineteenth century investigators apparently had younger, heavier, specimens. One of Harless's Munich subjects was a "young, executed man"; the other subject was age 29. Of Braune and Fischer's five Leipzig subjects, the ages of two are listed as 45 and 50 years; the ages of the others are not given. The German authors especially mentioned certain subjects as being "muscular" or "well-built," but the only way we can compare the builds of their subjects and the Michigan series is through a height-weight ratio. The height-to-cube-root-of-weight indices of the present group of subjects, calculated in the metric system, varied from 41.5 to 45.0 (medium builds); plus one of 46.2 (a more slender build). Indices of the five Leipzig subjects ranged from 41.4 to 43.6, while the two Munich subjects showed indices of 43.2 and 46.5.

It should be obvious that information based on so meager a sampling of subjects must be applied to other populations with discretion; prudently treated, of course, even sketchy data on one or two subjects may have value for first approximations. Except for the limited data of Fujikawa ('63) none of the usable cadaver information on body segments was derived from infants, children, females, or different races or builds. An examination of the data themselves, however, will show the variability and consistency of the available measurements. It should also suggest the special characteristics of the research material and the degree of confidence one

might expect from extrapolations to living subjects of different height, weight, build, or tissue composition.

PROCEDURES

Plan of dismemberment. In this study of cadaver material, the attempt was to obtain the maximum possible amount of data from every specimen. Consequently, each cadaver was subjected to a battery of standardized procedures including: (1) screening, selection, and preliminary measurement; (2) preparation for dismemberment according to a pattern believed to be functionally meaningful; (3) the actual separation and weighing of segments; (4) measurement of the linear dimensions of segments; (5) location of segment centers of mass; (6) determination of segment volumes; and (7) determinations of the specific gravity of tissue. In addition, (8) measurements were made of the frequencies of segments considered as pendulums. The latter data, along with segment lengths and masses, permit determinations of radius of gyration and moment of inertia of segments, factors pertinent to dynamic analyses. (The data dealing with radius of gyration and moment of inertia will be treated in a later paper.) The different phases of the procedure were often handled concurrently with a designated person under supervision assigned to each activity.

The procedures for dismemberment were based on the following rationale. Since segments are in fact continuous, any separation of segments is arbitrary. It is obvious that the soft tissues of such parts as the head, thorax, forearm, foot, and so on, move *en masse* with the more-or-less rigid elements of the body framework, but these units cannot be separated for measurement simply by cutting through the soft tissues and disarticulating joints. A more fundamental understanding of body mechanics is required if the parts measured are to be meaningfully defined.

The links or straight-line distances that span between adjacent joint centers make up the effective core-lines of the body segments. The length of each link is related to the solid structural element or elements in a segment that provide the lever system of the body mechanism. (The link

concept has been developed in detail by Dempster, '55a, b, '61, '65, and Dempster, Sherr and Priest, '64.) Each link in the body is enveloped by such tissues as skin, muscles, and bone, and the composite becomes a mass segment. But the link, like the link in a machine, is the structural unit or functional length of such a unit necessary for any valid consideration of body mechanics. A body segment length is the same as its link, and this length, rather than a length from arbitrary surface landmarks, is needed in locating center of mass or in determining radius of gyration and moment of inertia. Consequently, segments must be separated at joint-centers rather than at joint-surfaces.

Braune and Fischer (1889) separated joints at joint-centers and they described their technique in some detail. In contrast, Harless (1860) dismembered certain limb segments of his specimens by disarticulating the joints but he cut other joints at joint-centers; he spoke, however, of segment lengths as from joint center to joint center. Meeh (1895) also disarticulated joints in his work, following Harless's method.

Braune and Fischer sawed across frozen, straightened limb joints of the supine body at the level of the joint centers. Our basic plan, in contrast, was to freeze joints at the midposition of their movement range, relative to all possible directions of movement, and to bisect the resulting joint-angles by sawcuts through joint centers. Our assumption was that separation across either straightened joints or fully-flexed joints would divide the segments into masses that would not be representative of a large range of joint postures; the bisecting of a joint angle by sawcuts across a midrange position, however, should provide a meaningful compromise for the separation of mean segment masses.

Initial dismemberment techniques. Each cadaver was lashed to a work board, and hip and shoulder joints were bent to their midrange positions (fig. 1A). Thus, the humerus was flexed 60°, abducted 45° and medially rotated 23°; the thigh was flexed 57°, abducted 10° and laterally rotated 3°. A protractor with a movable arm was used to set up these midrange postures based on joint-range measurements of liv-

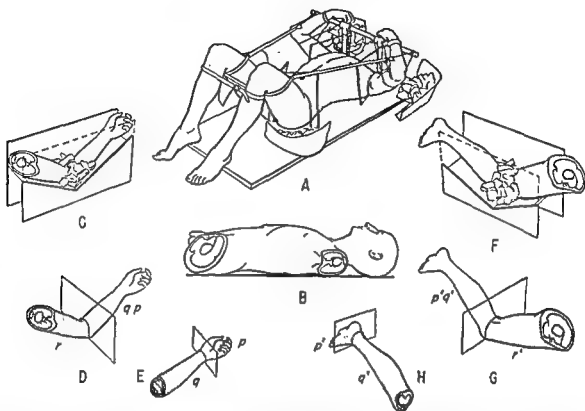


Fig. 1A A cadaver with the hips and shoulders trussed into midrange positions. Sheet metal containers about each joint are heaped with dry ice. Shaded planes show where sawcuts were made to bisect the midrange joint angulations. B, The head and trunk section after removal of limbs. C and F, Whole upper and lower limbs in special troughs with dry ice to freeze elbows and knees in a semiflexed midrange position. D and G, Planes show location of sawcuts that bisect the midrange joint angulations. E and H, Planes of sawcuts at wrist and ankle. Segments coded with single letters, *p*, *q*, and *r* (or *p'*, *q'*, and *r'*), or stippled, are unitary segments; whole limbs and composite distal segments (*q*, *p*, and *p'*, *q'*) are not stippled.

ing subjects (Dempster, '55a). To simplify bending at the hip joint and to assure accurate localization of the femoral head, an incision between the scrotum and thigh was continued down to the ischiopubic ramus; each of the muscles arising from the outer aspect of the ischium and pubis was then dissected from its periosteal attachment and from the obturator membrane. This procedure facilitated positioning of the hip joint and accurate palpation of the femur head. Similar probing incision to permit accurate location of the humeral heads were also made through the deltoid muscles. Once positioned, the limbs were secured with rope to posts on the work board. Dry ice (solid carbon dioxide) was then packed about the four joints (fig. 1, A) and the body, trussed in this manner, was placed in a cold room overnight.

The joints, frozen solidly in position, were severed by saw cuts the next morning to provide five body parts for subsequent procedures: trunk-with-head, right and left upper limbs, and right and left lower limbs, (fig. 1B, C, F). Surface landmarks which defined the plane of the sawcut at the shoulder (fig. 2A, B) were: (a) a point on the anterior axillary fold immediately superficial to the medial contour of the arm, (b) a similar point on the posterior axillary fold, and (c) the palpable sulcus between the bones at the acromioclavicular joint. These points define a plane which simultaneously bisects the midrange angle of the joint and passes through the center of the head of the humerus.

Landmarks for our saw plane through the hip joint (fig. 2B) were: (d) a point on the skin at the symphyseal end of the ischiopubic ramus at the origin of the ad-

ductor longus muscle, (e) along the ischiopubic ramus to the ischial tuberosity and the origin of the hamstring muscles, and (f) a point just inferior to the anterior superior iliac spine.

This represented a compromise plane, since a true bisecting plane for the mid-range position of the hip joint will pass obliquely across the hip mass from the femoral trochanter and posttrochanteric dimple laterally — along Holden's line (an inch or two below the inguinal ligament: Jones, '20) — to an oblique transacetabular line between the anterior inferior iliac spine and the lesser sciatic notch of the ischium. If such a sawcut were used, an additional sawcut at an angle, along the

outer face of the ischium and pubis, would be required to separate the limb from the trunk. It should be noted that the landmarks, and plane, actually used (fig. 2B, d, e, f) represent a compromise that cuts the center of the femoral head but does not bisect the joint angle. No saw cut in a single plane will simultaneously: (1) separate the thigh from the trunk with a flat surface, (2) bisect the joint angle, (3) cut through the joint center, and (4) provide good landmarks. The hip landmarks finally chosen were decided upon because correlated measurements of limb volume on living subjects, using water-immersion techniques, were feasible with the same landmarks. Our shoulder landmarks,

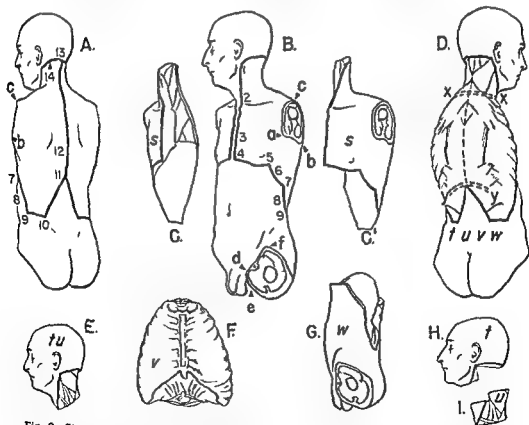


Fig. 2 Stages in segmentation of the head and trunk. A and B show a sequence of landmarks for incisions used in removing the limbs (letters) and the shoulder mass (figures). C and C', Right and left frozen shoulder masses after removal from plaster moulds. D, Composite head and trunk section to be disarticulated. Lines x-x and y-y suggest the level for severing deep back muscles prior to disarticulating cervical from thoracic and thoracic from lumbar vertebrae. E, Composite head, abdominopelvic complex, head, and neck. F, G, H, and I, Individual segments: Thorax, Head, Neck, and Abdominopelvic complex.

which required no such compromise, permitted similar measurements on living subjects for the upper limbs.

Five composite parts resulted from the first dismemberment procedure (fig. 1B, C, F). As in the studies by Harless and by Braune and Fischer, measurements were made on each of these composites, and the following cadaver-by-cadaver measurements for eight specimens (Dempster, '55a) are on record: (1) weight, (2) location of center of mass, (3) moment of inertia, and (4) volume after thawing of the limbs.

Since the Michigan data, and the older German records, too, showed considerable variation in the center of mass and moment of inertia of composite parts, a variability that could be attributed to differences in angulation of the elbow, wrist, fingers, knee, or angle, only unitary limb segments are dealt with in this paper. The dimensions, location of centers of mass, and radius of gyration of such limb composites as whole limbs, forearm-with-hand, and shank-with-foot (fig. 1D, G, E, H) are better derived mathematically from unitary data than by using the variable information from direct measurements. As will be noted, however, composite parts did have indirect value in verifying the mass and volume data of unitary limb segments.

Dismemberment of limbs. The elbows and knees of the detached upper and lower limbs were bent to arbitrary midrange positions of 70° and 62° respectively, based on the literature concerning joint-range in living subjects (Dempster, '55a). The forearm was then given a semi-prone position, and the foot was rotated laterally until a toe-to-heel line averaged 5° from the plane of knee-bending. So positioned, the limbs were placed in troughs (fig. 1C, F), and again dry ice was packed about the joints until they were frozen solid. Sawcuts were then made that passed through each joint center and bisected each joint angle (fig. 1D, G).

Anatomical landmarks defining the proper plane for the sawcuts at each elbow (fig. 1D) were as follows: (1) lower border of medial epicondyle of the humerus; (2) a point on the capitulum of the humerus (at the lateral epicondyle),

8 mm proximal to the palpable groove between the circumference of the radius and the humeral capitulum; and (3) the antecubital flexure crease of the skin. Landmarks for the knee (fig. 1G) were: (1) center of the posterior curvature of the medial femoral condyle, as palpated; (2) same for the lateral condyle; (3) the mid-region of the popliteal flexure crease of the skin; and (4) a point below the upper margin of the patella. Incisions through the skin with a scalpel were an aid when saw cuts were made.

Eight new limb segments were produced by the above procedure; that is, two upper- and two lower-limb segments on each side. Of these, the four proximal segments were unitary, the four distal binary. In figure 1, shaded parts represent the four unitary segments; upper-limb segments are designated by the letters p, q, and r; while lower-limb segments are indicated by p', q', and r'. The four distal segments (fig. 1E, H) were then severed by sawcuts at the wrist and ankle, producing eight new unitary segments (a total of 12 segments for the four limbs).

In these last procedures, the intent was again to separate limb segments in accordance with the link concept; consequently, joints were positioned and frozen before cutting, and landmarks were determined to define sawcut planes that would bisect joint-angles and also pass through joint-centers. Thus, wrists were frozen unflexed and adducted about 10°. Landmarks beginning on the palmar aspect of the hand were: (1) midpoint of pisiform bone, (2) distal wrist crease at palmaris longus tendon, and (3) proximal palpable part of the scaphoid bone at the base of the thenar eminence; and, on the dorsum of the hand, (4) palpable sulcus between lunate and capitate bones. This cut typically passes through the center of the head of the capitate bone at approximately the functional center of the wrist joint (fig. 1E).

For similar reasons the feet were frozen with the sole of each at a right angle to the shank axis. Landmarks for this positioning were: (1) superior border of calcaneus just anterior to the Achilles tendon as palpated medially and laterally, (2) upper border of the head of the talus, and (3) lower tip of the fibula. This cut

passes through the center of curvature of the talus bone at the ankle joint (fig. 1H). Often it was convenient to transect the calcaneal tendon at its insertion to permit the foot to dorsiflex enough for freezing; skin incisions ordinarily were an aid in determining bony landmarks with certainty, and skin pencil lines or scalpel scratches were used routinely as guides for sawcuts.

During this sequence of dismemberments, some 20 limb parts were available at different times for measurement. Of these, 12 italicized here and represented with single letters were unitary segments, and eight were composites of two or three units. The parts were: right and left total upper-limbs (*pqr*), right and left total lower-limbs (*p'q'r'*), right and left arms (*r*), right and left forearms with hands (*pq*), right and left thighs (*r'*), right and left legs with feet (*p'q'*), right and left forearms (*q*), right and left hands (*p*), right and left shanks (*q'*), and right and left feet (*p'*). For later measurements and center-of-gravity determinations, the fingertips were sewn flexed to the thenar eminence, just proximal to the palpable uncinate process of the hamate bone, in a radioulnar sequence approximating a "rest" position (fig. 4A).

Further dismemberment of body. Although the studies of Harless and of Braune and Fischer carried the dismemberment of the central body mass only as far as separating the head from the trunk, we separated the total trunk-with-head into five unitary parts (fig. 2): (1) right shoulder segment (*s*), (2) left shoulder segment (*s*), (3) head (*t*), (4) thorax (*v*), and (5) abdominopelvic segment (*w*). The pelvic mass could not be treated as a unit separable from the abdominal mass, as is commonly done in the constructive sketches of art anatomy texts, since the abdominopelvic viscera would be unrestrained if the body wall and peritoneum were transected. Composite segments (fig. 2A, D, E), analogous to those for the limb procedures, were available for measurement at interim stages of the dismemberment: (1) trunk-with-head-with-shoulders (*s + t u v w*), (2) trunk-with-head-minus-shoulders (*t u v w*), and (3) head-with-neck (*t u*). These composites were not

contaminated by the above-mentioned errors that varied from specimen to specimen because of angulation differences in limb composites. Data on composite segment (1), the trunk-with-head-with-shoulders unit, may be of more value practically than those of the unitary segments of the axial region, hence, these will be presented and discussed.

The shoulder section (fig. 2A, B, C, C') was defined as the shoulder girdle and all muscles operating on the girdle, together with the overlying subcutaneous tissue and skin. So defined, the two shoulder masses fit over the upper trunk like a cape. Each side attaches to the thorax in front along a line that coincides with the origins of the pectoralis major and serratus anterior muscles. Posteriorly, the girdle muscles of each side attach to the rear portion of the skull, to the vertebral spine, to the thoracodorsal (lumbodorsal) aponeurosis, and to the crest of the ilium.

Accordingly, incisions were made following the sequence of numbers shown in figures 2A and 2B: from (1) the mastoid process to (2) the suprasternal notch along the anterior edge of the sternocleidomastoid muscle, (3) along the medial border of the pectoralis major muscle about a centimeter lateral to the midline, (4) to the seventh chondrosternal junction, then laterally (5) to the lateral limit of the origin of the pectoralis major muscle. The incision, then followed (6) the origin of the serratus anterior muscle to (7) the anterior margin of the latissimus dorsi muscle; it continued (8) along the anterior edge of the latissimus dorsi muscle to the crest of the ilium, then posteriorly along (9) the crest of the ilium to (10) the lateral border of the thoracodorsal aponeurosis. From this point, the incision was carried to (11) the twelfth thoracic spine and along (12) the spines of the thoracic and cervical vertebrae to (13) the skull. The skin incision was completed by following (14) the nuchal line to the mastoid process.

The trapezius and sternocleidomastoid muscles were detached from the skull; the sternoclavicular joint on each side was disarticulated; the pectoralis major and pectoralis minor muscles were separated from the thoracic wall, as were the serratus

anterior and latissimus dorsi muscles. The latter muscle was also detached from the crest of the ilium and the thoracodorsal aponeurosis. The trapezius and rhomboid muscles were separated from the vertebral column. The levator scapulae muscle was detached from the cervical transverse processes, and the omohyoid muscle was cut at the anterior margin of the sternocleidomastoid muscle. The whole mass was then separated along the loose shearing plane next to the thoracic and abdominal walls. Finally, the brachial plexus and axillary artery and vein were separated at the outer margin of the first rib. Through these dissection procedures, the two shoulder masses were entirely separated from the trunk (fig. 2A, B, C, C' and D).

After removal of the two shoulder masses, the remaining integument on the trunk consisted of: (1) a continuous covering of the skull vault and face above and anterior to the nuchal line and mastoid processes; (2) a v-shaped area between the sternocleidomastoid muscles that continued downward as a narrow strip anterior to the sternum; (3) a larger covering overlying the rectus sheath, the lateral abdominal muscles, the groin, genitalia, perineum, medial buttock region, and sacrum; and (4) a triangular sheet of integument over the thoracodorsal aponeurosis that converged on the apex of the spine of the vertebra T-12.

It was essential that the detached shoulder masses, which consisted partly of semi-rigid tissues, retain their natural shapes during the procedures intended to locate the center of gravity of each mass and determine the period of oscillation of each part when considered as a pendulum. Accordingly, it was necessary to freeze these parts rigidly in the shape they had while in the trunk. A plaster of paris mold was therefore made of each side of the trunk, completely overlapping each shoulder mass, before the removal of these parts. The detached masses were later fitted into these molds and packed with dry ice; upon removal, the frozen parts retained their original shapes (fig. 2C and C').

After removal of the shoulder masses, the remaining trunk (fig. 2D, t u v w) was separated into three smaller sections:

head-with-neck (t u), *thorax* (v) and *abdominopelvic segment* (w). Thus, the *head-with-neck* composite (fig. 2E) was cut from the trunk (1) along a plane that coincided with the upper borders of the first rib, (2) by disarticulating the joints between vertebrae C-7 and T-1, and (3) by severing the remaining soft tissues at the same level (fig. 2D, x-x). The *thorax* (fig. 2F) was separated from the lower trunk (1) by using blunt dissection between the peritoneum and the lower surface of the diaphragm, (2) by disarticulating the column between T-12 and L-1, and (3) by severing the deep muscles of the back at the same level (fig. 2D, Y-Y). The *abdominopelvic segment* (fig. 2G) was the remaining mass of the trunk.

Finally, after measurements on the composite, the *head-with-neck* segment (t u) was separated (fig. 2H, I) into the *head* proper (t) and the *neck* (u). The neck, it will be recalled, lacks sternocleidomastoid and trapezius muscles and the overlying integument. The procedure adopted was simply (1) the making of a transverse cut just below the hyoid level and across the neck viscera to the level of the prevertebral fascia; (2) blunt dissection between the neck viscera anteriorly and the prevertebral fascia posteriorly to the level of the skull base; (3) severing the deep muscles of the neck from the occipital and temporal bones; and (4) separation of the skull from the column by disarticulating the atlantooccipital joint and by cutting the longus and rectus muscles. The head so-defined is both anatomically and mechanically correct, in contrast to the simple straight cut of Harless, Meek, and Braune and Fischer. Measurements were made of the head segment alone but not of the neck alone, since measurements on a block of tissues representing cervical vertebrae, deep back muscles, and the neck viscera would have little meaning.

Although considerable tissue retraction after cutting across the limbs was noted by Harless who adjusted for this by stretching the skin and stitching it over the cut ends, this was not a significant feature for either the unpreserved or preserved material of this study. Whether it was the time interval after death, the freezing of

joints prior to sawing or a generally older group of subjects, some factor or combination of factors must have reduced tissue elasticity.

Linear measurements. Linear measurements of the body parts were made in the metric system, using a standard anthropometer for larger measurements, a spread-

ing caliper for measurements of parts of intermediate size, and a sliding caliper for measurements of small parts (hand and foot). Table 1 shows the end-points used for caliper measurements relating to the limb segments (links) after they were separated into units. The same instruments were also used in measurements

TABLE 1
End points for caliper link lengths and related dimensions

Body part	Superior (proximal) end point	Inferior (distal) end point
1 Shoulder	(a) center of articular face of sternal end of clavicle	(b) center of curvature of humeral head (proximal surface of cut that bisects midrange joint angle)
2 Arm	(a) same as 1b (distal face of cut)	(b) junction, transverse axis of trochlea of humerus at narrowest cross section of ulnar articulation
3 Forearm	(a) same as end point 2b (distal face of cut)	(b) center of curvature of proximal end of capitate bone (proximal face of cut)
4 Hand	(a) same as 3b (distal surface of cut)	(b) proximal interphalangeal knuckle of finger II, position of rest
5 Thigh	(a) center of curvature of femoral head	(b) middle of a line through the center of curvature of the posterior aspect of the two femoral condyles (proximal face of cut)
6 Shank	(a) same as 5b (distal face of cut)	(b) center of the area of the cut body of the talus (proximal face of cut)
7 Foot	(a) same as 6b (distal face of cut)	(b) tip of great toe
8 Entire head and trunk	(a) vertex of head	(b) midpoint of the transacetabular line
9 Head and neck	(a) vertex of head	(b) center of cut intervertebral disc at lower face of centrum of vertebra C-7
10 Thorax	(a) midpoint of disc tissue at superior face of centrum of vertebra T-1	(b) midpoint of disc tissue of inferior face of centrum of vertebra T-12
11 Abdomino-pelvic segment	(a) midpoint of disc tissue, superior face of centrum of vertebra L-1	(b) same as 8b
Widths and a Height — End Points		
12 Transhumeral width	Span between points 1b of right and left sides	
13 Transacetabular width	Span between centers of femoral heads of right and left sides, measured after removal of lower limbs	
14 Hip-to-shoulder height	Vertical distance between lines 12 and 13	

anterior and latissimus dorsi muscles. The latter muscle was also detached from the crest of the ilium and the thoracodorsal aponeurosis. The trapezius and rhomboid muscles were separated from the vertebral column. The levator scapulae muscle was detached from the cervical transverse processes, and the omohyoid muscle was cut at the anterior margin of the sternocleidomastoid muscle. The whole mass was then separated along the loose shearing plane next to the thoracic and abdominal walls. Finally, the brachial plexus and axillary artery and vein were separated at the outer margin of the first rib. Through these dissection procedures, the two shoulder masses were entirely separated from the trunk (fig. 2A, B, C, C' and D).

After removal of the two shoulder masses, the remaining integument on the trunk consisted of: (1) a continuous covering of the skull vault and face above and anterior to the nuchal line and mastoid processes; (2) a v-shaped area between the sternocleidomastoid muscles that continued downward as a narrow strip anterior to the sternum; (3) a larger covering overlying the rectus sheath, the lateral abdominal muscles, the groin, genitalia, perineum, medial buttock region, and sacrum; and (4) a triangular sheet of integument over the thoracodorsal aponeurosis that converged on the apex of the spine of the vertebra T-12.

It was essential that the detached shoulder masses, which consisted partly of semi-rigid tissues, retain their natural shapes during the procedures intended to locate the center of gravity of each mass and determine the period of oscillation of each part when considered as a pendulum. Accordingly, it was necessary to freeze these parts rigidly in the shape they had while in the trunk. A plaster of paris mold was therefore made of each side of the trunk, completely overlapping each shoulder mass, before the removal of these parts. The detached masses were later fitted into these molds and packed with dry ice; upon removal, the frozen parts retained their original shapes (fig. 2C and C').

After removal of the shoulder masses, the remaining trunk (fig. 2D, t u v w) was separated into three smaller sections:

head-with-neck (t u), *thorax* (v) and *abdominopelvic segment* (w). Thus, the *head-with-neck composite* (fig. 2E) was cut from the trunk (1) along a plane that coincided with the upper borders of the first rib, (2) by disarticulating the joints between vertebrae C-7 and T-1, and (3) by severing the remaining soft tissues at the same level (fig. 2D, x-x). The *thorax* (fig. 2F) was separated from the lower trunk (1) by using blunt dissection between the peritoneum and the lower surface of the diaphragm, (2) by disarticulating the column between T-12 and L-1, and (3) by severing the deep muscles of the back at the same level (fig. 2D, Y-Y). The *abdominopelvic segment* (fig. 2G) was the remaining mass of the trunk.

Finally, after measurements on the composite, the *head-with-neck segment* (t u) was separated (fig. 2H, I) into the *head proper* (t) and the *neck* (u). The neck, it will be recalled, lacks sternocleidomastoid and trapezius muscles and the overlying integument. The procedure adopted was simply (1) the making of a transverse cut just below the hyoid level and across the neck viscera to the level of the prevertebral fascia; (2) blunt dissection between the neck viscera anteriorly and the prevertebral fascia posteriorly to the level of the skull base; (3) severing the deep muscles of the neck from the occipital and temporal bones; and (4) separation of the skull from the column by disarticulating the atlantooccipital joint and by cutting the longus and rectus muscles. The head so-defined is both anatomically and mechanically correct, in contrast to the simple straight cut of Harless, Meck, and Braune and Fischer. Measurements were made of the head segment alone but not of the neck alone, since measurements on a block of tissues representing cervical vertebrae, deep back muscles, and the neck viscera would have little meaning.

Although considerable tissue retraction after cutting across the limbs was noted by Harless who adjusted for this by stretching the skin and stitching it over the cut ends, this was not a significant feature for either the unpreserved or preserved material of this study. Whether it was the time interval after death, the freezing of

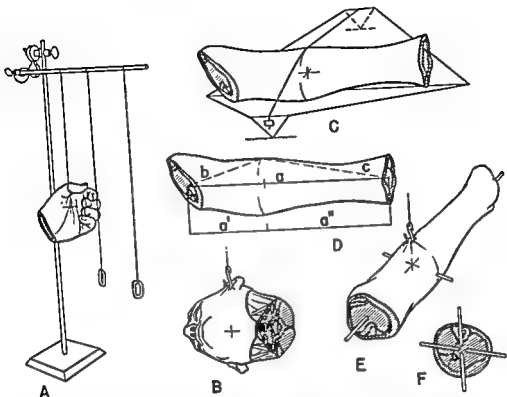


Fig. 4A. Method for locating center of mass on hands (or feet and thorax) by suspension from the different points, sighting across plumb lines, and marking. B, Special suspension method for the head, keeping the sagittal plane horizontal. C, Special sheet metal balance plate for locating center of mass of the long limb segments and the abdominopelvic complex. D, Geometry for determining of mass of the long limb segments and the abdominopelvic complex. E, Suspension of long limb segments so that drill holes and dowels will intersect at the center of mass of a cross section. F, A sawcut section through a limb segment at a plane marked by dowels which point toward the center of mass to be located anatomically.

the skin. Then the part was rotated about its longitudinal axis, balanced, and marked again; the encircling line clearly demarcated the transverse level of the center of mass for that segment.

Suspension of the various limb segments endwise from the joint centers confirmed Braune and Fischer's comment (1889) that segment centers of mass fall on or near a line interconnecting joint centers. Since the plane of balance was marked with a skin pencil on the surface of a segment, however, the relative distance of the center of mass from the two ends along this straight line was not immediately available. The following procedure was required to obtain this information for each part (fig. 4D): a caliper measurement (distance a) was made spanning from end

to end of the segment; two more measurements (b and c) were made, each from one end to a point on the skin surface at the transverse level of the center of mass, that is, at the skin-pencil mark. These three caliper measurements (a , b , and c), when plotted, made up the sides of a flat scalene triangle. A calculation involving simple geometrical ratios gave the proper value; thus the corrected distance of the center of mass from the proximal end of the segment (a') was:

$$a' = \frac{b^2 - c^2 + a^2}{2a}$$

After all other measurements were made, the location of the center of mass of each limb segment, relative to anatomical landmarks, was determined by the fol-

relating to center of gravity. All unitary segments were measured in this way.

As stated earlier, anterior, posterior and left side photographs had been made of the body as suspended by tongs. The camera, equipped with a ten inch lens, was at a standard distance at hip height and a 5×7 film was exposed in a triple back to show each view of the body at a height of four and one-half to four and three-fourths + inches on the ground glass; a measuring scale and plumb line were included in the field of view. After enlarged positives were made of the views, calipered stature and link dimensions could be scaled off on the photographs with the links meeting at best estimated joint center positions. Each side was a check on the other. Several additional dimensions on the photographs were scaled off and corrected using a reduction factor based on cadaver and photograph size. These gave enough secondary measurements to allow the outline of figure 3 to be drawn. Apart from the outline, figure 3 is a stick figure in which the lengths are shown as a percentage of stature.

Location, centers of mass. Both suspension and balancing methods were used for locating the center of mass (gravity) of the body parts; the method was varied with the purpose of the measurement and with the part studied. Figure 4A shows a suspension system, roughly comparable with that of Braune and Fischer, (1889), with two plumb lines for sighting. This system was used alone for such nonlinear parts as the head (fig. 4B), hand, shoulder, and thorax; successive suspensions from at least three widely separated points permitted the center of mass to be located at a single point in space, that is, the intersection point of three planes.

For elongate limb segments, a balancing plate was used as shown in figure 4C. This system permitted one to locate a transverse plane through the center of mass, relative to the length of the part. The plane of balance was identified by stretching a thread over the specimen from balance point to balance point, and the line of thread contact was marked on

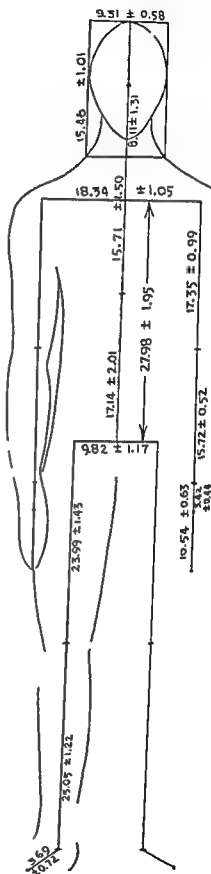


Fig. 3 Link figure with mean dimensions of each link stated in terms of percentage of stature.

Figure 3

that any errors caused by immersion and blood loss, were negligible.

For many of the weighings and volumetric measurements, however, three separate determinations on different segment composites could be used as checks on the size of the component parts and these values could be averaged. With regard to the hand, for instance, the records included: (1) a direct measurement of mass (and volume) for the hand (p) as a separate segment, (2) an indirect determination derived from the value for the entire upper-limb (p q r) minus the values for the forearm (q) and arm (r), and (3) an indirect value calculated from data for forearm-with-hand (q p) minus the forearm (q). Similarly, one direct and two subtraction values for mass (and for volume) were possible for the forearm (q) and for the arm (r). Analogous calculations were possible with each of the lower-limb segments also, giving three values of mass (or volume) for each.

In the midbody section, similar determinations were possible for both masses and volumes; thus shoulders (s) were measured separately, but the trunk-minus-shoulders mass (t u v w) could also be subtracted from the trunk-minus-limbs mass (s s t u v w) to give an indirect value for the right-plus-left-shoulder mass. Using comparable additions and subtractions, it was possible to supplement a direct measurement with indirect measurements for the mass and volume of both shoulders together (s + s), of the initial head and trunk part (s s t u v w), and of the shoulderless head and trunk (t u v w). Additionally, the mass (and volume) of

each of the separate axial units, the head and neck (t u), thorax (v), abdominopelvic complex (w), could be both measured directly and subtracted from the t-u-v-w mass (and volume) giving indirect values for each component. These multiple mass and volume determinations were of special value in working over data on body segments long since measured and discarded.

Density. The density or specific gravity of each part for each specimen was simply the mathematical quotient of mass divided by volume.

Tissue density. Following the location of segment centers of mass anatomically and before material was discarded, each segment was again weighed, then it was dissected into (1) skin and subcutaneous tissues, (2) muscle and associated tissues (including fasciae, tendons, blood vessels, and nerves), and (3) bone and joint. Each of these components was weighed and then it was immersed in a graduate cylinder containing a measured amount of water — bubbles were avoided. The mass divided by the volume of water displaced gave the density of the component.

RESULTS

The anatomical end points used in this study for the measurements of link lengths and the locations of the center of mass are given in table 1. The dimensions of the various links calipered in the Michigan cadaver material as well as the Braune and Fischer data can be found in table 2. These are expressed in centimeters and also as per cent of total stature. Table 3 lists the location of segment centers of

TABLE 2
Link dimensions of cadavers in relation to stature

	Michigan data		Leipzig data (Braune and Fischer)	
	cm	%	cm	%
Thigh link	40.56 \pm 2.42 (18)	23.99 \pm 1.43	43.32 \pm 1.21 (10)	24.26 \pm 0.74
Shank link	42.36 \pm 2.07 (18)	25.05 \pm 1.22	40.55 \pm 1.43 (10)	24.72 \pm 0.87
Foot link	6.23 \pm 1.22 (18)	3.694 \pm 0.720		
Lumbocoxal link	28.99 \pm 3.40 (8)	17.14 \pm 2.01		
Thoracic link	26.57 \pm 2.54 (8)	15.71 \pm 1.50		
Cranio cervical link	13.71 \pm 2.21 (8)	8.11 \pm 1.31		(10.6) ¹
Arm link	29.34 \pm 1.67 (18)	17.35 \pm 0.99	29.41 \pm 1.12 (6)	17.93 \pm 0.68
Forearm link	26.58 \pm 0.87 (18)	15.72 \pm 0.52	27.42 \pm 1.25 (4)	16.72 \pm 0.76
Hand link	5.777 \pm 0.745 (18)	3.422 \pm 0.441	5.38 \pm 0.33 (6)	3.28 \pm 0.20
Transpelvic	16.32 \pm 1.79 (19)	9.82 \pm 1.17 (19)	16.73 \pm 0.48 (3)	10.20 \pm 0.29

¹ Only one measurement available.

lowing procedure. Each part was refrozen and, if necessary, rebalanced so that the next encircling line at the plane of balance could be marked again. Next, by either successive suspensions or through successive balancings, two or three diameters through the encircling mark and the center of mass were defined. After end points of two or three diameters had been marked, drill holes were then made into the part along the marked diameters, and pointed one-fourth inch dowels were driven into the holes. The center of mass was then transected by a sawcut in the plane of the sticks. A detailed anatomical study of the cut surface, together with some dissection of the part when the tissues thawed, permitted an exact anatomical location of the center of mass relative to muscles, tendons, and bones of the segment.

To locate the center of mass of the head-neck segment anatomically, a special technique was followed. The mass was suspended from several trial points on the skin until the head hung with its sagittal plane horizontally (fig. 4B). After proper suspension points for both right and left sides were found, lead-headed tacks were pushed into the skin to mark these points. Lateral x-ray films were then made of the segment to locate its center of mass; this lay at the point where a line between the lead-headed tacks intersected the plane of the midsagittal bony anatomy. Alternately, drill holes were made at both suspension points, each aiming towards the other, and a pointed dowel was driven through the whole width of the head; a sagittal sawcut showed the cut dowel which marked the location of the center of mass. In two instances, the center of mass of the head alone (t) was also determined. The x-ray method was advantageous in that it required neither sagittal sawcuts nor drill holes, and parts could remain intact.

Weighting techniques. For those body parts with a mass of less than 20 kg critical weighings were made on a solution balance calibrated in grams and accurate with any combination of counterbalancing weights to within one or two grams — less than 0.5% error for the smallest part weighed. Larger masses, such as those of the total trunk, or abdominopelvic mass,

were measured to the nearest quarter-pound on a 300 lb. av. Fairbanks grain scale, then expressed in metric units. Total body mass was measured by placing the body on two bathroom scales; data were corrected and converted to metric units later. A measurement error of within $\pm 1.0\%$ may be assumed for the two latter techniques.

Volumetric measurements. All determinations of volume were made using a procedure of double weighings based on Archimides's principal of water displacement. Thus, the difference between the weight of the part in air and the weight submerged in water represented the mass of water displaced; this value, assuming a water density of 1.0, gave the corresponding volume of the part. The heavier body parts were encircled with cord, lifted with block and tackle, and lowered into a cylindrical tank of water. If the part contained air, a lead weight of known mass and volume was attached to assure submersion; this extra factor was allowed for in the calculations. After the part was submerged, it was disconnected from the block and tackle and suspended from a 15 kg Chatillon autopsy spring scale previously attached to the block and tackle.

Lighter body parts were weighed in air attached by a cord and submerged by hand and then connected directly to the scales. These submerged weighings took only a moment or two and the parts were immediately drained and dried; thus later weighings were not noticeably contaminated through absorbing water in earlier immersions. It was critically important, however, following each freezing and sawing phase that the parts be entirely thawed, to avoid volume measurements that would be too high because of low density ice in the tissues. Weighings under water were not as accurate for the smaller parts, such as the hands, as for those of larger size. In retrospect a method involving the spillover and weighing of displaced water would have been preferable for volumes of a liter or less.

As the larger segments (head and trunk, abdominopelvic segment, thigh) drained after the immersion, they sometimes noticeably dripped blood. However, reweighings before and after immersion indicated

mass measured from the proximal end points and given as per cent of the total link length. The anatomical locations of the average centers of mass are shown in figures 5 and 6. The elliptical shape of the loci \square to represent the mean deviation of these centers. The mean mass and per cent of total mass of body segments for

the Michigan and the Leipzig cadavers are listed in table 4. The mean volume of our cadaver segments and their ratio to total body volume are in table 5. In seven bodies the limb segments were further dissected to determine the proportion of skin and fascia, muscle, and bone. These results are shown in table 6 as per cent of

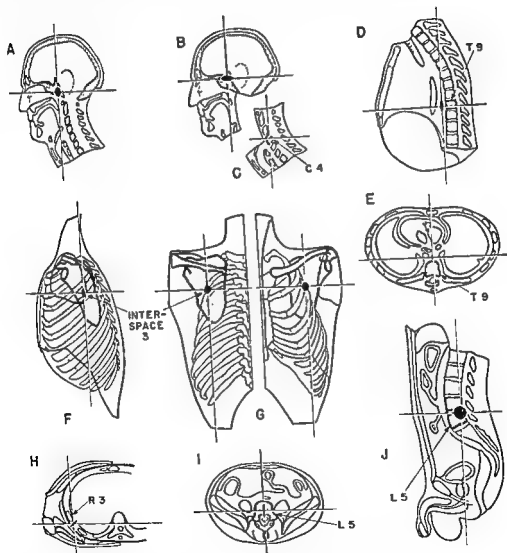


Fig. 6 Center of mass location in segments of the head and trunk. A, Location in the head and neck; dotted line, ear outline. B and C, Locations in the head alone and in the neck. D and E, Center of mass of the thorax anterior to vertebral body T-9. F, G, and H, Center of mass of shoulder segment below rib 3. I and J, Abdominopelvic center of mass in the vertebral body of L-5. The relative vertical and horizontal dimensions of the black ellipse at the center of mass of the segment indicates the variability of position in the cardinal axes of the part (cf. fig. 5).

TABLE 3

Distance between proximal end point and segment center of mass

	Michigan data	Leipzig data (Braune and Fischer)
	% of link	% of link
Thigh	$42.78 \pm 2.05(18)$	$43.68 \pm 2.50(10)$
Shank	$42.64 \pm 2.32(18)$	$42.14 \pm 0.99(10)$
Foot	100.00	
Lumbocoxal segment	$54.85 \pm 7.46(8)$	
Thorax	$66.10 \pm 6.39(8)$	
Arm	$43.74 \pm 3.03(18)$	$45.90 \pm 2.38(10)$
Forearm	$42.93 \pm 2.13(18)$	$42.12 \pm 1.07(6)$
Hand	100.00	100.00

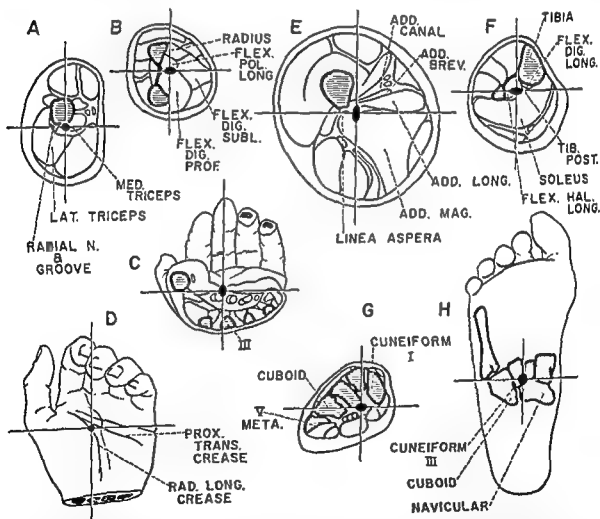


Fig. 5. Anatomical locations of center of mass in the limb segments. The relative heights and widths of the black spots that are centered over the average location of the center of mass reflect the relative variability in the two directions; each height and width correspond with the plus and minus mean deviations of position of the center of mass. The bones in the section are shaded and the more relevant muscles and other landmarks are labeled. A, Arm section. B, Section through the more relevant muscles and other landmarks in the arm. C and D, Center of mass location in the hand. E, Center of mass location in the thigh segment. F, Location in the leg. G and H, Location of center of mass of the foot segment.

total weight. The data from a similar study of the shoulder segment of three of the bodies are also tabulated in this table. Finally, the average density of body segments for our cadaver material and the Harless data are presented in table 7. All of the tabulated values include the standard deviation and the sample numbers are given in parentheses.

DISCUSSION

From the descriptions of the techniques used by earlier workers, it is evident that this data, if it is to be used, cannot be amalgamated for comparison but must, rather, be interpreted in the light of the investigator's individual data gathering idiosyncrasies. The very small samples, peculiarities of determining segments, disarticulation, loss of body fluids, position of limbs, etc. have marked effects on body constant values. The measurement of segments from the proximal to the distal extremity of the bone is not the value re-

quired for link length. This dimension must be based on the mean interaxial distance of the segment. Hence, joints should not be disarticulated. Measurements based on surface landmarks must be understood, equilibrated, or standardized. We have attempted to identify superficial, palpable landmarks to locate link end-points which can be duplicated in further investigations by later workers on cadaver or living material. Similarly, it is equally important to use a standardized, if nevertheless arbitrary, limb position. Obviously, the soft tissues overlying articulations will share their mass with adjacent links; the degree to which they contribute to the links will vary with the degrees of freedom and position exhibited by the joint. The fluidity of this mass distribution will effect not only mass values for links but the locations of segment centers of gravity and other body constants as well. Our efforts were directed toward establishing mid-

TABLE 6
Mass in per cent of total weight

	Skin and fascia	Muscle	Bone
Thigh	29.0 ± 3.31(14)	59.6 ± 2.81(14)	11.5 ± 1.78(14)
Shank	22.2 ± 2.98(14)	45.6 ± 2.85(14)	32.3 ± 2.56(14)
Foot	29.2 ± 4.30(14)	20.3 ± 4.25(14)	50.7 ± 7.35(14)
Arm	26.0 ± 3.85(14)	56.8 ± 4.74(14)	18.0 ± 1.61(14)
Forearm	18.7 ± 4.25(14)	53.2 ± 4.90(14)	28.2 ± 3.99(14)
Hand	28.4 ± 3.04(13)	27.6 ± 2.98(13)	44.0 ± 3.27(13)
Shoulders (left side only)	36.5 ± 3.34(6)	53.9 ± 4.09(6)	9.6 ± 3.76(6)

TABLE 7
Average density of body segments of cadavers¹

	Michigan data (Demyster)	Harless data
	Density (gm/cm ³)	Density
Whole body ²	1.003	
Head and trunk	1.0138 ± 0.0260(18)	
Trunk minus shoulders	1.0083 ± 0.0319(18)	
Head and neck	1.1708 ± 0.1825(14)	1.0851(1) ³
Shoulders	1.0925 ± 0.1318(34)	
Thorax	0.9573 ± 0.1284(16)	
Abdominopelvic mass	1.0297 ± 0.0424(18)	
Arm	1.0676 ± 0.0266(42)	1.0887 ± 0.0036(5)
Forearm	1.1015 ± 0.0430(42)	1.1097 ± 0.0040(5)
Hand	1.0696 ± 0.3491(42)	1.1126 ± 0.0064(5)
Thigh	1.0401 ± 0.0170(41)	1.0685 ± 0.0149(6)
Shank	1.0789 ± 0.0288(41)	1.1000 ± 0.0217(6)
Foot	1.0664 ± 0.1474(41)	1.0893 ± 0.0089(6)

¹ Mass in air divided by volume.

² From literature.

³ Head alone.

TABLE 4
Mean weights of male cadaver segments and ratio to total body weight

	Michigan data (Dempster)		Leipzig data (Braune and Fischer)	
	Mean weights (gm)	% of Total	Mean weights (gm)	% of Total
Total body weight	61190 \pm 8137 (7)	100	58895	(5)
Head and trunk	34637 \pm 5607 (18)	56.34 \pm 2.45 (6)	30824	(5) 52.21 \pm 2.97(5)
Head and trunk minus shoulders	28077 \pm 3994 (18)	46.02 \pm 2.23(5)		
Head and neck	5119 \pm 838 (16)	7.92 \pm 0.85 (7)		
Shoulders	3401 \pm 843 (34)	5.27 \pm 0.54(14)		
Thorax	7669 \pm 2270 (17)	10.97 \pm 1.52(7)		
Abdomino-pelvic headless trunk	16318 \pm 2505 (18)	26.39 \pm 2.90(7)		
Arm	1636 \pm 350 (42)	2.64 \pm 0.29(14)	2017 \pm 406 (22)	3.167 \pm 0.27 (10)
Forearm	947 \pm 199 (42)	1.531 \pm 0.165(14)	1342 \pm 242 (18)	2.087 \pm 0.245(6)
Hand	378.3 \pm 71.7(42)	0.612 \pm 0.058(14)	536.1 \pm 84.4(18)	0.833 \pm 0.045(6)
Thigh	609.6 \pm 985 (41)	10.008 \pm 1.197(14)	6632 \pm 783 (22)	10.924 \pm 0.769(10)
Shank	2852 \pm 695 (41)	4.612 \pm 0.534(14)	2924 \pm 379 (22)	4.680 \pm 0.353(10)
Foot	884 \pm 178 (41)	1.431 \pm 0.142(14)	1072 \pm 106 (22)	1.765 \pm 0.194(10)

TABLE 5
Mean volumes of male cadaver segments and ratio to body volume

	Michigan data (Dempster)	
	Volume (cm ³)	Ratio
Total body volume ¹	61,190 \pm 8137	54.877 \pm 2.280(6)
Head and trunk	33,970 \pm 4570 (18)	45.545 \pm 1.377(5)
Head and trunk minus shoulders	27,815 \pm 3687 (18)	
Head and neck	4,508 \pm 818 (14)	7.178 \pm 0.709(7)
Shoulders	3,172 \pm 919 (34)	5.063 \pm 0.563(14)
Thorax	7,752 \pm 1978 (16)	12.109 \pm 1.370(7)
Abdominopelvic mass	15,854 \pm 2366 (18)	26.274 \pm 3.361(7)
Arm	1,533 \pm 332 (42)	2.439 \pm 0.294(14)
Forearm	857 \pm 180 (42)	1.531 \pm 0.167(14)
Hand	342.7 \pm 73.8(42)	0.612 \pm 0.057(14)
Thigh	5,865 \pm 969 (41)	9.588 \pm 1.142(14)
Shank	2,643 \pm 654 (41)	4.221 \pm 0.502(14)
Foot	833 \pm 174 (41)	1.294 \pm 0.143(14)

¹ Total body volume equals weight divided by density of 1.0.

total weight. The data from a similar study of the shoulder segment of three of the bodies are also tabulated in this table. Finally, the average density of body segments for our cadaver material and the Harless data are presented in table 7. All of the tabulated values include the standard deviation and the sample numbers are given in parentheses.

DISCUSSION

From the descriptions of the techniques used by earlier workers, it is evident that this data, if it is to be used, cannot be amalgamated for comparison but must, rather, be interpreted in the light of the investigator's individual data gathering idiosyncrasies. The very small samples, peculiarities of determining segments, disarticulation, loss of body fluids, position of limbs, etc. have marked effects on body constant values. The measurement of segments from the proximal to the distal extremity of the bone is not the value re-

quired for link length. This dimension must be based on the mean interaxial distance of the segment. Hence, joints should not be disarticulated. Measurements based on surface landmarks must be understood, equilibrated, or standardized. We have attempted to identify superficial, palpable landmarks to locate link endpoints which can be duplicated in further investigations by later workers on cadaver or living material. Similarly, it is equally important to use a standardized, if nevertheless arbitrary, limb position. Obviously, the soft tissues overlying articulations will share their mass with adjacent links; the degree to which they contribute to the links will vary with the degrees of freedom and position exhibited by the joint. The fluidity of this mass distribution will effect not only mass values for links but the locations of segment centers of gravity and other body constants as well. Our efforts were directed toward establishing mid-

TABLE 6
Mass in per cent of total weight

	Skin and fascia	Muscle	Bone
Thigh	29.0 ± 3.31(14)	59.6 ± 2.81(14)	11.5 ± 1.78(14)
Shank	22.2 ± 2.98(14)	45.6 ± 2.85(14)	32.3 ± 2.56(14)
Foot	29.2 ± 4.30(14)	20.3 ± 4.25(14)	50.7 ± 7.35(14)
Arm	26.0 ± 3.85(14)	56.8 ± 4.74(14)	18.0 ± 1.61(14)
Forearm	18.7 ± 4.25(14)	53.2 ± 4.90(14)	28.2 ± 3.89(14)
Hand	28.4 ± 3.04(13)	27.6 ± 2.98(13)	44.0 ± 3.27(13)
Shoulders (left side only)	36.5 ± 3.34(6)	53.9 ± 4.09(6)	9.6 ± 3.76(6)

TABLE 7
Average density of body segments of cadavers^a

	Michigan data (Dempster)	Harless data
	Density (gm/cm ³)	Density
Whole body ^b	1.003	
Head and trunk	1.0138 ± 0.0260(18)	
Trunk minus shoulders	1.0088 ± 0.0319(18)	
Head and neck	1.1708 ± 0.1825(14)	1.0851(1) ^c
Shoulders	1.0925 ± 0.1318(34)	
Thorax	0.9573 ± 0.1284(16)	
Abdominopelvic mass	1.0297 ± 0.0424(18)	
Arm	1.0576 ± 0.0266(42)	1.0887 ± 0.0036(5)
Forearm	1.1015 ± 0.0430(42)	1.1097 ± 0.0040(5)
Hand	1.0696 ± 0.3491(42)	1.1126 ± 0.0064(5)
Thigh	1.0481 ± 0.0170(41)	1.0685 ± 0.0149(6)
Shank	1.0789 ± 0.0288(41)	1.1000 ± 0.0217(6)
Foot	1.0664 ± 0.1474(41)	1.0893 ± 0.0089(6)

^a Mass in air divided by volume.

^b From literature.

^c Head alone.

range joint positions which could be identified, duplicated, and described.

In considering the Michigan data, we must remember that we are dealing with a sample which was older and below average stature and weight when compared with the national average. Nor do we have information on the body constants of infants, children, young adults, and females. These values also vary with body type. We did analyze the amount of bone, muscle, skin and fascia in several specimens but much additional information is needed to determine the relationship which exists between body physique and the distribution of mass as well as the center of mass. Physiological status also effects the distribution of volume and mass. The exact degree of this effect is another area of investigation.

LITERATURE CITED

- Barter, J. T. 1957 Estimation of the mass of body segments. WADC Technical Report 57-260.
- Bernstein, N. 1935 Untersuchungen über die Biodynamik des Ganges des normalen erwachsenen Mannes. Inst. Exper. Med. d. Soviet Union, Moscow. 243 pp. (In Russian; German summary)
- Braune, W., and O. Fischer 1889 Über der Schwerpunkt des Menschlichen Körpers mit Rücksicht auf die Ausrüstung des Deutschen Infanteristen. Abhandl. d. Kl. sächs. Ges. Wiss. Math. Phys. Kl., 15 (7): 561-672.
- 1892 Bestimmung der Trägheitsmomente des menschlichen Körpers und seiner Glieder. Abhandl. d. Kl. sächs. Ges. Wiss. Math. Phys. Kl., 18 (8): 409-492.
- Contini, R., R. J. Drillis and M. Bluestein 1963 Determination of body segment parameters. Human Factors, 5: 493-504.
- Dempster, W. T. 1955a Space requirements of the seated operator. WADC Technical Report 55-159.
- 1955b The anthropometry of body action. Ann. N. Y. Acad. Sci., 63: 559-585.
- 1961 Free-body diagrams as an approach to the mechanics of human posture and motion. In F. G. Evans et al., Biomechanical studies of the musculo-skeletal system. Charles C Thomas, Springfield, Ill. Chap. 5, 81-135.
- 1965 Mechanisms of shoulder movement. Arch. Phys. Med. & Rehabilitation, 46: 49-70.
- Dempster, W. T., L. A. Sherr and J. G. Priest 1964 Conversion scales for estimating humeral and femoral lengths and the lengths of functional segments in the limbs of American caucasoid males. Human Biol., 36: 246-262.
- Duggar, B. C. 1962 The center of gravity of the human body. Human Factors, 4: 131-148.
- Elftman, H. 1939 The Rotation of the Body in Walking. Arbeitsphysiol., 10 (5): 477-484.
- Fischer, O. 1892 Ein zweiter Mechanismus zur Bestimmung der Lage des Schwerpunktes eines Systems von in beliebiger Weise durch Gelenke mit einander verbundenen Körpern; Einige Gelenkmechanismen; Mechanismus zur Bestimmung der Lage des Schwerpunktes des menschlichen Körpers und seiner Teile. Katalog math. u. math.-phys. Modelle, Apparate u. Instrumente. 100-104, 350-359.
- 1904 Der Gang des Menschen. Abh. d. Math.-Phys. Cl. d. k. Sächs. Gesellsch. d. Wiss., 28: 319-418.
- 1906 Theoretische Grundlagen für eine Mechanik der lebenden Körper. B. G. Teubner, Leipzig u. Berlin, 372 pp.
- Fujikawa, K. 1963 The center of gravity in the parts of the human body. Okajimas Fol. Anat. Jap., 39: 117-126.
- Harless, E. 1857 Lehrbuch der plastischen Anatomie, enthaltend die Gesetze für organische Bildung und künstlerische Darstellung der menschlichen Gestalt im Allgemeinen und in den einzelnen Situationen. 2 vol., 170 pp., 180 pp., Ebner u. Seubert, Stuttgart.
- 1860 Die statischen Momente der menschlichen Gliedmassen. Abhandl. d. k. bayer. Akad. d. Wissensch., 8: 71-96, 259-294.
- Jones, F. W. 1920 The principles of anatomy as seen in the hand. P. Blakiston's Son, Phila., 325 pp.
- Krause, C. F. T. 1843 Handbuch der menschlichen anatomie. Hahn'schen Hofbuchhandlung, Hanover, 1274 pp.
- Krogman, W. M., and F. E. Johnston 1963 Human mechanics: four monographs abridged. Tech. Doc. Rep. AMRL-TDR-63-123.
- Meeh, C. 1895 Volummessungen des menschlichen Körpers und seiner einzelnen Theile in den verschiedenen Altersstufen. Ztschr. f. Biol., 31: 125-147.
- Meyer, G. H. 1873 Die Statik und Mechanik des Menschlichen Knochengerüsts. Wilhelm Engelmann, Leipzig, 402 pp.
- Sheldon, W. H., C. W. Dupertuis and E. McDermott 1954 Atlas of men. Harper & Bros., New York, 357 pp.
- Sheldon, W. H., S. S. Stevens and W. B. Tucker 1940 The varieties of human physique. Harper & Bros., New York, 347 pp.
- Spector, W. S. (ed.) 1956 Handbook of biological data. W. B. Saunders, Phila., 584 pp.
- Valentin, G. G. 1850 Lehrbuch der Physiologie des Menschen. (2 vols. bound in 3), F. Vieweg u. Sohn, Braunschweig, 420 pp., 731 pp., 316 pp.
- Vierordt, H. 1893 Anatomische, physiologische und physikalische Daten und Tabellen zum Gebrauche für Mediciner. G. Fischer, Jena, 400 pp.
- Williams, H. R., and M. Williams 1962 Biomechanics of human motion. W. B. Saunders, Phila., 147 pp.
- Zook, D. E. 1932 Physical growth of boys: a study by means of water displacement. Am. J. Dis. Child., 43: 1347-1432.

A Study of Mineral Density Surrounding Resorption Sites in Teeth

J. K. AVERY, R. A. MEYERS AND L. E. HALE

Department of Oral Biology, School of Dentistry and Department of Anatomy, Medical School, University of Michigan, Ann Arbor, Michigan

ABSTRACT An investigation of mineral density surrounding lacunar resorption sites in cases of both internal and external root resorption, was carried out on 37 human primary and permanent teeth. In addition, equivalent areas of the roots of 14 normal appearing teeth were studied for comparison. Thirty-two of the teeth were analyzed using microradiographic and microhardness techniques and the remainder were studied microscopically after histologic preparation. The teeth used for microradiographic analysis were embedded in plastic, bisected and half of each tooth was sectioned at 70-100 μ . Microradiographs were taken at 9.5 kv and exposed to 30 milliamperes for 25 to 40 minutes. The other halves of the teeth were used for microhardness tests using a Tukon Microhardness Tester. One series of microhardness measurements was made 10 to 40 μ from sites of active resorption in root dentin and a second series was made 250 to 500 μ from these sites. The hardness measurements of the first series were found to be significantly lower than those of the second in cases of both external and internal resorption. Hardness values of the surface of normal appearing roots were also less than areas 250 to 500 μ deeper in the dentin. Microradiographs did not reveal any definite zone of subsurface demineralization although some resorption sites were bordered by irregular areas of decreased radio-density which may be due to superimposition of several resorption sites within the thickness of the tooth section. Histologic observations did not reveal a definite subsurface demineralization gradient. The lacunar resorption front was found to be a multilocular and completely interconnected system.

The cause of tooth resorption other than that related to the process of eruption and shedding of teeth, has interested numerous investigators for many years. The condition of irregular cavities within teeth resulting in "pink spots" was noted as early as 1890 by Miller, in 1894 by Gaskill and in 1920 by Mummery. There have been numerous studies of the characteristics of this pathologic process as well as a number of investigations concerned with its etiology.

To gain information concerning the prevalence of root resorption Massler and Malone ('54) examined the radiographs of permanent teeth of 708 persons and found 86.4% of the teeth examined or an average of 16 teeth in each person undergoing resorption to some extent. Thoma ('35) pointed out that tooth resorption may originate either on the internal or the external surfaces of the root. Considering the latter type, Henry and Weinmann ('51) found approximately 77% of external root resorption occurring in the apical third of the tooth, 20% in the middle third and

only 4% in the gingival third. It was located most often on the mesial and the buccal surfaces of the roots. They concluded resorption occurs more readily on those root surfaces facing physiologic movement, the areas where trauma was the greatest. They also found, as did Warner et al. ('47) that repair of roots with cementum or dentin-like substance occurred in a high percentage of the cases. Stafne and Slocumb ('44) found the central incisor the most frequently involved tooth. In consideration of causes, most investigators believed trauma was an important factor. This may be caused by occlusal interferences, (Orban, '28) orthodontic appliances, (Ketcham, '29; Hemley, '41; Oppenheim, '42) or chemical agents used in restoring teeth (Via, '55; Cabrini et al., '57; Rabinowitch, '57). Also the prolonged effects of inflammation is believed an important predisposing factor to this disease. Again Cahn ('32) and Scopp ('56) believe that idiopathic resorption may be due to an increase of pulpal blood supply which aids in the resorption

of calcium salts. Others believe systemic factors, perhaps hormonal, such as hyperthyroidism as suggested by Becks ('33) and by Henry and Weinmann ('51) or hyperparathyroidism which according to Young ('63) may predispose this process in experimental animals. There are many causes of resorption of both the internal and external surfaces of the root however, which cannot be explained by any of the above mentioned causes.

Recently modern scientific methods have been used in an attempt to gain further insight into the etiology of this process. Burstone ('53) found the ground substance of dentin adjacent to the area of internal resorption to contain more than normal amounts of glycoprotein material. He theorized this increase may be due in part to proteolytic activity of pulpal bacteria superimposed on the primary processes of resorption. Sognnaes ('59) utilizing microradiographic techniques found no evidence of a demineralization gradient in tooth resorption. In 1961, utilizing electron microscopy, he found a half micron alteration of the dentin surrounding a Howship's lacunae. There has been much work done on bone resorption and several investigations are pertinent to this discussion. Greulich ('61) utilizing high resolution, ultrasoft microradiography studied the distribution of organic mass at the sites of bone resorption. He observed a band or rind approximately 1-1.5 μ in width at the point of junction of the osteoclast. Goldhaber and Barnett ('60) demonstrated succinic dehydrogenase in osteoclasts and Burstone ('60) found dehydrogenase, acid phosphatase and leucine aminopeptidase in osteoclasts. Balough ('63) found osteoclasts to contain DPNH diaphorase, TPNH diaphorase, lactic and succinic dehydrogenase. Fullmer ('64) also noted osteoclasts contain high amounts of the latter. Ultrastructural studies by Hancox and Boothroyd ('63) revealed mineral crystals in the vacuoles of the osteoclasts and the resulting exposed collagen was noted to be enclosed in the folds of the cells' ruffled border. It was suggested that an initial mineral loss is followed by digestion of the fibrous matrix.

In an attempt to gain further information of the characteristics of the mineral density of the calcified tissue surrounding lacunar resorption sites in dentin, the present study was planned and has employed microradiographic, microhardness and histologic techniques.

MATERIALS AND METHODS

A. Microradiography

Thirty-two primary and permanent teeth showing areas of external and internal resorption were fixed in 10% neutral formalin and then embedded in bioplastic. The teeth were then cut in half, one half being used for microhardness studies and the other half for microradiography. Sections were cut for microhardness on a water cooled, hard tissue sectioning machine¹ at 70-100 μ . The thickness of each section was measured with a micrometer to determine the proper time for radiographic exposure. These were stored in tap water until they were used. At that time they were allowed to air dry for 5-10 minutes, the excess bioplastic removed from the sections and then they were cemented with acetone onto Saran Wrap which had been cut into strips. These strips bearing the sections were adapted onto 1 \times 3 spectroscopic plates² in the dark room. These plates were placed in a camera bottom so that the source-object distance was 5.5 inches. A shutter was used with a film holder to make the bottom light tight so the film could be carried to and from the machine and the dark room.

The x-ray machine used was a Picker 50 K.V. industrial unit with a type AEG 50 machlett tube operated at 38 primary volts and 30 milliamperes which produced 9.5 K.V. This voltage gives x-rays of a wave length of approximately 2.2 \AA which is the proper wave length for maximal absorption by calcium ions. Exposures varied from 25-40 minutes depending upon the thickness of the sections. After exposures were made the plates were developed in Kodak D-19 at 68°F for five minutes, washed, fixed and dried. They were studied and photographed on a microscope.

¹ Gillings Hamco Thin Sectioning Machine, Hamco Machines Inc., Rochester, New York.
² Kodak type 649-D.

B. Microhardness

The undecalcified halves of the teeth used for microhardness were sliced into slabs averaging one-half millimeter thick and smoothed by hand on a glass slab using no. 60 wet sand paper. Final polishing was accomplished with a felt wheel at high speed for ten seconds. The sections were then affixed to glass slides and tested for microhardness² using a 25 gm weight. The instrument was standardized each day to assure consistent results. Only uniform indentations showing diamond-shaped impressions with the long axis seven times greater than the width were used. The areas considered to be undergoing resorption, were those showing obvious scalloping either on the internal or external surfaces of the tooth root. The diamond indenter was positioned to gain measurements in two areas. The first area was as close as possible to the zones of resorption. These were all within 10-40 μ from these sites. A second area studied for comparison was 250 to 500 μ from these areas. To facilitate interpretation of the areas of the crown measured, the tooth sections were magnified and tracings of each section were made. Another series of five normal appearing teeth were studied in the same manner. The hardness of the root surface area underlying cementum was compared in an area again 250 to 500 μ away in the dentin.

C. Histologic

Another series of normal appearing human teeth and some undergoing resorption were fixed in formalin, decalcified with formic citrate and then sectioned, mounted, stained with hemotoxylin and eosin and Mallory's connective tissue stain and examined microscopically. Attempts were made to examine similar areas as evaluated by the microradiographic and hardness techniques. Photomicrographs were then made of sections believed pertinent to this study.

RESULTS

Microhardness study

The average mean Knoop hardness (KHN) of dentin 10 to 40 μ from sites of active root resorption was found to be

37.6 in primary teeth and 43.1 in permanent teeth or an average of 40.4 KHN for both series of teeth. The KHN of dentin 250 to 500 μ from these zones was found to be 52.8 in primary teeth and 56.1 in permanent teeth. It is observed that this is a difference of 15.2 KHN in primary teeth and 13.0 in permanent teeth between the areas of resorption and the areas deeper in dentin. An explanation of these findings is shown in figures 1, 2 and 3 and in tables 1 and 2.

A test of the significance of the hardness of the dentin at the resorption fronts as compared to areas of non-resorbing dentin was done by calculating the "T" values of the mean hardness of the two areas in each individual tooth. Most of them were found to be significantly different at the 95% level of confidence. Also the teeth were found to show some variation in hardness within the two locations studied. It was noted that the mean hardness of the resorbed area in permanent teeth was greater than that of the primary teeth by only 5.5 KHN and in the non-resorbed area 3.3 KHN. There was an indication of a slightly increased hardness of the permanent dentition over the primary.

In an attempt to gain more information about the characteristics of the surface as opposed to deeper areas in dentin, it was decided to analyze a series of normal appearing teeth. Five teeth with normal appearing roots were prepared in the manner previously indicated and indentations were made 10-40 μ from the surface of the root dentin immediately underlying the cementum. A second series of indentations were obtained 250 to 500 μ deeper in the dentin. The surface dentin underlying cementum was found to be less hard than that situated deeper in the root (table 3 and fig. 4). An average mean hardness of 42.0 KHN was found for the surface and 62.2 KHN for the deeper dentin or a difference of 20.2 Knoop Hardness Numbers. Using a one way analysis of variants the F ratio revealed this difference between the means to be significant at the 99% confidence level. There appears thus to be a band of softer peripheral dentin of the root underlying the cementum. The

² Tukon Microhardness Tester with Knoop Diamond Indenter.

TABLE 1
Primary teeth

Tooth no.	Resorbed areas			Non-resorbed areas			Calculations	
	No. of indents	KHN	S.D.	No. of indents	KHN	S.D.	"T" value	Signif.
D-1	26	30.6	5.9	8	40.9	3.0	3.6	yes
D-2	30	29.9	2.1	8	43.3	1.3	7.8	yes
D-3	19	31.7	7.9	5	58.8	2.3	3.9	yes
D-4	32	31.0	7.9	8	41.8	3.5	3.6	yes
D-5	37	35.1	3.2	13	45.8	1.0	8.2	yes
D-6	34	31.9	3.6	12	45.7	4.2	3.3	yes
D-7	13	31.8	2.0	11	54.0	4.8	6.1	yes
D-8	20	29.1	2.8	10	56.6	4.1	20.7	yes
D-9	21	38.6	4.5	12	61.9	6.3	7.8	yes
M-1	25	52.2	10.2	29	58.5	13.1	1.9	no
M-2	15	45.1	6.3	24	58.2	11.3	3.9	yes
M-3	10	44.5	17.3	27	50.0	12.4	1.3	no
M-4	11	45.5	14.5	17	53.2	14.3	1.3	no
M-5	25	41.8	10.7	16	51.4	15.1	2.1	yes
C-1	27	55.2	13.4	17	55.5	14.2	0.08	no
Total	351			217				
Average		37.6			52.8			

TABLE 2
Permanent teeth

Tooth no.	Resorbed areas			Non-resorbed areas			Calculations	
	No. of indents	KHN	S.D.	No. of indents	KHN	S.D.	"T" value	Signif.
IR-12 area 1	28	49.9	7.7	9	55.6	6.7	1.5	no
IR-12 area 2	33	44.9	3.6	10	56.9	4.0	6.5	yes
IR-13	16	39.8	4.2	11	54.6	3.7	7.2	yes
IR-14	28	53.1	8.1	13	59.7	2.3	2.7	yes
IR-15	10	33.6	2.2	10	60.3	4.0	73.1	yes
IR-16 area 1	24	36.5	2.7	10	58.3	1.1	7.5	yes
IR-16 area 2	20	31.8	2.9	14	48.9	2.9	16.3	yes
Total	159			77				
Average		43.1			56.1			

TABLE 3
Permanent teeth. Normal appearing root dentin

Tooth no.	Surface			Below surface		
	No. of indents	KHN	S.D.	No. of indents	KHN	S.D.
N-1	28	35.1	4.6	28	64.0	6.4
N-2	17	43.5	4.0	17	59.0	6.1
N-3	26	43.8	3.6	26	62.9	5.3
N-4	26	43.8	5.5	26	65.4	7.1
N-5	14	43.1	8.3	14	59.8	5.3
Total	111			111		
Average		42.1			62.2	

surface measurements of both series of permanent teeth at 10 to 40 μ from the surface of dentin were found to have very similar hardness values. The normal appearing surface was 42.0 KHN and the abnormal 43.1 KHN.

It is of interest that because of the extent of resorption, the location of some of the microhardness measurements were located near central root dentin or the area where the hardness was originally the greatest.

Microradiographic study

Microradiographs of the 70–100 μ thick dentin specimens revealed the oval shape of the resorption cavities and the interrelationship of large groups of these spaces (figs. 5, 6). It is of interest to observe that as many as 50 to 75 may be present in the thickness of a 70–100 μ slab. Many of the lacunae appear to range from 30 to 200 μ or more in size and in some cases a number of smaller ones appear in contact with a larger cavity (fig. 6). The larger cavity may be termed "primary" sites and the smaller lacunae associated with the larger areas "secondary" sites. The multilocular areas in figures 5 and 6 reveal how a number of lacunae may be grouped, many of them appear superimposed in the radiograph. No evidence appears of a gradient of mineral resorption around the sites. The resorption cavities shown in figures 5 and 6 were from a case where little tissue destruction had occurred. This could be considered a young active site. The lacunae appear smaller and more numerous than those of figures 7 and 8. The site shown in figure 7 is from an advanced case of internal resorption and much dentin was missing. This probably is an older site which has lost some of the spicules of dentin which helped define the smaller sites. As these sites expanded the spicules are eliminated resulting in the formation of larger sites. The edges of the resorption cavities appear equally as dense as the adjacent areas with the exception of the small area appearing in the center and upper left of figure 7. This area again may consist of a number of smaller sites, however, which are associated with the adjacent larger one. The microradiograph shown as figure 8 is of a

deep, tunnel-type defect. This kind of defect was found in several of the teeth and is thought to be related to an accessory root canal. This theory is substantiated by the fact that this microradiograph was taken of an area near the apical canal. The boundaries of this space appear to be altered by numerous small lacunar sites. Many of the resorption fronts revealed areas of repair. Microradiographic appearance of areas of secondary deposition of bony or cementum-like substance on the root surface are shown in figures 9 and 10. Figure 9 is from an area of internal resorption and figure 10 from an external site. In a few areas, what appeared as a sub-surface demineralization front was observed (fig. 11). As this is from an area of internal resorption, it is possible that the less radiopaque area represents predentin. A possible similar area can be seen in figure 13 where the resorption is in an early stage and some of the predentin is still present. Predentin is quite radiolucent and may appear as shown in figure 13. The diagram shown in figure 12 is an interpretation of the multilocular nature of the resorption sites and their various means of communication. All of the sites are connected with the surface of the advancing front and each site is usually connected with the smaller ones above, below and/or the one to the right and left of it. By this means a vast surface area is maintained and small islands of dentin are produced and efficiently eliminated.

Histologic study

The microscopic studies were of teeth some with internal and others with external resorption sites and the observations clarified some of the previous findings. Figure 13, as previously noted, was a primary site probably caused by chemical trauma on the pulp, $\text{Ca}(\text{OH})_2$. The initial stage of resorption is indicated by the degenerating odontoblasts and little loss of tissue at this time except the uncalcified predentin. It also appears that predentin deposition has ceased. Figure 14 illustrates a dense staining zone bordering a resorption site and may be indicative of such chemical changes as mineral loss to the depth of several microns. Functional dentin appears on the right with the proto-

TABLE 1
Primary teeth

Tooth no.	Resorbed areas			Non-resorbed areas			Calculations	
	No. of indents	KHN	S.D.	No. of indents	KHN	S.D.	"T" value	Signif.
D-1	26	30.6	5.9	8	40.9	3.0	3.6	yes
D-2	30	29.9	2.1	8	43.3	1.3	7.8	yes
D-3	19	31.7	7.9	5	58.8	2.3	3.9	yes
D-4	32	31.0	7.9	8	41.8	3.5	3.6	yes
D-5	37	35.1	3.2	13	45.8	1.0	8.2	yes
D-6	34	31.9	3.6	12	45.7	4.2	3.3	yes
D-7	13	31.8	2.0	11	54.0	4.8	6.1	yes
D-8	20	29.1	2.8	10	56.6	4.1	20.7	yes
D-9	21	38.6	4.5	12	61.9	6.3	7.8	yes
M-1	25	52.2	10.2	29	58.5	13.1	1.9	no
M-2	15	45.1	6.3	24	58.2	11.3	3.9	yes
M-3	16	44.5	17.3	27	50.0	12.4	1.3	no
M-4	11	45.5	14.5	17	53.2	14.3	1.3	no
M-5	25	41.8	10.7	16	51.4	15.1	2.1	yes
C-1	27	55.2	13.4	17	55.5	14.2	0.08	no
Total	351			217				
Average		37.6			52.8			

TABLE 2
Permanent teeth

Tooth no.	Resorbed areas			Non-resorbed areas			Calculations	
	No. of indents	KHN	S.D.	No. of indents	KHN	S.D.	"T" value	Signif.
IR-12 area 1	28	49.9	7.7	8	55.6	6.7	1.5	no
IR-12 area 2	33	44.9	3.6	10	56.9	4.0	6.5	yes
IR-13	16	39.8	4.2	11	54.6	3.7	7.2	yes
IR-14	28	53.1	8.1	13	59.7	2.3	2.7	yes
IR-15	10	33.6	2.2	10	60.3	4.0	73.1	yes
IR-16 area 1	24	36.5	2.7	10	58.3	1.1	7.5	yes
IR-16 area 2	20	31.8	2.9	14	48.9	2.9	16.3	yes
Total	159			77				
Average		43.1			56.1			

TABLE 3
Permanent teeth. Normal appearing root dentin

Tooth no.	Surface			Below surface		
	No. of indents	KHN	S.D.	No. of indents	KHN	S.D.
N-1	28	36.1	4.6	28	64.0	6.4
N-2	17	43.5	4.0	17	59.0	6.1
N-3	26	43.8	3.6	26	62.9	5.3
N-4	26	43.8	5.5	26	65.4	7.1
N-5	14	43.1	8.3	14	59.8	5.3
Total	111			111		
Average		42.1			62.2	

structural studies of Hancox and Bothroyd ('63) on avian bone revealed a mineral loss lining a lacunae. Further, they found crystals in the vacuoles of the osteoclasts and exposed collagen fibrils were found enclosed in the folds of the cell membrane. They believe this is suggestive of a process of continuous digestion. Other investigators who have not found demineralized collagen fibers believe the primary change to be solution of the collagen fibers; Scott and Pease ('56); Gonzales and Karnovsky ('61); and Dudley and Spiro ('61).

Whether the mechanism involves first the alteration of the collagen fibril resulting in a subsequent release of mineral and final digestion of the fibril or vice versa is yet to be answered. It is hoped the present observations of a possible subsurface demineralization front may aid in the clarification of this complex process.

CONCLUSIONS

1. The microhardness 10 to 40 μ from lacunar resorption sites was consistently less than that of dentin 250 to 500 μ from these sites.
2. The various amounts of root dentin lost during resorption resulted in measurements of some lacunar sites which were located in areas previously highest in mineral density.
3. Microhardness of normal appearing dentin 10 to 40 μ near the root surface was consistently less than that of dentin 250 to 500 μ from these sites.
4. Microradiographs of resorption sites revealed some to be bordered by irregular areas of decreased radiodensity which was believed to be caused by superimposition of several resorption sites in the thickness of the slab or to zones of predentin.
5. Microradiographs of resorption sites in dentin revealed the lacunae to be oval shaped, multilocular and a completely inter connected system, with themselves and with the surface of the front.

Author's Note

The authors would like to dedicate this paper to Professor Wilfrid T. Dempster, a friend, an associate and a constant inspiration in teaching and research.

LITERATURE CITED

- Avery, J. K., R. L. Visser and D. E. Knapp 1961 The pattern of the mineralization of enamel. *J. Dent. Res.*, 40: 1004-1019.
- Balogh, K. J. 1963 Histochemical study of oxidative enzyme systems in teeth and periodontal tissues. *J. Dent. Res.*, 42: 1457-1466.
- Becks, H. 1933 Root resorptions and their relation to pathologic bone formations I. Statistical data and roentgenographic aspect. *Am. Soc. Ortho.*, 33: 84-121.
- Burstone, M. S. 1953 The ground substance of abnormal dentin, secondary dentin, and pulp calcification. *J. Dent. Res.*, 32: 269-279.
- 1960 Hydrolytic enzymes in dentinogenesis and osteogenesis. In: *Calcification in Biological Systems*. Ed., R. F. Sognnaes. Publication No. 64 of the A.A.S., Washington, pp. 217-243.
- Cabrini, R. I., O. A. Maisto and E. E. Manfredi 1957 Internal resorption of dentine. *Oral Surg., oral Med., and Oral Path.*, 10: 90-96.
- Cahn, L. R. 1932 A case of bone metaplasia in the pulp canal of a tooth. *Dent. Items of Interest*, 54: 518-520.
- Craig, R. G., and F. A. Peyton 1958 The microhardness of enamel and dentin. *J. of Dent. Res.*, 37: 661-668.
- Dudley, H. R., and D. Spiro 1961 The fine structure of bone cells. *J. Biophys. and Biochem. Cytol.*, 11: 627-649.
- Fullmer, H. M., C. C. Link and M. J. Baer 1964 A stain for bone—illustrating apposition and absorption in two colors. *Stain Tech.*, 39: 71-73.
- Gaskill, H. J. 1894 Report of a case in which dentine of a tooth was absorbed by the pulp. *Dental Cosmos*, 36: 1019-1020.
- Goldhaber, P., and R. J. Barnett 1960 Succinic dehydrogenase in osteoclasts in resorbing-bone tissue cultures. *J. Dent. Res.*, 39: 728.
- Gonzalez, F. and M. J. Karnovsky 1961 Electron microscopy of osteoclasts in healing fractures of rat bone. *J. Biophys. and Biochem. Cytol.*, 9: 299-316.
- Greulich, R. G. 1961 Organic mass distribution in bone matrix undergoing osteoclastic resorption. *Arch Oral Biol.*, 3: 137-142.
- Hancox, N. M., and B. Bothroyd 1963 Structure-function relationship in the osteoclast. In: *Mechanisms of Hard Tissue Destruction*. Ed., R. F. Sognnaes. Am. Assoc. for Adv. of Science, Washington. Chapter 18, 497-514.
- Hemley, S. 1941 The incidence of root resorption of vital permanent teeth. *J. Dent. Res.*, 20: 133-141.
- Henry, J. L., and J. P. Weinmann 1951 The pattern of resorption and repair of human cementum. *J. Am. Dent. Assoc.*, 42: 270-290.
- Ketcham, A. H. 1929 A progress report of an investigation of apical root resorption of vital permanent teeth. *Inter. J. Ortho.*, 15: 310-328.
- Masser, N., and A. J. Malone 1954 Root resorption in human permanent teeth, a roentgenographic study. *Am. J. Ortho.*, 40: 619-633.

plasmic processes of the odontoblasts still in the dentinal tubules. Figures 15 and 16 both are from early and acutely active resorption fronts. In both figures observe the area of predentin (P) still present along the pulp border. It is apparent how this zone is bypassed along with an attached spicule of dentin as the front moves deep into the tissue. Close association of cells in the lacunae and the fibrous appearing substance in the background is evident. Finally, no definite subsurface alteration was revealed in the histologic study.

DISCUSSION

Analysis of the mineral density at 10 to 40 μ from lacunar resorption sites by microhardness measurements revealed a significant decrease in amount. If this is a stage in this pathologic process then it should be considered relative to the series of events that characterize resorption. Before doing this it is best to consider several technical factors that might lead to misinterpretation of the data. First, it is possible to produce a curved surface on the edge of a bone or tooth sample bordered by a softer substance such as plastic by over polishing. It has been noted by other investigators, Craig and Peyton ('58) and Rautiola and Craig ('61) that curved surfaces may produce distorted indentations. In the present study several precautions were taken to prevent this possible error. (1) Polishing was limited to ten seconds and (2) only diamond shaped indentations in which the long axis was seven times the width were used. Any distortion in this pattern caused immediate rejection of the measurement. Again possible false readings might be obtained from measurements taken in an area undermined with resorption sites. However only a few of the teeth were noted to be affected in this manner as discussed in the microradiographic findings. Measurements in such areas could produce distorted impressions yet few were obtained and these were excluded from the study.

The finding of less hard peripheral dentin underlying cementum in normal appearing roots is in agreement with the findings of Rautiola and Craig ('61). They found a narrow band of peripheral dentin

located between the central root and cementum to have a KHN of 38. Central root dentin on the other hand, had a mean KHN of 69. These figures for permanent teeth agree closely with the findings in the present study of normal permanent teeth which was 42 KHN for peripheral dentin and 62 KHN for areas of one-fourth to one-half millimeter nearer the central root. These are also similar to the findings of 56 KHN for non-resorbed areas of the pathologic permanent teeth. Again the extent of resorption in each tooth was different so the location of the hardness measurements would vary. In one case the resorption front would be located in central root dentin and in the next it would be nearer the periphery. That is why no overall statistical correlations were attempted, only the statistical difference between each resorption site and the area deeper in the same tooth. It is of interest that 17 to 22 resorbing teeth showed significant differences in the hardness of the two areas. Therefore if all technical errors have been excluded it is possible that a subsurface demineralization gradient exists. Such a gradient of 10 to 40 μ was not apparent microradiographically although it has been shown previously by Avery et al. ('61) that Tukon microhardness measurements reflect changes in mineral density that are not discernable by microradiography. This is true at least under the limitations of the equipment and techniques used.

Other investigators have noted the surface of root dentin to be less hard. It has been termed the "granular layer" as it appears microscopically to contain interglobular spaces. It is described as a developmental feature by Orban ('62).

Resorption of mineral to the depth of 1 to 2 μ have been described by a number of authors. Sognnaes et al. ('61) with the electron microscope described the characteristics of resorption surfaces of dentin and noted distinct ultrastructural changes to the depth of 0.6 μ . This change involved a reduced electron density and evidence of denuded fibrillar material. He stated he found no evidence of demineralization beyond the half micron. He also stated this in an earlier study in 1959 in which he used microradiography. The ultra-

structural studies of Hancox and Bothroyd ('63) on avian bone revealed a mineral loss lining a lacunae. Further, they found crystals in the vacuoles of the osteoclasts and exposed collagen fibrils were found enclosed in the folds of the cell membrane. They believe this is suggestive of a process of continuous digestion. Other investigators who have not found demineralized collagen fibers believe the primary change to be solution of the collagen fibers: Scott and Pease ('56); Gonzales and Karnovsky ('61); and Dudley and Spiro ('61).

Whether the mechanism involves first the alteration of the collagen fibril resulting in a subsequent release of mineral and final digestion of the fibril or vice versa is yet to be answered. It is hoped the present observations of a possible subsurface demineralization front may aid in the clarification of this complex process.

CONCLUSIONS

1. The microhardness 10 to 40 μ from lacunar resorption sites was consistently less than that of dentin 250 to 500 μ from these sites.

2. The various amounts of root dentin lost during resorption resulted in measurements of some lacunar sites which were located in areas previously highest in mineral density.

3. Microhardness of normal appearing dentin 10 to 40 μ near the root surface was consistently less than that of dentin 250 to 500 μ from these sites.

4. Microradiographs of resorption sites revealed some to be bordered by irregular areas of decreased radiodensity which was believed to be caused by superimposition of several resorption sites in the thickness of the slab or to zones of predentin.

5. Microradiographs of resorption sites in dentin revealed the lacunae to be oval shaped, multilocular and a completely interconnected system, with themselves and with the surface of the front.

Author's Note

The authors would like to dedicate this paper to Professor Wilfrid T. Dempster, a friend, an associate and a constant inspiration in teaching and research.

LITERATURE CITED

- Avery, J. K., R. L. Visser and D. E. Knapp 1961 The pattern of the mineralization of enamel. *J. Dent. Res.*, 40: 1004-1019.
- Balogh, K. J. 1963 Histochemical study of oxidative enzyme systems in teeth and periodontal tissues. *J. Dent. Res.*, 42: 1457-1466.
- Becks, H. 1933 Root resorptions and their relation to pathologic bone formations I. Statistical data and roentgenographic aspect. *Am. Soc. Ortho.*, 33: 84-121.
- Burstone, M. S. 1953 The ground substance of abnormal dentin, secondary dentin, and pulp calcification. *J. Dent. Res.*, 32: 269-279.
- 1960 Hydrolytic enzymes in dentinogenesis and osteogenesis. In: *Calcification in Biological Systems*. Ed., R. F. Sognnaes. Publication No. 11 of the A.A.A.S., Washington, pp. 217-243.
- Cabrini, R. I., O. A. Maisto and E. E. Manfredi 1957 Internal resorption of dentine. *Oral Surg., oral Med., and Oral Path.*, 10: 90-96.
- Cahn, L. R. 1932 A case of bone metaplasia in the pulp canal of a tooth. *Dent. Items of Interest*, 54: 518-520.
- Craig, R. G., and F. A. Peyton 1958 The microhardness of enamel and dentin. *J. of Dent. Res.*, 37: 661-668.
- Dudley, H. R., and D. Spiro 1961 The fine structure of bone cells. *J. Biophys. and Biochem. Cytol.*, 11: 627-649.
- Fullmer, H. M., C. C. Link and M. J. Baer 1964 A stain for bone—Illustrating apposition and absorption in two colors. *Stain Tech.*, 39: 71-73.
- Gaskill, H. J. 1894 Report of a case in which dentine of a tooth was absorbed by the pulp. *Dental Cosmos*, 36: 1019-1020.
- Goldhaber, P., and R. J. Barnett 1960 Succinic dehydrogenase in osteoclasts in resorbing-bone tissue cultures. *J. Dent. Res.*, 39: 728.
- Gonzalez, F. and M. J. Karnovsky 1961 Electron microscopy of osteoclasts in healing fractures of rat bone. *J. Biophys. and Biochem. Cytol.*, 9: 299-316.
- Greulich, R. C. 1961 Organic mass distribution in bone matrix undergoing osteoclastic resorption. *Arch Oral Biol.*, 3: 137-142.
- Hancox, N. M., and B. Bothroyd 1963 Structure-function relationship in the osteoclast. In: *Mechanisms of Hard Tissue Destruction*. Ed., R. F. Sognnaes. Am. Assoc. for Adv. of Science, Washington. Chapter 18, 497-514.
- Hemley, S. 1941 The incidence of root resorption of vital permanent teeth. *J. Dent. Res.*, 20: 133-141.
- Henry, J. L., and J. P. Weinmann 1951 The pattern of resorption and repair of human cementum. *J. Am. Dent. Assoc.*, 42: 270-290.
- Ketcham, A. H. 1929 A progress report of an investigation of apical root resorption of vital permanent teeth. *Inter. J. Ortho.*, 15: 310-328.
- Massler, M., and A. J. Malone 1954 Root resorption in human permanent teeth, a roentgenographic study. *Am. J. Ortho.*, 40: 619-633.

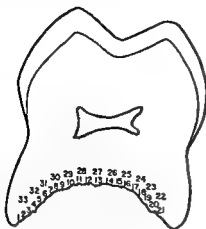
- Miller, W. D. 1890 Action of the products of fermentation of the different structures of the mouth. S. S. White Dental Mfg. Co., Philadelphia. Chapter 6, 123.
- Mummery, J. H. 1920 The pathology of "pink spots" on teeth. *Erit. Dent. J.*, 41: 301-311.
- Oppenheim, A. 1942 Human tissue response to orthodontic intervention of short and long duration. *Am. J. Ortho. and Oral Surg.*, 28: 263-301.
- Orban, B. 1928 Tissue changes in traumatic occlusion. *J. Am. Dent. Assoc.*, 15: 2090-2106.
- 1962 Dentin. In: Orban's Oral Histology and Embryology. Ed., H. Sicher, C. V. Mosby Co., St. Louis. Chapter IV, 120.
- Rabinowitch, B. Z. 1957 Internal resorption. *Oral Surg., Oral Med., Oral Path.*, 10: 193-206.
- Rautiola, C. A., and R. G. Craig 1961 The microhardness of cementum and underlying dentin of normal teeth and teeth exposed to periodontal disease. *J. Perio.*, 32: 113-123.
- Scopp, I. W. 1956 Resorption of dentin and cementum in teeth. *J. Dent. Med.*, 11: 220-224.
- Scott, B. L., and D. C. Pease 1956 Electron microscopy of the epiphyseal apparatus. *Anat. Rec.*, 126: 465-495.
- Sognnaes, R. F. 1959 Microradiographic observations of demineralization gradients in the pathogenesis of hard-tissue destruction. *Arch. Oral Biol.*, 1: 106-121.
- Sognnaes, R. F., J. T. Albright and R. M. Frank 1961 Electron-microscopic surface changes in lacunar resorption. *Inter. Assoc. Dent. Res., Abstracts 39th Gen. Meeting, J. Dent. Res.*, 40: 672.
- Stafne, E. C., and C. H. Slocumb 1944 Idiopathic resorption of teeth. *Am. J. Ortho. and Oral Surg.*, 30: 41-49.
- Thoma, K. H. 1935 Central osteoclastic resorption of dentine and complete repair with osteo-dentine in the permanent tooth of an adult. *Dental Items of Interest*, 57: 23-38.
- Warner, G. R., B. Orban, M. K. Heine and B. T. Ritchey 1947 Internal resorption of teeth: Interpretation of histologic findings. *J. Am. Dent. Assoc.*, 34: 468-483.
- Via, W. F. 1955 Evaluation of deciduous molars treated by pulpotomy and calcium hydroxide. *J. Am. Dent. Assoc.*, 50: 34-43.
- Young, R. W. 1963 Histophysical studies on bone cells and bone resorption. In: *Mechanisms of Hard Tissue Destruction*. Ed. R. F. Sognnaes. Am. Assoc. for Adv. of Science, Washington. Chapter 17, 417-496.

PLATE 1

EXPLANATION OF FIGURES

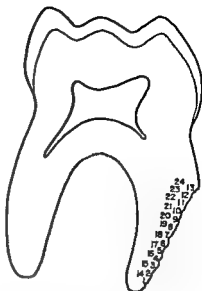
Figures 1 thru 4 are projection diagrams of sections of human teeth to show the location of the microhardness measurements. The area indicated by the lower series of numbers was taken within 10-40 μ from resorption sites as seen in figures 1, 2 and 3 and 10-40 μ from the surface of the normal appearing root in figure 4. The higher series of numbers were taken one-fourth to one-half millimeter from these areas. The figures are expressed as Knoop Hardness Numbers.

- 1 A primary molar undergoing external resorption probably related to the process of eruption of its permanent successor. Orig. Mag. $\times 4$.
- 2 A primary molar tooth undergoing external resorption of the lateral surface of only one root. Orig. Mag. $\times 4$.
- 3 A projection diagram of a human permanent tooth undergoing internal resorption. The superficial zone adjacent to the pulp has smaller Knoop Hardness Number indicating it is not as hard as the deeper dentin seen. Orig. Mag. $\times 4$.
- 4 A projection diagram of a normal appearing human tooth. In this case the peripheral zone of the root dentin immediately underlying the cementum was found to be softer than adjacent deeper root dentin. orig. Mag. $\times 4$.



Knoop Hardness Numbers

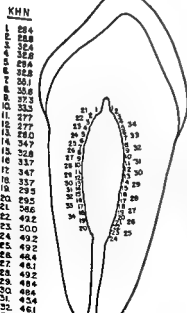
1. 32.8	12. 33.3	23. 56.6
2. 47.6	13. 37.8	24. 56.6
3. 40.7	14. 37.3	25. 55.6
4. 40.1	15. 36.9	26. 56.6
5. 48.9	16. 37.6	27. 56.6
6. 37.3	17. 40.7	28. 61.9
7. 28.0	18. 45.4	29. 69.6
8. 39.5	19. 37.3	30. 68.2
9. 36.9	20. 36.2	31. 69.6
10. 39.5	21. 39.5	32. 69.2
11. 38.3	22. 53.7	33. 69.2



Knoop Hardness Numbers

1. 23.4	9. 24.2	17. 41.9
2. 23.4	10. 24.0	18. 36.2
3. 17.7	11. 24.2	19. 34.7
4. 23.1	12. 17.7	20. 34.2
5. 23.4	13. 22.1	21. 34.7
6. 21.9	14. 50.0	22. 34.2
7. 21.9	15. 36.8	23. 34.2
8. 20.9	16. 41.9	24. 34.7

2



KHN

1. 28.9	12. 36.9
2. 39.5	13. 37.8
3. 36.9	14. 37.3
4. 36.9	15. 37.3
5. 36.3	16. 37.3
6. 39.5	17. 37.3
7. 37.8	18. 37.3
8. 37.3	19. 37.3
9. 37.3	20. 37.3
10. 37.3	21. 37.3
11. 37.3	22. 37.3
12. 36.8	23. 37.3
13. 37.8	24. 37.3
14. 36.3	25. 37.3
15. 37.3	26. 37.3
16. 27.7	27. 37.3
17. 33.7	28. 37.3
18. 32.6	29. 37.3
19. 33.3	30. 37.3
20. 33.3	31. 37.3
21. 35.6	32. 37.3
22. 35.1	33. 37.3
23. 35.6	34. 37.3
24. 36.9	
25. 36.6	
26. 37.6	
27. 37.6	
28. 37.6	
29. 37.6	
30. 37.6	
31. 37.6	
32. 37.6	
33. 37.6	
34. 37.6	

KHN

1. 42.6	12. 36.9
2. 41.9	13. 37.8
3. 35.6	14. 37.3
4. 33.3	15. 37.3
5. 30.3	16. 37.3
6. 33.3	17. 37.3
7. 36.9	18. 37.3
8. 32.8	19. 37.3
9. 33.7	20. 37.3
10. 29.9	21. 37.3
11. 34.2	22. 37.3
12. 29.1	23. 37.3
13. 31.9	24. 37.3
14. 29.8	25. 37.3
15. 36.2	26. 37.3
16. 36.9	27. 37.3
17. 34.2	28. 37.3
18. 35.5	29. 37.3
19. 31.5	30. 37.3
20. 40.7	31. 37.3
21. 40.1	32. 37.3
22. 35.3	33. 37.3
23. 43.3	34. 37.3
24. 44.0	
25. 38.3	
26. 40.1	
27. 39.5	
28. 38.1	

KHN

29. 69.8	40. 56.6
30. 71.0	41. 56.6
31. 68.2	42. 63.1
32. 71.0	43. 46.9
33. 68.2	44. 56.6
34. 69.8	45. 59.7
35. 67.8	46. 65.7
36. 64.8	47. 68.2
37. 65.7	48. 68.9
38. 56.6	49. 61.9
39. 53.6	50. 71.0
40. 56.6	51. 68.2
41. 56.6	52. 69.6
42. 63.1	53. 68.2
43. 46.9	54. 65.7
44. 56.6	55. 68.9
45. 59.7	56. 71.0

4

PLATE 2

EXPLANATION OF FIGURES

- 5-6 Microradiographs of areas of internal resorption of root dentin. These lesions were from areas of very little tissue destruction. It is noted that all of the resorption cavities are of similar size and not very large. The numerous radiolucent resorption cavities appear superimposed in those sections 70-100 μ in thickness. No distinct demineralization gradient appears around the sites. (D), Dentin. Orig. Mag. $\times 450$.
- 7 Microradiograph of an advanced area of internal resorption. In this case much of the root dentin was missing. Larger resorption cavities appear in the remaining dentin than in the cases shown in figures 5 and 6. The radiopacity is generally uniform except in the center of the picture where secondary sites are noted. Orig. Mag. $\times 100$.
- 8 Microradiograph of an area of internal resorption located near the apical foramina. Numerous resorption cavities appear along the walls of this deep defect which may be an accessory root canal. Orig. Mag. $\times 100$.



PLATE 3

EXPLANATION OF FIGURES

- 9 A resorption site which originated along the pulpal aspect of a human tooth. The dentinal tubules are visible as is the ragged edge of the resorption front. No mineralization gradient is seen. An area of bony repair can be seen partially filling a defect, (R), Repair. Orig. Mag. $\times 100$.
- 10 A resorption site located on the external aspect of a tooth. The areas of repair appear extensive. It is probable that this bone or cementum has also undergone some resorption with a cavity resulting in the central area of the secondary deposition. Orig. Mag. $\times 100$.
- 11 A microradiograph of a resorption site originating from the internal aspect of a tooth. The dentin tubules are faintly visible as is an area of radiolucent matrix. This appears as an area of decreased mineral content. Because of its location it is possible that this area represents predentin. Orig. Mag. $\times 540$.
- 12 A diagram of a resorption front in dentin representing an interpretation of the microradiographic data. The relationship of the dentinal tubules and the numerous lacunar sites are shown. Each site is connected with another as well as to the surface of the primary site. As the oval shaped sites are expanded they isolate small islands of dentin which in turn are then finally resorbed.

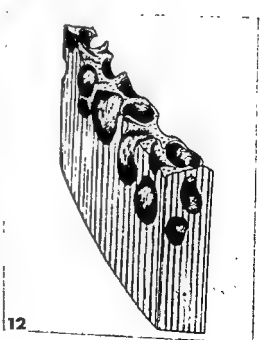


PLATE 4

EXPLANATION OF FIGURES

- 13 Photomicrograph of an initial or early site of internal resorption revealing a loss of some predentin. The odontoblasts have degenerated and the degenerative changes in the pulpal connective tissue can be seen. Some predentin, but not dentin, has already been destroyed. Vascular granulation tissue has invaded this area adjacent to a site of amputation of the pulp with calcium hydroxide. This amputation was done necessarily to remove a necrotic area of the pulp. (P), Predentin, (D), Dentin. Hematoxylin and eosin stain. Orig. Mag. $\times 450$.
- 14 Photomicrograph of an area of internal resorption revealing a dense staining of the matrix immediately adjacent to the resorption front to a depth of several microns. This may be indicative of chemical changes related to the resorption process such as demineralization of the matrix. Mallory's connective tissue stain. Orig. Mag. $\times 450$.
- 15 Photomicrograph of an area of internal resorption showing the dentinal tubules *in cross section* and a remaining spicule of dentin and attached predentin, (P), predentin and (arrows) indicating predentin. The normal architecture of the pulp is lost and some large multinucleated cells appear along the resorption front. Hematoxylin and eosin stain. Orig. Mag. $\times 450$.
- 16 Photomicrograph of an area of active internal resorption. The cross sectioned dentin tubules and the lacunar resorption sites can be seen. Note the cells and fibrous appearing material within the lacunae. Below can be seen a spicule of dentin and adjacent attached predentin, (P), Predentin, and (arrows) indicating predentin. It would appear as if the resorption front is skirting this area. Hematoxylin and eosin stain. Orig. Mag. $\times 450$.

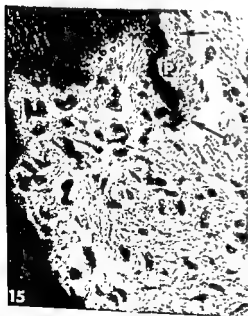
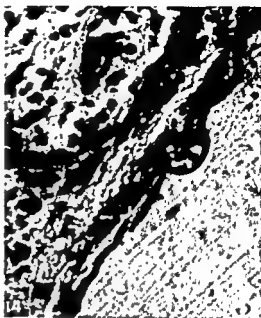


PLATE 4

EXPLANATION OF FIGURES

- 13 Photomicrograph of an initial or early site of internal resorption revealing a loss of some predentin. The odontoblasts have degenerated and the degenerative changes in the pulpal connective tissue can be seen. Some predentin, but not dentin, has already been destroyed. Vascular granulation tissue has invaded this area adjacent to a site of amputation of the pulp with calcium hydroxide. This amputation was done necessarily to remove a necrotic area of the pulp. (P), Predentin, (D), Dentin. Hematoxylin and eosin stain. Orig. Mag. $\times 450$.
- 14 Photomicrograph of an area of internal resorption revealing a dense staining of the matrix immediately adjacent to the resorption front to a depth of several microns. This may be indicative of chemical changes related to the resorption process such as demineralization of the matrix. Mallory's connective tissue stain. Orig. Mag. $\times 450$.
- 15 Photomicrograph of an area of internal resorption showing the dentinal tubules in cross section and a remaining spicule of dentin and attached predentin, (P), predentin and (arrows) indicating predentin. The normal architecture of the pulp is lost and some large multinucleated cells appear along the resorption front. Hematoxylin and eosin stain. Orig. Mag. $\times 450$.
- 16 Photomicrograph of an area of active internal resorption. The cross sectioned dentin tubules and the lacunar resorption sites can be seen. Note the cells and fibrous appearing material within the lacunae. Below can be seen a spicule of dentin and adjacent attached predentin, (P), Predentin, and (arrows) indicating predentin. It would appear as if the resorption front is skirting this area. Hematoxylin and eosin stain. Orig. Mag. $\times 450$.

The Interrelation of the Digestive and Skeletal Systems as Determinants of Tooth Position¹

ALLAN G. BRODIE

Department of Orthodontics, University of Illinois
at the Medical Center, Chicago, Illinois

ABSTRACT In spite of the many differences between teeth and bone in their phylogenetic and embryologic origins, modes of growth, disease and repair processes, the two continue to be equated together in most matters relating to their functioning positions.

On the basis of a variety of studies by others and recent quantitative longitudinal investigations by himself the author seeks to demonstrate that the positions of the teeth are under the control of different body systems, viz., the skeletal and the digestive. The first controls the root apices, the second the crowns.

The numerous and distinct differences between teeth and jaw bones, e.g., their phylogenetic and embryological origins, modes of growth, processes of repair and adjustment, and disease processes have been recognized for many years. However, they continue to be equated together in matters dealing with the positions of the teeth, i.e., with their occlusion or mal-occlusion. The studies herein reported point to the necessity of considering this matter as the resultant of the dual influences of the skeleton and the foregut.

One of these influences is muscular and acts on the crowns of the teeth. It is contributed by the muscle forces of the tongue acting from within the dental arches and those of the lips and cheeks which act from without. These are the contributors of the forces from the digestive system.

The ends of the tooth roots are under the control of the skeletal system, specifically the maxilla and mandible. They move in response to the growth of the jaw. The alveolar process serves to adjust the teeth to the two sets of influences and maintains them in their functional relationships. It is not part of the true skeleton. A brief review of certain evidence seems indicated here to support the above concept.

The enamel epithelium is derived from the epithelium of the stomodeum via the dental lamina and in turn initiates the formation of the dentin and the periodontal membrane. The periodontal membrane is responsible for cementum formation at the proximal and alveolar bone at the dis-

tal ends of its fibers. The alveolar bone becomes attached to the inner surfaces of the bony troughs of the maxillae and mandible which are thereafter indistinguishable. All of these stages have been demonstrated in transplants of the enamel organ placed in various connective tissue beds of the body (Hoffman, '60).

It is only after the teeth have begun their development that the bone destined to become the jaws appears. In the mandible, it is initiated by Meckel's cartilage, well below the forming teeth. From here successive layers of bone are developed and constantly remodeled. These will become the outer and inner walls and lower border of the mandibular body (Bhaskar, '53; fig. 1). A similar enclosing of the tooth germs occurs in the maxillae but its initiation seems to reside in the mesenchyme itself rather than in a transitory cartilage.

The outer and inner walls of the maxillae and mandible grow in height, and their edges approach each other but do not close over the underlying tooth germs. The margins are separated by connective tissue which is covered by the oral epithelium. The teeth, while thus enclosed, are carried passively by the growth of the jaws and thus are completely under the influence of the skeletal system during this period.

The tongue, already large in the embryo, rather completely fills the mouth at

¹This study was supported in part by Research grant D-1468 from the National Institute for Dental Research, U. S. Public Health Service.



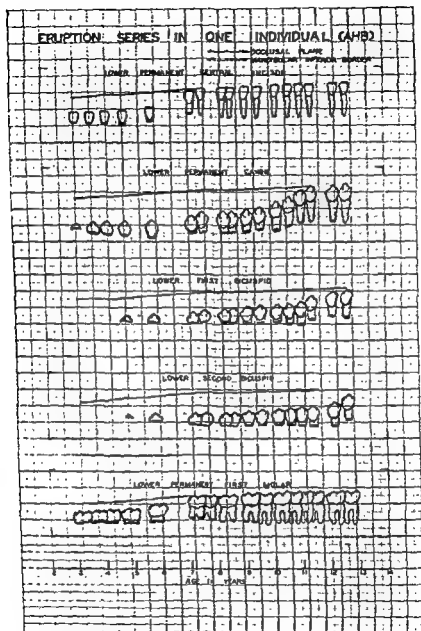


Fig. 2 Tracings of serial cephalometric x-rays of development and eruption of mandibular teeth of one child. (After Carlson.)

from the first to the third permanent molar.

The different influences working at the level of the tooth crowns are reflected in the arrangement of the teeth as these are

seen in the mouth. Anterior to the first permanent molar they follow the curved course of the outer surfaces of the maxillae and mandible, i.e., they stand fairly upright over the bone of the jaws that sup-

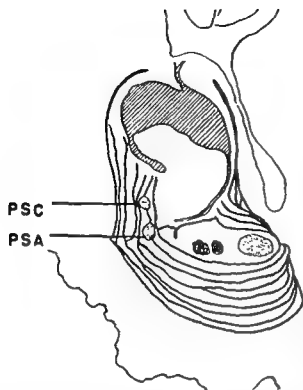


Fig. 1 Camera lucida drawing of frontal section through first molar region of the mandible in an *ia* rat embryo 20 days insemination age. ($\times 25$.) In this mutant strain the deposition of bone appears to be normal but it is not accompanied by remodeling resorption. PSC, perichondral splint, condylar cartilage. PSA, perichondral splint, angular cartilage. (After Bhaskar.)

birth and flows over the free margins of the jaws to contact the inner surface of the cheeks and lips. The erupting teeth separate these two muscle masses for the first time and are guided by them into an arch arrangement that reflects the forces operating between them. Henceforth their crowns will remain largely under this environmental control — that of the digestive system.

When a tooth is studied longitudinally through its periods of growth and eruption it is found that the complete development of the crown is not accompanied by any perceptible change of its position within the mandible (Carlson, '44; fig. 2). With the beginning of root formation it starts its eruptive movement and until it has reached its occlusal position the rate of this movement exceeds that of root formation. Having attained this level, remaining root formation takes place by downward growth into the bone.

Throughout the period of jaw growth the root ends of the teeth maintain constant proportional mediolateral positions within the jaws. In this they follow the behavior of inclusions within all growing bones, e.g., marrow spaces, sinuses, foramina. The outer surfaces of their roots remain close to the surfaces of the bones that contain them. Both the maxillae and the mandible grow in width by surface additions to their buccal surfaces but this does not lead to disproportionate thickness of the bone covering the roots. The alveoli of the teeth move with them by corresponding resorptive and appositional processes of their walls. This has been demonstrated with vital dyes such as madder, alizarin Red 'S' and lead acetate. How closely they follow can be observed in any collection of skulls. Certain of these will reveal the exposed root ends of the maxillary canine and the mesiobuccal root of the first permanent molar.

In the mandible this close relationship of the roots of the molars to the outer table is less apparent because of the external oblique ridge that becomes continuous with the coronoid process. The crowns of the teeth add to the illusion, being placed well medially to the ramus. Posteroanterior x-rays of the mandible reveal that each of the permanent molars form laterally to the dental arch and are inclined medially at an angle so that their occlusal surfaces face medially, forward and upward.

Dempster et al. ('63; fig. 3) demonstrated the close relation that always seems to exist between the roots of the teeth and the outer surfaces of the maxillae and mandible. They drilled holes through the long axes of the teeth and extended the holes through to outside surfaces. They placed stiff wires in the holes and found that the upper wires were disposed in an arch arrangement similar to that formed by the crowns of the teeth. This was true also of the lower wires which passed through the succedaneous teeth. Beginning with the permanent molars the wires revealed increasing lateral deviation of their roots, i.e., they followed the divergence of the lower border of the mandible. The crowns, on the other hand, were inclined increasingly toward the lingual

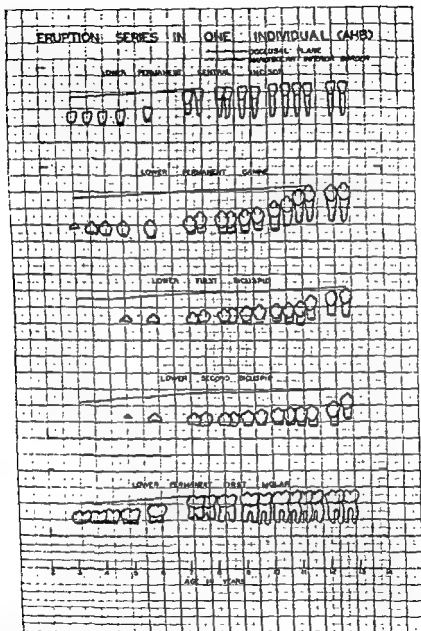


Fig. 2 Tracings of serial cephalometric x-rays of development and eruption of mandibular teeth of one child. (After Carlson.)

from the first to the third permanent molar.

The different influences working at the level of the tooth crowns are reflected in the arrangement of the teeth as these are

seen in the mouth. Anterior to the first permanent molar they follow the curved course of the outer surfaces of the maxillae and mandible, i.e., they stand fairly upright over the bone of the jaws that sup-

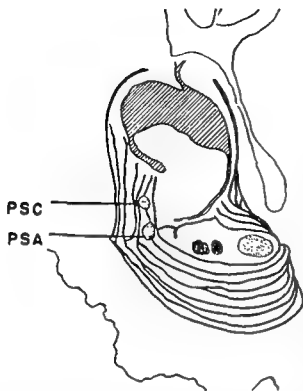


Fig. 1 Camera lucida drawing of frontal section through first molar region of the mandible in an *Ia* rat embryo 20 days in gestation age. ($\times 25$.) In this mutant strain the deposition of bone appears to be normal but it is not accompanied by remodeling resorption. PSC, perichondral splint, condylar cartilage. PSA, perichondral splint, angular cartilage. (After Bhaskar.)

birth and flows over the free margins of the jaws to contact the inner surface of the cheeks and lips. The erupting teeth separate these two muscle masses for the first time and are guided by them into an arch arrangement that reflects the forces operating between them. Henceforth their crowns will remain largely under this environmental control — that of the digestive system.

When a tooth is studied longitudinally through its periods of growth and eruption it is found that the complete development of the crown is not accompanied by any perceptible change of its position within the mandible (Carlson, '44; fig. 2). With the beginning of root formation it starts its eruptive movement and until it has reached its occlusal position the rate of this movement exceeds that of root formation. Having attained this level, remaining root formation takes place by downward growth into the bone.

Throughout the period of jaw growth the root ends of the teeth maintain constant proportional mediolateral positions within the jaws. In this they follow the behavior of inclusions within all growing bones, e.g., marrow spaces, sinuses, foramina. The outer surfaces of their roots remain close to the surfaces of the bones that contain them. Both the maxillae and the mandible grow in width by surface additions to their buccal surfaces but this does not lead to disproportionate thickness of the bone covering the roots. The alveoli of the teeth move with them by corresponding resorptive and appositional processes of their walls. This has been demonstrated with vital dyes such as madder, alizarin Red 'S' and lead acetate. How closely they follow can be observed in any collection of skulls. Certain of these will reveal the exposed root ends of the maxillary canine and the mesiobuccal root of the first permanent molar.

In the mandible this close relationship of the roots of the molars to the outer table is less apparent because of the external oblique ridge that becomes continuous with the coronoid process. The crowns of the teeth add to the illusion, being placed well medially to the ramus. Posteroanterior x-rays of the mandible reveal that each of the permanent molars form laterally to the dental arch and are inclined medially at an angle so that their occlusal surfaces face medially, forward and upward.

Dempster et al. ('63; fig. 3) demonstrated the close relation that always seems to exist between the roots of the teeth and the outer surfaces of the maxillae and mandible. They drilled holes through the long axes of the teeth and extended the holes through to outside surfaces. They placed stiff wires in the holes and found that the upper wires were disposed in an arch arrangement similar to that formed by the crowns of the teeth. This was true also of the lower wires which passed through the succedaneous teeth. Beginning with the permanent molars the wires revealed increasing lateral deviation of their roots, i.e., they followed the divergence of the lower border of the mandible. The crowns, on the other hand, were inclined increasingly toward the lingual

scribed. Thus they would accompany the growth of the jaws and would not be disturbed by the loss of the alveolar process.

There are no landmarks which denote any junction of the alveolar processes and the skeletal bone of the jaws, but Axel Lundstrom ('25) declared that there were zones at the level of the tooth apices that could not be modified by movement of the teeth. He called these zones the "apical bases" of the jaws. Tentative acceptance of Lundstrom's postulate and the constant relation of the root ends of the teeth to the outer surfaces of the jaws suggested the possibility of measuring the areas enclosed by the peripheries of the maxillary apical base and dental arch (Richardson and Brodie, '64). Applying the method to the

longitudinal records of growing children (Brodie, '65) demonstrated striking differences between the size, form and growth of the dental arch at the level of the tooth crowns and that at the level of their root ends. The apical base was shown to increase in the same manner as that of other skeletal parts to 18 years, the age limit of the study, while the curve of the dental arch flattened abruptly between the twelfth and the thirteenth years. Records of a sample of older individuals revealed increases of the apical base for a number of years beyond 18. This seems to explain why it has never been possible to find correlations between the dental arches and dimensions of the facial skeleton (Meredith and Higley, '51).

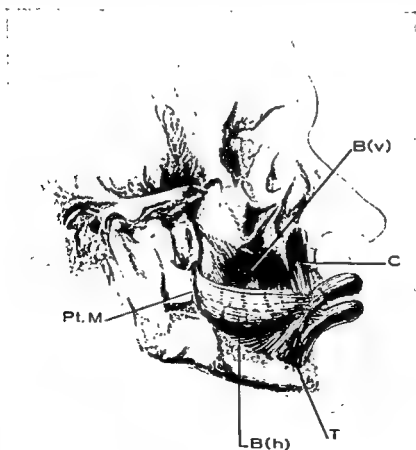


Fig. 4 Buccinator muscle as revealed by dissection of 200 cadavers. B(v), vertical fibers; B(h), horizontal portion; Pt.M., pterygomandibular raphe; C, m. caninus; T, m. triangularis.

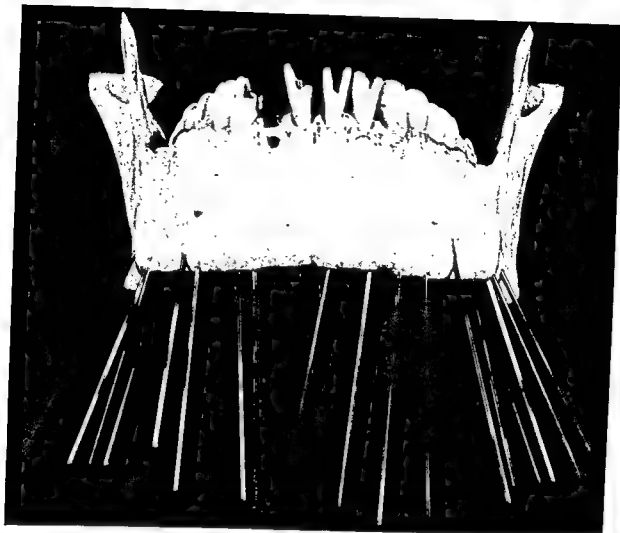


Fig. 3 Anterior view of mandible with wires indicating axial positions of lower teeth, as demonstrated by Dempster et al. (Courtesy, Dept. of Anatomy, Univ. of Michigan.)

ports them. This relation prevails as well in the maxillary molar series. In the mandible the relation of the molars changes. The crowns follow the same course as the upper teeth while their roots follow the lateral divergence of the body of the mandible as it runs to the ramus. The reason for these differences appears to lie in the muscular environment of the teeth at the level of the crowns.

The principal muscle involved is the Buccinator, which has recently been shown to be more complex than it has been pictured in anatomy texts (Howland and Brodie, '66; fig. 4). It consists of a central portion whose fibers run in a horizontal direction at the level of the crowns of the teeth. In back, it crosses unattached from the buccal to the lingual sides of the mandible to be attached to the pterygo-

mandibular raphe, which structure also serves as the anterior attachment of the constrictor pharyngis superior, making the mouth and pharynx continuous.

The horizontal portion of the buccinator is firmly attached below to the external oblique ridge which it leaves as it crosses the mandibular body. Above, it is suspended from the surface of the maxilla by a thin sheet of fibers which are attached slightly above the level of the root ends of the teeth. Anteriorly, at the canine-first premolar region, these fibers run almost vertically but become increasingly oblique as they approach and pass around the back of the maxilla to take attachment on its infratemporal surface. From this it can be realized that all of the attachments of this muscle are to the skeletal bone of the jaws, not to the alveolar process, as usually de-

ing jaws gradually provide more room for the aligning of the teeth.

Quantitative data are lacking on muscular influences that seem to be of significance in the positioning of the teeth, viz., the tongue and circumoral muscles. Although there is ample clinical and investigative evidence that these muscles exert profound influences on tooth position there is no available information on such matters as timing and rate of growth, associated states of tensions, etc. It would be reasonable to expect that variables with considerable ranges would be found in these areas as well as in those already considered and that the end result would depend on how the three sets of variables were integrated in the individual.

LITERATURE CITED

- Abelson, S. M., A. G. Brodie, J. P. Bronstein and S. L. Schreiber 1941 Muscular macroglossia: Five year observation with cephalometric and speech studies in a case of spontaneous resolution. *Am. J. Dis. Child.*, 62: 624-628.
- Bhaskar, S. N. 1953 Growth pattern of the rat mandible from 13 days insemination to 30 days after birth. *Am. J. Anat.*, 92: 1-53.
- Brodie, A. G. 1953 Late growth changes in the human face. *Angle Orthod.*, 23: 146-157.
- 1965 Muscles, growth and the apical base. *Dent. Practitioner*, 15: 343-357.
- Carlson, H. 1944 Studies on the rate and amount of eruption of certain human teeth. *Am. J. Orthod. and Oral Surg.*, 30: 575-588.
- Dempster, W. T., W. J. Adams and A. A. Duddles 1963 Arrangement in the jaws of the roots of teeth. *J. Am. Dent. Assoc.*, 67: 779-797.
- Enlow, D. E. 1963 *Principles of Bone Remodeling*. Charles C Thomas, Springfield, Ill.
- Hoffman, R. L. 1960 Formation of periodontal tissues around subcutaneously transplanted teeth. *J. Dent. Res.*, 39: 781-798.
- Howland, J. P., and A. G. Brodie 1968 Pressures exerted by the buccinator muscle. *Angle Orthod.*, 36: 1-12.
- Lundstrom, Axel F. 1925 Malocclusion of the teeth regarded as a problem in connection with the apical base. *Internat. J. Orthod.*, 11: 591-609; 724-731; 793-812; 933-941; 1022-1042 and 1109-1131.
- Meredith, H. V., and L. B. Higley 1951 Relationships between dental arch widths and widths of the face and head. *Am. J. Orthod.*, 27: 193-204.
- Richardson, E. R., and A. G. Brodie 1964 Longitudinal study of growth of maxillary width. *Angle Orthod.*, 34: 1-15.
- Subtelny, J. S., and A. G. Brodie 1954 An analysis of orthodontic expansion in unilateral cleft lip and cleft palate patients. *Am. J. Orthod.*, 40: 686-697.

There is a great deal of additional evidence, both clinical and investigative, to support the concept that the positions of the teeth are determined to a large extent by muscular forces acting at the level of the crowns and skeletal factors working at the level of the root ends. Following surgical repair of the lip alone in cleft lip and palate anomalies, there is a rapid decrease in the dimensions of the dental arch (Subtelny and Brodie, '54); microglossia has been shown to be accompanied by diminutive dental arches while macroglossia is characterized by outward tipping and spacing of the teeth. Remission of the macroglossia is followed by closing of spaces and recovery of axial inclinations (Alelson et al., '40; Brodie, '54).

Longitudinal x-ray series of growing individuals from 9 to 17 years (Brodie, '53; fig. 5) revealed that during puberty the dental arches began to fall behind the skeletal parts of the face as the face develops. This resulted in the incisors becoming more upright and the mouth less prominent as age advanced. It is a matter of common observation that this change continues into senility. Even in those individuals who retain all of their teeth the dental arches are shortened by their interproximal wear and adjustment to this wear takes place in a posterior direction.

The restraining force of the lips and cheeks is exercised principally through the buccinator muscle, which, if considered as a forward extension of the pharyngis constrictor superior, is ultimately attached behind to the pharyngeal tubercle of the

occipital bone and the prevertebral fascia of the upper cervical region. This restraining force acts on the crowns of the teeth and the dental arches which they form. The root ends follow the forward and lateral growth of the jaw bones proper.

DISCUSSION

If it be granted that the positions of the teeth are under the influences of two distinctly different body systems the reasons for the prevalence of malocclusion in the population becomes more readily comprehensible. It appears to be a matter of how the variables of the two systems, as well as those of the teeth themselves, are integrated in the individual.

A great amount of research germane to the present discussion has been done on the teeth and on the skeletal systems but very little that is equally applicable has been conducted on the musculature of the foregut (pharyngeal derivatives).

Studies on the teeth have revealed large ranges in the timing and order of their eruption. Although those of the primary set have been shown to have sufficient room in most infants for their accommodation, even if they all erupted simultaneously, the six anterior teeth of the permanent set are one-third wider than their predecessors. Furthermore, their crowns have attained their full size deep in the jaws, long before they erupt. To be accommodated within the young child's jaw at this stage they are crowded and jumbled. The order and time of their eruption in relation to the level of development of the jaws are decisive factors in determining whether they will be normally arranged, crowded or spaced.

The growth of the jaws, while usually an even and orderly process, exhibits variables of time and rate in attaining its potential among individuals. Within the individual, growth is a continuous variable. Eruption, on the other hand, is a discontinuous variable because a whole tooth must be accommodated at one time. Thus it can be realized that unless the variables of tooth eruption and jaw growth are harmoniously integrated there will be derangement of the teeth of one sort or another. Such disharmonies have been shown to be transitory in many cases as the grow-

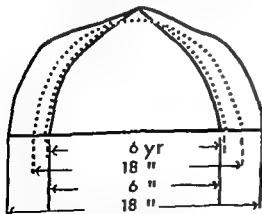


Fig. 5 Growth increases in areas of dental arch, dotted line, and apical base, solid line, in a single individual from 6 to 18 years.

Differences and Relationships Between the Physical Properties and the Microscopic Structure of Human Femoral, Tibial and Fibular Cortical Bone¹

F. GAYNOR EVANS AND SEONG BANG
The University of Michigan, Ann Arbor, Michigan

ABSTRACT Coefficients of correlation between certain physical properties and the histological components of the break area were calculated on an IBM 7090 computer for 56 femoral, 79 tibial and 37 fibular specimens of embalmed cortical bone of standardized size and shape. Strong positive correlations (0.01–0.02 significance level) were found between tensile strength and the percentage of interstitial lamellae in the break area; between hardness and the number of osteons/mm²; and between hardness and the percentage of osteons in the break area. Equally high negative correlations were found between tensile strength and percentage of osteons in the break area; between shearing strength and average area/osteon remnant; between elastic modulus and percentage of spaces in the break area; and an even higher correlation (0.001) between hardness and percentage of spaces in the break area. Negative correlations (at slightly more than 0.05 significance level) were found between shearing strength and modulus and average area/osteon. Osteons tend to reduce the tensile strength and elastic modulus of bone while interstitial lamellae tend to increase them. The probable reason is the relatively greater amount of cement lines, which are sites of weakness where failure can occur, in Haversian bone as compared with lamellar bone. The predominant orientation of collagen fibers and the amount and distribution of calcium may also be involved. These factors are now being investigated.

The present paper is a supplement to our previous one ('66) on the relations between statistically significant differences in the physical properties and microscopic structure of adult human femoral and fibular cortical bone. The physical properties investigated (ultimate tensile strength, single shearing strength, tensile strain, tangent modulus of elasticity, hardness, density, and the ratio of single shearing strength to ultimate tensile strength) and their relation to osteons, remnants or fragments of osteons, interstitial lamellae, and spaces are the same as in our previous investigation.

Our studies relate more physical properties of bone to its microscopic structure than do the investigations of Maj and Toajari ('37), Olivo, Maj and Toajari ('37), Olivo ('37), Maj ('38), Toajari ('38, '39), Evans ('57, '58), Currey ('59, '62, '64), Dempster and Coleman ('61), and Heft et al. ('65). The majority of these investigations were on the relation of tensile strength and/or modulus of elasticity of

bone to the osteons or collagen fiber distribution although Currey ('64) discussed the possible relation of bone strength to the spatite crystals while Heft et al. ('65) investigated the relation of compressive strength, impact bending strength and microhardness to primary and Haversian bone. Nonhuman bone was usually used in these studies but none of them related statistically significant differences in the physical properties of the bone to its microscopic structure.

MATERIALS AND METHODS

The physical properties investigated in the present study were determined for 405 femoral, 193 tibial and 37 fibular specimens of cortical bone which were machined to a standardized size and shape from the proximal, the middle and the distal thirds of the shaft of the respective bones. The specimens were obtained from

¹ This research was supported (in part) by Research grant AM-03865-07 from the National Institutes of Health, U.S. Public Health Service.

Differences and Relationships Between the Physical Properties and the Microscopic Structure of Human Femoral, Tibial and Fibular Cortical Bone¹

F. GAYNOR EVANS AND SEONG BANG
The University of Michigan, Ann Arbor, Michigan

ABSTRACT Coefficients of correlation between certain physical properties and the histological components of the break area were calculated on an IBM 7090 computer for 56 femoral, 79 tibial and 37 fibular specimens of embalmed cortical bone of standardized size and shape. Strong positive correlations (0.01-0.02 significance level) were found between tensile strength and the percentage of interstitial lamellae in the break area; between hardness and the number of osteons/mm²; and between hardness and the percentage of osteons in the break area. Equally high negative correlations were found between tensile strength and percentage of osteons in the break area; between shearing strength and average area/osteon remnant; between elastic modulus and percentage of spaces in the break area; and an even higher correlation (0.001) between hardness and percentage of spaces in the break area. Negative correlations (at slightly more than 0.05 significance level) were found between shearing strength and modulus and average area/osteon. Osteons tend to reduce the tensile strength and elastic modulus of bone while interstitial lamellae tend to increase them. The probable reason is the relatively greater amount of cement lines, which are sites of weakness where failure can occur, in Haversian bone as compared with lamellar bone. The predominant orientation of collagen fibers and the amount and distribution of calcium may also be involved. These factors are now being investigated.

The present paper is a supplement to our previous one ('66) on the relations between statistically significant differences in the physical properties and microscopic structure of adult human femoral and fibular cortical bone. The physical properties investigated (ultimate tensile strength, single shearing strength, tensile strain, tangent modulus of elasticity, hardness, density, and the ratio of single shearing strength to ultimate tensile strength) and their relation to osteons, remnants or fragments of osteons, interstitial lamellae, and spaces are the same as in our previous investigation.

Our studies relate more physical properties of bone to its microscopic structure than do the investigations of Maj and Toajari ('37), Olivo, Maj and Toajari ('37), Olivo ('37), Maj ('38), Toajari ('38, '39), Evans ('57, '58), Currey ('59, '62, '64), Dempster and Coleman ('61), and Heft et al. ('65). The majority of these investigations were on the relation of tensile strength and/or modulus of elasticity of

bone to the osteons or collagen fiber distribution although Currey ('64) discussed the possible relation of bone strength to the apatite crystals while Heft et al. ('65) investigated the relation of compressive strength, impact bending strength and microhardness to primary and Haversian bone. Nonhuman bone was usually used in these studies but none of them related statistically significant differences in the physical properties of the bone to its microscopic structure.

MATERIALS AND METHODS

The physical properties investigated in the present study were determined for 405 femoral, 193 tibial and 37 fibular specimens of cortical bone which were machined to a standardized size and shape from the proximal, the middle and the distal thirds of the shaft of the respective bones. The specimens were obtained from

¹ This research was supported (in part) by Research grant AM-03865-07 from the National Institutes of Health, U.S. Public Health Service.

The physical property and histological data were subjected to an analysis of variance on an IBM 7090 computer in The University of Michigan Computing Center to determine if the differences between the means for the various physical properties and histological elements were statistically significant. Coefficients of correlation between the physical properties and histological elements were also computed. Since 5% variation is generally assumed to be normal in biological material, only differences with a significance level greater than 0.05 were considered.

RESULTS

Average values for the various physical properties of the femoral, the tibial and the fibular specimens (figs. 1, 2) showed that the tibial specimens had the greatest ultimate tensile and single shearing strength and were the densest. The fibular specimens were the stiffest (highest modulus of elasticity) and had the greatest tensile strain (1% elongation). The femoral specimens were the hardest, the weakest

(tensile and shearing strength), the least stiff and had the least tensile strain. The fibular specimens were the softest and the least dense.

An analysis of variance of these data revealed differences, at the 1% or better significance level, between the physical properties of the different specimens. Comparison of the femoral and the tibial specimens showed that the latter were significantly stronger (ultimate tensile and shearing strength), stiffer (modulus of elasticity), denser and exhibited greater tensile strain than did the femoral specimens. The fibular specimens also had a significantly greater ultimate tensile strength and a higher modulus of elasticity than the femoral specimens. The tibial specimens were significantly denser than the fibular ones.

The single shearing strength of the fibular specimens was greater than that of the femoral ones but the latter were denser than the former at the 5% significance level. There were no significant differ-

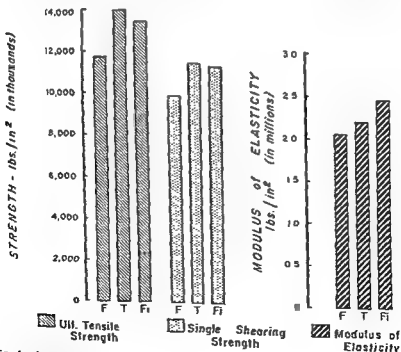


Fig. 1 Average values for tensile and shearing strength and modulus of elasticity of human bone. The number of specimens is indicated above the bars.

the embalmed bodies of 11 white males, one Negro male and four white females ranging from 33 to 98 years of age. None of the individuals had died from primary bone diseases (table 1) and all the bones appeared to be normal. The older individuals, especially the women, very probably had senile osteoporosis although this was not confirmed by x-ray examination. Embalmed material was used because the only unembalmed femoral material was from above-knee amputations in which only the distal third of the femur was present. Wet specimens were used for all determinations of physical properties except density.

The methods for determining the physical properties of the specimens were the same as those employed by Evans and Lebow ('51, '52). Some comments on the determination of hardness and density may be helpful because the hardness of bone has not been investigated much in the past and the method of determining density was especially developed by Evans, Coolbaugh and Lebow ('51) for their studies on bone.

The hardness of the specimens was determined with a Rockwell superficial hardness tester (see Cowdrey and Adams, '44, for details) which measures the resistance of a material to penetration by a hardened steel ball or by a diamond cone. Two scales of values, B for ball and C for cone, are available for use. The B scale was used in the present studies in which a steel ball, one-eighth inch in diameter, was loaded with 45 kg for ten seconds. The

value for hardness was obtained from the average of four tests, two on each side of the specimen. With the Rockwell method any penetration less than a certain depth gave a negative (-) value for the hardness of the material being tested. This explains the presence of negative hardness values for some of the specimens.

The density determinations were made on air dried specimens to prevent moisture from being entrapped within the spaces of the specimens. Corrections were not made for air in the spaces because they would not cause any significant differences in the results. Strontium 90 was used in the density determinations, the density of the specimen being based upon the percentage of transmission of beta rays through the specimen in a given amount of time (see Evans, Coolbaugh and Lebow, loc. cit., for details).

Transverse sections, taken as near the fracture site as possible, of randomly selected specimens were analyzed with respect to the percentage of spaces, osteons, remnants or fragments of osteons and interstitial lamellae in the sections. Photographs of the sections were taken under ordinary light with a Zeiss photomicroscope and prints, enlarged to a standardized size, were made on photographic paper of a constant known weight. The enlarged prints were then analyzed with respect to the above mentioned histological elements by the photomicrograph-weight method used by Evans ('58) and Evans and Bang ('66).

TABLE 1

Cadaver no.	Age	Sex	Race	Cause of death
1342	33	Female	White	Severe uterine hemorrhage
657	64	Male	White	Myocardial infarct
987	70	Male	White	Pulmonary tuberculosis
1112	63	Male	White	Pneumonia
1081	65	Male	White	Cerebral hemorrhage
804	50	Male	White	Infectious hepatitis
1070	47	Male	White	Pul. Tb.
1087	78	Male	White	Coronary occlusion
213	81	Male	White	Arteriosclerotic heart disease
1434	69	Female	White	Cerebral vascular hemorrhage
1121	36	Male	White	Pul. Tb.
1143	47	Male	White	Bronchiogenic carcinoma
1240	66	Male	White	Myocardial infarct
1128	72	Male	Negro	Pul. Tb.
1742	90	Female	White	Arteriosclerotic heart disease
1552	98	Female	White	Acute myocardial infarct

The physical property and histological data were subjected to an analysis of variance on an IBM 7090 computer in The University of Michigan Computing Center to determine if the differences between the means for the various physical properties and histological elements were statistically significant. Coefficients of correlation between the physical properties and histological elements were also computed. Since 5% variation is generally assumed to be normal in biological material, only differences with a significance level greater than 0.05 were considered.

RESULTS

Average values for the various physical properties of the femoral, the tibial and the fibular specimens (figs. 1, 2) showed that the tibial specimens had the greatest ultimate tensile and single shearing strength and were the densest. The fibular specimens were the stiffest (highest modulus of elasticity) and had the greatest tensile strain (1% elongation). The femoral specimens were the hardest, the weakest

(tensile and shearing strength), the least stiff and had the least tensile strain. The fibular specimens were the softest and the least dense.

An analysis of variance of these data revealed differences, at the 1% or better significance level, between the physical properties of the different specimens. Comparison of the femoral and the tibial specimens showed that the latter were significantly stronger (ultimate tensile and shearing strength), stiffer (modulus of elasticity), denser and exhibited greater tensile strain than did the femoral specimens. The fibular specimens also had a significantly greater ultimate tensile strength and a higher modulus of elasticity than the femoral specimens. The tibial specimens were significantly denser than the fibular ones.

The single shearing strength of the fibular specimens was greater than that of the femoral ones but the latter were denser than the former at the 5% significance level. There were no significant differ-

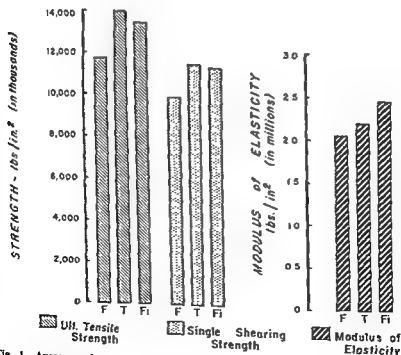


Fig. 1 Average values for tensile and shearing strength and modulus of elasticity of human bone. The number of specimens is indicated above the bars.

ences in the hardness of the various specimens.

The results of the histological analysis of the corrected break area of the specimens, in terms of the percentage of the

area formed by the various histological components of the sections, are presented diagrammatically in figure 3. The corrected break area is obtained by subtracting the area of spaces (Haversian canals, resorp-

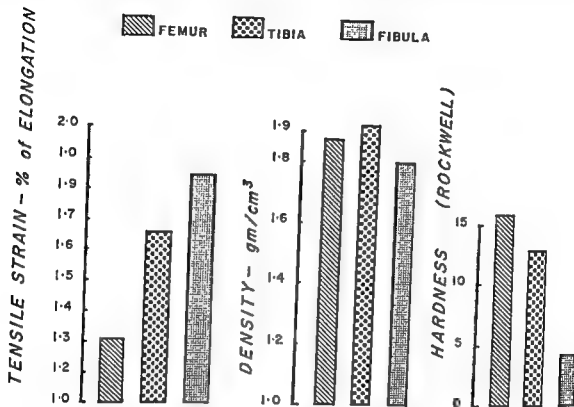


Fig. 2 Average values for tensile strain (% elongation), density and hardness of human bone.

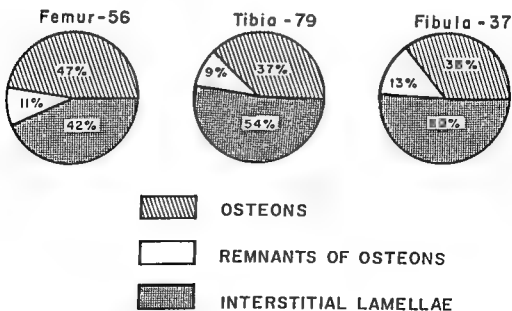


Fig. 3 Percentage of corrected break area formed by various histological components of bone. See text for definition of corrected break area.

tion spaces, etc.) from the original break area of the specimen as measured with calipers at the time of the test. The corrected break area was always smaller than the original break area because the caliper measurements of the break area did not allow for irregularities in the margins of the section nor for spaces within the section.

Comparison of the histological components of the corrected break area of the femoral, the tibial and the fibular specimens showed that the percentage of the area formed by osteons was the greatest in the femoral sections and the least in the fibular ones. The fibular sections had the highest percentage of the area formed by remnants of the osteons; the tibial sections the lowest percentage. The proportion of interstitial lamellae was greatest in the tibial sections and least in the femoral ones.

The sections from the three bones also exhibited differences in the average number of osteons and osteon remnants per square millimeter (fig. 4) and in the aver-

age area (square micra) per osteon and per osteon remnant (fig. 5). The femoral sections had the largest number of osteons/mm² while the fibular sections had the fewest. The largest number of osteon fragments/mm² was found in the tibial sections and the lowest in the femoral sections. The fibular sections had the largest osteons and osteon fragments; the tibial sections the smallest ones.

An analysis of variance between the histological components of the femoral and tibial sections revealed the following differences at the 1% or better significance level. The femoral sections had larger osteons and remnants of osteons (area in square micra) than did the tibial sections and they formed a larger percentage of the corrected break area. The percentage of the original break area formed by spaces and of the corrected break area formed by interstitial lamellae was significantly greater in the tibial sections than in the femoral ones.

Similar comparison of the femoral and fibular sections showed that the femoral

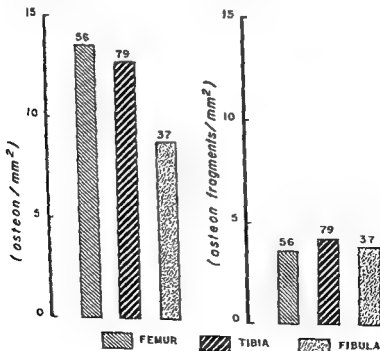


Fig. 4 Average number of osteons and their fragments per mm² of human bone.

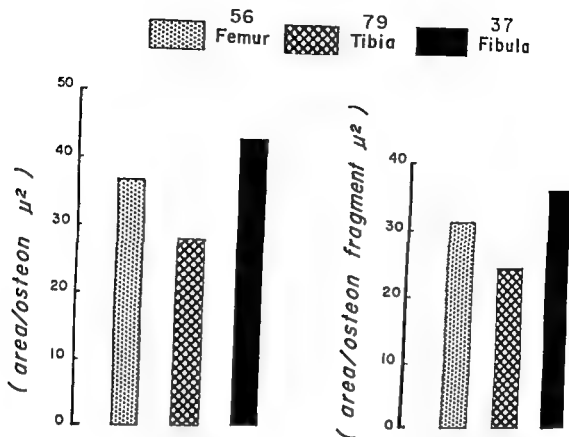


Fig. 5. Average area (μ^2) per osteon and per osteon fragment in human bone.

sections had significantly more osteons/mm² and a significantly greater percentage of the corrected break area formed by osteons than did the fibular sections. The latter had a significantly greater percentage of the corrected break area formed by interstitial lamellae.

An analysis of the tibial and the fibular sections revealed that the tibial sections had significantly more osteons/mm² and a greater percentage of the corrected break area formed by interstitial lamellae than did the fibular sections. However, the fibular sections had significantly larger osteons and osteon remnants (area in square micra) than did the tibial sections.

DISCUSSION

The finding of some highly significant differences between certain physical properties and histological components of human cortical bone raises the question as to whether or not differences in the physical properties of bone show a significant correlation with its histological components. In order to answer this question

coefficients of correlation between the physical properties and histological components of more than 100 transverse sections of standardized specimens of human femoral, tibial and fibular bone were calculated on an IBM 7090 computer in The University of Michigan Computing Center.

The results of this analysis (table 2) reveal a high positive correlation between ultimate tensile strength (UTS) and the percentage of the corrected break area (CBA — see text for definition) formed by interstitial lamellae; between hardness and the number of osteons/mm²; and between hardness and the percentage of the corrected break area formed by osteons.

High negative correlations are found between ultimate tensile strength and the percentage of the corrected break area formed by osteons; between the modulus of elasticity (E) and the average area/osteon; between the modulus of elasticity and the percentage of the original break area (OBA — see text for definition) formed by spaces; between single shearing (punching) strength (SSS) and the average area/

TABLE 2

Correlation between physical properties and histological elements of embalmed human cortical bone (femur, tibia and fibula)

Variables	Adjusted number	Correlation coefficient (R)	T-test (T)	Significance level
E vs avg area/osteon	115	-0.195	-2.109	> 0.05
E vs % OBA-spaces	115	-0.242	-2.648	> 0.01
UTS vs % CBA-osteons	119	-0.236	-2.628	> 0.01
UTS vs % CBA-interop. lamellae	119	0.233	2.592	> 0.02
SSS vs avg area/osteon	118	-0.188	-2.060	> 0.05
SSS vs avg area/osteon remnant	118	-0.230	-2.541	> 0.02
Hardness vs no. osteon/mm ²	113	0.259	2.827	> 0.01
Hardness vs % CBA-osteons	113	0.246	2.675	> 0.01
Hardness vs % OBA-spaces	113	-0.367	-4.158	> 0.001

E, Tangent modulus of elasticity.

OBA, Original break area.

UTS, Ultimate tensile strength (stress).

CBA, Corrected break area.

SSS, Single shearing strength (stress).

No. Number of specimens.

osteon; between single shearing strength and the average area/osteon fragment; and between hardness and the percentage of the original break area formed by spaces.

The high positive correlation between ultimate tensile strength and the percentage of the corrected break area formed by interstitial lamellae and the slightly higher negative correlation between the same physical property and the percentage of the corrected break area formed by osteons suggest that interstitial lamellae tend to increase the tensile strength of cortical bone while osteons tend to reduce it. These correlations explain, in part, the significantly greater ultimate tensile strength of the tibial and the fibular specimens in comparison with that of the femoral ones because the two former kinds of specimens had a significantly greater proportion of their corrected break area formed by interstitial lamellae while the femoral specimens had a significantly greater proportion of osteons (fig. 3).

The probable reason, as we pointed out previously (Evans and Bang, '66), that an abundance of osteons and their remnants (fragments) tends to reduce the tensile strength of cortical bone is that Haversian bone, i.e., bone consisting mainly of Haversian systems (osteons) and their remnants, has a proportionately greater amount of cementing substance than does lamellar bone. Each osteon and osteon remnant is surrounded by a well

defined cement line; therefore, the more osteons and their remnants in a given area of bone the more cement lines or cementing substance. The cement lines are not crossed by collagen fibers and represent the weakest material in bone as evidenced by the fact that fractures tend to follow the cement lines rather than to cross osteons or interstitial lamellae (Maj and Toajari, '37; Dempster and Coleman, '61; Evans and Bang, '66). Consequently, femoral bone, since it has proportionately more osteons (fig. 3) in the corrected break area as well as more osteons/mm² (fig. 4) than does tibial or fibular bone, has proportionately more cement lines at which failure can occur.

The greater number of osteons/mm² in femoral bone as compared with tibial and fibular bone (fig. 4) tend to reduce its strength for another reason. Any holes in a material tend to weaken it because each hole acts as a stress raiser, i.e., an area of higher stress concentration, where failure of the material is apt to be initiated. The Haversian canals and lacunae, as noted by Currey ('62), act as stress raisers in bone; therefore, the more osteons in a given area of bone, the more stress raisers or areas of higher stress concentration where failure can start. However, as also pointed out by Currey, the Haversian canals and the lacunae tend to limit the propagation of a microfracture because the fracture is stopped whenever it comes to a hole in the bone.

The significantly greater single shearing strength of the tibial and the fibular specimens in comparison with the femoral ones is probably related to the fact that they have fewer osteons/mm² than the femoral specimens (fig. 4). Consequently, the tibial and fibular specimens have fewer cement lines where shearing can occur. The negative correlation (table 2) between single shearing strength and the average area per osteon and per osteon remnant may also be a contributing factor although the correlation between shearing strength and average area/osteon was only a little better than the 0.05 significance level.

The greater size (area) of the fibular osteons in comparison with the femoral ones (fig. 5) may be a contributing factor to the significantly greater modulus of elasticity of the fibular specimens because a weak negative correlation (table 2) was found between modulus and average area/osteon. A more important factor, as previously suggested by Evans ('58) from polarized light studies, is the orientation of the collagen fibers which in the fibular specimens is predominantly parallel to the long axis of the specimen while in the femoral specimens the collagen fibers are more obliquely oriented. Therefore, the collagen fibers of the fibular specimens are in a better position to resist tensile forces than are those of the femoral specimens. Evans' suggestion has recently been confirmed by Ascenzi and Bonucci ('64) and by Ascenzi, Bonucci, and Checcucci ('66) who have shown that the tensile strength and modulus of elasticity are higher in osteons with collagen fibers nearly parallel to the long axis of the osteon. A more detailed investigation, by means of polarized light, of the relation between the physical properties and collagen fiber orientation of femoral, tibial and fibular cortical bone is now in progress in our laboratory.

The strong positive correlation between hardness and the number of osteons/mm² as well as the percentage of the corrected break area formed by osteons (table 2) aids in explaining the differences in the hardness of the specimens. Thus, the femoral specimens, which were the hardest (fig. 2), had the most osteons/mm² as well as the greatest percentage of the corrected break area formed by osteons (fig.

3) while the fibular specimens, which were the softest, had the fewest osteons/mm² and the lowest percentage of the corrected break area formed by osteons. However, as previously mentioned, none of the differences between the hardness of the various types of specimens was at the 0.05 or better significance level. The amount and distribution of calcium in the specimens, in addition to the relative number of older and younger osteons, are also probably related to hardness and some of the other physical properties of bone. These factors are now being investigated in our laboratory.

As would be expected, a high negative correlation was found between the amount of spaces in the original break area and the hardness and modulus of elasticity of the specimen as determined at the time of testing. However, as mentioned previously, the value for these physical properties changed somewhat when correction was made for the spaces (Haversian canals, resorption, etc.) in the original specimens.

Osteons, as we discussed in our earlier paper (Evans and Bang, '66), are not simple spool-like structures but branch or bifurcate. Consequently, the histological composition of a cross section of a specimen changes along the length of the specimen. However, the fact that the specimen failed where it did indicates that the histological composition of the specimen at the level of the fracture was weaker than in other levels of the specimen.

CONCLUSIONS

1. The ultimate tensile and single shearing strength, tensile strain, modulus of elasticity, density and hardness were determined for 405 femoral, 193 tibial and 37 fibular specimens of cortical bone of a standardized size and shape. The methods of determining the physical properties are described.

2. The specimens were obtained from embalmed bodies of 11 white males, one Negro male, and four white females ranging from 33 to 98 years of age. None of the individuals had died from primary bone disease and all the bones appeared to be normal.

3. The histological composition of transverse sections of the specimens at the level of the fracture site was studied by the photomicrograph-weight method used in previous studies.

4. Analyses of variance were calculated on an IBM 7090 computer to determine significant differences between the physical properties and histological components of the various specimens.

5. The following differences, at the 0.01 or better significance level, were found between the physical properties of the specimens:

a. The tibial specimens had a higher tensile and shearing strength, tensile strain, modulus of elasticity and density than the femoral specimens.

b. The fibular specimens had a higher tensile and shearing strength and a higher modulus of elasticity than the femoral specimens.

c. The tibial specimens had a higher density than the fibular specimens.

6. The following differences, at the 0.01 or better significance level, were found between the histological components of 56 femoral, 79 tibial and 37 fibular transverse sections of the specimens at the level of the fracture site:

a. The femoral sections had larger osteons and remnants of osteons (square micra) and they formed a greater percentage of the break area than in the tibial sections.

b. The tibial sections had a larger percentage of the break area formed by interstitial lamellae than did the femoral sections.

c. The femoral sections had more osteons/mm² and a greater percentage of the break area formed by osteons than did the fibular sections.

d. The fibular sections had a larger percentage of the break area formed by interstitial lamellae than did the femoral sections.

e. The number of osteons/mm² and the percentage of the break area formed by osteons was greater in the tibial than in the fibular sections.

f. The fibular sections had larger osteons and remnants of osteons than the tibial sections.

7. A strong positive correlation (0.02 significance level) was found between the ultimate tensile strength of the specimens and the percentage of interstitial lamellae in the transverse sections at the level of the fracture site.

8. Hardness also showed a strong positive correlation (0.01 significance level) with the number of osteons/mm² and the percentage of osteons in the transverse sections at the level of the fracture.

9. Strong negative correlations (0.02 or better significance level) were found between ultimate tensile strength and the percentage of the break area formed by osteons; between single shearing strength and the average area/osteon remnant; and between hardness and the percentage of spaces in the break area.

10. Significant differences in the physical properties of femoral, tibial and fibular cortical bone are explained and discussed in terms of differences in the histological composition of the specimens at the level of the fracture site.

LITERATURE CITED

- Ascenzi, A., and E. Bonucci 1964 The ultimate tensile strength of single osteons. *Acta anat. (Basel)*, 58: 160-183.
- Ascenzi, A., E. Bonucci and A. Checcucci 1966 The Tensile Properties of Single Osteons Studied Using a Microwave Extensometer. In: *Studies on the Anatomy and Function of Bone and Joints*. Ed. by F. G. Evans. Springer-Verlag, Heidelberg. 121-141.
- Cowdrey, I. H., and R. G. Adams 1944 *Materials Testing: Theory and Practice*. John Wiley and Sons, Inc., New York, 1-158.
- Currey, J. D. 1959 Differences in the tensile strength of bone of different histological types. *J. Anat.*, 93: 87-95.
- 1962 Stress concentrations in bone. *J. Microscopical Sci.*, 103: 111-133.
- 1964 Mechanical aspects of the structure of bone. (Abstract presented at the Bone and Tooth Society, London, September 25, 1963). *J. Bone Joint Surg.*, 46B: 356.
- Dempster, W. T., and R. F. Coleman 1961 Tensile strength of bone along and across the grain. *J. Appl. Physiol.*, 16: 355-360.
- Evans, F. G. 1957 *Stress and Strain in Bones*. Charles C Thomas, Springfield, Ill., 1-245.
- 1958 Relations between the microscopic structure and tensile strength of human bone. *Acta Anat.*, 35: 285-301.
- Evans, F. G., and S. Bang 1966 Physical and Histological Differences between Human Fibular and Femoral Compact Bone. In: *Studies on the Anatomy and Function of Bone and Joints*. Ed. by F. G. Evans. Springer-Verlag, Heidelberg. 142-155.

The significantly greater single shearing strength of the tibial and the fibular specimens in comparison with the femoral ones is probably related to the fact that they have fewer osteons/mm² than the femoral specimens (fig. 4). Consequently, the tibial and fibular specimens have fewer cement lines where shearing can occur. The negative correlation (table 2) between single shearing strength and the average area per osteon and per osteon remnant may also be a contributing factor although the correlation between shearing strength and average area/osteon was only a little better than the 0.05 significance level.

The greater size (area) of the fibular osteons in comparison with the femoral ones (fig. 5) may be a contributing factor to the significantly greater modulus of elasticity of the fibular specimens because a weak negative correlation (table 2) was found between modulus and average area/osteon. A more important factor, as previously suggested by Evans ('58) from polarized light studies, is the orientation of the collagen fibers which in the fibular specimens is predominantly parallel to the long axis of the specimen while in the femoral specimens the collagen fibers are more obliquely oriented. Therefore, the collagen fibers of the fibular specimens are in a better position to resist tensile forces than are those of the femoral specimens. Evans' suggestion has recently been confirmed by Ascenzi and Bonucci ('64) and by Ascenzi, Bonucci, and Checcucci ('66) who have shown that the tensile strength and modulus of elasticity are higher in osteons with collagen fibers nearly parallel to the long axis of the osteon. A more detailed investigation, by means of polarized light, of the relation between the physical properties and collagen fiber orientation of femoral, tibial and fibular cortical bone is now in progress in our laboratory.

The strong positive correlation between hardness and the number of osteons/mm² as well as the percentage of the corrected break area formed by osteons (table 2) aids in explaining the differences in the hardness of the specimens. Thus, the femoral specimens, which were the hardest (fig. 2), had the most osteons/mm² as well as the greatest percentage of the corrected break area formed by osteons (fig.

3) while the fibular specimens, which were the softest, had the fewest osteons/mm² and the lowest percentage of the corrected break area formed by osteons. However, as previously mentioned, none of the differences between the hardness of the various types of specimens was at the 0.05 α better significance level. The amount and distribution of calcium in the specimens, in addition to the relative number of older and younger osteons, are also probably related to hardness and some of the other physical properties of bone. These factors are now being investigated in our laboratory.

As would be expected, a high negative correlation was found between the amount of spaces in the original break area and the hardness and modulus of elasticity of the specimen as determined at the time of testing. However, as mentioned previously, the value for these physical properties changed somewhat when correction was made for the spaces (Haversian canals, resorption, etc.) in the original specimens.

Osteons, as we discussed in our earlier paper (Evans and Bang, '66), are not simple spool-like structures but branch or bifurcate. Consequently, the histological composition of a cross section of a specimen changes along the length of the specimen. However, the fact that the specimen failed where it did indicates that the histological composition of the specimen at the level of the fracture was weaker than in other levels of the specimen.

CONCLUSIONS

1. The ultimate tensile and single shearing strength, tensile strain, modulus of elasticity, density and hardness were determined for 405 femoral, 193 tibial and 37 fibular specimens of cortical bone of a standardized size and shape. The methods of determining the physical properties are described.

2. The specimens were obtained from embalmed bodies of 11 white males, one Negro male, and four white females ranging from 33 to 98 years of age. None of the individuals had died from primary bone disease and all the bones appeared to be normal.

Microradiographic Visualization of Structure in Bones of the Masked Shrew, *Sorex cinereus*¹

WILLIAM J. L. FELTS² AND FRANCIS A. SPURRELL³
University of Minnesota, Minneapolis

ABSTRACT *Sorex cinereus*, the masked shrew, is nearly the smallest of mammals. The femur, metatarsal, phalanges and mandible of wild-trapped animals were examined by a variation in the technique of contact microradiography. Purpose of the investigation is the exploration of some aspects of the question of size as a factor in structural complexity in bone, as well as the possibilities of the shrew in studies of skeletal aging. Comparison is made with bones of the laboratory mouse and rat.

Limb bones of the masked shrew are avascular. Vascularity of the mandible appears related primarily to maintenance of dental tissues. The femur is comparatively simple, its sparse spongiosa consisting of relatively large trabeculae. Diaphyseal compacta appears to be of maximum thickness for the avascular state. Tubular foot bones are without spongiosa and bone on their articular surfaces is nearly as thick as that in the diaphysis. Metatarsals and phalanges of mice have the same gross structure but are vascular. These bones in the rat have trabeculae in functional patterns.

The simplicity of structure of these minute bones, and the drastic structural modification of bones of apparently starved or stressed animals, indicates potential utility of the shrew in experimental investigations.

The primary aim of this paper is to present some observations on the structure of certain bones of the masked shrew, *Sorex cinereus*, and, where appropriate, to draw comparisons with the same bones in the much larger mouse and rat. The masked shrew is the smallest readily available member of Family Soricidae (Order Insectivora) in America. Only the rarer pygmy shrew, *Microsorex hoyi*, is smaller among American mammals, but specimens of that species overlap *S. cinereus* in dimensions. In the Great Lakes region (Burt, '48) adult specimens of *S. cinereus* may range in weight from 2.3 to 4.0 gm and in length (approximately half consisting of tail) from 80 to 109 mm. This minute, extremely active and short-lived mammal (Crowcroft, '57) is, therefore, roughly a sixth or less the size of the common laboratory mouse. Our attention was drawn to the shrew in the course of a rather broad examination of comparative mechanical organization of bones (Felts and Spurrell, '65; Felts, '66) and of skeletal growth and aging (Felts, '64; Felts and Grewe, '65; Spurrell, Felts and Baudin, '66). Realization of the minuteness of the shrew's bones led to the anticipation that these might be ap-

propriate subjects for exploration of some parameters of the relationship of bone size to structural complexity. The short life span, of approximately one year, and the possible simplicity of bone structure suggested also that they might be simple, ideal models for analysis of skeletal aging and of responses to environmental conditions. The information presented here is derived from wild-caught specimens. It constitutes only an introduction to the essentials of anatomy in selected bones, and it is but a preliminary statement on the questions raised. The presentation is not statistical and dimensions and weights will be given only as general indicators of size and mass. An attempt currently is underway to place the shrew under controlled laboratory conditions so that more detailed investigations may be carried out.

Our secondary aim is to demonstrate the practicability and utility of microradiography in analysis of structure in whole bones of small animals. Although contact microradiography is well-es-

¹Supported by U.S.P.H.S. grant HD 02119.

²Department of Anatomy, School of Medicine, Minneapolis Campus.

³Department of Veterinary Surgery and Radiology, College of Veterinary Medicine, St. Paul Campus.

- Evans, F. G., C. C. Coolbaugh and M. Lebow 1951 An apparatus for determining bone density by means of radioactive strontium (Sr^{90}). *Science*, 114: 182-185.
- Evans, F. G., and M. Lebow 1951 Regional differences in some of the physical properties of the human femur. *J. Appl. Physiol.*, 3: 563-572.
- 1952 The strength of human compact bone as revealed by engineering technics. *Am. J. Surg.*, 83: 326-331.
- Heft, J., P. Kučera, M. Vávra and V. Voleník 1965 Comparison of the mechanical properties of both the primary and haversian bone tissue. *Acta Anat.*, 61: 412-423.
- Maj, G. 1938 Osservazioni sulle differenze topografiche della resistenza meccanica del tessuto osseo di uno stesso segmento scheletrico. *Monitore Zool. Ital.*, 49: 139-149.
- Maj, G., and E. Toajari 1937 Osservazioni sperimentali sul meccanismo di resistenza del tessuto osseo lamellare compatto alle azioni meccaniche. *Chir. Organi Mov.*, 22: 541-557.
- Olivo, O. M. 1937 Rispondenza della funzione meccanica varia degli osteoni con la loro diversa minuta architettura. *Boll. Soc. Ital. Biol. Sper.*, 12: 400-401.
- Olivo, O. M., G. Maj and E. Toajari 1937 Sul significato della minuta struttura del tessuto osseo compatto. *Boll. Sci. Med. Bologna*, 109: 369-394.
- Toajari, E. 1938 Resistenza meccanica ed elasticità del tessuto osseo studiata in rapporto alla minuta struttura. *Monitore Zool. Ital.*, 48: 148-154.
- 1939 Differenze nella struttura e resistenza meccanica del tessuto osseo in due razze *Bos Taurus*. *Arch. Sci. Biol. (Bologna)*, 25: 544-557.

walled, avascular bone is not part of a mosaic that has dimensions beyond the single unit; it is a discrete entity with individual characteristics of growth, and it exists in an articulated system, subjected to mechanical forces which its individual organization must counter.

Apart from the incompletely understood relationship of vascularity to size, it seems that smaller bones should be less complex than larger bones in their gross internal architecture, i.e., in the proportions and distribution of compacta and spongiosa. In several parts of his classic treatise on form, Thompson ('42) discussed and illustrated relationships of structure to magnitude of the organism. Relative to mammalian bones this point is difficult to specify, but it is axiomatic in technology that one does not scale down strength of material when size of an object is reduced. Conversely, larger structures require more complicated distributions of material than do smaller ones of the same overall design and function. In regard to bone architecture, the consideration of structural complexity relative to size raises such questions as that of the ultimate simplicity possible in tubular bones of very small animals, the size level above which trabecular support (load distribution) is required within a bone, the least number of layers of bone that constitute an effective tubular unit, and the largest tubular form that may exist without the addition of internal vascular channels.

MATERIALS AND METHODS

Specimens of *Sorex cinereus* used in this study were drawn from a collection in the Museum of Natural History, University of Minnesota. The animals had been trapped by Dr. John R. Tester in the Waubun Prairie Research Area, Mahanomen County, Minnesota, between early spring and early winter of two years ('58-'59). The sample thus included a range of immature to mature animals in the year of their birth and mature animals that had been born the previous year. Crowcroft ('57) has shown the seasonal distribution of shrews according to length and to tooth wear. This pattern was considered in selecting a group of 42 speci-

mens almost evenly distributed over the range of length available, 62 to 92 mm. (It will be noted that the latter figure is considerably less than Burt's adult maximum of 109 mm. It is not known whether or not this represents an actual regional characteristic in growth and survival). Reproductive tracts of the selected animals then were examined by Dr. Albert Erickson of the MNH in order to determine sex and to permit classification as immature or mature. The group divided almost exactly into the two sexes in the two developmental levels. An additional male specimen, only 51 mm in length, was obtained later from another, but comparable, locale in Minnesota.

Several additional facts regarding site and method of collection and mode of preservation of these specimens of *S. cinereus* have bearing on the observations that follow. The animals were all from essentially a uniform ecological site. The traps were of the snap-kill type that insured that the animals did not starve to death. These two facts are important in view of the apparently great susceptibility of shrews to variations in diet and to even short-term deprivation of food (Crowcroft, '57). All specimens had been fixed whole, in neutral formalin, and were stored in a common container. Original identification tags were retained throughout. Finally, all were identified by the available morphological criteria as being *S. cinereus* rather than the rarer *Microsorex hoyi* or the quite common *Sorex palustris* (water shrew), that are, respectively, slightly smaller and considerably larger than *S. cinereus*. For comparative purposes, the femur of *M. hoyi* is illustrated in this report, and bones of both *M. hoyi* and *S. palustris* were examined radiographically.

After a general survey of the shrew skeleton, certain bones were chosen as being most useful for our purposes. None of these posed special problems of removal and handling, once procedures had been established. The femur was chosen because of its key role in locomotion and weight-bearing, and because so much is known of its structure in other species. Because they were the smallest tubular bones readily available in all specimens,

lished as a method in skeletal histology (e.g., ground sections, Jowsey et al., '65), it does not appear to have been applied in extenso to the investigation of whole-bone structure in either small laboratory animals or wild forms. "Contact" in this usage is something of a misnomer for a small bone usually cannot lie completely in contact with the emulsion. Our application of the method obviously is a direct parallel to classical radiography of whole large bones in which a conventional apparatus is used and the subjects are laid on standard radiographic films (e.g., Felts and Spurrell, '66). For very small bones, the radiation is from a low-energy source (soft x-rays) and the microradiographic emulsions have a grain size more appropriate to the absolute size of the bone. This variation in contact microradiography is in routine use in this laboratory in the analysis of age changes in bones of mice, and in the study of alveolar healing and mandibular reconstruction in young mice (Grewe, '66). It is thought that the use of contact microradiography in an analysis of shrew bones is perhaps the best possible demonstration of the capabilities of the technique.

That the internal structure of a bone is influenced by its size is implicit in various aspects of the literature on skeletal morphology and physiology. The most obvious fact in this regard is the domination of microscopic structure of large bones (i.e., those of large experimental animals and of man) by evidence of the requirement that all portions of the bone and its osteocytes be within a maximum optimum distance from the circulatory system (Ham, '57). In the thick walls of large bones, the complex of primary and secondary osteons (haversian systems), or in many species, the equally extensive plexiform system, is the solution to the biological problem (Enlow, '62b). (Actually, whether the problem is simply the metabolic requirements of cells or the greater need of the body for the most effective distribution of perivascular tissues with bone-building and bone-removing capacities, or whether it is both of these or more, has not been determined). The sequential pattern and fate of such perivascular aggregations of cells and in-

tercellular substance are the important criteria in typical microscopical investigations of structural changes in bone (e.g., McLean and Rowland, '63; Jowsey, '63; Spurrell et al., '66). Such bone is variably porous through time and according to regional subdivisions. Consequently, the mechanical capacity of a whole large bone is not simply a function of external form, diaphyseal wall thickness, dimensions of marrow cavities, and orientation of spongiosa and compacta. Quantity and distribution of space and quality (i.e., level of mineralization) of bone within the compacta must be considered in evaluation of skeletal aging and of skeletal responses to environmental conditions. If gross structure as a biomechanical unit is to be studied relative to age and the environment, it appears therefore that the animal of choice should be one with the simplest of vascular channels or, ideally, one with none at all. In either case, microdensitometric analysis of mineralization would be easier than in a larger bone having a greater number of differentially mineralized loci.

Comparative histology of bone (Enlow and Brown, '56; Enlow, '62a, b) has revealed that bones of smaller species have very simple patterns of vascular channels and distributions of bony tissue. The most simple form is that of nonhaversian, or primary vascular, channels not surrounded by concentric lamellae. The bones of the smallest of reptiles and mammals appear in sections to be without internal vascular channels. It is a reasonable assumption that their periosteal and endosteal vascular networks are close enough to the full depth of the bony wall to permit the same physiological processes as in larger bones with extensive intraosseous canals. In such avascular bones the gross dimensions, no matter how microscopic the entire bone may be, can be the prime criteria in evaluation of structural change relative to time and circumstance, and, indeed, mineralization patterns are relatively gross. One is tempted to regard such bones as being equivalent to single osteons. Lacroix ('51) has termed such a comparison unfortunate, and his position is wholly justified. Unlike an osteon, a minute, thin-

walled, avascular bone is not part of a mosaic that has dimensions beyond the single unit; it is a discrete entity with individual characteristics of growth, and it exists in an articulated system, subjected to mechanical forces which its individual organization must counter.

Apart from the incompletely understood relationship of vascularity to size, it seems that smaller bones should be less complex than larger bones in their gross internal architecture, i.e., in the proportions and distribution of compacta and spongiosa. In several parts of his classic treatise on form, Thompson ('42) discussed and illustrated relationships of structure to magnitude of the organism. Relative to mammalian bones this point is difficult to specify, but it is axiomatic in technology that one does not scale down strength of material when size of an object is reduced. Conversely, larger structures require more complicated distributions of material than do smaller ones of the same overall design and function. In regard to bone architecture, the consideration of structural complexity relative to size raises such questions as that of the ultimate simplicity possible in tubular bones of very small animals, the size level above which trabecular support (load distribution) is required within a bone, the least number of layers of bone that constitute an effective tubular unit, and the largest tubular form that may exist without the addition of internal vascular channels.

MATERIALS AND METHODS

Specimens of *Sorex cinereus* used in this study were drawn from a collection in the Museum of Natural History, University of Minnesota. The animals had been trapped by Dr. John R. Tester in the Waubun Prairie Research Area, Mahan County, Minnesota, between early spring and early winter of two years ('58-'59). The sample thus included a range of immature to mature animals in the year of their birth and mature animals that had been born the previous year. Crowcroft ('57) has shown the seasonal distribution of shrews according to length and to tooth wear. This pattern was considered in selecting a group of 42 speci-

mens almost evenly distributed over the range of length available, 62 to 92 mm. (It will be noted that the latter figure is considerably less than Burt's adult maximum of 109 mm. It is not known whether or not this represents an actual regional characteristic in growth and survival). Reproductive tracts of the selected animals then were examined by Dr. Albert Erickson of the MNH in order to determine sex and to permit classification as immature or mature. The group divided almost exactly into the two sexes in the two developmental levels. An additional male specimen, only 51 mm in length, was obtained later from another, but comparable, locale in Minnesota.

Several additional facts regarding site and method of collection and mode of preservation of these specimens of *S. cinereus* have bearing on the observations that follow. The animals were all from essentially a uniform ecological site. The traps were of the snap-kill type that insured that the animals did not starve to death. These two facts are important in view of the apparently great susceptibility of shrews to variations in diet and to even short-term deprivation of food (Crowcroft, '57). All specimens had been fixed whole, in neutral formalin, and were stored in a common container. Original identification tags were retained throughout. Finally, all were identified by the available morphological criteria as being *S. cinereus* rather than the rarer *Microsorex hoyi* or the quite common *Sorex palustris* (water shrew), that are, respectively, slightly smaller and considerably larger than *S. cinereus*. For comparative purposes, the femur of *M. hoyi* is illustrated in this report, and bones of both *M. hoyi* and *S. palustris* were examined radiographically.

After a general survey of the shrew skeleton, certain bones were chosen as being most useful for our purposes. None of these posed special problems of removal and handling, once procedures had been established. The femur was chosen because of its key role in locomotion and weight-bearing, and because so much is known of its structure in other species. Because they were the smallest tubular bones readily available in all specimens,

the metatarsal and the proximal and middle phalanges of the third digit, left hind foot, were used throughout this study. The front foot often had been damaged in the trap, and marginal digits of any foot often evidenced healed injuries, or were missing antemortem. The mandible was examined because it is relatively a very large bone in the shrew and because preliminary examination revealed a pattern of vascular channels. It should be noted that each bone, or region of a bone, of *S. cinereus* illustrated in this paper was selected as typical of at least three, or in some cases five, radiographed bones from specimens of the indicated sex and level of maturity. The only exceptions were the radiograph of the hind foot of a very young animal (fig. 9) and that of a varient femur (fig. 5). Bones of the mouse and the rat were selected on the same basis.

Bones were removed, with the aid of iridectomy scissors, fine scalpel and forceps, under a dissecting microscope. In many cases small fragments of muscles, tendons and joint capsules were left in place when removal would have damaged the fragile bones. In the case of the smallest, 51 mm specimen of *S. cinereus*, the metatarsal and phalanges could not be removed safely and the foot was dehydrated and radiographed as a unit). The essentially clean bones then were dehydrated in rapid changes of alcohols and in alcohol-ether and were allowed to dry in air. Subsequent paraffin sectioning of radiographed bones revealed that articular cartilages were mostly intact and that the body of marrow had shrunken and lay to one side or the other within the dried bones. The radiographic image of articular cartilage was visible in some radiographs. The mass of dehydrated marrow is actually visible in one radiograph (fig. 5).

Micro-radiographic exposures were made on Eastman High Resolution plates with a locally-produced apparatus. The x-ray tube is a Machlett Type A-2 with a chromium anode and a beryllium thin-window. The power supply and control unit are built for the tube and its mode of use. The tube is energized just above the voltage at which the copper absorber produces K-

characteristic radiation. A vanadium filter is interposed in the beam. Although the apparatus is equipped with an evacuation pump, no vacuum was produced between tube-window and film for the exposures made in this investigation. To facilitate handling and to insure proper orientation, the bones were mounted, singly or in groups, on strips of Scotch-Tape spanning the aperture in a broad ring of manilla stock. The ring then was turned over and placed so that the secured bones were in direct contact with the film. The tape was completely radiolucent at the energy levels involved. For a preliminary survey of all bones of the selected group, a target-film distance of 17 cm was employed, and exposure time ranged from 15 to 45 minutes depending on the specimens. In the definitive radiographs on which the illustrations are based, distance was increased to 31 cm to reduce parallax. Exposures then ranged from 45 to 240 minutes. Target-film distance in the apparatus is controlled by interchangeable lengths of stainless-steel tubes (20 cm diameter) that serve as the specimen and film chamber below the tube holder and above the pump fitting. The ultimate use of each radiograph in the definitive series dictated the specific exposures. Because of extreme regional distinctions in density, the radiograph for figure 1, for example, necessitated less exposure than usual in order to visualize both internal structure and the thin edges of a variety of femora. For figure 2, on the other hand, greater exposure was required to delineate sharply the diaphyseal walls and trabeculae, and in figure 15 to resolve the vascular pattern in the mandible. Figure 5 illustrates the problem of simultaneous radiography of two bones of radically different densities.

From the contact microradiographs, illustrations were prepared either by photographic means or through use of a camera lucida. For lower magnifications (i.e., groups of bones, individual femora and mandibles of the shrew, and all bones of rat and mouse), a Leitz macrophotographic apparatus was employed. For higher magnifications, the same apparatus was used in conjunction with a microscope. The film for microscopic work was

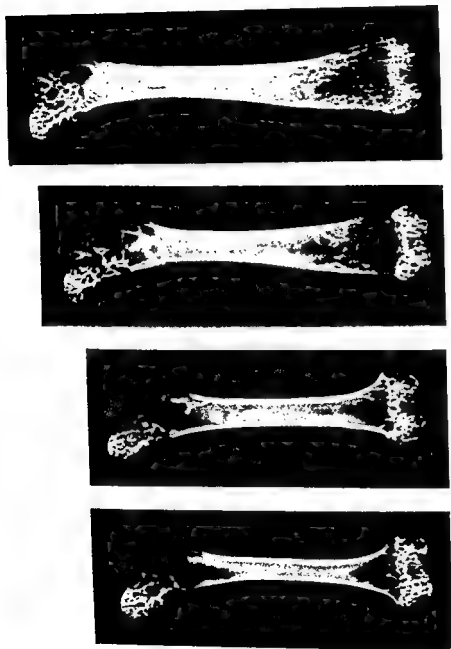


Fig. 1 Frontal (anterior-posterior) radiographs of left femora of specimens of *S. cinereus*. Left to right: immature male and female, mature male and female. Size difference between latter two does not imply a general sex difference in size. All radiographed on a single plate and photographed and printed as a unit. $\times 14$.

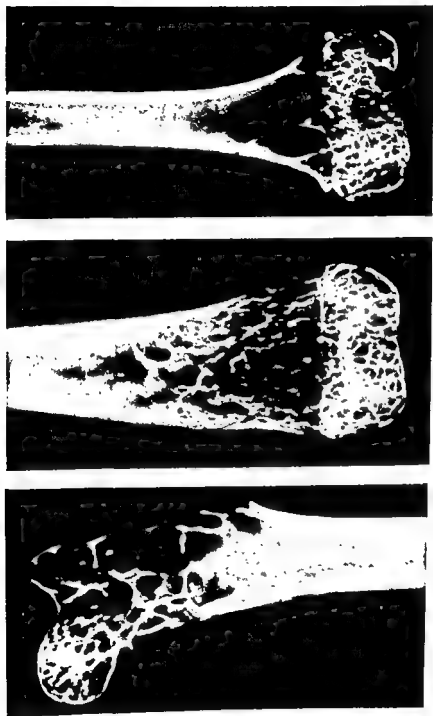


Fig. 2 Frontal radiographs of proximal end of femur of mature male *S. cinereus* (left) and distal ends of femur of mature (center) and immature (right) males. Contact prints of higher magnification negatives of the radiographs represented by first and third images in figure 1. $\times 26$.

Eastman Commercial Ortho, used with a conventional light source and a green filter, and for macroscopic illustrations, Eastman Plus-X. This selection was based on the excellent grey-scale obtained in trials. Contact printing was on a variety of Eastman papers, the choice depending on the contrast or fine detail to be emphasized in the illustrations. An enlarger was used only for figure 7 (see legend). Line drawings were made with a Wild microscope equipped with that maker's adjustable drawing tube. Measurements were taken directly from the radiographic plates on a Jones and Lamson optical comparator equipped with a vernier mechanical stage.

RESULTS AND DISCUSSION

Femur of the shrew

External configuration, general and regional internal architecture and other characteristics of femora of *S. cinereus*, *M. hoyi*, the mouse and the rat are presented in radiographs and in line drawings. Femora of immature and mature male and female specimens of *S. cinereus* are displayed in frontal view and at low magnification in figure 1. Proximal and distal regions of some of the same specimens are illustrated at higher magnification in figure 2, and figure 3 depicts the mature femur in lateral view. Typical and variant femora of young females are represented in figure 5. For comparison with that of the larger shrew, a femur of *M. hoyi* is shown in frontal view in figure 6. In order to compare structure and proportions between species without the difficulty imposed by size differences, figure 7 illustrates femora of *S. cinereus* and of the laboratory mouse and rat projected to a common length. A line drawing in figure 4 depicts essentials of later post-natal growth in the shrew femur, and figure 13 shows by line drawing the gross layering and cell distribution in a cross-section of the femur.

External configuration. In gross external form, femora of mature specimens of *S. cinereus* are of a rather common, unspecialized quadrupedal type (figs. 1, 3). The proximal and distal expansions (metaphyses and epiphyses) each occupy approximately a quarter and the diaphysis

a half of the length of the bone. In lateral view the femur typically is quite straight and tapers slightly toward the distal end. However, some otherwise normal mature femora (fig. 3) exhibit a posteriad deflection in the distal quarter. The curve of the condyles is carried far back in both forms. In frontal view (figs. 1, 2), the proximal end of the femur is flattened in the medial-lateral plane (compare with fig. 3), an appearance contributed to by the thinness of the greater trochanter and the gluteal crest below it, and by the mediad projection of the flattened lesser trochanter. The ovoid head is directed mediad and slightly anteriad from the low, broad neck. The diaphysis in the mature bone is cylindrical just distal to the proximal metaphysis, then becomes progressively more ovoid (long axis in



Fig. 3 Medial-lateral radiograph of femur of mature male specimen of *S. cinereus*. Enlargement of proximal end is from contact print of higher magnification negative of the radiograph represented by the whole-bone image. Detail of head is lessened by distance from emulsion. Note layering on to left (posterior) in each image. $\times 14$ and $\times 25$.

m-l plane) toward the distal metaphysis. It is without a *linea aspera*.

Between femora of mature and immature animals there is general agreement in configuration of the proximal region and a distinct difference in that of the distal region. In frontal view (fig. 2), the distal metaphysis of the mature bone (ovoid in cross-section) is relatively long and tapered, a virtually indistinguishable continuum between diaphysis and epiphysis. In the immature bone, however, this region is relatively short and it flares sharply in the medial-lateral plane. The relationship of this regional difference to growth and to internal architecture will be discussed in detail in a later paragraph.

The size of the femur of *S. cinereus* can be represented in essence by the following measurements. Femora of five mature males had a mean dry fat-free weight of 2.6 mg (1.8–2.9 mg). Overall length of these bones averaged 6.8 mm (6.5–7.2 mm), and midshaft diameter, 0.61 mm (0.58–0.63 mm). A comparison with femora of the mouse and the rat will be found in the final section of this paper.

General features of radiographic anatomy. Certain details in radiographs cannot readily be transferred effectively to photographs, or are below the level of magnification of the illustrations. In many places on the images, depending on structure, absolute thickness of bone and duration of exposure, osteocytic lacunae can be visualized. These are but point concentrations of silver salts, lacking specific margins and without trace of canaliculi. As Jowsey ('65) has indicated for contact microradiographs of ground sections from other species, such lacunar details are below the level of resolution of the emulsion. In sufficiently long exposures of the femur, lacunae are seen most readily in the diaphyseal wall that was adjacent to the emulsion. In projections of the edges of the tube, lacunae are visible in approximately the outer third and usually are invisible as thickness increases toward the marrow cavity. Images of lacunae are most obvious in the very thin walls of the metaphyses and epiphyses. In edge-projections of the thin cortices, two or three adjacent lacunae may cause the surface to appear faulted.

Cell-spaces within trabeculae usually cannot be distinguished with certainty from those of the wall against which they are projected. From these observations, it will be appreciated that lacunae are gross or macroscopic features relative to the very small absolute dimensions of bones of the shrew.

Careful examination of anterior-posterior, medial-lateral and oblique projections of shrew femora fails to reveal vascular channels other than those of nutrient vessels. The latter are of large diameter relative to their length and are most consistently present in the posteromedial wall of the upper diaphysis (figs. 1, 3) and on the posteromedial aspect of the distal metaphysis (fig. 2). In almost every femur, one projection may show a fine pattern of channels in the opposite wall (fig. 2), but in other projections of the same bone these are identifiable as merely surface (usually endosteal) impressions. The absence of intraosseous vascular channels is confirmed by ground sections and serial paraffin sections.

Frontal radiographs usually present a homogeneous image of the diaphysis (lacunae excepted). However, some radiographs taken in this plane have an indication of layering, i.e., long, faint lines separating a thick inner region from one or more outer, thinner regions of lower density. This is distinct from the slight gradient of density expected in the projection of a tube, and is not to be confused with the finer circumferential lamellae seen in paraffin sections but below the level of resolution of microradiographic emulsions. The presence of a surface deposit of lower radiodensity is almost a consistent finding in medial-lateral radiographs (fig. 3). This feature can be attributed to differential deposition of bone occurring as part of a posterolateral "drift" (term of Enlow, '62a), as shown in section in figure 13.

Articular cartilage cells are identifiable in short-exposure radiographs as a coarse "orange-peel" effect on the articular surfaces of the femur. In routine radiographs of longer exposures, surface outlines of osteocytic lacunae of smaller size are found in the same areas. These features too have been verified by paraffin

sections. Cartilage in the epiphyseal lines of immature femora (the distal only in the available specimens) cannot be distinguished radiographically, but a line of separation between primary and secondary centers is visible.

Compacta and spongiosa. Compacta in the femur of the shrew may be defined as the avascular bone of the diaphysis and of the surfaces or cortices of the metaphyses and epiphyses. Spongiosa is defined as the aggregation of trabeculae within the metaphyses and epiphyses, without regard to their number and diameter.

In femora of eight adult (male and female) specimens of *S. cinereus*, the diaphyseal compacta (midshaft in frontal radiographs) had a maximum thickness of 0.12 to 0.20 mm. The maximum, of course, would be slightly greater if measured through the region of low-density increment referred to above and depicted in figure 13. Thickness of compacta diminishes abruptly to the thin cortex over most of the metaphyses and epiphyses. In the proximal and distal ends of the femur, the surface layer is approximately 20 μ thick between trabecular contacts.

On its outer surface the diaphysis is smooth. The inner surface usually is of smooth contour as well, but in many specimens it is characterized by a number of long, shallow concavities, strongly suggestive that resorption (and deposition) in this small bone may occur in depth over relatively large regions of its endosteal surface. This feature is even more obvious in the femur of *M. hoyi* in figure 6. In the absence of properly fixed and stained sections of femora from shrews of several ages and physiological states, nothing more can be said regarding this feature.

The absolute and relative amount of spongiosa in the two ends of the femur requires an examination of the process by which its definitive form is attained. No femora included in this study had open epiphyseal lines in the head or trochanters. (From the single 51 mm specimen of *S. cinereus* it is known that these do exist.) The distal line was open in all femora from animals in the immature

category and was closed in over three-quarters of those from the mature group. Because of this developmental condition, it was possible to superimpose the proximal ends of the immature and mature femora, as in figure 4. Along the outlines of lesser trochanter, head and greater trochanter, femora of three animals of each sex in each category coincided so well that the two illustrated safely can be taken as typical. Points beside the drawings indicate the limits of the proximal and the distal spongiosa; differences between individuals and categories were so very slight that the one set of points indicates the situation in both stages.

On the basis of information in figures 2 and 4, the later growth of the femur can be summarized. After fusion of the proximal epiphysis, there are no significant changes in external configuration of the head or trochanters, nor in the extent of spongiosa within them. The rest of the proximal metaphysis and the diaphysis increase in diameter by periosteal depositions, while the discrepancy between endosteal resorption and external accretion is such that the compacta becomes thicker. The distal epiphyseal line continues to contribute to length; and there occurs a change in external form of the distal femur and in the amount of spongiosa within it. The abrupt flare from diaphysis to distal epiphyseal line that is characteristic of immature femora is replaced by a long, rather slight taper in mature ones. Clearly, this must be attributed to a change in the ratio of the rate of longitudinal growth to the rate of resorption on the surface of the metaphysis. Internally, the proximal limit of the distal spongiosa remains essentially where it was in the immature femur. This must represent another change in the ratios of rates of growth, i.e., that of longitudinal growth to that of resorption in the spongiosa. As a result of this pattern of developmental alteration, the amount of space occupied by spongiosa in the distal end of the femur increases not only in the absolute sense but in the relative one as well.

With the available material, nothing can be determined regarding physiological circumstances and timing of the shift

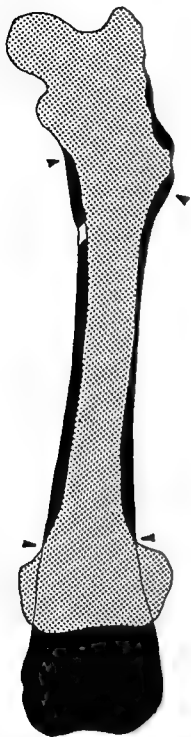


Fig. 4 Superimposed camera lucida drawings of typical femora of immature (shaded) and mature (black) male specimens of *S. cinereus*. Triangular pointers indicate limits of spongiosa in proximal and distal ends of both bones. Compare with distal ends of femora in figure 2.

in differential growth in the femur. A laboratory study of maturation, utilizing chemical and radiological markers for bone, would be needed to establish this

relationship. The most reasonable suspicion now is that the basic mechanism is simply an increase in the rate of longitudinal growth. It can be suspected too that femora of much older shrews (apparently available only if raised under laboratory conditions) would have thin walls in the distal region and that these would be supported by approximately the form of spongiosa seen in the proximal ends of the present series of bones. This statement is based on the assumption that differential resorption and remodeling eventually might produce the similarity in trabeculation found in the two ends of most mammalian limb bones (e.g., mouse and rat in fig. 7). This is suggested too by the state of trabeculation in the femur of *M. hoyi* in figure 6. The shift in differential growth apparently is not as great in that species as it is in *S. cinereus*, but in the mature specimen illustrated (with fused distal epiphysis), the proximal and distal spongiosae are more alike than in the available mature specimens of *S. cinereus*.

In *S. cinereus* the proximal spongiosa differs in detail between individual specimens, but there are certain basic features characteristic of all. The pattern may be termed coarse, for individual trabeculae are large (approximately 35 μ) in diameter relative to length and to size of the bone, and the ratio of space to bone is high (figs. 1, 2, 3). Thus, except in the center of the head, individual trabeculae can be traced in their extent and in their relationship to other trabeculae. There are no distinct interregional tracts of bone such as extend from the medial and lateral sides of the diaphysis to the head and to the trochanters in the femur of man (Koch, '17; Tobin, '55). The only consistent representation of such a load-distributing system in the shrew is an irregular grouping of trabeculae coursing from the lower buttress of the neck to the superior portion of the head. Visible as a radiodense array in all femora of *S. cinereus* and in the femur of *M. hoyi* (fig. 6), this tract is comparable to the very obvious and more regular one in the mouse femur and to a less obvious, fine-structured one in that of the rat (fig. 7). Except for this particular aggregation, trabeculae appear

to be variably arranged so as to interconnect the thin walls of the trochanters and of the gluteal crest, and to relate them to the thicker anterior and posterior surfaces of the metaphysis and epiphysis (compare figs. 2, 3). Within the head, the primary distribution of trabeculae is radial, with those on the lateral side extending into the neck. Throughout the spongiosa, the intersections of trabeculae, as well as their unions with the walls, are paired out so that the region is characterized by large and small apertures of various shapes. Within the head, this gives the appearance of rounded chambers just beneath the cortex.

Spongiosa within the distal end of the femur is generally more dense and fine-structured than that in the proximal end.

It is difficult to trace the extent and interconnections of individual trabeculae. In immature specimens the more proximal trabeculae in the mass are relatively large (figs. 1, 2), but the remainder are of far lesser diameter than those in the other end of the femur. Interconnected bars and plates relate the terminal plate of the metaphysis to the substantial distal cortex. Beyond the epiphyseal line (which can be traced in all radiographs) the distribution of trabeculae within the thin-walled secondary center appears in frontal view to be confused. In lateral radiographs, however, many of these trabeculae are seen to extend from the curved terminal plate of the epiphysis to the much greater curvature of the articular surface. In the more extensive spongiosa of mature



Fig. 5. Frontal views of left femora of two young female specimens of *S. cinereus*. Detailed description of typical (left) and variant femora is given in text. Both radiographed on same plate, at exposure suitable for typical femur, and pairing was maintained through final contact printing. $\times 17$.

femora the more robust trabeculae are in the proximal — distal axis. Unless the primary and secondary centers are joined, trabeculae of the secondary center retain the orientation described above. If the centers are united, the terminal plates may be interrupted and metaphyseal trabeculae are continuous with those in the epiphysis that terminate on the deep face of the articular surface. In none of the available mature specimens were there discrete curvilinear trabecular lines extending in the frontal plane from the diaphysis to the articular region, as in man; nor was there evidence of reorganization tending to produce larger trabeculae.

The diminution of femoral structure in response to adverse physiological or environmental conditions was obvious in three females and two males in the series. None of the females were pregnant, but lactation was a possibility in two. The most interesting example is represented in figure 5, in which one typical and one variant femur are shown as radiographed at an exposure appropriate for the typical bone. These femora were from two female specimens of *S. cinereus* trapped on the same day in the same area. The animals differed in overall length by only 2 mm (76 and 74 mm, left to right), and, on the basis of enlarged reproductive tracts but immature mammary glands, they were considered to be in or near first estrus. (Weights at trapping are unknown). The femur of the one is of typical radiodensity, and can be classified as immature on the basis of the developmental status of its distal end. The other femur was so delicate that the proximal metaphysis fractured during removal. The wall of the diaphysis is only about a fifth as thick as that of the typical femur, and the cortices of the metaphyses and epiphyses can hardly be visualized on the radiograph. Trabeculae are few in number and extremely thin. The outline of the proximal end parallels that of the typical femur, but the distal end is malformed. The masking effect of the thin bone shell is so slight that the dehydrated, shrunken marrow is visible within the diaphysis. Radiographic images of other bones of this particular animal were in keeping with that of the femur.

In wild-trapped animals, of course, neither the etiology nor the duration of such an obvious wasting of the skeleton are known. That the illustrated case may be a relatively acute one is suggested by the general comparability of the two females and by the maturational status of the femur and other bones. This may be a striking skeletal manifestation of starvation in keeping with Crowcroft's ('57) observations on weight loss of shrews when deprived of a daily food intake roughly equal to their weight. The drastic response of gross features to metabolic conditions suggests the utility of such bones in laboratory investigations in aging, nutrition and endocrinology.



Fig. 6 Frontal radiograph of left femur of mature male specimen of *M. hoyi*. $\times 18$.

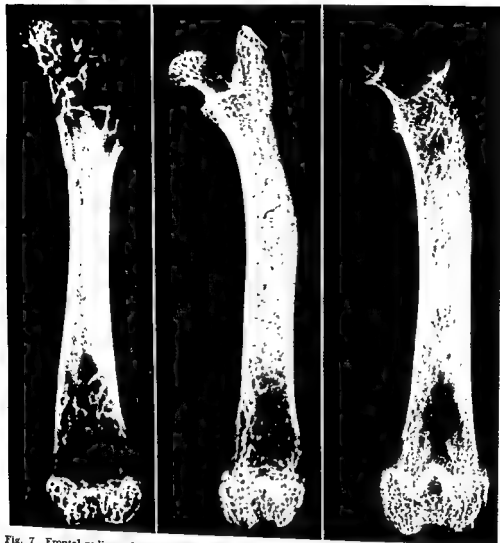


Fig. 7 Frontal radiographs of femora of *S. cinereus* (left), C57 black mouse (center) and albino rat (right) projected to common height (medial condyle to greater trochanter). Each bone radiographed at exposure suitable for its density and structure. Enlarger used in printing, on polycontrast paper with filters and dodging employed for the maximum representation of anatomical features across the series. See p. 21 for description and discussion of relative and absolute dimensions.

Metatarsal and phalanges of the shrew

External configuration and internal anatomy of the metatarsal and proximal and middle phalanges of *S. cinereus* are illustrated in figure 8. These are typical of the group studied; the dorsal-plantar view of the metatarsal and phalanges are from one adult male, while the lateral views are from another male and illustrate

variations in nutrient vessels. The metatarsal-phalangeal region of the intact foot of a very young male, 51 mm in length, in figure 9 shows the developmental status of these bones in a shrew recently out of the nest. Metatarsals of *S. cinereus*, the mouse and the rat are shown at common length in figure 10, and the proximal phalanges of these species are so depicted in figure 11. Figure 12 represents the arrangement

femora the more robust trabeculae are in the proximal — distal axis. Unless the primary and secondary centers are joined, trabeculae of the secondary center retain the orientation described above. If the centers are united, the terminal plates may be interrupted and metaphyseal trabeculae are continuous with those in the epiphysis that terminate on the deep face of the articular surface. In none of the available mature specimens were there discrete curvilinear trabecular lines extending in the frontal plane from the diaphysis to the articular region, as in man; nor was there evidence of reorganization tending to produce larger trabeculae.

The diminution of femoral structure in response to adverse physiological or environmental conditions was obvious in three females and two males in the series. None of the females were pregnant, but lactation was a possibility in two. The most interesting example is represented in figure 5, in which one typical and one variant femur are shown as radiographed at an exposure appropriate for the typical bone. These femora were from two female specimens of *S. cinereus* trapped on the same day in the same area. The animals differed in overall length by only 2 mm (76 and 74 mm, left to right), and, on the basis of enlarged reproductive tracts but immature mammary glands, they were considered to be in or near first estrus. (Weights at trapping are unknown). The femur of the one is of typical radiodensity, and can be classified as immature on the basis of the developmental status of its distal end. The other femur was so delicate that the proximal metaphysis fractured during removal. The wall of the diaphysis is only about a fifth as thick as that of the typical femur, and the cortices of the metaphyses and epiphyses can hardly be visualized on the radiograph. Trabeculae are few in number and extremely thin. The outline of the proximal end parallels that of the typical femur, but the distal end is malformed. The masking effect of the thin bone shell is so slight that the dehydrated, shrunken marrow is visible within the diaphysis. Radiographic images of other bones of this particular animal were in keeping with that of the femur.

In wild-trapped animals, of course, neither the etiology nor the duration of such an obvious wasting of the skeleton are known. That the illustrated case may be a relatively acute one is suggested by the general comparability of the two females and by the maturational status of the femur and other bones. This may be a striking skeletal manifestation of starvation in keeping with Crowcroft's ('57) observations on weight loss of shrews when deprived of a daily food intake roughly equal to their weight. The drastic response of gross features to metabolic conditions suggests the utility of such bones in laboratory investigations in aging, nutrition and endocrinology.



Fig. 5 Frontal radiograph of left femur of mature male specimen of *M. hoyi*. $\times 18$.

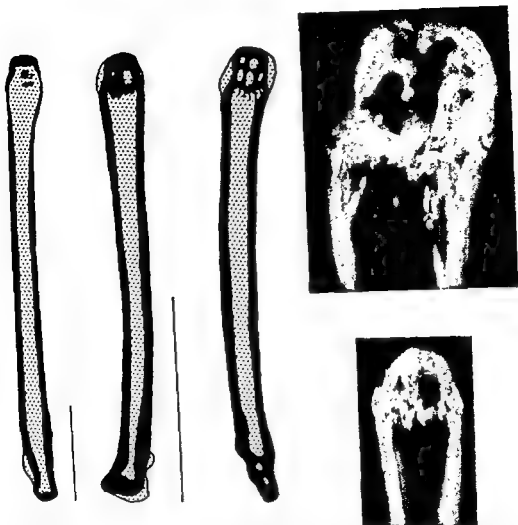


Fig. 10 Third metatarsals of *S. cinereus*, mouse (center) and rat (right). Drawn from radiographs projected to common height. Vertical lines indicate size of the two smaller bones relative to given size of rat's bone. Photographs at right (both at $\times 25$) illustrate details of distal ends of metatarsals of mouse (below) and rat. Compare with metatarsal in figure 8.

The proximal and middle phalanges differ from each other chiefly in size and in the configuration of their proximal articular surfaces. Each is generally symmetrical in frontal view and is tapered in lateral view. The attachment of the flexor sheath on the edges of the distal plantar surface is not associated with processes and the plantar surface is not grooved for a flexor tunnel. The proximal and distal phalanges of the adult in figure 8 weigh approximately 0.2 and 0.1 mg and are 1.48 and 0.98 mm in length, respectively.

Radiographic anatomy. The internal anatomy of shrew metatarsals and phalanges is most simple. Close examination of all radiographs in the series revealed no vascular channels in the compact walls. Apertures for nutrient vessels penetrate the walls in the proximal and distal quarters of the metatarsals, the exact site being quite variable. In the phalanges, these openings usually are paired and at mid-length. Osteocytic lacunae are prominent in all radiographs, but layering of bone is less obvious than in radiographs of the

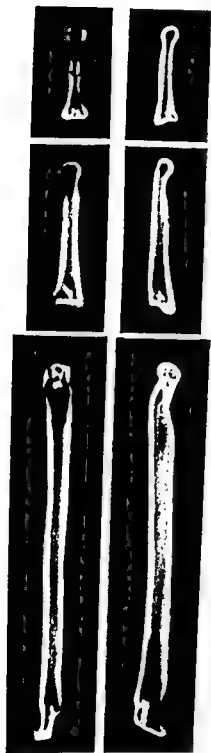


Fig. 8 Dorsal-plantar (left) and medial-lateral radiographs of third metatarsal and proximal and middle phalanges of third digit of adult male specimens of *S. cinereus*. Three bones to left are from one animal and those on right, at slightly less exposure, from another. In each case, metatarsals and phalanges were radiographed on a single plate and photographed and printed as a unit. $\times 24$.



Fig. 9 Dorsal-plantar radiograph of right foot of male specimen of *S. cinereus* 51 mm in length. First digit to left. (Image of skin visible to left of it.) Fifth digit removed in course of skinning of foot. $\times 45$.

of bone trabeculae in a metatarsal of *M. hoyi*.

External configuration. The configuration of the metatarsal and phalanges of the shrew is so simple and so evident in the illustrations that little description is required. The metatarsal is a simple tubular bone. In the proximal region, where it articulates with the tarsals and with neighboring metatarsals, the bone is somewhat flattened in the dorsal-plantar plane, and the articular facets complicate interpretation of radiographs. The distal articular surface is a low dome and the region immediately proximal to this is thin in lateral view and broad in frontal view. Between the para-articular regions the metatarsal is nearly a uniform cylinder, being slightly deeper than broad. The typical adult metatarsal in figure 8 weighs 0.4 mg, is 3.02 mm in length and at midlength has a diameter of 0.26 mm.

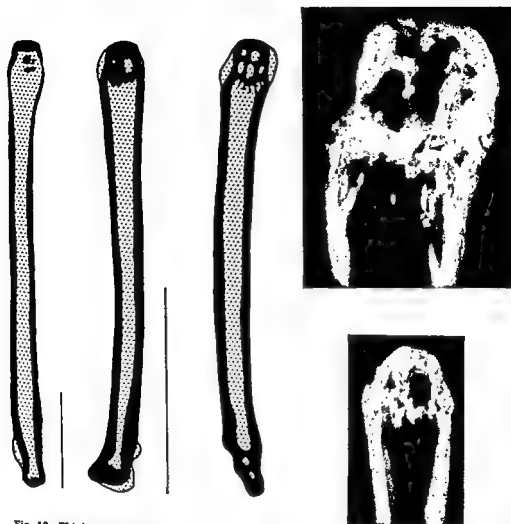


Fig. 10 Third metatarsals of *S. cinereus*, mouse (center) and rat (right). Drawn from radiographs projected in common height. Vertical lines indicate size of the two smaller bones relative to given size of rat's bone. Photographs at right (both at $\times 25$) illustrate details of distal ends of metatarsals of mouse (below) and rat. Compare with metatarsal in figure 8.

The proximal and middle phalanges differ from each other chiefly in size and in the configuration of their proximal articular surfaces. Each is generally symmetrical in frontal view and is tapered in lateral view. The attachment of the flexor sheath on the edges of the distal plantar surface is not associated with processes and the plantar surface is not grooved for a flexor tunnel. The proximal and distal phalanges of the adult in figure 8 weigh approximately 0.2 and 0.1 mg and are 1.48 and 0.98 mm in length, respectively.

Radiographic anatomy. The internal anatomy of shrew metatarsals and phalanges is most simple. Close examination of all radiographs in the series revealed no vascular channels in the compact walls. Apertures for nutrient vessels penetrate the walls in the proximal and distal quarters of the metatarsals, the exact site being quite variable. In the phalanges, these openings usually are paired and at mid-length. Osteocytic lacunae are prominent in all radiographs, but layering of bone is less obvious than in radiographs of the

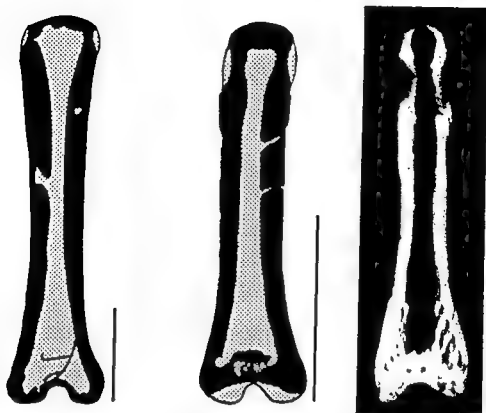


Fig. 11 Proximal phalanges of *S. cinereus*, mouse (center) and rat (right). Camera lucida drawings and radiograph to common height. Vertical lines indicate size of two smaller bones relative to given size of rat's bone ($\times 14$). Middle phalanges are of comparable structure.

femora. Layering does occur and is shown in section in figure 13.

In metatarsals of adults, the compacta is quite uniform in thickness (± 0.11 mm) throughout the entire central tube, although it varies in general between individual bones and is very slightly thinner in those from the immature group. In dorsal-plantar radiographs, it is thinnest immediately proximal to the distal epiphysis; in lateral radiographs, the only consistently thin point is on the plantar surface immediately distal to the proximal articular surface. Unlike the condition in femora, the wall of the metatarsal is thick over most of the articular surfaces. Compacta in the phalanges is, in general, as thick as that of the metatarsal. It is thin only at the middle of the distal articular surface (frontal view) and at the lateral points in the proximal end of the bone.

There is no real spongiosa in the metatarsals and phalanges of *S. cinereus*. In the proximal end of the marrow cavity of

the metatarsal, there are ridges of bone deep to angles of the external articular facets; multiple-position radiographs show these are not free-standing trabeculae. In the distal end of the cavity there also are such ridges, seen best in lateral views (fig. 8). In addition there are thick bony remnants of the distal (and only) epiphyseal line. These vary greatly from specimen to specimen, and may be a thick central mass (as in fig. 8, dorsal-plantar view) or only raised points on the wall. In general, the quantity of such bone is less in the more mature specimens.

In phalanges, the proximal end of the marrow cavity may be marked by variable low ridges. The radiograph of the proximal phalanx in figure 11 shows the most obvious mass encountered in any of the specimens. These, too, appear to be associated with the (proximal only) line of epiphyseal fusion and are less obvious or absent in the more mature bones. The distal end of the marrow cavity in pha-



Fig. 12 Camera lucida drawing from medial-lateral (left) and dorsal plantar radiographs of proximal end third metatarsal of a mature specimen of *M. hoyi*. Represented in grey-tone is a septum-like mass of bone within the marrow cavity, found in one specimen of this species but not in *M. cinereus*. Note isolated trabecula at top of drawing. Shown also are apertures for nutrient vessels and less dense (thinner) protrusions of bone beyond major image of wall. $\times 75$.

anges is a simple, smooth-walled chamber.

In a single specimen of *M. hoyi*, there was an array of trabeculae, forming a perforated septum in the medial-lateral plane near the proximal end of the meta-

tarsal (fig. 12). Two free-standing trabeculae spanned the side of the marrow cavity further distad in that bone. In the proximal phalanx, there were two trabeculae in a cruciform arrangement at the proximal end of the marrow cavity. Other bones of that specimen of the pygmy

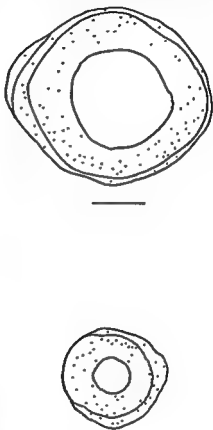


Fig. 13 Camera lucida drawings of midlength cross-sections of left femur and left third metatarsal of mature male specimen of *S. cinereus*. Posterolateral to left. Scale below each indicates 1/5 mm. Dots represent individual osteocytes in lacunae. Empty lacunae and fine circumferential lamellae are not indicated. One complete and one localized increment (identified in radiographs as less dense zones) are shown outside main mass of femoral section. Compare with figure 3. Relationship of increments to second season growth not known for certain. The incomplete layer of new bone on metatarsal was not identifiable on gross radiograph. Based on paraffin sections and undecalcified ground sections. $\times 65$.

shrew did not have unexpected numbers of trabeculae. The rationale for these small masses of bone is, of course, unknown. However, the occurrence of trabeculae in bones that otherwise do not, apparently, require them for mechanical integrity suggests a relationship to hormone balance or nutrition that is worthy of investigation.

The radiograph of the hind foot of a 51 mm, very young male of *S. cinereus* (fig. 9) reveals several interesting features of earlier development of the metatarsal and the phalanges. At the stage shown, endochondral ossification in metatarsals 2, 3 and 4 has progressed all the way proximad and the configuration of that end is essentially that of the adult in figure 8. Endochondral ossification is advancing distad, and there is an ample primary spongiosa. The (distal) growth cartilage is very thick and, in the original radiograph, the image of calcified cartilage could be seen adjacent to the primary spongiosa. The secondary center of the metatarsal is represented only by the very intense mass of calcified cartilage, as is the adjacent secondary center of the proximal phalanx. The most unexpected feature is the state of the diaphysis. This consists of a shell of woven bone interspersed with relatively large spaces. While there is nothing unusual in the basic pattern of development, the fact that a complex of bones of this

developmental status is used in weight-bearing and locomotion by a weaned animal suggests that the foot of living shrews, serially radiographed, might be an excellent indicator in nutritional studies.

Mandible of the shrew

The entire right mandible of an adult specimen of *S. cinereus* is shown in a lateral (lateral-medial) radiograph in figure 14. Portions of the same mandible are represented at higher magnification in figure 15. Figure 16 depicts schematically the distribution of bone and of vascular channels in selected cross-sections of the left mandible.

External configuration. The mandible (fig. 14) consists of an elongated body occupied largely by the alveoli of the teeth, a ramus terminating superiorly in a triangular coronoid process (ramus-coronoid process), a condylar process and a very thin, rod-like gonial process. The length of the illustrated mandible, from tip of incisor to posterior point on condyle, is 8.42 mm and its weight (teeth included) is 6.7 mg.

The body of the mandible is smooth on the medial, lateral and inferior surfaces. A good share of the superior surface is hidden by the overhang of the molars. The teeth are: one incisor, one cuspid, one premolar and three molars. Tooth-wear in shrews is severe because of the abrasive



Fig. 14 Lateral-medial radiograph of right mandible of mature male specimen of *S. cinereus*.
× 15.

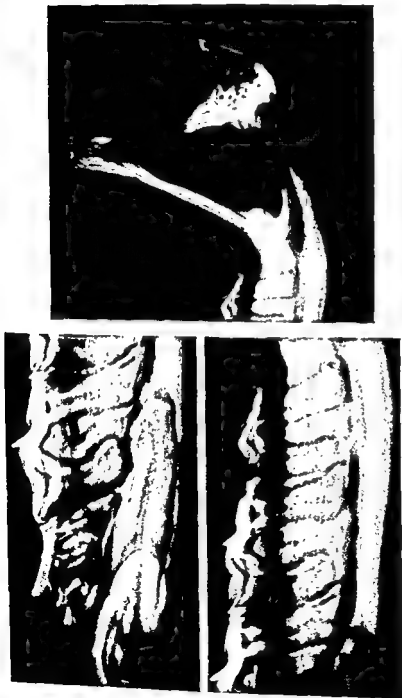


Fig. 15 Lateral-medial radiographs of portions of right mandible of *S. cinereus*. Contact prints of higher magnification negatives of the radiograph represented in figure 14. Right: posterior portion of mandible, including third molar ($\times 20$). Upper left: region of root of incisor and cuspid, premolar and first molar ($\times 33$). Lower left: region of first to third molars ($\times 33$). Cementum obscures some details of roots of teeth and of vascular channels in bone about teeth.

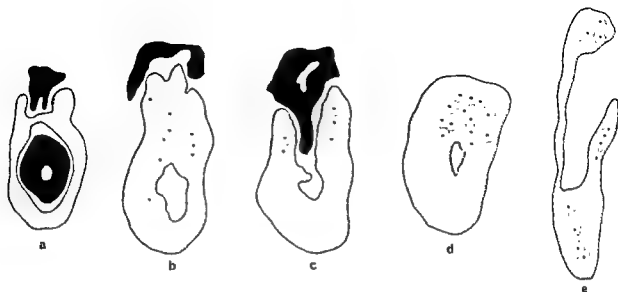


Fig. 16 Camera lucida drawings of selected cross-sections of left mandible of a mature male specimen of *S. cinereus*. Represented are: teeth (black), mandibular canal and alveoli (white), bone (shaded), vascular channels (dots placed, for clarity, in white fields). Sections pass through: a, anterior edge of premolar and middle of incisor; b, middle of second molar and its interradicular bone, and mandibular canal immediately posterior to incisor; c, anterior root of third molar; d, body of mandible posterior to third molar; e, the ramus-coronoid process posterior to its apex and to the mandibular foramen, and anterior to the gonial process. $\times 30$.

grit taken in with food. The heavy wear in the specimen illustrated is typical of mature animals in the size range above 80 mm.

The medial face of the ramus-coronoid process (fig. 15) is marked by a large depression occupied in life by the internal pterygoid muscle. The lower portion of this fossa lies below a sill and the lateral wall is exceedingly thin (fig. 16e). The margins of the fossa (and thus of the ramus-coronoid process) literally are thick rods bordering a triangular bony diaphragm. The condyle, at the posteroinferior corner of the fossa, is as deep in the medial-lateral axis as it is long in the anterior-posterior. (Growth and mechanics of the jaw and of the temporomandibular joint will be the subject of a paper in preparation.) The gonial process arises from the posteroinferior curve of the mandible inferior to the pterygoid fossa. Typically, it ends in a small knob.

Radiographic anatomy. The entire body of the mandible is compacta. The mandibular canal, from the mandibular foramen (inferior to the pterygoid fossa) to the mental foramen (lateral to the incisor) is the only large cavity within the body. From posterior to anterior, the canal com-

municates broadly with the alveoli of the molars and with the incisive alveolus where the canal passes lateral to it. The alveoli of the cuspid and premolar enter the roof of the incisive alveolus. The rest of the mandible, except for the condyle, also is made up of compacta. The thick margins of the pterygoid fossa appear in radiographs as a hollow triangle, for the thin wall of the fossa is almost always invisible at exposures suitable for the more massive portions of the mandible. The same is true of the very thin gonial process.

The only spongiosa in the mandible is in the condylar process. Trabeculae of various thicknesses extend from the anterior to the posterior and from the medial to the lateral walls of a marrow cavity that approximates the external form of the condyle and its articular surfaces.

Unlike the other bones dealt with thus far, the mandible has vascular channels obvious in both radiographs (fig. 15) and cross-sections (fig. 16). One or more channels can be identified in the thick anterior and posterior margins of the ramus-coronoid (figs. 15, 16e). In the apex of the process, there is a labyrinth, the form and size of which vary with the specimen.

The channels in the posterior margin of the ramus-coronoid process connect with the marrow cavity within the condyle. From that cavity, channels can be traced anteroinferiorly to a point slightly anterior to the base of the gonial process, where they connect with the mandibular canal and with channels in the gonial process (which begin in a sizable dilation). Forward of a point just anterior to the base of the gonial process, no vascular channels are found in the bone below the mandibular canal (figs. 15, 16b, c, d). In serial sections, only one channel was found lateral to and paralleling the mandibular canal (fig. 16b). However, in both radiographs and sections, vascular channels are present in the alveolar bone around and between the molars and the premolar. The bone around the cuspid and the incisor, on the other hand, is avascular.

The connections of vascular channels in alveolar bone of the molars and the premolar are quite extensive. Channels immediately posterior to the third molar (fig. 16d) connect with the mandibular canal, and with channels in the anterior margin of the ramus-coronoid process and in the sill of the pterygoid fossa (and thus with the marrow cavity within the condyle). Connections also can be traced to the region about the base of the gonial process (fig. 15). Channels can be followed from the postmolar region anteriorly along the sides of the molar and premolar alveoli. Interradicular and septal bone has channels that penetrate the alveolar cavities and extend to the mandibular canal directly. In figure 15, large vertical channels in the interradicular bone of the first and second molars course upward from the mandibular canal and have lateral connections to the alveoli and to channels in the bone lateral to them. External connections of the intrasosseous channels are difficult to trace in detail. Channels penetrate the compacta around the condylar neck, along the length of the ramus-coronoid process and in a few places on the lateral and medial surfaces of the body.

Paraffin sections of the mandible reveal the vascular channels to be of the primary vascular or non-haversian type. In figure 16, the positions of sectioned channels are

indicated by clear circles; the black points within these are a reasonable approximation of the size of the channels themselves. Although the present material is inadequate for a proper and complete histological analysis, it appears from the regional stain reaction and the distribution of empty lacunae that much of the deep bone below the mandibular canal may be necrotic.

Comparison of bones of shrew, mouse and rat

In figure 7, femora of the shrew, the mouse and the rat are represented by frontal radiographs projected to common (medial condyle to greater trochanter) length. The bones were selected as typical of those of five each of the following: mature male specimens of *S. cinereus* approximately 3 gm in weight; male C57 black mice, 8 months of age, of 29.6 gm mean weight; and male albino rats of 320 gm mean weight. Mean lengths of femora were, respectively, 6.8 mm (6.5–7.2 mm), 14.8 mm (14.5–15.7 mm) and 32.0 mm (31.7–33.0 mm). Mouse and rat femora, thus, are approximately 2.2 and 4.7 times as long as that of the shrew. Mean weights of femora were: shrew, 2.6 mg (1.8–2.9 mg); mouse, 30.0 mg (25.5–36.0 mg); and rat, 348.8 mg (313.8–372.3 mg). The femur of the mouse, thus, weighs approximately 11 times, and of the rat 134 times, that of the shrew. In view of the great differences in body weight, and in weight and length of femur, among the three species, it is important to consider whether the femur of any of these species might in life be subjected to greater loadings than those of the others. Calculation of the ratio of femur weight to body weight (actually, quarter-body weight, as an approximation) yields the same range of values for all three, i.e., approximately 0.25 gm body weight per milligram of femur weight. While this calculation refers to static rather than dynamic loading, it is reasonable in view of the generally comparable postural and locomotory habits in the three species.

Comparison of size and of proportions between bones of the shrew, mouse and rat is not without some danger. It is easy to be superficial and difficult to be complete in distinguishing between size-related

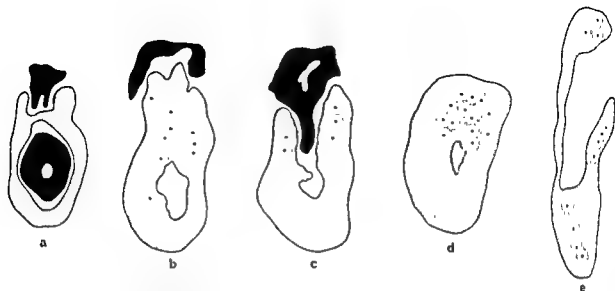


Fig. 16 Camera lucida drawings of selected cross-sections of left mandible of a mature male specimen of *S. cinereus*. Represented are: teeth (black), mandibular canal and alveoli (white), bone (shaded), vascular channels (dots placed, for clarity, in white fields). Sections pass through: a, anterior edge of premolar and middle of incisor; b, middle of second molar and its interradicular bone, and mandibular canal immediately posterior to incisor; c, anterior root of third molar; d, body of mandible posterior to third molar; e, the ramus-coronoid process posterior to its apex and in the mandibular foramen, and anterior to the gonial process. $\times 30$.

grit taken in with food. The heavy wear in the specimen illustrated is typical of mature animals in the size range above 80 mm.

The medial face of the ramus-coronoid process (fig. 15) is marked by a large depression occupied in life by the internal pterygoid muscle. The lower portion of this fossa lies below a sill and the lateral wall is exceedingly thin (fig. 16e). The margins of the fossa (and thus of the ramus-coronoid process) literally are thick rods bordering a triangular bony diaphragm. The condyle, at the posteroinferior corner of the fossa, is as deep in the medial-lateral axis as it is long in the anterior-posterior. (Growth and mechanics of the jaw and of the temporomandibular joint will be the subject of a paper in preparation.) The gonial process arises from the posteroinferior curve of the mandible inferior to the pterygoid fossa. Typically, it ends in a small knob.

Radiographic anatomy. The entire body of the mandible is compacta. The mandibular canal, from the mandibular foramen (inferior to the pterygoid fossa) to the mental foramen (lateral to the incisor) is the only large cavity within the body. From posterior to anterior, the canal com-

municates broadly with the alveoli of the molars and with the incisive alveolus where the canal passes lateral to it. The alveoli of the cuspid and premolar enter the roof of the incisive alveolus. The rest of the mandible, except for the condyle, also is made up of compacta. The thick margins of the pterygoid fossa appear in radiographs as a hollow triangle, for the thin wall of the fossa is almost always invisible at exposures suitable for the more massive portions of the mandible. The same is true of the very thin gonial process.

The only spongiosa in the mandible is in the condylar process. Trabeculae of various thicknesses extend from the anterior to the posterior and from the medial to the lateral walls of a marrow cavity that approximates the external form of the condyle and its articular surfaces.

Unlike the other bones dealt with thus far, the mandible has vascular channels obvious in both radiographs (fig. 15) and cross-sections (fig. 16). One or more channels can be identified in the thick anterior and posterior margins of the ramus-coronoid (figs. 15, 16e). In the apex of the process, there is a labyrinth, the form and size of which vary with the specimen.

The channels in the posterior margin of the ramus-coronoid process connect with the marrow cavity within the condyle. From that cavity, channels can be traced anteroinferiorly to a point slightly anterior to the base of the gonial process, where they connect with the mandibular canal and with channels in the gonial process (which begin in a sizable dilation). Forward of a point just anterior to the base of the gonial process, no vascular channels are found in the bone below the mandibular canal (figs. 15, 16b, c, d). In serial sections, only one channel was found lateral to and paralleling the mandibular canal (fig. 16b). However, in both radiographs and sections, vascular channels are present in the alveolar bone around and between the molars and the premolar. The bone around the cuspid and the incisor, on the other hand, is avascular.

The connections of vascular channels in alveolar bone of the molars and the premolar are quite extensive. Channels immediately posterior to the third molar (fig. 16d) connect with the mandibular canal, and with channels in the anterior margin of the ramus-coronoid process and in the sill of the pterygoid fossa (and thus with the marrow cavity within the condyle). Connections also can be traced to the region about the base of the gonial process (fig. 15). Channels can be followed from the postmolar region anterior along the sides of the molar and premolar alveoli. Interradicular and septal bone has channels that penetrate the alveolar cavities and extend to the mandibular canal directly. In figure 15, large vertical channels in the interradicular bone of the first and second molars course upward from the mandibular canal and have lateral connections to the alveoli and to channels in the bone lateral to them. External connections of the intraosseous channels are difficult to trace in detail. Channels penetrate the compacta around the condylar neck, along the length of the ramus-coronoid process and in a few places on the lateral and medial surfaces of the body.

Paraffin sections of the mandible reveal the vascular channels to be of the primary vascular or non-haversian type. In figure 16, the positions of sectioned channels are

indicated by clear circles; the black points within these are a reasonable approximation of the size of the channels themselves. Although the present material is inadequate for a proper and complete histological analysis, it appears from the regional stain reaction and the distribution of empty lacunae that much of the deep bone below the mandibular canal may be necrotic.

Comparison of bones of shrew, mouse and rat

In figure 7, femora of the shrew, the mouse and the rat are represented by frontal radiographs projected in common (medial condyle to greater trochanter) length. The bones were selected as typical of those of five each of the following: mature male specimens of *S. cinereus* approximately 3 gm in weight; male C57 black mice, 8 months of age, of 29.6 gm mean weight; and male albino rats of 320 gm mean weight. Mean lengths of femora were, respectively, 6.8 mm (6.5–7.2 mm), 14.8 mm (14.5–15.7 mm) and 32.0 mm (31.7–33.0 mm). Mouse and rat femora, thus, are approximately 2.2 and 4.7 times as long as that of the shrew. Mean weights of femora were: shrew, 2.6 mg (1.8–2.9 mg); mouse, 30.0 mg (25.5–36.0 mg); and rat, 348.8 mg (313.8–372.3 mg). The femur of the mouse, thus, weighs approximately 11 times, and of the rat 134 times, that of the shrew. In view of the great differences in body weight, and in weight and length of femur, among the three species, it is important to consider whether the femur of any of these species might in life be subjected to greater loadings than those of the others. Calculation of the ratio of femur weight to body weight (actually, quarter-body weight, as an approximation) yields the same range of values for all three, i.e., approximately 0.25 gm body weight per milligram of femur weight. While this calculation refers to static rather than dynamic loading, it is reasonable in view of the generally comparable postural and locomotory habits in the three species.

Comparison of size and of proportions between bones of the shrew, mouse and rat is not without some danger. It is easy to be superficial and difficult to be complete in distinguishing between size-related

characteristics and those more directly relatable to evolved functional interactions between bone and muscle in insectivores and in rodents. The latter category is exemplified by the similarity of outlines of the upper half of the femur of the two rodents, yet the gluteal crest of the mouse is very large and is reflected in internal structure of the diaphysis while that of the rat is smaller and has little influences on internal structure.

The most obvious proportional distinction between the femur of the shrew and those of the mouse and the rat is in the dimensions and distribution of compacta and spongiosa. Relative to length the femur of the shrew has the narrowest diaphyseal midsection but the thickest compacta. Unlike that in the rodents, it tapers sharply to the thin surfaces of the metaphyses and epiphyses, especially at the proximal end. The cortex of the proximal and distal ends is proportionally thicker in the shrew than in the mouse and the rat. Within the metaphyses and epiphyses, there are relatively fewer trabeculae but they are relatively thicker than in the other species.

Comparison of both relative and absolute thickness of the diaphyseal compacta reveals a most interesting condition. The diaphyseal wall thickness at midlength in the shrew femur is approximately 70% and 46% of that in femora of the mouse and rat, respectively; in proportion to the differences in femoral length, one would expect these to be approximately 46% and 21%. This poses an enigma. The compacta of the femoral diaphysis is vascularized in both the mouse and the rat, as has been described by Enlow ('62a, b), while the femur of the shrew is avascular. The distance between a mid-depth osteocyte or lamina of bone and either the periosteal or endosteal surface in the shrew (fig. 13) is greater than the distances we have observed between such points and either a surface or a vascular channel in sections of femora from the mouse and rat. As was stated in regard to the mandible, the present material is not such as to allow a suitable analysis of the possible relationship of this spatial condition to apparently acellular (vacant lacunae) areas found in paraffin sections. However, the available information does lead to the

conclusion that the femur of the shrew must have the thickest avascular compacta that one should expect to find in limb bones in a mammal. That avascularity is not a mandatory characteristic of the shrew skeleton is shown by the presence of vessels in the mandible. However, the specific location and the number of channels adjacent to teeth implies that these are for the maintenance of dental tissues. Clearly, there is a threshold for vascularity of both femora and tubular foot bones somewhere between the size of those in the shrew and those in the mouse.

Metatarsals and proximal phalanges of the shrew, the mouse and the rat are shown at common length in figures 10 and 11 respectively. For the gross structure of the entire metatarsal of the shrew, a line drawing suffices (Compare figs. 8, 10); for the mouse and rat, line drawings are supplemented by radiographs of the distal regions. The proximal phalanges of the shrew and the mouse also can be represented adequately by line drawing, but the entire phalanx of the rat is shown in a radiograph. The radiographs in figures 10 and 11 show the vascularity of the bones of the mouse and rat, and sections have revealed channels like those in their femora.

Except in the distal regions, gross structure of metatarsals of the three species is very similar (fig. 10). Species differences in articulations aside, the proximal ends of metatarsals of the mouse and the rat are, as in the shrew, thick-walled and without trabeculae. The fused distal epiphyseal line in the metatarsal of the mouse (fig. 10) resembles the irregular mass of bone seen at the same place in the metatarsal of the shrew (fig. 8); however, in the mouse there are several small cavities within the mass and, where it attaches to the wall, minute buttresses can be identified. In the rat, the terminal plates of the distal metaphysis and of the secondary center are supported by true trabeculae. Below the epiphyseal line these rods of bone extend distad and centrad from the wall to the terminal plate; about the epiphyseal line an irregular pattern of trabeculae extend from side to side within the secondary center and relate the ter-

minal plate and the articular surface. In all three species there is considerable individual variation in relative thickness of the diaphyseal wall, but in general the proportion to length is in the same range in the shrew and the mouse, and is slightly less in the rat. In the rat metatarsal, the wall thins out in the region where the trabeculae are attached.

The distal regions in the proximal phalanges of all three species are thick-walled and free of trabeculae (fig. 11). The proximal ends of these bones in the shrew and mouse are without spongiosa but have the ridges and the remnants of epiphyseal fusion described earlier. The proximal end of the phalanx of the rat, however, has essentially the same trabecular structure as the distal end of the metatarsal.

The fact that the femora of all three species have spongiosa, and that the tubular foot bones of the shrew and mouse do not, implies that the presence of spongiosa in a particular bone is a matter of its size. Metatarsals and phalanges of large animals have tapered diaphyseal walls, thin cortices on the metaphyses and epiphyses, and an organized pattern of relatively fine trabeculae. In the same bones in the rat, a few trabeculae are present as a simple load-distributing system. In the mouse and shrew, these bones are without spongiosa and the proximal and distal ends are thick-walled. Primary spongiosa forms during endochondral ossification in the tubular foot bones of the shrew and the mouse, and is not modified and retained in the adult. It may be assumed, therefore, that there is a need for trabecular support within metatarsals and phalanges of mammals somewhat larger or heavier than mice. In the femur of the shrew a very few trabeculae, relatively thick but absolutely not much finer than those in the mouse and rat, serve the function of dozens or hundreds of trabeculae in larger femora. Perhaps this is best exemplified by the simple compression tract in the neck and head. One might theorize that a mammal a bit smaller than the shrew would have no femoral spongiosa, but would have thick walls in its metaphyses and epiphyses. In the absence of such a mammal, perhaps the bones of small reptiles will yield information on this point.

ACKNOWLEDGMENTS

The authors are most appreciative of the assistance of the staff members of the University of Minnesota Museum of Natural History named in the introductory text. Microradiographs were prepared by Mr. O. V. Heath of our laboratory and photography was by members of the Department of Medical Art and Photography. Manuscript preparation was by Mrs. Sharon Waldstein.

LITERATURE CITED

- Burt, W. 1948 Mammals of Michigan. University of Michigan Press, Ann Arbor.
- Crowcroft, P. 1957 The Life of the Shrew. Max Reinhardt, London.
- Enlow, D. H. 1962a A study of the post-natal growth and remodeling of bone. *Am. J. Anat.*, 110: 79-102.
- 1962b Functions of the haversian system. *Am. J. Anat.*, 110: 269-306.
- Enlow, D. H., and S. O. Brown 1956 A comparative histological study of fossil and recent bone tissues. Part I. *Tex. J. Sci.*, 8: 405-443.
- Felts, W. J. L. 1964 The determination of bending and of transverse breaking strength in femora of inbred mice. (*Abst.*) *Anat. Rec.*, 148: 281.
- 1966 Some structural and functional characteristics of flippers and flukes in cetaceans. In: *Whales, Porpoises and Dolphins*, K. S. Norris, ed. University of California Press, Los Angeles.
- Felts, W. J. L., and J. M. Grewe 1965 Microradiographic and histologic appearance of mouse mandibles after extraction of mandibular incisors. (*Abst.*) *Anat. Rec.*, 151: 349.
- Felts, W. J. L., and F. A. Spurrell 1965 Structural orientation and density in cetacean humeri. *Am. J. Anat.*, 116: 171-203.
- 1966 Some structural and developmental characteristics of cetacean (odontocete) radii. A study of adaptive osteogenesis. *Am. J. Anat.*, 118: 103-134.
- Grewe, J. M. 1966 Histologic and microradiographic investigation of the consequences of mandibular incisor extraction in the young mouse. Thesis (Ph.D.), University of Minnesota, Minneapolis.
- Ham, A. W. 1957 Histology (third edition). J. P. Lippincott, Philadelphia.
- Jowsey, J. 1963 Microradiography of bone resorption. In: *Mechanisms of Hard Tissue Destruction*, R. F. Sognnaes, ed. *Am. Assoc. Adv. Sci.*, Washington, D. C.
- Jowsey, J., P. G. Kelly, L. Riggs, A. J. Bianco, Jr., D. A. Scholtz and J. J. Cohen 1965 Quantitative microradiographic studies of normal and osteoporotic bone. *J. Bone and Joint Surg.*, 47-A: 785-807.
- Koch, J. C. 1917 The laws of bone architecture. *Am. J. Anat.*, 21: 177-298.
- Lacroix, P. 1951 The Organization of Bones. Translated by S. Güder. The Blakiston Company, Philadelphia.

- McLean, F. C., and R. E. Rowland 1963 Internal remodeling of compact bone. In: Mechanisms of Hard Tissue Destruction, R. F. Sognnaes, ed. Am. Assoc. Advance. Sci., Washington, D. C.
- Spurrell, F. A., W. J. L. Felts and L. V. Baudin 1966 Osteon development in swine. In: Swine in Biomedical Research, L. K. Bustad and R.

- O. McClellan, ed. Frayn Printing Company, Seattle, Washington.
- Tobin, W. J. 1955 The internal architecture of the femur and its clinical significance. J. Bone and Joint Surg., 37-A: 57-73.
- Thompson, D' A. W. 1942 On Growth and Form (second edition). Cambridge University Press, Cambridge.

Tolerance of the Facial Bones to Impact

VOIGT R. HODGSON

Biomechanics Research Center, Wayne State University,
Detroit, Michigan

ABSTRACT A study of the tolerance of the facial bones to blunt impact has been conducted for the purpose of determining the mechanics and important parameters affecting fracture. Such information is urgently needed for the safe design of vehicles and protective equipment, and would serve a useful purpose as an aid in the diagnosis and treatment of facial injuries. Work to date has been concentrated around the zygomatic bone because of its amenability to mathematical analysis and susceptibility to damage due to its relative fragility and prominence. The force to fracture the bone has been found to be time dependent. For example, high forces up to 1,000 pounds can be tolerated for extremely short time durations of 3 milliseconds or less. Impacts lasting beyond 4 milliseconds produce fracture near 200 pounds. These figures are for a 1 inch square area, and it has been found that for impulses lasting longer than 4 milliseconds the tolerance of the zygomatic bone can be raised by a factor of 150 to 250% if the load is distributed over the entire bone. A linear fracture around one zygomatic bone has been found not to affect the structural integrity of the opposite side of the face, which fact has been very useful in comparing parameters on the same cadaver. In comparing the impact strength of three facial bones on each of four cadavers, the frontal bone has been found to tolerate a force three or four times higher than the mandible and zygomatic bone which are about equal.

This study was begun in 1960 by Patrick and Lange ('65) to determine the important parameters affecting injury to the facial bones. The initial approach to the problem was with the use of static loads on Stresscoat-covered human skulls to determine the critical areas in terms of susceptibility to damage due to prominence and/or fragility. The areas chosen for closer scrutiny in the dynamic phase of the experiment were in the vicinity of the zygomatic bone, zygomatic arch, maxilla, and the neck of the mandible.

A mathematical model was introduced which described the response of the zygomatic bone and the zygomatic arch of embalmed human cadavers to blunt, rigid body impact sufficiently well to clarify the mechanics involved (Hodgson, Talwalker and Nakamura, '66). These two bones are uniquely shaped and situated as to allow a deflection measurement relative to the skull to be taken and thereby establish a correlation between static and dynamic response necessary for analysis. The conclusions drawn from this study were that the parameters which determine tolerance to a blow were force and time duration of impact, and load distribution. Force and time of impact, in turn, are dependent

upon impact velocity, elastic and/or plastic properties of the bone and colliding surface, and the mass of the head and colliding body. The load distribution is dependent upon the skin thickness and the shape and deformation properties of the colliding surface (Hodgson, Lange and Talwalker, '66).

In this phase of the investigation the previous knowledge and experience was applied specifically to the zygomatic bone: to determine its tolerance, effect of load distribution and compare its strength to other bones of the face.

MATERIALS AND METHODS

A machine was designed to deliver controlled energy blows at precise blow locations by accelerating solid metal cylinders ranging in weight from 2 to 16 pounds to velocities up to 100 feet per second. Essentially, the machine consists of a high pressure air tank, a fast-acting valve, and an air cylinder. The compressed air drives the piston rod of the cylinder through the valve to a point approximately six inches short of impact with the target at which time a striker slides out of the end of the piston rod of the air cylinder past two magnetic probes spaced three inches apart

and then strikes the face. The velocity of the striker is obtained from the time required to sweep past the two magnetic probes. An accelerometer mounted on the rear of the striker determines the deceleration of the striker at impact from which the force as a function of time is obtained.

The cadaver material used in these experiments came from the same source as that used to supply the medical school students. A list of cadavers and physical descriptions is shown in table 1. There was considerable variation in bone structure and soft tissue among the cadavers which were generally over 60 years of age, and ranged in weight from 116 to 238 pounds. The cadavers are prepared by flexing the joints until they can be strapped in a sitting position. Initially, a modified operating chair was used to hold the cadaver, but this has been replaced by a swing as shown in figure 1. A crystal-type accelerometer is mounted opposite the blow location to record head response to the blow.

During the investigation, blows have been delivered directly from metal to bone, with soft tissue intact, and through various types and thicknesses of padding. However, most of the blows have been delivered to the intact soft tissue over an area of 1 square inch. Several blows were also distributed over 5.2 square inches, the

area obtained with a 2.563-inch diameter striker which circumscribes the zygoma bone of most cadavers. For all the experiments the bone and tissue were kept as moist as practically possible, and during test intermissions the face was covered with wet gauze and a plastic bag.

The shape of the striker accelerometer pulse was used as a guide to determine the fracture threshold. For a blow to an intact bone, the pulse has an approximately half sine shape typical of an elastic impact. When a bone is fractured, some of the energy is dissipated in scraping and tearing, and this fact is revealed in the form of jagged or high frequency components superimposed upon the main pulse. This method of detection made it possible to terminate an experiment very close to the fracture threshold. The number of blows to cause fracture was kept at a minimum, usually five or six. The fractures were located by x-rays of the subject before and after the experiment and by reflecting the soft tissue after the experiment.

RESULTS

The oscillograph records shown in figure 2 illustrate clearly how fracture threshold and depressed fractures from subsequent blows can be detected. These are records of striker and head acceleration for blows to the left zygoma of cadaver

TABLE 1
Vital statistics of cadaver material

Cad. no.	Age	Weight	Date of death	Cause of death	Date of embalming	Date of test	No.
594	74	149	12-12-63	M. I.	12-14-63	4-21-64	1
569	64	218	8-29-63	Coronary occlusion	9-27-63	6-12-64	2
685	73	125	6-23-64	Cancer of esophagus	6-29-64	8-17-64	3
661	73	184	4-26-64	Lumbar pneumonia	4-28-64	9- 8-64	4
595	72	168	12-12-63	Cerebral vascularity	12-14-63	10- 5-64	5
717	72	150	8- 2-64	Acute coronary occlusion	8- 4-64	8-30-65	6
847	67	180	8-12-65	Bilateral pneumonia	8-17-65	9-23-65	7
770	82	116	1-23-65	Myocardial infarction	1-26-65	10- 1-65	8
837	53	238	7-24-65	Uremia and pulmonary edema	7-27-65	10- 4-65	8
807	75	146	4-30-65	Pneumonia	5- 3-65	10-11-65	10
494	67	170	3-19-63	Cerebral thrombosis	3-25-63	10-12-65	11
821	60	180	5-29-65	Natural causes	6- 3-65	10-14-65	12
812	72	125	5-12-65	Pneumonia	6- 2-65	12-16-65	13
772	81	172	1-24-65	Cancer of liver	1-29-65	12-21-65	14
785	74	140	3- 4-65	Cerebral vascular accident	3- 9-65	12-28-65	15
905	74	140	12-10-65	Carotid heart disease	12-10-65	1-19-66	16
907	59	120	12- 9-65	Cancer of pancreas	12-10-65	1-24-66	17
771	84	170	1-24-65	Septicemia	1-26-65	1- 6-66	18
738	87	130	10- 8-64	Pneumonia	10-10-64	1- 4-66	19



Fig. 1 Cadaver positioned in a swing to receive a blow to the left zygomatic bone with a 12 pound striker.

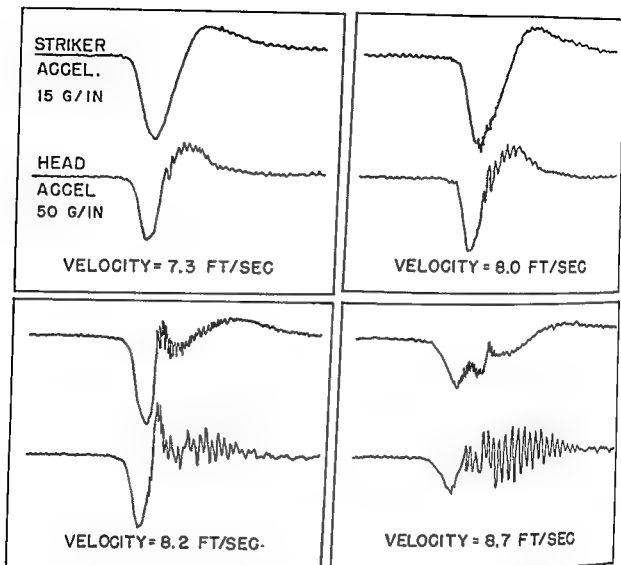


Fig. 2 Oscillograph records of striker and head accelerations due to a blow to the zygomatic bone of Cadaver 847. The striker curve indicates an elastic impact in the upper left; a linear fracture in the upper right; subsequent depressed fractures in lower photographs.

no. 847 using a 12-pound striker with the blow distributed over an area of 1 square inch through intact soft tissue and a 0.250 inch soft rubber pad. The striker accelerometer, which communicates with the blow site through the rigid striker, is usually the best criterion of fracture, and its trace will be used in the following discussion. In the upper left photograph, the trace indicates that the energy delivered to the bone has been stored and released elastically as indicated by the near half sine wave response. In the upper right trace it can be observed that a high frequency component has been added to the response pulse near and just beyond the peak de-

celeration of the striker. This indicates that some of the energy absorbed by the bone has been dissipated in the tearing and scraping action of fracture. Subsequent blows as shown in the lower part of the figure are indicative of a depressed fracture.

Further refinement of the technique of detecting the threshold of fracture can be obtained by plotting force versus velocity for all the blows up to and including fracture threshold. Figure 3 is a plot of data from blows to the face of cadaver 717 with a 12-pound striker with the blow distributed over an area of one square inch through a 1-inch thick vinyl pad with soft

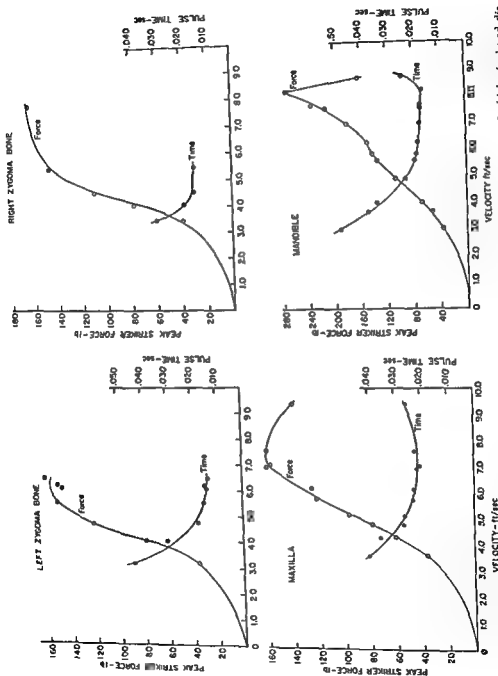


Fig. 3 Tolerance curves for the facial bones of Cadaver 717. The blows were delivered through one inch thick vinyl pad distributed over one square inch. Deflection characteristics of the padding predominate below a velocity of 4 ft/sec above which the elastic properties of the bone are dominant until failure occurs.

tissue removed from the bone. The purpose of removing the soft tissue was to eliminate a variable and replace it with a consistent energy absorber thick enough to distribute the force over the convex surface of the bone. Velocity of impact is plotted on the abscissa versus peak striker force on the left ordinate and base line pulse time on the right ordinate. The interpretation of the curves for the left zygomatic bone in the upper left are as follows: The lower portion of the force versus velocity curve takes its shape due to the predominant characteristics of the vinyl foam at low impact velocities. At higher velocities, the padding is squeezed between the striker and the facial bone to the point where most of the air has been extruded so that the elastic properties of the bone predominate causing a nearly linear relationship between force and velocity from 80 up to about 150 pounds force. At or near this point the load falls off abruptly. The maximum energy-absorbing capability of the bone has been reached for this type of load application and failure in the form of a linear fracture occurs.

The time versus velocity curve has a similar interpretation. At the lower impact velocities the relatively soft characteristics of the vinyl foam predominate and the impact pulse time varies with velocity. Over the portion of the curve corresponding to the nearly linear portion of the force versus velocity curve, the pulse time versus velocity curve is essentially constant. The plot of points for the other bones follows a similar pattern.

Figure 4 is a plot of data for the right and left zygomatic bones of cadavers showing the relationship between peak striker force and base line pulse time for blows with strikers ranging in weight from 1 to 12 pounds. The curved line has been drawn as the best fit through the points which were obtained by striking an area of 1 square inch. Normally, a blow by a rigid body to a facial bone will produce an impact with an extremely short time duration in the neighborhood of 1 to 3 milliseconds as measured on the base line of the pulse. Consequently, in order to produce the spread of pulse time shown, the impact conditions were varied from direct impact to the soft tissue covered

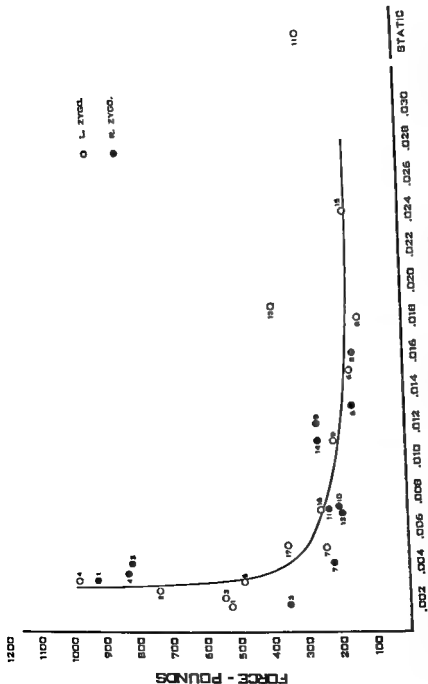
bone, to 1 inch of padding over the intact soft tissue. Much of the data obtained for this plot were from both the right and left zygomatic bones of the same cadaver.

Below 4 milliseconds the data tended to be erratic. For instance, Cadaver 1¹ fractured on the right side at 930 pounds, 3 milliseconds, and fractured on the right side at 530 pounds, one and one-half milliseconds. Other values below four milliseconds varied between 350 and 975 pounds. Beyond 5 milliseconds most of the data lie between 150 and 250 pounds. Cadaver 11 was struck on the right side with a resultant tolerance figure of 230 pounds and seven milliseconds. The left side was loaded statically and fractured at a force of 275 pounds.

Most cadavers fractured on each side of the face at approximately the same force level (see, for example, cadavers 6, 7, 8, and 9). Cadaver 13 which fractured at 375 pounds, 19 milliseconds was the strongest cadaver in the group. It is the only cadaver which departed significantly from the fracture band of 150-250 pounds for impacts lasting beyond 5 milliseconds. As the tests continue, undoubtedly more data points will fall outside of this band, particularly above it. However, it is doubtful if many will fall below the 140 pounds recorded for cadaver 8, an 82 year old, 116 pound male. Presumably, the female population might fall on the lower edge of or below the data obtained from this experiment in which all of the subjects were old, embalmed males and in which the fine-featured individuals tended to be lowest. However, in some cases the fine features were associated with a compactness which increased their strength, so that fine features in themselves are not criteria of weakness.

In table II are given the associated forces, pulse time, velocity, energy and load distribution factors as a basis for comparison of the frontal bone, mandible, and the zygomatic bone of four cadavers. All tests were conducted with the load distributed over 5.2 square inches of area and using 1 inch of polyurethane padding with intact soft tissue. The range of force and time to fracture the frontal, mandible and zymo-

¹ Cadaver numbers have been shortened on figure 4 for convenience. See table 1.



PULSE TIME - SECONDS

Fig. 4 Force and pulse base line time to cause linear fracture for the zygomatic bone of the embalmed cadaver. Note the similar fracture levels for right and left side of Cadavers 6, 7, 8, and 9. Impacts below 0.004 seconds were more erratic, viz: Cadavers 1, 2, 3, and 4.

TABLE 2

Comparison of tolerance to blunt¹ impact of frontal, mandible and zygomatic bone of embalmed male cadavers

Cadaver	Age	Weight	Blow location	Peak force	Base time	Velocity	Energy	Location of fracture ²
		lb		lb	sec	ft/sec	ft-lb	
905	74	140	Fr.	2050	0.004	25.0	117	Blow site to R. and L. orbit
			M.	576	0.008	16.1	48	4R, 4L
			R. Z.	396	0.014	15.6	45	1, 2, 3
907	59	120	Fr.	1980	0.004	28.0	146	Blow site to R. orbit
			M.	588	0.005	15.6	45	4L
			R. Z.	648	0.009	17.2	55	1, 2, 3
738	87	130	Fr.	1660	0.004	17.9	60	Blow site to R. orbit
			M.	600	0.008	14.3	38	4R, 4L
			R. Z.	390	0.019	13.2	33	2
771	84	170	Fr.	943	0.005	17.3	56	Blow site to R. orbit
			M.	360	0.008	11.9	26	4L, 4R
			R. Z.	360	0.014	12.5	29	1, 2, 3

¹ All blows distributed over 5.2 sq in area.

² Refer to figure 5.

Fr. — Frontal.

M. — Mandible.

R. Z. — Right Zygomatic.

matic bones were, respectively: 943 to 2050 pounds, 4 or 5 milliseconds; 360 to 600 pounds, 5 to 8 milliseconds; and 360 to 648 pounds, 9 to 19 milliseconds. The data is limited but is included in order to impart some idea of the magnitude of the agents involved in a fracture-producing impact to the facial bones under these specific sets of conditions, and also to show the strength of the zygomatic bone relative to the other bones of the face. For the frontal blows the head of the cadaver was tipped forward so that the striker delivered the blow flush and centered on the forehead. The mandible blows were delivered to the symphysis menti with line of action through the temporomandibular joint. Blows to the zygomatic bone were delivered to the most prominent point directly under the zygomatico facial foramen with line of action horizontal and 30 degrees to the median sagittal plane with the cadaver sitting erect. For these tests the body of the cadaver was restrained from moving by being situated in an operating chair. However, the head was free to move.

Fractures of the frontal bone had no set pattern but generally ran down into one or both of the orbits. The mandible generally fractured on one or both necks, but in one other case dislocation of the

head and temporomandibular joint occurred along with fracture on both sides approximately through the mental foramen. The zygomatic bone invariably fractured at or near one of the sutures through which it articulates with the zygomatic processes of the zygomatic arch, temporal bone, and maxilla. See figure 5 for fracture locations.

The effect of increasing the load distribution area from 1.0 to 5.2 square inches for the zygomatic bone is shown in table 3. The force to fracture generally increased from 150 to 250% with a somewhat corresponding energy increase required to obtain fracture at the larger area, which is listed second for each cadaver except 738. Blows to both left and right zygomatic bones of cadaver 738 were distributed over an area of 5.2 square inches and fractured at nearly the same force and location. The other cadavers almost all fractured at similar locations on the right and left side also.

DISCUSSION

A collision between two bodies results in an equal and opposite force, varying in time, which acts on each body during the period of contact. The integral with respect to time over the contact period of this force is referred to as impulse. For

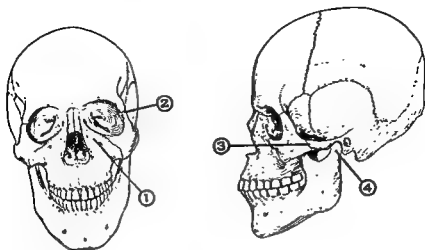


Fig. 5 General location of fractures to the zygomatic bone and mandible. Corresponding locations were found on the right side.

TABLE 3
Comparison of effect of increasing load distribution from 1 sq in to 5.2 sq in¹

Cadaver	Peak force lb	Base time sec	Velocity ft/sec	Energy ft-lb	Location of fracture ²
772-R	252	0.016	15.0	42	1, 2, 3
772-L	583	0.026	25.8	124	1, 2, 3
812-L	374	0.019	14.5	39	1, 2
812-R	756	0.020	25.4	120	1, 3
821-L	190	0.007	12.8	30.5	—
821-R	480	0.009	17.4	57	—
905-L	252	0.007	8.6	11	1, 2, 3
905-R	396	0.014	15.6	44	1, 2, 3
907-L	348	0.005	11.4	24	1, 2, 3
907-R	648	0.009	17.2	53	1, 2, 3
738-L	360	0.019	13.2	33	2
738-R	390	0.019	13.2	33	2

¹ One square inch data listed first for each cadaver except 738 in which both tests were with 5.2 sq in area.

² Refer to figure 5.

impact involving a given amount of energy, the resultant impulse experienced by the body of interest, in this experiment a cadaver with the force exerted on a facial bone, will be the same whether the blow is received directly on the bone or through energy-absorbing material. The difference will be in the shape of the impulse, or force-time curve (see fig. 2). With no padding material, the force will be high and time duration extremely short, while the force will be lower and of longer dura-

tion in the case with an energy absorber. If the velocity of impact through an energy-absorbing material is increased, the pulse time will continue to decrease down to a minimum duration determined by the load-deflection characteristics of the bone and material, while the force will continue to rise, limited only by the fracture tolerance of the bone. At some force-time combination, the strain energy at a point in the bone will reach a limit and the bone will fail. The energy required to produce

this failure is thus seen to depend upon, among other things, the material interposed between the striking object and the bone which, of course, includes the highly variable soft tissue.

The amount of energy also depends upon the restraint imposed upon the body. This is to say, for example, the energy to produce fracture for a cadaver sitting in an immovable operating chair will be different and less than that required to produce fracture with a cadaver sitting in a swing free to move since in the latter case energy is expended in moving the cadaver. However, this difference will also depend upon the relative sizes of the mass of the head and the striking device. For example, given two moving projectiles with the same energy ($E = \frac{1}{2} mv^2$), proportionately more of the energy of the smaller, faster-moving object will be spent in producing local deformation at the impact site, than that of the heavier, slower-moving body which will tend to cause more head movement.

Another factor which must be considered is the force distribution. It is difficult on the face to determine quantitatively the effect of varying the area of impact because of undulating surface, but there is no question that increasing the area increases the amount of energy which can be absorbed before fracture occurs (see table 3). Swearingen ('65) found that a machine which readily produced fracture of individual facial bones of cadavers could not produce a fracture when the impact was distributed over the entire face by means of a molded block.

It is apparent that the manner in which energy is dissipated or transferred in a collision is dependent upon boundary and impact surface conditions so that a tolerance based upon tests conducted on an intact human cadaver in terms of energy is practically impossible to attain. Striker force has been used as the tolerance parameter in these experiments because it can be conveniently measured by the use of today's fast response accelerometers and signal conditioning equipment. Also, the force sensed by the striker is that part of the original kinetic energy which is doing work on the bone even though the associated deflection cannot generally be measured.

Any tolerance values, if they are to be useful, should be given for the most critical loading condition; i.e., line of action, center of load application, and area of distribution. It is not feasible to determine tolerance for every size of area, but a choice was made of one square inch. This constitutes a convenient unit area which is standard with which to compare as more becomes known about the effect of load distribution. Also, it constitutes a convenient size which is large enough to be considered blunt, but small enough to be distributed over any protuberance of the face. As such, it is felt that data obtained for the zygomatic bone approximates the most critical condition for this bone based upon laboratory and clinical experience, and therefore will have the broadest application for those interested in protecting the face. Tests comparing impact to fresh and embalmed cadavers are now being conducted.

ACKNOWLEDGMENT

The author gratefully acknowledges the initial guidance and continued support and direction of Professor Lawrence M. Patrick and William A. Lange, M.D., and also the dedicated technical assistance of Mr. Eugene Dupuis in conducting the experiments.

LITERATURE CITED

- Hodgson, V. R., W. A. Lange and R. K. Talwalker 1966 Injury to the Facial Bones. The Ninth Stapp Car Crash Conference Proceedings, The Nolte Center for Continuing Education of the General Extension Division of the University of Minnesota, Minneapolis, Minnesota.
- Hodgson, V. R., R. K. Talwalker and G. S. Nakamura 1966 Response of the Facial Structure to Impact. The Eighth Stapp Car Crash Conference Proceedings, Wayne State University Press, Detroit, Michigan.
- Patrick, L. M., W. A. Lange, and V. R. Hodgson 1965 Facial Injuries — Causes and Prevention. The Seventh Stapp Car Crash Conference Proceedings, Charles C Thomas, Publisher, Springfield, Illinois.
- Swearingen, J. J. 1965 Tolerances of the Human Face to Crash Impact. Federal Aviation Agency, Office of Aviation Medicine, Civil Aeromedical Research Institute, Oklahoma City, Oklahoma.

Bone Fractures Produced by High Velocity Impacts¹

DONALD F. HUELKE, LYNN J. BUEGE, AND JAMES H. HARGER
*Department of Anatomy, The University of Michigan,
Ann Arbor, Michigan*

ABSTRACT The effects of high velocity impact to the distal end of 122 human femurs were studied using one-quarter inch steel spheres as projectiles, with impact velocities from 500 to 1700 feet per second. In the lower velocity range, a "drill hole" fracture was produced with low energy expenditure, and the diameter of this type of fracture was increased as a function of increasing velocity. At the higher impact velocities the bone exploded with a violent radial displacement of the material surrounding the missile path, similar to the cavitation effect often seen in soft tissues. At increasing impact velocities, increasing amounts of energy were expended in producing the fracture.

Although there have been many experimental studies on the effects of high velocity impacts to animals or animal tissues (Dziemian et al., '61; Harvey et al., '47; Harvey and McMillen, '47; and Krauss, '57), only a few have been concerned primarily with bone (Horsley, 1894; Keith and Hall, '19; and Grundfest, '45). The literature on the effects of high velocity impacts has been summarized in *Wound Ballistics* (Coates and Beyer, '62), an outstanding compilation and review of the pertinent studies in this field.

Most studies have dealt with the response of soft tissues to high velocity impacts. In these studies tissue damage has been attributed to not only the direct impact of the projectile but also to the rapid radial displacement of the tissues. As the projectile passes through the tissue, radial displacement of the tissue about the path of the projectile produces a temporary cavity of very short duration and many times the diameter of the projectile. Infrequently it has been noted that bones located near but not in the missile's path can be fractured by this cavitation phenomenon. The presence of a temporary cavity in bone has been suggested by Harvey, et al. ('62) and Huelke and Darling ('64).

Most previous studies on the effects of high velocity impact on human bone have been limited to clinical descriptions of wartime wounds or museum specimens (LaGarde, 1895; Keith and Hall, '19; and Harvey et al., '62). Because of the sig-

nificant differences between animal and human bone in density, strength, and bone architecture, extrapolation of the data from animal subjects to human material is open to question.

In this report, therefore, we will describe the effects of impacts of steel spheres at various impact velocities on the distal end of human femurs.

MATERIALS AND METHODS

In this study 122 embalmed human femurs were used. The popliteal surface between and slightly above the condyles was the target point. In this region the bone consists of a thin cortical shell enclosing a core of cancellous bone. Throughout the study one-quarter inch diameter, 16.1 grain steel spheres were used as projectiles.

By using steel spheres instead of bullets, the problems of pitch and yaw of the projectile were eliminated. The non-deformable sphere presented the same surface area to the target at all times, whereas the nose of a bullet tends to flatten or mushroom, thereby changing the surface area presented to the target specimen.

The steel spheres were fired from a specially designed helium-operated gun. Projectile velocities between 500 and 1700 ft/sec were used in this study by varying

¹This research was supported by U.S.P.H.S. grant AC-00196 from the Division of Accident Prevention, Bureau of State Services, and, in part, by the General Research Support grant FR-05383-04 to The University of Michigan Medical School.

the gas pressure in the gun. The gun, positioned on a rigid table approximately six feet from the securely mounted bone, was fired with a pneumatic valve activated by a Wollensak Control Unit (model WF-301). Behind the bone a projectile recovery box filled with sand and lined

with one-quarter inch steel plate prevented the escape or ricochet of the spent projectile. The impact velocity was determined by measuring the time duration of the projectile's passage through two thin electronic grids positioned exactly one foot apart. When the projectile

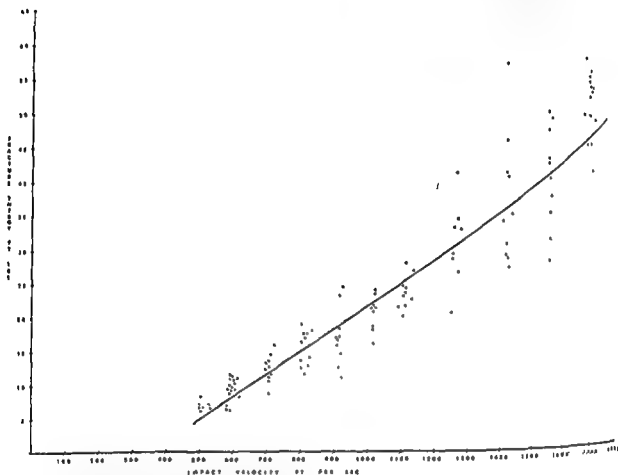


Fig. 1 The relation between impact velocity and energy expended in fracturing the distal area of human femurs by one-fourth inch steel spheres.

TABLE 1
Average values for distal femoral impacts with one-fourth inch spheres

No. of tests	Entrance velocity	Exit velocity	Entrance energy	Exit energy	Energy expended	Percentage energy loss
	ft/sec	ft/sec	ft-lbs	ft-lbs	ft-lbs	%
10	508	175	9.2	1.6	7.6	82.6
16	590	272	12.3	2.9	9.5	76.8
10	701	359	17.4	4.8	12.7	72.6
11	806	453	23.0	7.5	15.5	67.3
10	905	563	29.0	11.6	17.4	59.9
10	1006	624	35.8	14.1	21.7	60.7
10	1101	735	42.9	19.2	23.8	55.3
8	1250	821	55.3	24.2	31.1	56.0
11	1410	957	70.3	33.1	37.2	53.0
10	1548	1111	84.9	45.4	40.8	48.0
14	1697	1198	101.9	51.0	51.0	50.0

pierces the first grid, a counter chronograph (Electronic Counters, Inc., model 464T) is activated; when the second grid is pierced, the counter stops. The effect of the paper grids on projectile velocity is demonstrably insignificant.

In order to measure the exit velocity of the projectile, a Dynafax high speed camera (Beckman and Whitley model 326) was used to record the motion of the

projectile after bone impact; and two electronic flash units (Beckman and Whitley model 358) were used as light sources. The camera has adjustable framing rates up to 26,000 frames per second. The flash units are also adjustable, generating light pulses for durations of 2.7, 5.4, or 10.8 milliseconds, depending on the framing rate of the camera. For example, a high framing rate required (1) a shorter

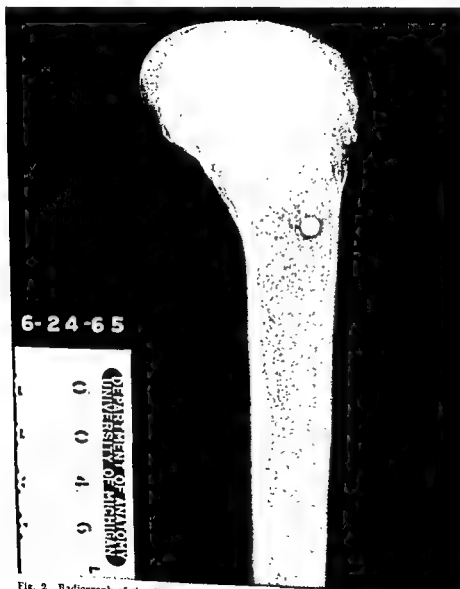


Fig. 2. Radiograph of the distal femur showing a one-fourth inch steel sphere imbedded in the bone. Impact velocity was 483 ft/sec. The projectile entered the bone from the left.



Fig. 3 Exit hole of an embalmed human femur impacted by a one-fourth inch steel sphere at 700 ft/sec.

flash duration to avoid multiple exposures of the film, and (2) a more intense flash to assure that sufficient light reaches the briefly exposed film. After bone impact the projectile passed above a scale standard, two pointed markers set exactly six inches apart. The flash units were synchronized with the event by a Pulse In-

terval Generator (Electronic Counters, Inc. model 565T). This generator was activated by the projectile's piercing the second electronic grid, and, after a given delay, it triggered the flash units. By using a camera pulse counter (Hewlett-Packard model 5512A), a constant read-out of the revolutions per second of the

camera's film carriage was obtained; the readout was automatically stopped when the gun was fired. Using this readout value, calculations of the camera's framing rate at the exact moment of exposure could be made.

Enlarged photographs of the sphere's motion over the scale standard were made and used to measure the distance traveled by the projectile between each frame. The exit velocity of the projectile was then calculated from the camera framing rate and the distance traveled by the sphere between each frame. The residual kinetic energy of the projectile was then computed. The difference between the impact energy and the residual energy represents the amount expended in producing the fracture.

A Fastax high speed camera (Wollensak model WF-1) was used to record the projectile-bone impact phenomenon. This camera was synchronized with gun firing by the WF-301 Control Unit, and the electronic flash units were used as the light source.

RESULTS

The data indicated that as the impact velocity increases, more energy is expended in producing the fracture (fig. 1). The straight line in figure 1 closely follows the average values of the energy expended at each velocity level, as shown in table 1. In three of the ten specimens at the lowest impact velocity (approximately 500 ft/sec) the projectile did not exit from the bone, indicating that this velocity and corresponding impact energy are near the minimum necessary to completely penetrate the distal end of the femur (fig. 2). Damage to the bone at low velocities consisted of entrance and exit holes with minimal cortical fragmentation about the margins of the exit hole (fig. 3); no linear or comminuted fractures were found in these specimens. This "drill hole" fracture was only slightly larger than the diameter of the projectile itself. In producing this type of fracture an average energy of 7.6 ft-lbs was expended, with a range for the various bones of 6.1 to 9.8 ft-lbs. The high speed film segment (fig. 4) shows the production of this drill hole fracture.

At impact velocities of 500 to 1000 ft/sec the impact energy of the sphere is in-

creased, and there was an enlargement of the projectile path through the cancellous bone. Also, the exit hole was noticeably enlarged. High speed films of tests in this velocity range showed large amounts of

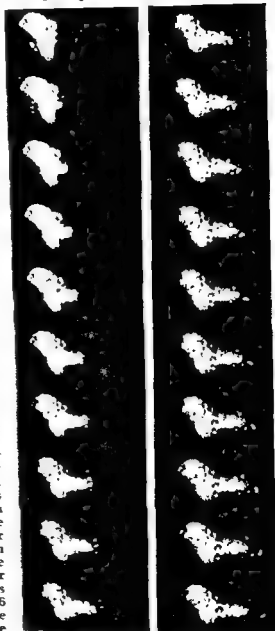


Fig. 4 High speed film segment (14,824 frames/sec) of a one-fourth inch steel sphere impacting the femur shown in figure 3. The femur is mounted in an inverted position. The sequence begins in the top left frame.

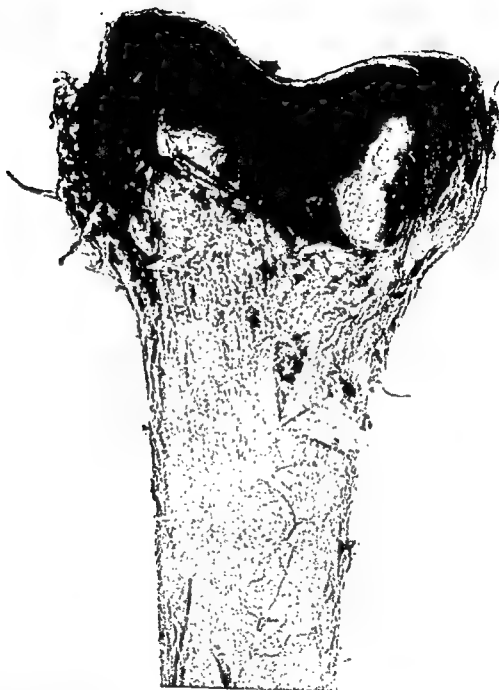


Fig. ■ Exit hole of an embalmed human femur impacted by a one-fourth inch steel sphere at 700 ft/sec.

flash duration to avoid multiple exposures of the film, and (2) a more intense flash to assure that sufficient light reaches the briefly exposed film. After bone impact the projectile passed above a scale standard, two pointed markers set exactly six inches apart. The flash units were synchronized with the event by a Pulse In-

terval Generator (Electronic Counters, Inc. model 565T). This generator was activated by the projectile's piercing the second electronic grid, and, after a given delay, it triggered the flash units. By using a camera pulse counter (Hewlett-Packard model 5512A), a constant read-out of the revolutions per second of the

camera's film carriage was obtained; the readout was automatically stopped when the gun was fired. Using this readout value, calculations of the camera's framing rate at the exact moment of exposure could be made.

Enlarged photographs of the sphere's motion over the scale standard were made and used to measure the distance traveled by the projectile between each frame. The exit velocity of the projectile was then calculated from the camera framing rate and the distance traveled by the sphere between each frame. The residual kinetic energy of the projectile was then computed. The difference between the impact energy and the residual energy represents the amount expended in producing the fracture.

A Fastax high speed camera (Wollensak model WF-1) was used to record the projectile-bone impact phenomenon. This camera was synchronized with gun firing by the WF-301 Control Unit, and the electronic flash units were used as the light source.

RESULTS

The data indicated that as the impact velocity increases, more energy is expended in producing the fracture (fig. 1). The straight line in figure 1 closely follows the average values of the energy expended at each velocity level, as shown in table 1. In three of the ten specimens at the lowest impact velocity (approximately 500 ft/sec) the projectile did not exit from the bone, indicating that this velocity and corresponding impact energy are near the minimum necessary to completely penetrate the distal end of the femur (fig. 2). Damage to the bone at low velocities consisted of entrance and exit holes with minimal cortical fragmentation about the margins of the exit hole (fig. 3); no linear or comminuted fractures were found in these specimens. This "drill hole" fracture was only slightly larger than the diameter of the projectile itself. In producing this type of fracture an average energy of 7.6 ft-lbs was expended, with a range for the various bones of 6.1 to 9.8 ft-lbs. The high speed film segment (fig. 4) shows the production of this drill hole fracture.

At impact velocities of 800 to 1000 ft/sec the impact energy of the sphere is in-

creased, and there was an enlargement of the projectile path through the cancellous bone. Also, the exit hole was noticeably enlarged. High speed films of tests in this velocity range showed large amounts of

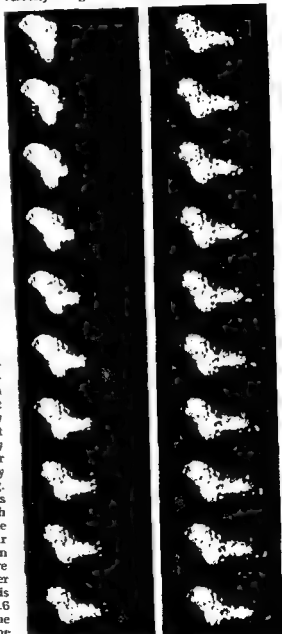


Fig. 4 High speed film segment (14,824 frames/sec) of a one-fourth inch steel sphere impacting the femur shown in figure 3. The femur is mounted in an inverted position. The sequence begins in the top left frame.

debris (bone fragments and marrow) being ejected from the exit hole after the projectile had passed through. At 800 ft/sec an average energy of 15.5 ft-lbs was expended in producing the fracture, and at

1000 ft/sec the average energy expended was 21.7 ft-lbs.

At an impact velocity of 1400 ft/sec the projectile path and exit hole were greatly enlarged, and in six of the 11 specimens



Fig. 5 Human femur impacted by a one-fourth inch steel sphere at 1709 ft/sec.

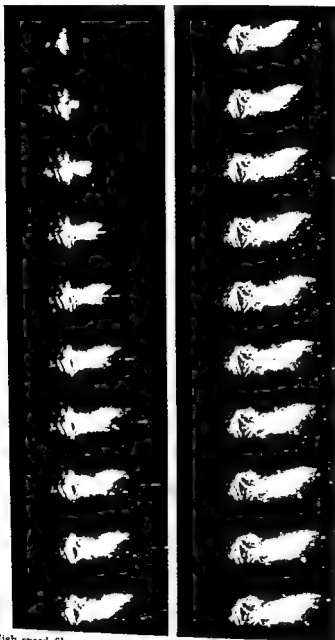


Fig. 11 High speed film segment (14,856 frames/sec) of a one-fourth inch steel sphere impacting the femur shown in figure 5. The femur is mounted in an inverted position. The sequence begins in the top left frame.

in this sample there was complete separation of the distal end from the femoral shaft with many comminuted fragments. High speed films of these impacts showed great amounts of cancellous bone frag-

ments, marrow, and embalming fluid being explosively expelled from the exit hole. At this velocity an average energy of 37.2 ft-lbs was used in producing the fractures. At the highest impact velocity, 1700 ft/

sec, almost all bones had extensive comminuted fractures which completely separated the distal end from the shaft (fig. 5). In these tests the high speed films clearly demonstrate the enormous explosive effects of such high velocity impacts (fig. 6). The average energy expenditure in producing these fractures was 51.1 ft-lbs.

DISCUSSION

As a projectile passes through soft tissue it imparts radial velocity to the surrounding medium, thereby causing a large temporary cavity. During its brief lifetime the temporary cavity in soft tissue will pulsate several times before it subsides (French and Callender, '62). This displaced tissue may damage other structures some distance from the projectile's path before returning to its original position. The relative lack of elasticity in bone led Ilterget ('53) to suggest that true cavitation does not occur in bone, but other investigators have noticed an explosive effect on animal bone directly impacted *in situ* at high velocities (Harvey et al., '62).

The mechanism of the cavitation in bone seems not unlike that in soft tissue: the projectile, after penetrating one cortical plate, encounters the marrow-filled cancellous bone and propels the marrow radially at high velocity, breaking the very thin plates of cancellous bone. When the projectile penetrates the second cortical plate, the exit hole is also enlarged by the cavitation in the cancellous material. Due to the relatively inelastic nature of bone, the temporary cavity thus formed in the cancellous bone also becomes the permanent cavity. Therefore, a relatively large internal cavity may remain whereas in soft tissue it collapses: whether this cavity in bone is called temporary or permanent is only a question of semantics. In addition, as has been observed in soft tissues, the cavitation phenomenon in bone produces an exit hole larger than the entrance hole. In the higher velocity impacts (1400 to 1700 ft/sec) the cavitation phenomenon produced an explosion of the tissue, destroying the greater portion of the cancellous bone and fragmenting the surrounding cortical bone.

Examination of femurs after impact disclosed that some had little embalming

fluid or marrow within the cancellous bone (due to excessive drying). In these bones the cavitation effects were diminished and the energy expended in producing the fractures was lower than average for the specific impact velocity. Furthermore, in some preliminary studies of high velocity impacts to dried and degreased femurs, it was found that drill hole fractures were produced at the same impact velocities that produced extensive damage to the marrow-filled cadaver specimens. In the dry femurs there is no mass of tissue or fluid to be radially displaced; thus without the effects of cavitation, extensive fractures, as described above, are not produced.

At the lower impact velocities the radial displacement of the cancellous material is minimal: little cavitation is noted in the velocity range below 800 ft/sec. Callender and French ('35) indicated that the degree of destruction caused by identical projectiles is significantly dependent upon the density of the tissue and upon the impact velocity of the projectile. In more dense material and/or with greater impact velocity more tissue destruction is found. In a fluid system such as soft tissues, resistance to penetration increases with the impact velocity; so if the impact velocity is increased sufficiently the resistance of less dense tissues approaches the resistance offered at lower impact velocities by more dense tissues. For example, fluid-filled viscera, blood vessels, and other soft tissues such as muscle will literally explode when impacted by a high velocity projectile. Since cancellous bone is actually filled with a soft tissue, the marrow, we feel that the explosive nature of the femoral fractures from impacts at the higher velocities is not unlike that seen in impacts to soft tissues.

The linear increase in the energy expended to produce fractures as a function of impact velocity is due to the resistance of the material. This resistance is not only dependent upon the hardness and elasticity of the tissue but also on its density. At velocities above that necessary for penetration the projectile will dissipate a greater proportion of its energy in the tissue as the impact velocity increases because of increasing resistance.

Biological variation between the femurs is well demonstrated in figure 1. At each impact velocity there is a scattering of the data points. This is not due to errors of measurement or recording, for calculations show that our total error is 3% or less. Four important parameters influence this biological variation. One is the total thickness of the bone at the impact point. Micrometer measurements of the specimens along the projectile path indicate that in the thicker specimens more energy is expended to produce the fracture. The second factor is the thickness of the cortical bone at the points of impact and exit of the missile. The third variable is the density of the cortical bone and of the enclosed cancellous bone. The fourth factor is the amount of marrow and/or embalming fluid within the cancellous spaces. These parameters then can produce variations in the amount of energy expended by the projectile at a given impact velocity.

Preliminary studies using fresh unembalmed human femurs have shown that at the various impact velocities the data points fall within the range of those plotted in figure 1 for embalmed bone. Thus there do not appear to be any significant differences between embalmed and unembalmed human bone in response to high velocity impact.

LITERATURE CITED

- Callender, G. R., and R. W. French 1935 Wound ballistics: Studies in the mechanism of wound production by rifle bullets. *Military Surg.*, 77: 177-201.
- Coates, J. B., and J. C. Beyer 1962 Wound Ballistics. Office of the Surgeon General, Department of the Army, Washington, D. C.
- Dziemian, A. J., J. A. Mendleson and D. Lindsey 1961 Comparison of the wounding characteristics of some commonly encountered bullets. *J. of Trauma*, 1: 341-353.
- French, R. W., and G. R. Callender 1962 Wound Ballistics. Ed. by J. B. Coates and J. C. Beyer. Office of the Surgeon General, Department of the Army, Washington, D. C. Chapter II, 91-142.
- Grundfest, H. 1945 Penetration of Steel Spheres into Bone. Missiles Casualty Report no. 10, National Research Council, Division of Medical Science, Office of Research and Development.
- Harvey, E. N., J. M. Korr, G. Oster and J. H. McMillen 1947 Secondary damage in wounding due to pressure changes accompanying the passage of high velocity missiles. *Surgery*, 21: 218-239.
- Harvey, E. N., and J. H. McMillen 1947 An experimental study of shock waves resulting from the impact of high velocity missiles on animal tissues. *J. Exper. Med.*, 83: 321-328.
- Harvey, E. N., J. H. McMillen, E. G. Butler and W. O. Puckett 1962 Wound Ballistics. Ed. by J. B. Coates and J. C. Beyer. Office of the Surgeon General, Department of the Army, Washington, D. C. Chapter III, 143-236.
- Herget, C. M. 1953 Surgery of Trauma. Ed. by W. F. Bowers. J. B. Lippincott Co., Philadelphia. Chapter 23, 494-510.
- Horsley, V. 1894 The destructive effects of projectiles. Notices of the proceedings of the Royal Institute of Great Britain, 14: 228-238.
- Huelke, D. F., and J. H. Darling 1964 Bone fractures produced by bullets. *J. of For. Sci.*, 9: 461-469.
- Keith, A., and M. E. Hall 1919 Bones showing the effects of gunshot injuries, in the army medical collection now on display in the Museum of the Royal College of Surgeons of England. *Brit. J. of Surg.*, 24: 537-565.
- Krauss, M. 1957 Studies in wound ballistics: Temporary cavity effects in soft tissues. *Military Med.*, 4: 221-231.
- LaGarde, L. A. 1895 Gunshot wounds. Report of the Surgeon General of the Army, 73-95.

Continuous Attachment of the Periodontal Membrane

ALLAN G. KRAW AND DONALD H. ENLOW

Department of Anatomy and The Center for Human Growth and Development, The University of Michigan, Ann Arbor, Michigan

ABSTRACT A polychrome stain for differentiating precollagenous and collagenous fibers, and tetracycline for labeling bone changes were used in young rats to trace adjustments involved in movements of teeth within bone. Distinct differences were seen in fibrous attachments on depository and resorptive bone surfaces. These are associated with shifts of the periodontal membrane as the root and surrounding bone undergo drift. Some resorptive areas receive total destruction of fibrous attachment. Other areas involve a process of fibrous conversion as ordinary fibers of the bone matrix become uncovered during bone removal and function as periodontal fibers anchored into the receding bone surface. An intermediate zone of the periodontal membrane functions to progressively shorten distal ends of these same fibers and to relink them with newly formed precollagenous fibrils. These become continuous with mature fibers attached to the cementum. On depository surfaces, outer fibers of the membrane become embedded into new alveolar bone, and former precollagenous fibrils of the inward-shifting intermediate zone translocate to become the new outer zone. Continuous relinkage is simultaneously maintained between the inner and outer zones. Haversian remodeling occurs beneath resorptive surfaces and re-anchorage is thereby established in specific areas where total destruction of fibrous connection had previously occurred.

The purpose of this report is (1) to describe and interpret the response of the young, growing periodontal membrane to differential polychrome staining for collagen and precollagen; (2) to describe the nature of periodontal attachments on the various resorptive and depository surfaces of alveolar bone; and (3) to correlate the distribution of underlying Haversian remodeling, using tetracycline labeling, with periodontal anchorage on resorptive surfaces of bone.

Teeth are firmly attached to the bony alveolar wall by a dense connective tissue bridge, the periodontal membrane. Parallel bundles of collagenous fibers extend from the cementum of the tooth across the span between root and bone and are embedded in the alveolar wall. The continuous maintenance of this attachment, however, is complicated by several factors associated with growth, including differential growth rates between bone and teeth, progressive eruption, rotation and tilting movements of teeth, drifting, and continuous rebuilding changes taking place in the bone of the growing maxilla and mandible. Because spatial relationships between teeth and alveolar bone constantly change during

these movements, adjustment mechanisms necessarily exist that function to maintain firm and continuous attachment of the periodontal membrane to both tooth and bone. Sicher ('23, '42) reported the presence of an "intermediate plexus" in the periodontal membrane of rodents that is located in the approximate middle third of the membrane. He suggested that this plexus, containing an abundance of argyrophilic fibers, functions to splice collagenous fibers embedded in the bone on one side and the cementum on the other. The tooth can undergo eruption and at the same time maintain its attachment by a continuous resplicing of the new and old fibers as they become relocated during tooth movement. Orban ('27) later extended this explanation to human dentition. The presence of an intermediate plexus has also been reported in the guinea pig (Hunt, '59) and in the spider monkey (Goldman, '57). Several workers, however, have questioned the existence of this plexus, including Eccles ('59), Trott ('62), and Zwarych and Quigley ('65). Sicher ('65) suggests that the presence and relative prominence of an intermediate plexus is dependent upon the degree of tooth movement at the time observed. Dur-

ing quiescent periods, this plexus presumably becomes obscured.

An important factor involved in movements of teeth within bone is the common occurrence of alveolar bone surfaces which are *resorptive* in character, rather than *depository*. This growth factor is associated with progressive movements of a tooth directly into areas previously occupied by bone. Such movements take place during both drift and eruption, and they involve the widespread resorptive removal of bone on contact surfaces between the alveolar wall and the periodontal membrane. New bone deposition occurs on the opposite (endosteal) side of the same alveolar wall. By this combined process, the entire plate of bone moves in a direction corresponding to the movement of the tooth. It is currently believed that bone resorption, in general, represents a total process of removal, including bone cells, the entire fibrous matrix, and the ground substance. It is also generally assumed that the resorption of alveolar bone, into which periodontal fibers are anchored, similarly results in a total destruction of periodontal attachment in such areas. Gottlieb ('42) has estimated that as much as 20 percent of the total alveolar bony lining can represent such a resorptive surface with corresponding fibrous detachment. Sicher and Weinmann ('44, '65) suggest that intermittent, scattered spot deposition of reparative bone on such surfaces functions to temporarily maintain partial attachment during tooth movements.

In the present report, an expansion of the concept of an intermediate plexus will be made, and additional observations and interpretations dealing with the nature of its mechanism will be presented. The critical problem of attachment and successive reattachment onto resorptive bone surfaces will be examined, and new information will be presented relative to processes involved.

MATERIALS AND METHODS

Maxillary bones from a total of 62 female albino rats of the Sprague-Dawley strain were used for study. The animals ranged from 60 to 75 days in age and averaged 215 gm in weight. Maxillary

specimens were fixed in formalin acetic alcohol (10:5:85), decalcified in Decal (Winthrop Laboratories), double-embedded in celloidin, and serially sectioned at 10 μ . A variety of horizontal, vertical, and frontal sections were prepared. Sections were stained with a polychrome stain (Herovici, '63) to differentiate mature collagenous fibers from formative (precollagenous) fibrils. This procedure was used in order to identify and localize sites of collagen formation and to correlate their distribution with changes in the periodontal membrane and alveolar bone during drift and eruption. Using this stain, mature fibers appear red (acid fuchsin), and precollagenous fibrils appear blue (methylene blue). A number of representative sections were also stained with standard Hematoxylin and eosin and with Mallory-Heidenhain for comparison with the polychrome stain.

Tetracycline hydrochloride (30 mg/kg body weight) was also administered to a group of 14 animals in a series of three intraperitoneal injections at 48-hour intervals. This procedure was used to identify and localize remodeling changes in the bone tissue of the alveolar wall associated with tooth movements and periodontal adjustments. Tetracycline becomes incorporated within newly formed bone, and layers or zones of such bone can be visualized by the use of ultraviolet microscopy (Behatia and Sognnaes, '63; Gregg and Avery, '64; Owen, '63; Bevelander, Nakahara, and Rolle, '60).

OBSERVATIONS

Alveolar bone surfaces and fibrous anchorage. Two general kinds of bone surfaces, depository and resorptive, line the alveolar cavity, and each is readily identifiable in routine preparations using medium power magnification. Depository surfaces are characterized by an accumulation of successive layers composed either of lamellar or non-lamellar bone tissue. As new bone is deposited, bundles of periodontal fibers become incorporated within the bone in a manner comparable with Sharpey's fibers in areas of muscle or tendon attachment (fig. 3). The resulting bone type is distinctive in structure and is commonly termed "bundle bone."

Although this alveolar bone type represents the predominant bone tissue present beneath depository surfaces, some scattered areas may also be observed in which such fibrous attachment does not occur. In this instance, the only direct interconnection between bone and the periodontal membrane is by vascular bundles and cell processes. Both types of periodontal bone, which correspond to periosteal bone tissue, are formed in areas where movements of teeth proceed in a general direction away from the bone surface. Progressive new bone deposition on the alveolar surface serves to maintain a constant bone-tooth position as the tooth shifts in location due to drift or eruption.

Resorptive alveolar surfaces are characterized by a scalloped margin (fig. 4) and an abundant distribution of prominent osteoclasts. Such surfaces are located in areas involving progressive movement of the root in a direction toward the bone surface. The resorptive removal of bone from this outer periodontal surface, together with new bone deposition on the opposite (endosteal) side, serves to move this entire area of the alveolar wall in a direction corresponding to the movement of the advancing tooth.

In contrast with the depository surfaces just described, resorptive surfaces can be observed in which fibrous continuity with the periodontal membrane has become severed as a result of the resorptive destruction of alveolar bone tissue during tooth movements. This situation is typically seen in those areas in advance of vascular bundles as they enter the bone within formative resorption spaces (figs. 1, 4). The resorptive surface of the bone is discontinuous with the periodontal membrane, and fibrous attachment between the two is lacking in such areas.

Another common relationship occurs between the periodontal membrane and resorptive bone surfaces, however, that has been previously unrecognized. A significant distribution of resorptive surfaces were observed in which direct fibrous continuity between the bone and the adjacent periodontal membrane was not detached or destroyed as a result of bone removal. In this situation, the movement of the alveolar wall in an endosteal direction

(away from the advancing root of the tooth) leaves a trail of uninterrupted and apparently undisturbed collagenous fibers that were once a component part of the ordinary bone matrix but which had become progressively uncovered as the remainder of the bone around them was removed (fig. 4). They then become directly incorporated into the shifting and continuously reforming periodontal membrane. This observation is in contradiction with the widespread belief that bone resorption necessarily results in a total destruction of the entire bone matrix. This can be true in areas adjacent to blood vessels, as described in the previous paragraph, and in such regions bone resorption results in total fibrous detachment. In contrast, however, resorptive surfaces that are not directly associated with periodontal vascular bundles are characterized by a retention of collagenous fibers released from the bone matrix as a result of bone resorption. As they are uncovered from the receding bone surface, these bone matrix fibers become actual periodontal fibers that insert into the remaining bone and retain direct continuity with those matrix fibers still enclosed as a part of the bone tissue. Uninterrupted and continuous attachment is thereby maintained in such areas. As bone fibers are uncovered to become periodontal fibers, they subsequently undergo a process of shortening and relinkage with precollagenous fibrils within the periodontal membrane in order to accommodate membrane shifts and tooth movements. This process will be outlined in later paragraphs.

Bone matrix fibers that become exposed as a result of the removal of bone from around them are not "Sharpey's fibers" of the kind present within bundle bone beneath depository surfaces. The latter are periodontal fibers that become embedded within new bone deposits as special anchoring fibers and represent inclusions within the ordinary intercellular bone matrix. In contrast, fibers that are uncovered and preserved during resorption undergo a converse developmental sequence. They are ordinary bone fibers that subsequently become converted into periodontal fibers. Within the matrix of

the bone, they are not arranged in coarse, parallel bundles oriented in a perpendicular plane. Rather, they enter the bone and merge directly with the general fibrous matrix (Compare fig. 3 with fig. 4). It is noteworthy that a comparable process of fibrous exposure, conversion, and subsequent relinkage also occurs on resorptive periosteal bone surfaces in which muscles and tendons insert (Enlow, '62b, '65b; Hoyte and Enlow, '66).

Four contrasting situations are, thus, characteristic of various depository and resorptive surfaces in contact with the periodontal membrane. These are (1) depository surfaces involving embedded Sharpey's fibers (bundle bone), (2) depository surfaces in which periodontal fibers do not become embedded during bone deposition, thereby leaving bone and periodontal membrane without local fibrous attachment, (3) resorptive surfaces involving a total destruction of fibrous connection and continuity as a consequence of bone removal, and (4) resorptive surfaces in which bone matrix fibers survive bone resorption and are retained as new periodontal fibers directly continuous with remaining alveolar bone matrix fibers. On depository surfaces, the first circumstance above has been most frequently encountered. On resorptive surfaces, both situations described are widespread and routinely seen in varying combinations. They appear approximately equal in total distribution, although quantitative determinations have not been made. As will be pointed out in later paragraphs, a number of related considerations are involved in each of the mechanisms outlined above.

Distribution of precollagen and collagen. In the descriptions that follow, the fibers of the periodontal membrane will be grouped into three component zones: the anchoring fibers of the cementum (the inner zone), the anchoring fibers of the alveolar bone (outer zone), and an intermediate zone joining the inner and outer zones (figs. 2-4). The fibers of the intermediate zone will be termed linkage fibers.

The inner zone, adjacent to the root, typically contains large collagenous fibers arranged into coarse bundles which insert

into the cementum. These fibers are composed largely of mature collagen and appear red with polychrome staining. The outer zone, adjacent to the alveolar wall, contains coarse fibers that pass directly into the bone. In general, the outer zone is more labile than the characteristically stable inner zone in that extensive fiber recombination is typically active in this area. Goldman ('57) has also reported the more stable nature of the inner as compared with the outer zone. In those regions of the alveolar wall involving depository surfaces and the formation of periodontal bundle bone, the fibers are colored a deep red with the differential polychrome stain. These fibers continue into the bone as Sharpey's fibers and retain their red color within the bone tissue. They represent mature collagen, and they have a large diameter and are arranged into coarse bundles.

Adjacent to resorptive surfaces, the fibers of the outer zone also stain with a red color, and they represent the mature collagenous fibers of the old bone matrix that have been uncovered during progressive resorption and which now serve as periodontal fibers. Mixed with these mature, red-stained fibers, however, are large numbers of fine, blue-stained, precollagenous fibrils that continue directly into the predominantly precollagenous intermediate zone. The fibers of the intermediate zone, thus, grade for a considerable distance into the outer zone. These overlapping precollagenous fibrils may extend close to the resorbing bone surface, and in this area of fiber convergence, direct blending and linkage of old and new fibers can be observed. On depository surfaces, an overlap between the young fibrils of the intermediate zone and the mature, coarse fibers of the outer zone is also seen, but the degree of overlap is less marked. The reason for this lies in the differing functions of the intermediate zone on resorptive as compared with depository surfaces, as described in other paragraphs. Large numbers of sizable osteoclasts are usually observed on the receding bone surface interspersed among the bundles of fibers. Using Mallory's stain, numerous, large, eosinophilic cytoplasmic granules of

in undetermined nature are seen within these osteoclasts.

The intermediate zone spanning between the inner and outer zones ordinarily contains a few scattered, red-stained mature fibers in varying stages of recombination and shortening. The great majority of fibers observed in the intermediate zone, however, are delicate, blue-stained precollagenous fibrils. They form a relatively dense mesh and are interspersed with abundant fibroblasts and scattered vessels. The functional significance of the intermediate zone with its characteristic overlap into both the inner and outer zones will be evaluated in the later discussion.

In some scattered areas, the three-part zoning just described is not evident. Here, the majority of fibers throughout the entire thickness of the periodontal membrane are all coarse-bundled, mature collagenous fibers and respond with a typical red color to the polychrome stain. Such areas may be interpreted as stable at that particular time, and bone deposition or resorption was not then active. Since shifts of the periodontal membrane and linkage adjustments in response to bone movements were not involved, the entire fibrous component of the intermediate zone had progressed to maturity.

Remodeling changes in alveolar bone. In contrast to the unmodified and primary nature of periodontal bone beneath depository alveolar surfaces, endosteal bone tissues underlying resorptive surfaces are often characterized by marked internal remodeling changes (figs. 2, 4). Just beneath the surface, large resorption canals following the course of pre-existing primary vascular canals extend in a progressive direction deeper into the bone, thereby keeping pace with the advancing resorptive front of the entire receding bone surface. These erosion canals subsequently receive new deposits of bone within their enlarged lumina and are thereby converted into secondary osteones (Haversian systems). The fibrous matrix of these newly formed osteones is directly continuous with the fibers of the adjacent periodontal membrane. As the resorptive front (resorbing alveolar surface) continues to advance into the bone, the osteones un-

dergo resorptive removal in turn, but their uncovered matrix fibers are converted into periodontal fibers retaining connection with the fibers of the remaining bone. The fibers of the Haversian system matrix, thus, are not subject to immediate destruction as the bone itself undergoes removal, and they thereby become incorporated directly as the new outer zone of the periodontal membrane as the latter follows the drift of the bone surface. The red-stained, mature fibers released from the resorbing osteones blend directly with the elongating precollagenous fibrils of the intermediate zone. This sequence is progressive, and the continued formation of resorption canals and new secondary osteones continues in advance of the resorbing surface of the alveolar wall. Such internal Haversian reconstruction deep to a resorptive surface is characteristic, in contrast to the unremodeled, primary nature of the bone beneath depository surfaces. This general process is comparable with the situation seen in long bones in which Haversian remodeling occurs within bone in relation to muscle and tendon attachment on resorptive surfaces (Enlow, '62b).

In tetracycline labeled bone specimens, the remodeling sequence outlined above is effectively demonstrated (fig. 1). Fluorescence is observed (1) on the surface of the depository side of a tooth socket, and (2) within the enlarged canals and resorption spaces deep to the bone surface on the resorptive side of the socket. Using H³ Proline, Stallard ('63) also demonstrated bone deposition within the spaces of bone associated with resorptive alveolar surfaces.

Haversian reconstruction in tooth-bearing bone is most widespread beneath those resorptive surfaces in which the underlying bone is relatively thick. In some areas, the intervening wall of alveolar bone between a resorptive surface on one side and a depository surface on the other can be quite thin (fig. 4). In such locations, the remodeling sequence described above does not occur since the plate of bone is not sufficiently thick to contain large resorption canals or osteones. In these locations, the functional role of Haversian remodeling is not involved be-

the bone, they are not arranged in coarse, parallel bundles oriented in a perpendicular plane. Rather, they enter the bone and merge directly with the general fibrous matrix (Compare fig. 3 with fig. 4). It is noteworthy that a comparable process of fibrous exposure, conversion, and subsequent relinkage also occurs on resorptive periosteal bone surfaces in which muscles and tendons insert (Enlow, '62b, '65b; Hoyte and Enlow, '66).

Four contrasting situations are, thus, characteristic of various depository and resorptive surfaces in contact with the periodontal membrane. These are (1) depository surfaces involving embedded Sharpey's fibers (bundle bone), (2) depository surfaces in which periodontal fibers do not become embedded during bone deposition, thereby leaving bone and periodontal membrane without local fibrous attachment, (3) resorptive surfaces involving a total destruction of fibrous connection and continuity as a consequence of bone removal, and (4) resorptive surfaces in which bone matrix fibers survive bone resorption and are retained as new periodontal fibers directly continuous with remaining alveolar bone matrix fibers. On depository surfaces, the first circumstance above has been most frequently encountered. On resorptive surfaces, both situations described are widespread and routinely seen in varying combinations. They appear approximately equal in total distribution, although quantitative determinations have not been made. As will be pointed out in later paragraphs, a number of related considerations are involved in each of the mechanisms outlined above.

Distribution of precollagen and collagen. In the descriptions that follow, the fibers of the periodontal membrane will be grouped into three component zones: the anchoring fibers of the cementum (the inner zone), the anchoring fibers of the alveolar bone (outer zone), and an intermediate zone joining the inner and outer zones (figs. 2-4). The fibers of the intermediate zone will be termed linkage fibers.

The inner zone, adjacent to the root, typically contains large collagenous fibers arranged into coarse bundles which insert

into the cementum. These fibers are composed largely of mature collagen and appear red with polychrome staining. The outer zone, adjacent to the alveolar wall, contains coarse fibers that pass directly into the bone. In general, the outer zone is more labile than the characteristically stable inner zone in that extensive fiber recombination is typically active in this area. Goldman ('57) has also reported the more stable nature of the inner as compared with the outer zone. In those regions of the alveolar wall involving depository surfaces and the formation of periodontal bundle bone, the fibers are colored a deep red with the differential polychrome stain. These fibers continue into the bone as Sharpey's fibers and retain their red color within the bone tissue. They represent mature collagen, and they have a large diameter and are arranged into coarse bundles.

Adjacent to resorptive surfaces, the fibers of the outer zone also stain with a red color, and they represent the mature collagenous fibers of the old bone matrix that have been uncovered during progressive resorption and which now serve as periodontal fibers. Mixed with these mature, red-stained fibers, however, are large numbers of fine, blue-stained, precollagenous fibrils that continue directly into the predominantly precollagenous intermediate zone. The fibers of the intermediate zone, thus, grade for a considerable distance into the outer zone. These overlapping precollagenous fibrils may extend close to the resorbing bone surface, and in this area of fiber convergence, direct blending and linkage of old and new fibers can be observed. On depository surfaces, an overlap between the young fibrils of the intermediate zone and the mature, coarse fibers of the outer zone is also seen, but the degree of overlap is less marked. The reason for this lies in the differing functions of the intermediate zone on resorptive as compared with depository surfaces, as described in other paragraphs. Large numbers of sizable osteoclasts are usually observed on the receding bone surface interspersed among the bundles of fibers. Using Mallory's stain, numerous, large, eosinophilic cytoplasmic granules of

heir component fibers. The entire periodontal membrane on this side of the tooth (the "tension" side) thereby keeps proportionate position between bone and cementum by its own mechanism of drifting. In this process, thus, the fibrils of the intermediate zone elongate on one side to keep pace with the fibers of the moving inner zone, and on the other side they become converted into the fibers of the outer zone which, in turn, become progressively embedded into newly forming alveolar bone.

On the opposite side of the root (the "pressure" side), an equivalent but fundamentally different process is involved. As the root drifts to the right in diagrams 4-6 of figure 5, the alveolar wall simultaneously shifts in a like direction. This is brought about by the resorptive removal of bone from this bone surface together with corresponding bone deposition on the opposite endosteal side. The proportionate thickness of the alveolar wall is thereby maintained. As previously described, inward-advancing, resorptive bone surfaces involve two general circumstances. First, some areas of surface resorption result in a total destruction of the bone, including its fibrous connection with the periodontal membrane. These areas typically occur around vascular bundles as they course into the alveolar bone from the periodontal membrane. Second, resorptive removal of surface bone in other areas leaves a distinct trail of mature collagenous fibers which were once a part of the bone matrix, prior to resorption, but which have become translocated as the fibrous outer zone in contact with the resorptive bone surface. As the root moves progressively in a direction toward the receding bone surface, a constant shortening of these same fibers occurs as they grade into the labile intermediate zone. At the same time, continued elongation of precollagenous fibrils takes place within the outer part of the intermediate zone, and these young fibrils link with the constantly shortening, mature fibers of the outer zone as the latter become successively uncovered from the bone matrix as a result of surface resorption. Whether such shortening involves an actual dissolution and subsequent reattachment of the mature fibers with precollagenous fibrils, or

whether a process of progressive molecular recombination and conversion takes place is not now known. However, direct continuity can be traced between the matrix of the resorbing alveolar bone, the fibers of the outer zone, and the new fibrils of the intermediate zone. Fibrous connection, thus, is not interrupted as a consequence of surface bone removal.

The inner zone of the periodontal membrane, anchored into the cementum, is composed of mature, coarse-bundled fibers. As the root drifts, these same fibers are carried in a corresponding direction. Continuous relinkage occurs in the overlap area between the stable inner and the labile intermediate zones as the constantly reforming precollagenous fibrils of the latter layer become bonded as extensions of the inner mature fibers.

The complex sequence of adjustments involved in the drift of the membrane in a direction toward the alveolar bone surface involves, in summary, a direct conversion of former bone matrix fibers released during resorption into the new fibers of the outer periodontal zone. Since these fibers retain direct continuity with the fibrous matrix of the remaining bone deep to the resorptive surface, attachment is maintained between bone and membrane. Second, in the overlap zone between the outer and intermediate zones, a progressive shortening (or de-differentiation) of these same fibers occurs and relinkage takes place with a simultaneous elongation of the intermediate precollagenous fibrils. These newly formed young fibrils, in turn, become successively reformed and sequentially relinked with the stable fibers of the inner zone attached to the cementum of the tooth. This combined sequence of changes permits a "drift" of the entire periodontal membrane in such a manner that it maintains proportionate thickness during such movement. It provides, further, continued attachment of teeth to the alveolar wall.

The movements and changes just described represent, in part, the special mechanism adapted to the horizontal drifting of teeth within bone. Two separate and distinct processes are involved, one associated with the tension side and the other with the pressure side of a moving

cause the relatively rapid formation and destruction of the entire thickness of the alveolar wall obviates the functional role of internal remodeling, as described below.

DISCUSSION

Movements of teeth and alveolar bone.

The basic movements of teeth involve eruption and a progressive drifting in either a mesial or a distal direction depending upon species considered. The mechanism of drift functions to maintain firm contact between adjacent teeth as contact surfaces undergo wear, thereby bracing the entire dental arch. Teeth also experience tilting and rotating movements during drift and eruption. Another kind of tooth movement occurs which is not generally realized. The growth of any bone, including the mandible and maxilla, involves a process of continuous relocation of its component areas as the entire bone increases in overall size. As the various regions of a bone undergo such consecutive repositioning, the teeth located within these areas experience corresponding and simultaneous shifts in position in order to retain their relative position in the bone as a whole. This process of relocation in conjunction with bone changes due to growth contributes to the functional basis for the process of mesial drift (Enlow, '65a).

The drifting process of the periodontal membrane. The structure of the periodontal membrane provides an intrinsic mechanism by which the membrane itself can continuously move in a manner corresponding to the complex variety of tooth and bone movements outlined above. Just as both teeth and bone drift together in a horizontal plane, the intervening periodontal membrane also undergoes "drift." At the same time, it permits differential vertical movements between a tooth and the surrounding bony alveolar wall. Throughout these progressive changes, the periodontal membrane maintains firm attachment between teeth and supporting bone.

The horizontal drift of a tooth and the corresponding movements of its bony socket and periodontal membrane is schematized in figure 5. The three zones of

the periodontal membrane are shown, including the inner and outer layers containing large numbers of coarse, mature fiber bundles. The intermediate zone, with its mesh of delicate precollagenous fibrils, overlaps and blends well into both the inner and outer zones. This overlap is particularly prominent between the intermediate and the outer zones. In diagrams 1, 2, and 3 of figure 5, the tooth is drifting in a direction toward the right (away from the bone surface shown). Periodontal fibers that were once a component part of the outer zone have now become embedded within the periodontal bundle bone as Sharpey's fibers. As mentioned earlier, scattered areas of new bone formation can also occur in which fibers of the periodontal membrane do not become bound as inclusions within formative bone tissue, and direct fibrous connection between the alveolar wall and the membrane is lacking in such locations. The arrangement shown in the growth stages 1-3, however, is more commonly found. Progressive inclusion of periodontal fibers has occurred as new bone is laid down on the alveolar surface by the periodontal membrane. As seen in this figure, the outer zone is composed of coarse, mature collagenous fibers. This same area was formerly located as the intermediate zone of a previous growth stage. They were once precollagenous, finely-bundled fibrils formerly positioned in the intermediate zone but have become mature, coarsely-bundled fibers translocated into the new outer zone. The continuously shifting intermediate zone has moved in a direction to the right. It is composed of newly formed fibrils that represent an elongation of the fibrils of the old intermediate zone which, in turn, have become the mature, coarse fibers of the new outer zone. As the root of the tooth drifts to the right, the mature fibers of the inner zone, attached to the cementum, move to the right with the moving tooth. These fibers are stable and undergo relatively little turnover. The young fibrils of the continuously reforming intermediate zone become elongated behind the moving fibers of the inner zone, and they keep constant bond with them. The overlap between these two zones represents the constantly moving site of linkage between

their component fibers. The entire periodontal membrane on this side of the tooth (the "tension" side) thereby keeps proportionate position between bone and cementum by its own mechanism of drifting. In this process, thus, the fibrils of the intermediate zone elongate on one side to keep pace with the fibers of the moving inner zone, and on the other side they become converted into the fibers of the outer zone which, in turn, become progressively embedded into newly forming alveolar bone.

On the opposite side of the root (the "pressure" side), an equivalent but fundamentally different process is involved. As the root drifts to the right in diagrams 4-6 of figure 5, the alveolar wall simultaneously shifts in a like direction. This is brought about by the resorptive removal of bone from this bone surface together with corresponding bone deposition on the opposite endosteal side. The proportionate thickness of the alveolar wall is thereby maintained. As previously described, inward-advancing, resorptive bone surfaces involve two general circumstances. First, some areas of surface resorption result in a total destruction of the bone, including its fibrous connection with the periodontal membrane. These areas typically occur around vascular bundles as they course into the alveolar bone from the periodontal membrane. Second, resorptive removal of surface bone in other areas leaves a distinct trail of mature collagenous fibers which were once a part of the bone matrix, prior to resorption, but which have become translocated as the fibrous outer zone in contact with the resorptive bone surface. As the root moves progressively in a direction toward the receding bone surface, a constant shortening of these same fibers occurs as they grade into the labile intermediate zone. At the same time, continued elongation of precollagenous fibrils takes place within the outer part of the intermediate zone, and these young fibrils link with the constantly shortening, mature fibers of the outer zone as the latter become successively uncovered from the bone matrix as a result of surface resorption. Whether such shortening involves an actual dissolution and subsequent reattachment of the mature fibers with precollagenous fibrils, or

whether a process of progressive molecular recombination and conversion takes place is not now known. However, direct continuity can be traced between the matrix of the resorbing alveolar bone, the fibers of the outer zone, and the new fibrils of the intermediate zone. Fibrous connection, thus, is not interrupted as a consequence of surface bone removal.

The inner zone of the periodontal membrane, anchored into the cementum, is composed of mature, coarse-bundled fibers. As the root drifts, these same fibers are carried in a corresponding direction. Continuous relinkage occurs in the overlap area between the stable inner and the labile intermediate zones as the constantly reforming precollagenous fibrils of the latter layer become bonded as extensions of the inner mature fibers.

The complex sequence of adjustments involved in the drift of the membrane in a direction toward the alveolar bone surface involves, in summary, a direct conversion of former bone matrix fibers released during resorption into the new fibers of the outer periodontal zone. Since these fibers retain direct continuity with the fibrous matrix of the remaining bone deep to the resorptive surface, attachment is maintained between bone and membrane. Second, in the overlap zone between the outer and intermediate zones, a progressive shortening (or de-differentiation) of these same fibers occurs and relinkage takes place with a simultaneous elongation of the intermediate precollagenous fibrils. These newly formed young fibrils, in turn, become successively reformed and sequentially relinked with the stable fibers of the inner zone attached to the cementum of the tooth. This combined sequence of changes permits a "drift" of the entire periodontal membrane in such a manner that it maintains proportionate thickness during such movement. It provides, further, continued attachment of teeth to the alveolar wall.

The movements and changes just described represent, in part, the special mechanism adapted to the horizontal drifting of teeth within bone. Two separate and distinct processes are involved, one associated with the tension side and the other with the pressure side of a moving

root. Differential movements between teeth and the adjacent alveolar wall, as in eruption and rotation, are also brought about by this sequence of progressive fibrous re-linkage between the intermediate and the inner and outer zones of the periodontal membrane.

Another basic process contributes to the constant maintenance of tooth attachment to bone during their respective movements. This mechanism involves the continuous formation and reformation of secondary (Haversian) bone in advance of *resorptive* surfaces (figs. 2, 4). As a bone surface in contact with the periodontal membrane is destroyed, erosive penetration of resorption canals into the bone take place, and new bone is subsequently laid down within these enlarged spaces. The resulting secondary bone has a fibrous matrix that is directly continuous with the fibers of the outer zone of the shifting periodontal membrane and provides localized attachment between the membrane and the alveolar wall during this process of resorptive movement. As older Haversian systems are destroyed by the advancing resorptive front, fibers are uncovered from their matrix in the manner described in previous paragraphs. They become incorporated in turn into the outer periodontal zone where they undergo linkage with the fibrils of the correspondingly moving intermediate zone. As this occurs, new generations of resorption spaces develop in advance of the blood vessels entering the bone from the periodontal membrane, and new Haversian systems are then formed within these spaces. This process of Haversian remodeling functions as a reattachment mechanism in two specific instances. First, it occurs beneath those particular surface areas deep to a resorptive front in which bone removal has resulted in a total destruction of the bone matrix, including its fibers. This characteristically takes place in locations next to and on either side of periodontal blood vessels. Continuations of these vessels pass into the resorption spaces and eventually become the central blood vessels within Haversian canals following the formation of secondary osteones. The overall process provides a means by which reattachment of fibers becomes established in those local-

ized areas where former attachment was destroyed. Haversian remodeling may also be involved in regions where firm fibrous anchorage was previously lacking. This situation, noted earlier, has been found in some scattered areas where formative periodontal bone does not embody periodontal fibers as it is laid down. Although not widespread in the rat, secondary bone reconstruction with Haversian system formation apparently can provide fibrous continuity between the alveolar wall and the membrane where such regions become involved in subsequent bone and tooth movements.

It is noteworthy that Haversian remodeling also occurs in long bones on those particular surfaces where muscles and tendons are attached (Enlow, '62b). Significantly, secondary Haversian systems are characteristically lacking in the bone of rats (and many other species) except in specific areas, such as the periodontal membrane, which involve resorptive surfaces in association with fibrous reattachment. In the skeleton of very young individuals, bone tissues are typically fine-cancellous in structure. The canals within this type of bone are large, and a process of compaction by bone deposition within these available spaces results in the formation of primary osteones (Enlow, '63). This developmental sequence functions in fibrous reattachment in a manner comparable with secondary Haversian remodeling in that both involve the deposition of new bone within large canals or spaces. In very young individuals, the distribution of primary osteones parallels that of the secondary osteones in older individuals.

CONCLUSIONS

Sections of decalcified maxillary bones from a group of young, rapidly growing white rats were stained with a differential collagenous and precollagenous polychrome stain. A second group of rats was treated with tetracycline, a vital bone-marking dye, and their maxillae were then sectioned and studied by fluorescence microscopy. The purpose of these procedures was to trace the sequence of adjustments that take place in the periodontal membrane and alveolar bone dur-

ing facial growth and the complex movements of teeth.

The different kinds of bone surfaces lining the alveolar socket are described. Of special interest is the finding that resorptive surfaces adjacent to the root are associated with two separate circumstances. First, approximately half of the total resorptive surface area involves total fibrous destruction and loss of attachment. This occurs primarily in regions adjacent to vascular bundles within the periodontal membrane. On remaining surfaces of resorptive bone, some fibers within the original bone matrix are not destroyed but become uncovered during bone removal and are subsequently incorporated into the laterally-moving periodontal membrane. These fibers retain direct connection with the fibrous matrix of the alveolar bone and provide fibrous attachment and anchorage between the resorptive surface of the drifting bone and the contiguous periodontal membrane.

Deep to resorptive surfaces of alveolar bone, enlarged resorption canals containing blood vessels extend into the bone in advance of the resorptive front. Progressive deposition of bone within these erosion spaces takes place, and the fibrous matrix of the resulting secondary Haversian systems is in direct continuity with the fibers of the periodontal membrane. Repetition of this remodeling process occurs as resorption of the alveolar surface continues. This mechanism provides attachment and subsequent reattachment between bone and tooth in those particular areas which previously had involved total destruction of fibrous connection between the periodontal membrane and alveolar bone. As each Haversian system undergoes removal, in turn, the fibers of the Haversian matrix become released and serve as transient periodontal fibers that retain continuity with the remaining bone. Surface remnants of such secondarily-formed bone, as it undergoes progressive destruction during resorption, represent in part the localized areas previously attributed to "spot" deposition and repair during resorption.

Just as the root of a tooth and its surrounding bone undergo a process of drift, the periodontal membrane itself experi-

ences corresponding movement. Drifting of the periodontal membrane involves two basic and different processes. One represents a mechanism associated with depository surfaces and the other with resorptive surfaces. In all areas, the actively moving periodontal membrane is composed of three zones. The inner zone is attached to the cementum and contains mature collagenous fibers which are relatively stable. The outer zone also contains mature, coarse-bundled fibers that are anchored in the alveolar bone as attachment fibers. The intermediate zone, comparable with the intermediate plexus of Sicher, contains an abundant distribution of young, precollagenous fibrils. Adjacent to depository surfaces of alveolar bone, these young fibrils are converted into the coarse fiber bundles of the outer zone as the entire membrane shifts and as former outer fibers become embedded into new surface bone. The young, labile precollagenous fibrils of the intermediate zone also provide continuous linkage with the mature, stable fibers of the inner zone attached to the cementum. Adjacent to resorptive bone surfaces, fibers released from the resorbing bone matrix become progressively shortened within the intermediate zone as the periodontal membrane drifts in a direction toward the receding bone surface. Continuous re-linkage occurs between the newly-formed fibrils of the intermediate zone and these fibers of the resorbing bone matrix which serve as the transient outer fibrous zone of the periodontal membrane. Linkage adjustments simultaneously occur in the overlap area between the intermediate and inner zones. Actual mechanisms of linkage and subsequent re-linkage at the molecular level are not now known.

The combination of processes outlined above provides continuous attachment of the tooth to its alveolar wall during the complex variety of movements that take place as teeth undergo relocation due to maxillary and mandibular growth, eruption, drifting, rotation, and tilting.

ACKNOWLEDGMENTS

This study was supported in part by U.S.P.H.S. grant DE-01903 and by summer student fellowships awarded by the Uni-

root. Differential movements between teeth and the adjacent alveolar wall, as in eruption and rotation, are also brought about by this sequence of progressive fibrous re-linkage between the intermediate and the inner and outer zones of the periodontal membrane.

Another basic process contributes to the constant maintenance of tooth attachment to bone during their respective movements. This mechanism involves the continuous formation and reformation of secondary (Haversian) bone in advance of resorptive surfaces (figs. 2, 4). As a bone surface in contact with the periodontal membrane is destroyed, erosive penetration of resorption canals into the bone take place, and new bone is subsequently laid down within these enlarged spaces. The resulting secondary bone has a fibrous matrix that is directly continuous with the fibers of the outer zone of the shifting periodontal membrane and provides localized attachment between the membrane and the alveolar wall during this process of resorptive movement. As older Haversian systems are destroyed by the advancing resorptive front, fibers are uncovered from their matrix in the manner described in previous paragraphs. They become incorporated in turn into the outer periodontal zone where they undergo linkage with the fibrils of the correspondingly moving intermediate zone. As this occurs, new generations of resorption spaces develop in advance of the blood vessels entering the bone from the periodontal membrane, and new Haversian systems are then formed within these spaces. This process of Haversian remodeling functions as a reattachment mechanism in two specific instances. First, it occurs beneath those particular surface areas deep to a resorptive front in which bone removal has resulted in a total destruction of the bone matrix, including its fibers. This characteristically takes place in locations next to and on either side of periodontal blood vessels. Continuations of these vessels pass into the resorption spaces and eventually become the central blood vessels within Haversian canals following the formation of secondary osteones. The overall process provides a means by which reattachment of fibers becomes established in those local-

ized areas where former attachment was destroyed. Haversian remodeling may also be involved in regions where firm fibrous anchorage was previously lacking. This situation, noted earlier, has been found in some scattered areas where formative periodontal bone does not embody periodontal fibers as it is laid down. Although not widespread in the rat, secondary bone reconstruction with Haversian system formation apparently can provide fibrous continuity between the alveolar wall and the membrane where such regions become involved in subsequent bone and tooth movements.

It is noteworthy that Haversian remodeling also occurs in long bones on those particular surfaces where muscles and tendons are attached (Enlow, '62b). Significantly, secondary Haversian systems are characteristically lacking in the bone of rats (and many other species) except in specific areas, such as the periodontal membrane, which involve resorptive surfaces in association with fibrous reattachment. In the skeleton of very young individuals, bone tissues are typically fine-cancellous in structure. The canals within this type of bone are large, and a process of compaction by bone deposition within these available spaces results in the formation of primary osteones (Enlow, '63). This developmental sequence functions in fibrous reattachment in a manner comparable with secondary Haversian remodeling in that both involve the deposition of new bone within large canals or spaces. In very young individuals, the distribution of primary osteones parallels that of the secondary osteones in older individuals.

CONCLUSIONS

Sections of decalcified maxillary bones from a group of young, rapidly growing white rats were stained with a differential collagenous and precollagenous polychrome stain. A second group of rats was treated with tetracycline, a vital bone-marking dye, and their maxillae were then sectioned and studied by fluorescence microscopy. The purpose of these procedures was to trace the sequence of adjustments that take place in the periodontal membrane and alveolar bone dur-

PLATES

versity of Michigan School of Dentistry. Diagrams used in this report were prepared by Mr. William L. Brudon.

LITERATURE CITED

- Behatla, H. L. and R. F. Sognnaes 1963 Tetracycline discoloration and labelling of teeth and bone. A review. *J. South. California D. A.*, 31: 215.
- Bevelander, G., H. Nakahara and G. Rolle 1960 The effect of tetracycline on the development of the skeletal systems of the chick embryo. *Develop. Biol.*, 2: 298.
- Bevelander, G., G. Rolle and S. Cohlan 1961 The effect of administration of tetracycline on the development of teeth. *J. Dent. Res.*, 40: 1020.
- Ecclies, J. D. 1959 Studies on the development of the periodontal membrane: The principal fibers of the molar teeth. *Dental Practit. Dent. Rec.*, 10: 31-35.
- Enlow, D. H. 1962a A study of the post-natal growth and remodeling of bone. *Am. J. Anat.*, 110: 79-102.
- 1962b Functions of the haversian system. *Am. J. Anat.*, 110: 269-306.
- 1963 Principles of Bone Remodeling. Charles C Thomas, Publisher, Springfield, Ill.
- 1964 A study of the postnatal growth of the human mandible. *Am. J. Orthodontics*, 50: 25-50.
- 1965a Growth and remodeling of the human maxilla. *Am. J. Orthodontics*, 51: 446-464.
- 1965b The problem of muscle tension and the stimulation of bone growth. *Anat. Rec.*, 131: 3, 451.
- Finerman, G., and R. A. Milch 1963 In vitro binding of tetracycline to calcium. *Nature*, 198: 486.
- Goldman, H. M. 1957 Histologic structure of the attachment apparatus. *Alpha Omegan*, 25: 102.
- Goto, S. 1952 Studien über die fastern des plexus intermedius der zahnwurgelhaut. *Anat. Inst. Med. Fak., University of Okazama*, 4: 177.
- Gottlieb, B. 1942 Some histologic facts useful in orthodontic practice. *Am. J. Orthodontics*, 28: 167.
- Gregg, J. M., and J. K. Avery 1964 Studies of alveolar bone growth and tooth eruption using tetracycline-induced fluorescence. *J. Oral Ther. and Pharm.*, 1: 268-281.
- Herovici, C. 1963 A polychrome stain for differentiating precollagen from collagen. *Stain Tech.*, 38: 204-205.
- Hoyte, D. A. N., and D. H. Enlow 1966 Wolff's law and the problem of muscle attachment on resorptive surfaces of bone. *Am. J. Phys. Anthro.*, 24: 205-214.
- Humason, G. L. 1962 *Animal Tissue Techniques*. W. H. Freeman and Co., San Francisco. 151-152.
- Hunt, A. M. 1959 Description of the molar teeth and investing tissues of normal guinea pigs. *J. Dent. Res.*, 38: 216-231.
- Orban, B. 1927 Beziehungen zwischen zahn und knochen. *Bewegung der zahn keime*. Z. f. Anat. u. Entw., 83: 804.
- Owen, L. N. 1963 The effects of administering tetracyclines to young dogs with particular reference to localization of drugs in the teeth. *Arch. Oral Biol.*, 8-715.
- Sicher, H. 1923 Bau und funktion des fixationsapparat der meerschweinchenmolaren. *Z. f. Stomat.*, 21: 580.
- 1942 Tooth eruption: The axial movement of continuously growing teeth. *J. Dent. Res.*, 21: 201-210.
- Sicher, H., and J. P. Weinmann 1944 Bone growth and physiologic tooth movement. *Am. J. Ortho. and Oral Surg.*, 30: 109.
- 1954 Principal fibers of the periodontal membrane. *The Bur.*, 55: 2-4.
- 1965 *Oral Anatomy*. C. V. Mosby, St. Louis. 276-277.
- Stallard, R. E. 1963 The utilization of H^3 -proline by the connective tissue elements of periodontium. *Periodontics*, 1: 185-188.
- Stein, G., and J. P. Weinmann 1925 Die physiologische wanderung der Zähne. *Z. f. Stomat.*, 23: 733.
- Tomes, C. S. 1923 *A Manual of Dental Anatomy*. Ed. by H. W. Tims and C. B. Henry. MacMillan Co., New York. 128-132.
- Trott, J. R. 1962 The development of the periodontal attachment in the rat. *Acta anat. (Basel)*, 51: 313-328.
- Weinmann, J. P. 1954 The adaptation of the periodontal membrane to physiologic and pathologic changes. *J. Oral Sur., Oral Med. and Oral Path.*, 8: 977.
- Zwarych, P. D., and M. B. Quigley 1965 The intermediate plexus of the periodontal ligament: History and further investigations. *J. Dent. Res.*, 44: 383-391.

PLATE 1

EXPLANATION OF FIGURES

- 1 Photomicrograph of a tetracycline-injected specimen using ultraviolet light. New bone deposition (light-appearing band) occurs on the alveolar surface (A) at the tension side of the socket. In contrast, bone formation on the pressure side takes place deep to the surface within resorption spaces (B). $\times 50$.
- 2 The periodontal membrane is composed of an inner zone (A) adjacent to the cementum, an intermediate zone (B), and an outer zone (C) continuous with the fibrous matrix of the alveolar wall. The bone surface seen in this section is resorptive, and resorption spaces and secondary Haversian systems (osteones) form and continuously reform (D) deep to the surface in advance of the drifting resorptive front. $\times 100$.
- 3 On the depository alveolar surface (tension side of socket), the inner zone (A), intermediate zone (B), and the outer zone (C) of the periodontal membrane are apparent, although the sequence of changes involved in periodontal drift differs from that on the pressure (resorptive) side. Compare with figure 5. Note the embedded periodontal fibers within the bone. $\times 200$.
- 4 A thin alveolar wall separates two adjacent sockets. The bone surface on the left (C) is resorptive, and that on the right (E) is depository. The inner (A), intermediate (B), and outer (C) zones of the periodontal membrane are seen. As the resorptive surface drifts toward the right, bone matrix fibers are uncovered and become the fibers of the outer zone (C). A trail of such fibers can be seen exiting from primary alveolar bone tissue as well as from secondary Haversian bone. Note that total fiber destruction and loss of attachment occurs, however, in advance of blood vessels (D). Such an area will later become partially filled with bone to become a secondary Haversian system. Note also that Haversian remodeling occurs only in the thicker areas of the alveolar wall and is absent from very thin, transient regions (compare area D with E). $\times 100$.

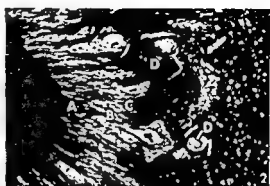
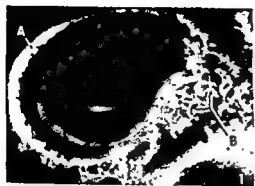


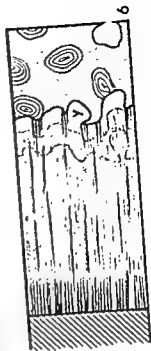
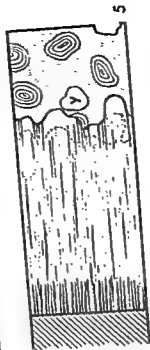
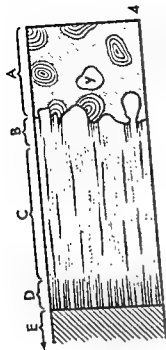
PLATE III

EXPLANATION OF FIGURE

This schematic series of diagrams is an interpretation of adjustment mechanisms involved in the movements of the periodontal membrane during bone and tooth shifts. They illustrate successive and sequential changes that occur in the alveolar bone (A), the outer periodontal zone (B), intermediate periodontal zone (C), inner periodontal zone (D), and the cementum of the root (E) as both the bone and tooth drift to the right (arrows). The increment "U" designates an arbitrary distance moved during each growth stage. The illustrations on the left (1, 2, 3) represent the series of drift changes on the depository (tension) side of the alveolar socket, and the illustrations on the right (4, 5, 6) show changes on the resorptive (pressure) side. The points "x" and "y" are included as random position markers so that movements relative to a fixed point can be visualized.

On the tension side (1, 2, 3), increments of new bundle bone are deposited on the alveolar surface, thereby progressively enclosing the fibers of the outer zone B. At the same time, the peripheral ends of the fibrils in the intermediate zone C are converted into the new fibers of the outer zone as the latter shifts to the right. The stable fibers of the inner zone D are pulled to the right and maintain constant linkage with the labile fibrils of the intermediate zone C. These latter fibrils constantly elongate in a direction toward the right as they simultaneously become converted to outer zone fibers on the left.

On the pressure side (4, 5, 6), the stable fibers of the inner zone are moved to the right and similarly maintain constant linkage with the shortening inner ends of the fibrils in the intermediate zone. Bone-matrix fibers are constantly uncovered from the resorbing surface of A to become the fibers of the outer periodontal zone B. The inner ends of these same fibers are then converted successively into the elongating outer ends of the linkage fibrils in the intermediate zone. Direct fibrous continuity can be traced through each zone from A to E. Extensive bone reconstruction is seen deep to the resorptive alveolar surface, in contrast to the depository side, and resorption canals and secondary osteones are formed. This remodeling mechanism provides re-attachment in those localized areas that previously involved total resorptive destruction of fibrous anchorage. Such alternating areas are shown along the contact between A and B.



Morphogenesis of the Palate in Normal Human Embryos with Special Emphasis on the Mechanisms Involved¹

ALPHONSE R. BURDI AND KATHLEEN FAIST

Department of Anatomy, 2500 East Medical Building,
The University of Michigan, Ann Arbor, Michigan

ABSTRACT The aim of this study was to re-evaluate the classical description of fusion as the closure mechanism of both the hard and soft palates in normal human embryos. Does the soft palate develop by a posterior continuation of shelf apposition, epithelial lamination and disintegration, and by mesenchymal cell fusion as described for the hard palate? Or does the soft palate develop by proliferation and migration of subepithelial mesenchymal growth centers at the posterior edge of the fused hard palate so that the early furrow which separates the two primordial processes of the soft palate is progressively obliterated by mesenchymal merging at the furrow base?

Observations of human embryos prior to, during, and after palatal closure (7-12 wks, 18-75 mm C-R length) indicated (1) an anteroposterior gradient of palatal closure beginning at the primary palate and (2) epithelial fusion remnants found only in the hard palate regions. These observations suggest that the soft palate develops by a displacement of epithelium by mesenchymal merging rather than by epithelial fusion of the entire secondary palatine processes.

The human palate has been traditionally described as forming during the third month of development from the midline fusion of the palatine shelves with each other, with the free margin of the nasal septum, and with the primary palate (Keith, '33; Patten, '53; Kernahan and Stark, '58; Schour, '60; Hamilton, Boyd, Mossman, '62; Wood and Kraus, '62; Ballard, '64; Arey, '65; Maisels, '66). These descriptions further indicated an anteroposterior gradient of closure and epithelial fusion along the entire length of the shelves forming the secondary palate, which includes the hard and soft palates as contrasted to the premaxilla or primary palate.

The purpose of this study is to re-evaluate the traditional description of normal human palatal formation. What are the possible morphogenic mechanisms involved in the early formation of the secondary palate, and, in specific, the formation of the soft palate and uvula? Does the soft palate region develop as a posterior continuation of the epithelial fusion of the more anterior regions of the palatine shelves? Or does the soft palate develop by growth, migration, and coalescence (merging) of subepithelial mesenchymal centers along the posterior edge of the fused future hard palate? The latter mechanism, unlike palatal shelf fusion, does not involve the sequence of epithelial abutment, lamination, and subsequent breakdown.

MATERIALS AND METHODS

Thirty-one human embryos ranging in size from 18 to 75 millimeters crown-rump length and in age from 7 to 12 weeks were studied (table 1). This series represented the secondary palate before, during, and after its closure.

Each embryo was routinely fixed in 10% neutral buffered formalin, histologically prepared and sectioned frontally at either 10 or 15 μ . Sections were serially mounted and alternately stained with a Masson triple stain and with hematoxylin and eosin. Each embryo was then studied by (1) light microscopy to describe any developmental tissue changes and (2) by graphic reconstruction. The latter technique is similar to classic waxplate reconstruction. Each serial section was pro-

¹ This investigation was supported by research grant HD 00178 from the National Institute of Child Health and Human Development and a National Science Foundation Summer Undergraduate Research Fellowship (CE-6283) to K. F.

TABLE 1
Developmental and estimated chronologic
ages of embryos

Human embryo no. ¹	C-R length	Age ²
	mm	weeks
EH 650	18	7
EH 619	18	7
EH 358	18	7
EH 933	20	7
EH 600	20	7
EH 592	21	7
EH 739	22	7
EH 598	22	7
EH 419	23	7
EH 880-A	24	7
EH 591	25	8
EH 938	26	8
EH 589	26	8
EH 892	27	8
EH 840	28	8
EH 512	29	8
EH 882	29	8
EH 15-A	30	8
EH 377	32	8
EH 946	34	8
EH 785	35	9
EH 523	36	9
EH 479	36	9
EH 746	37	9
EH 621	38	9
EH 17-E	39	9
EH 909	40	9
EH 18	45	9
EH 784	55	10
EH 198	58	11
EH 628	75	12

¹ From The University of Michigan Embryological Research collection.

² Chronologic ages determined upon basis of crown-rump length according to Wood and Kraus ('62).

jected and traced at a predetermined magnification ($\times 50$). A reference perpendicular line was then drawn on each tracing so that it passed through the middle of the frontally sectioned nasal septum and, if present, through the epithelial remnants of palatal shelf fusion which were evident in the midline.

The actual graphic reconstruction of the palatal region called for millimeter-ruled graph paper upon which was arbitrarily placed a line corresponding to the constructed reference line on each tracing. Space on each graph was allotted to equal the thickness of each projected serial section multiplied by the magnification factor, e.g., 10μ section thickness $\times 100$ times enlargement = 1000μ or 1.0 mm of graph space. Then, distances of the dental lamina and enamel organs were measured

from the perpendicular on the tracing and each value plotted on the graph paper. In this manner, the contour of the entire dental arch was reconstructed and taken to represent the margins of the developing palatal region. The locations of the future incisive and greater palatine foramina, the greater palatine nerves, the palatine processes of the maxillary bones, and the loss of connection between the palate and the nasal septum were landmarks also indicated on each graphic reconstruction. The number of epithelial fusion remnants per section evident along the midpalatal line was mapped on the graphic reconstruction by a color key: 0-3 remnants — blue, 4-6 remnants — red, 7-9 remnants — green, and orange for ten or more remnants.

RESULTS

During the seventh and early eight weeks, 18-25 mm C-R length embryos had separate palatine shelves. At seven weeks in utero (EH 650 and 619), the palatine shelves appeared as slight projections extending medially from each maxillary process. In the nine older specimens of this group (19-25 mm C-R length), each palatine shelf was greater in volume and was obliquely to vertically oriented. Anteriorly, each shelf was thick and triangular in shape and conformed in shape to the lateral contour of the interposed tongue mass. The posterior shelf regions of these same embryos were long, slender, and vertical in position.

The secondary palate was also open in the 26-29 mm C-R length group. Unlike the previous group, these five embryos showed a clear regional difference in the position of the palatine shelves. Anteriorly, each shelf was horizontally oriented and grew toward the midline above the tongue. Posteriorly, the palatine shelves remained as slender, vertically oriented projections extending inferomedially to the base of the tongue. This characteristic transition between the anterior and posterior regions was identified by (1) the presence of the nerves descending to the vomeronasal (Jacobson's) organs, (2) the distal extent of the two paraseptal cartilages underlying the anterior-most portion of the septum, and (3) the first indication of vomerine ossification centers underlying the pos-

erior area of the cartilaginous septum in the midline.

Closure of the secondary palate was first observed at eight weeks in one transitional embryo at 29 mm C-R length (EH 882) and in seven other embryos ranging in crown-rump length from 30 to 37 mm. Regions of the palatine shelves which were horizontally oriented in the younger group were the first palatal shelf segments in contact (1) each other, (2) the primary palate, and (3) the inferior edge of the nasal septum. Subsequent fusion occurred first in the region of the future incisive canal as evidenced by the oblique course of the descending nasopalatine nerves in the canal. Septopalatine contact followed both anteroposterior and superoinferior gradients (figs. 1-2).

The oldest series of embryos (38-75 mm C-R length) verified these gradients of palatine closure observed earlier and also indicated a difference in the developmental fate of the epithelium covering the future hard and soft palate regions of the palatine shelves. The anatomical distinction between these two palatal regions was made by locating (1) the change in direction of the descending palatine nerves from vertical to anteroposterior in the palatal shelf mesenchyme which corresponded in position to the future greater palatine foramen, and (2) the posterior-most connection between the nasal septum and palate immediately anterior to Rathke's pocket which arose as a midline diverticulum from the early oral cavity. The primary differences observed were related

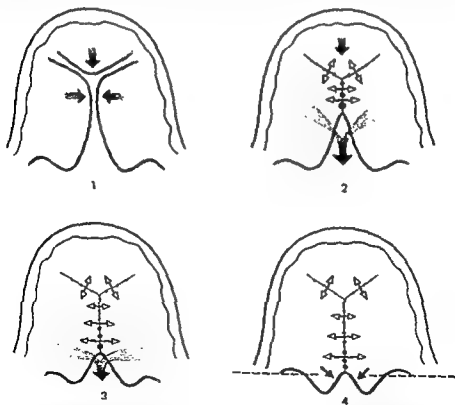


Fig. 1 Fusion mechanism of the hard palate. Inferior view of the palatine shelves showing the gradients of anteroposterior closure (large stippled arrows). Note the sequential changes in size and distribution of epithelial remnants along junction lines and true fusion by intersheaf mesenchymal bridges (open arrows) between remnants. Solid arrows in stage 4 represent the merging mechanism of the soft palate.

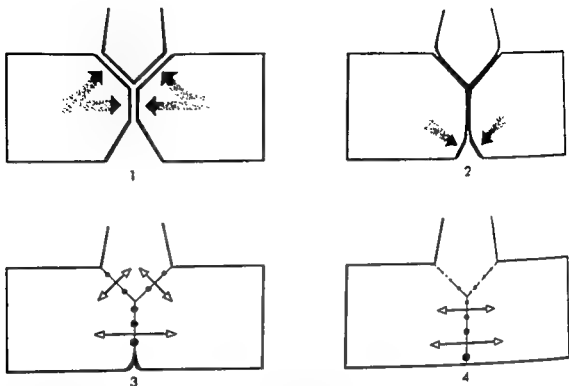


Fig. 2 Fusion mechanism of the hard palate. Stages of septopalatine closure illustrating super inferior contact fusion gradients as seen in frontal section.

to the sequential development of a laminated fusion epithelium between the shelves, breakdown of the raphe, and, later, the occurrence and distribution of midline epithelial remnants.

Following initial midline contact and the formation of the incisive canal, the abutting layers of cuboidal epithelium covering each palatine shelf fused to form a laminated epithelial raphe. Graphic reconstructions of intermediate and older embryos (30-75 mm C-R length) demonstrated progressive changes in this early raphe. First, as more posterior regions of the shelves contact each other, the raphe formed earlier in the anterior areas became attenuated and interrupted by mesenchymal cells bridging from one shelf to another, i.e., true fusion. The number of epithelial remnants in the first areas of shelf fusion then decreased from ten or more per serial section to zero to three per section with a concomitant increase in the areas of the intersheaf mesenchymal bridges between remaining remnants. According to this developmental gradient, newer areas of shelf fusion had the greatest number of epithelial remnants and the

least amount of mesenchymal bridging whereas the older areas of fusion had fewer epithelial remnants and larger areas of mesenchymal cells bridging between shelves. This anteroposterior change in epithelial development was observed for only the developing hard palate.

Neither a midline epithelial raphe nor epithelial remnants were found in the area of newly formed soft palate and uvula. This was clearly demonstrated in the embryos from late nine through twelve weeks, where the soft palate was progressively closing its intersheaf furrow without demonstrating a fusion epithelium. The absence of epithelial involvement in the soft palate was compared with the hard palate areas in these same embryos which continued to show a series of epithelial remnants. These remnants were especially pronounced along the junction lines in the posterior half of the hard palate.

The bilateral soft palatine shelves continued to consolidate by a condensation of mesenchyme in the midline. Our graphic reconstructions showed a gradual obliteration of the original intersheaf furrow in both the anteroposterior and superoinferior

directions (fig. 3). Complete closure of the soft palate by mesenchymal bridging was seen at 12 weeks in the 75 mm C-R length embryo.

The abutting surfaces of the palatine shelves and the nasal septum were covered by a single layer of cuboidal cells. This epithelium at eight weeks became progressively stratified and laid on a distinct basement membrane. The outermost layer of cells remained cuboidal. Stratification continued in the oldest embryos studied (55-75 mm C-R length) followed by a clear differentiation of more regional types of epithelium. A non-keratinized stratified squamous epithelium lined the oral surface of the entire palate whereas the septum and the nasal surface of the palate were covered by a pseudostratified columnar epithelium with goblet cells. The

stratified epithelium on the oral surface of the palate was thickest in the midline and anterior regions and became thinner and attenuated in the soft palate.

Histological observations of embryos seven through eight weeks (18-32 mm C-R length) generally showed little cellular differentiation in the bulk of palatal shelf mesenchyme. Older specimens of the series from nine through 12 weeks did show blood vessels close to the oral surface of the shelves. In addition, there were increasing amounts of bone extending toward the midline from premaxillary and maxillary ossification centers as discontinuous spicules.

DISCUSSION

In the present study, observations of the secondary palate prior to, during, and

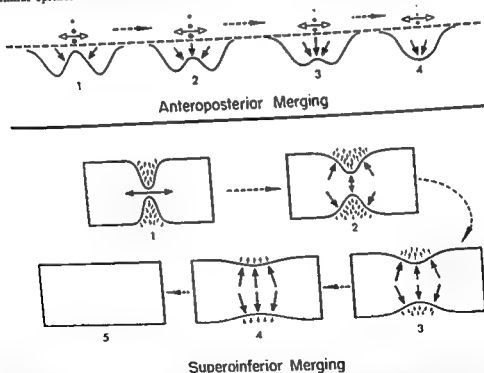


Fig. 3 Merging mechanism of the soft palate. In the sequence summarizing anteroposterior merging, stage one is identical to the posterior region of stage four in figure 1. Directions of subepithelial mesenchymal growth and resultant obliteration of the intersheft furrow are shown by the large-solid merging arrows. Note epithelial remnants remaining anteriorly in the hard palate. The superoinferior merging sequence also illustrates the differential growth of subepithelial mesenchymal centers with the progressive obliteration (small solid arrows) of the furrow which normally indents the superior and inferior surfaces of the developing soft palate. Mesenchymal hypoplasia during any of these stages could lead to submucous clefts.

Immediately following closure suggest that fusion may not be the only mechanism involved as classically described. This classical description of palatal closure involves, in sequence, the midline contact of the palatine shelves with each other and with the nasal septum, the contact, fusion, and lamination of abutting epithelial surfaces, the subsequent breakdown of the laminated midline raphe into epithelial aggregates, and then true fusion of the shelves by mesenchymal cells bridging from one shelf to the other between the epithelial aggregates. These developmental events could only be verified for regions of the secondary palate destined to become hard palate.

The idea that another mechanism is involved in secondary palate closure stems from the developmental occurrence, distribution, and longevity of midline epithelial remnants of the secondary palate. These remnants are characteristically arranged either as an uninterrupted raphe or as isolated epithelial aggregates separated by mesenchymal cells. More importantly, however, they are only found in the hard palate regions of the secondary palate. This observation on the regional distribution of epithelial remnants is supported by Bergengrün ('09) who found that epithelial remnants formed a continuous raphe in the midline of only the hard palate in the embryo. His observations are complemented by other studies. Schumacher ('27) reported that these cornified remnants regress rapidly after birth and usually disappear by the third year; Wood and Kraus ('62) have verified these observations more recently.

In the embryo these residual epithelial cells of the palate can continue to differentiate, proliferate, and gradually acquire the character of enlarged epithelial "pearls" (Barry, '61). Further differentiation of these pearls can result in pathologic median palatine fissural cysts. Interestingly, except for one clinical case that will be cited later, these midpalatine cysts have only been seen, diagnosed, and reported as occurring in the hard palate (Orban, '57; Ash, '61; Thoma, '63; Clark, '65; Kerr and Ash, '65). It seems reasonable to explain this regional limitation of palatal cysts postnatally on the basis that midpalatine

epithelial fusion remnants, from which these cysts arise, occur only in the hard palate region of the embryo during palatal closure.

If the entire secondary palate were to close by fusion, and the longevity of resultant epithelial remnants were the same along the entire line of palatal fusion extending from the incisive canal to the uvula, it is both anatomically and clinically significant to ask why midpalatine epithelial remnants are not also found in the soft palate as it closes.

As the secondary palatine shelves unite by fusion in an anteroposterior gradient, the posterior unfused regions of the shelves destined to become soft palate are united by a common base of mesenchyme at the posterior edge of the future hard palate. Thus, after the hard palate fuses two small mesenchymal processes covered by epithelium extend posteriorly toward the oropharynx. Continued development of these mesenchymal processes is dependent on localized rate changes in proliferation, aggregation, and posterior migration of mesenchymal cells in the common base area and in the two soft palate processes springing from it. Obviously, the most critical component in this merging mechanism of the soft palate and uvula is mesenchymal growth and migration.

The essential difference between fusion and merging mechanisms relates to the method by which the palatal shelf epithelium is pushed out or displaced from between the two soft palatal processes by merging of subepithelial growth centers instead of epithelial abutment and disintegration as in fusion. Figure 5 summarizes the two mechanisms of palatal closure suggested by this study. The formation of the soft palate by mesenchymal merging and epithelial displacement provides some explanation as to why epithelial pearls and potential cysts are restricted to the hard palate.

Streeter ('51) recognized the importance of this growth mechanism in smoothing out the various surface swellings and ridges of the human face during the first three months in utero. He considered each swelling as corresponding to growth centers in the underlying common mesen-

chyme. The furrows that lie between the swellings were progressively obliterated as the proliferation and merging cells filled in at the base of the furrow. This called for a relatively more rapid rate of merging at the furrow base than laterally in the processes surrounding the furrow. Peter ('13) earlier had found that grooves separating the embryonic facial processes do not disappear as a result of epithelial fusion but that they become shallower and eventually obliterated, as the increase in the subepithelial mass produced a new surface level. Stimulated by these early descriptions, Patten ('61) called this a merging mechanism.

That this merging mechanism is not specific to the development of the soft palate is further illustrated by the normal formation of the philtrum of the lip. During the sixth and seventh weeks in utero, two nasomedial processes lie between the nasal pits and are separated from each other along their labial surfaces by a normal midline furrow. This furrow is progressively smoothed out during the eighth week by a merging of its underlying frontal mesenchyme which, if it doesn't occur, can lead to a midline cleft of the philtrum, i.e., a true harelip. The development of the philtrum also indicates how a mesenchymal process and its surface epithelium can be regionally affected by different developmental mechanisms as fusion and merging. Bilateral or unilateral cleft lip stems from a failure in the fusion mechanism between the nasomedial and maxillary processes of the upper jaw during the second month.

Similar to the developing philtrum, the development of the soft palate and uvula involves the obliteration of midline furrows which not only separate the two soft palate processes but also indent the superior and inferior surfaces of the soft palate as it coalesces in an anterior to posterior direction. Defects in the merging mechanism of the soft palate involving mesenchymal hypoplasia, and/or a reversal of localized growth rates, could result in such clinical entities as cleft or bifid uvulae, submucous clefts, and, possibly, uvular cysts.

Patten ('61) explains how a cyst can develop through a defect in the merging

mechanism. Unlike the normal obliteration of a furrow by merging, the mesenchymal cells at the base of the furrow are relatively inactive as compared to the cells in the processes themselves. As a result of this abnormal reversal of growth rate, the original furrow is not obliterated but instead deepened by the mesenchymal growth surrounding it laterally. Continued hypoplasia at the base of the furrow and relatively faster growth in the lateral processes would result in a deepened furrow. Varying degrees of cleft soft palates are

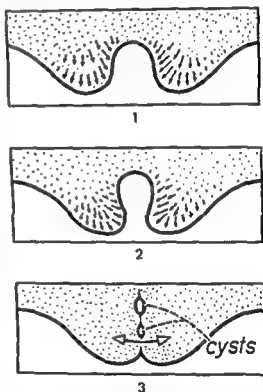


Fig. 4 Schematic diagrams suggesting how a reversal of normal gradients of subepithelial mesenchymal merging can result in an epithelial inclusion cyst. Mesenchymal cells at the furrow base are relatively inactive as compared with cells laterally in the two processes of the soft palate (stage 1). As a result of this abnormal rate reversal, the original midline furrow can deepen anteroposteriorly (stage 2). Compare this stage with the normal obliteration of the furrows shown in figure 3. Continued abnormal growth toward the midline could result in a localized fusion epithelium and a potential cyst. Once having formed an isolated cyst, the surrounding mesenchyme can again resume merging and posterior growth of the soft palate (stage 3).

immediately following closure suggest that fusion may not be the only mechanism involved as classically described. This classical description of palatal closure involves, in sequence, the midline contact of the palatine shelves with each other and with the nasal septum, the contact, fusion, and lamination of abutting epithelial surfaces, the subsequent breakdown of the laminated midline raphe into epithelial aggregates, and then true fusion of the shelves by mesenchymal cells bridging from one shelf to the other between the epithelial aggregates. These developmental events could only be verified for regions of the secondary palate destined to become hard palate.

The idea that another mechanism is involved in secondary palate closure stems from the developmental occurrence, distribution, and longevity of midline epithelial remnants of the secondary palate. These remnants are characteristically arranged either as an uninterrupted raphe or as isolated epithelial aggregates separated by mesenchymal cells. More importantly, however, they are only found in the hard palate regions of the secondary palate. This observation on the regional distribution of epithelial remnants is supported by Bergengrün ('09) who found that epithelial remnants formed a continuous raphe in the midline of only the hard palate in the embryo. His observations are complemented by other studies. Schumacher ('27) reported that these cornified remnants regress rapidly after birth and usually disappear by the third year; Wood and Kraus ('62) have verified these observations more recently.

In the embryo these residual epithelial cells of the palate can continue to differentiate, proliferate, and gradually acquire the character of enlarged epithelial "pearls" (Barry, '61). Further differentiation of these pearls can result in pathologic median palatine fissural cysts. Interestingly, except for one clinical case that will be cited later, these midpalatine cysts have only been seen, diagnosed, and reported as occurring in the hard palate (Orban, '57; Ash, '61; Thoma, '63; Clark, '65; Kerr and Ash, '65). It seems reasonable to explain this regional limitation of palatal cysts postnatally on the basis that midpalatine

epithelial fusion remnants, from which these cysts arise, occur only in the hard palate region of the embryo during palatal closure.

If the entire secondary palate were to close by fusion, and the longevity of resultant epithelial remnants were the same along the entire line of palatal fusion extending from the incisive canal to the uvula, it is both anatomically and clinically significant to ask why midpalatine epithelial remnants are not also found in the soft palate as it closes.

As the secondary palatine shelves unite by fusion in an anteroposterior gradient, the posterior unfused regions of the shelves destined to become soft palate are united by a common base of mesenchyme at the posterior edge of the future hard palate. Thus, after the hard palate fuses two small mesenchymal processes covered by epithelium extend posteriorly toward the oropharynx. Continued development of these mesenchymal processes is dependent on localized rate changes in proliferation, aggregation, and posterior migration of mesenchymal cells in the common base area and in the two soft palate processes springing from it. Obviously, the most critical component in this merging mechanism of the soft palate and uvula is mesenchymal growth and migration.

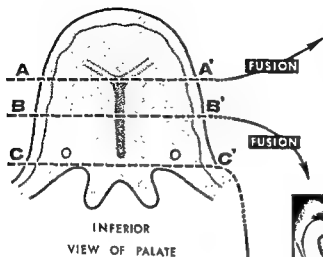
The essential difference between fusion and merging mechanisms relates to the method by which the palatal shelf epithelium is pushed out or displaced from between the two soft palatal processes by merging of subepithelial growth centers instead of epithelial abutment and disintegration as in fusion. Figure 5 summarizes the two mechanisms of palatal closure suggested by this study. The formation of the soft palate by mesenchymal merging and epithelial displacement provides some explanation as to why epithelial pearls and potential cysts are restricted to the hard palate.

Streeter ('51) recognized the importance of this growth mechanism in smoothing out the various surface swellings and ridges of the human face during the first three months in utero. He considered each swelling as corresponding to growth centers in the underlying common mesen-

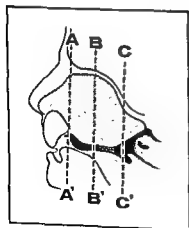
thus explainable (Berans, 1893; Stark, '61; Meskin, Gorlin, Isaacson, '64). The epithelial lining of each side of the furrow could also approximate and contact to form a localized fusion epithelium and possibly a cyst (fig. 4). To our knowledge, there has been only one observation of a single soft palate, i.e., uvular, cyst (Andrews, '62).

LITERATURE CITED

- Andrews, B. F. 1962 Epidermal inclusion cyst of the uvula in infancy. *Am. J. Dis. Child.*, 103: 174-176.
- Arey, L. B. 1965 *Developmental Anatomy*. W. B. Saunders Co., Philadelphia, 7th Ed., Chap. XIII, pp. 213-244.
- Ash, M. M., Jr. 1961 *A Handbook of Differential Oral Diagnosis*. C. V. Mosby Co., St. Louis, Chap. D, pp. 70-71.
- Ballard, W. W. 1964 *Comparative Anatomy and Embryology*. The Ronald Press Co., New York, Chap. 13, pp. 227-240.
- Barry, A. 1961 Development of the branchial region of human embryos with special reference to the fate of epithelia. In: *Congenital Anomalies of the Face and Associated Structures*. Ed. by S. Pruzansky, Charles C Thomas Co., Springfield, pp. 46-62.
- Berans, C. 1893 *Anomalies of the uvula*. *Philadelphia Med. Bull.*, 15: 177-179.
- Bergengrün, P. 1909 "Epithelperlen" und Epithelstränge in der Raphe des harten Gaumens. *Arch. Entw. Mech. Org.*, 28: 277-326.
- Clark, H. B., Jr. 1965 *Practical Oral Surgery*. Lea & Febiger, Philadelphia, 3rd Ed., Chap. 9, pp. 255-297.
- Davies, J. 1963 *Human Developmental Anatomy*. The Ronald Press Co., New York, Chap. 11, pp. 123-134.
- Hamilton, W. J., J. D. Boyd and H. W. Mossman 1962 *Human Embryology*. Williams and Wilkins Co., Baltimore, 3rd Ed., Chap. X, pp. 203-266.
- Kelth, A. 1933 *Human Embryology and Morphology*. William Wood & Co., Baltimore, 5th Ed., Chap. XIII, pp. 182-206.
- Kernahan, D. A., and R. B. Stark 1958 A new classification for cleft lip and cleft palate. *Plastic and Reconstruct. Surg.*, 22: 435-441.
- Kerr, D. A., and M. M. Ash, Jr. 1965 *Oral Pathology*. Lea & Febiger, Philadelphia, 2nd Ed., Chap. 3, pp. 29-57.
- Maisels, D. O. 1966 Early orthopaedic treatment of clefts of the primary and secondary palates: A surgeon's view. *Cleft Palate J.*, 3: 76-86.
- Meskin, L. H., R. J. Gorlin and R. J. Isaacson 1964 Abnormal morphology of the soft palate: I. The prevalence of the cleft uvula. *Cleft Palate J.*, 1: 342-346.
- Orban, B. J. 1957 *Oral Histology and Embryology*. C. V. Mosby Co., St. Louis, 4th Ed., Chap. 1, pp. 17-33.
- Patten, B. M. 1953 *Human Embryology*. McGraw-Hill Book Co., Inc., New York, 2nd Ed., Chap. 14, pp. 427-459.
- 1961 The normal development of the facial region. In: *Congenital Anomalies of the Face and Associated Structures*. Ed. by S. Pruzansky, Charles C Thomas Co., Springfield, pp. 11-45.
- Peter, K. 1913 *Atlas der Entwicklung der Nase und des Gaumens beim Menschen, mit Einschluss der Entwicklungsstörungen*. Jena, Gustav Fischer, vii and 130.
- Schour, I. 1960 *Noyes' Oral Histology and Embryology*. Lea & Febiger, Philadelphia, 8th Ed., Chap. 2, pp. 29-43.
- Schumacher, S. 1927 *Die Mundhöhle*. In: *Handbuch der Mikroskopischen Anatomie des Menschen*. Ed. by W. VonMollendorff, Springer, Berlin, Vol. 5, pp. 1-32.
- Stark, R. B. 1961 *Embryology, pathogenesis and classification of cleft lip and cleft palate*. In: *Congenital Anomalies of the Face and Associated Structures*. Ed. by S. Pruzansky, Charles C Thomas Co., Springfield, pp. 66-84.
- Streeter, G. L. 1951 *Developmental Horizons in Human Embryos*. Age Groups XI to XXIII. *Carnegie Contrib. to Emb.*, Reprint Vol. 2.
- Thoma, K. H. 1963 *Oral Surgery*. C. V. Mosby Co., St. Louis, 4th Ed., Chap. 35, pp. 886-895.
- Wood, P. J., and D. S. Kraus 1962 Prenatal development of the human palate. *Archiv. Oral Biol.*, 7: 137-150.



SAGITTAL
VIEW OF PALATE



MERGING



PLATE 1

EXPLANATION OF FIGURE

- 5 *Summary of fusion and merging mechanisms underlying palatal closure.* Closure of the future hard palate by fusion is shown by representative frontal sections beginning at the junction of the primary and secondary palates (A-A') and extending along the entire hard palate (B-B') as indicated by the full length of the nasal septum (heavy-stippled midline area in diagram of inferior view of palate). Serial section C-C' represents the formation of the soft palate by sub-epithelial mesenchymal merging in regions posterior to the septum and the greater palatine nerves.

Number key for anatomical landmarks

- | | |
|-----------------------------------|---------------------------------------|
| (1) nasal cavity | (16) greater wing of sphenoid bone |
| (2) nasal septum | (17) ocular muscles |
| (3) paraseptal cartilages | (18) vomerine bone |
| (4) lateral wing of nasal capsule | (19) maxillary bone |
| (5) dental lamina | (20) tongue muscle |
| (6) eye | (21) palatine shelf and blood vessels |
| (7) epithelial fusion remnants | (22) body of sphenoid bone |
| (8) oral cavity | (23) Rathke's pocket |
| (9) tongue | (24) nasopharynx |
| (10) Meckel's cartilage | (25) oropharynx |
| (11) mandible | (26) maxillary blood vessels |
| (12) premaxillary bone | (27) soft palate |
| (13) eyelids | (28) submandibular gland |
| (14) forebrain | (29) hyoid bone |
| (15) nerves to vomeronasal organs | |

An Electron Microscopic and Radioautographic Study of the Rat Parotid Gland after Actinomycin D Administration¹

SEONG S. HAN

Departments of Oral Biology and Anatomy, The University of Michigan
School of Dentistry and Medical School, Ann Arbor, Michigan

ABSTRACT Rat parotid glands have been examined by electron microscopy and radioautography (³H-leucine incorporation) at various intervals following an injection of actinomycin D in the amount of 0.125 µg per gram of body weight. Light microscopic observations confirmed results from previous experiments similar to this. Radioautographs showed a definite drop in number of silver grains in acinar cells of the parotid from experimental animals. This was most pronounced in 7-day rats which received ³H-leucine four hours prior to sacrifice. Electron microscopic observations revealed a generalized reduction in number and degree of the organization of organelles concerned with protein synthesis. Furthermore, frequent appearances of lipid droplets, cytolysosomes and crystalloid structures were noted. Changes of the nucleolus included the reduction of its size and the formation of spherical encapsulated bodies. A brief discussion is made of these results in relation to the biochemical nature of actinomycin effects on protein producing cells.

During the past several years numerous biochemical and radioautographic workers have taken advantage of the unique effect of actinomycin D on RNA and protein biosyntheses. Results from these studies show that most, if not all, of the cytoplasmic RNA is derived from the nucleus and that the administration of actinomycin D brings forth a substantial reduction of protein and total inhibition of RNA syntheses (Tamaoki and Mueller, '62; Caspersson et al., '63; Franklin, '63; Levy, '63; and Merits, '63), although there has been some conjecture regarding the resistance of four sRNA synthesis (Franklin, '63). The degradation of ribosomes by actinomycin D has been observed both under *in vivo* (Staehelin et al., '63) and *in vitro* conditions (Wiesner et al., '65).

Insofar as the structural reflection of these chemical effects is concerned, remarkable nuclear and nucleolar changes following the administration of the antibiotic in a massive dose have attracted the attention of several electron microscopists (Journey and Goldstein, '61; Goldstein et al., '60; Schoeffl, '64; and Jezequel and Bernhard, '64). Few described any modification of cytoplasmic structures in those studies dealing with the acute effect.

On the other hand, serious alterations in histological and cytochemical characteristics of rat salivary glands have been observed following a sublethal dose of the actinomycin D (Jhee and Han, '64; and Jhee, Han and Avery, '65). The cytological changes observed in the salivary gland cells include: an early nuclear pycnosis and decrease in number of nucleoli, loss of the cytoplasmic basophilia, and vacuolization and rarification of the cytoplasm. The aim of the present communication is to describe the fine structural changes of the rat parotid gland following a sublethal dose injection of actinomycin D. A limited number of light micrographs and radioautographs which illustrate the picture of ³H-leucine incorporation will be presented for the purpose of orientation and correlation.

MATERIAL AND METHODS

Adult male Sprague-Dawley rats were paired according to weight and one of each pair was injected with 0.125 µg actinomycin D/g body weight. Three pairs as a group were sacrificed on days 1, 3, 5, 7, 10, 14 and 21 after the injection. One pair

¹This study was supported in part by grants from U.S.P.H.S. (DE-1620) and from American Cancer Society (1N-40-F).

An Electron Microscopic and Radioautographic Study of the Rat Parotid Gland after Actinomycin D Administration¹

SEONG S. HAN

Departments of Oral Biology and Anatomy, The University of Michigan
School of Dentistry and Medical School, Ann Arbor, Michigan

ABSTRACT Rat parotid glands have been examined by electron microscopy and radioautography (³H-leucine incorporation) at various intervals following an injection of actinomycin D in the amount of 0.125 µg per gram of body weight. Light microscopic observations confirmed results from previous experiments similar to this. Radioautographs showed a definite drop in number of silver grains in acinar cells of the parotid from experimental animals. This was most pronounced in 7-day rats which received ³H-leucine four hours prior to sacrifice. Electron microscopic observations revealed a generalized reduction in number and degree of the organization of organelles concerned with protein synthesis. Furthermore, frequent appearances of lipid droplets, cytolysomes and crystalloid structures were noted. Changes of the nucleolus included the reduction of its size and the formation of spherical encapsulated bodies. A brief discussion is made of these results in relation to the biochemical nature of actinomycin effects on protein producing cells.

During the past several years numerous biochemical and radioautographic workers have taken advantage of the unique effect of actinomycin D on RNA and protein biosyntheses. Results from these studies show that most, if not all, of the cytoplasmic RNA is derived from the nucleus and that the administration of actinomycin D brings forth a substantial reduction of protein and total inhibition of RNA syntheses (Tamaoki and Mueller, '62; Caspersson et al., '63; Franklin, '63; Levy, '63; and Lerits, '63), although there has been some conjecture regarding the resistance of four RNA synthesis (Franklin, '63). The degradation of ribosomes by actinomycin D has been observed both under *in vivo* (Staehelin et al., '63) and *in vitro* conditions (Wiesner et al., '65).

Insofar as the structural reflection of these chemical effects is concerned, remarkable nuclear and nucleolar changes following the administration of the antibiotic in a massive dose have attracted the attention of several electron microscopists (Journey and Goldstein, '61; Goldstein et al., '60; Schoeff, '64; and Jezequel and Bernhard, '64). Few described any modification of cytoplasmic structures in those studies dealing with the acute effect.

On the other hand, serious alterations in histological and cytochemical characteristics of rat salivary glands have been observed following a sublethal dose of the actinomycin D (Jhee and Han, '64; and Jhee, Han and Avery, '65). The cytological changes observed in the salivary gland cells include: an early nuclear pyknosis and decrease in number of nucleoli, loss of the cytoplasmic basophilia, and vacuolization and rarification of the cytoplasm. The aim of the present communication is to describe the fine structural changes of the rat parotid gland following a sublethal dose injection of actinomycin D. A limited number of light micrographs and radioautographs which illustrate the picture of ³H-leucine incorporation will be presented for the purpose of orientation and correlation.

MATERIAL AND METHODS

Adult male Sprague-Dawley rats were paired according to weight and one of each pair was injected with 0.125 µg actinomycin D/g body weight. Three pairs as a group were sacrificed on days 1, 3, 5, 7, 10, 14 and 21 after the injection. One pair

¹ This study was supported in part by grants from U.S.P.H.S. (DE-1620) and from American Cancer Society (IN-40-F).

of these were intracardially injected with H^3 -leucine in the amount of 2.5 μ C/g body weight ten minutes prior to sacrifice, whereas the remaining two pairs were given the same injection 30 minutes and four hours before the sacrifice respectively.

Under ether anesthesia small pieces of the parotid gland were dissected out by iridectomy scissors and fixed either in 2% OsO_4 in M/10 phosphate buffer at pH 7.4 or in 2% glutaraldehyde followed by OsO_4 post-fixation. The tissues were dehydrated, embedded in Epon in a routine manner, sectioned on a LKB ultramicrotome and studied in a Hitachi HU-11 electron microscope.

For radioautography, pieces of the parotid gland were fixed in Bouin's solution, double-embedded in parlodion and paraffin, sectioned at 6 μ , coated with Kodak NTB-3 liquid nuclear track emulsion and kept in an air-tight slide box containing Drierite stored at 4° C. After 4 to 6 weeks of exposure the slides were developed in Dolmi, stained with hematoxylin and eosin, and observed under a Zeiss photomicroscope.

OBSERVATIONS

Histologic and radioautographic appearance

The microscopic appearance of parotid cells confirmed data from previous studies. In control animals, acinar cells were well defined containing a distinct basophilic region at the base and a supernuclear accumulation of zymogen granules. The nucleus was large, rounded and vesicular in appearance having one or more prominent nucleoli (fig. 1). One day after the administration of actinomycin D, the pycnosis of acinar nuclei became apparent. By day 3, many acinar cells had condensed pycnotic nuclei with an apparent reduction of the cytoplasmic basophilia (fig. 2). By the end of the first week, the nuclear pycnosis had progressed further and occasional vacuoles were seen in association with the nucleus (fig. 3). The cytoplasm of the cell became less dense and gave the impression of a generalized rarification. By day 10, nuclei started to return to normalcy assuming a rounded contour with the re-appearance of nucleoli and by day 14

many acinar cells showed a fair amount of the basal basophilia (fig. 4).

In addition radioautographic slides showed the following results. Ten minutes and 30 minutes after injection of H^3 -leucine, silver grains were more or less diffusely distributed throughout the gland cell both in control and experimental animals, although in the former group more silver grains appeared to be concentrated in the basal and supernuclear Golgi region of the cell after 30 minutes of H^3 -leucine injection. By four hours after injection the number of grains in experimental animals were reduced in number and they were distributed evenly throughout the entire cell (fig. 5). This was most obvious in the day 7 animal. In contrast to this, cells from control glands after four hours of H^3 -leucine injection showed a definite concentration of silver grains in the apical cytoplasm which corresponded to the area of zymogen accumulation (fig. 6).

Electron microscopy

Acinar cells. For the convenience of description most of the micrographs to be presented will be from rats sacrificed seven days after actinomycin D. As has been shown by previous workers, acinar cells from control animals contained numerous profiles of regularly arranged rough-surfaced endoplasmic reticulum (RER) which were basally located and occasional mitochondria being interposed between membranes of the RER (figs. 7, 9). Supernuclearly, a large Golgi complex was located. The Golgi complex was made up of 4 or 5 units, each one of which was composed of several stacks of flattened membranes and a large number of small vesicles and a few vacuoles. Elsewhere the apical cytoplasm was filled with zymogen granules. Under conditions of the fixation zymogen granules had a somewhat homogeneous, finely granular interior of moderate electron density and the surrounding membrane often showed irregularities and possible breakages. Only occasional granules showed the bizonal appearance, i.e. a darker outer zone with a lighter interior.

In comparison to this, cells from experimental animals were usually smaller, containing fewer profiles of the RER in the basal region (fig. 8). Despite the reduction

in total number of ribosomes in experimental animals, a fair amount of polysomes were seen, whenever the RER was oriented in a favorable plane. The Golgi apparatus was definitely reduced in its degree of organization and only 1 or 2 units of stacked membranes were visualized in any single cell at a given plane of section. Individual units of the Golgi complex were small and were devoid of or drastically reduced in number of the vesicles (fig. 10). Many zymogen granules gained peripheral density showing the bizonal appearance, while others have lost the clarity of the outer limiting membrane (fig. 8).

In certain cells zymogen granules formed aggregates of various sizes by fusion of several to a dozen or more granules (fig. 11). Although the preservation of membranes surrounding the circumference of such aggregates was questionable in osmium fixed preparations, clear-cut limiting membranes were observed following glutaraldehyde fixation. Occasionally the aggregates contained other cytoplasmic organelles such as ribosomes, RER, mitochondria and what appeared to be lipid droplets. In many instances, the zymogen granules contained within the aggregate body maintained its own limiting membranes. They were similar in appearance to typical cytoisosomes which primarily contained mitochondria and degraded products of the RER, and increased in number towards the end of the first week (fig. 12). A number of lipid droplets appeared at this time especially in the basal region of cells, some of them in close proximity to the nuclear membrane (fig. 14). Large crystalloid structures were often present in acinar cells.

Modifications of nuclear structures induced by actinomycin in the parotid acini were of the following two types. First, there was a remarkable reduction in size of the nucleolus which appeared to have lost most, if not all, of the 150 Å unit granules associated with the structure (figs. 15, 16). The second change was the formation of small encapsulated areas of nucleoli (figs. 17, 18, 19, 20). It appeared that a finely filamentous substance developed around pieces of degenerating nucleoli which would eventually surround and

separate that portion of the nucleolus from the rest of the nucleoplasm forming a spherical body as judged by observations on a large number of sections. Such encapsulated bodies contained the ribosome-like granules as well as dense homogeneous portion of the nucleolus.

Ducts. Essentially no alterations were observed in the structure of intercalated duct cells which appeared to maintain a normal complement of the RER, ribosomes, a small Golgi apparatus and mitochondria. No significant change was observed in the intercellular relationship.

Some of the cells making up the secretory duct, however, showed the following differences (figs. 21, 22, 23). The appearance of mitochondria, basal infoldings of the plasma membrane and intercellular interdigitations was largely unchanged, although mitochondria often became smaller and denser than those of control animals (fig. 13). More significantly, small vacuoles of irregular shape which characterized the apical cytoplasm of secretory duct cells were increased in number (figs. 22, 23). They were also larger, many of them showing an irregular stellate contour and contained a fairly electron dense matrix.

DISCUSSION

The light microscopic observation made in conjunction with radioautographic studies confirms results obtained from previous works (Jhee and Han, '64) and provides for further support that actinomycin D does induce serious morphological defects in cells of the parotid gland which produce proteinaceous enzymes. Furthermore, the differences in appearance of grain distribution observed in radioautographs of day 7 rat especially after four hours of H-leucine injection indicates a definite damage done to the synthetic machinery responsible for H-leucine incorporation. The elegant work by Warshawsky et al. ('63) has also shown that at four hours H-leucine accumulates maximally in the zymogen region of pancreatic acinar cells which are not unlike parotid gland cells, although our recent observation indicates that pancreatic cells show more discreet pattern of H-leucine distribution than parotid cells (Han, '66).

The electron microscopic observation of cells taken from the same tissue as used for radioautography provides a definite support for the conclusion derived from radioautographic data. Thus, all intracellular structures identified so far to be parts of the synthetic apparatus for proteins showed serious reduction in degree of the organization or in their number. In addition the appearance of other structures that have been observed in situations of altered glandular metabolism, such as the formation of crystalloids or fat droplets, add to the evidence that the physiology of the acinar cells is definitely altered. Of interest is to note the persistence of polyosomes in insulted cells which might be related to the smaller dose employed in this study. However, it is also possible that they represent more resistant polyosomes as implied by previous biochemical studies (Staehelin, '63) which showed only 50 to 80% breakdown of polyosomes even after a massive amount of actinomycin capable of total inhibition of RNA synthesis.

It is difficult to assess, although highly desirable, exactly what is the primary morphological effect of any insult on the cell. In electron microscopy, the difficulty is doubled because of problems related to differentiating and quantitating changes. Based on what has been known from biochemical studies, one might arbitrarily define the primary structural effect of actinomycin D to be changes in the nucleolar structure and number of ribosomes, whereas alterations of the membrane system of the ER, Golgi apparatus and number of zymogen granules might be taken as necessary consequences of reduced secretory function. The formation of cytolysosomes, lipid droplets and crystalloids, might be regarded as further adaptive changes related to abrupt imbalance of various intermediary metabolic processes which might also come after other types of physiologic insults. For instance, the formation of lipid droplets in fibroblast cells from scorbutic guinea pigs were related to reduced synthesis of collagen in healing wounds (Ross and Benditt, '62) and the increase in cytolysosomes has been related to various aspects of reduced or upset cellular functions (Novikoff, '63). The formation of crystalloids similar to

what has been observed in this study was observed by Scott and Pease ('64) in parotid acinar cells, although they found them in relation to a heightened functional status.

Nucleolar alterations observed in this study are somewhat different from the acute effect of actinomycin D observed in pancreatic acinar cells (Jezequel and Bernhard, '64) and cultured kidney cells (Schoeffl, '64) and from the chronic effect on the fibroblast of the dental pulp (Han et al., '66). Rather than showing the segregation of nucleolar components, nucleoli in experimental animals in our hands showed a drastic reduction in number of ribosome-like granules and might be of significance in view of the role nucleoli play in RNA metabolism (Perry et al., '61). The formation of encapsulated bodies within the nucleus has been occasionally observed in some of the lymphoid cells as well as in duct cells of salivary glands (Han, '66), although none of these previously noticed intranuclear bodies contained what could be identified as materials originating from the nucleolar structure; namely, the ribosome-like granules and the homogeneous dense substance of the nucleolus.

The real significance of the phenomenon of nucleolar encapsulation remains to be elucidated. It is tempting, however, to speculate on the following possibilities on purely logical grounds: It might represent a means by which the cell might preserve a vital intranuclear organelle concerned with RNA metabolism during a period of time when RNA synthesis is severely restricted; or alternately it might be an expression of the final stage of nucleolar deterioration which may result in the extrusion of the encapsulated matters into the cytoplasm. The latter possibility is particularly intriguing, since the nuclear extrusion has been observed in other types of cells (Bak, '66). Furthermore, the extrusion might be a mandatory affair, if the content of encapsulated bodies were degraded masses destined to be hydrolyzed by lysosomal enzymes which, so far as known, are exclusively cytoplasmic.

The lack of effect on intercalated duct cells indicates the limitedness of the role that duct cells might play in protein bio-

synthesis of the organ. On the other hand, cells in the secretory duct apparently show accumulation of apical vacuoles with an increase in electron density of their content and, if one were to presume that dense vacuoles or granules might represent secretory product by the cell, the observation could be regarded as expressing a possible retention of secretory products as the result of hypofunctioning of duct cells. In fact a similar situation was observed following fasting and atropin administration, conditions which are known to suppress duct functions (Scott and Pease, '64).

LITERATURE CITED

- Bak, I. J. 1966 The ultrastructure of the substantia nigra and candidate nucleus and the cellular localization of catechol amines. *Exp. Brain Res.*, in press.
- Caspersson, T., S. Farver, G. E. Foley and D. Killander 1963 Cytochemical observations on the nucleolus-ribosome system. Effect of actinomycin D and nitrogen mustard. *Exp. Cell Res.*, 32: 529-552.
- Franklin, R. M. 1963 The inhibition of ribonucleic acid synthesis in mammalian cells by actinomycin D. *Biochem. Biophys. Acta*, 72: 555-565.
- Goldstein, M. N., I. J. Slotnick and L. J. Journey 1960 In vitro studies with HeLa cell lines sensitive and resistant to actinomycin. *Ann. N. Y. Acad. Sci.*, 89: 474-483.
- Han, S. S. 1966 Unpublished observations.
- Han, S. S., J. K. Avery and J. S. Bang 1967 The effect of actinomycin D on the fibroblast of the incisor pulp of the rat, a study by quantitative radioautography and electron microscopy. *Arch. Oral Biol.*, in press.
- Jezequel, A. M., and W. Bernhard 1964 Modifications ultrastructurales du pancreas exocrine de rat sous l'effet de l'actinomycine D. *J. Microscopie*, 3: 279-296.
- Jhee, H. T., and S. S. Han 1964 Effects of actinomycin D on the salivary glands of the rat. *Life Sci.*, 3: 1239-1247.
- Jhee, H. T., S. S. Han and J. K. Avery 1965 A study of salivary glands of rats infected with actinomycin D. *Am. J. Anat.*, 116: 631-652.
- Journey, L. J., and M. N. Goldstein 1961 Electron microscope studies on HeLa cell lines sensitive and resistant to actinomycin D. *Cancer Res.*, 21: 929-932.
- Levy, H. B. 1963 Effect of actinomycin D on HeLa cell nuclear RNA metabolism. *Proc. Soc. Exp. Biol. Med.*, 113: 886-889.
- Novikoff, A. B. 1963 Lysosomes in the physiology and pathology of cells: contribution of staining methods. In: *Lysosomes*, Ciba Foundation Symposium, pp. 36-73.
- Perry, R. P., A. Hell and M. Errera 1961 The role of nucleolus in ribonucleic acid and protein synthesis. *Biochim. Biophys. Acta*, 49: 47.
- Ross, R., and E. P. Benditt 1962 Wound healing and collagen formation. II. Fine structure in experimental scurvy. *J. Cell Biol.*, 12: 533-551.
- Schoeff, G. E. 1964 The effect of actinomycin D on the fine structure of the nucleolus. *J. Ultrastr. Res.*, 10: 224-243.
- Scott, B. L., and D. C. Pease 1964 Electron microscopy of induced changes in the salivary gland of the rat. In: *Salivary Glands and Their Secretions*, Internat'l Ser. Monogr. Oral Biol., ed. by L. M. Sreebny and L. Meyer, Macmillan, N. Y., pp. 13-43.
- Staehelin, T., F. O. Wettstein and H. Noll 1963 Breakdown of rat liver ergosomes in vitro after actinomycin inhibition of messenger RNA synthesis. *Science*, 140: 180-183.
- Tamsaki, T., and G. E. Mueller 1962 Synthesis of nuclear and cytoplasmic RNA of HeLa cells and the effect of actinomycin D. *Biophys. Biochem. Res. Comm.*, 9: 451-454.
- Wartbawsky, H., C. P. Leblond and E. Droz 1963 Synthesis and migration of proteins in the cells of the exocrine pancreas as revealed by specific activity determination from radioautographs. *J. Cell Biol.*, 16: 1-21.
- Wiesner, R., C. Acs, E. Reich and A. Shafit 1965 Degradation of ribonucleic acid in mouse fibroblasts treated with actinomycin. *J. Cell Biol.*, 27: 47-52.

The electron microscopic observation of cells taken from the same tissue as used for radioautography provides a definite support for the conclusion derived from radioautographic data. Thus, all intracellular structures identified so far to be parts of the synthetic apparatus for proteins showed serious reduction in degree of the organization or in their number. In addition the appearance of other structures that have been observed in situations of altered glandular metabolism, such as the formation of crystalloids or fat droplets, add to the evidence that the physiology of the acinar cells is definitely altered. Of interest is to note the persistence of polysomes in insulted cells which might be related to the smaller dose employed in this study. However, it is also possible that they represent more resistant polysomes as implied by previous biochemical studies (Stachelin, '63) which showed only 50 to 80% breakdown of polysomes even after a massive amount of actinomycin capable of total inhibition of RNA synthesis.

It is difficult to assess, although highly desirable, exactly what is the primary morphological effect of any insult on the cell. In electron microscopy, the difficulty is doubled because of problems related to differentiating and quantitating changes. Based on what has been known from biochemical studies, one might arbitrarily define the primary structural effect of actinomycin D to be changes in the nucleolar structure and number of ribosomes, whereas alterations of the membrane system of the ER, Golgi apparatus and number of zymogen granules might be taken as necessary consequences of reduced secretory function. The formation of cytolysosomes, lipid droplets and crystalloids, might be regarded as further adaptive changes related to abrupt imbalance of various intermediary metabolic processes which might also come after other types of physiologic insults. For instance, the formation of lipid droplets in fibroblast cells from scorbutic guinea pigs were related to reduced synthesis of collagen in healing wounds (Ross and Benditt, '62) and the increase in cytolysosomes has been related to various aspects of reduced or upset cellular functions (Novikoff, '63). The formation of crystalloids similar to

what has been observed in this study was observed by Scott and Pease ('64) in parotid acinar cells, although they found them in relation to a heightened functional status.

Nucleolar alterations observed in this study are somewhat different from the acute effect of actinomycin D observed in pancreatic acinar cells (Jezequel and Bernhard, '64) and cultured kidney cells (Schoeff, '64) and from the chronic effect on the fibroblast of the dental pulp (Han et al., '66). Rather than showing the segregation of nucleolar components, nucleoli in experimental animals in our hands showed a drastic reduction in number of ribosome-like granules and might be of significance in view of the role nucleoli play in RNA metabolism (Perry et al., '61). The formation of encapsulated bodies within the nucleus has been occasionally observed in some of the lymphoid cells as well as in duct cells of salivary glands (Han, '66), although none of these previously noticed intranuclear bodies contained what could be identified materials originating from the nucleolar structure; namely, the ribosome-like granules and the homogeneous dense substance of the nucleolus.

The real significance of the phenomenon of nucleolar encapsulation remains to be elucidated. It is tempting, however, to speculate on the following possibilities on purely logical grounds: It might represent a means by which the cell might preserve a vital intranuclear organelle concerned with RNA metabolism during a period of time when RNA synthesis is severely restricted; or alternately it might be an expression of the final stage of nucleolar deterioration which may result in the extrusion of the encapsulated matters into the cytoplasm. The latter possibility is particularly intriguing, since the nuclear extrusion has been observed in other types of cells (Bak, '66). Furthermore, the extrusion might be a mandatory affair, if the content of encapsulated bodies were degraded masses destined to be hydrolyzed by lysosomal enzymes which, so far as known, are exclusively cytoplasmic.

The lack of effect on intercalated duct cells indicates the limitedness of the role that duct cells might play in protein bio-

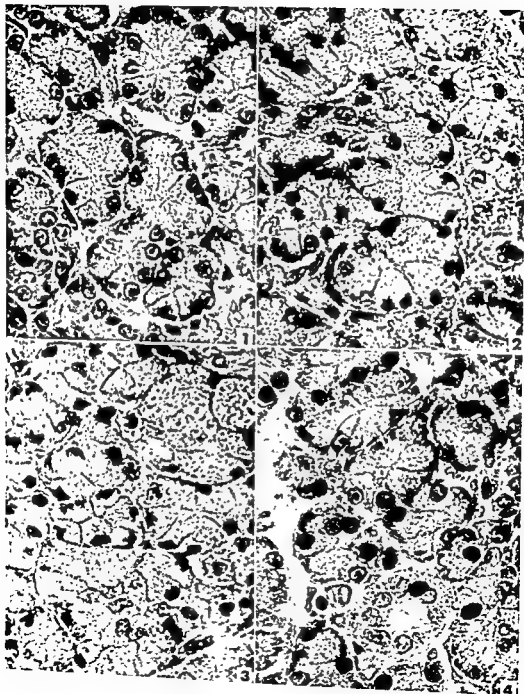


PLATE 1

EXPLANATION OF FIGURES

- 1 A portion of the parotid gland from a control animal. Notice well-defined large cells with distinct basal basophilia and large nucleus containing prominent nucleoli. Approximately $\times 840$. Fixed in Bouin's solution, and stained with hematoxylin and eosin.
- 2 A portion of the parotid gland of a rat injected with actinomycin D three days prior to sacrifice. The pycnosis of acinar nuclei is evident in most cells and the cytoplasm appears rarified with a loss of the basophilia. Approximately $\times 840$. Fixed in Bouin's solution, and stained with hematoxylin and eosin.
- 3 A portion of the parotid gland from a rat injected with actinomycin D seven days prior to sacrifice. Further degeneration is noted in the cytoplasm, including the formation of vacuoles which often are associated with nucleus. Approximately $\times 840$. Fixed in Bouin's solution, and stained with hematoxylin and eosin.
- 4 A portion of the parotid from a rat injected with actinomycin D 14 days prior to sacrifice. Note the restoration of the nucleolar structure as well as the recovery of basophilic materials in the cytoplasm.

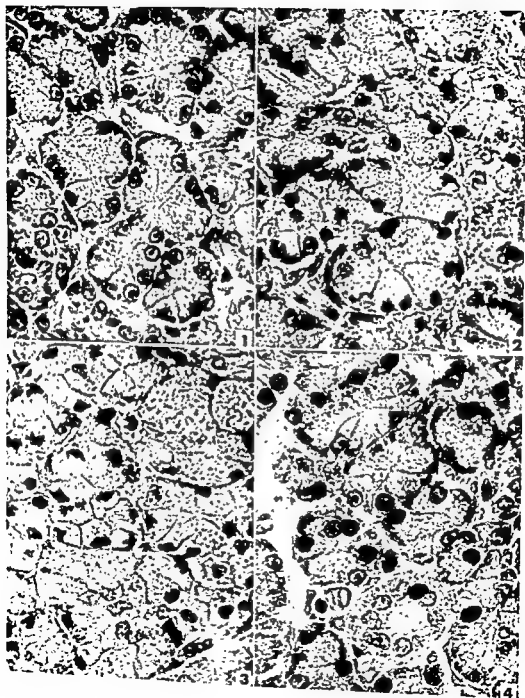


PLATE ■

EXPLANATION OF FIGURES

- A radioautograph of the parotid from a 7-day experimental animal, which was given an injection of H_3 -leucine four hours prior to sacrifice. The cytoplasmic degeneration depicted in preceding photographs is evident. Silver grains are distributed throughout the glandular tissue without any preferential pattern of localization. Approximately $\times 920$. Fixed in Bouin's solution, and stained with hematoxylin and eosin after development of the radioautograph.
- A radioautograph of the parotid from a 7-day control rat, which was given H_3 -leucine injection four hours prior to sacrifice. The silver grains are predominantly located in the supernuclear region where the accumulation of zymogen granules occurs. Approximately $\times 920$. Fixed in Bouin's solution, and stained with hematoxylin and eosin after development of the radioautograph.

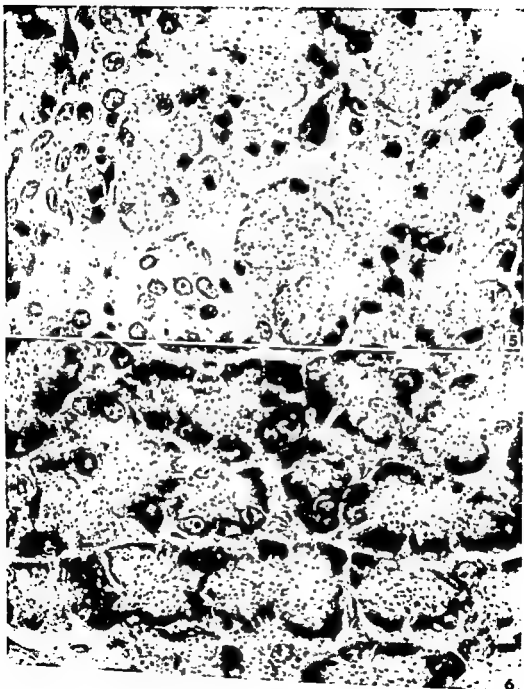


PLATE 2

EXPLANATION OF FIGURES

- 5 A radioautograph of the parotid from a 7-day experimental animal, which was given an injection of H_3 -leucine four hours prior to sacrifice. The cytoplasmic degeneration depicted in preceding photographs is evident. Silver grains are distributed throughout the glandular tissue without any preferential pattern of localization. Approximately $\times 920$. Fixed in Bouin's solution, and stained with hematoxylin and eosin after development of the radioautograph.
- A radioautograph of the parotid from a 7-day control rat, which was given H_3 -leucine injection four hours prior to sacrifice. The silver grains are predominantly located in the supernuclear region where the accumulation of zymogen granules occurs. Approximately $\times 920$. Fixed in Bouin's solution, and stained with hematoxylin and eosin after development of the radioautograph.

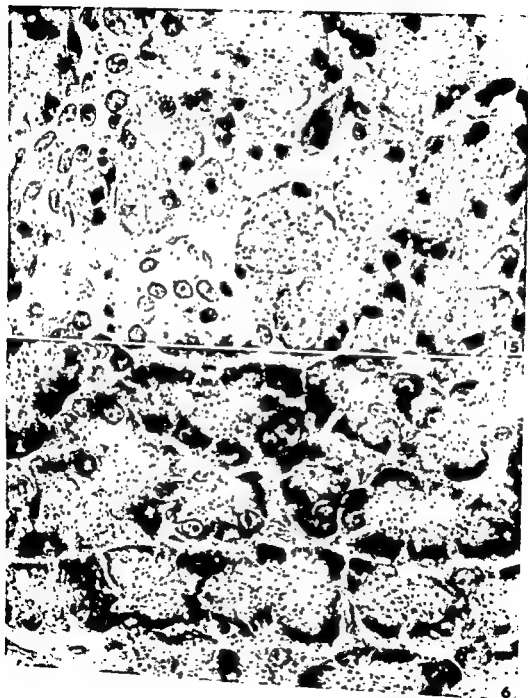


PLATE 3

EXPLANATION OF FIGURES

- 7 A low power electron micrograph of an acinar cell of the parotid gland from the 7-day control rat. The basal portion of the cytoplasm is packed with a well-developed RER and numerous ribosomes, whereas the supernuclear portion contains several well-organized Golgi units and numerous zymogen granules. OsO_4 fixation. Approximately $\times 8,600$.
- 8 A low power electron micrograph of an acinar cell of the parotid gland of a 7-day experimental rat. Notice the reduction in organization of the RER at the base of the cell. Only a few units of the Golgi apparatus are visible and many of the zymogen granules show the bizonal appearance. OsO_4 fixation. Approximately $\times 9,400$.

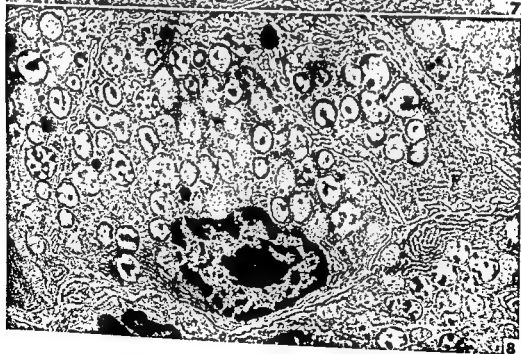
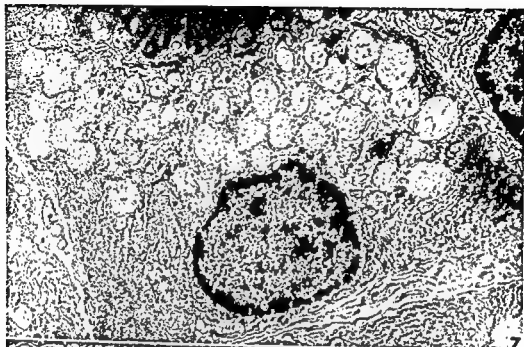


PLATE 4

EXPLANATION OF FIGURES

- 9 One of several units of the Golgi apparatus of an acinar cell of the parotid gland from a control rat. Notice the extensiveness of membranous elements and numerous small vesicles associated with them. OsO_4 fixation. Approximately $\times 14,000$.
- 10 A profile of the Golgi apparatus of an acinar cell of the parotid gland from an experimental animal. Compared to figure 9, this unit is smaller and the number of associated vesicles is much fewer. OsO_4 fixation. Approximately $\times 18,600$.

PAROTID GLAND AND ACTINOMYCIN
Seong S. Han

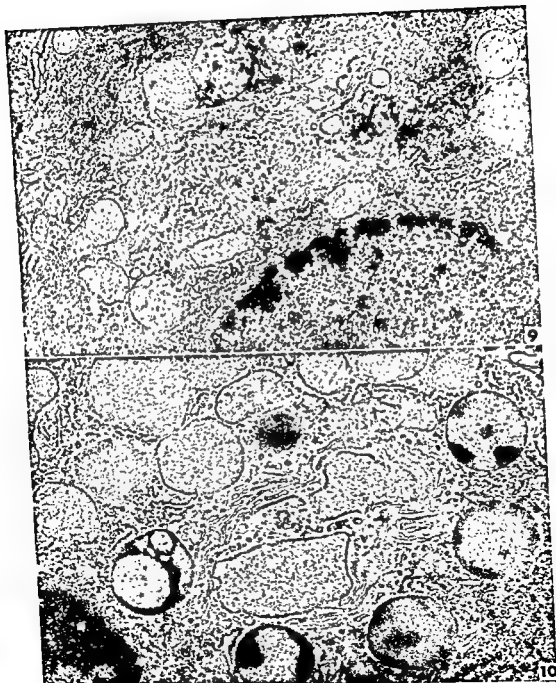


PLATE 5

EXPLANATION OF FIGURES

- 11 The appearance of aggregated zymogen granules in parotid acinar cells from an experimental rat, fixed in glutaraldehyde. Notice the presence of ribosomes, the RER, mitochondria and many zymogen granules. The outer limiting membrane of such aggregates as well as that of zymogen granules appears to be intact. Approximately $\times 18,000$.
- 12 A portion of an acinar cell of the parotid gland from an experimental animal, demonstrating a small cytolysome which contains a degenerating mitochondrion and ribosomes. OsO_4 fixation. Approximately $\times 32,600$.
- 13 A portion of a secretory duct cell of the parotid gland from an experimental rat. Notice the rounded appearance of mitochondria, one of which seems to have become condensed but showing distorted cristae and an intact intramitochondrial granule. OsO_4 fixation. Approximately $\times 28,400$.
- 14 Portions of acinar cells of the parotid gland from an experimental animal. Notice the formation of lipid droplets in the cytoplasm, many of which are located in association with the somewhat irregular nuclear membrane. OsO_4 fixation. Approximately $\times 9,200$.

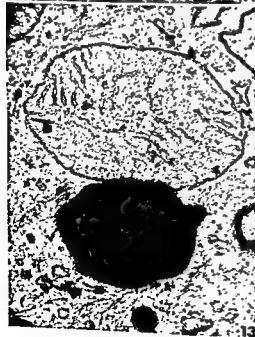


PLATE 6

EXPLANATION OF FIGURES

- 15 A nucleolus of an acinar cell of the parotid from a control animal. Notice the large size of this nucleolus which shows an impressive accumulation of ribosome-like granules associated with it. OsO₄ fixation. Approximately $\times 98,800$.
- 16 A nucleolus of an acinar cell of the parotid from an experimental animal. The size of the nucleolus is smaller than the one shown above and it is practically denuded of the ribosome-like granules. OsO₄ fixation. Approximately $\times 102,000$.

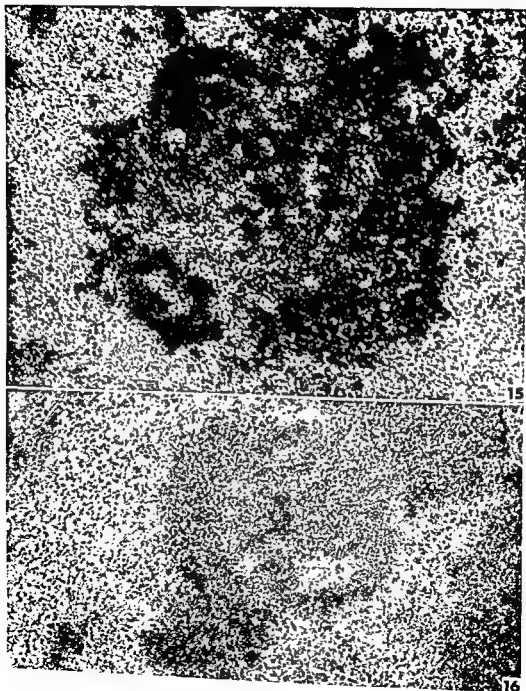


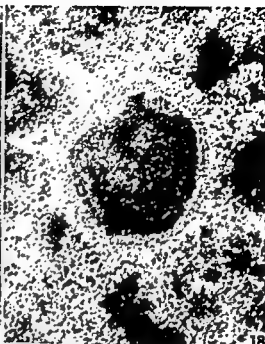
PLATE 7

EXPLANATION OF FIGURES

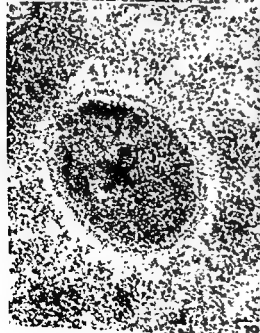
- 17-20 The formation of encapsulated nucleolar bodies. Note the appearance of the finely fibrillar structure surrounding a portion of the already small nucleolus in figure 21. The structure on figure 22 suggests that the fibrillar material has almost surrounded the small piece of nucleolar substances. Figures 23 and 24 show profiles of encapsulated bodies as found most frequently. The spherical bodies appear to contain a fair amount of ribosome-like granules as well as the homogeneously dense nucleolar structure. OsO₄ fixation. Approximately $\times 88,400$.



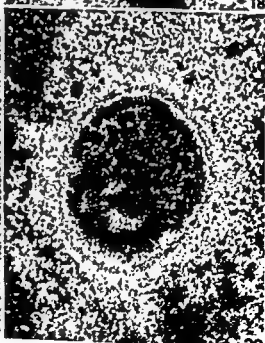
17



18



19



20

PLATE 8

EXPLANATION OF FIGURE

- 21 A portion of a secretory duct of the parotid gland from a control rat. The tall cell body contains a large number of basally located mitochondria in association with the infolded plasma membrane. A limited number of apical vacuoles may be seen. OsO_4 fixation. Approximately $\times 8,600$.



PLATE 8

EXPLANATION OF FIGURE

- 21 A portion of a secretory duct of the parotid gland from a control rat. The tall cell body contains a large number of basally located mitochondria in association with the infolded plasma membrane. A limited number of apical vacuoles may be seen. OsO_4 fixation. Approximately $\times 8,600$.

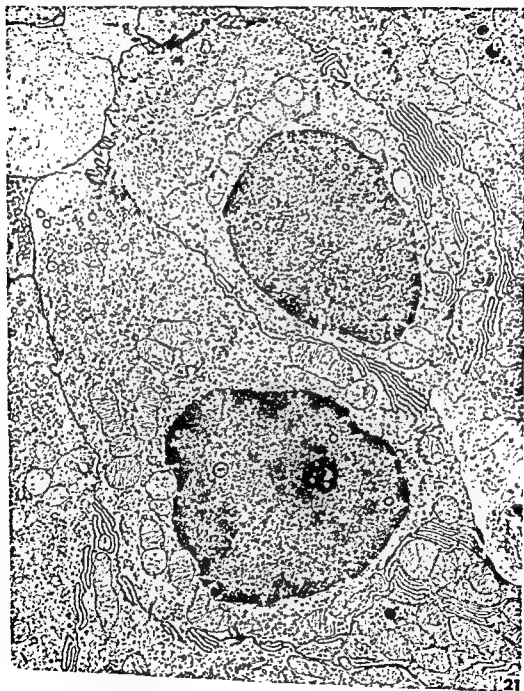


PLATE 8

EXPLANATION OF FIGURE

- 21 A portion of a secretory duct of the parotid gland from a control rat. The tail cell body contains a large number of basally located mitochondria in association with the infolded plasma membrane. A limited number of apical vacuoles may be seen. OsO_4 fixation. Approximately $\times 8,600$.

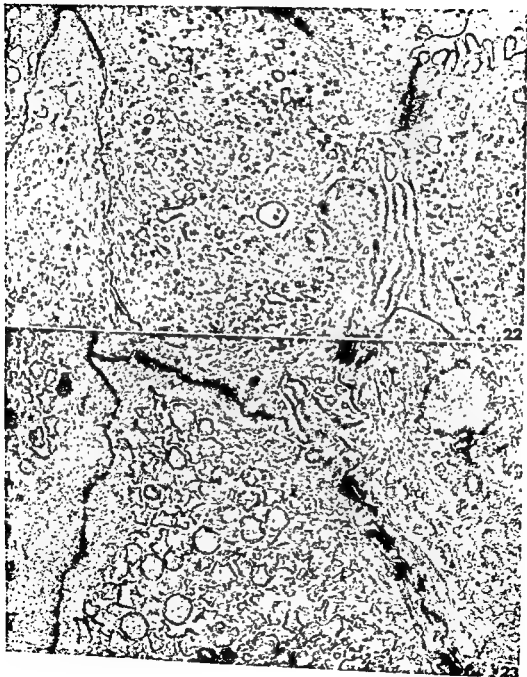


PLATE 9

EXPLANATION OF FIGURES

- 22 Portions of the apical cytoplasm of secretory duct cells from a control animal. Notice the small number of cytoplasmic vesicles or vacuoles in addition to the usual structure. OsO_4 fixation. Approximately $\times 14,800$.
- 23 Portions of the apical cytoplasm of secretory duct cells from an experimental animal. Notice the increased number of apical vacuoles which also have gained electron density of their content. OsO_4 fixation. Approximately $\times 14,800$.

A Morphological Analysis of the Early Implantation Stages in the Rat¹

ALLEN C. ENDERS and SANDRA SCHLAFKE

Department of Anatomy, Washington University Medical School,
St. Louis, Missouri

ABSTRACT By making use of the known sequence of ovulation and fertilization in Holtzman rats, the Pontamine Blue reaction, and electron microscopy, the first stages in implantation were studied. Implantation is initiated when the blastocyst becomes clasped by the endometrium and hence assumes a fixed position (evening of day 5). At this stage, the trophoblast cells are in close association with the uterine epithelial cells, with interdigitating microvilli in places, but decidualization of the fibroblasts is just beginning. In the second stage of implantation the decidualized fibroblasts form a cup around the luminal epithelium. Evidence of adhesion of the cell membranes of trophoblast cells with the cell membranes of luminal epithelial cells can be seen at this time. The layer of fibroblasts immediately surrounding the luminal epithelium becomes epitheloid, resulting in a relative isolation of the luminal epithelium from its vascularization. This stage is well-developed by the afternoon of day 6. By the morning of day 7, the luminal epithelium has disappeared from the region of the forming ectoplacental cone down to the level of the abembryonic trophoblast. The trophoblast cells on the lateral aspect of the blastocyst are directly in contact with the residual basement membrane of the luminal epithelial cells, and are separated by this structure and a small connective tissue cleft from the stromal cells. The importance of the relative isolation of the epithelium by the stromal reaction and the adhesion of the cell membrane of the trophoblast cells to the cell membranes of epithelial cells with regard to removal and phagocytosis of epithelial elements are discussed, and many of the cytological features observed during the process are described.

The ready availability of the rat and mouse have made these animals favorite objects for the study of implantation. Duval (1891) took advantage of the abundance of rats in the slaughterhouses of Paris for his study materials. However, he used Lataste's collection of mouse reproductive tracts for the comparison of stages and the timing of these stages. His studies, plus those that followed in the next two decades dealing with both the mouse (Burckhard, '01; Sobotta, '03) and the rat and mouse (Melissinos, '07), established many of the essential features of implantation in these myomorph rodents. The mouse was the major subject of these studies, and little distinction was made between the mouse and rat, which were considered to be in the same genus at that time. Although these studies predated a precise knowledge of the reproductive cycle, timed implantation stages were obtained by using Sobotta's method of placing female mice that had given birth to litters 21 days previously with males, then

examining them subsequently for copulation plugs.

The most comprehensive study of implantation in the rat is that of Huber ('15). He reviewed not only the literature on implantation in the mouse mentioned above, but also the less distinguished literature on the rat. He took advantage of the large Wistar colony to obtain material from a series of observed matings, and thus made it clear that most of the major features of implantation in the mouse previously observed could be observed in the rat with equal facility. He reserved the subject of decidualization for a further paper (which regrettably never appeared), but carefully described elongation of the blastocyst, formation of the ectoplacental cone, entypy or germinal inversion, and the relation of the trophoblast cells to the maternal epithelium in these stages of implantation.

Although the morphological features of early implantation are reviewed periodi-

¹This work was supported by grant GB-2476 from the National Science Foundation.

were rinsed in buffer for one to two hours, and post fixed in 2% buffered osmium tetroxide for two hours. The post fixed tissue was then dehydrated in a cold graded series of alcohols, passed through propylene oxide, and embedded in araldite (Durcupan). The majority of implantation sites were sectioned sagittally, as it was found that the actual region of contact between the trophoblast and the uterus could be reached more rapidly with this approach. Other pieces were sectioned transversely, and a few specimens were sectioned from the antimesometrial face to aid in determining the shape of the implantation chamber. Phase sections were examined routinely during the cutting process to determine the orientation of the implantation site. In a number of instances, all sites from an individual animal were prepared in this fashion, and phase sections were stained with the periodic acid-Schiff method and with azure B.

Sections taken for examination with the electron microscope were made with diamond blades on a Porter-Blum MT-2 microtome. They were examined in an RCA EMU 3G electron microscope.

The blastocysts and implantation sites used in this study were obtained from 16 rats on the afternoon and evening of day 5 of pregnancy, 29 rats on day 6, and nine on the morning of day 7. In all instances the time of day (Central Standard Time) at which the rats were killed was recorded. In general, the rats were grouped in time periods of three to four hours. For the convenience of the reader and in the interest of accuracy, the precise time when killed will be used in the text, but the implication of greater accuracy than three to four hours in chronology of development is not warranted.

DESCRIPTION

Preimplantation stage

In agreement with Dickmann and Noyes ('61), we find that on the late afternoon of day III of pregnancy most of the blastocysts have lost their zonae, but are still implanted. A Pontamine Blue reaction is not usually found at this time. This stage therefore constitutes a good reference point with which to compare the stages of implantation.

The blastocysts at this stage are situated in the periodic shallow depressions that constitute the antimesometrial floor of the uterine lumen. They are slightly more elongated than they are prior to loss of the zona, and deviate from a truly spherical shape in two respects. The embryonic hemisphere of the blastocyst is slightly smaller than the abembryonic hemisphere, and the blastocysts are flattened in a plane normal to the embryonic-abembryonic axis. It appears probable that they are thus situated not only antimesometrially with the embryonic hemisphere oriented mesometrially, but in addition that the wider portion of their transverse axis is oriented along the cranio-caudal axis of the uterine lumen. In some instances the abembryonic trophoblast cells are rounded, but more commonly they are distinctly flattened cells.

Blastocyst. Cytologically the trophoblast cells do not appear to be greatly altered from the stage preceding loss of the zona. They have short irregular microvilli on their free surface, well developed junctional complexes, and an irregular but not highly folded internal border. Areas which are largely filled by the fibrous plaques so characteristic of the mature ovum and cleavage stages (Szollosi, '65; Enders and Schlafke, '65) can still be seen, although the diameter of these plaques appears somewhat reduced and the margins of the regions are not always as distinct as in earlier stages. Polyribosomes are extremely numerous in the cytoplasm, and strands of granular endoplasmic reticulum are common but are not extensive. The Golgi zones are now discrete areas near the nucleus, but do not show any distinct apical or basal polarity. A few large inclusion bodies are present in many of the cells (apparent derivatives of the previous yolk bodies), and frequently some of the trophoblast cells contain a few lipid droplets. At this stage there do not appear to be any cytological differences between the trophoblast of Rauber's layer and the abembryonic trophoblast. The embryonic cell mass cells constitute a discrete mass with numerous intercellular spaces. Cytologically these cells are similar to the trophoblast cells. The cells of the embryonic cell mass

cally (Mossman, '37; Amoroso, '52; Blandau, '61), subsequent individual studies have tended to center on specific features of interest, especially the process of decidualization, the role of the epithelium in implantation, and the activity of the blastocyst at implantation. Examples of some of the important contributions of this type are illustrative. Krehbiel's ('37) careful morphological study of the decidual reaction in the rat included both a description of the formation of decidual tissue in normal implantation and as a response to experimental trauma. An extensive series of studies examining the physiological basis of decidual formation has appeared recently (Velardo et al., '53; Shellesnyak, '62; De Feo, '63). Such physiological studies naturally tend to emphasize the maternal organism. A number of studies on the epithelium at implantation have also been made, of which Alden's ('47) paper on lipid in the uterine epithelium is noteworthy. Alden concluded that there was an epithelial response to the blastocyst which precipitated decidualization. Blandau ('49), using paraffin and glass beads the size of blastocysts, showed that in the rat there could be epithelial loss when implantation crypts were induced by these inert objects.

The tendency of the blastocyst to continue its development in extra-uterine sites was shown in the rat by Nicholas ('42), and carried on extensively by others using the mouse (Runner, '47; Fawcett, '50; Kirby, '63) and rat (Jollie, '61). Other observations have tended to emphasize the interrelationship of the blastocyst and endometrium in early implantation. The observation that decidualomata could be produced while the blastocysts remained unimplanted (Krehbiel, '41), and the use of the transfer technique with its evidence suggesting the necessity of appropriate age correlations between endometrium and blastocyst (Noyes and Dickmann, '60) are particularly striking evidence of the precision of interaction at this stage.

The introduction of a method for localizing early implantation stages by intravascular injection of dye (Psychoyos, '60; Orsini, '63), coupled with the availability of more suitable methods of preservation of larger pieces of tissue for electron mi-

croscopy, presented an opportunity to study the fine structure of the early implantation site. In this manner, not only could the morphological features of implantation be reexamined in greater detail, but in addition the timing of the first implantation stages could be followed more precisely.

MATERIALS AND METHODS

Rats of the Holtzman strain were kept on a constant light cycle consisting of 14 hours of light, ten hours of dark. Virgin female rats with estrous smears were placed with males in the afternoon. The next morning they were examined; if sperm were found in the vaginal smear, that day was designated day 1 of pregnancy. (Szollosi and Ris ('61) found that with this lighting regime, the Holtzman strain of rats follows closely the schedules published by Austin ('51) and Odor and Blandau ('51) with regard to ovulation, sperm penetration, and early pronuclear development.) When implantation sites were to be collected, the rats were anesthetized and 0.25 ml Pontamine Blue was injected into the femoral vein 15 minutes before collecting the tissue. In some instances the rats were killed and the regions of the uterus exhibiting blue spots cut out and placed in fixative. In other instances, the initial fixative was injected into the abdominal aorta while the animal was under anesthesia. When perfusion by this latter method was successful, the uterine horns had a firm rubbery consistency and no contraction of the muscle could be seen when portions of the uterus were sliced. Pieces of the perfused uterus exhibiting the blue reaction were placed in either 3% glutaraldehyde in phosphate buffer or Karnovsky's ('65) formalin-glutaraldehyde fixative (depending on which of these was used for perfusion). After a few minutes in the initial fixative, most of the slices were trimmed to 1-2 mm in width. In many instances the sites of the contralateral horn were also preserved so that all of the sites from a single animal could be observed. In other instances the contralateral horn was flushed with fixative to collect the blastocysts.

Following two hours initial fixation in the aldehyde fixative, the pieces of tissue

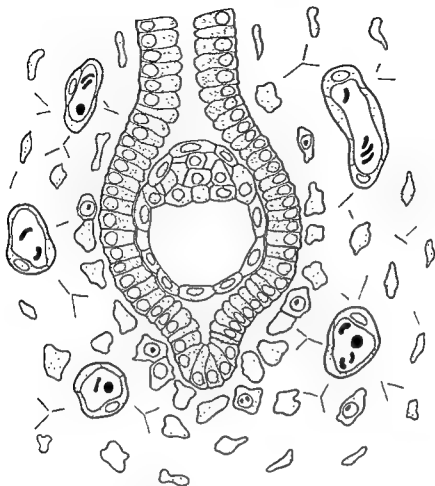


Fig. 1 A diagrammatic representation of the first stage in implantation, in which the edematous uterus clamps the blastocyst.

Blastocyst. The blastocysts at this stage are neither greatly altered in shape nor in cytology from the previous stage described (fig. 5). In those blastocysts showing the greatest amount of change, a few alterations in the direction of later changes can be discerned. A few granules of glycogen are found in some of the abembryonic trophoblast cells, and occasionally several of these cells are slightly swollen. Lipid droplets are usually more numerous throughout the trophoblast at this stage. Where the trophoblast cells are in apposition to the uterine epithelium, the microvilli interdigitate in a rough fashion, and occasionally one can see the tip of a

uterine microvillus projecting into a caveola of the trophoblast (figs. 6, 7). A single trophoblast cell extends over several uterine epithelial cells and may be slightly indented by those cells. In one instance, two of the six sites examined from a single rat had small portions of the zona pellucida trapped between the trophoblast and luminal epithelium.

Uterine epithelium. In the area of close apposition between the luminal epithelial cells and the blastocyst, the apical surface of the epithelial cells closely follows the general contour of the trophoblast cells and is somewhat modified. In addition to short digitiform microvilli seen previously,

which border on the cavity of the blastocyst are usually flattened in cross-section and will occasionally show more extensive cisternae of the endoplasmic reticulum than in other embryonic cell mass cells.

Luminal epithelium. The luminal epithelial cells of the uterus are columnar in the antimesometrial region where blastocysts are found. The apical borders of these cells have numerous fairly regular but short microvilli. At the bases of the microvilli are numerous acinar invaginations characterized by a slightly denser membrane and radial projections into the cytoplasm, of a type variously designated caveolae, acanthosomes, micropinocytotic vesicles, protein pits, etc.

At the cell margins, the junctional complexes have terminal bar substance in the areas of close apposition. Towards the basal end of the lateral borders adjacent cell membranes are interdigitated. The basal surface of the epithelial cells projects toward the stroma in an irregular fashion, especially in cells situated on the lateral walls of the lumen. Within the epithelial cells there is a zonation in distribution of inclusions and organelles. Basally, there are numerous large lipid droplets. The mitochondria are short rod-like forms, and cisternae of the endoplasmic reticulum are extensive. Distal to the nucleus is a well-formed Golgi region of membranes and vesicles. A few lipid droplets and several denser inclusions, some of which include lipid pigments, are found in this region. Above the Golgi zone in the apical region of the cell is a zone in which there are numerous mitochondria and rather unusual vesicular-appearing structures as well as tubular invaginations. (Since these vesicular structures usually have an irregular shape, are indented by tongues of cytoplasm, and otherwise vary from the typical vesicles normally described, it is apparent that simply calling them vesicles does not adequately characterize these structures.)

Lymphocytes are commonly found between the bases of epithelial cells. No other intraepithelial leucocytes were seen at this stage.

Stroma. The stroma immediately around the antimesometrial luminal epithelium is

rich in fibroblasts. (This zone from the epithelium to the first layer of vessels constitutes the primary decidual zone of Krehbiel ('37), and is the only area which will be described.) The fibroblasts in this zone are more numerous and are more compact cells than are the fibroblasts in the uteri of many animals that do not exhibit a decidual reaction. At this stage, the connective tissue around the vessels appears slightly edematous (see fig. 4), and the clusters of collagen fibrils are widely dispersed.

Cytologically, the fibroblasts are characterized by their numerous undilated cisternae of the endoplasmic reticulum, and polyribosomes both associated with the endoplasmic reticulum and free in the cytoplasm. Small lipid droplets are frequent inclusions, and microtubules can often be found in the cytoplasm, but there is very little fibrous material. The mitochondria are typically rod-shaped with lamelliform cristae. The nucleoli are prominent but are not unusually large. Occasional caveolae are seen on the free surface. Each fibroblast has several regions of contiguity with neighboring cells. Macrophages are commonly found in this region of the uterus, but mast cells are not.

Implantation stage 1

Implantation can be considered to start when a fixed position of the blastocyst in relation to the uterus has been established. By the evening of day 5, in most of the rats the blastocysts are held in position within the uterine lumen (fig. 1). It should be pointed out that this is the earliest time at which a distinct Pontamine Blue reaction can be elicited. Nevertheless, all of the blastocysts can be readily flushed from the uterus at this stage with no evidence of any damage. Furthermore decidualization is barely beginning. In tissues fixed by perfusion, the blastocysts are almost entirely encompassed by the uterine epithelium and are situated close to the antimesometrial end of the uterine lumen, with their embryonic cell masses oriented mesometrially. The stroma of the uterus appears edematous and the lateral margins of the uterine lumen are apposed.

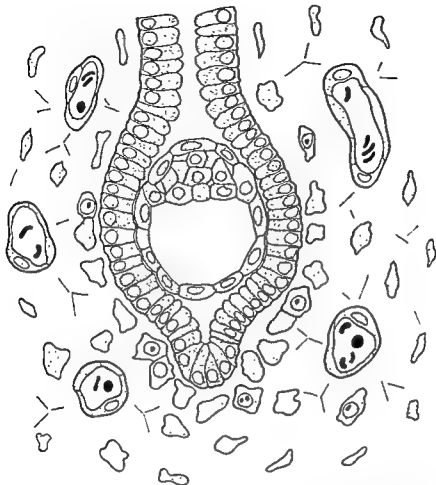


Fig. 1 A diagrammatic representation of the first stage in implantation, in which the edematous uterus clasps the blastocyst.

Blastocyst. The blastocysts at this stage are neither greatly altered in shape nor in cytology from the previous stage described (fig. 5). In those blastocysts showing the greatest amount of change, a few alterations in the direction of later changes can be discerned. A few granules of glycogen are found in some of the abembryonic trophoblast cells, and occasionally several of these cells are slightly swollen. Lipid droplets are usually more numerous throughout the trophoblast at this stage. Where the trophoblast cells are in apposition to the uterine epithelium, the microvilli interdigitate in a rough fashion, and occasionally one can see the tip of a

uterine microvillus projecting into a caveola of the trophoblast (figs. 6, 7). A single trophoblast cell extends over several uterine epithelial cells and may be slightly indented by those cells. In one instance, two of the six sites examined from a single rat had small portions of the zona pellucida trapped between the trophoblast and luminal epithelium.

Uterine epithelium. In the area of close apposition between the luminal epithelial cells and the blastocyst, the apical surface of the epithelial cells closely follows the general contour of the trophoblast cells and is somewhat modified. In addition to short digitiform microvilli seen previously,

numerous more irregular knoblike protrusions of the apical cytoplasm are found. In some instances there is also a reduction in vesiculation in these cells. Little alteration from the previous described condition could be observed at this time in the epithelial cells peripheral to the blastocyst.

Stroma. A few changes can be seen in some of the stromal cells surrounding the implantation site, particularly at the anti-mesometrial extremity. In this location some of the fibroblasts are a little more cuboidal in shape than previously, and frequently strands of three or four of these cells may be seen lying parallel to the lumen and abutting one another over a broad region (fig. 8). Many of these fibroblasts have one or two enlarged nucleoli with the nucleolonema exhibiting clumping at the periphery of each nucleolus. The cytoplasm of the fibroblasts is rich in polyribosomes and has numerous strands of granular endoplasmic reticulum. However, the cisternae of the endoplasmic reticulum are not dilated. A few lipid droplets are found in these cells but little or no glycogen. Small capillaries are situated about 10μ from the luminal epithelium. They are loosely surrounded by pericytes with only connective tissue situated between them and the luminal epithelium. As in the previous stage, a few macrophages are usually seen in this region.

Implantation stage 2

Day II is a time of rapid change. During day 6 the blastocyst elongates (losing in the process its previous slightly flattened condition), and an implantation chamber is formed (fig. 2). Although some of the blastocysts may be flushed from the uterus at this stage without apparent damage, the recovery rate is low, and when fixed implantation chambers are dissected, the blastocyst is usually found to be adhering to one side of the chamber. (The blastocysts can, however, be dislodged by touching with a sharp dissecting needle.) Mitotic figures are numerous in the blastocyst, stromal cells and endothelial cells. Because of the rapid changes occurring, the variation seen in different implantation sites is also large.

In the early stages of chamber formation, the implantation chamber is shallow with a heavy concentration of decidualizing cells antimesometrially. As the chamber becomes more fully formed, it resembles in shape a thick-walled testtube shoved into a ball of clay, the clay made to adhere by extending it slightly up the walls of the test tube, (the test tube being the luminal epithelium, the surrounding clay the dense decidual cells).

The cytological description which follows is based on the condition in the afternoon of day 6, a time at which the implantation chamber is well formed. This time is roughly the mid-point between the previous stage described and the subsequent stage at which the epithelium is lost.

Blastocyst. As well as elongating, the blastocysts show a number of cytological changes. The abembryonic trophoblast cells accumulate large amounts of glycogen, and lipid droplets are more prominent (figs. 9, 10). Many of these cells round up, and their cytoplasm appears less dense than in the previous stage. Although plaques can still be found, deposition of glycogen is occurring in these areas, and individual profiles of the former inclusion are shorter and less distinct. The trophoblast cells show numerous protrusions, some of which are microvillous, toward the cavity of the blastocyst and the cells of Raubers' layer are more distinctly separated from the underlying embryonic cell mass cells. The embryonic cell mass in many instances is more dispersed than during the previous stage and individual cells (presumptive endoderm) are seen apparently migrating down along the trophoblast. The embryonic cell mass cells do not accumulate glycogen to the extent that the trophoblast cells, especially abembryonic trophoblast cells, do. They do, however, contain lipid droplets and in the case of some of the endoderm cells have more extensive granular endoplasmic cisternae. In some places where the trophoblast cells are closely associated with the epithelium, there are broad regions where the cell membrane of the trophoblast cells is directly apposed to that of the luminal epithelial cells. In these regions, microvilli are no longer

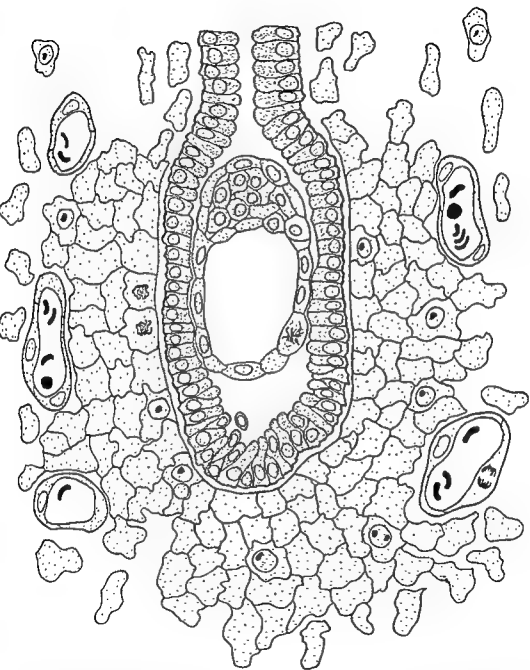


Fig. 2 A diagrammatic representation of the second stage in implantation. The fibroblasts have transformed into decidual cells, leaving a connective tissue cleft between the luminal epithelial cells and the transformed decidua. The trophoblast cells of the blastocyst adhere to the epithelial cells in a number of places, but loss of epithelium has not occurred.

prominent. The cell faces are roughly parallel and in tangential sections show regions where it is difficult to discern an intervening space. In other instances where trophoblast cells have shrunk away from the epithelium, strands of cytoplasm stretch between the apposed surfaces as though they had been pulled away by the separation.

Epithelium. In agreement with Krehbiel ('37), we find at this stage that a zonation of luminal epithelial cells occurs. Attention has been focused in this work only on the cells adjacent to the blastocyst and in the base of the implantation crypt.

The cells adjacent to the blastocyst are little altered. Their free surface has many blunt irregular projections, a few vesicles and, in those areas immediately apposed to the blastocyst, shows a slight increase in density beneath the membrane. Frequently clusters of filaments are seen within this apical cytoplasm, often coursing parallel to the surface. Occasionally such filaments are seen in the basal cytoplasm also. The blunt surface projections of the epithelial cells are generally knobby, and for the most part are unlike the more uniform projections normally described as microvilli (fig. 11).

In the antimesometrial portion of the crypt the epithelium is irregular, showing some stratification. Occasional cells appear to be free in the lumen, and often cellular debris only roughly showing indications of a cell outline is found. Some of the cells in this region show a dilation of the endoplasmic reticulum, the Golgi zones, and of the basal intercellular space.

Stroma. By the afternoon of day 6, the stroma has formed a distinct cup around the epithelium. Mitotic figures are abundant, particularly in the periphery of this region and in the endothelial cells of the vessels around the cup. Immediately underlying the epithelium the fibroblasts have hypertrophied to the extent that they constitute a continuous layer, leaving a connective tissue cleft between the basement membrane of the epithelium and the surface of the decidualizing fibroblasts (fig. 12). Into this connective tissue cleft a few short folds and processes of the fibroblasts extend. All of the fibroblasts in this region have enlarged and can now

be considered decidual cells. Through the more solid portions of the decidual cup, residual collagen fibers are present in depressions surrounded by processes of adjacent cells. In the small pockets of connective tissue space remaining between these closely apposed cells is a granular material in clumps which resembles in density the material of the basement membrane.

At the periphery of the decidual cups, the fibroblasts are less cuboidal and are elongated in such a way that they appear to radiate from the clustered mass of cells. It is in this peripheral position that the vessels of this region are found.

A number of modifications occur in the individual fibroblasts. They accumulate fibrillar material (fig. 13). Frequently a meshwork of filaments is oriented roughly parallel to the surface of the implantation chamber within the individual cells. In addition, glycogen begins to accumulate in some of the cells, particularly near lipid droplets (fig. 14). Other cells have isolated masses of glycogen granules. The cisternae of the granular endoplasmic reticulum are extensive and some dilation can be seen, particularly at the confluence between two or more cisternae (fig. 15). Frequently the cisternae appear to abut the cell membrane. In some instances the material within the slightly dilated cisternae has a density similar to the extracellular material seen between the decidual cells. The contact between decidual cells is extensive, and in some areas of contact, junctional complexes of sorts are formed in which the cell membranes are closely apposed (fused?) for short segments, and where there is a slight increase in density of the adjacent cytoplasm.

Implantation stage 3

The elongation of the implantation site initiated in the previous stage continues during the evening of day 6 and the morning of day 7 (fig. 3). The decidualization of the stroma is more extensive and isolates the small amount of epithelium in immediate association with the blastocyst from the rest of the uterine epithelium in the cranio-caudal direction, but as yet not mesometrially. The stromal blood ves-

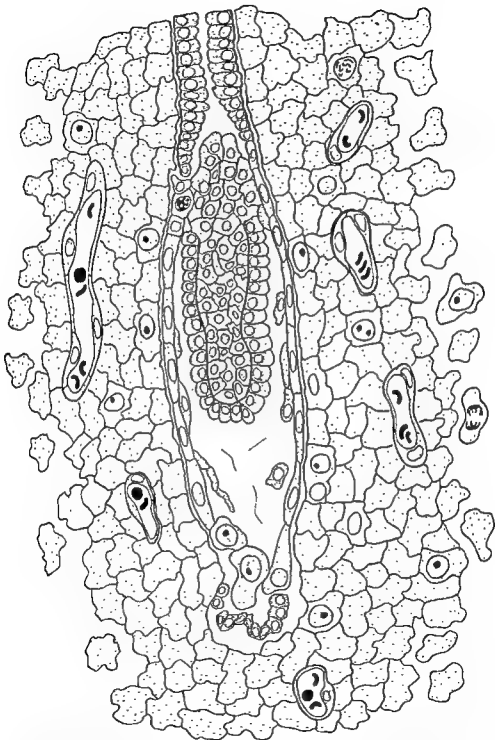


Fig. 3 A diagrammatic representation of the relationship in the implantation site at stage 3 of implantation, showing that the luminal epithelium is no longer present along the lateral margins of the implantation site.

sels are now surrounded by decidua, and appear to be reinvading and hence coming closer to the implanting blastocyst. It is during this period of time that trophoblast cells first come into contact with the stroma. That is, regions are found in which no luminal epithelium intervenes between the trophoblast and decidua.

The blastocyst changes rapidly during this period. In the early stages, it is characterized by its elongate tubular shape and the fact that in thick sections Rauber's layer is distinct, as is the endoderm. By the end of this period (morning of day 7) there is a small but distinct ectoplacental cone, and entypy or "germinal inversion" has converted the embryonic cell mass into an "egg cylinder."

"Penetration" of the uterine epithelium. The earliest we have observed contact of the trophoblast with the stroma was in implantation sites from a single animal taken at 3 A.M. on day 7. In still earlier animals occasional instances can be seen where an epithelial cell has rounded up and come loose from its basement membrane, but contact between the trophoblast and the denuded region has not been established. The region at which the trophoblast is first seen applied to the underlying stroma is generally the margins of the embryonic cell mass. Here the trophoblast lies in close contact with the thin connective tissue covering the decidual cells, i.e., it is still separated by the cleft between the basement membrane previously underlying the epithelium and the decidual cells. As the area in which no epithelial cells intervene between the trophoblast and decidua increases, three zones develop. Mesometrially the margins of the forming ectoplacental cone are in close association with the luminal epithelium (fig. 16). (The apex of the ectoplacental cone lies free in the lumen.) These marginal cells closely abut the individual epithelial cells which form the limits of the remaining mesometrial epithelium. They adhere along these lateral borders and may occasionally extend for short distances between the basement membrane and the overlying epithelial cells. In other instances, the marginal epithelial cells may already be loosened and be situated 2-3 μ into the uterine lumen. Nevertheless, a

considerable portion of their surface will be in contact with the trophoblast. In some of the more highly denuded sites, considerable epithelial debris, including whole nuclei with surrounding cytoplasm, are seen within the trophoblast cells at the margin of the ectoplacental cone, but at this stage no penetration of the trophoblast through the connective tissue cleft overlying the stromal cells is found (fig. 18).

Along the lateral margins of the cavity of the blastocyst, the trophoblast cells are slender and lie against the residual basement membrane of the epithelial cells (fig. 17). In the antimesometrial extension of the blastocyst (3rd zone), conditions are different. The epithelial cells are frequently sloughed into the residual uterine lumen. Debris is abundant. The trophoblast cells are irregular, protrude in among the residual cellular elements, and are increased in size. Cellular debris is common within these cells, and some of them (primary giant cells) extend for appreciable distances away from the general surface of the blastocyst. In this region all types of relationship with the epithelial cells may be found: trophoblast overlying the epithelial cells, surrounding epithelial cells, with engulfed fragments, etc. The total impression received of the relationship of the blastocyst to the implantation site at this time is that the margin of the ectoplacental cone constitutes a collar at which progressive dislocation of the epithelial cells occurs. On the lateral wall of the blastocyst, the trophoblast is directly apposed to the epithelial surface of the residual cleft formed by decidualization. Abembryonically the trophoblast cells are transforming into primary giant cells, and their relationship to one another and to the residual lumen with its debris is irregular.

Blastocyst. A number of cytological changes as well as important cellular translocations occur in the blastocyst by the morning of day 7. As implied in the previous section, the trophoblast cells exhibit regional differences in cytology. Along the lateral margins of the blastocyst, the trophoblastic cells are extremely thin and their nuclei are flattened. At the antimesometrial pole, however, the cells are larger, having large nuclei, and numerous large processes extend toward the residual debris

in the lumen of the uterus (fig. 19). These primary giant cells are characterized by abundant polyribosomes, but relatively few cisternae of the granular endoplasmic reticulum and a sparse distribution of mitochondria. Numerous lipid droplets may be seen in some of these cells. The cytology of the trophoblast cells in other regions of the blastocyst is less highly altered from the previous stage. However, polyribosomes are abundant, no areas of yolk plaques can be found, and most of the glycogen of the previous stage has disappeared. Few microvilli are present on any of the trophoblast cells, even where they are overlying residual epithelium or are free in the uterine lumen.

The cells of the ectoplacental cone form an irregular mass extending toward the mesometrial end of the uterine lumen. In light micrographs their cell boundaries are not always distinct, but they are distinctly cellular in electron micrographs. The embryonic cell mass begins to undergo entopy on the morning of day 7. That is, the embryonic cell mass grows down into the cavity of the blastocyst, resulting in a protrusion whose outer surface is covered by visceral endoderm, and within which is a solid mass of cells. The more antimesometrial portion of this enclosed mass will eventually form the embryo with the proamniotic cavity extruding mesometrially. However, no cavity formation is apparent at this stage. These inner cells of the egg cylinder are typically embryonic in cytological features, having many polyribosomes, a few strands of granular endoplasmic reticulum, scattered small mitochondria, and few inclusions (fig. 20). The visceral endodermal cells are characteristically cuboidal in shape and have distinct dilations at the junctions of cisternae of the endoplasmic reticulum (fig. 21). Between these endodermal cells are junctional complexes, and intervening between this layer and the rest of the embryonic cell mass is a well-formed basement membrane. (In earlier stages extracellular material accumulates against the bases of and occasionally between these endodermal cells.) The parietal endodermal cells extend along the trophoblast both singly and as isolated groups. They are flattened against the trophoblast and show little evi-

dence of formation of Reichert's membrane until the middle of day 7.

Epithelium. As previously mentioned the epithelium shows signs of detachment from its basement membrane as early as the morning of day 6. By the morning of day 7, not only is the epithelium gone over the lateral margins of the implantation site, but those cells which are beneath the site (antimesometrial) have largely loosened from their basement membrane and moved into the uterine lumen. Various stages of disintegration of epithelial cells may be seen. Individual cells constituting the margins of a group of cells still attached to the basement membrane round up, the nuclei become rounder with fewer indentations, microvilli tend to be lost, and lipid droplets apparently increase in size. Where the epithelium remains intact the microvilli are generally reduced. Vesicles in the apical cytoplasm are relatively few, but otherwise the cells do not appear to be greatly altered.

Stroma. The process of decidualization progresses both with regard to the extent of the stroma involved and the degree of decidualization of the cells involved. Glycogen becomes more abundant, especially in individual cells. Although most of the decidual cells do not show dilated endoplasmic reticulum, a few of the cells begin to show quite extensive dilation. Fibrous material is abundant in the cytoplasm of most decidual cells, but has a less ordered arrangement with regard to the direction of the margins of the implantation cavity than earlier. Lipid droplets are abundant in most of the decidual cells. As in the previous stage, the decidual cells bordering the uterine lumen constitute a complete layer, separated now from the trophoblast only by the residual connective tissue cleft between the basement membrane of the departed epithelium and the stroma itself. Into this region the decidual cells extend blunt scattered processes. At the margins of the decidual cells just underlying this space are distinct junctional complexes. The epithelioid transformation of these stromal elements has thus been completed. The small size of the blood vessels and their greater proximity to the implantation site than in the previous stage suggest a

reinvasion, but hemorrhage into the sub-epithelial space is rare at this stage.

At the periphery of the primary decidual zone occasional unmodified macrophages are seen. In addition, in this region there is a tendency toward two types of decidual cell. The second cell type is characterized by having more irregular cisternae of the endoplasmic reticulum with more scattered ribosomes along the membranes, but is otherwise quite similar to the other decidual cells.

DISCUSSION

Although it is generally understood what is meant when referring to implantation of the blastocyst in the endometrium, or nidation, difficulties arise when attempts are made to establish the time of initiation of implantation, the duration of this stage, or when a comparison of the features of implantation is made between different species of mammals. Since the intimacy of association between the fetal and maternal tissues, as well as such other features as the site of implantation and the degree of swelling of the blastocyst, are different in different species, not all of the stages of implantation will be identical. Nevertheless, the first stage of implantation must be the assumption of a fixed position of the blastocyst with regard to the uterus, no matter what the eventual degree of trophoblastic penetration (Fainstat and Chapman, '65). Before such a time, the blastocyst is unattached and hence unimplanted. It is quite possible that this early association can be disrupted without injury to either the blastocyst or the uterus, as it can be in the rat, but as long as it is relatively fixed under normal conditions, it should be considered implanted.

In the rat, the first attachment is apparently achieved by a decrease in width of the uterine lumen, resulting in a clasp of the blastocyst. From our observations of edema, the known presence of edema in early pseudopregnancy (Jollie and Bencosme, '65) and the well-known effect of estrogen in producing edema (Pappas and Blanchette, '65), it appears feasible at the present time to consider that it is an estrogen-induced edema which results in the clasp of the blastocyst. Once the blastocyst is clasped it can then act as a stimulus

to decidualization, thus resulting in a localized transformation of the fibroblasts to decidual cells, concomitant with a transient local enhancement of the vascular permeability, which can be visualized grossly by the Pontamine Blue reaction, or in the electron microscope by permeability of the vessels to thorotrast. Since Blandau ('49) has shown that blastocyst-sized particles are effective in producing a local decidual reaction in the rat, this effect of the blastocyst might well be largely or entirely mechanical. In this case, some continued contraction of the myometrium would probably aid the blastocyst in being an irritant.

The process of decidualization results in a tubular pit surrounding the blastocyst, the antimesometrial extreme of the uterine lumen, and extending beyond these structures. The cells which undergo transformation to decidual cells are the somewhat peculiar large-bodied fibroblasts which surround the uterine lumen. No evidence of migration of cells from around the blood vessels, etc., was observed in our material. Some of the changes which we have observed (increased fibrillar material, formation of glycogen, dilation of the endoplasmic reticulum) have been observed previously by Jollie and Bencosme ('65), in induced decidualomata. However, the decidual changes occur more rapidly in the normal implantation site, the formation of glycogen in particular appearing much earlier in normal implantation than in the decidualomata, studied by Jollie. The eventual transformation of the fibroblast cells surrounding the uterine lumen to decidual cells with an epithelioid character and well-formed junctional complexes must result in a modification of the connective tissue space intervening between the luminal epithelium and its vascular bed. The relative isolation resulting from these modifications might contribute to the sloughing of the epithelial cells from the basement membrane, a phenomenon which has not been observed in our preparations before decidualization.

The mechanism by which the blastocyst comes to have a more intimate association with the stroma has long been a subject of speculation. Blandau ('49) points out that apparently the trophoblast of the rat is less invasive than that of the guinea pig, and

that it fails to exhibit proteolytic activity in his *in vitro* test system. Needless to say, observations of individual fixed specimens do not give a continuous record of the dynamic activity of the cells involved. However, there are a number of implications which can be gained from these observations with the electron microscope. The sloughing of whole luminal epithelial cells and clumps of these cells from their basement membrane some distance from the vicinity of the trophoblast and the finding of individual isolated cells in the lumen indicate that in the region of the decidual cup the luminal epithelium is no longer a typical viable epithelium tending to maintain its surface intact. The absence of any specific breakdown of individual cells in contact with the trophoblast (but not phagocytized by the trophoblast) is evidence against extracellular enzymatic lysis of the epithelium by the trophoblast. Where the trophoblast is in intimate contact with the epithelium (especially at the margin of the forming ectoplacental cone) it is possible, and indeed appears probable, that the growing trophoblast mechanically dislocates some of the epithelium. However, at no time are large sheets removed in this fashion, nor does there appear to be any penetration of the epithelium until some disruption of this layer has taken place. Particularly striking is the membrane-to-membrane adherence of the trophoblast to the epithelial cells. In this regard it is interesting that in the oldest stage we have examined (day 7) the trophoblast has not penetrated the stroma and in most places has not even penetrated through the residual basement membrane and other connective tissue elements, overlying the stroma. This observation would also indicate that some type of membrane-to-membrane adherence which could contribute to the phagocytic process is the important factor in activity of the trophoblast, rather than any histolytic action which might be expected to be reflected in loosening or destruction of the connective tissue remaining between the basement membrane of the epithelium and the stroma. Only at the antimesometrial extreme of the blastocyst do the trophoblast cells grow out from the general surface of the blastocyst. In

this position, their cell processes are extending into cellular debris as these trophoblast cells undergo transformation into primary giant cells.

In summary, the histolytic and invasive properties of the early trophoblast of the rat appear to be very feeble in the first stages of normal implantation, but adherence of the trophoblastic cell membrane to the cell membranes of the epithelial cells appears to be an important process with regard to translocation of some epithelial cells and phagocytosis of sloughed cells.

LITERATURE CITED

- Alden, R. H. 1947 Implantation of the rat egg. II. Alterations in osmophilic epithelial lipids of the rat uterus under normal and experimental conditions. *Anat. Rec.*, 97: 1-19.
- Amoroso, E. C. 1952 Placentation. In: Marshall's Physiology of Reproduction, A. S. Parkes, ed., Longmans, Green and Company, New York.
- Austin, C. R. 1951 The formation, growth and conjugation of the pronuclei in the rat egg. *J. Roy. Micro. Soc.*, 71: 295-306.
- Blandau, R. J. 1949 Embryo-endometrial interrelationship in the rat and guinea pig. *Anat. Rec.*, 104: 331-359.
- . 1961 Biology of eggs and implantation. In: Sex and Internal Secretions, W. C. Young, ed., Williams and Wilkins, Baltimore.
- Burckhard, G. 1901 Die Implantation des Eies der Maus in die Uterusschleimhaut und die Umbildung derselben zur Decidua. *Archiv. für Micro. Anat.*, 37: 528-569.
- De Feo, V. J. 1963 Temporal aspect of uterine sensitivity in the pseudopregnant or pregnant rat. *Endocrinol.*, 72: 305-316.
- Dickmann, Z., and R. W. Noyes 1961 The zona pellucida at the time of implantation. *Fertil. Steril.*, 12: 310-318.
- Duval, M. 1891 Le placenta des rongeurs. Le placenta de la souris et du rat. *J. Anat. et Physiol.*, 27: 24-73.
- Enders, A. C., and S. J. Schlafke 1965 The fine structure of the blastocyst: some comparative studies. In: Preimplantation Stages of Pregnancy, Wolstenholme and O'Connor, eds., Churchill, London.
- Fainstat, T., and G. B. Chapman 1965 Microvilli of endometrial epithelium in relation to ovulation. *Am. J. Ob. Gyn.*, 91: 852-861.
- Fawcett, D. W. 1950 Development of mouse ova under the capsule of the kidney. *Anat. Rec.*, 108: 71-92.
- Huber, G. C. 1915 The development of the albino rat, *Mus norvegicus albinus*. I. From the pronuclear stage to the stage of mesoderm anlage; end of the first to the end of the ninth day. *J. Morph.*, 26: 247-358.
- Jollie, W. P. 1961 The incidence of experimentally produced abdominal implantations in the rat. *Anat. Rec.*, 141: 159-167.

reinvasion, but hemorrhage into the sub-epithelial space is rare at this stage.

At the periphery of the primary decidual zone occasional unmodified macrophages are seen. In addition, in this region there is a tendency toward two types of decidual cell. The second cell type is characterized by having more irregular cisternae of the endoplasmic reticulum with more scattered ribosomes along the membranes, but is otherwise quite similar to the other decidual cells.

DISCUSSION

Although it is generally understood what is meant when referring to implantation of the blastocyst in the endometrium, or nidation, difficulties arise when attempts are made to establish the time of initiation of implantation, the duration of this stage, or when a comparison of the features of implantation is made between different species of mammals. Since the intimacy of association between the fetal and maternal tissues, as well as such other features as the site of implantation and the degree of swelling of the blastocyst, are different in different species, not all of the stages of implantation will be identical. Nevertheless, the first stage of implantation must be the assumption of a fixed position of the blastocyst with regard to the uterus, no matter what the eventual degree of trophoblastic penetration (Fainstat and Chapman, '65). Before such a time, the blastocyst is unattached and hence unimplanted. It is quite possible that this early association can be disrupted without injury to either the blastocyst or the uterus, as it can be in the rat, but as long as it is relatively fixed under normal conditions, it should be considered implanted.

In the rat, the first attachment is apparently achieved by a decrease in width of the uterine lumen, resulting in a clasping of the blastocyst. From our observations of edema, the known presence of edema in early pseudopregnancy (Jollie and Bencosme, '65) and the well-known effect of estrogen in producing edema (Pappas and Blanchette, '65), it appears feasible at the present time to consider that it is an estrogen-induced edema which results in the clasping of the blastocyst. Once the blastocyst is clasped it can then act as a stimulus

to decidualization, thus resulting in a localized transformation of the fibroblasts to decidual cells, concomitant with a transient local enhancement of the vascular permeability, which can be visualized grossly by the Pontamine Blue reaction, or in the electron microscope by permeability of the vessels to thorotrast. Since Blandau ('49) has shown that blastocyst-sized particles are effective in producing a local decidual reaction in the rat, this effect of the blastocyst might well be largely or entirely mechanical. In this case, some continued contraction of the myometrium would probably aid the blastocyst in being an irritant.

The process of decidualization results in a tubular pit surrounding the blastocyst, the antimesometrial extreme of the uterine lumen, and extending beyond these structures. The cells which undergo transformation to decidual cells are the somewhat peculiar large-bodied fibroblasts which surround the uterine lumen. No evidence of migration of cells from around the blood vessels, etc., was observed in our material. Some of the changes which we have observed (increased fibrillar material, formation of glycogen, dilation of the endoplasmic reticulum) have been observed previously by Jollie and Bencosme ('65), in induced deciduomata. However, the decidual changes occur more rapidly in the normal implantation site, the formation of glycogen in particular appearing much earlier in normal implantation than in the deciduomata, studied by Jollie. The eventual transformation of the fibroblast cells surrounding the uterine lumen to decidual cells with an epitheloid character and well-formed junctional complexes must result in a modification of the connective tissue space intervening between the luminal epithelium and its vascular bed. The relative isolation resulting from these modifications might contribute to the sloughing of the epithelial cells from the basement membrane, a phenomenon which has not been observed in our preparations before decidualization.

The mechanism by which the blastocyst comes to have a more intimate association with the stroma has long been a subject of speculation. Blandau ('49) points out that apparently the trophoblast of the rat is less invasive than that of the guinea pig, and

EARLY IMPLANTATION IN THE RAT
Allen C. Enders and Sandra Schlafke

- Jollie, W. P., and S. A. Bencosme 1965 Electron microscopic observations on primary decidua formation in the rat. *Am. J. Anat.*, 116: 217-236.
- Karnovsky, M. J. 1965 A formaldehyde-glutaraldehyde fixative of high osmolarity for use in electron microscopy. *J. Cell Biol.*, 27: 137A.
- Kirby, D. R. S. 1963 The development of mouse blastocysts transplanted to the scrotal and cryptorchid testis. *J. Anat.*, 97: 119-130.
- Krehbiel, R. H. 1937 Cytological studies of the decidua reaction in the rat during early pregnancy and in the production of deciduomata. *Physiol. Zool.*, 10: 212-234.
- 1941 The production of deciduomata in the pregnant lactating rat. *Anat. Rec.*, 81: 67-77.
- Melissinos, K. 1907 Die Entwicklung des Eies der Mause. *Achiv. für mikr. Anat.*, 70: 577-628.
- Mossman, H. W. 1937 Comparative morphogenesis of the fetal membranes and accessory uterine structures. *Contrib. Embryol. Carneg. Inst.*, 26: 129-246.
- Nicholas, J. S. 1942 Experiments on developing rats. IV. The growth and differentiation of eggs and egg-cylinders when transplanted under the kidney capsule. *J. Exp. Zool.*, 90: 41-64.
- Noyes, R. W., and Z. Dickmann 1960 Relationship of ovular age to endometrial development. *J. Reprod. Fert.*, 1: 186-196.
- Odor, D. L., and R. J. Blandau 1951 Observations on fertilization and the first segmentation division in rat ova. *Am. J. Anat.*, 89: 29-61.
- Orsini, M. W. 1963 Morphological evidence on the intrauterine career of the ovum. In: *Delayed Implantation*, A. C. Enders, ed., U. Chicago Press, Chicago.
- Pappas, G. D., and E. J. Blanchette 1965 Transport of colloidal particles from small blood vessels correlated with cyclic changes in permeability. *Invest. Ophthalmol.*, 4: 1026-1036.
- Psychoyos, A. 1960 La réaction deciduale est précédée de modifications précoces de la perméabilité capillaire de l'utérus. *C. R. Soc. Biol.*, 154: 1384-1387.
- Runner, M. N. 1947 Development of mouse eggs in the anterior chamber of the eye. *Anat. Rec.*, 98: 1-17.
- Shelesnyak, M. C. 1962 Decidualization: The decidua and the deciduoma. *Perspect. Biol. Med.*, 5: 503-518.
- Sobotta, J. 1903 Die Entwicklung des Eies der Maus vom Schlusse der Furchungsperiode bis zum Auftreten der Aminosalten. *Archiv. für Mikr. Anat.*, 61: 274-330.
- Szollosi, D. G. 1965 Development of "follicle substance" in some rodent eggs. *Anat. Rec.*, 151: 424.
- Szollosi, D. G., and H. Ris 1961 Observations on sperm penetration in the rat. *J. Biophys. Biochem. Cytol.*, 10: 275-283.
- Velardo, J. T., A. B. Dawson, A. G. Olsen and F. L. Hisaw 1953 Sequence of histological changes in the uterus and vagina of the rat during prolongation of pseudopregnancy associated with the presence of deciduomata. *Am. J. Anat.*, 93: 273-306.

PLATE 1

EXPLANATION OF FIGURE

- 4 Venule (right) and fibroblast in the endometrium from an animal killed at 3 P.M. day 5. Note that thorotrast has leaked from the vessel and has accumulated between it and the fibroblast at the left of the picture (0.5 cm³ thorotrast injected into the femoral vein 20 minutes before fixation of the tissue). Apparently edema of the endometrium has already begun by this stage. $\times 22,500$.



PLATE 2

EXPLANATION OF FIGURE

- 5 Section of a blastocyst from 9 P.M. day 5. In this region Rauber's layer (upper right) overlies the embryonic cell mass. Note the presence of regions devoid of organelles and containing plaques. $\times 16,700$.

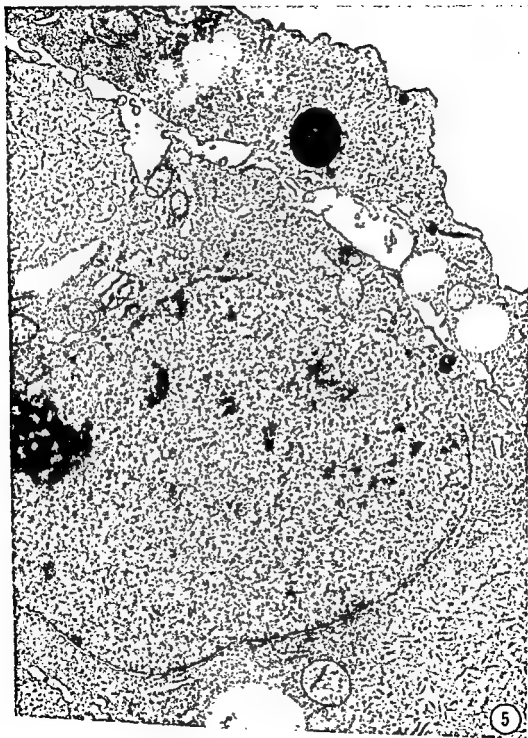


PLATE 2

EXPLANATION OF FIGURE

- 5 Section of a blastocyst from 9 P.M. day 5. In this region Rauber's layer (upper right) overlies the embryonic cell mass. Note the presence of regions devoid of organelles and containing plaques. $\times 16,700$.



PLATE 3

EXPLANATION OF FIGURE

- 6 A trophoblast cell (upper right) associated with three uterine epithelial cells, from an animal killed at 9 P.M. on day 5. Note the particularly close association of the central epithelial cell with the trophoblast. Lipid droplets (L) characteristic of the basal portion of epithelial cells of this stage can be seen in the lower left corner. LP, lipid pigment. $\times 10,700$.

EARLY IMPLANTATION IN THE RAT
Allen C. Enders and Sandra Schlafke

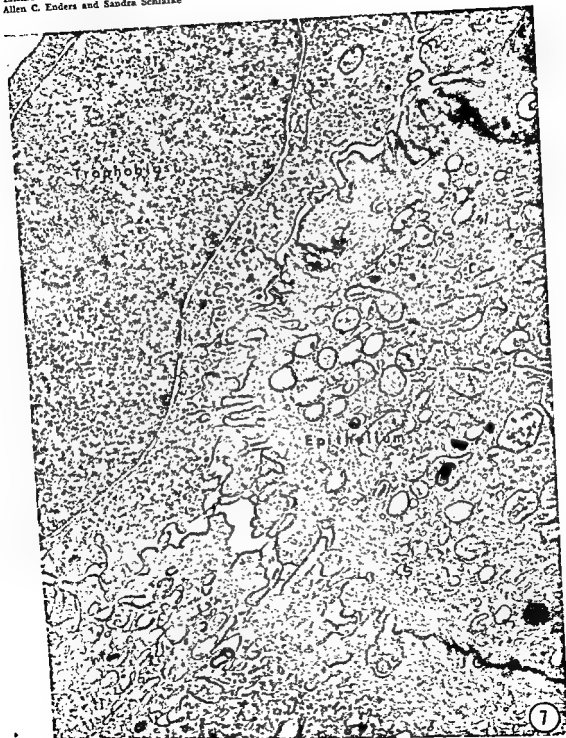


PLATE 4

EXPLANATION OF FIGURE

- 7 Higher magnification of a similar area to that shown in the previous figure. Note the interdigitation of projections from the trophoblast and luminal epithelial cells. A few fine granules of glycogen can be seen in the trophoblast cell. The peculiar vesiculations of the epithelial cell (dilated in the cell at the right, more horseshoe-shaped in the cell on the left) are shown clearly here, as is a typical junctional complex (JC). 9 P.M. day 5. $\times 24,700$.

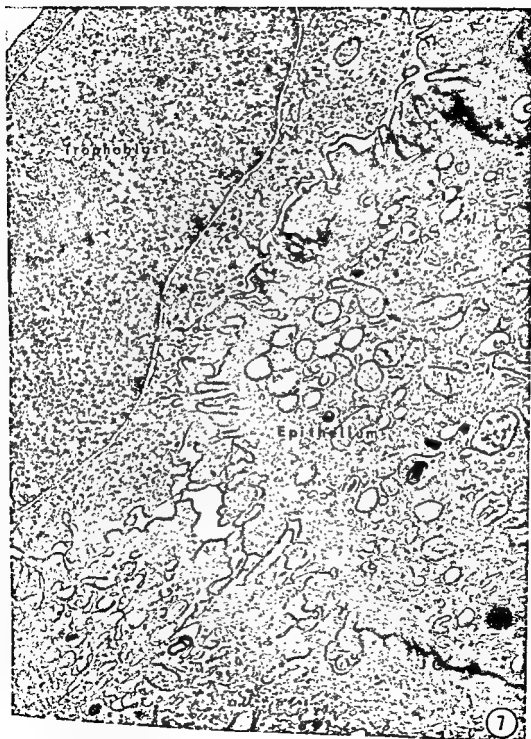


PLATE 5

EXPLANATION OF FIGURE

- 8 Several fibroblasts from around the antimesometrial luminal epithelium (upper right) at 9 P.M. on day 5. There are large areas of contiguity between the cells but the endoplasmic reticulum is undilated and the cytoplasm in general appears relatively unmodified. $\times 6,000$.

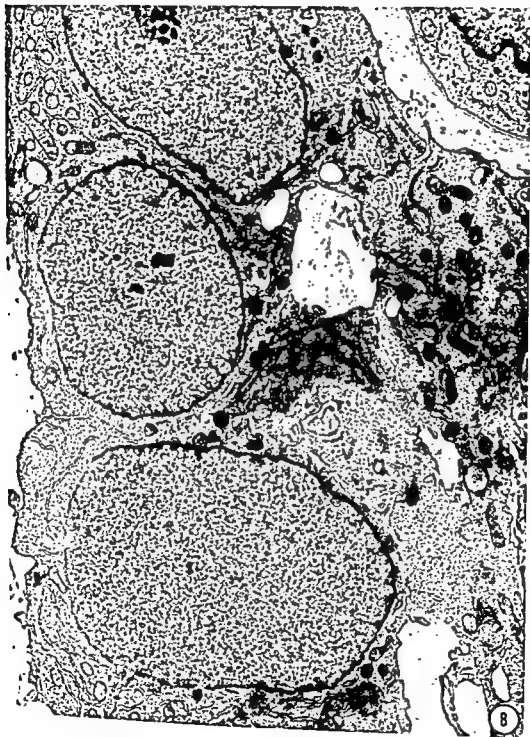


PLATE 6

EXPLANATION OF FIGURE

- Abembryonic trophoblast cells from an animal killed at 10 A.M. on day 6. There is an abundance of glycogen and lipid in the dividing cell at the left. The junctional complex seen in the upper right beneath the free surface of the blastocyst is typical of this stage. $\times 19,000$.



PLATE III

EXPLANATION OF FIGURE

- Ⓚ Abembryonic trophoblast cells from an animal killed at 10 A.M. on day 6. There is an abundance of glycogen and lipid in the dividing cell at the left. The junctional complex seen in the upper right beneath the free surface of the blastocyst is typical of this stage. $\times 19,000$.



PLATE 7

EXPLANATION OF FIGURE

- 10 A high magnification of a mid body between two dividing trophoblast cells. The parallel array of microtubules is seen here, as are a number of cytoplasmic folds at the right of the picture. The shape of the glycogen granules can be seen in the lower right corner and the upper left beneath the lipid droplet. 10 A.M. day 6. $\times 25,500$.

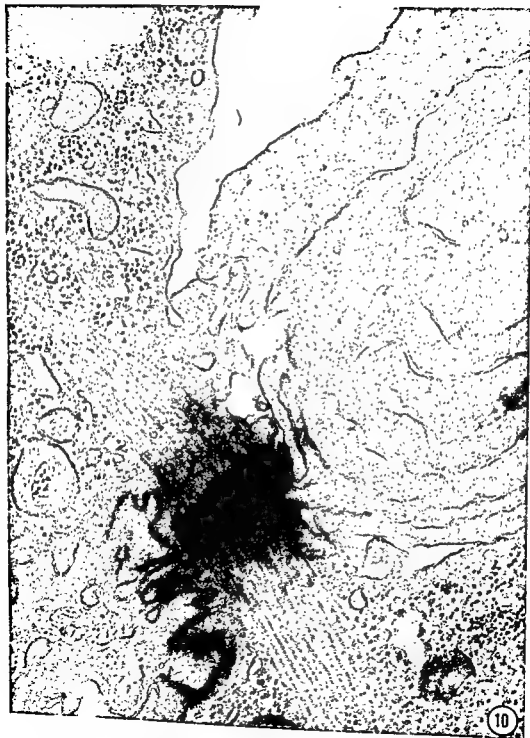


PLATE 8

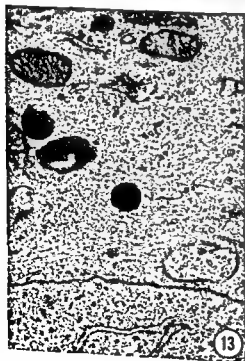
EXPLANATION OF FIGURE

- 11 The apical surface of an epithelial cell from an animal killed at 10 A.M. day 6, showing the knobby and irregular nature of the surface projections. The apical vesicles (arrows) are mostly in a collapsed form in this cell. Their exact nature is yet to be elucidated. $\times 37,000$.



EXPLANATION OF FIGURES

- 12 This micrograph illustrates the cleft which becomes delineated between the luminal epithelium (upper right) and the decidualized fibroblasts (lower left) by the morning of day 6. Parts of three fibroblasts constitute the bordering decidua. They form a continuous sheet. Note the flocculent material (arrows) in the connective tissue cleft in addition to the collagen fibrils (C) and basement membrane (BM). $\times 13,500$.
- 13 The fibrillar material in the decidual cell at the top of this picture is characteristic of this cell type. 5 P.M. day 6. $\times 25,800$.
- 14 Dense glycogen granules frequently appear first in association with the lipid droplets in the decidual cells, as illustrated here. ■ P.M. day 6. $\times 16,200$.



EXPLANATION OF FIGURES

- 12 This micrograph illustrates the cleft which becomes delineated between the luminal epithelium (upper right) and the decidualized fibroblasts (lower left) by the morning of day 6. Parts of three fibroblasts constitute the bordering decidua. They form a continuous sheet. Note the flocculent material (arrows) in the connective tissue cleft in addition to the collagen fibrils (C) and basement membrane (BM). $\times 13,500$.
- 13 The fibrillar material in the decidual cell at the top of this picture is characteristic of this cell type. 5 P.M. day 6. $\times 25,800$.
- 14 Dense glycogen granules frequently appear first in association with the lipid droplets in the decidual cells, as illustrated here. 5 P.M. day 6. $\times 16,200$.

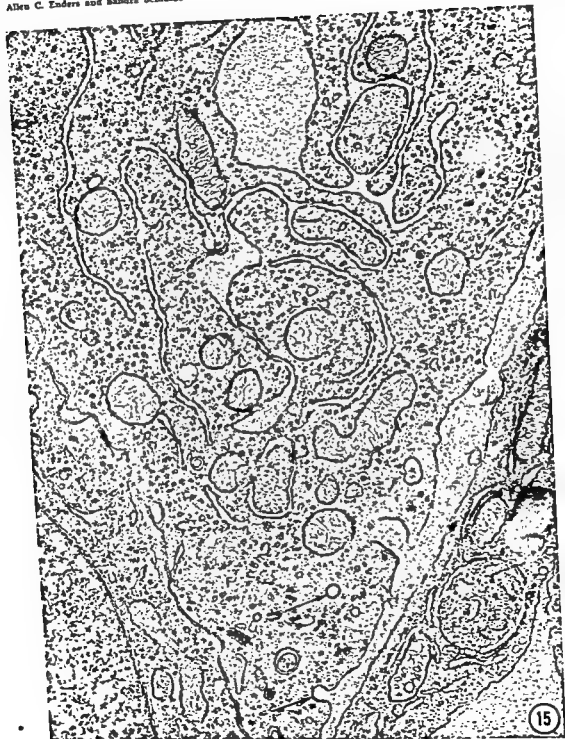
EARLY IMPLANTATION IN THE RAT
Allen C. Enders and Sandra Schlafke

PLATE 10

EXPLANATION OF FIGURE

- 15 Dilation of the cisternae of the endoplasmic reticulum can be seen in this decidualizing fibroblast fixed at 5 P.M. day 6. Note the similarity in density of the material within the cisternae and that in the intracellular space between this fibroblast and the adjacent endothelial cell in the lower right corner. F, fibrillar material; arrows, caveolae. $\times 26,800$.



PLATE 12

EXPLANATION OF FIGURE

- 17 Lateral margin of an advanced implantation site from 9 A.M. day 7, showing the typical arrangement of this region. Apparently Reichert's membrane is just beginning to form (arrows). The visceral endothelial cell at the top of the picture illustrates clearly the advanced differentiation of the apical cytoplasm of these cells. CT, connective tissue cleft; P.End., parietal endoderm; Tr, trophoblast. $\times 8,700$.

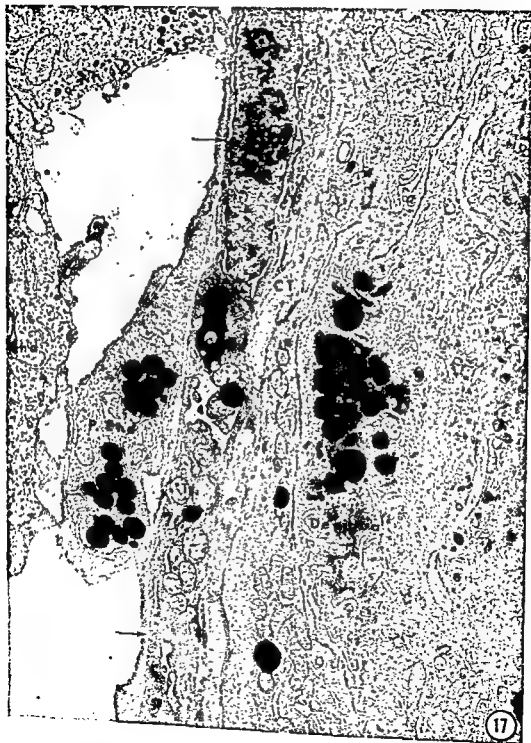


PLATE 12

EXPLANATION OF FIGURE

- 17 Lateral margin of an advanced implantation site from 9 A.M. day 7, showing the typical arrangement of this region. Apparently Reichert's membrane is just beginning to form (arrows). The visceral endothelial cell at the top of the picture illustrates clearly the advanced differentiation of the apical cytoplasm of these cells. CT, connective tissue cleft; P.End., parietal endoderm; Tr, trophoblast. $\times 8,700$.



EXPLANATION OF FIGURES

- 18 In the upper right corner of this micrograph from a stage III implantation site, a tongue of trophoblast (Tr) surrounds an epithelial cell nucleus (Ep). Cell processes, collagen, fibrils, and an amorphous ground substance can be seen in the connective tissue cleft between the residual basement membrane (BM) and the decidual cell. 9 A.M. day 7. $\times 13,800$.
- 19 At the top center of this micrograph a large abembryonic trophoblast cell (primary giant cell) is extending a process to the residual basement membrane within the epithelial debris of the antimesometrial lumen. Note that there is still no penetration into the underlying stroma. 9 A.M. day 7. $\times 3,200$.

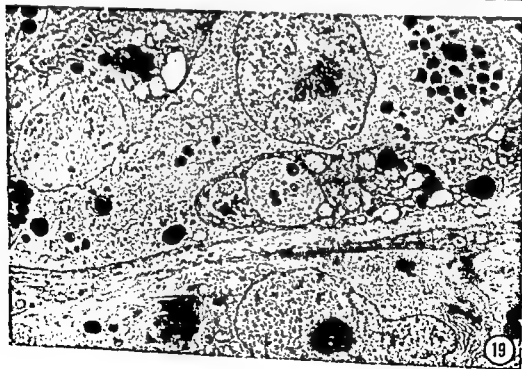
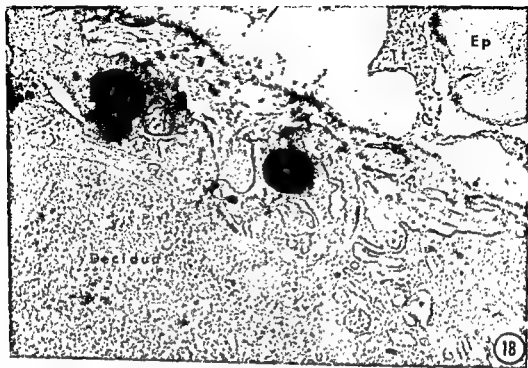
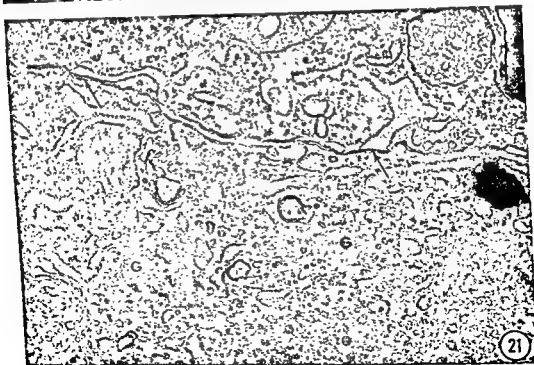
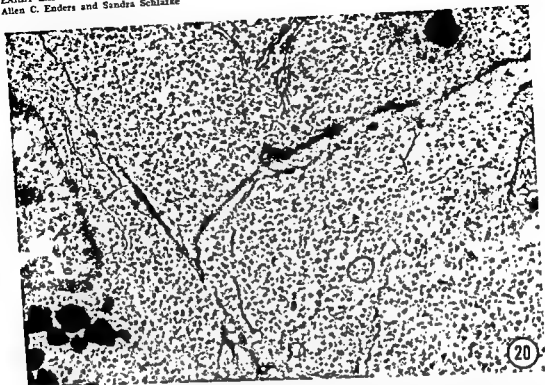


PLATE 14

EXPLANATION OF FIGURES

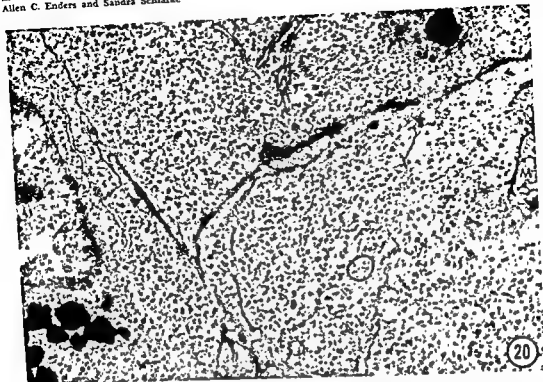
- 20 Inner cells of the egg cylinder. These cells are now completely differentiated from the specialized cytoplasm of the early fertilized egg, and have become typically embryonic, with many polyribosomes, a few strands of endoplasmic reticulum, occasional mitochondria, and relatively few inclusions. L, lipid. 9 A.M. day 7. $\times 16,400$.
- 21 Small portions of two adjacent visceral endodermal cells are shown in this micrograph. The dilation of the cisternae of the endoplasmic reticulum and the close apposition of smooth portions of the reticulum to the basement membrane (arrows) are seen both in these cells and in decidual cells. The large juxtannuclear Golgi zone (G) seen in the bottom cell is a further indication of the extent of differentiation of these endodermal cells. 10 A.M. day 7. $\times 33,000$.

EARLY IMPLANTATION IN THE RAT
Allen C. Enders and Sandra Schlafke



EXPLANATION OF FIGURES

- 20 Inner cells of the egg cylinder. These cells are now completely differentiated from the specialized cytoplasm of the early fertilized egg, and have become typically embryonic, with many polyribosomes, a few strands of endoplasmic reticulum, occasional mitochondria, and relatively few inclusions. L, lipid. 9 A.M. day 7. $\times 16,400$.
- 21 Small portions of two adjacent visceral endodermal cells are shown in this micrograph. The dilation of the cisternae of the endoplasmic reticulum and the close apposition of smooth portions of the reticulum to the basement membrane (arrows) are seen both in these cells and in decidual cells. The large juxtannuclear Golgi zone (G) seen in the bottom cell is a further indication of the extent of differentiation of these endodermal cells. 10 A.M. day 7. $\times 33,000$.

EARLY IMPLANTATION IN THE RAT
Allen C. Enders and Sandra Schlafke

The Mechanism of Spermiation in the Toad^{1,2}

M. H. BURGOS AND R. VITALE-CALPE³

Instituto de Histología y Embriología,
Facultad de Ciencias Médicas, U.N.C.,
Mendoza — Argentina

ABSTRACT The present paper is the first demonstration, at the ultrastructural level, of the mechanism of sperm release from the Sertoli cells. The main target of the immediate effect of LH is the cytoplasm of the Sertoli cells.

Three main stages are recognized in the cellular response: (1) swelling of the endoplasmic reticulum, (2) swelling of the apical cytoplasm, (3) the apical detachment.

The preservation of the nucleated basal portion of the Sertoli cells after the stage of apical detachment is assured by a mechanism of protective overlapping of residual membranes.

It has also been shown that LH is able to increase water and sodium content in the toad testis. It is postulated that water enters after the injection of the LH into the channels of the endoplasmic reticulum, then the water moves into the apical cytoplasm attracted by hydrophilic products derived from enzymatic splitting of cytoplasmic mucoproteins. Finally water passes into the lumen of the seminiferous tubules simultaneously with cell debris and the liberated spermatozoa. The lysosomes present in the cytoplasm of the Sertoli cell in this mucolytic action may be involved.

The first observations contributing to an explanation of the mechanism of the release of spermatozoa under gonadotrophic stimulation were reported in 1945 and 1946 by De Robertis, Burgos and Breyter. It was suggested that the target cell of gonadotrophin was the Sertoli cell which showed a remarkable cytoplasmic vacuolization, rupture of the apical vacuoles and concurrent release of fluid and spermatozoa into the lumen of the seminiferous tubules. A few years later, knowledge of this rapid effect of gonadotrophins upon the toad testis, led to its clinical application in the toad test for diagnosis of pregnancy (Calli Mainini, '47). At the same time it was shown that gonadotrophins also act directly upon the testis isolated *in vitro* (Burgos and Mancini, '47) and that a highly hydrophilic mucoprotein was probably involved in the mechanism of release of spermatozoa (Mancini and Burgos, '48). Working along a similar line but with *Rana temporaria*, the school of van Oordt (van Oordt et al., '54) studied the mechanism of release of spermatozoa and described swelling of large vacuoles of Sertoli cells with distension of the tubules, increase in their water content, and the presence of a metachromatic substance (van Dongen et al., '58, '60 and '62). Both

groups of investigators recognized the increase in water content of the seminiferous tubules as an important factor in sperm release. Houssay et al., 1929 (for a complete review see Houssay, '54) had earlier reported an increase in water content of the testis when they demonstrated that pituitary extract caused an increase in weight and volume of the testis accompanied by a translucent appearance and distension of the tubules. Astrada and Taleisnik ('57) studying the effect of pituitary extracts on isolated toad testis in saline solution, concluded that water was pumped against the concentration gradient.

In the work reported here, we have succeeded in demonstrating the ultrastructural basis for release of the spermatozoa. An increase in water content has been confirmed and an increase in sodium content has been shown to result from the administration of purified LH. Luteinizing hormone has been found to have a remark-

¹This work was introduced at the VI Meeting of the Asociación Latinoamericana de Ciencias Fisiológicas (Member of the International Union of Physiological Sciences) held at Viña del Mar (Chile) in November, 1964.

²Supported by a grant from the Population Council M-63-121 and a school grant RF 62051 from the Rockefeller Foundation.

³Research Assistant supported by the Population Council grant M-63-121.

in the cloacal fluid was observed 30 minutes after the injection and continued positive during the entire period of observation. Control animals were also checked in a similar way.

Testes were carefully exposed 30, 60 and 120 minutes after the end of the intravenous injections. Ten percent Acrolein in cold phosphate buffer (Millonig) at pH 7.4 plus 0.33 M sucrose plus 0.04 % CaCl_2 , was dropped upon the testes over a period of 10 minutes. The testes were then dissected from the mesorchium, cut with a sharp razor into slices about 3 mm thick and immersed for 20 minutes in the same fixative at room temperature. Slices were transferred and washed in the same buffer solutions for 15 min-

utes after the end of the injection. After direct or LRI injection, the cytoplasm is paler, the cluster appears less close packed and farther removed from the nucleus of the Sertoli cell (fig. 11). Finally, the Sertoli cell still attached to the basement membrane and partially vacuolated, shows a loss of part of its apical cytoplasm concurrently with the release of spermatozoa (fig. 12).

Control Sertoli cell

In electron micrographs (fig. 7, 9) cell limits are clearly resolved and the contact surfaces between sustentacular cells (Sertoli cells) show desmosomes and frequent interdigitations, especially in their basal portion. A clearly defined basement membrane is found at the interface between Sertoli cells and the surrounding

The Sertoli cell nucleus is irregular in shape and has a large nucleolus. The heterogeneous cytoplasm contains areas which show a striking development of the smooth endoplasmic reticulum, Golgi complex and numerous mitochondria. Running between those zones rich in organelles are bundles of delicate fibrils (fig. 9) which surround the nucleus and extend toward the cell periphery. The apical cytoplasm immediately surrounding the heads of maturing spermatozoa is clear, devoid of organelles and consists of a fine filamentous material of low electron density (fig. 9).

LH treated Sertoli cell

There are three recognizable stages in the mechanism of spermiation as revealed in electron micrographs. The first of these may be designated the *stage of swelling of the endoplasmic reticulum*. In this stage the Sertoli cells show a remarkable development of the smooth endoplasmic reticulum (ER). Channels become more numerous and dilated. Vacuoles and cisternae swell markedly, and the distended reticulum comes to occupy much of the cytoplasm (figs. 2, 13). A watery content fills the channels and vacuoles of the ER (figs. 14, 15). The swelling of this organelle produces an increase in size of the Sertoli cell as a whole which becomes tall and columnar owing mainly to an expansion of the supranuclear and apical cytoplasm. At the same time the tips of the spermatozoa are pushed away from the nuclear and basal zone by the swelling of the ER in the apical region of the cell (fig. 2). In the basal zone, there are frequent openings of the channels of ER onto the basement membrane (figs. 2, 14). Basal infoldings become shorter and diminish in number (figs. 2, 13) or disappear altogether (fig. 13). The implanted spermatozoa become separated from one another by the swelling of the interspersed ER (figs. 2, 13, 15). Among the profiles of the ER, are lysosomes and mitochondria with a dense matrix and wide intracristal spaces.

Following the stage of distension of the endoplasmic reticulum is the *stage of swelling of the apical cytoplasm*. The apical cytoplasm which surrounds the sper-

matozoa becomes paler and bulges upward and laterally (figs. 3, 16). Gradually the volume of the apical cytoplasm increases while at the same time the distended ER collapses (fig. 16, arrow). This swelling, progressively effaces the apical recesses which contain the spermatozoa and thus pushes the spermatozoa further towards the tubular lumen (figs. 3, 17).

The third phase of the process is the *stage of the apical detachment*. The extreme swelling of the apical cytoplasm results in the formation of cupola-like projections (fig. 17) or irregular cytoplasmic blebs (fig. 18). Concomitant with the rupture and disintegration of the apical cytoplasm, spermatozoa, fluid and cellular debris are discharged into the lumen. Numerous narrow channels and collapsed membranes are seen in the supranuclear region of the cells which are now lower owing to loss of their apical cytoplasm. These membranes apparently are formed by the apposition of flattened vesicles and cisternae of the endoplasmic reticulum and by the overlapping of the residual cell surface membrane. These piles of membranes formed thus may represent a mode of repair of the cells after abscission of their apical cytoplasm. At this stage a typical Golgi complex is frequently observed (fig. 19). Mitochondria are similar to those of the previous stages. They are elongated with dense matrix and wide intracristal clefts. Lysosomes are rarely seen in the cytoplasm of the Sertoli cells.

Figure 18 shows part of the cytoplasm of Sertoli cells after the release of spermatozoa. A few vacuoles and an overlapping of membranes remain near the lumen. The rest of the cytoplasm shows a pale nucleus, surrounded by numerous fibrils, typical channels of rough endoplasmic reticulum containing a filamentous material of low electron density and vacuoles, lacunae and channels of the smooth endoplasmic reticulum. The basement membrane shows absence of infoldings.

Water, sodium and potassium content

As shown in figure 5 and table 1, the mean values of the water content in the toad testis, which is in control animals

able effect on the Sertoli cell cytoplasm and its junction with the sperm cells. The process has been followed from the very beginning to the end, and three main stages have been recognized.

MATERIALS AND METHODS

Forty adult male toads, *Bufo arenarum* Hensel, were collected in the Mendoza area during fall, winter and early spring. They were divided into two lots, pithed and injected via the abdominal vein. The control lot (20) with 1 ml isotonic saline and the experimental lot (20) with 1 ml isotonic saline containing 1 mg purified luteinizing hormone (LH).⁴ All the experimental animals were examined for a positive response to LH before dissecting the testis. The presence of spermatozoa in the cloacal fluid was observed 30 minutes after the injection and continued positive during the entire period of observation. Control animals were also checked in a similar way.

Testes were carefully exposed 30, 60 and 120 minutes after the end of the intravenous injections. Ten percent Acrolein in cold phosphate buffer (Millonig) at pH 7.4 plus 0.33 M sucrose plus 0.04 g % CaCl_2 , was dropped upon the testes over a period of 10 minutes. The testes were then dissected from the mesorchium, cut with a sharp razor into slices about 3 mm thick and immersed for 20 minutes in the same fixative at room temperature. Slices were transferred and washed in the same buffer solutions for 15 minutes, cut into smaller pieces (1 mm³) and refixed in cold 1% OsO_4 buffered with phosphate at pH 7.4 plus 0.33 M sucrose plus 0.04 g % CaCl_2 . Blocks dehydrated through ethyl alcohol and propylene oxide were embedded in Epon (Luft). Thin sections were obtained on a Huxley or Porter-Blum ultramicrotome with glass knives and examined in a Siemens Elmiskop I after uranyl acetate and lead citrate stain (Reynolds). One micron sections stained with PAS and with toluidine blue-borax were studied with the light microscope.

The water content of testes dissected from 50 animals was determined in a control group and in a group killed 120 minutes after injection by comparison of

wet weight of recently dissected testes and dry weight of the same testes after 3 days in a 100°C oven. Milliequivalents of sodium and potassium were also determined in the same testes by the technique of flame photometry in a Hilger spectrophotometer.⁵

RESULTS

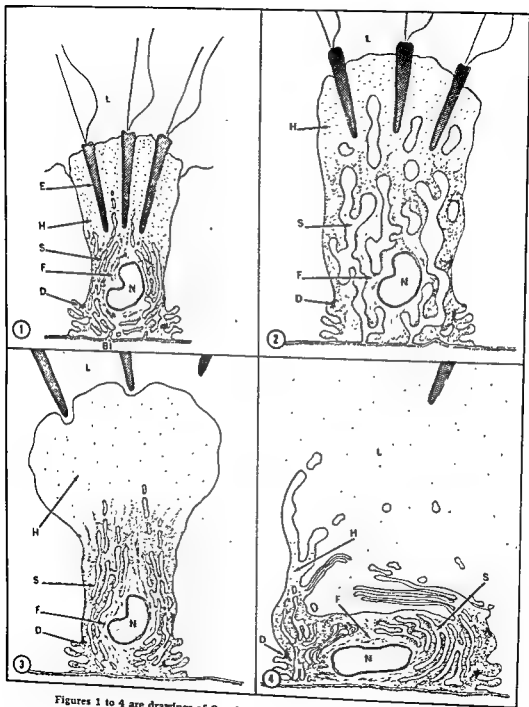
Three familiar images from light microscopy are presented in figures 10, 11 and 12 to summarize the mechanism of spermiation under gonadotrophin stimulation (LH). The control Sertoli cell shows a closely packed cluster of spermatozoa deeply embedded in its apical cytoplasm in very close proximity to the nucleus (fig. 10). At the beginning of the effect of LH injection, the cytoplasm is paler, the cluster appears less closely packed and farther removed from the nucleus of the Sertoli cell (fig. 11). Finally, the Sertoli cell still attached to the basement membrane and partially vacuolated, shows a loss of part of its apical cytoplasm concurrently with the release of spermatozoa (fig. 12).

Control Sertoli cell

In electron micrographs (fig. 7, 9) cell limits are clearly resolved and the contact surfaces between sustentacular cells (Sertoli cells) show desmosomes and frequent interdigitations, especially in their basal portion. A clearly defined basement membrane is found at the interface between Sertoli cells and the surrounding connective tissue. The seminiferous tubules often show basement membrane material extending into infoldings or pliations of the basal surface of the sustentacular cells (fig. 8). The cytoplasm at the apical portion of the columnar supporting cells contains the late spermatids and spermatozoa. These germ cells occupy deep recesses in the irregular luminal surface of the Sertoli cells. The contact surface between Sertoli cells and germ cells is smooth and lacks desmosomes.

⁴ Ovine LH, lot NIH-LH-S-1, was kindly supplied by the Endocrinological Study Section of the National Institutes of Health.

⁵ Sodium and potassium determinations have been made by Dr. R. I. Stancioni and Dr. J. C. Romero from the Department of Physiology. This collaboration is gratefully acknowledged.



Figures 1 to 4 are drawings of Sertoli cells which summarize the different stages of the release of spermatozoa.

TABLE 1
Toad testis water content

	Total body weight	Testis wet weight	Testis dry weight	Water content
	$P < 0.3$	$P < 0.005$	$P < 0.07$	$P < 0.07$
Control	45.2 ± 0.45	73.7 ± 0.10	10.0 ± 0.13	63.7
Experimental	46.1 ± 0.50	117.0 ± 0.12	11.3 ± 0.26	105.7

This table shows the different water content of the testis of normal and L.H. treated toads.

of the order of 63.7 mg increases after gonadotrophin stimulation in 2 hours to 105.7 mg. The total increase expressed as the difference between both mean values is 42.0 mg. We can also express these values as percent of testicular dry weight. The control animals have 63.7 mg per 100 mg of testicular dry weight, the experimental ones 94.1 mg per 100 mg, the total increase in water being 30.4 mg per 100 mg dry weight.

Sodium milliequivalents per cent of dry weight (fig. 6) also increases from 46 in the control to 64 in the experimental testes. Potassium appears to move in the opposite direction to a less significant degree, from 40 meq % to 37 meq % of dry weight.

DISCUSSION

The observations presented in this paper constitute the first demonstration at the level of the electron microscope of the mechanism of sperm release in the toad. The injection of LH in the male toad evokes spermiation as well as ovulation in the female. The term spermiation introduced by van Oordt ('46), as the counterpart of ovulation, is widely accepted by workers in reproduction. The immediate effect of LH in the male toad

is mainly on the cytoplasm of the Sertoli cell where the hormone produces several changes beginning with marked swelling of the cytoplasm, unfolding of the apical recesses and finally release of spermatozoa.

In the spermiation produced by experimental hormonal treatment, three main stages have been recognized. In the first stage, the hormone produces an increase in the area occupied by the smooth endoplasmic reticulum (ER). It is likely that the swelling of the ER is a consequence of, or an adaptation to, the increase in water content in the cells. At this stage an important increment in water and sodium content of the testes was found. These results are in agreement with the observations of Astrada and Taleisnik ('57) that the water penetrates testes, which have been immersed in saline, against a concentration gradient. The striking elaboration of channels and cytoplasmic membranes may be related to a mechanism of active transport whereby the water and sodium are pumped into the cell.

In the second stage, the apical cytoplasm of the Sertoli cell becomes swollen concomitant with the collapse of the ER. We interpreted this change as a result of

Fig. 1 In the heterogeneous cytoplasm of the control Sertoli cell are shown: the endoplasmic reticulum (S); the apical cytoplasm (H) and the bundles of fibrils (F). The sperm heads occupying deep apical recesses (E). Basal infoldings are present (BI). Desmosomes are found connecting adjacent Sertoli cells (D). Nucleus (N). Lumen (L).

Fig. 2 Stage of swelling of the endoplasmic reticulum. The cell becomes taller and more columnar. Spermatozoa are pushed away from the nuclear zone. Basal infoldings become wider, shorter and then disappear.

Fig. 3 Stage of swelling of the apical cytoplasm. A progressive unfolding of the apical recesses which contain the spermatozoa, pushes the spermatozoa farther toward the tubular lumen. At the same time the endoplasmic reticulum collapses.

Fig. 4 Stage of the apical detachment. The apical cytoplasm disintegrates and spermatozoa, fluid and cellular debris pass into the lumen. The loss of this zone leaves the rest of the cytoplasm, protected only by the apposition of membranes.

the passage of water from the lumen of the ER into the ground substance of the apical cytoplasm. Mancini and Burgos ('47) and van Dongen ('60) postulated that the main cause of spermiation is an enzymatic splitting of a mucoprotein. The present observations would lead us to assume that this hypothetic enzymatic mechanism takes place in the apical cytoplasm at this second stage. It is well known after de Duve ('61) that the lysosomes contain all the acid hydrolases present in the cell; the lysosomes are found in the Sertoli cells but they are rarely seen after the first stage of spermiation. These lysosomes may be the source of the above postulated mucolytic enzyme. The swelling of the apical cytoplasm is presumed to be causally related to the unfolding of the apical invaginations and consequent discharge of the spermatozoa. The swollen cytoplasm may also contribute a certain amount of liquid to the lumen thus serving to increase the intratubular pressure, to open the efferent ducts and to carry forward the content of the tubules.

The preservation of the nucleated basal portion of the Sertoli cell after the third stage of apical detachment, is an interesting example of how a cell is protected from being completely evacuated into the lumen in the course of apocrine secretion. Probably a similar mechanism of protective overlapping of membranes may happen in other cells suffering a partial elimination of the cytoplasm in apocrine secretion.

This study has also shown that LH is able to move water and sodium into the toad testis; the Sertoli cells are the main target of LH action, and probably the recipients of a large part of the sodium and water increase. The effect of LH is similar to the effect of human chorionic gonadotrophin (HCG) injected into the toad. As HCG is able to evoke spermiation "in vitro," from isolated portions of the toad testis (Burgos and Mancini, '47), we believe that LH acts directly upon the toad testis and not by way of any other endocrine mediator.

LITERATURE CITED

- Astrada, J. J., and S. Taleisnik 1957 Inhibición y espermatoliberación del testículo de sapo por soluciones salinas o hipofísicas. *Rev. Soc. argent. Biol.*, 33: 340-346.
- Burgos, M. H., and D. W. Fawcett 1956 An electron microscope study of spermatid differentiation in the toad *Bufo arenarum* Hensel. *J. Biophys. Biochem. Cytol.*, 2: 223-240.
- Burgos, M. H., and R. E. Mancini 1947 Expulsión de espermatozoides por acción de las gonadotrofinas en el testículo de sapo "in vitro." *Rev. Soc. argent. Biol.*, 23: 165-175.
- de Duve, C. 1963 The lysosomes concept. In: *Lysosomes* Ciba Foundation Symposium, Ed. Churchill, London.
- De Robertis, E. D. P., M. H. Burgos and E. Breyer 1945 Acción de la hipófisis sobre la célula de Sertoli y el proceso de expulsión de los espermatozoides en los anfibios. *Rev. Soc. argent. Biol.*, 4: 21-25.
- 1946 Action of anterior Pituitary on Sertoli cells and on the release of toad spermatozoa. *Proc. Soc. Exper. Biol.*, N. Y., 61: 20-22.
- Galli Mainini, C. 1947 Reacción diagnóstica de erobarazo en la que se usa el sapo macho como animal reactivo. *La Semana Médica*, 54: 337-340.
- Houssay, B. A. 1954 Hormonal regulation of the sexual function of the male toad. *Acta Physiol. Latinoamer.*, 4: 1-41.
- Luft, J. M. 1961 Improvements in epoxy resin embedding methods. *J. Biophys. Biochem. Cytol.*, 9: 409-414.
- Mancini, R. E., and M. H. Burgos 1948 Mucopolisacáridos en la espermatogénesis del sapo. *Rev. Soc. argent. Biol.*, 24: 318-327.
- Millonig, G. 1962 Further observations on a phosphate buffer for osmium solutions. VI. Int. Congress for Electron Microscopy, Philadelphia, Academic Press, ed., p. 8.
- Reynolds, E. S. 1963 The use of lead citrate at high pH as an electron opaque stain in electron microscopy. *J. Cell Biol.*, 17: 208-212.
- van Dongen, W. J. 1958 The function of polysaccharides in the spermiation of *Rana temporaria*. *Acta Physiol. Pharm. Neerl.*, 7: 535-536.
- 1962 Spermiation in *Rana temporaria*. In: G. J. van Oordt, his contributions to science. G. W. van der Wiel and Co., Arnhem. The Netherlands.
- van Dongen, W. J., R. E. Ballieux, H. J. Ceursew and T. Offermans 1960 Spermiation in the common frog (*Rana temporaria*). III. Histochemical and chemical investigations. *Proc. Kon. Ned. Akad. Wetensch. Amsterdam (c)*, 63: 257-263.
- van Oordt, G. J., AM. Th. Beenackers, P. G. W. J. van Oordt and A. M. Stadhouder 1954 On the mechanism of the initial stages of spermiation in the Grass Frog, *Rana temporaria*. *Acta Endocrinol.*, 17: 294-300.
- van Oordt, G. T., and H. Klomp 1946 Effects of oestrone and gonadotrophin administration in the male toad (*Bufo bufo*). *Proc. Kon. Ned. Akad. Wetensch. Amsterdam*, 49: 565-570.

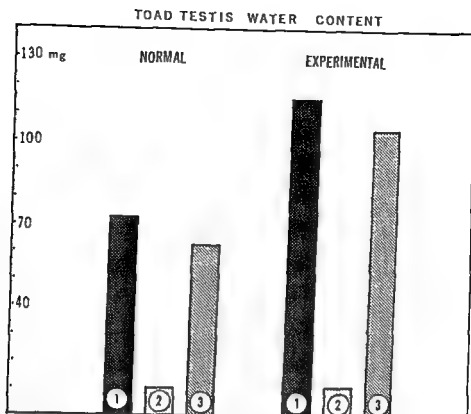


Fig. 5 Changes in water content. Column 1 represents the total weight of both control and experimental testes. Column 2 represents the dry weight and column 3 is the difference between 1 and 2 which corresponds to the water content.

TOAD TESTIS SODIUM AND POTASSIUM CONTENT

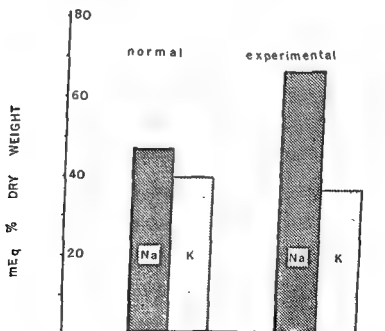


Fig. 6 Total sodium content increases 18 milliequivalents per cent of testicular dry weight after LH treatment. Potassium decreases to a less significant degree.

SPERMATION IN THE TOAD
M. H. Burgos and R. Vitale-Calpe

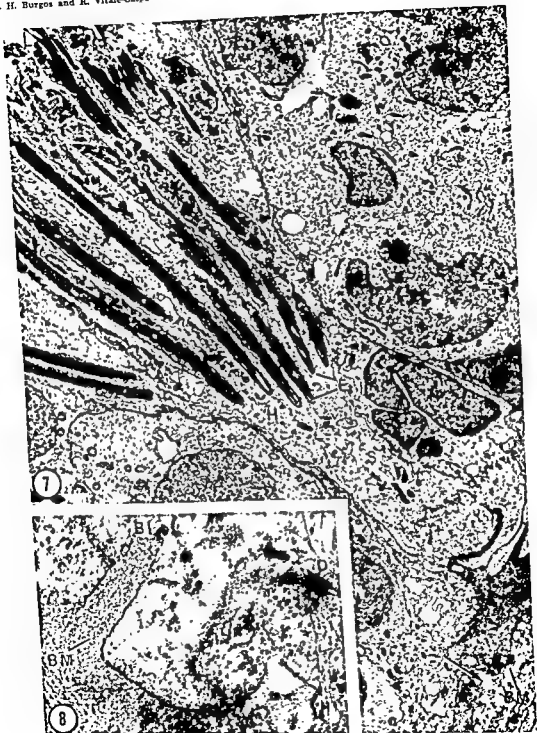


PLATE I

EXPLANATION OF FIGURES

Figures 7 to 9 correspond to electron micrographs of the normal toad testis stained with the combined lead-uranyl stain.

- 7 A survey view of the control Sertoli cell, showing a closely packed cluster of spermatozoa (E); the apical cytoplasm containing embedded spermatozoa (II); the region of the endoplasmic reticulum (S); the basal membrane (BM); the lumen (L) and the arrow that points to a basal infolding. 4,000 \times .
- 8 Higher magnification of the basal region with a basal infolding (BI), desmosome (D) and the basement membrane (BM). 30,000 \times .



PLATE 2

EXPLANATION OF FIGURE

- 9 Portion of the cytoplasm of two Sertoli cells. Late spermatid E_1 and spermatozoa E_2 appear embedded in the apical cytoplasm. Irregular nucleus (N) of scalloped outline. Three zones are recognized in the cytoplasm; bundles of fibrils (F), apical cytoplasm (H) and endoplasmic reticulum (S). 25,000 \times .



PLATE 3

EXPLANATION OF FIGURES

Figures 10, 11, 12 present the light microscopic appearance of $1\ \mu$ sections of portions of Epon embedded toad testis stained with toluidine blue-borax. 1,300 \times .

- 10 Control Sertoli cell (SC) with a closely packed cluster of spermatozoa near the nucleus (E).
- 11 Experimental Sertoli cell (SC) at the beginning of the effect of LH injection. The cluster of spermatozoa appears less closely packed and more distant from the nucleus of the Sertoli cell. The cell increases in length and becomes paler and vacuolated.
- 12 Experimental Sertoli cell (SC) at the end of the LH effect. Loss of the apical cytoplasm of the Sertoli cell and release of spermatozoa into the lumen (L).

Figures 13 to 21 are electron micrographs of the LH treated toad testes, stained with the combined lead-uranyl stain.

- 13 Portions of the cytoplasm of 3 Sertoli cells at the beginning of the effect of LH. Increase in the number and diameter of the channels, lacunae (La) and vacuoles of the endoplasmic reticulum (S). The upper cytoplasm contains spermatozoa; the middle one shows two sections of the same nucleus, the bundles of fibrils (F), mitochondria (M), lysosomes (Ly) and the endoplasmic reticulum (S). Arrow points to a basal invagination at the basement membrane. $\times 12,500$.

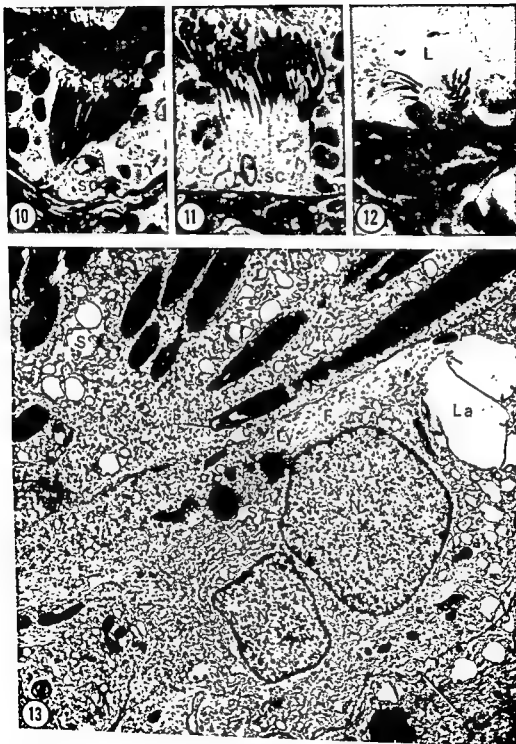


PLATE 3

EXPLANATION OF FIGURES

Figures 10, 11, 12 present the light microscopic appearance of $1\ \mu$ sections of portions of Epon embedded toad testis stained with toluidine blue-borax. $1,300\times$.

- 10 Control Sertoli cell (SC) with a closely packed cluster of spermatozoa near the nucleus (E).
- 11 Experimental Sertoli cell (SC) at the beginning of the effect of LH injection. The cluster of spermatozoa appears less closely packed and more distant from the nucleus of the Sertoli cell. The cell increases in length and becomes paler and vacuolated.
- 12 Experimental Sertoli cell (SC) at the end of the LH effect. Loss of the apical cytoplasm of the Sertoli cell and release of spermatozoa into the lumen (L).

Figures 13 to 21 are electron micrographs of the LH treated toad testes, stained with the combined lead-uranyl stain.

- 13 Portions of the cytoplasm of 3 Sertoli cells at the beginning of the effect of LH. Increase in the number and diameter of the channels, lacunae (La) and vacuoles of the endoplasmic reticulum (S). The upper cytoplasm contains spermatozoa; the middle one shows two sections of the same nucleus, the bundles of fibrils (F), mitochondria (M), lysosomes (Ly) and the endoplasmic reticulum (S). Arrow points to a basal invagination at the basement membrane. $\times 12,500$.



PLATE 4

EXPLANATION OF FIGURE

- 14 Basal portion of a Sertoli cell stimulated by LH during the stage of endoplasmic reticulum swelling. The channels of the endoplasmic reticulum (S) widely open show communications with the extracellular compartment (arrow). Mitochondria (M) with dense matrix and open intracristal space. Dense particles (P) scattered in the cytoplasm. Basement membrane (BM) and lamina propria (LP).
× 62,000.



PLATE 5

EXPLANATION OF FIGURE

- 15 Apical portion of an LII stimulated Sertoli cell, showing the widely dilated cisternae, channels and vacuoles during the stage of swelling of the endoplasmic reticulum (S). In the upper right corner is a portion of the head of a spermatozoon (E) and the intercellular space limited by the cell membranes of both (IS), spermatozoa and Sertoli cell. The star indicates the light filamentous component of the apical cytoplasm. Arrow points to the opening of a channel into a cisterna. $\times 62,000$.

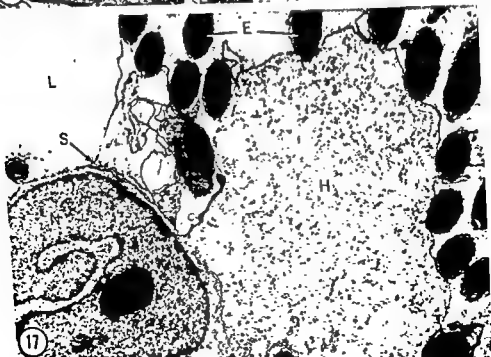
SPERMATION IN THE TOAD
M. H. Burgos and R. Vitale-Calpe

PLATE 6

EXPLANATION OF FIGURES

- 16 Portions of the cytoplasm of 3 Sertoli cells, the middle one in stage of swelling of the apical cytoplasm shows cross and oblique sections of sperm heads (E). Between the nucleus (N) and (H) the apical cytoplasm, are stacks of collapsed channels and cisternae of the endoplasmic reticulum (arrow). Lumen (L). $\times 12,500$.
- 17 Stimulated Sertoli cell during the stage of swelling of the apical cytoplasm. The unfoldings of the apical recesses form a cupola-like projection and pushes the spermatozoa (E) further into the lumen (L). Between the nucleus and the apical cytoplasm (H) few parallel arrays of membranes of the endoplasmic reticulum are shown (S). $\times 12,500$.



PLATE 7

EXPLANATION OF FIGURE

- 18 Portion of a Sertoli cell, during the last stage of apical detachment. The disorganized apical cytoplasm shows many irregular cytoplasmic blebs (CB) formed at expenses of the swollen apical cytoplasm, dense particles and some channels of the endoplasmic reticulum. In the remaining part of the cytoplasm, the nucleus (N) is surrounded by mitochondria (M) and three lacunar spaces (La) related to the channels (arrow). $\times 60,000$.



PLATE 8

EXPLANATION OF FIGURES

- 19 Persisting portion of a Sertoli cell at the end of the stage of apical detachment. Two large lacunae (La) and collapsed channels contribute to the overlapping of membranes (arrow) near the lumen (L). Close to the irregular nucleus (N) the cytoplasm shows many irregular channels and vacuoles, a Golgi complex (GC), dense mitochondria (M), few fibrils (F) and a desmosome (D). $\times 31,000$.
- 20 Stage of the apical detachment. Overlapping of membranes (arrow). The lumen (L) contains cellular debris and spermatozoa. Mitochondria (M). $\times 37,000$.

SPERMATION IN THE TOAD
M. H. Burgos and R. Vitale-Calpe

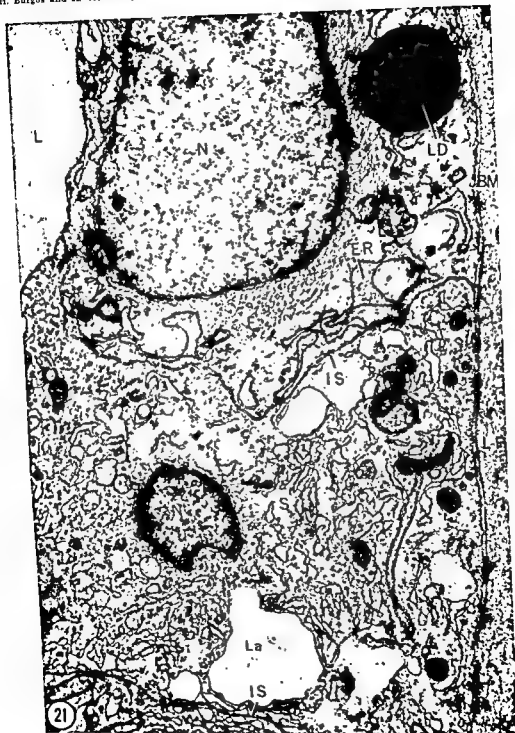


PLATE 9

EXPLANATION OF FIGURE

- 21 Part of the cytoplasm of three Sertoli cells after the release of spermatozoa and elimination of the apical cytoplasm. The bundles of fibrils surround a pale and swollen nucleus (N). Typical channels of rough endoplasmic reticulum contain a filamentous (Er) material of low electron density. Large lacunae (La) and channels of the endoplasmic reticulum (S) surround a small portion of another nucleus (N). Two intercellular spaces (IS), a lipid droplet (LD), dense mitochondria (M) and the basement membrane without infoldings. Lamina propria (LP). $\times 25,000$.

SPERMATION IN THE TOAD
M. H. Burgos and R. Vitale-Calpe



An Experimental Study of Microscopic and Submicroscopic Lipid Inclusions in Hepatic Cells of the Mouse¹

HAROLD F. PARKS

Professor of Anatomy, University of Kentucky Medical Center,
Lexington, Kentucky

ABSTRACT Lipid spherules of microscopic (1- μ) and submicroscopic (300-1000 Å) dimensions were studied by electron microscopy in livers of mice that were normally fed, fasted, refed, or fed fat-free or high-fat diets. Tissues were fixed by perfusion with osmium and post-osmicated at 37°C.

Submicroscopic inclusions were present in Golgi complex, endoplasmic reticulum, cytoplasmic vesicles near space of Disse, and in the space itself. The lipid of these inclusions was sufficiently unsaturated to be fixed and rendered insoluble by post-osmication in all animals save those that were fed a diet rich in saturated fat or a fat-free high-carbohydrate diet (which induces synthesis of saturated fatty acids); in animals fed the two latter diets, the central mass of the inclusions escaped fixation and was dissolved during dehydration and imbedding. The inclusions were thus shown to reflect the character of the fatty acids most freely available in the cytoplasm of the hepatic cell in a given physiological state. On the basis of morphological and biochemical considerations, the submicroscopic inclusions were identified as secretion antecedents, elaborated by the liver for export to the blood.

The larger lipid inclusions, which did not dramatically reflect changes in the degree of saturation of fatty acids available in the liver cell, were concluded to represent a more stable storage pool of hepatic-cell neutral lipid.

In addition to the relatively large (1- μ) lipid droplets of hepatic cells that have been known to cytologists for several decades, membrane-enclosed osmophilic spherules or granules of diameters usually in the range 300-1000 Å have been observed in electron-microscopic studies of normal livers of mice (Parks, '56, '62; Caesar, '61; and Daems, '61), rats (Fawcett, '55; Rouiller, '56; Watson, '58; Caesar, '61; and Reynolds, '63, '65), guinea pigs (Caesar, '61), and hamsters (Chandra, '63). The small granules have also figured with varying prominence in reports of experimental studies involving (1) ethanol treatment (Hartoft and Porta, '64; Ashworth et al., '65), (2) orotic acid-induced hypolipemia (Novikoff et al., '64), (3) carbon tetrachloride intoxication (Ashworth et al., '63; Reynolds, '63; and Smuckler, et al., '62), (4) ethionine intoxication (Baglio and Farber, '65), (5) cerium poisoning (Magnusson, '63), (6) phosphorus poisoning (Jézéquel, '58), (7) effects of administration of the carcinogen dimethylnitrosamine (Emmelot and Benedetti, '60; Mukherjee et al., '63), (8)

ischemia (Bassi and Bernelli-Zazzero, '64), (9) the breathing of pure oxygen (Schaffner and Felig, '65), (10) leukemia (DeHarven and Friend, '58), (11) starvation (Parks, '60, '62), (12) the feeding of fat (Ashworth et al., '60, '61, '65; Parks, '62), and (13) sequelae of partial hepatectomy (Jordan, '64; Trotter, '64, '65). The nature and physiological significance of these granules have not been fully established. Many of the authors named above have considered them to be lipid on the basis of their appearance, fixation properties, increase in numbers in fat-feeding experiments, etc. As for the physiological significance of the granules, their frequently observed presence in the perisinusoidal space of Disse (as well as in hepatic cells) has suggested to some authors the interpretation that they are extruded by the hepatic cell into the blood plasma; to other authors it has suggested that the granules are engulfed by the hepatic cell from the blood plasma.

¹Supported by National Science Foundation grant GD-3030.

The present paper correlates the nature of the membrane-enclosed osmiophilic granules with the dietary intake of the animal. It describes the granules in relation to starvation and refeeding and in relation to other experimental conditions involving the feeding of high-fat or fat-free high-carbohydrate diets. It furnishes additional evidence of the lipid character of the osmiophilic granules by demonstrating that they exhibit a state of saturation comparable to that of the fatty acids entering the liver from the blood plasma. It further indicates that when fatty acids are not freely available to the liver from the blood, the granules can be synthesized from non-lipid precursors. Finally it provides evidence that the lipid granules are discharged into the space of Disse and are therefore to be regarded as secretion antecedents, probably beta lipoproteins. The larger lipid droplets in the hepatic cell are shown to represent a more stable pool of lipid whose character is less dramatically affected by changes in the character of fatty acids entering the liver.

MATERIAL AND METHODS

This report is based on the study of hepatic tissue from a total of 142 young male and female CFW mice that were in various nutritional states at the time of death. All of the animals had free access to drinking water at all times. Twelve animals representing a "normal" nutritional state were maintained on Purina Laboratory Chow until the time of sacrifice. The experimental mice were also given Purina Laboratory Chow from the day of weaning until experimental treatment was begun.

Thirty-one mice were fasted from 1 to 5 days before hepatic tissue was taken for examination. Eight others were fasted four days and re-fed at two, three and a half, or eight hours before death.

The remaining animals all received special diets. Usually they were weaned at 21 days of age and fed a "normal" diet for one or two weeks before being given special diet.

Forty-eight animals were given a "fat-free test diet" (Nutritional Biochemicals Corp., Cleveland, Ohio) containing 58% sucrose as carbohydrate for 4-9 days. Seventeen animals were fed the "fat-free

test diet" for a period of 6 to 9 days and subsequently starved 24-48 hours before death.

The high-fat diets used consisted of 75-90% "fat-free test diet" and 25-10% fat. Sixteen animals were fed for 3 to 8 days on a high-fat diet in which the (25%) fat component was a hydrogenated (and therefore largely saturated) vegetable oil ("Hydrol 100," Durkee Famous Foods, Cleveland, Ohio). A diet rich in unsaturated fats (10-25% corn oil) was given to ten animals for a period of 3 to 5 days before death.

The livers of the majority of animals used were fixed by perfusion with Palade's ('52) veronal-acetate buffered osmium tetroxide solution containing 0.22 M sucrose (cf. Caulfield, '57). Laparotomy was performed on supine animals during deep anesthesia produced by intraperitoneal injection of 0.4-0.5 ml of 12% urethane, and the hepatic portal vein exposed by gently lifting the intestines on the right side of the body and displacing them to the left. After a curved no. 30 needle which was attached to a 1-ml tuberculin syringe was inserted into the portal vein, the abdominal aorta and vena cava were severed with scissors and 1 ml of fixative solution injected during a period of approximately one minute. Small pieces of liver were subsequently placed in cold (4°C) fixative for 1 to 4 hours. After dehydration in ethyl alcohol, the blocks were imbedded in butyl methacrylate by polymerizing for 36 hours at 58-60°C in the presence of 1% benzoyl peroxide. Silver sections were cut with glass knives on a Porter-Blum microtome, mounted on carbon coated grids, stained with lead- or barium hydroxide (Watson, '58), "sandwiched" with carbon (cf. Watson, '57), and examined with a Siemens Elmiskop I at 60 KV. The majority of exposures were taken at magnifications of 10,000 to 15,000.

Early in the study a tendency was noted for the centers of lipid inclusions to be dissolved during dehydration and imbedding procedures, thus leaving a shell or "rim" of lipid in the sections. In an attempt to correct this tendency by insuring maximal osmication of triglyceride inclusions, tissues from the majority of animals were post-osmicated overnight at

37°C in 2% osmium tetroxide solution. This procedure, while tending to remove glycogen from the sections, successfully preserved all lipid inclusions except those consisting predominantly of saturated fat.

OBSERVATIONS

Background or reference description of osmiophilic spherules in liver cells of the normally fed mouse. Two morphologically distinguishable types of osmiophilic inclusions which will here be described as lipid spherules are seen on ultrastructural examination of the hepatic cell of the CFW mouse.

One type of inclusion lies free in the ground cytoplasm; i.e., is not enclosed within a membrane. It is relatively large, being of the order of 1 μ in diameter. It is microscopically visible, can be stained in frozen sections with oil-soluble dyes, dissolves in fat solvents, and is therefore demonstrably fatty in nature. It is the writer's experience that, in electron-microscopic preparations of mouse liver fixed 1 to 2 hours in cold 1% osmic acid solution and imbedded in methacrylate, the centers of these inclusions often dissolve, leaving a peripheral shell of fat surrounding an empty space (cf. figs. 9, 10). However, post-osmication at 37°C for 24 hours fixes the entire inclusion, rendering it insoluble in alcohol and methacrylate. The electron density imparted to the fat by osmium tetroxide appears to be enhanced by staining with barium hydroxide (cf. Watson, '58).

The lipid inclusions constituting the second type are smaller, most falling in the diameter range of 300-1000 Å, and are separated from the ground cytoplasm by a membrane. They occur singly, being sparsely distributed in the granular and agranular endoplasmic reticulum (figs. 1, 2, 5), or in groups of varying sizes. The membrane-enclosed groups or clusters often occur as swollen cisternae of the Golgi apparatus (cf. figs. 1, 4, 5). Since the latter organelle usually lies near the bile canaliculus, the majority of small lipid granules tend to be concentrated in this vicinity. Despite this suggestive proximity, however, the writer has never seen an indication that the lipid granules are discharged into the bile channel. On the other

hand, granules of the same type are also to be seen as membrane-enclosed clusters ("bags" of granules) at or near the edges of the cell bordering on the perisinusoidal space of Disse, and as free individuals in the space itself (cf. figs. 6, 8). In some instances, the membrane of the cytoplasmic vesicle containing the granules exhibits a continuity with the plasma membrane of the cell (cf. figs. 7, 8). Profiles showing this relationship reveal a continuity of the "lumen" of the (intracellular) vesicle with the (extracellular) perisinusoidal space which makes possible a movement of granules between the two spaces. It is therefore obvious that the granules do move from one compartment to the other. The direction in which such granules move must be interpreted tentatively for obvious reasons; however, the fact that the granules tend to be tightly packed in the intracytoplasmic inclusions and in various states of dispersion in the extracellular space argues that they are extruded from, rather than ingested by, the cell — it would appear that the Brownian movement to which they would be subject would tend to make them move from a higher concentration toward a lower one.

In addition to the "bags" of granules, individual membrane-enclosed granules are also occasionally seen near, or with membrane showing a continuity with, the plasma membrane bordering the space of Disse. Morphological study of this type of inclusion in sections of course gives no clue as to whether the lipid granule in question was moving into, or out from, the cell at the time of fixation.

The small membrane-enclosed lipid granules in routinely fixed liver exhibit varying degrees of density. Some are dark (cf. fig. 5); some relatively light (cf. fig. 4); and some darkened so slightly by osmic acid that their outlines are difficult to distinguish (cf. fig. 1). In many cases they have relatively light centers with darker peripheries. The observation that they tend to be darker near the outer edge of a section than in more centrally located parts indicated that longer treatment with osmic acid might improve fixation and visualization; and it was found that when fixation was extended to include

overnight treatment with 2% osmic acid at 37°C, the lipid granules were more intensely darkened (fig. 2).

Results of starvation. Both the large fat droplets and the small membrane-enclosed lipid granules of the starving animal, although changed in numbers, exhibited the same distribution and the fixation-and-staining characteristics as those of their counterparts in the normally-fed animal. An earlier light-microscopic study (Parks, '58) had shown that the relatively large lipid droplets of hepatic cells increase greatly in number in animals starved 12 hours or longer, and that mitochondria tend to apply themselves in cap-like fashion to the surfaces of the fat droplets. In the present electron-microscopic study varying degrees of intimacy between fat and mitochondria were observed (figs. 9, 10).

In the majority of cases, mitochondria that had not changed their normal shape appeared to be touching a neighboring fat droplet with a relatively small part of their surface. In many instances, though, mitochondria developed concavities that made possible a greater area of intimate relationship with a adjacent fat droplets. In these areas of close relationship, a thin layer of ground cytoplasm or some smooth endoplasmic reticulum was often interposed between mitochondrion and fat, but broad areas of contact were also frequently seen. The fatty liver characteristic of starvation persisted until the animal's depot fat was exhausted or until it was refed.

A distinct impression was gained that the small, membrane-enclosed lipid granules of hepatic cells also increased in number during starvation. They were seen in greater numbers in the endoplasmic reticulum, and while in many cases the Golgi complexes appeared not to contain more granules than those of the well-fed animal, some were conspicuously laden with granules. In the liver of one animal that had been starved 24 hours all or most of the Golgi bodies seen contained a very large number of granules. The largest of these Golgi complexes contained 55 profiles of rounded membranous vesicles in one section, 18 of which exhibited ten or more granules within the profile. A part of this

organelle is seen in figure 5. Small lipid granules were also plentiful in cytoplasmic vesicles bordering on or opening into the space of Disse, in the space of Disse, and in passage between the two compartments.

Because of their great variability in size it is not possible to state whether the membrane-enclosed granules in the fasting animal were generally larger than those of the well-fed; however, two unusually large ones were seen in the Golgi (peribiliary) region of hepatic cells in animals starved 24 hours. Each appeared to be the sole occupant of its membranous envelope; they were 0.3 and 0.6 μ in diameter respectively. A third granule 0.4 μ in diameter was seen in company with several small ones in the space of Disse in another animal that had been starved 24 hours.

In animals starved for prolonged periods, the small lipid granules were to be found in Golgi complex, endoplasmic reticulum, cytoplasm near space of Disse, and in space of Disse as long as the fatty-liver condition (i.e., profusion of large fat inclusions) characteristic of starvation was maintained. After the animal had exhausted its available depot fat and its liver ceased to be fatty, small lipid granules were also absent from the hepatic cells. Golgi bodies, usually the richest repositories of such granules, were reduced to small stacks of flattened, empty cisternae accompanied by typical small spherical Golgi vesicles (fig. 11).

Since both the large and the small lipid spherules of hepatic cells increased in number during starvation, it was natural to suspect the possibility that one form of inclusion might be the precursor of the other. In no case, however, was a profile seen which could be interpreted to suggest that small granules fuse together (losing their membranes) to form large ones, or that small granules lose their membranes and fuse with larger spherules, thus increasing the size of the latter inclusions.

Starvation and refeeding. The most conspicuous change seen in the livers of animals starved four days and refed 2 to 8 hours before death was the rapid reappearance of glycogen. This material was present in some cells at two hours and had become very plentiful in all cells by eight hours. No remarkable changes in the amount of intracellular lipid were seen to

take place during these early hours after refeeding; however, the livers of two animals (at 2 hours and at 3½ hours after refeeding) were seen to contain an unusual form of membrane-enclosed lipid granules. These granules occurred as localized groups of individually-enclosed spherules 700–4000 Å in diameter. Their centers had been dissolved out, leaving a peripheral shell of fat surrounding an empty space (fig. 3). Since the tissues in question had not been post-osmicated, this appearance was thought to be due to incomplete fixation.

Results of feeding saturated fats. The large (1-μ) fat spherules in the livers of all animals given a diet containing 25% "Hydrol 100" exhibited two markedly different degrees of solubility in alcohol and methacrylate following postosmication. Some of the fat droplets were fully fixed, darkened, and rendered insoluble by the fixative. The others had resisted fixation and were largely dissolved during dehydration and imbedding procedures, leaving a residue that appeared in section as a thin but dense outer shell surrounding a central area which was empty or contained a sparse lacework of low-density osmophilic material. Formations of smooth endoplasmic reticulum were closely applied to a large part of the surface of most of these "soluble" lipid droplets (fig. 13). In the majority of animals that were fed a diet high in saturated fat, the "soluble" lipid droplets in hepatic cells were considerably more plentiful than insoluble ones. In view of the fact that osmium tetroxide does not fix-and-blacken saturated fats, the "soluble" lipid droplets were interpreted to consist largely of saturated fat.

The small membrane-enclosed lipid granules in liver cells of animals fed a high saturated fat diet were abundantly present both as individuals in the endoplasmic reticulum and as membrane-enclosed clusters in Golgi complex and in the cytoplasm bordering the space of Disse. Their character varied with the weight-gaining history of the animal eating the diet: the majority of animals lost weight initially and slowly gained it back, eventually exceeding their initial weight by a small margin. In the liver of these ani-

mals the membrane-enclosed granules were unusually small (200–400 Å in diameter) and consisted of a relatively dense outer layer surrounding a low-density or optically empty central part (fig. 12). One group of four animals gained well, however, increasing their body weight 15–30% in six days. Although the small membrane-enclosed granules in their hepatic cells had the same basic structure and distribution as those of the animals that did not gain weight well, they were considerably larger and their centers more obviously dissolved out (fig. 14). Failure of the central parts of these granules to be fixed and rendered insoluble by post-osmication was taken to mean that the granules consisted largely of saturated fat. No granules were recognized in the space of Disse although continuities between cytoplasmic vesicles and plasma membrane were seen. It is probable that the outer shells of granules lying free in the blood plasma, and thus deprived of the support of a cytoplasmic membranous enclosure, were too fragile to remain intact when their triglyceride centers were dissolved.

Results of feeding unsaturated fat. The large lipid spherules in the hepatic cells of mice fed a diet containing 10–25% corn oil were totally fixed and rendered insoluble by osmic acid. Some of these spherules were closely invested by formations of smooth endoplasmic reticulum (fig. 16), thus paralleling a relationship observed in livers of animals fed diets high in saturated fat (fig. 13). This relationship was not seen with the same frequency, however, as in animals fed saturated fat.

The small membrane-enclosed granules were conspicuous, not only as membrane-bound individuals (fig. 15) and clusters (fig. 16) in cells, but also in the space of Disse. In addition, a few granules were seen between the two membranous layers of the nuclear envelopes in some cells. All of the small lipid granules of these animals exhibited a high, uniform density in sections stained with barium hydroxide.

Results of feeding a fat-free high-carbohydrate diet. Most of the animals receiving this diet gained weight steadily after an initial loss in weight that was restored during the first two or three days. A large proportion of the large fat spher-

overnight treatment with 2% osmic acid at 37°C, the lipid granules were more intensely darkened (fig. 2).

Results of starvation. Both the large fat droplets and the small membrane-enclosed lipid granules of the starving animal, although changed in numbers, exhibited the same distribution and the fixation-and-staining characteristics as those of their counterparts in the normally-fed animal. An earlier light-microscopic study (Parks, '58) had shown that the relatively large lipid droplets of hepatic cells increase greatly in number in animals starved 12 hours or longer, and that mitochondria tend to apply themselves in caplike fashion to the surfaces of the fat droplets. In the present electron-microscopic study varying degrees of intimacy between fat and mitochondria were observed (figs. 9, 10).

In the majority of cases, mitochondria that had not changed their normal shape appeared to be touching a neighboring fat droplet with a relatively small part of their surface. In many instances, though, mitochondria developed concavities that made possible a greater area of intimate relationship with an adjacent fat droplets. In these areas of close relationship, a thin layer of ground cytoplasm or some smooth endoplasmic reticulum was often interposed between mitochondrion and fat, but broad areas of contact were also frequently seen. The fatty liver characteristic of starvation persisted until the animal's depot fat was exhausted or until it was refed.

A distinct impression was gained that the small, membrane-enclosed lipid granules of hepatic cells also increased in number during starvation. They were seen in greater numbers in the endoplasmic reticulum, and while in many cases the Golgi complexes appeared not to contain more granules than those of the well-fed animal, some were conspicuously laden with granules. In the liver of one animal that had been starved 24 hours all or most of the Golgi bodies seen contained a very large number of granules. The largest of these Golgi complexes contained 55 profiles of rounded membranous vesicles in one section, 18 of which exhibited ten or more granules within the profile. A part of this

organelle is seen in figure 5. Small lipid granules were also plentiful in cytoplasmic vesicles bordering on or opening into the space of Disse, in the space of Disse, and in passage between the two compartments.

Because of their great variability in size it is not possible to state whether the membrane-enclosed granules in the fasting animal were generally larger than those of the well-fed; however, two unusually large ones were seen in the Golgi (peribiliary) region of hepatic cells in animals starved 24 hours. Each appeared to be the sole occupant of its membranous envelope; they were 0.3 and 0.6 μ in diameter respectively. A third granule 0.4 μ in diameter was seen in company with several small ones in the space of Disse in another animal that had been starved 24 hours.

In animals starved for prolonged periods, the small lipid granules were to be found in Golgi complex, endoplasmic reticulum, cytoplasm near space of Disse, and in space of Disse as long as the fatty-liver condition (i.e., profusion of large fat inclusions) characteristic of starvation was maintained. After the animal had exhausted its available depot fat and its liver ceased to be fatty, small lipid granules were also absent from the hepatic cells. Golgi bodies, usually the richest repositories of such granules, were reduced to small stacks of flattened, empty cisternae accompanied by typical small spherical Golgi vesicles (fig. 11).

Since both the large and the small lipid spherules of hepatic cells increased in number during starvation, it was natural to suspect the possibility that one form of inclusion might be the precursor of the other. In no case, however, was a profile seen which could be interpreted to suggest that small granules fuse together (losing their membranes) to form large ones, or that small granules lose their membranes and fuse with larger spherules, thus increasing the size of the latter inclusions.

Starvation and refeeding. The most conspicuous change seen in the livers of animals starved four days and refed 2 to 8 hours before death was the rapid reappearance of glycogen. This material was present in some cells at two hours and had become very plentiful in all cells by eight hours. No remarkable changes in the amount of intracellular lipid were seen in

reflect to some extent that of the fatty acids entering the liver in a given set of circumstances, advantage has been taken of the fact that the degree to which osmium tetroxide combines with a fatty substance depends on the number of double bonds present in the constituent fatty acids (Wigglesworth, '57; Riemersma and Booi, '62; Stoeckenius, '62a,b). Thus, a fat inclusion rich in unsaturated fatty acids is fixed, densified, and rendered insoluble by osmium fixation while a relatively saturated fat inclusion may resist fixation to the extent that it is dissolved by dehydrating and imbedding media.

Liver of the normally fed animal. Two morphological types of osmiophilic spherule are distinguishable in hepatic cells of the normally fed mouse. This observation is in harmony with the inference of Maling et al. ('62) and Stein and Shapiro ('60) that two or more pools of triglyceride are present in the liver and the observation of Havel et al. ('62) and other authors that fractionated liver cell preparations contain triglyceride associated with membranous fractions as well as in "floating" fat droplets. As stated above, the large inclusions are readily identifiable as lipid by reason of their affinity for oil-soluble dyes. The fatty nature of the membrane-enclosed granule has been inferred by many authors including Emmelot and Benedetti ('60) who found that only the outer shell of the granule was rendered insoluble in acetone by potassium permanganate fixation.

The physiological significance of the lipid inclusions in liver cells can not be deduced from morphological observations on the livers of normally fed animals. Profiles showing groups of the membrane-enclosed type in passage between liver cell and space of Disse suggest an extrusion phenomenon in which the granules represent lipoprotein particles being secreted into the blood. However, a firm conclusion to this effect would not be fully warranted in view of conflicting biochemical and morphological interpretations bearing on the subject. Biochemical evidence presented by Dole and Hamlin ('62), Robinson ('64), and Rodbell et al. ('64) and electron microscopic observations (Ashworth et al., '60; Parks, '62) have been interpreted as indicating that triglyceride

particles were taken up bodily by hepatic cells. Fawcett ('64), however, has pointed out that the interpretations based on morphological observation are of doubtful validity, being "subject to the possible interpretation that the [membrane-enclosed] lipids [within hepatic cells] were hydrolyzed before passage across the cell membrane and that triglycerides were reconstituted within the cell cytoplasm." Also, a biochemical study of chylomicron uptake by isolated liver cells has indicated that hydrolysis of chylomicron fat takes place at the cell surface (Green and Webb, '64), and the authors question the validity of data indicating that unhydrolyzed triglycerides actually enter liver cells. The difficulty of deciding, on morphological grounds, the direction of movement of small lipid granules between liver cell and space of Disse is illustrated by the following divergence of interpretation: the granules have been considered as secretion antecedents explicitly by Parks ('56), Jezéquel ('58), Chandra ('63), and Ashworth et al. ('56) and implicitly by Baglio and Farber ('65). They have been regarded as lipid particles phagocytosed by the cell by Ashworth et al. ('60, '61, and '65), Caesar ('61), Parks ('62), Jordan ('64), and Trotter ('65). The question is not made easier by the observation of Heimberg et al. ('62) that both uptake and release of triglyceride by the liver appear to take place simultaneously.

Data presented by Allman and Gibson ('65) indicate that the liver of the normally fed mouse contains a greater proportion of saturated fatty acids (and a correspondingly smaller proportion of unsaturated fatty acids) than is present in dietary fat. The probable explanation for this relationship is that hepatic lipogenesis, which accounts for some of the fatty acid content of the liver cell, favors the formation of saturated over unsaturated fatty acids (White et al., '64). The lipid spherules of the mouse livers studied were, in any event, rich enough in unsaturated fat to be appropriately fixed with osmic acid, especially if tissues were post-osmicated at 37°.

Liver in starvation. It is generally known from chemical (e.g., Hodge et al., '41) and light-microscopic studies (e.g.,

ules of hepatic cells appeared to be homogeneously fixed in post-osmicated tissues (fig. 18), indicating an appreciable content of unsaturated fat. The others exhibited a manifestation of incomplete fixation, however, by shrinking to a smaller diameter than that of the cytoplasmic space originally occupied by them. These inclusions appeared as central masses of darkened fat surrounded by a shrinkage space that was empty except for some irregular thread-like extensions from the central mass to the ambient cytoplasm. This characteristic artifact was interpreted as indicating that the inclusions in question contained a greater proportion of saturated fatty acids than corresponding inclusions in starving or normally-fed animals. Unlike those of the animals fed saturated fat, however, these lipid droplets were not surrounded by formations of endoplasmic reticulum.

The membrane-enclosed lipid granules in the livers of these mice resembled those of animals that had gained weight well on a diet rich in saturated fat, i.e., they appeared as "ghosts" consisting of a dense thin membrane surrounding an "empty" spherical center (figs. 17 to 20). Failure of the center to be preserved and darkened by osmic acid was taken to indicate that the center consisted mainly of saturated fat. These lipid granules, which were present in all livers examined, were especially abundant in animals that were gaining weight at a rapid rate (one-half gram or more per day) at the time of death. They were seen in large numbers in the Golgi cisternae and endoplasmic reticulum and as individuals and clusters in the cytoplasmic areas near perisinusoidal spaces. Although no granules ("ghosts") were identified in the perisinusoidal space, continuities of the investing membranes of clusters (fig. 20) as well as individual granules (fig. 19) with the plasma membrane of hepatic cells revealed that granules were passing between the intra- and extra-cellular spaces. As in the case of animals eating a high saturated fat diet, failure to recognize granules in the space of Disse could be explained in terms of the absence of a structural element to support the delicate outer shell of a granule after its lipid center was dissolved. For

reasons which are set forth in the discussion section of this paper, this relationship between membrane-enclosed granules and the perisinusoidal space is interpreted as a manifestation of secretory activity by the liver cell.

Results of fasting following a fat-free high-carbohydrate diet. The lipid inclusions in animals that were fasted for 24 or 48 hours after being fed fat-free high-carbohydrate diet were found to have the same distribution and fixation-and-staining characteristics as those of animals starving after cessation of a normal dietary intake; i.e., the inclusions were darkened and rendered insoluble by osmic acid fixation.

DISCUSSION

General considerations. It is known from a large volume of biochemical and physiological literature that the liver plays a major role in the fat metabolism of the body. It functions as the major site of degradation and synthesis of fatty acids while adipose tissue serves as the major site of storage (White et al., '64). In a continuous interchange of fat between adipose tissue and liver (the "triglyceride cycle" of Rees and Shotlander, '63), the liver functions as an important source of plasma triglyceride: fat depots release free fatty acids (FFA) into the blood plasma (cf. Williamson, '64); hepatic cells remove them from the blood, re-esterifying them as triglycerides and incorporating the triglycerides into lipoproteins, which are then secreted into the blood (e.g., Rohlf and Eder, '61; Robinson, '64) and thus returned to the adipose tissues (cf. Markscheid and Shafir, '65). In addition to these and many other functions in fat metabolism, the liver figures prominently in the processing of dietary fat, removing it from the blood plasma (Robinson, '64), and secreting a portion as lipoprotein after re-esterification of its fatty acids (Dole and Hamlin, '62).

The present study, which was undertaken as a search for morphological correlates of some of the liver's known functions in the metabolism of fat, has relied in part on a behavioral characteristic of osmic acid. In view of the expectation that the state of saturation of the neutral lipid inclusions of the hepatic cell should

mainder presumably being metabolized or stored. Morphological findings on fat-fed animals were consistent with the implications of these considerations.

Feeding of saturated fat to mice produced changes in the character of many of the large lipid droplets and all of the small membrane-enclosed particles, the alteration being in the direction of increased saturation. These changes were not unexpected since the affected livers were in effect flooded with relatively highly saturated fatty acids. The small lipid granules presumably consisted very largely of saturated fat, with only the most peripheral layer containing enough double bonds and/or protein to be fixed and densified by osmium. The large droplets whose lipid content was relatively saturated were also apparently derived largely from dietary fatty acids since hepatic lipogenesis (which favors production of saturated fatty acids) is depressed by fat feeding (Bortz et al., '63). The fact that all droplets were not uniformly affected suggests that all fat droplets in a cell are not equally active metabolically. The observation that the saturated fat droplets were frequently invested with formations of endoplasmic reticulum suggests that that organelle may have functioned in some capacity in the deposition or removal of fat. An esterifying action of liver microsomes has been found in the chicken (Weiss et al., '60) but not in the rat (Senior and Isselbacher, '62). The latter authors did find, however, that rat liver microsomes actively cleaved monoglyceride to glycerine and fatty acid.

The livers of animals fed large quantities of unsaturated fats contained solidly-fixed and densified inclusions corresponding to all intracellular structures that were identified as lipid inclusions in animals eating saturated fat. In addition, small lipid granules were found in the space of Disse as well as in membranous vesicles in hepatic-cell cytoplasm bordering the space, thus indicating that passage of lipid granules between cellular and extracellular compartments takes place in fat-fed animals although extracellular granules were not demonstrated in animals fed saturated fat. Some of the large lipid droplets were invested with endoplasmic reticulum

formations, once again indicating that in livers which are flooded with fatty acids, the endoplasmic reticulum functions in the transfer of fatty material to or from the droplets.

The fixation characteristics of the small membrane-enclosed granules in fat-fed animals tend to support the conclusion of other authors that the granules are fatty in nature; it also indicates that the fat in the granules is derived from the fatty acids that are most freely available to the liver cell in a given set of physiological conditions. However, these observations do not contribute in a major way to the question of whether the granules are secretion antecedents or ingested particles.

Livers of animals fed fat-free diet. A high-carbohydrate, fat-free diet is known to inhibit release of FFA from depots (Jeanrenaud, '61) and increase lipogenesis in the liver (Bortz et al., '63). In the mouse liver it produces a marked increase in the activity of enzymes catalyzing the synthesis of long-chain, saturated fatty acids (Allman and Gibson, '65) and causes concurrent depletion of linoleic (18:2) acid. In a condition characterized by absence of fatty acids from dietary sources, reduced inflow of fatty acids from fat depots, depleted stores of dienoic fatty acid, and increased *de novo* synthesis of saturated fatty acids, all recently formed hepatic triglyceride inclusions could be expected to manifest their relatively saturated state by a low affinity for osmium. The present study has shown that in the livers of animals fed a fat-free diet, the centers of all of the small lipid granules escaped fixation and some of the large lipid droplets were incompletely fixed.

The fact that all of the large lipid droplets contained a large enough proportion of unsaturated fatty acids to be partially or totally fixed indicates that these inclusions are storage deposits with a slower metabolic turnover than the small granules, or that oxidatively desaturated (see White et al., '64) or other available unsaturated fatty acids are preferentially located in the large droplets. The absence of membranous formations of endoplasmic reticulum in relation to these droplets suggests that endoplasmic reticulum is not involved in the deposition of fat in these inclusions; the

Parks, '58) that the mouse, as well as numerous other species (Feigenbaum and Fisher, '63), develops a fatty liver during starvation. The present study reveals that the increase in lipid content is reflected by increases in number of both the submicroscopic membrane-bound lipid inclusions and the larger, microscopically visible lipid spherules. This finding indicates that both types of lipid inclusion are derived largely if not entirely from mobilized depot fat in the starving animal, since starvation favors release of free fatty acids (FFA) from depots (Jeanrenaud, '61; Mead, '63) and inhibits hepatic lipogenesis (Bortz et al., '63; Masoro et al., '62).

The larger lipid spherules could conceivably be formed directly by intracytoplasmic esterification of FFA entering the liver cell from the blood, or by loss-of-membranes-and-fusion of the smaller lipid granules. Since no indications of the latter possibility were seen, it appears that the former process accounts for their formation. The large droplets apparently represent storage deposits of fatty acids destined to be oxidized or, possibly, de-esterified and re-incorporated into different structures. The tendency for mitochondria to develop close physical relationships with fat droplets during starvation, which was first pointed out by Palade and Schidlowsky ('58) and Parks ('58), is most probably related to the fact that oxidation of fat is carried out principally by mitochondria (Wakil, '62).

The mode of formation and metabolic significance of the small membrane-enclosed lipid granules can not be interpreted with complete confidence from observations on starving animals. Since lipogenesis is inhibited in starvation, the granules must derive mainly from blood-borne FFA or represent triglyceride particles ingested bodily from the blood. Ashworth et al. ('65) regard the membrane-enclosed granules of the fasting liver as beta lipoproteins elaborated by the liver, largely on the grounds that they obviously could not represent chylomicrons derived from intestinal absorption of dietary fat. Although this interpretation is probably correct, at least for the majority of granules, account should be taken of Baxter's ('66) observation that some circulating triglyceride par-

ticles in the blood of the rat derive neither from dietary fat nor hepatic lipoprotein secretion, but are elaborated by the gut. The fatty acids of these particles in the rat (Baxter, '66) contained a concentration of double bonds comparable with that of liver triglyceride in the normally fed mouse or rat (Nelson, '62); the particles could therefore reasonably be expected to be preserved and densified by osmium fixation. Thus, the possibility should be recognized that low-density lipoprotein particles of non-hepatic provenience could conceivably be ingested by hepatic cells in the starving animal and appear in them as membrane-enclosed granules.

At any rate the small lipid granules were frequently seen in passage between hepatic-cell cytoplasm and space of Disse in the present study. Since the liver is the chief source of plasma triglyceride in the fasting animal (Robinson, '64), it appears likely that electron-micrograph profiles showing granules passing from one compartment to another represent manifestations of the extrusion of beta lipoprotein particles into the blood plasma.

Liver of starved-and-refed animals. Two starved-and-refed animals showed membrane-enclosed fat inclusions with "empty" centers in the early hours after refeeding. In view of the small number of animals studied, this observation can not be taken to represent an established phenomenon; it would not have been considered worth recording without more extensive experimentation had not Hartoft and Porta ('64) reported similar inclusions in hepatic cells of rats in the early hours after alcohol administration. Hartoft and Porta's ('64) "hollow rims of lipid ... surrounded by a single membrane" became solid by eight hours following treatment. Possibly a similar change took place in refed animals; no hollow lipid inclusions were noticed at eight hours after refeeding. The basis for the hollow centers of these inclusions is not understood.

Liver of fat-fed animals. Absorbed dietary fatty acids enter the blood stream as triglycerides in chylomicra, some 40% of which are taken up by the liver (Robinson, '64). A proportion of these fatty acids are released into the blood again in low-density lipoproteins (Robinson, '64), the re-

mainder presumably being metabolized or stored. Morphological findings on fat-fed animals were consistent with the implications of these considerations.

Feeding of saturated fat to mice produced changes in the character of many of the large lipid droplets and all of the small membrane-enclosed particles, the alteration being in the direction of increased saturation. These changes were not unexpected since the affected livers were in effect flooded with relatively highly saturated fatty acids. The small lipid granules presumably consisted very largely of saturated fat, with only the most peripheral layer containing enough double bonds and/or protein to be fixed and densified by osmium. The large droplets whose lipid content was relatively saturated were also apparently derived largely from dietary fatty acids since hepatic lipogenesis (which favors production of saturated fatty acids) is depressed by fat feeding (Bortz et al., '63). The fact that all droplets were not uniformly affected suggests that all fat droplets in a cell are not equally active metabolically. The observation that the saturated fat droplets were frequently invested with formations of endoplasmic reticulum suggests that that organelle may have functioned in some capacity in the deposition or removal of fat. An esterifying action of liver microsomes has been found in the chicken (Weiss et al., '60) but not in the rat (Senior and Isselbacher, '62). The latter authors did find, however, that rat liver microsomes actively cleaved monoglyceride to glycerine and fatty acid.

The livers of animals fed large quantities of unsaturated fats contained solidly-fixed and densified inclusions corresponding to all intracellular structures that were identified as lipid inclusions in animals eating saturated fat. In addition, small lipid granules were found in the space of Disse as well as in membranous vesicles in hepatic-cell cytoplasm bordering the space, thus indicating that passage of lipid granules between cellular and extracellular compartments takes place in fat-fed animals although extracellular granules were not demonstrated in animals fed saturated fat. Some of the large lipid droplets were invested with endoplasmic reticulum

formations, once again indicating that in livers which are flooded with fatty acids, the endoplasmic reticulum functions in the transfer of fatty material to or from the droplets.

The fixation characteristics of the small membrane-enclosed granules in fat-fed animals tend to support the conclusion of other authors that the granules are fatty in nature; it also indicates that the fat in the granules is derived from the fatty acids that are most freely available to the liver cell in a given set of physiological conditions. However, these observations do not contribute in a major way to the question of whether the granules are secretion antecedents or ingested particles.

Livers of animals fed fat-free diet. A high-carbohydrate, fat-free diet is known to inhibit release of FFA from depots (Jeanrenaud, '61) and increase lipogenesis in the liver (Bortz et al., '63). In the mouse liver it produces a marked increase in the activity of enzymes catalyzing the synthesis of long-chain, saturated fatty acids (Allman and Gibson, '65) and causes concurrent depletion of linoleic (18:2) acid. In a condition characterized by absence of fatty acids from dietary sources, reduced inflow of fatty acids from fat depots, depleted stores of dienoic fatty acid, and increased *de novo* synthesis of saturated fatty acids, all recently formed hepatic triglyceride inclusions could be expected to manifest their relatively saturated state by a low affinity for osmium. The present study has shown that in the livers of animals fed a fat-free diet, the centers of all of the small lipid granules escaped fixation and some of the large lipid droplets were incompletely fixed.

The fact that all of the large lipid droplets contained a large enough proportion of unsaturated fatty acids to be partially or totally fixed indicates that these inclusions are storage deposits with a slower metabolic turnover than the small granules, or that oxidatively desaturated (see White et al., '64) or other available unsaturated fatty acids are preferentially located in the large droplets. The absence of membranous formations of endoplasmic reticulum in relation to these droplets suggests that endoplasmic reticulum is not involved in the deposition of fat in these inclusions; the

droplets may be presumed to have been growing, since the diet being administered is known to cause the development of a fatty liver in mice (Allman and Gibson, '65).

The small membrane-enclosed lipid granules in animals fed a fat-free high-carbohydrate diet appeared to consist of a central mass of relatively saturated fat surrounded by a thin shell of osmiophilic material probably representing a surfactant layer of phospholipids and possibly an investment of protein (Dole and Hamlin, '62). The interpretation that the center is saturated fat is supported by the facts that (1) granules of this description are found in livers that are known to be synthesizing saturated fatty acids (Allman and Gibson, '65) and (2) they resemble corresponding inclusions in livers that are being flooded with saturated fatty acids. These granules are of special interest in this study as they bear on the question of whether membrane-enclosed lipid granules represent ingested particles or secretion antecedents. They appear *not* to represent ingested particles: (1) no dietary triglyceride enters the blood from the gut of the animal on fat-free diet; (2) depot fat mobilization is currently believed to involve exclusively the release of free fatty acids and not the release of particulate fat (Shapiro, '64) — if mobilized depot fat were to enter the space of Disse or the liver cell as triglyceride it would be solidly fixed by osmium and therefore recognizably different from the inclusions seen; and (3) endogenous low-density lipoprotein particles arising in the gut of animals on a fat-free diet, as described by Baxter ('66) would also contain enough double bonds to be solidly fixed by osmium. The granules *do* appear to represent secretion antecedents: (1) the liver is recognized as the chief source of circulating triglyceride derived from endogenous sources (see Havel et al., '62); (2) the granules exhibit size and structural characteristics suggesting that they are beta lipoprotein (cf. Casley-Smith, '62); and (3) electron micrographs demonstrate a morphological basis for transfer of small lipid granules between cellular and extracellular compartments, many of the profiles clearly sug-

gesting extrusion into the blood rather than ingestion into the cell (figs. 7, 8, 20).

Thus, in an experiment designed to drastically reduce the possibility of particulate fat entering the liver, the liver cells have continued to exhibit a large content of lipid granules and have continued to show manifestations of transfer of the granules between cells and blood plasma. Unless some large source of circulating endogenous particulate fat other than the liver can be identified, the membrane-enclosed granules must be recognized as secretion antecedents (beta lipoproteins) elaborated by the liver for export to the blood.

Starvation following administration of fat-free diet. This treatment produced a picture of hepatic cell lipid inclusions similar to that which accompanies starvation following a normal diet. Since in starvation the chief source of fatty acids available to the liver is depot fat, both types of lipid inclusion quickly assumed the degree of unsaturation characteristic of depot fat, and were well preserved by osmium.

Summary interpretation and discussion of lipid inclusions

The large lipid droplets of the hepatic cell appear to represent storage deposits whose fatty acids equilibrate relatively slowly with other intracellular fatty acids. Thus, when cells were in effect flooded with saturated fatty acids (from fat-feeding or from increased lipogenesis resulting from fat-free high-carbohydrate diet), the small membrane-enclosed lipid granules were strongly affected while only a part of the large droplets reflected the change. Also, since all large droplets were not equally affected, it is possible that all were not equally metabolically active. A special relation of lipid droplet to mitochondrion was seen during fasting; this physical intimacy is probably related to the role of the mitochondrion in the oxidation of fat. Another intimate relationship with agranular endoplasmic reticulum was seen in animals on a high-fat diet. The functional implications of this physical intimacy are not clearly evident at present.

The relationship between small membrane-enclosed granules and large droplets

is not clearly settled. Several authors (Trotter, '64; Ashworth et al., '65; Baglio and Farber, '65) report indications that the small inclusions fuse with the large ones. Mukherjee et al. ('63) indicate that, in cells damaged by dimethylnitrosamine, the small membrane-enclosed granules grow larger and lose their membranes. However, no electron micrographs clearly demonstrating fusion of small granules with large droplets have been published to the present writer's knowledge.

Observations on the small membrane-enclosed lipid granules in this study have pointed toward the conclusion that they are secretion antecedents elaborated by the hepatic cell for extrusion into the blood plasma. As such, their triglyceride content appears to be formed from fatty acids available in the ambient cytoplasm as a result of diffusion through the plasma membrane of FFA or of fatty acids derived from hydrolysis of particulate fat at the cell membrane, or from intracellular lipogenesis.*

There is reason to suspect that a coating of protein provided by the hepatic cell is necessary for the release of small granules into the blood. Substances that inhibit protein synthesis cause accumulation of the membrane-enclosed lipid granules in hepatic cells; e.g., ethionine (Baglio and Farber, '65), dimethylnitrosamine (Emmelot and Benedetti, '60; Mukherjee et al., '63; Rees and Shotlander, '63), and carbon tetrachloride (Smuckler et al., '62; Ashworth et al., '63; Reynolds, '63) which is also known to severely inhibit the release of triglyceride by liver (Meng, '64, p. 235). Orotic acid, which appears to depress lipoprotein synthesis without affecting other plasma proteins (see Meng, p. 230), also causes accumulation of small lipid granules in liver cells (Novikoff et al., '64). It is of course not clear whether these accumulations represent a back-up of secretion antecedents that can not be extruded because they are incomplete or abnormal, or a back-up of normal secretion antecedents which for some unknown reason can not be secreted. In any event, recovery from ethionine poisoning (Baglio and Farber, '65) and from fatty liver of acute phosphorus poisoning (Jézéquel, '58) appears to be accompanied by the appearance of fat granules in the space

of Disse, indicating a restoration of the ability to extrude lipid granules.

Partial hepatectomy or sham operation has been observed by Trotter ('65) to cause small lipid granules to become prominent in the liver cells and space of Disse of C₃H mice, the granules being most numerous in the perisinusoidal space during the period 10-120 minutes after operation. Trotter interprets this phenomenon as a phase in the entry of lipid granules into hepatic cells which is followed by incorporation of the small granules into the large fat droplets by fusion. An alternative explanation of the phenomenon is implicit in a number of observations (see Robinson, '64) to the effect that when labelled FFA are injected into the blood of a fasting rat with intact liver, labelled triglyceride in low-density serum lipoproteins can be detected within ten minutes following injection. The concentration of labelled triglycerides in the blood becomes maximal at 30 to 50 minutes, and then drops off. At the time of the peak concentration in the blood, considerable labelling is also detectable in hepatic-cell particulate fraction triglycerides. It therefore appears possible that relatively sustained (several minutes) mobilization of FFA by fat depots associated with the stress of operative procedure could result in entry of FFA into the liver cell, esterification to lipoprotein triglyceride, and subsequent extrusion into the space of Disse on a time schedule not unlike that described by Trotter. The phenomenon is worthy of further experimental analysis.

LITERATURE CITED

- Allmann, D., and D. Gibson 1965 Fatty acid synthesis during early linoleic acid deficiency in the mouse. *J. Lipid Research*, 6: 51-62.
 Ashworth, C. T., V. A. Stembridge and E. Sanders 1960 Lipid absorption, transport and hepatic assimilation studied with electron microscopy. *Am. J. Physiol.*, 198: 1326-1328.
 Ashworth, C. T., E. Sanders and N. Arnold 1961 Hepatic lipids; fine structural changes in liver cells after high-fat, high cholesterol, and choline-deficient diet. *A.M.A. Arch. Path.*, 72: 625-636.

* Morphologically, the formation of fat inclusions in liver cells could be said to parallel that of intestinal absorptive cells. Both cells form two kinds of inclusions from available precursors in the cytoplasm (see Strauss, '66): (1) larger droplets, which are not to be exported, lying free in the cytoplasm; and (2) smaller spherules, which are to be bodily extruded from the cell, enclosed within membranes.

- Ashworth, C., F. Luibel, E. Sanders and N. Arnold 1963 Hepatic Cell Degeneration. *A.M.A. Arch. Pathol.*, 75: 212-225.
- Ashworth, C. T., F. Wrightsman, B. Cooper and N. DiLuzio 1965 Cellular aspects of ethanol-induced fatty liver: a correlated ultrastructural and chemical study. *J. Lipid Research*, 6: 258-268.
- Baglio, C. M., and E. Farber 1965 Reversal by Adenine of the ethionine-induced lipid accumulation in the endoplasmic reticulum of the rat liver. A preliminary report. *J. Cell Biol.*, 27: 591-602.
- Bassi, M., and A. Bernelli-Zazzerio 1964 Ultrastructural cytoplasmic changes of liver cells after reversible and irreversible ischemia. *Exp. and Molec. Pathol.*, 3: 332-350.
- Baxter, J. H. 1966 Origin and characteristics of endogenous lipid in thoracic duct lymph in rat. *J. Lipid Research*, 7: 158-166.
- Bortz, W., S. Abraham and I. Chalkoff 1963 Localization of block in lipogenesis resulting from feeding fat. *J. Biol. Chem.*, 238: 1266-1272.
- Caesar, R. 1961 Elektronenmikroskopischer nachweis von fettpartikeln im disseschen raum. *Z. Zellforsch.*, 54: 793-802.
- Casley-Smith, J. R. 1962 The identification of chylomicra and lipoproteins in tissue sections and their passage into jejunal lacteals. *J. Cell. Biol.*, 15: 259-277.
- Caulfield, J. B. 1957 Effects of varying the vehicle of OsO₄ in tissue fixation. *J. Biophysic. and Biochem. Cytol.*, 3: 827-829.
- Chandra, S. 1963 Electron Microscopy of Hamster Liver. I. Morphology of Secretion. *J. Microscopie*, 2: 297-308.
- Daems, W. T. 1961 The micro-anatomy of the smallest biliary pathways in the mouse liver tissue. *Acta Anat.*, 46: 1-24.
- De Harven, E., and C. Friend 1958 Electron microscope study of a cell-free induced leukemia of the mouse. A preliminary report. *J. Biophysic. and Biochem. Cytol.*, 4: 151-155.
- Dole, V. P., and J. T. Hamlin 1962 Particulate fat in lymph and blood. *Physiol. Rev.*, 42: 674-701.
- Emmelot, P., and E. Benedetti 1960 Changes in the fine structure of rat liver cells brought about by dimethylnitrosamine. *J. Biophysic. Biochem. Cytol.*, 7: 393-396.
- Fawcett, D. W. 1955 Observations on the cytology and electron microscopy of hepatic cells. *J. Nat. Cancer Inst.*, 15: 1475-1502.
- 1964 Morphological consideration of lipid transport in the liver. In: *Proceedings of an International Symposium on Lipid Transport*, (Ed. by H. C. Meng) Charles C Thomas, Springfield, Illinois.
- Feigenbaum, A., and H. Fisher 1963 Changes in fatty acid composition in nutritional fatty degeneration of the liver. 1. Effect of starvation. *Brit. J. Nutrition*, 17: 31-37.
- Green, C., and J. Webb 1964 The uptake of chylomicron fatty acids by isolated liver cells. *Biochim. Biophys. Acta*, 84: 404-411.
- Hartroft, W., and E. Porta 1964 Ultrastructural hepatic changes in acute ethanol-treated rats. *Gastroenterology*, 46: 304-305.
- Havel, R., J. Felts and C. Van Duyne 1962 Formation and fate of endogenous triglycerides in blood plasma of rabbits. *J. Lipid Research*, 3: 297-308.
- Heimberg, M., I. Weinstein, H. Klausner and M. Watkins 1962 Release and uptake of triglycerides by isolated perfused rat liver. *Am. J. Physiol.*, 202: 353-358.
- Hodge, H. C., P. Mac Lachlan, W. Bloor, C. Stoneburg, M. Oleson and R. Whitehead 1941 Lipids of the fasting mouse. I. The relation between carcass lipids and liver lipids. *J. Biol. Chem.*, 139: 897-915.
- Jeanrenaud, B. 1961 Dynamic aspects of adipose tissue metabolism. *Metabolism*, 10: 535-581.
- Jezquel, A. M. 1958 Les effets de l'intoxication aiguë au phosphore sur le foie de rat. Etude au microscope électronique. *Ann. Anat. Pathol.*, 3: 512-537.
- Jordan, S. W. 1964 Electron microscopy of hepatic regeneration. *Exp. Mol. Pathol.*, 3: 183-200.
- Magnusson, G. 1963 The behavior of certain lanthanons in rats. *Acta Pharmacol. Toxicol. Suppl. no. 3*, 20: 1-95.
- Maling, H. M., A. Frank and M. C. Horning 1962 Effect of carbon tetrachloride on hepatic synthesis and release of triglycerides. *Biochim. Biophys. Acta*, 64: 540-545.
- Markscheide, L., and E. Schafritz 1965 Incorporation of lipoprotein-borne triglycerides by adipose tissue *in vitro*. *J. Lipid Research*, 6: 247-257.
- Masoro, E. J., E. Porter and H. Korchak 1962 Role of inhibitory mechanisms in physiological regulation of lipogenesis. *Am. J. Physiol.*, 202: 129-132.
- Meng, H. C. 1964 Proceedings of an International Symposium on Lipid Transport. Charles C Thomas, Springfield, Illinois.
- Mukherjee, T., R. Gustafsson, B. Afzelius and E. Arrhenius 1963 Effects of carcinogenic amines on amino acid incorporation by liver systems. II. Morphological and biochemical study on the effects of dimethylnitrosamine. *Cancer Res.*, 23: 944-953.
- Nelson, G. J. 1962 The lipid composition of normal mouse liver. *J. Lipid Res.*, 3: 256-262.
- Novikoff, A. B., P. S. Rohelm and N. Quintana 1964 Lipid in the liver cells of rats fed orotic acid and adenine. *Fed. Proc.*, 23: 126.
- Palade, G. E. 1952 A study of fixation for electron microscopy. *J. Exp. Med.*, 95: 285-297.
- Palade, G., and G. Schidlofsky 1958 Functional association of mitochondria and lipid inclusions. *Anat. Rec.*, 130: 352-353.
- Parks, H. F. 1956 The hepatic sinusoidal endothelial cell and its histological relationships. *Proc. Stockholm Conference on Electron Microscopy*, pp. 151-153.
- 1958 Observations on mitochondria in the fatty liver of the fasting mouse. *Anat. Rec.*, 130: 435-436.
- 1960 Electron microscopic study of hepatic cells of mouse during starvation and recovery following starvation. *Anat. Rec.*, 136: 255.

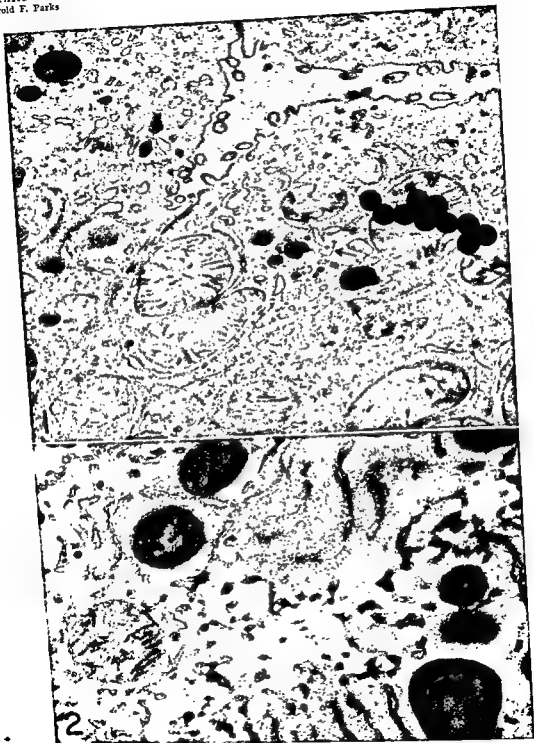
- 1962 On the uptake of chylomicrons by hepatic cells of mice. *Anat. Rec.*, 142: 320.
- Rees, K. R., and V. L. Shottlander 1963 Fat accumulation in acute liver injury. *Proc. Royal Soc. of London, Series B*, 157: 517-535.
- Reynolds, E. S. 1963 Liver Parenchymal Cell Injury. I. Initial alterations of the cell following poisoning with carbon tetrachloride. *J. Cell Biol.*, 19: 139-157.
- 1965 Liver Parenchymal Cell Injury. III. The nature of calcium-associated electron-opaque masses in rat liver mitochondria following poisoning with carbon tetrachloride. *J. Cell Biol.*, 25: 53-76.
- Riemersma, J., and H. Boel 1962 The reaction of osmium tetroxide with lecithin: application of staining procedures. *J. Histochem. Cytochem.*, 10: 89-95.
- Robinson, D. 1964 The uptake and release of lipids by the liver. In: *Proceedings of an International Symposium on Lipid Transport*. (H. Meng, Ed.) Charles C Thomas, Springfield, Illinois.
- Rodbell, M., O. Scow and S. Chernick 1964 Removal and metabolism of triglycerides by perfused liver. *J. Biol. Chem.*, 239: 385-391.
- Roheim, P. S., and H. A. Eder 1961 The formation of lipoproteins by the isolated perfused rat liver. *Circulation*, 24: 1101.
- Rouiller, C. 1956 Les Canalicules Biliaires. *Acta Anatomica*, 26: 94-109.
- Schaffner, F., and P. Felig 1965 Changes in hepatic structure in rats produced by breathing pure oxygen. *J. Cell Biol.*, 27: 505-518.
- Senior, J., and K. Isselbacher 1962 Direct esterification of monoglycerides with palmityl coenzyme A by intestinal epithelial subcellular fractions. *J. Biol. Chem.*, 237: 1454-1459.
- Shapiro, B. 1964 Enzymes in lipid transport. In: *Proceedings of an International Symposium on Lipid Transport*. (H. Meng, Ed.) Charles C Thomas, Springfield, Illinois.
- Smuckler, E. A., O. A. Iseri and E. P. Benditt 1962 An intracellular defect in protein synthesis induced by carbon tetrachloride. *J. Exp. Med.*, 116: 55-72.
- Stein, Y., and B. Shapiro 1960 Uptake and metabolism of triglycerides by the rat liver. *J. Lipid Res.*, 1: 326-331.
- Stoeckenius, W. 1962a Some electron microscopical observations on liquid-crystalline phases in lipid-water systems. *J. Cell Biol.*, 12: 221-229.
- 1962b The molecular structure of lipid-water systems and cell membrane models studied with the electron microscope. In: *The Interpretation of Ultrastructure*. (R. J. C. Harris, Ed.) Acad. Press, New York.
- Strauss, E. 1966 Electron microscopic study of intestinal fat absorption *in vitro* from mixed micelles containing linolenic acid, monolein, and bile salt. *J. Lipid Res.*, 7: 307-323.
- Trotter, N. 1964 A fine structure study of lipid in mouse liver regenerating after partial hepatectomy. *J. Cell Biol.*, 21: 233-244.
- 1965 Electron-opaque, lipid-containing bodies in mouse liver at early intervals after partial hepatectomy and sham operation. *J. Cell Biol.*, 25: 41-52.
- Wakil, S. J. 1962 Lipid Metabolism. *Ann. Rev. Biochem.*, 31: 369-406.
- Watson, M. L. 1957 Reduction of heating artifacts in thin sections examined in the electron microscope. *J. Biophysic. Biochem. Cytol.*, 3: 1017-1022.
- 1958 Staining of tissue sections for electron microscopy with heavy metals. II. Application of solutions containing lead and barium. *J. Biophysic. Biochem. Cytol.*, 4: 727-730.
- White, A., P. Handler and E. Smith 1964 *Principles of Biochemistry*, 3rd ed. Blakiston Div., McGraw-Hill, New York.
- Wigglesworth, V. B. 1957 The use of osmium in the fixation and staining of tissues. *Proc. Royal Soc. London, Series B*, 147: 185-199.
- Williamson, J. R. 1964 Adipose Tissue. Morphological changes associated with lipid mobilization. *J. Cell Biol.*, 20: 57-74.
- Weiss, S., E. Kennedy and J. Kiyasu 1960 The enzymatic synthesis of triglycerides. *J. Biol. Chem.*, 235: 40-44.

Note Added to Proof

The following relevant studies have been published or have otherwise come to the writer's attention since this manuscript was written:

- Hamilton, R. L., D. M. Regen, M. E. Gray, and V. S. LeQuire 1967 Lipid transport in liver. I. Electron microscopic identification of very low density lipoproteins in perfused rat liver. *Laboratory Investigation*, 17: February issue, in press.
- Jones, A. L., N. B. Huderman, and M. G. Herretz 1966 An electron microscopic study of lipoprotein production and release by the isolated perfused rat liver. *Proc. Soc. Exp. Biol. Med.*, 123: 4-9.
- Bruni, C., and K. R. Porter 1965 The fine structure of the parenchymal cell of the normal rat liver. *Am. J. Pathol.*, 46: 691-755.

- Ashworth, C., F. Luibel, E. Sanders and N. Arnold 1963 Hepatic Cell Degeneration. *A.M.A. Arch. Pathol.*, 75: 212-225.
- Ashworth, C. T., F. Wrightsman, B. Cooper and N. DiLuzio 1965 Cellular aspects of ethanol-induced fatty liver: a correlated ultrastructural and chemical study. *J. Lipid Research*, 6: 258-268.
- Baglio, C. M., and E. Farber 1965 Reversal by Adenine of the ethionine-induced lipid accumulation in the endoplasmic reticulum of the rat liver. A preliminary report. *J. Cell Biol.*, 27: 591-602.
- Bassi, M., and A. Bernelli-Zazzero 1964 Ultrastructural cytoplasmic changes of liver cells after reversible and irreversible ischemia. *Exp. and Molec. Pathol.*, 3: 332-350.
- Baxter, J. H. 1966 Origin and characteristics of endogenous lipid in thoracic duct lymph in rat. *J. Lipid Research*, 7: 158-166.
- Bortz, W., S. Abraham and I. Chaikoff 1963 Localization of block in lipogenesis resulting from feeding fat. *J. Biol. Chem.*, 238: 1266-1272.
- Caesar, R. 1961 Elektronenmikroskopischer nachweis von fettpartikeln im dissezierten raum. *Z. Zellforsch.*, 54: 793-802.
- Casley-Smith, J. R. 1962 The identification of chylomicra and lipoproteins in tissue sections and their passage into jejunal lacteals. *J. Cell. Biol.*, 15: 259-277.
- Caulfield, J. B. 1957 Effects of varying the vehicle of OsO_4 in tissue fixation. *J. Biophysic. and Biochem. Cytol.*, 3: 827-829.
- Chandra, S. 1963 Electron Microscopy of Hamster Liver. I. Morphology of Secretion. *J. Microscopie*, 2: 297-308.
- Daems, W. T. 1961 The micro-anatomy of the smallest biliary pathways in the mouse liver tissue. *Acta Anat.*, 46: 1-24.
- De Harven, E., and C. Friend 1958 Electron microscope study of a cell-free induced leukemia of the mouse. A preliminary report. *J. Biophysic. and Biochem. Cytol.*, 4: 151-155.
- Dole, V. P., and J. T. Hamlin 1962 Particulate fat in lymph and blood. *Physiol. Rev.*, 42: 674-701.
- Emmelot, P., and E. Benedetti 1960 Changes in the fine structure of rat liver cells brought about by dimethylnitrosamine. *J. Biophysic. Biochem. Cytol.*, 7: 393-396.
- Fawcett, D. W. 1955 Observations on the cytology and electron microscopy of hepatic cells. *J. Nat. Cancer Inst.*, 15: 1475-1502.
- 1964 Morphological consideration of lipid transport in the liver: In: *Proceedings of an International Symposium on Lipid Transport*, (Ed. by H. C. Meng) Charles C Thomas, Springfield, Illinois.
- Feigenbaum, A., and H. Fisher 1963 Changes in fatty acid composition in nutritional fatty degeneration of the liver. I. Effect of starvation. *Brit. J. Nutrition*, 17: 31-37.
- Green, C., and J. Webb 1964 The uptake of chylomicron fatty acids by isolated liver cells. *Biochim. Biophys. Acta*, 84: 404-411.
- Hartroft, W., and E. Porta 1964 Ultrastructural hepatic changes in acute ethanol-treated rats. *Gastroenterology*, 46: 304-305.
- Havel, R., J. Felts and C. Van Duyne 1962 Formation and fate of endogenous triglycerides in blood plasma of rabbits. *J. Lipid Research*, 3: 297-308.
- Heimberg, M., I. Weinstein, H. Klausner and M. Watkins 1962 Release and uptake of triglycerides by isolated perfused rat liver. *Am. J. Physiol.*, 202: 353-358.
- Hodge, H. C., P. Mac Lachlan, W. Bloor, C. Stoneburg, M. Oleson and R. Whitehead 1941 Lipids of the fasting mouse. I. The relation between carcass lipids and liver lipids. *J. Biol. Chem.*, 139: 897-915.
- Jeanrenaud, B. 1961 Dynamic aspects of adipose tissue metabolism. *Metabolism*, 10: 535-581.
- Jézéquel, A. M. 1958 Les effets de l'intoxication aiguë au phosphore sur le foie de rat. Etude au microscope électronique. *Ann. Anat. Pathol.*, 3: 512-537.
- Jordan, S. W. 1964 Electron microscopy of hepatic regeneration. *Exp. Mol. Pathol.*, 3: 183-200.
- Magnusson, G. 1963 The behavior of certain lanthanons in rats. *Acta Pharmacol. et Toxicol. Suppl. no. 3*, 20: 1-95.
- Maling, H. M., A. Frank and M. C. Horning 1962 Effect of carbon tetrachloride on hepatic synthesis and release of triglycerides. *Biochim. Biophys. Acta*, 64: 540-545.
- Markscheld, L., and E. Schafrir 1965 Incorporation of lipoprotein-borne triglycerides by adipose tissue *in vitro*. *J. Lipid Research*, 6: 247-257.
- Masoro, E. J., E. Porter and H. Korchak 1962 Role of inhibitory mechanisms in physiological regulation of lipogenesis. *Am. J. Physiol.*, 202: 129-132.
- Meng, H. C. 1964 *Proceedings of an International Symposium on Lipid Transport*. Charles C Thomas, Springfield, Illinois.
- Mukherjee, T., R. Gustafsson, B. Afzelius and E. Arrhenius 1963 Effects of carcinogenic amines on amino acid incorporation by liver systems. II. Morphological and biochemical study on the effects of dimethylnitrosamine. *Cancer Res.*, 23: 944-953.
- Nelson, G. J. 1962 The lipid composition of normal mouse liver. *J. Lipid Res.*, 3: 256-262.
- Novikoff, A. B., P. S. Roheim and N. Quintana 1964 Lipid in the liver cells of rats fed orotic acid and adenine. *Fed. Proc.*, 23: 126.
- Palade, G. E. 1952 A study of fixation for electron microscopy. *J. Exp. Med.*, 95: 285-297.
- Palade, G., and G. Schidlovsky 1958 Functional association of mitochondria and lipid inclusions. *Anat. Rec.*, 130: 352-353.
- Parks, H. F. 1956 The hepatic sinusoidal endothelial cell and its histological relationships. *Proc. Stockholm Conference on Electron Microscopy*, pp. 151-153.
- 1958 Observations on mitochondria in the fatty liver of the fasting mouse. *Anat. Rec.*, 130: 435-436.
- 1960 Electron microscopic study of hepatic cells of mouse during starvation and recovery following starvation. *Anat. Rec.*, 136: 255.

HEPATIC CELL LIPID INCLUSIONS OF MOUSE
Harold F. Parks

**Note: All illustrations are electron micrographs
of hepatic cells of CFW mice.**

PLATE 1

EXPLANATION OF FIGURES

- 1** Parts of three hepatic cells related to a bile canaliculus. Small lipid granules can be discerned in Golgi cisternae (upper left and lower center) and in the endoplasmic reticulum (arrows), but exhibit a low density presumably because of short exposure to fixative (one hour) and staining with lead hydroxide. The animal was starved 24 hours before sacrifice. $\times 22,000$.
- 2** Hepatic cell of a normally fed animal. The small lipid granules enclosed within the membranes of granular and agranular endoplasmic reticulum are much denser than those in figure 1 as a result of post-osmication overnight at 37°C . The section was stained with barium hydroxide. Glycogen is absent from the section, having been dissolved during the post-osmication. $\times 31,000$.

HEPATIC CELL LIPID INCLUSIONS OF MOUSE
Harold F. Parks

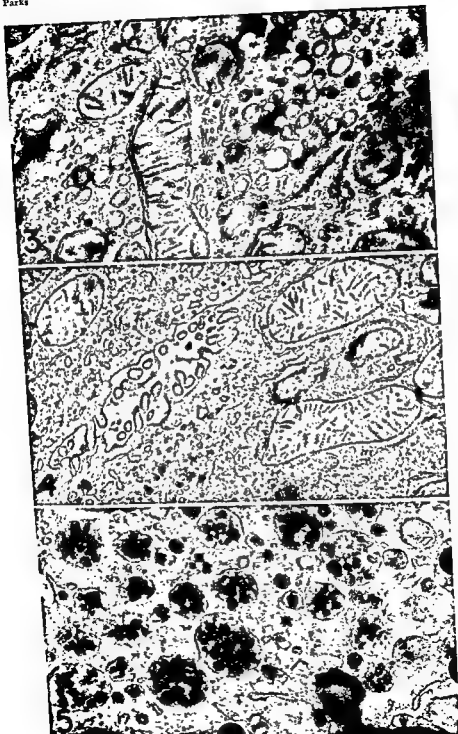


PLATE III

EXPLANATION OF FIGURES

- Membrane-enclosed lipid granules with centers dissolved out. The animal was fasted four days and refed two hours before hepatic tissue was removed and placed in cold fixative for approximately one hour. The section was stained with lead hydroxide, $\times 29,000$.
- 4 The micrograph shows a small Golgi complex above the bile canaliculus and a larger one below it. Both have rounded cisternae containing lipid granules. The animal was starved 24 hours. The tissue was fixed two hours in cold fixative and the section stained with lead hydroxide. $\times 24,000$.
- 5 Portion of a Golgi complex from liver of an animal that was fasted 24 hours. The large rounded cisternae contain numerous lipid granules which show no tendency to coalesce. Individual granules are also seen within small Golgi vesicles and in agranular (left side of picture) and granular (bottom) endoplasmic reticulum. A larger lipid spherule lying free in the cytoplasm is seen at the bottom right. A portion of another is below it. Fixation time in cold osmium tetroxide was two hours. The section was stained with barium hydroxide. $\times 32,000$.

HEPATIC CELL LIPID INCLUSIONS OF MOUSE

Harold F. Parks

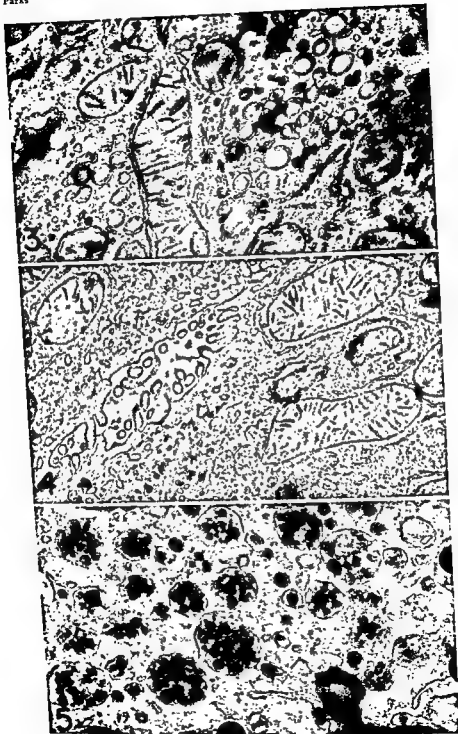


PLATE 3

EXPLANATION OF FIGURES

Note: These three figures show small lipid granules in the perisinusoidal space of Disse and/or the relationship of cytoplasmic "bags" of granules to the space. All were taken from liver following a 24-hour period of starvation. Tissues were fixed approximately two hours in cold fixative and sections stained with barium hydroxide.

- The micrograph shows part of an endothelial cell above, ■ hepatic cell below, and the space of Disse between them. In addition to a wisp of collagen (reticular fibril), numerous small lipid granules are seen in the space. One larger lipid droplet of the non-membrane-enclosed type and a part of another are seen in the hepatic cell. $\times 24,000$.
- 7 The lumen of a sinusoid is seen in the upper right. Between it and the space of Disse is a part of an endothelial cell, and a hepatic cell occupies the lower left part of the picture. A membranous vesicle enclosing a cluster of granules is prominent in the lower left center. Its membrane is continuous with the plasma membrane of the hepatic cell in such a way that the "lumen" of the vesicle is in communication with the perisinusoidal space through a constricted opening, thus providing a basis for the transfer of groups of granules between cellular and extracellular compartments. Colloidal mercuric sulfide particles are seen in a small vesicle in the endothelial cell in the upper left corner and on the surface of the endothelial cell. They were injected by caudal vein into a laparotomized animal 38 seconds before hepatic tissue was excised and fixed. $\times 32,000$.
- 8 Tangential section through space of Disse showing numerous small lipid granules. A vesicle containing a cluster of granules communicates via a constricted opening with the extracellular space near the upper right corner of the picture. A small portion of an endothelial cell is seen at the left side of the picture. $\times 22,000$.

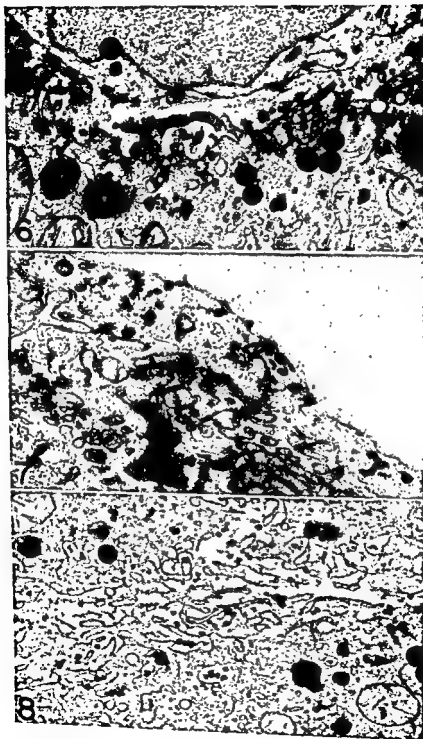


PLATE 4

EXPLANATION OF FIGURES

- 9-10 These micrographs each show a relatively large mitochondrion from the liver of a mouse that was starved for five days, but had not exhausted its depot fat reserves. Each illustration shows three degrees of intimacy between a mitochondrion and the fat droplets to which it is related: a part of the surface of each mitochondrion is in direct contact with a fat droplet; a part is separated from the neighboring fat droplet by a thin layer of ground cytoplasm; and a part has some smooth endoplasmic reticulum interposed between it and the fat droplet. The centers of the fat droplets have dissolved out as a result of incomplete fixation. The tissue was not post-osmicated. The section was stained with lead hydroxide. $\times 26,000$.
- 11 Two Golgi complexes (arrows) are shown in a hepatic cell from an animal that was starved five days and which had exhausted its depot fat. The Golgi cisternae are flattened and empty. A bile canaliculus is seen in the upper left. The tissue was fixed two hours in osmic acid and the section stained with lead hydroxide. $\times 18,000$.

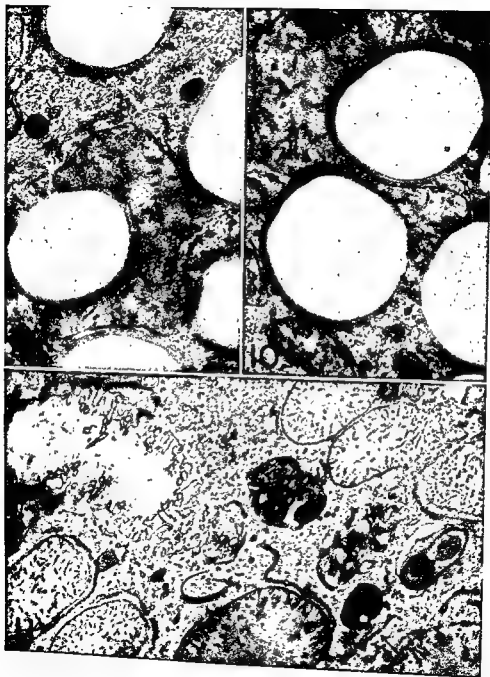


PLATE 5

EXPLANATION OF FIGURES

Note: Figures 12 through 20 are taken from tissues that were post-osmicated for 24 hours at 37°C. The normally present glycogen does not appear in the sections, having been dissolved out during post-osmication.

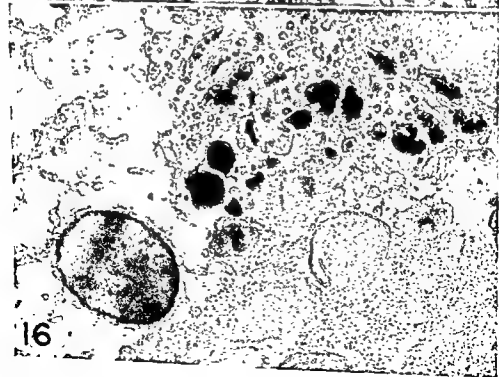
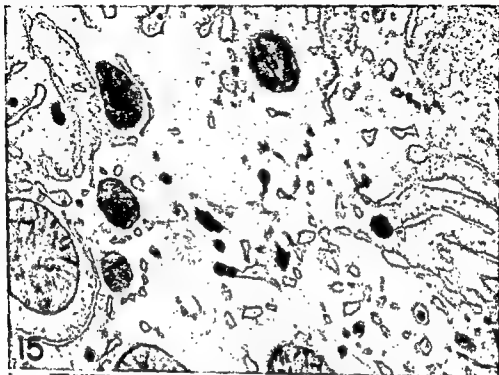
- 12 Hepatic-cell Golgi complex of animal that was fed a diet containing 25% "Hydrol 100" (a hydrogenated oil) for three days. The rounded cisternae contain numerous spherules whose centers have failed to become fixed and densified despite post-osmication. The outer shells of the granules, which are fixed, probably contain phospholipids and possibly protein. The section was stained with barium hydroxide. $\times 40,000$.
- 13 Large lipid droplet of the type that ordinarily lie free in the ground cytoplasm. With the exception of a thin peripheral shell, it has almost completely resisted fixation despite post-osmication. Most of its surface is closely invested with a formation of smooth endoplasmic reticulum. The animal was fed a diet containing 25% "Hydrol 100" for three days. The section was stained with barium hydroxide. $\times 42,000$.
- 14 Hepatic-cell Golgi complex of an animal that was fed a diet containing 25% "Hydrol 100" for six days. The lipid granules within the cisternae are larger than those in figure 12, but are similar in that their centers have also resisted fixation. $\times 45,000$.



PLATE 6

EXPLANATION OF FIGURES

- 15 Small lipid granules in hepatic-cell endoplasmic reticulum of an animal that was fed for five days a diet consisting of 75% fat-free test diet and 25% corn oil. The section was stained with barium hydroxide. $\times 36,500$.
- 16 Golgi complex and large fat droplet in hepatic cell of an animal that was fed for five days a diet consisting of 75% fat-free test diet and 25% corn oil. The cisternae of the Golgi complex are swollen with clusters of small lipid granules. The large fat droplet is closely invested with smooth endoplasmic reticulum. $\times 42,000$.



EXPLANATION OF FIGURES

- 17 Golgi complex of hepatic cell of an animal that was fed a fat-free high-carbohydrate diet for six days. The centers of the small lipid granules within cisternae have been dissolved out despite post-osmication. A large granule at the right (arrow) shows the structure of these inclusions to good advantage. The section was stained with barium hydroxide. $\times 36,500$.
- 18 Golgi complex and large fat droplet of animal that was fed a fat-free high-carbohydrate diet for six days. The centers of small lipid granules have failed to become fixed and densified by post-osmication, but the large lipid droplet (near center at bottom of picture) appears to be completely fixed. The dense object above the fat droplet is a microbody. The section was stained with barium hydroxide. $\times 50,000$.
- 19 The picture shows the space of Disse between an endothelial cell at the top and a hepatic cell at the bottom. The latter cell contains profiles of three individual membrane-enclosed lipid granules (arrows). The investing membrane of one inclusion is continuous with the plasma membrane of the hepatic cell, thus making possible a transfer of material between lumen of vesicle and the space of Disse. The animal was fed a fat-free high-carbohydrate diet for eight days. Post-osmication failed to fix the centers of the lipid granules. The section was stained with lead hydroxide. $\times 28,000$.
- 20 Parts of an endothelial cell (above), a hepatic cell (below), and the space of Disse between them. At the edge of the hepatic cell the membrane of a vesicle containing a group of lipid granules is continuous with the plasma membrane around a constricted opening that makes possible the passage of granules between vesicle and extracellular space. For reasons that are explained in the Discussion section of this paper, this kind of profile (and the similar relationship seen in fig. 19) is interpreted as demonstrating the morphological basis for the extrusion of low-density lipoprotein particles into the blood plasma. The animal was fed a fat-free high-carbohydrate diet for eight days. Post-osmication failed to fix the centers of the lipid granules. The section was stained with lead hydroxide. $\times 30,000$.



Central Projections of Portions of the Vestibular Ganglia Innervating Specific Parts of the Labyrinth in the Rhesus Monkey¹

BENNETT M. STEIN² AND MALCOLM B. CARPENTER

Department of Anatomy, College of Physicians and Surgeons,
Columbia University, New York, New York

ABSTRACT In 40 monkeys attempts were made to determine the central projections of cell groups in the superior and inferior vestibular ganglia (SVG, IVG) which innervate distinctive parts of the labyrinth, by: (1) severing peripheral branches of the ganglia, (2) resecting portions of the ganglia, and (3) producing discrete partial lesions in the ganglia. Serial sections of the temporal bones were stained with Sudan black B, and Nauta-stained sections of the brain stem were cut transversely and horizontally.

Section of peripheral branches of the vestibular ganglia produced no central degeneration and unreliable cell changes in the ganglia. Partial lesions of the SVG, innervating the cristae of the anterior and lateral canals, produced maximal degeneration in the superior and medial (rostral part) vestibular nuclei. Partial lesions of the SVG, innervating the macula of the utricle, produced maximal degeneration in the medial (caudal part) and inferior (mediodorsal part) vestibular nuclei. Some descending fibers related to the utricle entered the accessory cuneate nucleus.

Discrete lesions in portions of the IVG indicate relationships between: (1) the crista of the posterior canal and the superior vestibular nucleus (caudomedial part), and (2) the saccule and dorsolateral parts of the inferior vestibular nucleus. Cells of the vestibular ganglia innervating distinctive parts of the labyrinth have unique, as well as common, central projections within the vestibular nuclear complex.

Physiological studies indicate that anatomical components of the labyrinth each subserve distinctive functions. It appears established that the semicircular canals play a vital role in the maintenance of kinetic equilibrium and respond in a sensitive manner to angular rotation. The utricle, concerned primarily with static equilibrium, responds to changes in gravitational forces and to linear acceleration. The functions of the saccule are poorly defined, but anatomical evidence (Lorente de N6, '33) leaves little doubt that it is part of the complex vestibular end organ. Anatomical components of the labyrinth are innervated by peripheral processes of bipolar cells located in the superior and inferior vestibular ganglia. Anatomical studies (Alexander, '01; deBurlet, '24; Lorente de N6, '31) indicate that peripheral branches of the superior vestibular ganglion innervate: (1) the cristae of the anterior and lateral semicircular canals, (2) the macula of the utricle, and (3) a small dorsal part of the macula of the saccule. Peripheral branches of the inferior

vestibular ganglion innervate the crista of the posterior canal and the principal part of the macula of the saccule.

Attempts to precisely delimit cell groups within the ganglia which give rise to these peripheral branches have been only partially successful (Alexander, '01; Lorente de N6, '31, '33). The most extensive study (Lorente de N6, '31) of this subject, based upon silver impregnation methods in cat and mouse embryos, suggested that large cells in the superior vestibular ganglion innervating the crista of the anterior canal are most dorsal and distal. Large cells in the most medial and ventral parts of the superior ganglion were considered to innervate the macula of the utricle, and similar large cells, in an intermediate position, to project to the crista of the lateral canal. Certain small cells in the isthmus region, found at the junction of the supe-

¹This investigation was supported by grant NB-01538-08 from the Institute of Neurological Diseases and Blindness of the National Institutes of Health, Bethesda, Maryland.

²Special Fellow in neuroanatomy supported by training grant 5T1-NB-5242-07 from the Institute of Neurological Diseases and Blindness.

rior and inferior ganglia, were described as supplying fibers to parts of the macula of the utricle. Large cells in the lateral and inferior parts of the inferior vestibular ganglion were described as innervating the crista of the posterior canal. Both large and small cells located in medial and dorsal parts of the inferior ganglion projected to the macula of the saccule in the inferior saccular nerve. The author's description suggests that the superior saccular nerve actually arises from the same cell group, even though this nerve is considered as a branch of the superior vestibular ganglion. The principal point is that both nerves to the macula of the saccule were considered to arise from the same region of the inferior vestibular ganglion. Fibers innervating the macula of the utricle likewise arise from a localized region of the superior vestibular ganglion, but the nerves innervating the cristae of the semicircular canals arose from essentially similar cells in three distinct locations within the vestibular ganglia. Central branches of the vestibular nerve, according to Lorente de N6 ('31), formed three distinct bundles: (1) an anterior bundle containing the central processes of cells whose peripheral branches innervated the cristae of the three semicircular canals, (2) a middle bundle containing the central processes of cells which innervated the macula of the utricle, and (3) a posterior bundle of fibers from cells whose peripheral branches supplied the macula of the saccule.

The only detailed study of the central projections of the vestibular ganglia is that of Lorente de N6 ('33) based upon Golgi preparations of the mouse. Although this is a superb study, the terminology used for subdivisions of the vestibular nuclear complex is difficult to interpret in terms of the most widely used nomenclature for the vestibular nuclei (Brodal and Pompelano, '57; Brodal, Pompelano and Walberg, '62). This author subdivided the central projecting vestibular fibers into five groups, primarily on the basis of fiber size. Fibers of groups I (thin and medium-sized) and II (thick) arising from cells whose peripheral processes innervate the cristae of the semicircular canals, were located in the rostral part of the vestibular root. Upon entering the brain stem, these fibers bifurcated into:

- (1) ascending fibers which projected to the superior and medial vestibular nuclei, and
- (2) descending fibers which entered the lateral part of the inferior vestibular nucleus. Few, if any, of these fibers terminated in the lateral vestibular nucleus.

The thick and medium-sized fibers of group IV arose from cells innervating the macula of the utricle, and entered the ventral part of the lateral vestibular nucleus where they bifurcated. Descending branches of these fibers gave off collaterals to the ventral part of the lateral vestibular nucleus, while remaining fibers formed parallel descending fascicles in the dorso-medial part of the inferior vestibular nucleus. Less numerous ascending branches of group IV fibers were described as passing to the nucleus vestibulo-cerebellous, but not to the superior or medial vestibular nuclei.

Fibers of group V, chiefly medium-sized, arising from cells innervating the macula of the saccule, were located most caudally and laterally in the vestibular nerve root. Descending branches of bifurcating fibers of this group formed parallel fascicles in the dorsolateral part of the inferior vestibular nucleus, while ascending branches passed to laterocaudal parts of the nucleus vestibulo-cerebellous. The precise equivalent of the nucleus vestibulo-cerebellous in current terminology is uncertain, but the illustrations of Lorente de N6 ('33) suggest that this nuclear complex lies between the vestibular nuclei and the intrinsic cerebellar nuclei.

Fibers of group III, containing thick and medium-sized fibers, were described as occupying a position in the vestibular root caudal to that of the fibers of groups I and II. Although there is some uncertainty, these fibers were presumed to arise from cells which innervate the central part of the cristae and perhaps the dorsal part of the macula of the utricle. Ascending and descending branches of group III fibers appeared to be distributed to the same locations as those of group II; in addition, these fibers gave off collaterals to the ventral part of the lateral vestibular nucleus, as did the fibers of group IV.

The elegant studies of Lorente de N6 ('31, '33) indicated that the centrally projecting fibers from cells of the vestibular

ganglia have a partially distinctive and a partially common distribution within the vestibular nuclear complex. The central distribution of fibers from both maculae was similar, as was the central distribution of fibers from the cristae of the semicircular canals. Thus the otolithic organs and the membranous labyrinth, which are known to have different physiological functions, appeared in part to have separate central anatomical representation.

The object of the current study was to re-investigate the central projections of the vestibular ganglia innervating specific parts of the labyrinth in the rhesus monkey. While it seemed likely that the general organization of the central fibers of the vestibular ganglia in the monkey is basically similar to that of the mouse, certain important differences might exist in the primate. It also was felt that the utilization of the experimental method and some of the more recently developed staining techniques might contribute significant new data concerning the distinctive and overlapping central projections of primary vestibular fibers associated with the individual components of the complex vestibular end organ.

MATERIALS AND METHODS

Careful studies of the vestibular ganglia in the rhesus monkey were made in order to: (1) become familiar with the complex anatomy of the inner ear, and (2) establish the relationships between portions of the ganglia and peripheral branches innervating specific portions of the membranous labyrinth. These studies consisted of: (1) dissections of temporal bones done with a dental drill under an operating microscope, and (2) observations made from serial sections of decalcified temporal bones stained by various techniques. Temporal bones of different animals were sectioned horizontally and in the longitudinal axis of the vestibular nerve.

Forty rhesus monkeys were used in this study. Initially only unilateral operative procedures were carried out. Since all recent studies (Walberg, Bowsher and Brodal, '58; Carpenter, '60) indicate that primary vestibular fibers within the brain stem are entirely ipsilateral, bilateral procedures were done on most of the later

animals. This not only resulted in economies of time, effort, and material, but afforded an opportunity to compare central degeneration resulting from different peripheral lesions in the same animal.

A total of 59 separate operative procedures were done in 40 rhesus monkeys. Procedures performed were: (1) surgical section of single and multiple peripheral branches of the vestibular ganglia, (2) resection of all, or part, of particular vestibular ganglia, and (3) selective electrolytic destruction of portions of both the superior and inferior vestibular ganglia. Animals were anesthetized with intravenous Nembutal and surgery was performed under aseptic conditions.

Two operative approaches were used to expose the neural elements within the petrous bone: (1) a middle fossa transpetrosal approach to expose the superior vestibular ganglion and its branches, and (2) a transmastoid approach to expose the inferior vestibular ganglion and its branches. These procedures were as follows:

I. *Middle fossa, extradural, transpetrosal approach.* This procedure, described in man by Kurze and Doyle ('62), was modified for the monkey. The animal's head was immobilized in an inverted Lab-Tronics head holder; bayonet-type ear bars were used to raise the head above the horizontal bars of the stereotaxic frame. A large temporal craniotomy was made which extended from the floor of the middle fossa to the lateral border of the petrous ridge. An extradural exposure of the middle fossa was made using a self-retaining retractor to elevate the temporal lobe. This exposure of the anterior surface of the petrous pyramid provided important landmarks used in unroofing the internal auditory canal. These landmarks were: (1) the notch in the petrous ridge over the paraflocculus, (2) the facial hiatus, (3) the dural fold over the lateral border of the trigeminal nerve, and (4) the prominence of the petrous bone overlying the paraflocculus. To unroof the internal auditory canal, a high speed (24,000 r.p.m.) dental drill was used with diamond tipped dental bits of various sizes. The anterior portion of the petrous ridge, bounded medially by the trigeminal nerve, laterally by the paraflocculus and inferiorly by the facial hiatus,

was removed. A thin layer of bone was left overlying the internal auditory canal. After more precise identification of the medial and lateral borders of the internal auditory canal, this thin layer of bone was removed with a small pick. This exposure of the dorsal surface of the superior vestibular ganglion was used to: (1) section peripheral branches of the ganglion to the anterior and lateral canals, (2) place electrolytic lesions in dorsal and distal parts of the ganglion, and (3) resect the entire ganglion. Variations of this approach permitted exposure of the utricular nerve fibers and medial and inferior portions of the superior vestibular ganglion by opening the utricular cavity.

II. Transmastoid approach. This surgical approach was used to expose the inferior vestibular ganglion and its peripheral branches. The head was immobilized as previously described and an opening was made in the mastoid cavity with a large dental drill. This opening extended from the sigmoid sinus posteriorly to the middle ear. Further drilling superiorly in the mastoid cavity revealed the lateral and posterior semicircular canals. The inferior limb of the posterior canal was followed inward with the dental drill until the posterior canal nerve could be identified. A more anterior approach, avoiding the posterior canal nerve, was used to open the sacculle and expose the saccular nerve fibers as they passed through the macula cribrosa media. This thin plate of bone was broken to gain access to the part of the inferior vestibular ganglion supplying fibers to the sacculle. By these slightly different exposures lesions were placed in different parts of the inferior vestibular ganglion.

Electrolytic lesions, made after surgical exposures of the above types, were produced in the vestibular ganglia by fine monopolar electrodes, insulated except for 1 mm of a sharpened tip, using a direct current of 400 volts at 2 or 3 ma. Current was allowed to flow from 3 to 15 seconds. The electrode, held in a small insulated pin vise, was positioned manually with the aid of an operating microscope. Excision of the entire vestibular ganglion, or portions of the ganglion, was done with microsurgi-

cal scissors. Branches of the vestibular ganglia were cut similarly.

Prior to operation, the monkeys were observed in their cages for evidence of neurological disorder. On the day of operation each animal was examined neurologically in a restraining chair. Caloric responses were tested bilaterally, using an infusion of ice water with the lateral canal vertical and the ampulla of this canal directed upward.

Following surgery, animals were allowed to recover in their cages. Detailed observations were recorded daily by a number of observers. Periodic examinations were carried out in the restraining chair and all animals were tested for caloric responses prior to sacrifice.

Although abnormal physiological responses were observed in all animals following surgery, the results will not be reported. The significance of these responses was impossible to determine in most instances, since opening any portion of the membranous labyrinth subjects the entire system to deranged function. Facial palsy initially was frequent, occurring from cauterization of the stump of the greater superficial petrosal nerve, or from direct injury to the facial nerve. This complication was avoided in later animals.

Animals were sacrificed no sooner than 14 days after surgery and no later than 21 days. Animals were anesthetized with Nembutal and were sacrificed by intracardiac perfusion of a liter of normal saline followed by an equal volume of 10% neutral formaldehyde solution. The brains and spinal cords were removed *in toto* and further fixed in 10% neutral formaldehyde solution. That portion of the temporal bone containing the labyrinth, cochlea and their nerves was removed with a dental drill and placed in 10% neutral formaldehyde solution.

Histological studies of the vestibular nerves and ganglia. After adequate formalin fixation, two different methods were used to study the lesions of the vestibular ganglia and their peripheral nerve branches. Early in this study, the vestibular ganglia and their proximal and distal nerve fibers were dissected from the temporal bones, embedded in paraffin and sectioned serially. Sections of the vestibular

nerve in different animals were cut in horizontal and longitudinal planes. These sections were stained by the technics of Nissl, Weil, Bodian and Mason's trichrome. Because of inherent difficulties associated with the above methods, the Sudan black B method of Rasmussen ('61) was used in later phases of this study.

Trimmed petrous bones were stained with Sudan black B, decalcified in "Decal" solution² and embedded in gelatin. Sections were cut serially on a freezing microtome at 20 μ and mounted. Sections of the petrous bones were cut in horizontal or longitudinal planes of the vestibular nerve. These sections permitted accurate evaluations of the extent and position of lesions within the vestibular ganglia and provided information concerning the integrity of peripheral nerve fibers supplying sensory epithelium in different parts of the membranous labyrinth. Low magnification drawings of the vestibular ganglia and their peripheral nerve fibers were made from projections of these sections. Lesions of the superior vestibular ganglion could be evaluated most precisely in sections cut longitudinally, while horizontal sections of the petrous bone were most useful in evaluating lesions in the inferior vestibular ganglion.

In addition to the methods described above, attempts were made to stain the vestibular nerve by the Nauta and Gyax ('54) method both in specimens removed from the bone and in blocks of decalcified petrous bone. Because of difficulties in handling frozen sections, all material was embedded in paraffin. These variations of the method were unsuccessful and resulted in inconsistent staining of the myelin sheath with no staining of the degenerated axons. The Sudan black B technic was found to give a much clearer representation of the peripheral histology than any other method.

Histological studies of the brain stem. After adequate fixation, the brain stems of these animals were sectioned either transversely or horizontally. Blocks of tissue were cut at 20 μ on a freezing microtome and all sections were preserved in multi-compartment plastic boxes. Approximately 15 sections were placed in each numbered compartment. Multiple representative sec-

tions from all levels of the brain stem were stained by the method of Nauta and Gyax ('54). In addition certain sections through crucial areas of the vestibular nuclei were stained with cresyl violet. Written descriptions and drawings of the central degeneration were made independently by both authors. Discrepancies of observation were reviewed and restudied until both authors considered them resolved.

The original plan was to study each distinctive type of vestibular lesion in both horizontal and transverse sections. Although this remained our objective throughout this study, it was not always possible to produce identical lesions in two different animals.

OBSERVATIONS

Normal Anatomy of the Vestibular Ganglia

In over 50 specimens from the rhesus monkey the vestibular nerve, ganglia, and individual peripheral nerve branches were studied in detail. The vestibular nerve entered the petrous bone via the internal auditory meatus at an angle of approximately 40° with the sagittal plane of the skull. The vestibular ganglion lay within the auditory canal and was divided into two major portions, the superior and inferior vestibular ganglia (figs. 1, 3). These ganglia, for the most part, were distinctly separate and had only a small common junctional area of cells. The crista transversa, a ridge of bone at the lateral extremity of the internal auditory canal, separated the ganglia. At operation and in the study of histological specimens, this structure served as a useful and reliable landmark.

Superior vestibular ganglion. The superior vestibular ganglion, situated in a bony canal above the crista transversa, contained approximately two-thirds of the primary vestibular neurons. In the basal part of the superior ganglion, cells extended across the entire width of the vestibular nerve. In sections distal to this point, cells were distributed in a spiral fashion, tending to be located progressively more distal, dorsal and medial until they disappeared. Studies of normal Nissl, myelin sheath,

² Omega Decal solution, a product of Omega Chemical Corporation, New York, N. Y.

and Bodian stained sections suggested that cell groups located dorsomedially in the distal part of the ganglion gave rise to fibers passing to the crista of the anterior and lateral canals. Although some intermingling of fibers was seen, the majority of the fibers seemed to follow a fairly direct course. Even though it was not possible in normal stained preparations to sharply delimit cell groups of the anterior and lateral canals from each other, it was our impression that cells located most distally and dorsomedially projected fibers predominantly to the crista of the anterior semicircular canal. This impression was confirmed by data derived from localized lesions in this part of the superior vestibular ganglion. Fibers of the anterior and lateral canal nerves passed distally in small bony canals with the anterior canal nerve most dorsal. These bony canals were so close to each other that it was virtually impossible to destroy one of the nerves without injuring the other.

The large cell group of the superior vestibular ganglion, situated proximally and ventrally near the junction with the inferior vestibular ganglion, gave rise to numerous fine filaments which passed through small foramina in a bony septum (macula cribrosa superior) to innervate the macula of the utricle. Some of the fibers from the utricular region of the superior vestibular ganglion projected to superior portions of the macula of the saccule. The largest part of the fibers projecting to the macula of the saccule originated from a distinctive part of the inferior vestibular ganglion.

Inferior vestibular ganglion. The inferior vestibular ganglion, located below the crista transversa in a blunt bony canal, appeared divisible into two parts: (1) a larger part containing the saccular ganglion, situated inferiorly and slightly lateral to the axis of the superior vestibular ganglion, and (2) a smaller part consisting of cell groups protruding laterally at almost a right angle to the main mass of the inferior ganglion. The latter cell group appeared to give rise to the posterior canal nerve (figs. 1, 2). Cells of the saccular ganglion gave rise to numerous fine fibers which passed through a trabeculated bony septum (macula cribrosa media) to be

distributed to the macula of the saccule. Fibers from the distinctive lateral cell group passed through the foramen singulare as the posterior canal nerve and entered the crista of the posterior semicircular canal. Because of the distinctive arrangement of cell groups in the inferior vestibular ganglion, it seemed feasible to attempt to destroy each cell group separately.

The results of these observations suggest that definite cell groups within the vestibular ganglia give rise to peripheral fibers which innervate distinctive parts of the membranous labyrinth (fig. 1). Although these observations of normal specimens do not have the firm basis of those of Lorente de N6 ('33), done in the mouse and cat with the Golgi technic, the organization of cell groups in the monkey is remarkably similar. The schematic drawing of Lorente de N6 ('33; fig. 14) shows that the basic organization of the vestibular ganglia in lower forms is similar to that in the monkey, but in the primate the superior and inferior ganglia appear more sharply separated and cells are arranged in a distinctive, constant fashion.

More precise information concerning the cells of origin of peripheral processes of the vestibular ganglia might be obtained, if selective sectioning of these nerves were to produce retrograde cell changes in the ganglia. This was done as part of this study.

Total section of the vestibular nerve

In two animals (C-864 and C-965) the entire vestibular nerve was sectioned proximal to the vestibular ganglia following a middle fossa, transpetrosal exposure of the ganglia and nerve. In rhesus C-864 the vestibular ganglia were removed at surgery, embedded in paraffin, sectioned serially and stained with cresyl violet. Study of these sections indicated that both vestibular ganglia had been resected completely.

Brain stems of these animals were sectioned serially in transverse (C-864) and horizontal planes (C-965). Multiple representative sections from all levels of the brain stem were stained by the Nauta and Gyax method. Since degeneration in both animals was similar, it can be described synthetically. The entire vestibular root was degenerated; profuse degeneration was

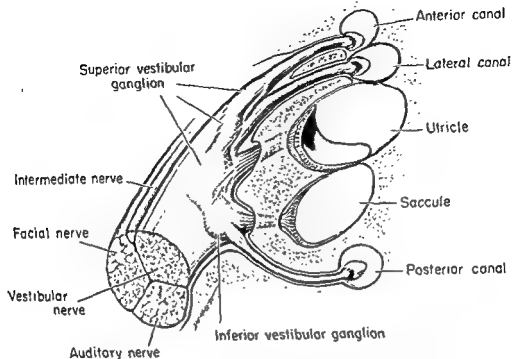


Fig. 1 Semischematic drawing of the vestibular ganglia and peripheral branches innervating anatomically distinctive portions of the labyrinth. Cells of the superior vestibular ganglion are arranged in a spiral fashion. The attenuated distal portion of the superior vestibular ganglion supplies fibers innervating the cristae of the anterior and lateral canals. Cells in the broader, proximal part of this ganglion innervate the macula of the utricle. The superior and inferior vestibular ganglia are joined by an isthmus of cells. Cells of the inferior vestibular ganglion innervate the macula of the saccule and the crista of the posterior canal.

seen about cells in all parts of the interstitial nucleus of the vestibular nerve. Relatively profuse degeneration, present in all vestibular nuclei, was distributed in a specific manner; certain regions of each vestibular nucleus were free of degenerated primary vestibular fibers. The differential pattern of distribution of primary vestibular fibers in the monkey appears similar to that described by Walberg, Bowscher and Brodal ('58) for the cat.

Profuse degeneration in the vestibular root entered the vestibular complex at the ventrolateral border of the lateral vestibular nucleus and passed both rostrally and caudally within the complex. Ascending fibers passed through the rostrolateral parts of the lateral vestibular nucleus, without apparent terminations, and entered ventrolateral portions of the superior vestibular

nucleus. Preterminal degeneration was distributed to the centrolateral region of this nucleus with particularly notable aborization about the larger cells located centrally. A moderate number of degenerated fibers passed through the ventromedial parts of the superior vestibular nucleus to reach the oral parts of the medial vestibular nucleus. A smaller number of the degenerated ascending fibers passed both medial and lateral to the superior cerebellar peduncle toward the cerebellum.

The degenerated fibers from the root entry zone which did not ascend directly, either passed medially in heavy bundles through the ventrocaudal aspect of the lateral vestibular nucleus and the rostral portion of the inferior vestibular nucleus, or descended in the inferior vestibular nucleus. The lateral vestibular nucleus was

for the most part free of degeneration except for the fibers passing through its lateral and ventral regions.

Degenerated fibers passing medially did not appear to arborize about the large cells of the lateral vestibular nucleus and arborizations about the smaller cells were not numerous. These fibers terminated in the oral pole of the medial vestibular nucleus or descended into lateral parts of the medial vestibular nucleus. The most profuse preterminal degeneration in this nucleus was located rostrally where arborizations were seen about larger cells. At caudal levels the amount of degeneration progressively diminished, so that only sparse degeneration was present in caudal portions of the nucleus.

The inferior vestibular nucleus contained abundant degeneration throughout its rostral part. Prominent fascicles of degenerated fibers descending in this nucleus occupied large parts of its transverse extent but were more numerous in the dorsal regions. Clusters of medium-sized cells throughout the nucleus were surrounded by profuse preterminal degeneration. No degenerated fibers entered the ventrolateral caudal portion of the inferior vestibular nucleus, designated as cell group f (Brodal and Pompeiano, '57).

A number of degenerated fascicles passed medially from all portions of the inferior vestibular nucleus to end about the cells of the lateral part of the medial vestibular nucleus. These fibers were most prominent in the rostral and midportions of the inferior vestibular nucleus.

A few degenerated fibers passed from the dorsolateral part of the inferior vestibular nucleus to end in oral parts of the accessory cuneate nucleus. These fibers entered the nucleus in small fascicles which became dispersed among clusters of large cells. Only a few of these fibers appeared to establish intimate contacts with cell somata.

Lesions of the vestibular ganglia and their peripheral branches

In 38 monkeys, 57 operative procedures on the vestibular ganglia and their peripheral branches were performed. Lesions considered suitable for detailed study of both peripheral and central degeneration

were produced on 33 different sides in 22 monkeys. Animals with poorly placed lesions, or lesions which could not be evaluated precisely, were omitted from the study.

Surgical section of peripheral branches of the vestibular ganglia. In seven monkeys peripheral branches of the superior and inferior vestibular ganglia were destroyed on nine sides without damaging the ganglia. Nissl-stained sections of the vestibular ganglia in three animals [C-870 (R), C-876 (L), and C-936 (R)], in which nerves to the anterior, posterior and lateral canals and to the utricle were sectioned, did not demonstrate chromatolytic cell changes or cell loss (fig. 2). Animals were sacrificed 5, 8 and 27 days after the nerves were sectioned. Nauta-stained sections of the brain stem did not reveal degeneration in the vestibular nerve root or in the vestibular nuclei.

Six lesions destroying branches of the vestibular ganglia innervating the utricle, saccule and posterior canal were produced electrolytically in four animals [C-931 (L), C-934 (B), C-937 (B), and C-945 (R)]. Temporal bones of these animals, stained with Sudan black B, were sectioned serially. None of the lesions destroyed any part of the vestibular ganglia. Although this staining method does not permit critical evaluation of cell changes, there were no apparent reductions of cell populations. No degeneration of the myelin sheath was seen in portions of the vestibular nerve proximal to the ganglia, and Nauta-stained sections did not reveal any degeneration in the brain stem on the side of the lesions.

The above data suggest that section of the peripheral branches of the vestibular ganglia: (1) does not produce readily detectable chromatolytic cell changes in the ganglia, and (2) does not cause degeneration of primary vestibular fibers in the brain stem.

Lesions of the superior vestibular ganglion

Total lesions of the superior vestibular ganglion. In four animals [C-863 (R), C-865 (R), C-866 (R), and C-890 (L)] the entire superior vestibular ganglion was resected following a transpetrosal exposure of the ganglion. The completeness of these

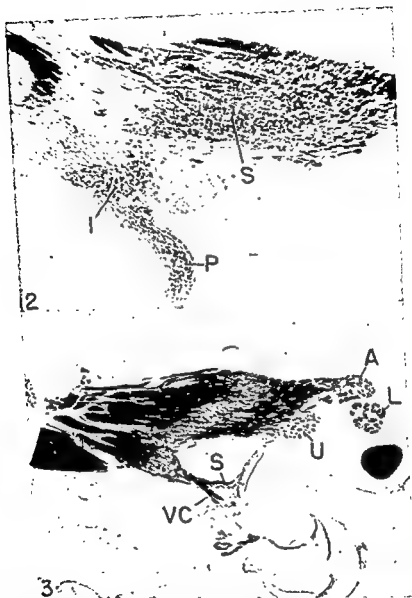


Fig. 2 Rhesus C-936. Photomicrograph of a longitudinal section of the right superior (S) and inferior (I) vestibular ganglia showing the disposition of cell groups. The posterior canal nerve (P) can be seen issuing from the lower part of the inferior vestibular ganglion. The posterior canal nerve was sectioned surgically distal to the ganglion, but no retrograde cell changes were evident in the ganglion. Nissl $\times 20$.

Fig. 3 Photomicrograph of the right, normal vestibular ganglia and peripheral branches in a section of the petrous bone. This section is cut in the longitudinal axis of the ganglia and demonstrates the anterior (A) and lateral (L) canal nerves as well as utricular fibers (U) arising from the superior vestibular ganglion. A few fibers of the saccular nerve (S) can be followed toward the macula of the saccule; ventral to these fibers is the vestibulo-cochlear (VC) anastomosis. Sudan black B $\times 15$.

for the most part free of degeneration except for the fibers passing through its lateral and ventral regions.

Degenerated fibers passing medially did not appear to arborize about the large cells of the lateral vestibular nucleus and arborizations about the smaller cells were not numerous. These fibers terminated in the oral pole of the medial vestibular nucleus or descended into lateral parts of the medial vestibular nucleus. The most profuse preterminal degeneration in this nucleus was located rostrally where arborizations were seen about larger cells. At caudal levels the amount of degeneration progressively diminished, so that only sparse degeneration was present in caudal portions of the nucleus.

The inferior vestibular nucleus contained abundant degeneration throughout its rostral part. Prominent fascicles of degenerated fibers descending in this nucleus occupied large parts of its transverse extent but were more numerous in the dorsal regions. Clusters of medium-sized cells throughout the nucleus were surrounded by profuse preterminal degeneration. No degenerated fibers entered the ventrolateral caudal portion of the inferior vestibular nucleus, designated as cell group f (Brodal and Pompeiano, '57).

A number of degenerated fascicles passed medially from all portions of the inferior vestibular nucleus to end about the cells of the lateral part of the medial vestibular nucleus. These fibers were most prominent in the rostral and midportions of the inferior vestibular nucleus.

A few degenerated fibers passed from the dorsolateral part of the inferior vestibular nucleus to end in oral parts of the accessory cuneate nucleus. These fibers entered the nucleus in small fascicles which became dispersed among clusters of large cells. Only a few of these fibers appeared to establish intimate contacts with cell somata.

Lesions of the vestibular ganglia and their peripheral branches

In 38 monkeys, 57 operative procedures on the vestibular ganglia and their peripheral branches were performed. Lesions considered suitable for detailed study of both peripheral and central degeneration

were produced on 33 different sides in 22 monkeys. Animals with poorly placed lesions, or lesions which could not be evaluated precisely, were omitted from the study.

Surgical section of peripheral branches of the vestibular ganglia. In seven monkeys peripheral branches of the superior and inferior vestibular ganglia were destroyed on nine sides without damaging the ganglia. Nissl-stained sections of the vestibular ganglia in three animals [C-870 (R), C-876 (L), and C-936 (R)], in which nerves to the anterior, posterior and lateral canals and to the utricle were sectioned, did not demonstrate chromatolytic cell changes or cell loss (fig. 2). Animals were sacrificed 5, 8 and 27 days after the nerves were sectioned. Nauta-stained sections of the brain stem did not reveal degeneration in the vestibular nerve root or in the vestibular nuclei.

Six lesions destroying branches of the vestibular ganglia innervating the utricle, saccule and posterior canal were produced electrolytically in four animals [C-931 (L), C-934 (B), C-937 (B), and C-945 (R)]. Temporal bones of these animals, stained with Sudan black B, were sectioned serially. None of the lesions destroyed any part of the vestibular ganglia. Although this staining method does not permit critical evaluation of cell changes, there were no apparent reductions of cell populations. No degeneration of the myelin sheath was seen in portions of the vestibular nerve proximal to the ganglia, and Nauta-stained sections did not reveal any degeneration in the brain stem on the side of the lesions.

The above data suggest that section of the peripheral branches of the vestibular ganglia: (1) does not produce readily detectable chromatolytic cell changes in the ganglia, and (2) does not cause degeneration of primary vestibular fibers in the brain stem.

Lesions of the superior vestibular ganglion

Total lesions of the superior vestibular ganglion. In four animals [C-863 (R), C-865 (R), C-866 (R), and C-890 (L)] the entire superior vestibular ganglion was resected following a transpetrosal exposure of the ganglion. The completeness of these

Dorsal and rostral portions of the lateral vestibular nucleus were free of degenerated fibers, except for those previously described as projecting to the superior vestibular nucleus. Through central portions of the vestibular root, where the lateral vestibular nucleus was well developed, virtually all root fibers were degenerated. These fibers arched medially over the spinal trigeminal tract and entered the ventral third of Deiters' nucleus. The majority of these fibers appeared to traverse the ventral third of the lateral vestibular nucleus until they reached its medial border where they projected dorsomedially into the medial vestibular nucleus. Virtually none of these fibers arborized about the large cells of Deiters' nucleus and good examples of arborizations about smaller cells were rare. A considerable number of root fibers from the superior division of the vestibular nerve traversed rostral parts of the inferior vestibular nucleus in a lateral to medial direction; most of these fibers entered lateral portions of the medial vestibular nucleus, but some appeared to terminate about cells in the rostral part of the inferior vestibular nucleus.

In the medial vestibular nucleus preterminal degeneration was most abundant in dorsolateral regions, especially rostral to, and at the level of, the vestibular root. Good quality arborizing networks of fibers were present in the medial vestibular nucleus near its mutual border with Deiters' nucleus. Profuse degeneration was seen also about a distinct collection of large cells in the more medial part of the medial vestibular nucleus. Caudal to the root entry zone, degeneration in the medial vestibular nucleus continued to be present in dorsolateral regions, but was relatively modest in amount. In horizontal sections a small number of fine descending degenerated fascicles were seen in this nucleus. Most of the degenerated fibers entering caudal parts of the medial vestibular nucleus appeared to come from the bundles of degenerated fibers descending in the inferior vestibular nucleus. These fibers separated from the main bundles at right angles and projected into lateral parts of the medial vestibular nucleus.

Fibers entering the inferior vestibular nucleus traversed the ventral parts of Deiters' nucleus and entered mainly rostromedial parts of the inferior vestibular nucleus. Very few, if any, fibers entered lateral portions of the inferior vestibular nucleus directly. These fibers, arranged in small fascicles, descended the length of the inferior vestibular nucleus, gradually diminishing at successively more caudal levels (figs. 31, 37). Some of the descending fibers tended to shift to lateral positions at more caudal levels. Distinct arborizations about groups of larger cells were seen clearly at various levels in horizontal sections (fig. 33). Degenerated fibers seen in both dorsal and ventral portions of the nucleus seemed to be greatest in more medial regions. As mentioned above, collateral fibers were given off at various levels to lateral and dorsal parts of the medial vestibular nucleus. No degenerated fibers entered the ventrolateral part of the inferior vestibular nucleus caudally. The large cells in this region constitute cell group f (Brodal and Pompeiano, '57). No distinct degeneration was seen in cell groups x or z as delimited by the above authors.

A small but distinct bundle of descending degenerated fibers, tending to occupy lateral portions of the inferior vestibular nucleus at caudal levels, was found to leave the vestibular nuclear complex and enter the most rostral part of the accessory cuneate nucleus. These fibers were never numerous but were consistently seen about the large cells in this part of the accessory cuneate nucleus. Caudal portions of this nucleus occasionally contained a few degenerated fibers. Preterminal degeneration in the accessory cuneate nucleus was not related to concomitant degeneration in the solitary fasciculus, or to injury of the spinal trigeminal tract since it was present in animals in which these structures were not injured. No degeneration was seen in the cuneate nucleus in any of these animals. This small fiber bundle passing to the accessory cuneate nucleus appeared to constitute the only brain stem projection from the vestibular root that passed beyond the limits of the vestibular nuclear complex.

resections were confirmed by histological sections of the surgical specimens and serial sections of the remaining vestibular ganglia and nerve fibers removed at autopsy. Sections stained by various methods indicated that the inferior vestibular ganglia and their central and peripheral processes were preserved except for a small number of cells near the junctional zone of the superior and inferior vestibular ganglia.

In three other monkeys [C-869 (R), C-927 (R), and C-928 (R)] electrolytic lesions were produced in the superior vestibular ganglia (fig. 4). Lesions in all animals of this group were made on the right side with small wire electrodes insulated except for the tip. At autopsy, the vestibular ganglia with central and peripheral fibers were dissected from the temporal bone in rhesus C-869 (R), dehydrated, embedded in paraffin, and cut serially. Sections were stained by the Nissl and Bodian methods. Examination of these sections disclosed virtually complete destruction of the superior vestibular ganglion; the inferior vestibular ganglion and its cell processes appeared normal.

Following sacrifice, the temporal bones of rhesus C-927 (R) and C-928 (R), stained with Sudan black B, revealed well localized electrolytic lesions in the superior vestibular ganglion associated with degeneration of all peripheral branches of this ganglion. The superior divisions of the vestibular nerve were totally degenerated, except in rhesus C-928 (R) where a few fibers in the dorsal part of this division appeared normal. The lesion in this animal spared a small part of the superior vestibular ganglion that gives rise to fibers of the anterior canal nerve.

Central degeneration in these seven animals with resection, or virtually total destruction, of the superior vestibular ganglia was essentially the same. Although sections of the brain stem were cut transversely (C-863, C-865, C-869, and C-890) and horizontally (C-866, C-927, and C-928) in different animals, these findings can be presented most conveniently in a synthetic fashion (fig. 6).

The spatial disposition of degeneration in the vestibular root following total lesions of the superior vestibular ganglion

was constant and characteristic. Near the site where the vestibular root enters the brain stem, degeneration was complete in rostral and lateral portions of the nerve (fig. 21). In transverse sections of the brain stem all fibers of the vestibular nerve were degenerated rostrally; but at successively more caudal levels, degenerated fibers were confined to lateral portions of the root and clearly demarcated from the normal fibers present medially. Sections through the caudal part of the vestibular root revealed almost exclusively normal fibers. Horizontal sections of the brain stem disclosed the same disposition of fibers from the superior division of the vestibular nerve, but indicated that these fibers comprised approximately two-thirds of the fibers in the vestibular nerve (fig. 25). Preterminal degeneration in the vestibular root arborized extensively about cells of the interstitial nucleus of the vestibular nerve located rostrally and laterally within the root, but cells of this nucleus in other parts of the root were free of degeneration.

Vestibular root fibers, entering rostrally, passed dorsally through lateral parts of the lateral vestibular nucleus to enter central and lateral portions of the superior vestibular nucleus (figs. 21, 27). A significant number of fibers skirted the lateral border of Deiters' nucleus in this projection. These fiber bundles arborized extensively about large-celled groups in central portions of the superior vestibular nucleus. Smaller individual fascicles of degenerated fibers were noted to enter more medial portions of this nucleus. In many cases distinct small bundles of degenerated fibers, passing rostrally and dorsally, were noted to enter the cerebellum along both sides of the superior cerebellar peduncle. Another small group of fibers from the rostral part of the vestibular root was observed to branch medially from the principal bundle described above; these relatively fine fascicles passed along the ventral border of the superior vestibular nucleus and entered rostral parts of the medial vestibular nucleus. Caudal portions of the superior vestibular nucleus contained smaller groups of degenerated fibers about large cells, but at these levels no vestibular root fibers could be seen entering the nucleus directly.

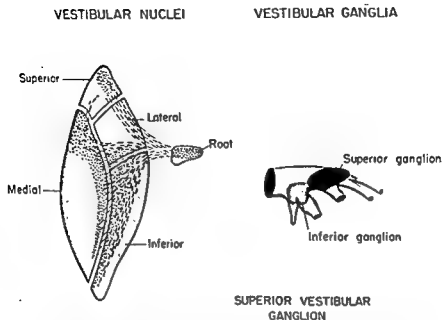


Fig. 6 Diagrammatic representation of the central distribution of degeneration in the vestibular nuclei resulting from a lesion of the superior vestibular ganglion. A lesion of this kind is shown in figure 4. The vestibular ganglia and their peripheral branches are shown on the right. The vestibular root and nuclei in horizontal orientation are on the left. The lesion is in black, while degeneration is represented by broken lines and dots.

Portions innervating the cristae of the anterior and lateral canals. Small electrolytic lesions in dorsal and peripheral parts of the superior vestibular ganglion were made on six sides in five animals [C-890 (R), C-899 (B), C-926 (R), C-927 (L), and C-931 (R)] (figs. 18, 19). After these animals were sacrificed, the temporal bones were removed, stained with Sudan black B, and cut serially in the longitudinal axis of the vestibular nerve. Determinations of the location and extent of the electrolytic lesions were made from these preparations. Relatively large lesions in rhesus C-899 destroyed virtually all parts of the superior vestibular ganglion bilaterally, except the part providing innervation to the maculae of the utricle. Degeneration emanating from the lesions could be followed in the anterior and lateral canal nerves to the cristae of these canals. The only one of these nerves not com-

pletely degenerated was the anterior canal nerve on the right side.

In the remaining four animals lesions of the superior vestibular ganglia were smaller and more superficial, involving predominantly dorsal and distal parts of the ganglia. The anterior canal nerve appeared completely degenerated while fibers of the lateral canal nerve were never all degenerated. None of these electrolytic lesions destroyed portions of the superior vestibular ganglion supplying fibers to the utricle and none involved any part of the inferior vestibular ganglion (fig. 5).

Preterminal degeneration in the brain stem of these animals was studied in transverse (C-890, C-926, and C-931) and horizontal (C-899 and C-927) sections stained by the Nauta and Gyax technic. Observations made in these animals can be presented in a composite manner because of their uniformity (fig. 7).

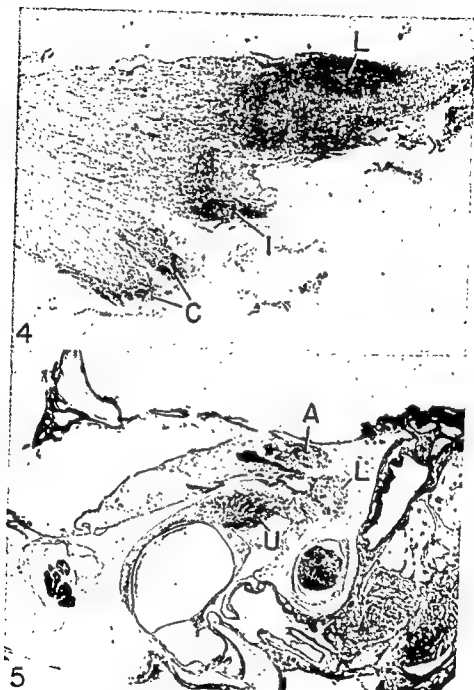


Fig. 4 Rhesus C-869. Photomicrograph of the right vestibular ganglia demonstrating a large electrolytic lesion (L) destroying the superior vestibular ganglion. The intact cells of the inferior vestibular ganglion (I) and a portion of the cochlear nerve (C) lie ventrally. Nissl $\times 15$.

Fig. 5 Rhesus C-926. Photomicrograph of the right petrous bone cut in the longitudinal axis of the vestibular nerve. A discrete lesion of the dorsolateral part of the superior vestibular ganglion produced peripheral degeneration in the fibers of the anterior (A) and lateral (L) canal nerves. Intact fibers supplying the utricle are designated by U. A part of the saccular epithelium is seen in cross section below the utricular fibers. Sudan black B $\times 15$.

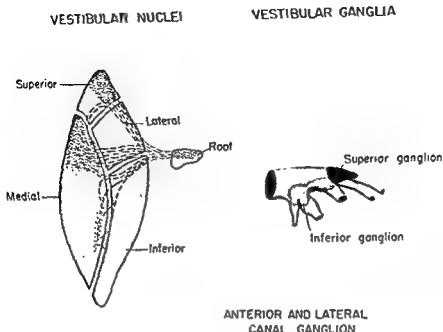


Fig. 7 Diagrammatic representation of the central distribution of degeneration resulting from a partial lesion in the superior vestibular ganglion destroying cells which innervate the cristae of the anterior and lateral canals. An example of degeneration in these canal nerves is shown in figure 5. For diagrammatic orientation, see figures 1 and 6. Note that the most profuse central degeneration is present in the superior vestibular nucleus and in rostral parts of the medial vestibular nucleus.

vestibular ganglion. Although the lesions in these animals destroyed exclusively inferior and medial cell groups within the superior vestibular ganglion, both lesions involved, to a small extent, cell groups in the junctional area between the two vestibular ganglia. It was virtually impossible to produce a lesion of any size in the utricular cell group without involving some cells in the junctional zone. The lesion in rhesus C-950 (L) appeared to destroy the entire cell group providing innervation for the macula of the utricle and spared cell groups innervating the cristae of the anterior and lateral canals (fig. 15). A smaller electrolytic lesion in rhesus C-955 (R) destroyed portions of the utricular ganglion and infringed upon the saccular ganglion (fig. 14).

Sections of the brain stem were cut horizontally [C-950 (L)] and transversely

[C-955 (R)]. Fiber degeneration in the vestibular root on the side of the lesion occupied a central band in horizontal sections which corresponded to the caudal part of the superior division of the root. Cells of the interstitial nucleus in this region were surrounded by degenerated fibers. A much smaller and less impressive group of degenerated fibers were seen in the caudal and medial parts of the vestibular root; these appeared to be fibers associated with the saccule.

Degenerated vestibular fibers at the root entry zone traversed ventral parts of the lateral vestibular nucleus, except for certain small fascicles that passed through lateral portions of the nucleus toward the superior vestibular nucleus. Relatively modest degeneration entered the superior vestibular nucleus ventrolaterally and arborized about some of the large cells in

Degenerated fibers within the vestibular nerve root were confined to rostral and lateral regions, but occupied a smaller fraction of the whole vestibular root than that described for total lesions of the superior vestibular ganglion (figs. 9, 23). In the four animals with lesions associated with complete degeneration in the anterior canal nerve and partial degeneration in the lateral canal nerve, central degeneration within the vestibular root was greatest in the most rostral part of the root and somewhat less laterally. These observations suggest that central fibers associated with the anterior canal are located most rostrally within the vestibular root, while those associated with the lateral canal are located rostromedially.

The most rostral degenerated fibers of the root retained this position upon entering the vestibular complex: fibers skirted and traversed dorsolateral parts of Deiters' nucleus *en route* to the superior vestibular nucleus. These fascicles entered the superior vestibular nucleus ventrolaterally and were distributed primarily to rostromedial parts of the nucleus (fig. 29). The majority of the fibers arborized extensively about large cells present in this region. Medial parts of the superior vestibular nucleus contained less degeneration, although a few fascicles of degenerated fibers frequently coursed along the ventral border of this nucleus toward the rostral pole of the medial vestibular nucleus. Caudal parts of the superior vestibular nucleus contained less profuse degeneration.

In sections through the central portion of the vestibular nerve root, degenerated fibers were confined to the lateral regions. At this location degenerated fibers coursed through ventral parts of the lateral vestibular nucleus and entered the medial vestibular nucleus. Degeneration within the medial vestibular nucleus, located mainly in dorsolateral regions, was profuse only in parts of the nucleus at, and above, the root entry zone. Notable arborizations of primary vestibular fibers frequently were seen about collections of relatively large cells in central parts of the nucleus (figs. 26, 35). Caudal to the vestibular root degeneration in the medial vestibular nu-

cleus was greatly reduced, and largely confined to lateral regions. While a modest number of primary vestibular fibers descended within this nucleus, most fibers entering caudal portions of the nucleus appeared to be given off from fascicles descending in the inferior vestibular nucleus.

Centrally projecting fibers from these partial lesions of the superior vestibular ganglia were relatively modest in the inferior vestibular nucleus. Descending fibers, traversing ventral and caudal parts of the lateral vestibular nucleus, entered the medial part of the inferior vestibular nucleus. Most of these descending fibers maintained this general position, giving off small groups of fibers to the medial vestibular nucleus at various locations. No primary vestibular fibers entered cell group f and none left the vestibular nuclear complex to enter adjacent cell groups.

The lateral vestibular nucleus was traversed ventrally by primary vestibular fibers passing to the medial and inferior vestibular nuclei, but few of these fibers established intimate relationships with cells of this nucleus.

Primary vestibular fibers in these animals entering portions of the interstitial nucleus of the vestibular nerve were located rostrally and laterally; other portions of this nucleus were free of degeneration.

The above observations suggested that the central projections of cell groups innervating the cristae of the anterior and lateral canals are predominantly to: (1) rostral and lateral portions of the superior vestibular nucleus, and (2) portions of the medial vestibular nucleus at, and above, the root entry zone. Even though the central distribution of these fibers is differential, some primary vestibular fibers from these canal nerves project to all subdivisions of the vestibular nuclear complex. No degenerated primary vestibular fibers from these partial lesions of the superior vestibular ganglion were observed to enter the accessory cuneate nucleus.

Portion innervating the macula of the utricle. In two animals [C-950 (L) and C-955 (R)] localized lesions were produced in the utricular part of the superior

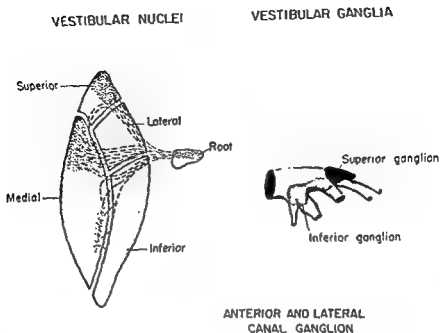


Fig. 7 Diagrammatic representation of the central distribution of degeneration resulting from a partial lesion in the superior vestibular ganglion destroying cells which innervate the cristae of the anterior and lateral canals. An example of degeneration in these canal nerves is shown in figure 5. For diagrammatic orientation, see figures 1 and 6. Note that the most profuse central degeneration is present in the superior vestibular nucleus and in rostral parts of the medial vestibular nucleus.

vestibular ganglion. Although the lesions in these animals destroyed exclusively inferior and medial cell groups within the superior vestibular ganglion, both lesions involved, to a small extent, cell groups in the junctional area between the two vestibular ganglia. It was virtually impossible to produce a lesion of any size in the utricular cell group without involving some cells in the junctional zone. The lesion in rhesus C-950 (L) appeared to destroy the entire cell group providing innervation for the macula of the utricle and spared cell groups innervating the cristae of the anterior and lateral canals (fig. 15). A smaller electrolytic lesion in rhesus C-955 (R) destroyed portions of the utricular ganglion and infringed upon the saccular ganglion (fig. 14).

Sections of the brain stem were cut horizontally [C-950 (L)] and transversely

[C-955 (R)]. Fiber degeneration in the vestibular root on the side of the lesion occupied a central band in horizontal sections which corresponded to the caudal part of the superior division of the root. Cells of the interstitial nucleus in this region were surrounded by degenerated fibers. A much smaller and less impressive group of degenerated fibers were seen in the caudal and medial parts of the vestibular root; these appeared to be fibers associated with the saccule.

Degenerated vestibular fibers at the root entry zone traversed ventral parts of the lateral vestibular nucleus, except for certain small fascicles that passed through lateral portions of the nucleus toward the superior vestibular nucleus. Relatively modest degeneration entered the superior vestibular nucleus ventrolaterally and arborized about some of the large cells in

the central region. A few distinct bundles of degenerated fibers passed along the lateral surface of the superior cerebellar peduncle while others entered the cerebellum via the juxtarestiform body.

Profuse degeneration was present in ventral parts of the lateral vestibular nucleus. A large part of these degenerated fibers appeared to merely traverse this nucleus, and descended in medial and central regions of the inferior vestibular nucleus. These degenerated fibers were arranged in fascicles which in horizontal sections could be followed for a considerable distance. Collaterals from these descending bundles passed medially into lateral parts of the medial vestibular nucleus. At various places descending fibers appeared to arborize about clusters of neurons. While degeneration was most profuse in the medial parts of the inferior vestibular nucleus, some degenerated fibers also were seen in dorsolateral regions. Degenerated fibers occupying dorsolateral

parts of the inferior vestibular nucleus appeared to be associated with fibers occupying the most caudal and medial part of the vestibular root. Evidence from other animals [C-928 (L) and C-955 (L)] suggested that these descending fibers probably were associated with the saccule.

Degeneration within the medial vestibular nucleus was located in dorsolateral regions of the nucleus; most of this degeneration was present at the root entry zone and in caudal parts of the nucleus. Fibers reaching caudal parts of the nucleus appeared to be derived largely from fascicles descending in the inferior vestibular nucleus. Oral parts of the medial vestibular nucleus were virtually free of degeneration (fig. 8).

The principal difference in the distribution of the central degeneration in rhesus C-950 (L) and C-955 (R) was that in rhesus C-955 (R) there was: (1) greater descending degeneration in the dorsolateral part of the inferior vestibular nucleus,

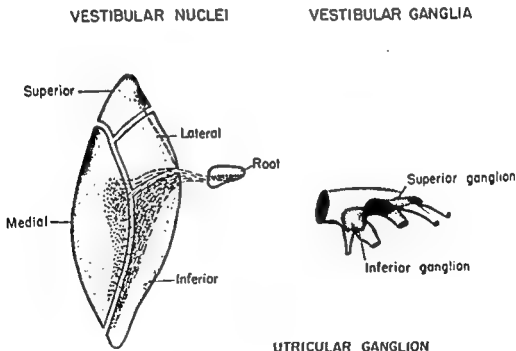


Fig. 8 Diagrammatic representation of the central distribution of degeneration within the vestibular nuclei resulting from a partial lesion of the superior vestibular ganglion destroying cells which innervate the macula of the utricle. Examples of lesions of this type are shown in figures 14 and 15. For diagrammatic orientation see figures 1 and 6. Note that the central degeneration is most profuse in the inferior and medial vestibular nuclei at, and below, the root entry zone.

and (E) more profuse degeneration in caudal parts of the medial vestibular nucleus. In both of these animals descending primary vestibular fibers passed caudally beyond the confines of the inferior vestibular nucleus to enter the accessory cuneate nucleus (fig. 36).

Lesions of the inferior vestibular ganglion

Portion innervating the macula of the saccule. Electrolytic lesions in two animals were produced in portions of the inferior vestibular ganglion considered to innervate the macula of the saccule. Lesions in rhesus C-928 (L) destroyed virtually all cells in this region of the ganglion. Lesions in rhesus C-955 (L) destroyed all of the cell group considered to innervate the macula of the saccule and about half of the cells giving rise to the posterior canal nerve (fig. 16). Lesions in both of these animals were confined to the inferior vestibular ganglion and did not appear to involve cells in the junctional zone.

Less well localized lesions in two other animals [C-945 (L) and C-949 (L)] destroyed parts of the cell group innervating the macula of the saccule but also involved ventral and medial parts of the superior vestibular ganglion (i.e., utricular region) to a lesser extent.

Nauta-stained sections of the brain stem were cut horizontally [C-928 (L) and C-945 (L)] and transversely [C-949 (L) and C-955 (L)].

Degeneration resulting from the lesion in C-928 (L) occupied the most caudal portion of the vestibular root (fig. 10). Upon reaching the vestibular nuclei, the majority of the degenerated fibers entered the dorsolateral part of the inferior vestibular nucleus without projecting in any appreciable numbers in the lateral vestibular nucleus (fig. 30). A smaller fascicle of degenerated fibers passed directly medial at caudal levels of the root entry zone; these fibers traversed ventrocaudal portions of the lateral vestibular nucleus and oral parts of the inferior vestibular nucleus in their passage to the lateral portions of the medial vestibular nucleus. There was none of the profuse degeneration in the rostral part of the medial vestibular nucleus char-

acteristically seen with lesions of the superior vestibular ganglion (fig. 11).

The most impressive degeneration seen descended in the dorsolateral part of the inferior vestibular nucleus. Degenerated fibers in this location extended throughout the rostrocaudal length of the inferior vestibular nucleus diminishing gradually at successively caudal levels. Distinct collections of degenerated fibers arborized about groups of cells in various locations, suggesting terminal arborizations. Medial and ventral regions of the inferior vestibular nucleus were virtually free of degeneration in this animal. Even though degenerated fibers in the inferior vestibular nucleus descended for long distances, none of the degenerated fibers was observed to pass beyond the vestibular nuclear complex. No degeneration was present in cell groups x or z and none was found in the accessory cuneate nucleus.

A small fascicle of degenerated fibers left the root entry zone and passed along the dorsolateral aspect of the lateral vestibular nucleus to arborize sparsely about the large cells in the centrolateral parts of the superior vestibular nucleus. In addition a few of these fibers passed through the lateral portions of the superior vestibular nucleus to enter the juxtarestiform body in a projection toward the cerebellum.

In rhesus C-955 (L) degeneration was confined to the caudal third of the vestibular root in a pattern suggesting incomplete degeneration of the inferior vestibular division (fig. 22). Degeneration within the vestibular nuclear complex was virtually identical with that described for rhesus C-928 (L) except for distinct areas of degeneration in: (1) the medial part of the superior vestibular nucleus, and (2) in the oral pole of the medial vestibular nucleus. The major descending degeneration was well localized to the dorsolateral part of the inferior vestibular nucleus. A few collaterals from these descending fascicles passed into lateral parts of the medial vestibular nucleus caudal to the root entry zone.

The lesions produced in rhesus C-945 (L) and C-949 (L) involved portions of the vestibular ganglia which innervate both the maculae of the saccule and the utricle, but the major part of these lesions involved

cell groups associated with the innervation of the sacculle.

In the vestibular root two separate bands of degeneration were found: (1) one located in the most caudal portion of the root similar to that described in rhesus C-928 (L), and (2) another band located at the junction of the posterior and middle thirds of the root, similar to that described in rhesus C-950 (L). The degeneration within the vestibular nuclei was qualitatively similar to that seen in C-928 (L), except for certain additions. At the mid-root entry zone, degenerated fibers traversed ventral portions of the lateral vestibular nucleus to end sparsely in the rostral parts of the medial vestibular nucleus. Degeneration in the inferior vestibular nucleus was more diffuse. Although the principal degeneration occupied the dorsolateral parts of the inferior vestibular nucleus, descending fascicles also were found in other parts of the nucleus. Medially projecting fibers from these descending bundles entered parts of the medial vestibular nucleus caudal to the root entry zone. Some degenerated fibers entered ventral parts of the lateral vestibular nucleus from which location they passed primarily to central parts of the superior vestibular nucleus. Oral parts of the medial vestibular nucleus contained little degeneration.

A small number of degenerated fibers passing from the inferior vestibular nucleus entered the oral pole of the accessory cuneate nucleus.

Portion innervating the crista of the posterior canal. Electrolytic lesions in three animals were produced in that portion of the inferior vestibular ganglion considered to innervate the crista of the posterior canal. These lesions, produced by exposures of the ganglion made through the mastoid region, destroyed approximately 25% of the cell group innervating the crista of the posterior canal in rhesus C-929 (L) and C-950 (R). A larger lesion in rhesus C-926 (L) destroyed virtually all cells which give rise to fibers of the posterior canal nerve and a small portion of those that innervate the sacculle (fig. 17). Sections of the brain stem were cut transversely [C-926 (L)] and horizontally [C-929 (L) and C-950 (R)]. Preterminal degeneration resulting from these lesions was

qualitatively similar and can be described in a composite fashion (fig. 12).

Degenerated fibers from that portion of the inferior vestibular ganglion giving rise to the posterior canal nerve, occupied a distinctive position within the vestibular root. These fibers formed a narrow band in the oral part of the caudal third of the vestibular nerve root (fig. 24). In transverse sections degenerated fibers passed obliquely from lateral to medial within the vestibular root as it entered the brain stem (fig. 20). These fibers maintained this medial position within the vestibular root throughout the intra-axial entry zone. As degenerated fibers reached the vestibular nuclear complex, a relatively large bundle of fibers coursed dorsally through central portions of the lateral vestibular nucleus and entered predominantly medial regions within the superior vestibular nucleus (fig. 28). The course and distribution of these fibers differed from that of fibers emanating from portions of the superior vestibular ganglion innervating the anterior and lateral canal nerves in that: (1) the number of degenerated fibers was appreciably less, (2) fibers passed more medially through Delters' nucleus, and (3) the areas of terminal arborization within the superior vestibular nucleus were more medial and caudal than those of the anterior and lateral canal nerves. Although these fibers passed to more medial parts of the superior vestibular nucleus, good quality preterminal arborizations were seen in the medial part of the large-celled central neurons (fig. 32).

From the root entry zone a modest number of degenerated fibers fanned out into ventral and caudal parts of the lateral vestibular nucleus (fig. 34). From this location fibers projected to: (1) medium-sized cells in rostral and lateral parts of the medial vestibular nucleus, and (2) rostro-medial portions of the inferior vestibular nucleus. These fibers seemed to be located in more dorsal regions than similar central fibers associated with the cristae of the anterior and lateral canals. Degenerated fibers in the areas described above tended to arborize in terminal fashion about larger cells. Only sparse degeneration was seen in caudal parts of the medial vestibular nucleus.

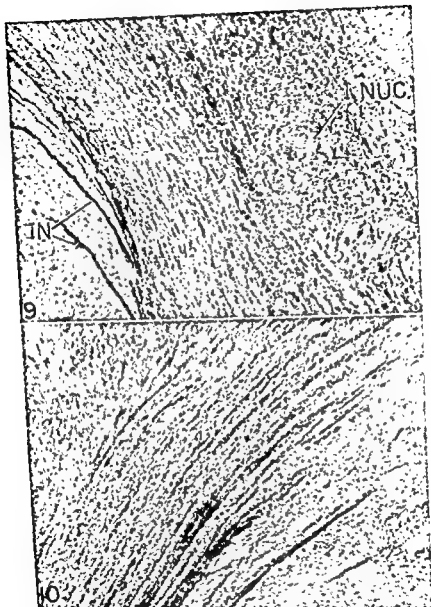


Fig. 9 Rhesus C-926. Photomicrograph of partial degeneration in the right vestibular nerve root resulting from a lesion of the superior vestibular ganglion destroying cells which innervate the cristae of the anterior and lateral canals. The lesion in the superior vestibular ganglion is shown in figure 18. Degeneration in the vestibular root was confined to rostro-lateral regions. Profuse preterminal degeneration is seen in that part of the interstitial nucleus (I. Nuc.) of the vestibular nerve surrounded by degenerated fibers. Degenerated fibers on the left are those of the intermediate nerve (IN) coursing through the spinal trigeminal tract. Nauta-Gygax $\times 95$.

Fig. 10 Rhesus C-955. Photomicrograph of partial degeneration in the caudal part of the left vestibular root resulting from a lesion (fig. 16) destroying cells of the inferior vestibular ganglion which innervate the macula of the saccule. These degenerated fibers occupied the most medial and caudal part of the vestibular root. Nauta-Gygax $\times 60$.

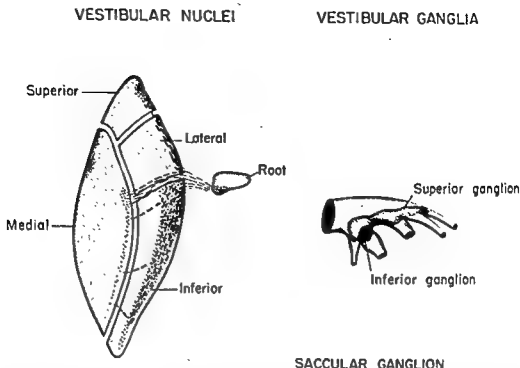


Fig. 11 Diagrammatic representation of the distribution of central degeneration within the vestibular nuclei resulting from a lesion of the inferior vestibular ganglion destroying cells which innervate the macula of the saccule. An example of this type of lesion is shown in figure 16. For diagrammatic orientation, see figures 1 and 6. The most abundant central degeneration resulting from this type of lesion is present in the dorsolateral part of the inferior vestibular nucleus.

An exception to the above pattern of fiber distribution was seen in the inferior vestibular nucleus in rhesus C-926 (L). In this animal a significant number of degenerated fibers descended in the dorsal part of the inferior vestibular nucleus. Quantitative and qualitative differences in these animals suggested that most of the descending degeneration seen in rhesus C-926 (L) was related to destruction of cells in the saccular portion of the inferior vestibular ganglion. This conclusion was supported by observations made in rhesus C-928 (L) where the saccular portion of the inferior vestibular ganglion was destroyed selectively.

Observations made in these animals suggested that relatively few central fibers, from cells innervating the crista of the posterior canal, terminate in the lateral vestibular nucleus. Most of the central fibers from this part of the inferior vestibular ganglion appeared to merely traverse parts of the lateral vestibular nucleus.

DISCUSSION

Most authors (Alexander, '01; DeBurler, '24; Lorente de N6, '31, '33; Shute, '51; Gacek, '66) accept the anatomical evidence that localized cell groups within the vestibular ganglia give rise to fibers that innervate particular parts of the labyrinth, as described in the introduction. Anatomical evidence supporting this organization within the vestibular ganglia is based upon studies of normal specimens using a variety of histological techniques. The most convincing data are based upon Golgi-stained preparations (Lorente de N6, '33). It would appear from the present study that precise information concerning the cells of origin of particular branches of the vestibular ganglion cannot be obtained by the retrograde cell technic. Surgical section of individual branches of the vestibular ganglion did not produce reliable retrograde cell changes within the ganglia. Thus the bipolar cells of the vestibular ganglia react differently than the pseudo-unipolar cells of

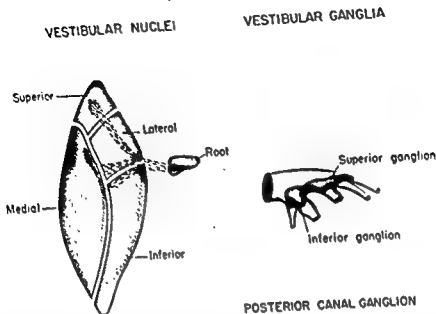


Fig 12 Diagrammatic representation of the distribution of central degeneration in the vestibular nuclei resulting from a lesion in the inferior vestibular ganglion destroying cells innervating the crista of the posterior canal. An example of a lesion of this type is shown in figure 17. For diagrammatic orientation see figures 1 and 6. The principal central degeneration from this type of lesion was found in the superior and medial vestibular nuclei.

the dorsal root ganglia (Hare and Hinsey, '40) and some cranial nerve ganglia (Amarillo, 1898; Yagita, '14).

Cells of the vestibular ganglion have been described as having two axons (Wersäll, '50), one peripheral and one central. This description conforms with the views of Bodian ('62) in his discussion of the generalized vertebrate neuron in which he regards the axon as only an elongated cytoplasmic extension that conducts the nerve impulse away from the dendritic zone. According to this thesis, dendrites are defined as neural processes concerned with response generator function. Thus in the case of the bipolar cells of the vestibular ganglion, axons occur on both sides of the cell body. Although the retrograde cell technique is the preferred experimental method for determining the origin of particular bundles of nerve fibers, another method must be used for the vestibular ganglia.

The method used in the current study was to produce small electrolytic lesions

in portions of the vestibular ganglia and to trace the resulting degeneration both peripherally and centrally. While the Sudan black B stain (Rasmussen, '61) used for study of peripheral degeneration is less specific than the Nauta and Gyax ('54) method, it offered the advantage of studying degenerated nerve fibers in serial sections of the petrous bone. Thus degenerated fibers could be traced into the specialized sensory epithelium of different parts of the labyrinth. This study of the central projections of portions of the vestibular ganglia using the Nauta and Gyax method was based on the premise that if lesions could be produced in localized parts of the ganglia and evaluated critically, it would be possible to determine experimentally the central projections of different parts of the ganglia. The disadvantage of this type of experiment is the technical difficulty of reproducing identical lesions in different animals.

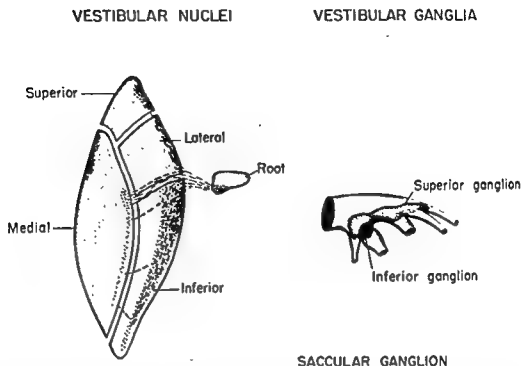


Fig. 11 Diagrammatic representation of the distribution of central degeneration within the vestibular nuclei resulting from a lesion of the inferior vestibular ganglion destroying cells which innervate the macula of the saccule. An example of this type of lesion is shown in figure 16. For diagrammatic orientation, see figures 1 and 6. The most abundant central degeneration resulting from this type of lesion is present in the dorsolateral part of the inferior vestibular nucleus.

An exception to the above pattern of fiber distribution was seen in the inferior vestibular nucleus in rhesus C-926 (L). In this animal a significant number of degenerated fibers descended in the dorsal part of the inferior vestibular nucleus. Quantitative and qualitative differences in these animals suggested that most of the descending degeneration seen in rhesus C-926 (L) was related to destruction of cells in the saccular portion of the inferior vestibular ganglion. This conclusion was supported by observations made in rhesus C-928 (L) where the saccular portion of the inferior vestibular ganglion was destroyed selectively.

Observations made in these animals suggested that relatively few central fibers, from cells innervating the crista of the posterior canal, terminate in the lateral vestibular nucleus. Most of the central fibers from this part of the inferior vestibular ganglion appeared to merely traverse parts of the lateral vestibular nucleus.

DISCUSSION

Most authors (Alexander, '01; DeBurlet, '24; Lorente de N6, '31, '33; Shute, '51; Gacek, '66) accept the anatomical evidence that localized cell groups within the vestibular ganglia give rise to fibers that innervate particular parts of the labyrinth, as described in the introduction. Anatomical evidence supporting this organization within the vestibular ganglia is based upon studies of normal specimens using a variety of histological techniques. The most convincing data are based upon Golgi-stained preparations (Lorente de N6, '33). It would appear from the present study that precise information concerning the cells of origin of particular branches of the vestibular ganglion cannot be obtained by the retrograde cell technique. Surgical section of individual branches of the vestibular ganglion did not produce reliable retrograde cell changes within the ganglia. Thus the bipolar cells of the vestibular ganglia react differently than the pseudo-unipolar cells of

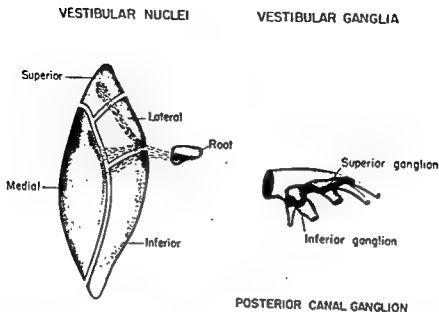


Fig. 12 Diagrammatic representation of the distribution of central degeneration in the vestibular nuclei resulting from a lesion in the inferior vestibular ganglion destroying cells innervating the crista of the posterior canal. An example of a lesion of this type is shown in figure 17. For diagrammatic orientation see figures 1 and 6. The principal central degeneration from this type of lesion was found in the superior and medial vestibular nuclei.

the dorsal root ganglia (Hare and Hinsey, '40) and some cranial nerve ganglia (Amabilino, 1898; Yagita, '14).

Cells of the vestibular ganglion have been described as having two axons (Wersäll, '60), one peripheral and one central. This description conforms with the views of Bodian ('62) in his discussion of the generalized vertebrate neuron in which he regards the axon as only an elongated cytoplasmic extension that conducts the nerve impulse away from the dendritic zone. According to this thesis, dendrites are defined as neural processes concerned with response generator function. Thus in the case of the bipolar cells of the vestibular ganglion, axons occur on both sides of the cell body. Although the retrograde cell technique is the preferred experimental method for determining the origin of particular bundles of nerve fibers, another method must be used for the vestibular ganglia.

The method used in the current study was to produce small electrolytic lesions

in portions of the vestibular ganglia and to trace the resulting degeneration both peripherally and centrally. While the Sudan black B stain (Rasmussen, '61) used for study of peripheral degeneration is less specific than the Nauta and Gyax ('54) method, it offered the advantage of studying degenerated nerve fibers in serial sections of the petrous bone. Thus degenerated fibers could be traced into the specialized sensory epithelium of different parts of the labyrinth. This study of the central projections of portions of the vestibular ganglia using the Nauta and Gyax method was based on the premise that if lesions could be produced in localized parts of the ganglia and evaluated critically, it would be possible to determine experimentally the central projections of different parts of the ganglia. The disadvantage of this type of experiment is the technical difficulty of reproducing identical lesions in different animals.

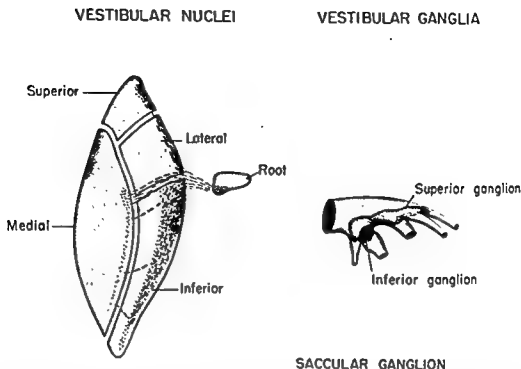


Fig. 11. Diagrammatic representation of the distribution of central degeneration within the vestibular nuclei resulting from a lesion of the inferior vestibular ganglion destroying cells which innervate the macula of the saccule. An example of this type of lesion is shown in figure 16. For diagrammatic orientation, see figures 1 and 6. The most abundant central degeneration resulting from this type of lesion is present in the dorsolateral part of the inferior vestibular nucleus.

An exception to the above pattern of fiber distribution was seen in the inferior vestibular nucleus in rhesus C-926 (L). In this animal a significant number of degenerated fibers descended in the dorsal part of the inferior vestibular nucleus. Quantitative and qualitative differences in these animals suggested that most of the descending degeneration seen in rhesus C-926 (L) was related to destruction of cells in the saccular portion of the inferior vestibular ganglion. This conclusion was supported by observations made in rhesus C-928 (L) where the saccular portion of the inferior vestibular ganglion was destroyed selectively.

Observations made in these animals suggested that relatively few central fibers, from cells innervating the crista of the posterior canal, terminate in the lateral vestibular nucleus. Most of the central fibers from this part of the inferior vestibular ganglion appeared to merely traverse parts of the lateral vestibular nucleus.

DISCUSSION

Most authors (Alexander, '01; DeBurlet, '24; Lorente de N6, '31, '33; Shute, '51; Gacek, '66) accept the anatomical evidence that localized cell groups within the vestibular ganglia give rise to fibers that innervate particular parts of the labyrinth, as described in the introduction. Anatomical evidence supporting this organization within the vestibular ganglia is based upon studies of normal specimens using a variety of histological techniques. The most convincing data are based upon Golgi-stained preparations (Lorente de N6, '33). It would appear from the present study that precise information concerning the cells of origin of particular branches of the vestibular ganglion cannot be obtained by the retrograde cell technic. Surgical section of individual branches of the vestibular ganglion did not produce reliable retrograde cell changes within the ganglia. Thus the bipolar cells of the vestibular ganglia react differently than the pseudo-unipolar cells of

markedly similar to the arrangement of specific cell groups in the vestibular ganglia. There is however a rotation, so that central processes of cells of the superior vestibular ganglia become rostral in the root and fibers from the inferior vestibular ganglia occupy caudal parts of the root.

It seems generally accepted (Koelliker, 1891; Held, 1892; Cajal, '09; Lorente de N6, '33) that virtually all primary vestibular fibers bifurcate into ascending and descending branches upon entering the vestibular nuclear complex. From studies (Walberg, Bowsher and Brodal, '58) of labyrinthectomized cats, it is known that primary vestibular fibers are distributed only to specific parts of each vestibular nucleus. Using the Golgi technic Lorente de N6 ('33) divided primary vestibular fibers into five groups on the basis of fiber size. With painstaking analysis this author was able not only to follow fibers from specific parts of the labyrinth to discrete portions of Scarpa's ganglion, but to determine the central distribution of these fibers within the vestibular nuclei. This formidable task is impressive considering the range of fiber size within the vestibular nerve. Fiber sizes within the vestibular nerve have been estimated differently by various authors (2-9 μ , Engstr6m and Rexed, '40; 1-9 μ , Wers6ll, '56; 2-5 μ , Gacek and Rasmussen, '61), but approximately 65% of the fibers fall within the 3-5 μ range (Wers6ll, '56). Since both the cristae and maculae are innervated by thick and thin fibers, an analysis of the central projections of fibers from particular parts of the labyrinth by the Golgi technic would seem to be exceedingly difficult. From this complex study of the central projections of vestibular fibers Lorente de N6 ('33) concluded: "The semicircular canals and the maculae have partly different and partly common central representation." It appears of special interest that he found fibers from both maculae to have an extremely similar central distribution.

According to Lorente de N6 ('33), bipolar ganglion cells innervating the cristae of the semicircular canals project ascending central branches to the superior vestibular nucleus (nucleus of Bechterew) and the nucleus vestibulo-cerebellousus. There is considerable doubt as to what is meant by

the term nucleus vestibulo-cerebellousus, which he refers to as a complex, but this seems to be a nucleus located between the vestibular nuclei and the intrinsic cerebellar nuclei. Descending branches of group I and II fibers from the semicircular canals are described as entering the inferior vestibular nucleus, with group I fibers lateral and group II fibers medial and ventral. Group II fibers are described as giving off short collaterals within the inferior vestibular nucleus and longer collaterals that sweep upward into the medial vestibular nucleus (nucleus angularis). All fibers of group I are reported to project collaterals in a medial direction with some ending in the inferior vestibular nucleus, and other longer and thicker fibers entering the medial vestibular nucleus, especially in dorsal regions.

Comparison of these findings with those of the current study indicates agreement with respect to the ascending branches of root fibers which appear to end mainly about large cells of the superior vestibular nucleus. Cells innervating the cristae of the anterior and lateral canals have central processes which appear to terminate in more rostral and lateral regions of the superior vestibular nucleus. Central fibers related to the crista of the posterior canal are distributed to medial and caudal regions of this nucleus. These data suggest that some central fibers related to the crista of each of the semicircular canals may be distributed to distinctive regions of the superior vestibular nucleus in a definite pattern.

The current study indicates that the central processes of cells innervating the cristae also have an important distribution within the oral part of the medial vestibular nucleus which seemed to be shared in common fashion. Most of these fibers traverse ventral parts of the lateral vestibular nucleus and oral portions of the inferior vestibular nucleus. Nauta-Gygax stained sections suggest that some of these fibers probably end in oral parts of the inferior vestibular nucleus. A smaller group of primary vestibular fibers related to the cristae descends in the inferior vestibular nucleus. Collaterals from these descending fibers project into dorsal parts of the medial vestibular nucleus. There appears to be little

Although experimental studies of the termination of primary vestibular fibers (Walberg, Bowsher and Brodal, '58) provide precise data concerning the selective distribution of these fibers in parts of the vestibular nuclei, they do not provide information concerning the central projections of cells innervating particular parts of the labyrinth. One important finding brought out by their study and that of Lorente de Nó ('33) is that primary vestibular afferents do not supply the entire territory of the four vestibular nuclei.

Physiological studies of the labyrinth have contributed greatly to our understanding of the function of this complex receptor, but relatively few studies have contributed information concerning the central projections of particular parts of the labyrinth. It is well known that a continuous barrage of afferent impulses reaches the vestibular nuclei even when an animal is at complete rest. Further, considerable activity in the vestibular nuclei remains after labyrinthectomy (Lorente de Nó, '26; Spiegel and Sato, '26) or after section of the vestibular nerve (Gernandt and Thulin, '52; DeVito, Brusa and Arduini, '56). However, spontaneous activity of single units in the vestibular nuclei can be modified by different forms of labyrinthine stimulation. The study of Adrian ('43) in the cat indicated that horizontal rotation of the head induced discharges in the oral part of the vestibular complex, while lateral tilting of the head and rotation in a transverse plane produced discharges in more caudal parts of the complex. Unfortunately, no attempts were made to localize histologically the units responding to these different forms of stimulation. According to Eckel ('54), neurons in the lateral and medial vestibular nuclei discharge in the rabbit in response to horizontal rotations, suggesting that some fibers from the crista of the lateral canal may reach portions of these nuclei. According to Kumoi, Hosomi and Matsumura ('63) stimulation of the ampullary nerve from the lateral canal evoked maximal potentials of short latency in the ipsilateral medial vestibular nucleus. These potentials were recorded in lateral parts of the medial vestibular nucleus near the root entry zone.

It is of great interest that in clinical studies of organic lesions of the vestibular system in man certain authors (Carmichael, Dix and Hallpike, '56, '65) have been able to postulate that specific labyrinthine functions probably are represented in different regions of the vestibular nuclear complex. These authors reported, "Thus, the tonus elements are found to be linked with those parts of the nuclei, in particular the lower part of the medial nucleus, which lie below the point of entry of the eighth nerve, while the canal elements are linked with those parts of the nuclei which lie above this level."

Lorente de Nó ('31) in his studies of the vestibular ganglia in the mouse and cat noted that cells innervating the cristae of the semicircular canals were widely separate, but that the central fibers of these cells merged into a common bundle in the most rostral part of the vestibular root. Central fibers from cells innervating the macula of the utricle were located caudal to those of the semicircular canals. The most caudally situated fibers in the vestibular root were those innervating the macula of the saccule. Observations made in the current study suggest a different arrangement in the monkey, even though basic similarities are obvious. Central fibers from cells of the superior vestibular ganglion innervating the anterior and lateral canals occupy rostral and lateral portions of the vestibular root. Our data suggest, but do not prove, that fibers from cells associated with the anterior canal probably occupy the extreme rostral position within the vestibular root. Cells of the inferior vestibular ganglion innervating the crista of the posterior canal do not appear to join those from other canals in any common bundle. Instead, these fibers are located in the anterior part of the caudal third of the vestibular root and tend to be concentrated most medially. In the monkey, fibers from cells innervating the macula of the utricle lie caudal to those related to the cristae of the anterior and lateral canals. Central fibers from cells supplying the macula of the saccule are located in the most caudal and medial part of the root. This orderly arrangement of fibers within the vestibular root and initial part of the root entry zone appears re-

markedly similar to the arrangement of specific cell groups in the vestibular ganglia. There is however a rotation, so that central processes of cells of the superior vestibular ganglia become rostral in the root and fibers from the inferior vestibular ganglia occupy caudal parts of the root.

It seems generally accepted (Koelliker, 1891; Held, 1892; Cajal, '09; Lorente de N6, '33) that virtually all primary vestibular fibers bifurcate into ascending and descending branches upon entering the vestibular nuclear complex. From studies (Walberg, Bowsher and Brodal, '58) of labyrinthectomized cats, it is known that primary vestibular fibers are distributed only to specific parts of each vestibular nucleus. Using the Golgi technic Lorente de N6 ('33) divided primary vestibular fibers into five groups on the basis of fiber size. With painstaking analysis this author was able not only to follow fibers from specific parts of the labyrinth to discrete portions of Scarpa's ganglion, but to determine the central distribution of these fibers within the vestibular nuclei. This formidable task is impressive considering the range of fiber size within the vestibular nerve. Fiber sizes within the vestibular nerve have been estimated differently by various authors (2-9 μ , Engström and Rexed, '40; 1-9 μ , Wersäll, '56; 2-5 μ , Gacek and Rasmussen, '61), but approximately 65% of the fibers fall within the 3-5 μ range (Wersäll, '56). Since both the cristae and maculae are innervated by thick and thin fibers, an analysis of the central projections of fibers from particular parts of the labyrinth by the Golgi technic would seem to be exceedingly difficult. From this complex study of the central projections of vestibular fibers Lorente de N6 ('33) concluded: "The semicircular canals and the maculae have partly different and partly common central representation." It appears of special interest that he found fibers from both maculae to have an extremely similar central distribution.

According to Lorente de N6 ('33), bipolar ganglion cells innervating the cristae of the semicircular canals project ascending central branches to the superior vestibular nucleus (nucleus of Bechterew) and the nucleus vestibulo-cerebellousus. There is considerable doubt as to what is meant by

the term nucleus vestibulo-cerebellousus, which he refers to as a complex, but this seems to be a nucleus located between the vestibular nuclei and the intrinsic cerebellar nuclei. Descending branches of group I and II fibers from the semicircular canals are described as entering the inferior vestibular nucleus, with group I fibers lateral and group II fibers medial and ventral. Group II fibers are described as giving off short collaterals within the inferior vestibular nucleus and longer collaterals that sweep upward into the medial vestibular nucleus (nucleus angularis). All fibers of group I are reported to project collaterals in a medial direction with some ending in the inferior vestibular nucleus, and other longer and thicker fibers entering the medial vestibular nucleus, especially in dorsal regions.

Comparison of these findings with those of the current study indicates agreement with respect to the ascending branches of root fibers which appear to end mainly about large cells of the superior vestibular nucleus. Cells innervating the cristae of the anterior and lateral canals have central processes which appear to terminate in more rostral and lateral regions of the superior vestibular nucleus. Central fibers related to the crista of the posterior canal are distributed to medial and caudal regions of this nucleus. These data suggest that some central fibers related to the crista of each of the semicircular canals may be distributed to distinctive regions of the superior vestibular nucleus in a definite pattern.

The current study indicates that the central processes of cells innervating the cristae also have an important distribution within the oral part of the medial vestibular nucleus which seemed to be shared in common fashion. Most of these fibers traverse ventral parts of the lateral vestibular nucleus and oral portions of the inferior vestibular nucleus. Nauta-Gygax stained sections suggest that some of these fibers probably end in oral parts of the inferior vestibular nucleus. A smaller group of primary vestibular fibers related to the cristae descends in the inferior vestibular nucleus. Collaterals from these descending fibers project into dorsal parts of the medial vestibular nucleus. There appears to be little

evidence to suggest that fibers from the cristae terminate in the lateral vestibular nucleus; most of the fibers seen within this nucleus appear to be fibers of passage.

Central fibers from cells of the vestibular ganglia innervating the maculae of the utricle and saccule appear to have a very different distribution than those related to the cristae. The utricle appears to have its major central representation in the inferior vestibular nucleus. These descending fibers enter the dorsomedial part of the inferior vestibular nucleus. In their descent within this nucleus collaterals are given off to dorsolateral parts of the medial vestibular nucleus. Relatively few primary vestibular fibers related to the macula of the utricle enter oral parts of the medial vestibular nucleus or the superior vestibular nucleus, but our studies do not indicate that these areas are devoid of central fibers related to the utricle. Since lesions restricted to the utricular part of the superior vestibular ganglion proved to be the most difficult to produce, this conclusion is based in part on comparisons of preterminal degeneration resulting from: (1) lesions destroying cells related to the nerves to the anterior and lateral canals, and (2) total resection of the superior vestibular ganglion. These data, plus those derived from lesions in the utricular part of the superior vestibular ganglia, leave little doubt that most of the utricular fibers descend in the inferior vestibular nucleus. While most of the central fibers related to the utricular portion of the superior vestibular ganglion traverse ventral portions of the lateral vestibular nucleus, almost no primary vestibular fibers appear to establish intimate synaptic contacts with giant cells. Since the Nauta-Gygax technic, as used here, does not permit evaluation of terminal degeneration in regions where many fibers are in passage, no definite conclusion concerning termination of utricular fibers in the lateral vestibular nucleus is possible. According to Walberg, Bowsher and Brodal ('58), primary vestibular fibers terminate only in rostroventral regions of the lateral vestibular nucleus. In view of the observations of Lorente de N6 ('33), it seems likely that some fibers related to the utricle do end in the lateral vestibular nucleus. However, it is our impression that a

larger number of fibers from this source descend in the dorsomedial part of the inferior vestibular nucleus.

Central fibers from cells of the inferior vestibular ganglion innervating the macula of the saccule likewise largely descend in the inferior vestibular nucleus. These fibers tend to occupy dorsolateral regions of the nucleus, and smaller numbers of these fibers were observed to enter the medial vestibular nucleus, except near the root entry zone. The central pattern of distribution of primary vestibular fibers from the maculae found in this study is essentially the same as described by Lorente de N6 ('33) (fig. 13).

One observation worthy of special note concerns descending primary vestibular fibers which pass laterally beyond the vestibular nuclear complex to enter the oral pole of the accessory cuneate nucleus. Degenerated fibers entered this nucleus, whenever peripheral lesions destroyed: (1) the entire vestibular nerve, (2) the superior vestibular ganglion, or (3) the utricular region of the superior vestibular ganglion. No degeneration in the accessory cuneate nucleus was associated with partial lesions of the vestibular ganglia, providing innervation to any of the cristae of the semicircular canals or the macula of the saccule. These data indicate that descending primary vestibular fibers to the accessory cuneate nucleus arise only from the utricular portion of the superior vestibular ganglion. Since virtually all cells of the accessory cuneate nucleus project to the cerebellum (MacNalty and Horsley, '09; Grant, '62), certain afferent impulses from the utricle must be relayed to the cerebellum via this nucleus, along with group IA and IB afferents from the upper extremity and the cervical musculature. It seems likely that interactions between vestibular afferents and muscle afferents in parts of this nucleus might play an important function in tonic neck reflexes and righting reactions. It is of interest that some trigeminal, glossopharyngeal and vagal root fibers (Rhoton, O'Leary and Ferguson, '66) also have been traced to the accessory cuneate nucleus in the monkey, suggesting that this nucleus serves as a cerebellar relay nucleus for impulses from both cranial and spinal nerves.

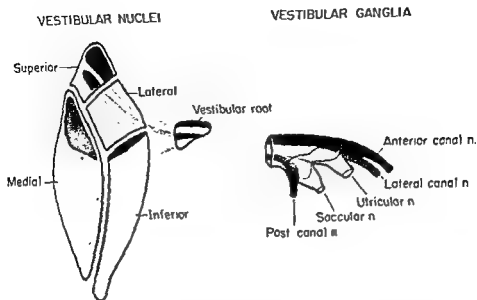


Fig. 13 Diagrammatic representation of relationships between portions of the vestibular ganglia and central projecting fibers within the vestibular nuclear complex. The vestibular ganglia and peripheral branches are shown on the right. The canal nerves and portions of the ganglia innervating the canal nerves are shown in red; the utricular part of the superior vestibular ganglion is yellow, while the saccular ganglion is in blue. On the left the vestibular nuclei and root are shown as they would appear in a horizontal section of the brain stem. Only the principal central projections of distinctive parts of the vestibular ganglia are shown. Portions of the vestibular ganglia innervating the cristae of the semicircular canals project primarily to the superior vestibular nucleus and oral parts of the medial vestibular nucleus. Portions of the vestibular ganglia innervating the macula of the utricle project primarily to parts of the medial and inferior vestibular nuclei. Central fibers from the saccular ganglion project mainly to dorsolateral parts of the inferior vestibular nucleus.

Cells of the interstitial nucleus of the vestibular nerve have been regarded as an aberrant cell group, probably belonging to the lateral vestibular nucleus (Cajal, '09; Fuse, '12; Brodal and Pompeiano, '57; Walberg, Bowsher and Brodal, '58). However, unlike the large cells of the lateral vestibular nucleus, these cells show preterminal arborization of primary vestibular fibers following lesions of the vestibular nerve (Walberg, Bowsher and Brodal, '58). These cells likewise are affected by retrograde cell changes following lesions in the medial longitudinal fasciculus (Brodal and Pompeiano, '57a), or spinal lesions (Pompeiano and Brodal, '57). Findings in the present study indicate that lesions in all parts of the vestibular ganglia produce preterminal degeneration within parts of the interstitial nucleus of the vestibular nerve. With lesions of por-

tions of the vestibular ganglia and partial degeneration of the vestibular nerve, only those parts of the interstitial nucleus situated among or within the degenerated fibers appear to have preterminal arborizations. These data suggest that different parts of the vestibular end organ probably project to specific parts of this small nucleus. Thus the interstitial nucleus may be the only nucleus of the vestibular complex to receive fibers from all parts of the end organ.

The interstitial nucleus of the vestibular nerve must be distinguished from another small group of cells located along the medial border of the vestibular root close to the ventral part of the spinal trigeminal tract. Cells of this nucleus are relatively uniformly small, and giant cells are never seen. This nucleus receives fibers from the intermediate nerve and has no con-

nections with the vestibular nerve. Rhoton, O'Leary and Ferguson ('66) have referred to this cell group as the paratrigeminal nucleus and have postulated that it may serve as a cerebellar relay nucleus. In our studies degeneration in this nucleus was present only when the intermediate nerve was injured.

The present study indicates that the central fiber projections from portions of the vestibular ganglia innervating specific parts of the labyrinth have unique as well as common areas of distribution within the vestibular nuclei. The fact that fibers related to the cristae of the semicircular canals project primarily to the superior vestibular nucleus and oral portions of the medial vestibular nucleus suggests that they probably play a dominant role in the control of eye movements. This observation would seem to conform to the conclusion reached by Brodal and Pompeiano ('57a) that ascending fibers in the medial longitudinal fasciculus are derived with some preponderance from the medial and superior vestibular nuclei. A recent physiological study (Shimazu and Precht, '65) demonstrated that second order neurons, mostly located in the superior and medial vestibular nuclei, were activated by excitation of receptors in the lateral semicircular canal. A study (Carpenter, '66; McMasters, Weiss and Carpenter, '66) of secondary vestibular fibers projecting to the nuclei of the extraocular muscles indicated that: (1) the superior vestibular nucleus gives rise to only uncrossed ascending fibers, and (2) the medial vestibular nucleus gives rise to predominantly ascending fibers which are both crossed and uncrossed. Although the lateral vestibular nucleus projects fibers to the nuclei of the extraocular muscles, these fibers appear to arise only from ventral parts of this nucleus. Relatively few ascending secondary vestibular fibers appear to arise from the inferior vestibular nucleus. Thus, these data suggest that the impulses arising in the cristae of the semicircular canals, and conveyed primarily to parts of the superior and medial vestibular nuclei, are concerned mainly with control of extraocular muscles.

The principal vestibular projection of fibers from the maculae of the utricle and

sacculle appears to coincide in part with portions of the inferior and medial vestibular nuclei which give rise to secondary vestibulocerebellar fibers (Brodal and Torvik, '57). This arrangement thus suggests that the inferior vestibular nucleus and laterocaudal parts of the medial vestibular nucleus probably are involved in the mechanism by which the otoliths influence muscle tone. Since the inferior vestibular nucleus does not project fibers to the spinal cord (Carpenter, '60a; Carpenter, Alling and Bard, '60; Nyberg-Hansen, '64) and descending ipsilateral fibers from the medial vestibular nucleus are modest in number (Nyberg-Hansen, '64; McMasters, Weiss and Carpenter, '66), it seems likely that vestibular impulses modifying muscle tone do so by relays that involve the cerebellum. On the basis of retrograde cell changes Brodal and Torvik ('57) concluded that secondary vestibulocerebellar fibers from parts of the inferior and medial vestibular nuclei project to the nodulus, the uvula, the flocculus, and the fastigial nuclei. Isolated lesions in the fastigial nucleus (Carpenter, Bard and Alling, '59) confirm that secondary vestibulocerebellar fibers arise predominantly from the inferior vestibular nucleus.

Physiological studies (DeVito, Brusa and Arduini, '56; Pompeiano and Cotti, '59) indicate that a certain number of units in the lateral vestibular nucleus do not respond to stimulation of the ipsilateral labyrinth. However, in decerebrate animals with intact cerebella, labyrinthine stimulation causes units to respond in all parts of the lateral vestibular nucleus (Pompeiano and Cotti, '59). These data suggest that a large number of units in the lateral vestibular nucleus probably are activated via impulses fed back from the cerebellum. Thus it seems likely that the otolithic portions of the labyrinth probably modify muscle tone by relaying impulses from parts of the inferior and medial vestibular nucleus to the cerebellum which, in turn, projects fibers back to the lateral vestibular nucleus via the fastigial efferent system. It is well recognized that the vestibulospinal tract, derived exclusively from cells of the lateral vestibular nucleus, is the principal pathway between the vestibular nuclei and the spinal cord (Pompe-

iano and Brodal, '57). This pathway is considered to exert facilitating influences upon postural tone and the reflex activity of the spinal cord (Brodal, Pompeiano and Walberg, '62). Recent studies (Shimazu and Precht, '65; Precht and Shimazu, '65) comparing the characteristics of "kinetic" and "tonic" vestibular neurons to vestibular nerve stimulation tend to support this thesis in that "tonic" vestibular neurons were reported to be activated by multi-synaptic mechanisms.

CONCLUSIONS

A study has been made of the central projections of portions of the vestibular ganglia recognized as innervating specific parts of the labyrinth. This investigation in the rhesus monkey was based upon: (1) the study of normal vestibular ganglia, (2) destruction of peripheral branches of the vestibular ganglia, (3) total and partial resections of the vestibular nerve and ganglia, and (4) discrete electrolytic lesions produced in localized parts of the vestibular ganglia. Degeneration resulting from discrete partial lesions in the superior and inferior vestibular ganglia was studied: (1) peripherally, in serial sections of the petrous bone decalcified and stained with Sudan black B, and (2) centrally, in representative sections throughout the vestibular nuclear complex stained by the Nauta-Gygax technic. Brain stem sections in different animals were cut in transverse and horizontal planes.

The following conclusions were drawn from this study:

1. Surgical section or destruction of peripheral branches of the vestibular ganglia in the monkey does not produce reliable retrograde cell changes in localized portions of the ganglia.

2. Vestibular root fibers arising from cells of the superior vestibular ganglion: (a) constitute approximately two-thirds of the fibers in the vestibular root, and (b) are grouped together in the rostral and lateral parts of the vestibular root. Central fibers from cells innervating the cristae of the anterior and lateral canals occupy the most rostral parts of the vestibular root, while central fibers from cells innervating the macula of the utricle are immediately caudal to these.

3. Vestibular root fibers arising from cells in the inferior vestibular ganglion: (a) constitute approximately one-third of the vestibular root, and (b) are grouped together in the caudal and medial parts of the vestibular root. Central fibers from cells innervating the crista of the posterior canal are rostral to those associated with the macula of the saccule.

4. Although central fibers from cells innervating the cristae of the semicircular canals are contained in both the superior and inferior divisions of the vestibular nerve, they have a remarkably similar principal central projection. These fibers project primarily to portions of the superior vestibular nucleus and to the oral parts of the medial vestibular nucleus. Central fibers related to the crista of the posterior canal are distributed to more medial and caudal regions of the superior vestibular nucleus.

5. Central fibers from cells innervating the macula of the utricle traverse, and give off collaterals to, ventral parts of the lateral vestibular nucleus and descend in the dorsomedial part of the inferior vestibular nucleus. Many of these fibers appear to terminate in the inferior vestibular nucleus; collaterals of these descending fibers project to the medial vestibular nucleus.

6. A small number of descending fibers from the utricular portion of the superior vestibular ganglion pass beyond the confines of the inferior vestibular nucleus and enter the accessory cuneate nucleus.

7. Central fibers from cells innervating the macula of the saccule enter the dorsolateral parts of the inferior vestibular nucleus and descend within this nucleus.

8. Some cells from the vestibular ganglia project fibers to parts of all of the four vestibular nuclei so that each specific part of the labyrinth has a unique as well as a common projection within the vestibular nuclear complex.

9. Primary vestibular fibers from all parts of the vestibular ganglia project fibers to parts of the interstitial nucleus of the vestibular nerve. With partial lesions of the vestibular ganglia, degeneration within the interstitial nucleus of the vestibular nerve is localized to that part of the nucleus situated among degenerated root fibers.

Two hypotheses are presented:

1. Central projections of cells of the vestibular ganglia innervating the cristae of the semicircular canals, passing primarily to the superior and oral parts of the medial vestibular nuclei, appear to be concerned largely with control of the extraocular muscles.

2. Central projections of cells of the vestibular ganglia innervating the maculae of the utricle and saccule, passing primarily to the inferior vestibular nucleus and caudal parts of the medial vestibular nucleus, appear to be concerned with neural mechanisms that modify muscle tone and spinal reflex activity. It seems likely that this mechanism involves secondary fibers which pass to parts of the cerebellum which, in turn, relays impulses back to the lateral vestibular nucleus.

LITERATURE CITED

- Adrian, E. D. 1943 Discharges from vestibular receptors in the cat. *J. Physiol.*, 101: 389-407.
- Alexander, G. 1901 Zur Anatomie des Ganglion Vestibulare der Säugetiere. *Arch. f. Ohrenheilk.*, 51: 109-125.
- Amabilino, R. 1898 Sul rapporto del ganglio geniculato con la corda del timpano e col faciale. *Pisani, Palermo*, 19: 123-140.
- Bodian, D. 1962 The generalized vertebrate neuron. *Science*, 137: 323-326.
- Brodal, A., and O. Pompeiano 1957 The vestibular nuclei in the cat. *J. Anat.*, 91: 438-454.
- 1957a The origin of ascending fibers of the medial longitudinal fasciculus from the vestibular nuclei. An experimental study in the cat. *Acta Morph.-Neerl.-Scand.*, 1: 306-328.
- Brodal, A., O. Pompeiano and F. Walberg 1962 The Vestibular Nuclei and Their Connections, *Anatomy and Functional Correlations*. Charles C Thomas, Springfield, Ill., 193 pp.
- Brodal, A., and A. Torvik 1957 Über den Ursprung der sekundären vestibulo-cerebellaren Fasern bei der Katze. *Arch. f. Psychiat. u. Ztschr. f. Neurol.*, 195: 550-567.
- Burlet, H. M. de 1924 Zur Innervation der Macula sacculi bei Säugetieren. *Anat. Anz.*, 58: 26-32.
- Cajal, S. R. 1909 *Histologie du Systeme Nerveux de l'Homme et des Vertébrés*. Paris, Maloine, Vol. 1, Chap. 27, 754-773.
- Carmichael, E. A., M. R. Dix and C. S. Hallpike 1956 Pathology, symptomatology and diagnosis of organic affections of the eighth nerve system. *Brit. Med. Bull.*, 12: 146-152.
- 1965 Observations upon the neurological mechanism of directional preponderance of caloric nystagmus resulting from vascular lesions of the brain-stem. *Brain*, 88: 51-74.
- Carpenter, M. B. 1960 Experimental anatomical physiological studies of the vestibular nerve and cerebellum. In *Symposium: Neural Mechanisms of the Auditory and Vestibular Systems* Ed., G. L. Rasmussen and W. F. Windle. Charles C Thomas, Springfield, Ill., Chap. 22, 297-323.
- 1960a Fiber projections from the descending and lateral vestibular nuclei in the cat. *Am. J. Anat.*, 107: 1-22.
- 1966 The ascending vestibular system and its relationship to conjugate horizontal eye movements. In: *The Vestibular System and Its Diseases*. Ed., R. J. Wolfson. University of Pennsylvania Press, Chap. 3, 69-98.
- Carpenter, M. B., F. A. Alling and D. S. Bard 1960 Lesions of the descending vestibular nucleus in the cat. *J. Comp. Neur.*, 114: 39-50.
- Carpenter, M. B., D. S. Bard and F. A. Alling 1959 Anatomical connections between the fastigial nuclei, the labyrinth and the vestibular nuclei in the cat. *J. Comp. Neur.*, 111: 1-26.
- Eckel, W. 1954 Elektrophysiologische und histologische Untersuchungen im Vestibulariskerngebiet bei Drehreizen. *Arch. Ohr., Heilk., usw. Z. Hals., usw.*, 164: 487-513.
- Engström, H., and B. Rexed 1940 Über die Kaliberverhältnisse der Nervenfasern im N. stato-acusticus des Menschen. *Z. mikr.-anat. Forsch.*, 47: 448-455.
- Fuse, G. 1912 Die innere Abteilung des Kleinhirnstieles (Meynert, I. A. K.) und der Deiters-Kern. *Arch. Hirnanat. Inst., Zurich*, 6: 29-267.
- Gacek, R. R. 1966 The vestibular efferent pathway. In: *The Vestibular System and Its Diseases*. Ed., R. J. Wolfson, University of Pennsylvania Press, Philadelphia, pp. 99-115.
- Gacek, R. R., and G. L. Rasmussen 1961 Fiber analysis of the stato-acoustic nerve of guinea pig, cat, and monkey. *Anat. Rec.*, 139: 455-463.
- Gernandt, B. E., and C. A. Thulin 1952 Vestibular connections of the brain stem. *Am. J. Physiol.*, 171: 121-127.
- Grant, G. 1962 Projections of the external cuneate nucleus onto the cerebellum in the cat: An experimental study using silver methods. *Exper. Neurol.*, 5: 179-195.
- Hare, W. K., and J. C. Hinsey 1940 Reactions of dorsal root ganglion cells to section of peripheral and central processes. *J. Comp. Neur.*, 73: 489-502.
- Held, H. 1892 Die Endigungsweise der sensiblen Nerven im Gehirn. *Arch. Anat. Physiol., Anat. Abt.*, 33-39.
- Koelliker, A. 1891 Der feinere Bau des verlängerten Markes. *Anat. Anz.*, 6: 427-431.
- Kumoi, T., H. Hosomi and H. Matsumura 1963 An analysis of the vestibular evoked potentials in response to stimulation of the ampullar nerve. *Kobe J. Med. Sci.*, 9: 79-88.
- Kurze, T., and J. B. Doyle 1962 Extradural intracranial (middle fossa) approach to the internal auditory canal. *J. Neurosurg.*, 19: 1033-1037.
- Lorente de Nó, R. 1926 Etudes sur l'anatomie de et la physiologie du labyrinthe de l'oreille et du VIII^e nerf. Part II. *Trav. du Lab. Rech. Biol., Univ. Madrid*, 24: 53-153.
- 1931 Ausgewählte Kapitel aus der vergleichenden Physiologie des Labyrinthes.

- Die Augenmuskelreflexe beim Kaninchen und ihre Grundlagen. *Ergeb. der Physiologie*, 32: 73-242.
- 1933 Anatomy of the eighth nerve. The central projection of the nerve endings of the internal ear. *Laryngoscope*, 43: 1-38.
- MacNalty, A. S., and V. Horsely 1909 On the cervical spinobulbar and spinocerebellar tracts and on the question of topographical representation in the cerebellum. *Brain*, 32: 237-255.
- McMasters, R. E., A. H. Weiss and M. B. Carpenter 1966 Vestibular projections to the nuclei of the extraocular muscles. Degeneration resulting from discrete partial lesions of the vestibular nuclei in the monkey. *Am. J. Anat.*, 118: 163-194.
- Nauta, W. J. H., and P. A. Gyax 1954 Silver impregnation of degenerating axons in the central nervous system. A modified technique. *Stain Tech.*, 29: 81-83.
- Nyberg-Hansen, R. 1964 Origin and termination of fibers from the vestibular nuclei descending in the medial longitudinal fasciculus. An experimental study with silver impregnation methods in the cat. *J. Comp. Neur.*, 122: 355-384.
- Pompeiano, O., and A. Brodal 1957 The origin of vestibulospinal fibres in the cat. *Arch. Ital. Biol.*, 95: 166-195.
- Pompeiano, O., and E. Cotti 1959 Analisi microelettronica delle proiezioni cerebellodeiteriane. *Arch. Sci. Biol.*, 43: 57-101.
- Precht, W., and H. Shimazu 1965 Functional connections of tonic and kinetic vestibular neurons with primary vestibular afferents. *J. Neurophysiol.*, 28: 1014-1028.
- Rasmussen, G. L. 1961 A method of staining the statoacoustic nerve in bulk with Sudan black B. *Anat. Rec.*, 139: 465-469.
- Rhoton, A. L., Jr., J. L. O'Leary and J. P. Ferguson 1966 The trigeminal, facial, vagal and glossopharyngeal nerves in the monkey. *Arch. Neur.*, 14: 530-540.
- Shimazu, H., and W. Precht 1965 Tonic and kinetic responses of cat's vestibular neurons to horizontal angular acceleration. *J. Neurophysiol.*, 28: 991-1013.
- Shute, C. C. D. 1951 The anatomy of the eighth cranial nerve in man. *Proc. Roy. Soc. Med.*, 44: 1013-1018.
- Spiegel, E. A., and G. Sato 1926 Experimentalstudien am Nervensystem. V. Über den Erregungszustand der medullären Zentren nach doppelseitiger Labyrinthausschaltung. *Pflügers Arch. ges. Physiol.*, 215: 106-119.
- Vito, R. V. De, A. Brusa and A. Arduini 1956 Cerebellar and vestibular influences on Deiterian units. *J. Neurophysiol.*, 19: 241-253.
- Walberg, F., D. Bowsher and A. Brodal 1958 The termination of primary vestibular fibers in the vestibular nuclei in the cat. An experimental study with silver methods. *J. Comp. Neur.*, 110: 391-419.
- Wersäll, J. 1956 Studies on the structure and innervation of the sensory epithelium of the cristae ampullares in the guinea pig. A light and electron microscopic investigation. *Acta oto-laryng.*, Stockholm, Suppl. 126, 1-85.
- 1960 Electron micrographic studies of vestibular hair cell innervation. In: *Neural Mechanisms of the Auditory and Vestibular Systems*. Ed. G. L. Rasmussen and W. F. Windle. Charles C Thomas, Springfield, Ill., Chap. 18, 247-257.
- Yagita, K. 1914 Einige Experimente an dem Nervus petrosus superficialis major zur Bestimmung des Ursprungsgebietes des Nerven. *Folia Neurobiol.*, 8: 361-382.

PLATE 1

EXPLANATION OF FIGURES

- 14 Rhesus C-955. Photomicrograph of the right petrous bone showing the vestibular ganglia cut in the longitudinal axis. A lesion (L) is present in the junctional area of the ganglia involving mainly the cells supplying fibers to the utricle and, to a lesser extent, cells supplying fibers to the saccule. Portions of the ganglia dorsal and ventral to the lesion are intact. Intact fibers to the anterior and lateral canals are seen in the upper right. Sudan black B $\times 10$.
- 15 Rhesus C-950. Photomicrograph of the left petrous bone showing the vestibular ganglia cut in the longitudinal axis. A lesion (L) is present in the cells supplying fibers to the utricle. Cells supplying fibers to the anterior and lateral semicircular canals are intact. A portion of the intact inferior vestibular ganglion (I) is seen ventrally, and below it, the cochlear nerve. Sudan black B $\times 10$.
- 16 Rhesus C-955. Photomicrograph of the left petrous bone showing the inferior vestibular ganglion cut in the horizontal axis. A lesion (L) destroyed cells and fibers supplying the macula of the saccule with encroachment on the cell group supplying fibers to the posterior canal. The cochlear nerve is seen on the right. Sudan black B $\times 10$.
- 17 Rhesus C-926. Photomicrograph of the left petrous bone showing the inferior vestibular ganglion cut in the horizontal axis. A lesion (L) destroyed that portion of the ganglion supplying fibers to the posterior canal. To the right of the lesion are shown the intact cells and fibers supplying the macula of the saccule. The cochlea is in the upper right and the macula of the saccule in the upper left. Sudan black B $\times 15$.
- 18 Rhesus C-926. Photomicrograph of the right petrous bone showing the superior vestibular ganglion cut in the longitudinal axis. A lesion (L) destroyed the cells supplying fibers to the anterior and lateral canals. Intact cells and fibers supplying the macula of the utricle are seen ventral to the lesion. The macula of the saccule is seen inferiorly and the partially degenerated seventh nerve is seen in cross section on the right. Sudan black B $\times 15$.
- 19 Rhesus C-931. Photomicrograph of the right petrous bone showing the vestibular ganglia cut in the longitudinal axis. A lesion (L) destroyed the cells supplying fibers to the anterior canal and some of the cells supplying fibers to the lateral canal. Remaining portions of the superior and inferior vestibular ganglia are intact. The partially degenerated seventh nerve is seen in cross section on the right. Sudan black B $\times 15$.

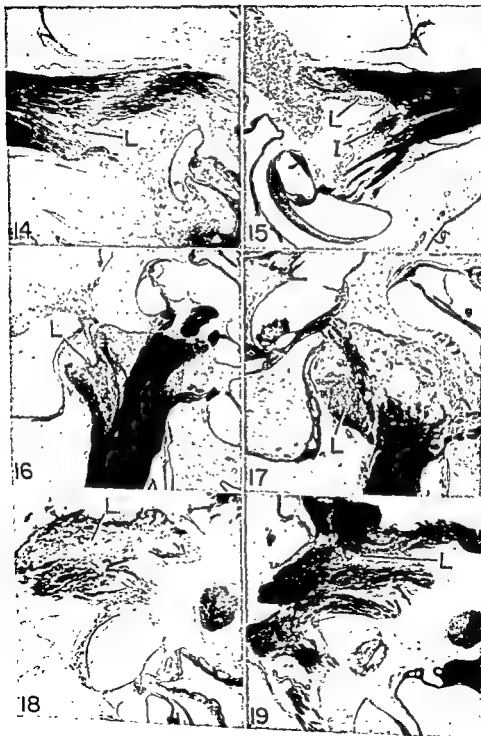


PLATE 1

EXPLANATION OF FIGURES

- 14 Rhesus C-955. Photomicrograph of the right petrous bone showing the vestibular ganglia cut in the longitudinal axis. A lesion (L) is present in the junctional area of the ganglia involving mainly the cells supplying fibers to the utricle and, to a lesser extent, cells supplying fibers to the saccule. Portions of the ganglia dorsal and ventral to the lesion are intact. Intact fibers to the anterior and lateral canals are seen in the upper right. Sudan black B $\times 10$.
- 15 Rhesus C-950. Photomicrograph of the left petrous bone showing the vestibular ganglia cut in the longitudinal axis. A lesion (L) is present in the cells supplying fibers to the utricle. Cells supplying fibers to the anterior and lateral semicircular canals are intact. A portion of the intact inferior vestibular ganglion (I) is seen ventrally, and below it, the cochlear nerve. Sudan black B $\times 10$.
- 16 Rhesus C-955. Photomicrograph of the left petrous bone showing the inferior vestibular ganglion cut in the horizontal axis. A lesion (L) destroyed cells and fibers supplying the macula of the saccule with encroachment on the cell group supplying fibers to the posterior canal. The cochlear nerve is seen on the right. Sudan black B $\times 10$.
- 17 Rhesus C-926. Photomicrograph of the left petrous bone showing the inferior vestibular ganglion cut in the horizontal axis. A lesion (L) destroyed that portion of the ganglion supplying fibers to the posterior canal. To the right of the lesion are shown the intact cells and fibers supplying the macula of the saccule. The cochlea is in the upper right and the macula of the saccule in the upper left. Sudan black B $\times 15$.
- 18 Rhesus C-926. Photomicrograph of the right petrous bone showing the superior vestibular ganglion cut in the longitudinal axis. A lesion (L) destroyed the cells supplying fibers to the anterior and lateral canals. Intact cells and fibers supplying the macula of the utricle are seen ventral to the lesion. The macula of the saccule is seen inferiorly and the partially degenerated seventh nerve is seen in cross section on the right. Sudan black B $\times 15$.
- 19 Rhesus C-931. Photomicrograph of the right petrous bone showing the vestibular ganglia cut in the longitudinal axis. A lesion (L) destroyed the cells supplying fibers to the anterior canal and some of the cells supplying fibers to the lateral canal. Remaining portions of the superior and inferior vestibular ganglia are intact. The partially degenerated seventh nerve is seen in cross section on the right. Sudan black B $\times 15$.

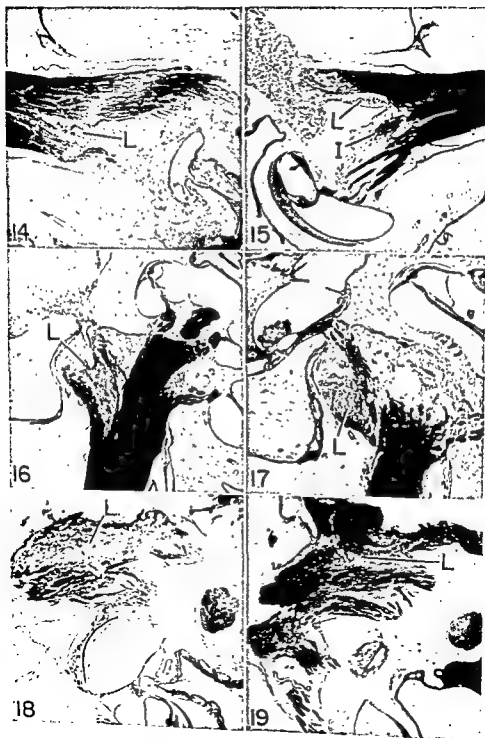


PLATE 2

EXPLANATION OF FIGURES

- 20 Rhesus C-926. Photomicrograph of the caudal portion of the left vestibular nerve root cut in the transverse plane showing a diagonal band of degeneration passing from lateral to medial. This degeneration resulted from a lesion destroying the posterior canal ganglion shown in figure 17. Nauta-Gygax $\times 50$.
- 21 Rhesus C-869. Photomicrograph of the right vestibular nerve root and superior vestibular nucleus cut in the transverse plane. Degeneration, resulting from destruction of the superior vestibular ganglion, is present throughout the rostral portion of the vestibular root and the central and lateral parts of the superior vestibular nucleus. The lesion of the superior vestibular ganglion is shown in figure 4. Nauta-Gygax $\times 15$.
- 22 Rhesus C-955. Photomicrograph of the caudal portion of the left vestibular nerve roots cut in the transverse plane showing degeneration in the medial aspect of the root which resulted from a lesion in the saccular ganglion. The lesion of the saccular ganglion is shown in figure 16. Nauta-Gygax $\times 40$.
- 23 Rhesus C-926. Photomicrograph of the right vestibular nerve root cut in the transverse plane. Degeneration, resulting from a lesion of the anterior and lateral canal ganglia, is located in the rostrolateral portion of the root. The few bands of degeneration along the medial border of the nerve root are the result of injury to the intermediate nerve. The lesion of the superior vestibular ganglion is shown in figure 18. Nauta-Gygax $\times 35$.
- 24 Rhesus C-929. Photomicrograph of the left vestibular root cut in the horizontal plane with the medial aspect of the root to the right. A narrow band of degenerated fibers, concentrated medially, is seen in the anterior part of the caudal third of the nerve root. This degeneration resulted from a lesion destroying the posterior canal ganglion (fig. 17). In the upper right is seen a small nucleus, free of degeneration which, in other animals, appeared to be related to the fibers of the intermediate nerve. Nauta-Gygax $\times 90$.
- 25 Rhesus C-927. Photomicrograph of the right vestibular root cut in the horizontal plane with the medial aspect of the root to the left. Degeneration, resulting from destruction of the superior vestibular ganglion, is located in the rostral two-thirds of the root. Nauta-Gygax $\times 35$.

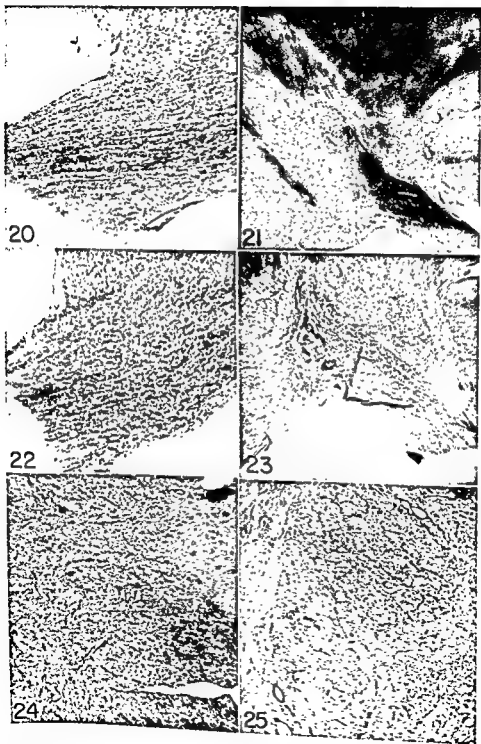


PLATE 2

EXPLANATION OF FIGURES

- 20 Rhesus C-926. Photomicrograph of the caudal portion of the left vestibular nerve root cut in the transverse plane showing a diagonal band of degeneration passing from lateral to medial. This degeneration resulted from a lesion destroying the posterior canal ganglion shown in figure 17. Nauta-Gygax $\times 50$.
- 21 Rhesus C-869. Photomicrograph of the right vestibular nerve root and superior vestibular nucleus cut in the transverse plane. Degeneration, resulting from destruction of the superior vestibular ganglion, is present throughout the rostral portion of the vestibular root and the central and lateral parts of the superior vestibular nucleus. The lesion of the superior vestibular ganglion is shown in figure 4. Nauta-Gygax $\times 15$.
- 22 Rhesus C-955. Photomicrograph of the caudal portion of the left vestibular nerve roots cut in the transverse plane showing degeneration in the medial aspect of the root which resulted from a lesion in the saccular ganglion. The lesion of the saccular ganglion is shown in figure 16. Nauta-Gygax $\times 40$.
- 23 Rhesus C-926. Photomicrograph of the right vestibular nerve root cut in the transverse plane. Degeneration, resulting from a lesion of the anterior and lateral canal ganglia, is located in the rostralateral portion of the root. The few bands of degeneration along the medial border of the nerve root are the result of injury to the intermediate nerve. The lesion of the superior vestibular ganglion is shown in figure 18. Nauta-Gygax $\times 35$.
- 24 Rhesus C-929. Photomicrograph of the left vestibular root cut in the horizontal plane with the medial aspect of the root to the right. A narrow band of degenerated fibers, concentrated medially, is seen in the anterior part of the caudal third of the nerve root. This degeneration resulted from a lesion destroying the posterior canal ganglion (fig. 17). In the upper right is seen a small nucleus, free of degeneration which, in other animals, appeared to be related to the fibers of the intermediate nerve. Nauta-Gygax $\times 90$.
- 25 Rhesus C-927. Photomicrograph of the right vestibular root cut in the horizontal plane with the medial aspect of the root to the left. Degeneration, resulting from destruction of the superior vestibular ganglion, is located in the rostral two-thirds of the root. Nauta-Gygax $\times 35$.

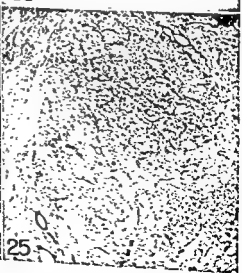
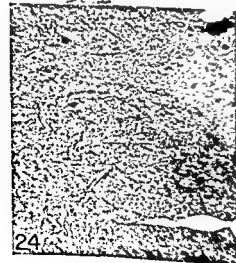
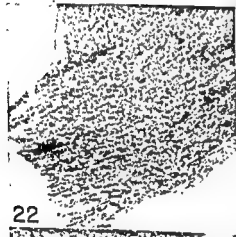


PLATE 3

EXPLANATION OF FIGURES

- 26 Rhesus C-931. Photomicrograph of the oral pole of the right medial vestibular nucleus cut in the transverse plane. Preterminal degeneration, resulting from destruction of the anterior and a portion of the lateral canal ganglia, is present about the large and medium sized cells. Nauta-Gygax $\times 200$.
- 27 Rhesus C-866. Photomicrograph of the right superior vestibular nucleus cut in the horizontal plane with the medial aspect to the left. Profuse preterminal degeneration, seen about the large cells in the central and lateral portions of this nucleus, resulted from resection of the superior vestibular ganglion. A bundle of degenerated fibers passing toward the cerebellum is seen on the right. Nauta-Gygax $\times 125$.
- 28 Rhesus C-926. Photomicrograph of the left superior vestibular nucleus cut in the transverse plane with the medial aspect of the nucleus on the right. There is modest preterminal degeneration passing diagonally into the most medial regions of the nucleus. This degeneration resulted from destruction of the posterior canal ganglion. A part of the superior cerebellar peduncle is in the extreme upper left. Nauta-Gygax $\times 125$.
- 29 Rhesus C-926. Photomicrograph of the right superior vestibular nucleus cut in the transverse plane with the medial aspect to the left. There is profuse degeneration passing diagonally into the central and lateral regions of this nucleus with preterminal degeneration about the larger cells. This degeneration resulted from destruction of cells of the anterior and lateral canal ganglia. The superior cerebellar peduncle borders the degeneration on the right. Nauta-Gygax $\times 50$.
- 30 Rhesus C-928. Photomicrograph of the dorsolateral portion of the left inferior vestibular nucleus cut in the horizontal plane with the medial aspect on the right. There are numerous fascicles of degenerated fibers descending among the cells of this nucleus. The peripheral lesion in this animal destroyed the saccular ganglion. Nauta-Gygax $\times 240$.
- 31 Rhesus C-866. Photomicrograph of the right inferior vestibular nucleus cut in the horizontal plane with the medial aspect to the left. There are dense descending fascicles of degenerated fibers and several collections of profuse preterminal degeneration about groups of cells in this nucleus. The superior vestibular ganglion was resected in this animal. Nauta-Gygax $\times 75$.

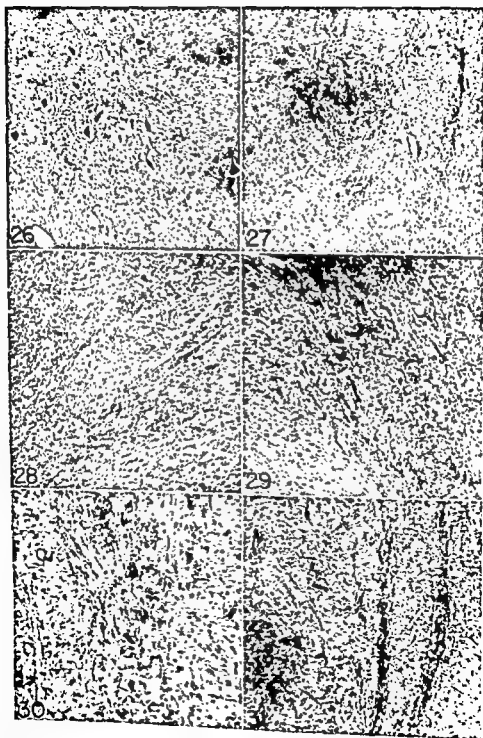
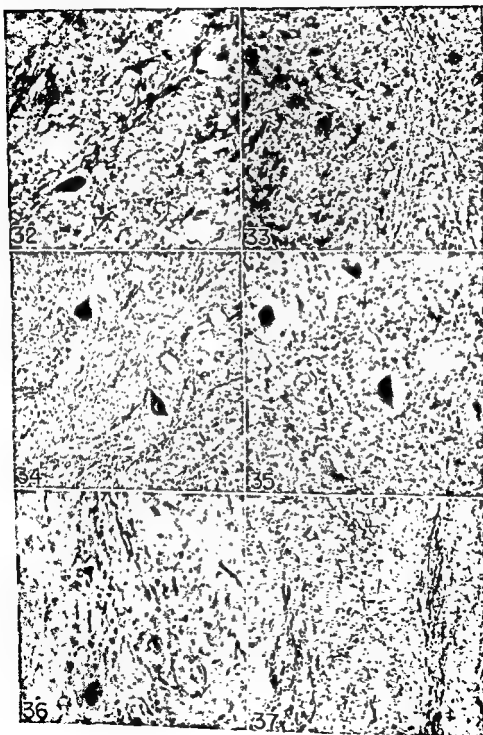


PLATE 4

EXPLANATION OF FIGURES

- 32 Rhesus C-926. Photomicrograph of the caudal and medial aspects of the left superior vestibular nucleus cut in the transverse plane with the medial aspect on the right. There is profuse preterminal degeneration arborizing about the cells of this region of the nucleus. The peripheral lesion destroyed the posterior canal ganglion. Nauta-Gygax $\times 450$.
- 33 Rhesus C-927. Photomicrograph of the right inferior vestibular nucleus cut in the horizontal plane with the medial aspect on the left. There are fine fascicles of descending degenerated fibers with some arborizations of fibers about cell groups in this nucleus. The peripheral lesion in this animal destroyed the superior vestibular ganglion. Nauta-Gygax $\times 250$.
- 34 Rhesus C-926. Photomicrograph of the left lateral vestibular nucleus cut in the transverse plane with the medial aspect on the right. Degenerated fibers are shown traversing the central portion of this nucleus without establishing close contact with the large cells. The peripheral lesion in this animal destroyed the posterior canal ganglion. Nauta-Gygax $\times 320$.
- 35 Rhesus C-931. Photomicrograph of the oral portion of the right medial vestibular nucleus showing preterminal degeneration about the cells. This degeneration resulted from destruction of the anterior, and a portion of the lateral, canal ganglia. Nauta-Gygax $\times 200$.
- 36 Rhesus C-950. Photomicrograph of the rostral portion of the left accessory cuneate nucleus cut in the horizontal plane. Degenerated fibers entered this nucleus from lateral portions of the inferior vestibular nucleus. Some fibers established close contact with large cells of this nucleus. The peripheral lesion in this animal destroyed the utricular ganglion. Nauta-Gygax $\times 500$.
- 37 Rhesus C-866. Photomicrograph of the right inferior vestibular nucleus cut in the horizontal plane with the medial aspect on the left. Dense bands of degenerated fibers are seen descending within this nucleus. The superior vestibular ganglion was resected in this animal. Nauta-Gygax $\times 200$.



Electron Microscopic Study of the Modification by Monosodium Glutamate of the Retinas of Normal and "Rodless" Mice¹

ADOLPH I. COHEN²

Departments of Anatomy and Ophthalmology, Washington University
School of Medicine, St. Louis, Missouri

ABSTRACT Sodium-L-glutamate was administered to post-natal Swiss albino and agouti C3H/HeJ "rodless" mice. In both cases there was at two months a marked reduction in myelinated axons of the optic nerve from about 25,000 to less than 225 axons but Swiss mice had more ganglion cell somas than axons. Glutamate-treated eyes seemed smaller and the lenses were 65% of the weight of control lenses. The inner nuclear layer of Swiss-glutamate retinas was reduced from 5-7 nuclei deep to 1-2. In treated Swiss mice the receptor concentration appears unchanged and electron microscopy revealed that both spheroidal and pedicular receptor terminals were contacted by presumed neurites of second order neurons. There was a small, relative increase in terminals of bipolar neurons in the markedly reduced inner plexiform layer. Relative to these findings a description is given of normal synaptic arrangements. In glutamate-treated "rodless" mice at two months the retina contained two rows of nuclei. Imbricated processes of glial cells of Müller faced the pigment epithellum and the retina contained scattered ganglion cells, bipolar cells, and other neurons less readily characterized. At two months most glutamate-treated mice, rod containing or "rodless," had a direct pupillary response and a detectable but obviously weaker consensual response. Preliminary examinations of animals one year after glutamate treatment showed receptor deterioration in albino animals and further retinal deterioration in both groups. The two surviving C3H-glutamate animals possessed milky cataractous lenses, however full but sluggish direct iris constrictions could be elicited.

In 1957 Lucas and Newhouse showed that monosodium glutamate administered suckling mice caused extensive destruction of the ganglion cell and inner nuclear layers of the retinas of these animals but spared the receptors. Potts, Adrell, and Kingsbury ('60) subsequently and only the "a" wave of the electroretinogram (ERG) in their glutamate treated mice, a finding consistent with current hypotheses relating the "a" wave of the electroretinogram to receptor activity. Since ganglion cell activity does not contribute to the electroretinogram the loss of the "b" wave must reflect changes in the inner nuclear layer. The effect of more lengthy degeneration on the ERG of glutamate treated rats has been described Potts, '65).

The residual retinal histology and physiology as evidenced in the above reports raises a number of interesting questions and possible opportunities for the student of retinal neuroanatomy and physiology. In a retina with normal concentrations of

receptors but a paucity of other neurons, what are the persisting synaptic arrangements? Would the simplified retina be useful in clarifying the synaptic connections of this complex organ? Are the normal concentrations of receptors in treated animals evidence that receptors may survive in the absence of synaptic connectives or have the remaining neurons of the inner nuclear layer adapted to contact more receptors than usual? Is the inner nuclear layer of the mouse retina populated largely by a cell which does not normally contact the receptors and is it this cell species which has diminished in sufficient numbers to account for the sharply reduced inner nuclear layer of these retinas?

To try to answer these questions the retinas of normal and glutamate treated animals were examined by electron mi-

¹This work was supported by grant NB-04818-03 of the National Institute of Neurological Diseases and Blindness of the National Institutes of Health.

²This work was performed during the tenure of a Career Development Award (5-K3-NB-3170) from the National Institutes of Health.

croscopy. To clarify further certain questions bearing on the factors influencing neuron survival, the glutamate experiments were extended to the C3H/HeJ strain of mouse which is homozygous for a recessive gene resulting in total receptor dystrophy.

MATERIAL AND METHODS

Six litters of Swiss albino mice (35 surviving experimental animals) and four litters of C3H/HeJ mice (10 surviving experimental animals) were used in these observations as well as control litters of the same races. The light microscope sufficed to show whether the glutamate effect occurred, as it invariably did, and electron microscopic examination was usually confined to one eye of an animal. As per the schedule of Potts et al. ('60), Swiss albino mice were given subcutaneous injections of monosodium glutamate for 18 days beginning on the second post-natal day but in later experiments it was observed that ten days of injection gave the full effect and this was employed with later groups of animals. Control injections of water or saline were given but proved to have no discernible effect. Lukas and Newhouse ('57) have explored compounds related to glutamate for their ability to induce this effect and the current investigation was not designed to explore further the mechanism of the glutamate effect.

Because in all animals the synaptic arrangements may differ in different retinal regions, an effort was made to make comparisons in similar retinal areas. Therefore, at a possible sacrifice of quality of fixation, the retina was fixed *in situ*. Some animal perfusions were tried but these did not give uniform fixation. In the final procedure adopted, the mice were decapitated, and the eyes were eviscerated and placed in fixative. The cornea was punctured and then dissected away with iridectomy scissors and a defect cut in the sclera to indicate the horizontal axis. The lens was then removed and the remainder of the eye allowed to fix. A variety of fixatives were explored, but best results were obtained by one hour's fixation in cold 2.5% glutaraldehyde in Earles saline containing 1 ml of 0.067 M KH_2PO_4 - KH_2PO_4 (pH 7.4) per 100 ml and 450 mg glucose per 100

ml followed without washing in buffer by overnight fixation in 2% osmium tetroxide in the same saline. The eyes were dehydrated in ethanol and embedded in epoxy-resin (Durcupan). The embedded eyes were cleaved along the horizontal axis and two regions were taken and mounted for examination. One, termed "central," was immediately temporal to the nerve head. The other, termed "peripheral," was the extreme periphery of the neural retina. Comparison of random fields at a standard magnification of $8000\times$ in both these areas in normal or experimental eyes gave estimates of the intrinsic variability in the frequency of those cell processes being studied. Sections were mounted on 1×2 mm single hole discs over Formvar films and stained with lead and uranium salts. Sections were studied with an Elmiskop 1A electron microscope.

Pupillary activity was crudely observed by leading light from a 6v microscope lamp to 1 cm in front of the eye by a fiber optic bundle while the eye was observed with a dissecting microscope. To test for a conscious eye response, one eye was stimulated as before and the other eye was observed using a red filter (Corning 2404) served using a red filter (Corning 2404) equipped 6v microscope lamp (AO) which was focused on the eye at a distance of eight inches from the eye. The effect of heat was ruled out in preliminary experiments by passing the light through one inch of a 10% copper sulfate bath without effecting the responsiveness. Animals were taped to a rubber hose stuffed with cotton during these examinations and were not anaesthetized.

RESULTS

The two day post-natal mouse had a largely undifferentiated retina with only ganglion cells demarked and these were putting forth dendrites and axons.

Two months following the glutamate treatment it was noted on removing the eyes of treated animals that they appeared smaller than those of controls from the same or other litters. No effort was made to quantitate this observation but the lens pairs were saved and weighed. The lenses of experimental animals averaged 65% of the weight of lenses of control animals with no overlap in weights of lenses from treated and untreated groups. (Pair

weights: controls 0.014 ± 0.001 gm; experimentals 0.009 ± 0.002 gm).

Figures 1 and 2 show paired light micrographs demonstrating the effect of the treatment on the retina, confirming earlier reports. The two-month-old animals showed a normal receptor concentration after treatment but in the inner nuclear layer the normal 5-7 tiers of nuclei were now 1-2 and only occasional ganglion cell somas were now evident. Cross-sections of the optic nerve of the normal two month mouse (fig. 3) revealed about 25,000 myelinated nerve fibers and electron microscopy of the nerve gave no evidence of non-myelinated fibers; the rare, isolated non-myelinated cross-sections seen being entirely accounted for as representing axons cut within nodes of Ranvier. Examination of the normal retina permitted the ready identification of fascicles of the non-myelinated axons (fig. 5) which only gain their sheathing on entering the optic nerve. Using this morphological guide, an inspection of the optic nerve of the two-day-old mouse, prior to glutamate treatment, revealed many non-myelinated axons in the nerve (fig. 6), however, their weaving made it difficult to obtain a precise numerical estimate since obliquely sectioned fibers with sparse neurotubules could be confused with slightly fibrous glial processes. Following the glutamate treatment from 0 to 225 myelinated axons were seen (fig. 4) in the optic nerves of two month animals. Since small volumes of highly concentrated solutions are injected subcutaneously part of this variation may be due to leakage. Since the number of surviving axons was substantially less than the number of optic nerve axons prior to treatment it demonstrates that the glutamate treatment has destroyed some axons.

In the retinas from glutamate treated animals there was an obvious reduction in the number of ganglion cell somas surviving at two months. Horizontal sections through two full normal retinas revealed by light microscopy some 200-250 ganglion cell somas whereas in two glutamate treated Swiss animals some 30-40 were seen. Flat retinal preparations were not made but it was highly probable that there were more somas than myelinated optic

nerve fibers in experimental animals since the ratio of myelinated fibers in the normal optic nerve to those in the experimental optic nerve is much greater than the ratio of somas in sections of the two retinas. The ganglion cell somas of experimental animals were clearly smaller than those of control animals. This most likely is an atrophy but could represent in part an enhanced survival of a smaller ganglion cell variety. One must also consider the possibility that these represent an intra-retinal ganglion cell as Gallego and Cruz ('65) have claimed to demonstrate in other species.

In examining the inner plexiform layer one is concerned with the interaction of ganglion cells, bipolar neurons, and amacrine cells. The ganglion cells are readily identified since they occur as a separate and innermost neural layer and in the mouse constitute a single line of cells (figs. 1, 7) above the layer of their axons, the optic fiber layer. This axonal layer is absent in glutamate-treated animals (fig. 8). The ganglion cells possess the largest somas of the retinal neurons with large nuclei with prominent nucleoli, prominent Golgi regions, a ribosome rich (Nissl) cytoplasm and frequent sub-membranal cisterns. Near the nerve head the adjoining ganglion cell somas were often contiguous (fig. 11) without intervening glia and a single cell at times possessed broad contiguities with as many as six adjoining cells. Ganglion cell axons were likewise not typically separated by glial processes. Surviving ganglion cell somas of glutamate-treated animals are similar in appearance to the normal ganglion cells except for size (fig. 8).

Stout apical dendrites contained microtubular elements similar to those in the axons. The dendrites extended outward toward the inner nuclear layer and branched. Ribosomes were not found in the finest branchings. At least some and perhaps all ganglion cell somas of glutamate-treated animals also send forth dendrites.

On the apex of the ganglion cells there were often found in contiguity the bag endings of the bipolar neurons (fig. 7), but these were also seen free of ganglion cell contact in the inner plexiform layer

(fig. 17). The bipolar neurons possessed a close morphological kinship to the receptors. Their nuclei lie in the inner nuclear layer and they send a stout, unbranched process into the inner plexiform layer which there terminates in a large, highly irregular bag filled with vesicles of 300-400 Å. These bags are clearly related to the receptor spherules and pedicles. The vesicle containing portion of the bag was somewhat branched or lobulated (fig. 17). In the mouse, as noted in other species (Missotten, '61; Fine, '62; Dowling and Boycott, '65), bipolar neurons possess at irregular intervals along the inner walls of the terminal bag curious plates arranged perpendicularly to the membrane. These plates or synaptic lamellae appear in shape and in cross-section as ribbons which, following appropriate staining, have a pentalaminar appearance (figs. 12, 13). The plates are surrounded by a halo of vesicles which stand off the plates as if a gel intervened. Between a small region of the basal curvature of the lunette plate and the cell membrane the arciform density, U-shaped in cross-section, is sometimes seen. Since nothing is known of the physiology of this apparatus it cannot be said whether cell contacts contiguous to the region containing this density differ in function from cell contacts in other lamella regions. This organelle is highly similar, except in size, to those in receptor bases as described by others (Ladman, '58; Lanzavecchia, '60; Cohen, '63). If the plane of section was satisfactory the synaptic lamella was included in a plane that typically passed between two cell processes terminating on the externum of the bag ending and the contacting membranes usually possessed an enhanced density when combined with uranium and lead staining were employed.

Dowling and Boycott ('65) have recently coined the useful term "dyad" for the paired external neurites opposite the synaptic lamellae of bipolar bags, following Missotten's ('64) use of "triad" for a slightly more complex system of external contacts at synaptic lamellae in pedicles of human cones. Although the bipolar bag must primarily be a presynaptic structure no vesicle clusters were seen anywhere against the inside of its cell membrane.

All the above bipolar features are essentially similar to those of the visual receptors from their nuclei to their terminations. In addition to the "dyad" contacts, bipolar bags were also contacted at clusters by processes which contained a cluster of vesicles in them and whose contact site is marked by a density (figs. 7, 17). These contacting processes had a typical "presynaptic" appearance according to the working hypotheses of most students of the fine structure of the central nervous system (Gray, '59). Moreover, as noted by Dowling and Boycott in primates ('65), one of the external dyad processes sometimes possessed a typical presynaptic contact on the bipolar bag thus suggesting possible bidirectional transmission or "feedback" arrangements (figs. 8, 15, 17). A reciprocal synaptic arrangement has recently been described in the olfactory bulb by Rall, Shepherd, Reese and Brightman ('66). Typical presumptive presynaptic contacts of unknown origin were sometimes seen on the apices of the somas of ganglion cells and on their dendritic extensions (fig. 10) but the contacts of the vesicle filled bipolar bags and ganglion cell somas seemed to be simple contiguities with no cell membrane specializations (fig. 9). Dowling and Boycott ('65) have recently claimed that such bipolar bag and ganglion cell contacts in primate and ganglion cell contacts in primate retinas may possess tight junctions but after an intensive search I have only seen one possible instance of this in the mouse, and I have failed to observe them in peripheral and central regions of human and macaque retinas. It might be noted that the very same sections in all these species routinely exhibit the tight junctions at the inner faces of the cells of the pigment epithelium so that the ability to preserve such junctions would not seem in doubt.

Amacrine cells have proven difficult to identify unequivocally in the mouse but the innermost (vitread) cell of the inner nuclear layer often had its nucleus surrounded by cytoplasm on all sides and its cytoplasm was rich in ribosomes (fig. 16). This concurs with Dowling and Boycott's identification ('65). Processes from these cells swept inwardly and laterally and differed from known bipolar axons in being less dense and often possessing ribosomes.

While these cells were the most likely candidates for amacrine cells, the presence of somas of amacrine cells in the midst of the inner nuclear tier was also likely but somewhat more difficult to establish since the distribution of cytoplasm differed in this compacted area. A working hypothesis suggested by Dowling and Boycott ('65) is that dyads usually represent a paired termination on the bipolar bag of a ganglion cell dendrite and an amacrine neurite, the latter alone possessing synaptic vesicles. While one often finds instances in the normal mouse where only one of the terminals possesses synaptic vesicles (fig. 12) and is the presumed amacrine neurite, it is not rare that one finds both dyad terminals with vesicles (figs. 14, 15), a situation similar to that in rod spherules of a number of species where both sublamellar processes usually possess vesicles. In fact in "dyad" pairs in the mouse instances of one, both, or rarely, neither (fig. 13) containing vesicles may be found. On the other hand, whether possessing vesicles or not, the two dyad processes usually differed in appearance, suggesting a different origin.

All the presumed synaptic arrangements seen in normal mice may be found in the inner plexiform layer of the glutamate-treated animals (fig. 8). There is a small but definite relative increase in the frequency of sections of bipolar bags both in central and peripheral retina suggesting that bipolar cell number is relatively less severely reduced than that of the amacrine and ganglion cells; or less likely, that more sections were being encountered because the bags had become larger and more branched or irregular.

The outer cells in the inner nuclear layer, to judge from other retinas, could be expected to include both horizontal cells and bipolar neurons although the latter are also found deeper in this layer. In the mouse all cells in this region possessed a cytoplasm that is rich in mitochondria and ribosomes and sent processes into the outer plexiform layer and toward the receptors (fig. 18). A reasonable working hypothesis is that with respect to the receptors, the bipolar processes are functionally post-synaptic elements, i.e., dendrites — processes which are ordinarily ex-

pected to be free of synaptic vesicles. If one considers an extension to mice of Polyak's ('41) description of horizontal cells in the primate retina and assumes horizontal cells to possess neuronal character, they would then link pedicles to spherules and pedicles. Thus their axonal terminals on rods would be telodendrites and might possess synaptic vesicles whereas their terminals on cones might either be vesicle-free dendrites or vesicle-containing telodendrites.

Turning to the mouse, a previous study of the receptors in this retina (Cohen, '60) showed that two receptor classes could be discerned on the basis of receptor terminals — i.e., a class ending in spherules like those of human rods and one ending in pedicles like those of human cones although but one class of outer segment was identified (figs. 19, 20, 21). These observations were confirmed. No significant changes in spherule and pedicle frequency were noted in comparisons of central and peripheral retina.

The spherules were spheroidal sacs containing numerous bare vesicles and some coated vesicles. Terminating neurites were deeply embedded in the spherule and were always contiguous to spherule membrane. Most deeply within the spherule one usually observed neurite terminations with a conspicuous although variable number of vesicles, mostly bare but occasionally coated. These were associated with synaptic lamellae, one or two, in the contiguous spherule cytoplasm. When the section plane through the lamella included the arciform density, it typically passed between two vesicle bearing processes but sometimes the processes lacked vesicles. Less deeply within the spherule were terminations of processes which were relatively clear in that they largely lacked vesicles although rare vesicular profiles were noted. While always contiguous to some internal surface of the spherule membrane, these clear terminations were typically not adjacent to lamellae. Where the clear processes entered the spherules, the adjacent spherule membrane often had enhanced density. The external spherule surface had process terminations containing synaptic vesicles (fig. 21). These exhibited enhanced membrane densities as

did points where sperules and pedicles were visibly contiguous and probably represent similar junctions. Sjöstrand ('58) showed a similar situation in the guinea pig. It did not prove possible by serial sectioning to trace the neurites within spherules to an identifiable cell of the inner nuclear layer, because the weaving of the neurites caused them to be lost in the plexiform area. In any event such tracing would have had limited value because the cells of the inner nuclear layers were not readily categorized.

In sections the pedicles possessed numerous basal contacts containing vesicles (fig. 20). These were on occasion traced to neurites containing ribosomes, an organelle not seen in receptor terminals. On other occasions serial sectioning showed apparent external contacts to be curled under portions of the same pedicle, the appearance resulting because the plane of the pedicle base was not perpendicular to the section plane. The pedicle synaptic lamellae were associated with a pair of neurites, which, in contradistinction to the typical situation in spherules, tended to be clear or relatively free of vesicles (fig. 20). Only occasional triad arrangements (Missotten, '64) were evident. Latent pedicle to pedicle contiguity was occasionally observed.

In glutamate-treated animals the frequency of receptor terminals possessing neurite contacts with second order neurons approached those of control animals (figs. 22, 23). On occasion one discerned a spherule with a clear area possibly suggesting loss of neurites but these were few. Slight differences in the nature of contacting neurites were suggested but not statistically established. Thus fewer vesicle containing endings were seen to terminate on the pedicles and some spherules seemed to lack vesicle containing processes. Apart from these suggestive alterations the area appeared surprisingly normal.

To see whether there would be less neuronal survival in the inner nuclear layer in a retina in which the chances of centripetal as well as centrifugal stimulation was reduced, glutamate was administered to post-natal mice of the C3H/HeJ strain. In this "rodless" strain the recep-

tors actually form during the first post-natal week but then degenerate. At two months only one row of receptor nuclei (but no inner or outer segments) and a vestige of the outer plexiform layer remain (fig. 24). Subsequently even these disappear. An electroretinogram was only obtained during the early period before receptor degeneration (Noell, '58, '65). The remainder of the retina and optic nerve were, however, quite normal in appearance by electron microscopy (Karli, '65; Cohen, unpublished observations). Another surprising but long known feature of "rodless" mice, including the animals employed here, but also albino "rodless" strains, is the persistence of a pupil response, both direct and consensual (Brückner, '51; review by Karli, '52). The iris also shows usual responses to constricting or dilating drugs (Brückner, '51).

Following glutamate treatment, the effect of this compound added to the dystrophic process yielding the comparison shown in figure 25. The retina was but two cells thick with a mixture of glial cells of Müller, ganglion cells, bipolar neurons and probably other neurons of the inner nuclear layer with a residuum of the inner plexiform layer (figs. 27, 28). The residuum of receptor nuclei and outer plexiform layer usually seen in two month C3H controls was absent. The optic nerve typically had less than 225 myelinated axons. The pigment epithelium appeared somewhat thinner but otherwise intact (figs. 25, 26). It faced a retinal surface of imbricated processes of Müller cells (fig. 26).

Remarkably enough, despite the reduction in optic nerve axons in glutamate-treated animals, at two months both treated Swiss albino and treated "rodless" animals had a vigorous direct pupil response and a detectable but less marked consensual response. An occasional two month "rodless"-glutamate animal gave no pupil response and the pupil was markedly dilated. This became more common in older animals. Unfortunately one two-month Swiss mouse with no axons evident in its optic nerve had been examined before residual pupillary activity had been noted. At one year after glutamate treatment, six albino animals showed receptor

deterioration with some retinal areas being devoid of receptors. Four of these showed a moderate to strong direct pupil response and weak consensual responses. The other two animals showed either slight or no direct pupil response and no consensual response. The two surviving C3H-glutamate mice both possessed milk-white cataractous lenses in both eyes and a full but sluggish direct pupil response. No consensual responses were elicitable. Their retinas suggested slight further deteriorations. Preliminary examinations of the irides of normal albino mice have revealed no unusual specializations.

The possibility of a pseudo-consensual response due to leakage of light from one eye to the other was explored. Using the heads of freshly decapitated normal Swiss albino mice and pigmented "rodless" mice where in both cases the pupil is markedly dilated, light was brought to one eye and the other observed. In a darkened room the contralateral albino eyes but not the pigmented eyes showed a faint but distinct glow. Accordingly, living non-glutamate treated Swiss albino and pigmented "rodless" animals were unilaterally enucleated. After 48 hours a glass ball was placed in the empty orbit after checking to see if the orbit was free of clotted blood which could block the transmission of light. Technical success was only achieved with two albino animals and one pigmented animal. In repeated observations on the unanaesthetized animals these exhibited strong direct reflexes but no pupil response was seen when the eyeless orbit was illuminated. In the case of the albinos the observation of iris movements is sufficiently difficult in red light so that very small movements might be overlooked.

DISCUSSION

With the exceptions of the spared receptors the effect of glutamate appears to represent randomized destruction in that some of everything persists. The retina in the mouse differentiates postnatally; thus opportunities for adaptive remodeling should be greatest since the glutamate is being applied at this time. An effect of glutamate on retinal vasculature is possible since growth of the lens, still vascularized in the post-natal period by the

hyaloid artery, a branch of the central retinal artery, is obviously retarded. However, this could be an indirect consequence of the retinal damage (see Coulombre and Coulombre, '66). The receptor sparing might represent an undamaged choroid blood supply or some intrinsic resistance of these cells. The relative bipolar sparing might have a similar origin.

The fact that no single class of neuron was eliminated in its entirety precluded an easy route to learning something new about the neuronal cytoarchitecture of the retina. Attempted detailed statistical analyses of types of processes were abandoned because in this small eye it was difficult to standardize location except grossly, and in a modified eye it is hard to decide what area corresponds to a given area in a normal eye. The thinner experimental retinas seemed somewhat better fixed than the controls. This could influence vesicle concentration which is one of the obvious things one might use to characterize cell processes. In other species a fortuitous distinctive character of some class of neurites would facilitate a statistical approach to retinal neural architecture. Because of the limitations of serial sectioning in tracing weaving processes in neuropil areas and in tracing processes travelling considerable distances, for most retinas a combined Golgi and electron microscopic serial section analysis would seem to offer the greatest promise (Stell, '65; Blackstad, '65).

A feature of special interest in the mouse is the presence of two receptor classes in this nocturnal animal. Is the pediculated receptor a photopic receptor? A recent report states that no duplex activity was detected physiologically in the mouse retina (Hellner, '66). Of general interest is the receptor-like morphology of the bipolar neuron. In addition to the evidence cited in this report, one may note that in many species retinas possess Landolt's Clubs (Landolt, 1871). These are processes from bipolar neurons that enter the ventricle of the retina between the receptor inner segments and Müller cell microvilli. The receptor-like aspects of the bipolar neurons suggest that it might

be worth considering that they possess similar electrophysiological characteristics.

The finding that almost all receptors are entered by neurites despite a drastic reduction in the inner nuclear layer suggests an adaptation by residual inner nuclear layer neurons to encompass more receptors. The validity of this surmise depends on how broad and overlapping bipolar and horizontal cell contacts with receptors may be in the normal retina and unfortunately this has not been established by Golgi methods, early efforts in this direction having failed. However, superior functional plasticity in the face of damage to the perinatal nervous system as compared to older nervous systems and classic neurological observation and suggestion that adaptation is a distinct possibility. Because of the possible importance of the above observations for the understanding of the factors influencing neural organization, further efforts to obtain successful Golgi preparations are clearly indicated.

The case of the C3H (rodless) mice shows that in the mice the conventional receptors are not necessary to obtain vigorous direct and consensual responses. This compels the conclusion that photoreceptive molecules are located in at least a second site in this eye. The existence of the consensual response says that information from one eye reaches the other eye and suggests involvement of the retina and optic nerve.

The fact that the glutamate-treated mice usually showed a strong direct but weaker consensual response suggests that the pigment site(s) in the stimulated eye is (are) essentially intact but that there is more difficulty in conveying the presence of light to the other eye than to the pupil of the stimulated eye.

In considering these phenomena one has to take into account possible intrinsic iris irritability as shown by Brown-Sequard (1859) for irides of certain fish and amphibians. Brückner ('51) obtained an iris response in the isolated mouse iris or eye with optic nerve sectioned but discounted the response as it possessed a long latency and required intense stimulation. It is possible, however, that mammalian irides have more fastidious re-

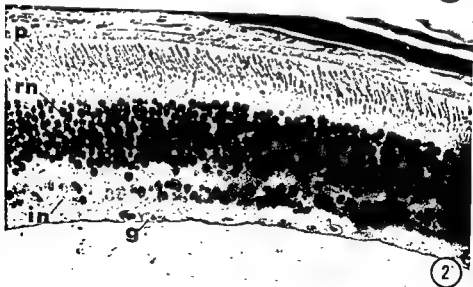
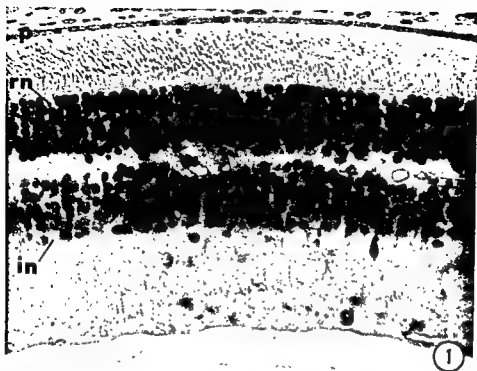
quirements for survival and function when removed from their blood supply. Karli ('54, '63), also pointing out that the iris response (latency 30 sec-1 min) under Brückner's conditions markedly differed from the quasi-normal threshold, latency, and speed of the *in vivo* response of the "rodless" mouse iris, has presented evidence for the need for an intact retina and optic nerve for the quasi-normal response. Indeed, Karli ('63) has presented evidence that his "rodless" mice can be taught to respond to an intense visual signal, that the peak wavelength of rhodopsin adsorption is also the peak wavelength for this learning, and that optic nerve section abolishes the response. It is not clear whether optic nerve sectioning in this small orbit was carried out without damage to the general blood supply of the eye. Karli suggests ('65) that rhodopsin in the pigment epithelium (none was detected in extracts in a procedure with limited sensitivity) is bleached and that electrical activity of these cells (Noell, '58, '65, did not detect any electrical activity) stimulates the bipolar neurons.

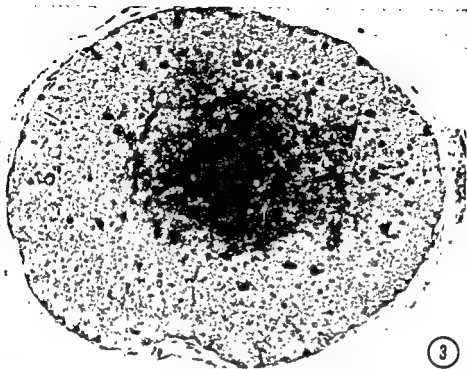
In the case of both rodless and rodless-glutamate treated mice in this study imbricated Müller cell processes intervened between any neurons and the cells of the pigment epithelium so that any stimulus could not be direct. It might be pointed out that the cells of the pigment epithelium are linked laterally by occluded cell junctions as part of their terminal bars (Cohen, '65) and that such junctions in other tissues have been said to represent paths of low resistance to ion currents (Dewey and Barr, '64). Since a chain of cells with such junctions extends all the way into the iris (Cohen, unpublished observations) one could consider a more direct path for iris stimulation. However, not only is the distance considerable even in this small mammal but no electrical activity to light was demonstrable in the "rodless" retina (Noell, '58, '65). One may always raise questions of sensitivity and speculate as to what would be an adequate stimulus. Karli's work ('63) and this report (consensual response) suggest at least a partial involvement of the retina and the questions of whether the retina is, in fact, involved and of a possible de-

gree of light sensitivity in bipolar or ganglion cells may have to be considered. A recent report describing experiments on cats suggests that the circulation may contribute to a consensual response under experimental conditions by bringing neurohumor released in one iris to the other (Kapp and Paulson, '66). In this case the second iris may have been rendered hypersensitive by the experimental procedures. However, to have this apply in "rodless" mice without intervention of the retina, neurohumor would have to be released by an intrinsically sensitive iris. This does not seem likely but should nonetheless be considered.

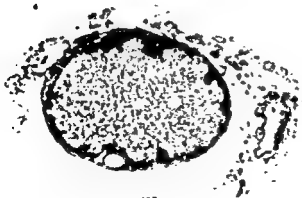
LITERATURE CITED

- Blackstad, T. W. 1965 Mapping of experimental axon degeneration by electron microscopy of Golgi preparations. *Zeit. f. Zellforschung*, 67: 819-834.
- Brown-Séquard, E. 1859 Recherches expérimentales sur l'influence excitatrice de la lumière, du froid et la chaleur sur l'iris, dans les cinq classes d'animaux vertébrés. *Journ. d. 1. Physiol. de l'homme et des animaux*, 2: 281-294; 451-460.
- Brückner, R. 1950 Spaltlampenmikroskopie und Ophthalmoskopie am auge von ratte und maus. *Documenta Ophthalmologica*, 7: 452-554.
- Cohen, A. I. 1960 The ultrastructure of the rods of the mouse retina. *Am. J. Anat.*, 107: 23-48.
- 1963 The fine structure of the visual receptors of the pigeon. *Exp. Eye Res.*, 2: 88-97.
- 1965 A possible cytological basis for the "R" membrane in the vertebrate eye. *Nature*, 205: 1222-1223.
- Coulombre, A. J., and J. L. Coulombre 1966 Growth of lens fiber mass. *Anat. Rec.*, 154: 335.
- Dewey, M. M., and L. Barr 1964 A study of the structure and distribution of the nexus. *J. Cell Biol.*, 23: 553-586.
- Dowling, J. E., and B. B. Boycott 1965 Neural connections of the retina: Fine structure of the inner plexiform layer. *Cold Spring Harbor Symposium on Quantitative Biology*, 30: 393-402.
- Fine, B. S. 1962 Synaptic lamellae in the human retina: An electron microscopic study. *J. Neuropath. Exp. Neurol.*, 22: 255-262.
- Galleo, A., and J. Cruz 1965 Mammalian Retina: Associational nerve cells in ganglion cell layer. *Science*, 150: 1313-1314.
- Gray, E. G. 1959 Axo-somatic and axodendritic synapses of the cerebral cortex: An electron microscope study. *J. Anat. (London)*, 93: 420-433.
- Helmer, K. A. 1966 Das adaptive Verhalten der Mausenhaut. *Albrecht v. Graefes Arch. klin. Exp. Ophthalm.*, 169: 166-175.
- Kapp, J., and G. Paulson 1966 Pupillary changes induced by circulatory arrest. *Neurology*, 16: 225-229.
- Karli, P. 1952 Rétines sans cellules visuelles. Recherches morphologiques, physiologiques et physio-pathologiques chez les Rongeurs. *Arch. Anat. Histol. Embryol.*, 35: 1-76.
- 1954 Etude de la valeur fonctionnelle d'une rétine dépourvue de cellules visuelles photo-réceptrices. *Arch. des Sciences Physiol.*, 8: 305-327.
- 1963 Les dégénérescences rétiniennes spontanées et expérimentales chez l'animal. *Progr. Ophthalm.*, 14: 51-69.
- Karli, P., M. E. Stoeckel and A. Porte 1965 Dégénérescence des cellules visuelles photo-réceptrices et persistance d'une sensibilité de la rétine à la stimulation photique. *Z. Zellforsch.*, 65: 238-262.
- Ladman, A. J. 1958 The fine structure of the rod bipolar synapse in the retina of the albino rat. *J. Biophys. Biochem. Cytol.*, 4: 459-466.
- Landolt, E. 1871 Beiträge zur anatomie der retina von frosch, salamander, und triton. *Arch. f. mikr. Anat.*, 7: 81-100.
- Lanzavecchia, G. 1960 Ultrastruttura dei coni e dei bastoncelli della retina de *xenopus laevis*. *Archivio italiano di anatomia e di Embriologia*, 65: 417-435.
- Lucas, D. R., and J. P. Newhouse 1957 The toxic effect of sodium L-glutamate on the inner layers of the retina. *AMA Arch. of Ophthalm.*, 58: 193-201.
- Missotten, L. 1961 Etude des synapses de la rétine humaine au microscope électronique. Ed. by A. L. Houwink and B. J. Spil. *The Proc. of the European Regional Conference on Electron Microscopy*, Delft, Netherlands, 2: 818-821.
- 1964 L'ultrastructure des tissus oculaires. *Bull. Soc. Belge d'Ophthalm.*, 136: 1-204.
- Noell, W. K. 1958 Studies on visual cell viability and differentiation. *Ann. N. Y. Acad. Sci.*, 74: 337-361.
- 1965 Aspects of experimental and hereditary retinal regeneration. *Biochem. of the Retina*, Academic Press, New York, edited by Clive N. Graymore.
- Polyak, S. L. 1941 The retina. University of Chicago Press (Chicago).
- Potts, A. M., K. W. Modrell and C. Kingsbury 1960 Permanent fractionation of the electroretinogram by sodium glutamate. *Am. J. Ophthalm.*, 50: 900-907.
- Potts, A. M. 1965 Selective action of chemical agents on individual retinal layers. *Biochem. of the Retina*, Academic Press, New York, edited by Clive N. Graymore, 155-161.
- Rall, W., G. M. Shepherd, T. S. Reese and M. Brightman 1966 Dendrodendritic synaptic



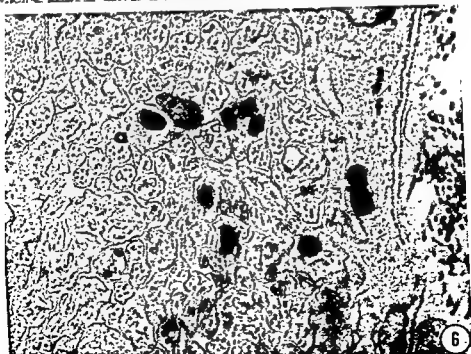
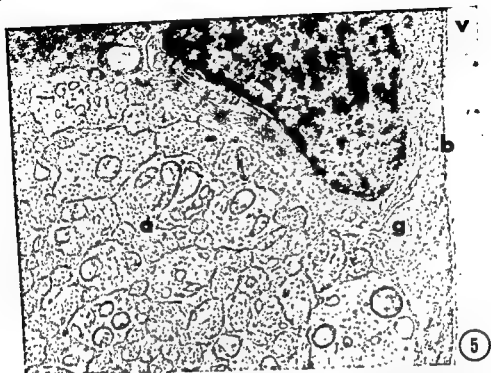


3



4

GLUTAMATE MODIFIED MOUSE RETINA
Adolph I. Cohen



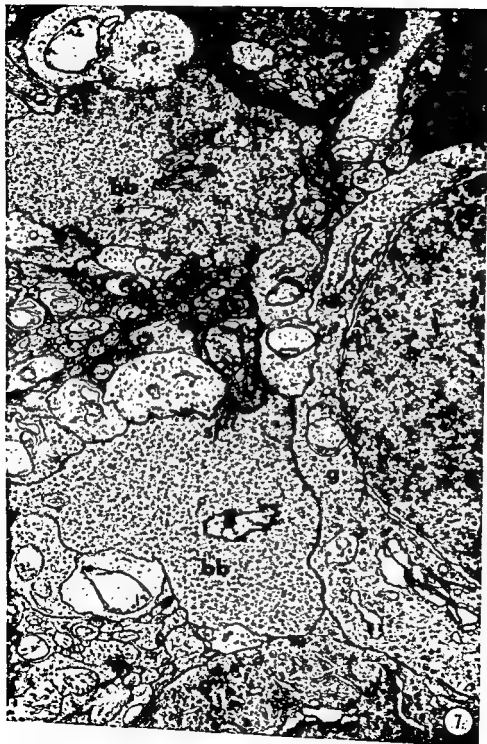


PLATE 5

EXPLANATION OF FIGURE

- An electron micrograph of the retinal surface of a glutamate-treated mouse. Facing the vitreous chamber (v) are processes of glial cells of Müller (m), artifactually somewhat dehydrated. No layer of ganglion cell axons is evident. A large ganglion cell (g) has contiguity with dyad processes opposite synaptic lamellae (sl). One of the dyad processes (arrow) also has a conventional synaptic contact on the bipolar bag. $\times 12,800$.



PLATE 5

EXPLANATION OF FIGURE

- 8 An electron micrograph of the retinal surface of a glutamate-treated mouse. Facing the vitreous chamber (v) are processes of glial cells of Müller (m), artifactually somewhat dehydrated. No layer of ganglion cell axons is evident. A large ganglion cell (g) has contiguity with dyad processes opposite synaptic lamellae (sl). One of the dyad processes (arrow) also has a conventional synaptic contact on the bipolar bag. $\times 12,800$.

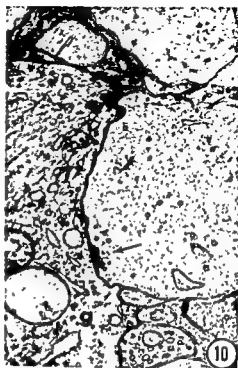
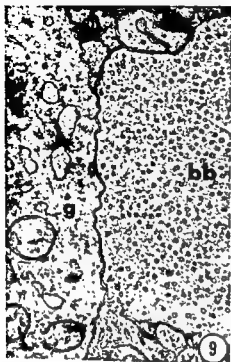


PLATE 6

EXPLANATION OF FIGURES

- 9 An electron micrograph from a control animal illustrating the contiguity of a bipolar ending (bb) and the apical surface of a ganglion cell (g). Note the absence of any membrane specialization at the junction. $\times 31,000$.
- 10 An electron micrograph from a control animal of a neurite contiguous with the apex of a ganglion cell (g) near its main dendrite. Note the presumptive synapse of conventional configuration (arrow). $\times 32,000$.
- 11 An electron micrograph of a control retina exhibiting contiguity of ganglion cell membranes. $\times 32,000$.

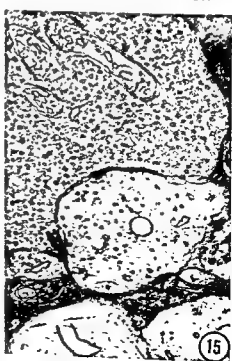


PLATE 7

EXPLANATION OF FIGURES

- 12 A common type of dyad contact in the inner plexiform layer from a control retina. The photograph exhibits the pentalaminar structure of the synaptic lamella (sl), the density of the opposed membranes of the dyad contacts, and vesicles in one of these contacts. A presumptive synapse of a conventional type is also seen (arrow). $\times 60,000$.
- 13 An infrequent variety of dyad contact from a control retina showing only sparse vesicular profiles in either dyad process. $\times 62,000$.
- 14 A dyad contact in the inner plexiform layer of a control retina showing vesicles in both contiguous neurites. While vesicles in both dyad contacts were often seen, it was unusual to have both neurites so similar in appearance. $\times 33,600$.
- 15 A dyad contact in the inner plexiform area of a glutamate-treated Swiss mouse showing dyad contacts differing in appearance but both containing vesicular profiles. $\times 33,000$.

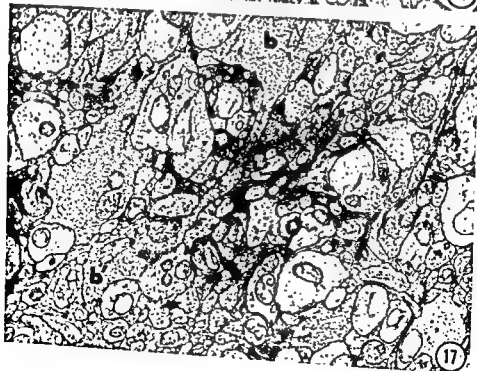
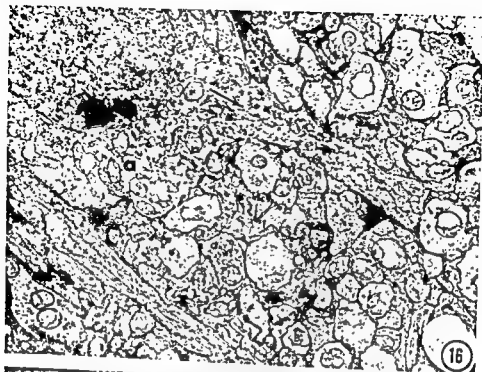


PLATE 8

EXPLANATION OF FIGURES

- 16 An electron micrograph of the inner aspect of the inner nuclear layer of a control retina showing a presumptive amacrine neuron (a) sending a process (arrow) into the inner plexiform layer. $\times 10,600$.
- 17 An electron micrograph of a section of a bipolar bag in the inner plexiform layer of a control retina showing two enlarged bag areas (b, b') connected by a narrower process. This illustrates the irregularity of the bipolar terminus. Also note vesicle containing endings on the bags, with the contacts exhibiting membrane density. $\times 28,500$.



PLATE 9

EXPLANATION OF FIGURE

- 18 An electron micrograph of the outer aspect of the inner nuclear layer from the retina of a glutamate-treated Swiss mouse illustrating the general cytoplasmic similarity of the neurons in this region. The cytoplasm is rich in ribosomes and mitochondria and often shows tubular elements (t). Fibril containing cytoplasm (f) of glial cells of Müller is also seen. $\times 21,600$.

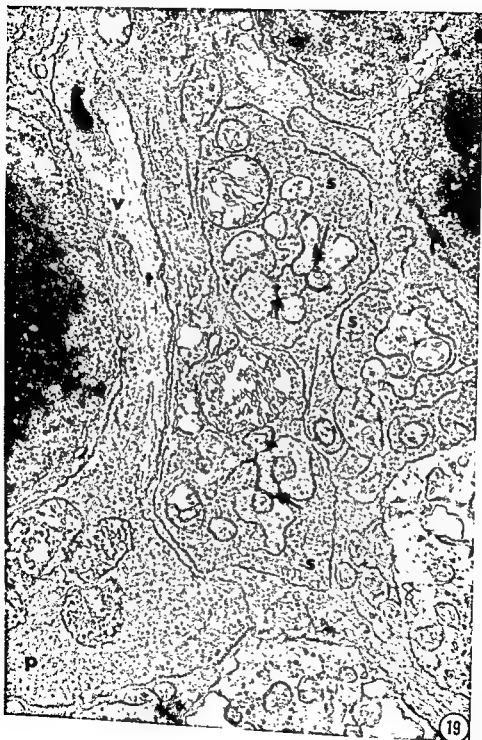


PLATE 10

EXPLANATION OF FIGURE

- 19 An electron micrograph of a control retina illustrating receptor spherules (s) and a portion of a pedicle (p). Note the neurotubules (t) and vesicles (v) in the pedicle stalk or axon. $\times 26,200$,

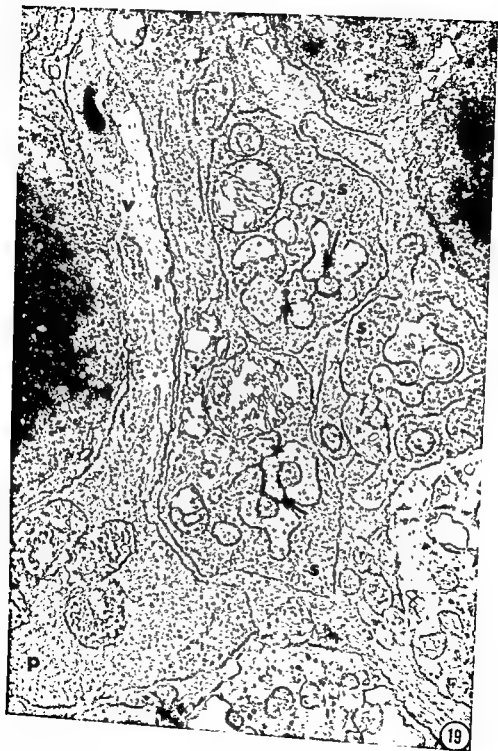


PLATE 11

EXPLANATION OF FIGURES

- 20 An electron micrograph of a control retina showing spherules (s) and a portion of a pedicle (p). The micrograph illustrates the typical situation that endings associated with synaptic lamellae in pedicles tend to lack vesicles while those associated with lamellae in spherules tend to possess them. Basal contacts on pedicles are rather numerous and possess vesicles and the contacting membrane are dense. $\times 34,500$.
- 21 An electron micrograph of a control retina illustrating additional spherule features. At the arrow is an external contact containing vesicles. This type of contact was occasionally traced to processes from pedicles. Note the U-shaped arciform densities between the synaptic lamellae (sl) and adjacent cell membrane. $\times 33,400$.

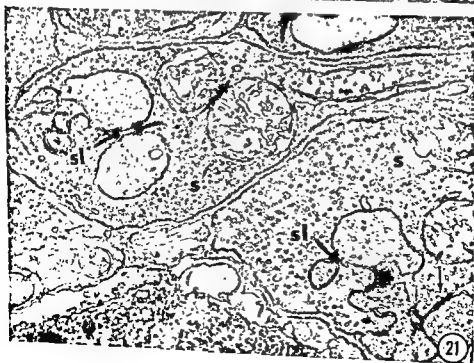


PLATE 11

EXPLANATION OF FIGURES

- 20 An electron micrograph of a control retina showing spherules (s) and a portion of a pedicle (p). The micrograph illustrates the typical situation that endings associated with synaptic lamellae in pedicles tend to lack vesicles while those associated with lamellae in spherules tend to possess them. Basal contacts on pedicles are rather numerous and possess vesicles and the contacting membrane are dense. $\times 34,500$.
- 21 An electron micrograph of a control retina illustrating additional spherule features. At the arrow is an external contact containing vesicles. This type of contact was occasionally traced to processes from pedicles. Note the U-shaped arciform densities between the synaptic lamellae (sl) and adjacent cell membrane. $\times 33,400$.

GLUTAMATE MODIFIED MOUSE RETINA
Adolph I. Cohen

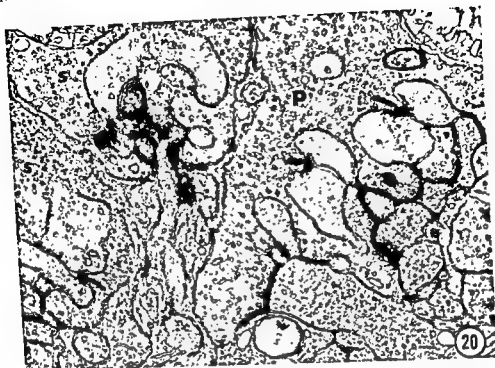


PLATE 12

EXPLANATION OF FIGURES

- 22 An electron micrograph of a glutamate-treated retina to illustrate the typical appearance of spherules. $\times 22,200$.
- 23 An electron micrograph of glutamate-treated retina to illustrate the typical appearance of a pedicle. There was a suggestion of somewhat fewer vesicle containing contacts on the pedicle base. $\times 42,700$.

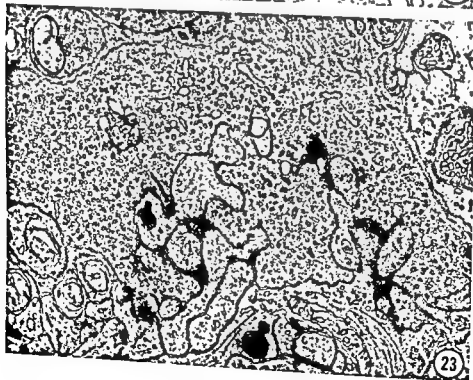
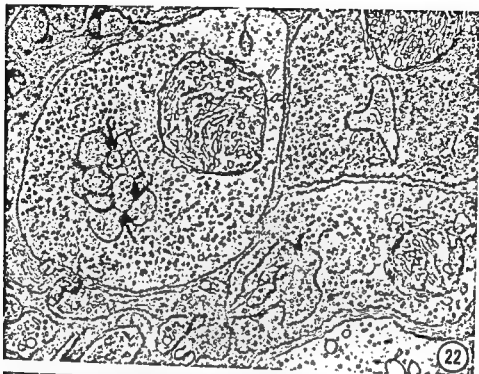
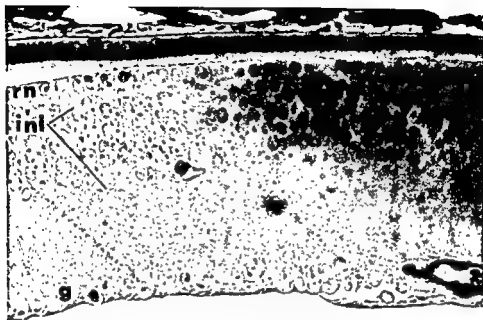


PLATE 13

EXPLANATION OF FIGURES

- 24 A light micrograph of the retina of C3H/HeJ mouse at two months of age. The pigment epithelium (p) abuts against the external limiting membrane. One remaining row of receptor nuclei (rn) is evident and below this is a residue of the outer plexiform layer. The inner nuclear (in) and ganglion cell (g) layers appear entirely normal. $\times 550$.
- 25 A light micrograph of a retina of a C3H/HeJ mouse treated with glutamate. The pigment epithelium (p) faces a retina with two rows of nuclei and an inner plexiform layer. $\times 540$.



(24)



(25)

PLATE 13

EXPLANATION OF FIGURES

- 24 A light micrograph of the retina of C3H/HeJ mouse at two months of age. The pigment epithelium (p) abuts against the external limiting membrane. One remaining row of receptor nuclei (rn) is evident and below this is a residue of the outer plexiform layer. The inner nuclear (in) and ganglion cell (g) layers appear entirely normal. $\times 550$.
- 25 A light micrograph of a retina of a C3H/HeJ mouse treated with glutamate. The pigment epithelium (p) faces a retina with two rows of nuclei and an inner plexiform layer. $\times 540$.

GLUTAMATE MODIFIED MOUSE RETINA
Adolph I. Cohen

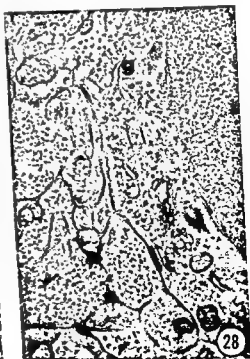


PLATE 14

EXPLANATION OF FIGURES

- 26 An electron micrograph of the apposition of the pigment epithelium and retina in a glutamate-treated C3H/HeJ mouse, showing the residual outer retinal surface consisting of imbricated processes of glial cells of Müller. $\times 15,500$.
- 27 An electron micrograph of the retina of a glutamate-treated C3H/HeJ mouse. A dyad synapse is evidence of the survival of some bipolar neurons as well as other neurons. $\times 32,000$.
- 28 An electron micrograph of the retina of a glutamate-treated C3H/HeJ mouse. The cell soma illustrated (g) appears to be that of a ganglion cell as also evidenced by the sub-membranal cistern (c) thus far only observed in the mouse retina in ganglion cells. $\times 19,800$.

The Development of the Facial Muscles in Man^{1,2}

RAYMOND F. GASSER³

Department of Anatomy, University of Alabama Medical Center,
Birmingham, Alabama

ABSTRACT Morphogenesis and histogenesis of the facial muscles is described in human embryos and fetuses 4.2–360.0 mm (crown-rump length). The microscopic study was performed on 50 specimens that had been variously serially-sectioned and stained. Graphic or wax reconstructions were made from transverse serial sections at 11 representative ages. Three late fetuses and a term infant were studied grossly.

Second branchial arch mesenchyme in early embryos (4.2–6.5 mm) becomes increasingly dense, but is not subdivided into distinct premuscle masses. By 8–20 mm, sheet-like collections (laminae) of premyoblasts and early myoblasts extend from the superficial part of the arch into the temporal, occipital, cervical and mandibular regions. Premuscle condensations deep in the arch become the stapedius, posterior digastric and stylohyoid muscles. The infraorbital lamina and the occipital platysma appear by 20–23 mm. The superficial muscles differentiate rapidly between 26 and 37 mm. Most are composed of myoblasts at 41 mm. By 80 mm, all the muscles contain myotubes and are in their definitive positions. At 80–140 mm, the myotubes become young muscle fibers. From 140 mm to 360 mm (term) the muscles increase in size and gain definitive attachments. Superficial muscles differentiate later than the deep and those in the cervicomandibular and occipital regions differentiate earlier than those in the frontal and midfacial regions. The muscle masses form *pari passu* with the muscular branches of the facial nerve which develop deep to them.

This paper presents a detailed description of the morphogenesis and histogenesis of the muscles innervated by the seventh cranial or facial nerve in man. Such a study may be helpful in understanding and explaining variations and anomalous arrangements of the facial musculature and the general patterns of development in the head and neck regions. Besides functioning to express the emotions of man, these muscles are also important in phonation, mastication, deglutition, audition and vision. This may help explain their extensive development and their unusual degree of individualization in the human subject. In comparison to the important role this musculature plays in the post-natal life of man, its embryology has received little attention. Since the time of Rahl (1887) and Gegenbaur (1890) the embryonic development of the facial muscles has been associated with the second branchial or hyoid arch. Futamura's ('06) paper is the most extensive report on the morphogenesis of these muscles and is widely quoted in the literature. He described the ontogeny of the muscles in the light of their phylogeny which makes an already difficult subject more complex. In

addition, the existence of primitive sphincter arrangements which he described at an early age around the eye, nose, mouth and ear is questionable. Because Popowsky (1895) and Huber ('31) used mainly fetal dissections as the source of their information, they could not adequately cover the early morphogenesis of the facial muscles and even many of the muscles in the fetal specimens were overlooked. Zuckermann-Zicha ('25) restricted her study to the development of only one facial muscle, the palpebral part of the orbicularis oculi. Both Futamura ('06) and Zuckermann-Zicha ('25) included statements on facial muscle histogenesis in their papers but more complete information during the early periods of prenatal life becomes significant in the light of Hooker's ('52, '58) and Humphrey's ('64) studies on the appearance of human fetal reflexes in the head and neck areas.

¹ Submitted in partial fulfillment of the requirements for the degree of Doctor of Philosophy in the Department of Anatomy in the Graduate School of the University of Alabama, University, Alabama, 1965.

² Added in part by grant HD-00230, National Institutes of Child Health and Human Development, National Institutes of Health to Dr. Tryphena Humphrey.

³ Present address: Department of Anatomy, Louisiana State University Medical Center, New Orleans, Louisiana.

muscle field were observed in ten variously stained, representative specimens 4.8 to 146.0 mm.³ After 26 mm, four regions were primarily observed, namely, occipital, orbicularis oris, orbicularis oculi and buccinator. The definitions of the various terms used for stages of histogenesis differ considerably from one author to another. In order to avoid this confusion, the terms suggested by Boyd ('60) for the histogenesis of nonsomitic muscles have been used, namely, *premyoblast*, *myoblast*, *myotube* and *muscle fiber*. In order to facilitate a better understanding of facial muscle histogenesis some of Boyd's stages have been subdivided. The definition of each stage and substage is as follows:

1. *Premyoblast*; a primordial muscle cell which cannot be distinguished from associated fibroblasts and is without orientation.

a. Early; an irregular stellate-shaped cell with little cytoplasm and a large, round, darkly-staining nucleus.

b. Late; an irregular stellate- or spindle-shaped cell with scant cytoplasm and an oval nucleus that stains lightly with finely clumped chromatin.

2. *Myoblast*; the cell may be uni- or multinucleated, has become elongated but shows no visible transverse striations and little or no cytoplasmic structure. Many groups of nuclei are oriented in the same direction.

a. Early; a uninucleated, short, spindle-shaped cell with the cytoplasm beginning to increase in amount and containing one oval or elongated, ellipsoidal nucleus with one or two nucleoli and finely clumped chromatin. No cytoplasmic structures are visible.

b. Middle; a uni- or multinucleated, long, spindle-shaped cell with elongated, ellipsoidal nuclei containing finely clumped chromatin. No cytoplasmic structures are evident. Cell shape and nucleus are similar to a short, smooth muscle cell.

c. Late; a multinucleated, very long, spindle-shaped cell with elongated nuclei containing finely clumped chromatin. Fine fibrils are sometimes evident in the cytoplasm. Groups of cells, in longitudinal section, have the appearance of long, parallel ribbons.

3. *Myotube*; a very elongated cell containing fibrils that show some transverse striations in the periphery and has an axial core of pale, homogeneous cytoplasm with ellipsoidal, central nuclei.

4. *Muscle Fiber*; a multinucleated cell with fully established, transverse striations and nuclei situated at the periphery.

a. Early; a muscle fiber with peripheral nuclei that are large in comparison to the total cross-section of the cell.

b. Late; the definitive muscle fiber.

DEVELOPMENTAL OBSERVATIONS

The sequence of development of the facial muscles is presented in five stages. Within each stage there are important, developmental changes, yet there is a natural overlap between stages.

As the individual muscles develop, they separate into a superficial and a deep group. When the separation becomes clear (Stage II), the development of the superficial muscles is presented before that of the deep muscles. The muscles innervated by the facial nerve are listed in table 1 where they are grouped according to their location (superficial or deep) and their common, premuscle condensation (lamina, mesenchymal collection or complex). The definitive location of the muscles is illustrated in figures 10 and 11 in the 80 mm fetus.

Stage I: second branchial arch mesenchyme (4.2 to 6.5 mm)

The mesenchyme of the second branchial arch in 4.2-6.5 mm embryos is most densely cellular in the middle and ventral regions of the arch. Midway in the arch it extends medially to join with the mesenchyme of the arch on the opposite side. When traced dorsally from the middle area it becomes less and less cellular (fig. 1). At the termination of the facial nerve, the mesenchyme surrounds the nerve and, at the level of the second arch epibranchial placode, it is located deep and caudal to the nerve. Dorsal to the arch, the mesenchyme is very much scattered with the cells becoming less numerous. The cells become slightly

³ A table giving in outline form the state of histogenesis for each of the ten specimens is in the author's dissertation. See footnote 4, page 358.

MATERIALS AND METHODS

The head and neck of 50 serially-sectioned human embryos and fetuses 4.2 to 146.0 mm crown-rump length (C-RL) were examined microscopically and segregated according to their state of development into four groups. Three aborted late fetuses (142, 210 and 270 mm C-RL) and a stillborn term infant (360 mm C-RL) were dissected. The three oldest dissected specimens comprised a fifth group. All future references to millimeter measurements in this paper will pertain to C-RL. All references to ages of the specimens studied will be menstrual age calculated from the C-RL according to the tables of Mall ('18) and Streeter ('20) for specimens under and over 100 mm, respectively.

The distribution of the sectioned specimens is as follows: Group I, four specimens 4.2 to 6.5 mm; group II, 20 specimens 8 to 20 mm; group III, 18 specimens 20 to 45 mm; group IV, 8 specimens 50 to 146 mm. The material had been sectioned in various planes and at various thicknesses, but most were cut transversely at 10 μ . Most of the youngest specimens (4.2-13.5 mm) had been stained with hematoxylin and eosin; specimens 13.5 to 37.0 mm had been stained with a variety of techniques, usually either protargol or a quadruple stain of hematoxylin, orange g, aniline blue and eosin. The 14 sectioned specimens over 37 mm had been stained with the quadruple stain.⁴

The right sides of 11 transversely-sectioned specimens at representative age levels were reconstructed, five graphically and six with wax. As many as 30 measurements were made on the right half of the projected image (17X to 70X) in the graphically-reconstructed specimens. A graph was constructed which consisted of horizontal parallel lines. The distance between the lines depended upon the thickness of the sections, their magnification and the number of sections measured. The measurements of the sections with the largest rostradorsal diameter were the first plotted on the graph followed by sections cranial and caudal to them. The picture constructed in this manner is a lateral view of the right half of the head and neck. The sections were subsequently ex-

amined microscopically in order to determine the location, arrangement and extent of the muscle precursors. Premuscle masses were plotted on graphs section by section in the form of dots (mesenchyme) and lines (myoblasts and myotubes). The lines had the same orientation as the premuscle cells in the sections.

The wax reconstructions resulted in essentially the same type of map with the added feature of having definite external contours. Their construction was similar to the method of Born (1883, 1888). Selected sections were projected (7X to 20X) onto sheets of dental tray spacer wax which had a uniform thickness (1.7 mm). The outlines of the projected images were cut into the wax sheets. Each sheet represented the same number of sections. The approximately 100 impressions were stacked in order and secured in position. The right side of the resulting model and a scale were photographed from a central lateral position and prints made at one-to-one magnification. The wax sheets in the model were represented in the print tracings as horizontal, parallel lines 1.7 mm apart. The sections were examined microscopically and the facial premuscle masses were plotted on the tracings in the same manner as above.

The dissected specimens were obtained relatively fresh and in good condition, embalmed by way of the umbilical vein with 10% buffered formalin, submerged in this fixative for two days and then washed in tap water for 24 hours. Then they were wrapped in cotton previously soaked in Kaiserling III solution, placed in plastic bags and stored as long as six months at 40°F. One week before their dissection, the heads and necks were lightly and carefully skinned and submerged in Bouin's fluid. At the time of their dissection, the fetuses were washed for one minute in water. The dissections were performed with a dissecting microscope at magnifications up to 40X using teasing needles, needle forceps and a small pair of scissors.

The types of primordial muscle cells present in various regions of the facial

⁴ A table giving a complete listing of pertinent data on each specimen is in the author's dissertation entitled "The development of the facial muscles and the facial nerve in human embryos," which is available at the Medical Center Library, University of Alabama Medical Center, Birmingham, Alabama.

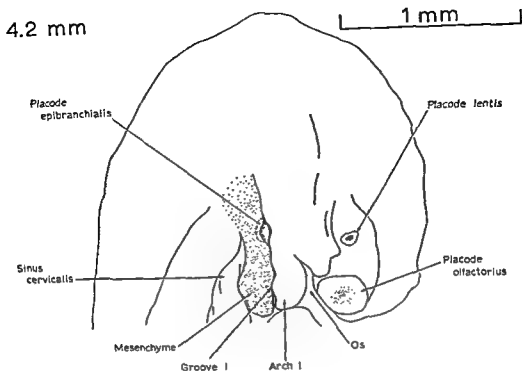


Fig. 1 The second branchial arch of a 4.2 mm embryo, six weeks, Holmes' silver stain. Taken from a graphic reconstruction. The mesenchymal cells in the second arch are shown as stipple.

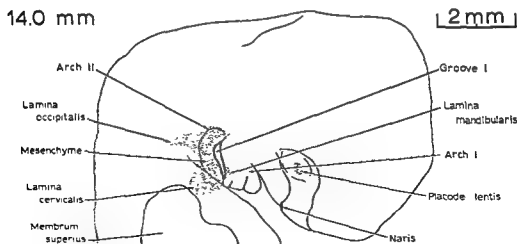


Fig. 2 The superficial part of the second branchial arch of a 14.0 mm embryo, eight weeks, Bodian's protargol stain. Taken from a graphic reconstruction. The mesenchymal cells in the superficial part of the arch with their extensions are shown as stipple.

TABLE 1

The superficial and deep facial muscles¹Stage II: facial premuscle masses
(8.0 to 20.0 mm)

- I. Superficial muscles**
- A. Temporal lamina
 - Auricularis superior m
 - B. Occipital lamina
 - Occipital belly of occipitofrontalis m (occipitalis m)
 - Auricularis posterior m
 - Transversus nuchae m
 - C. Cervical lamina
 - Cervical part of the platysma
 - D. Occipital platysma
 - Occipital part of the platysma
 - E. Mandibular lamina
 - Mandibular part of the platysma
 - Depressor labii inferioris m
 - Mentalis m
 - Risorius m
 - Depressor anguli oris m
 - Inferior part of the orbicularis oris m
 - Buccinator m (?)
 - Levator anguli oris m (?)
 - F. Infraorbital lamina
 - Zygomaticus major m
 - Zygomaticus minor m
 - Levator labii superioris m
 - Levator labii superioris alaeque nasi m
 - Superior part of the orbicularis oris m
 - Compressor naris m (?)
 - Dilator naris m (?)
 - Depressor septi m (?)
 - Orbicularis oculi m (?)
 - Frontal belly of occipitofrontalis m (frontalis m) (?)
 - Corrugator supercillii m (?)
 - Procerus m (?)
 - G. Mesenchymal cells adjacent to the first branchial groove
 - Auricularis anterior m
- II. Deep muscles**
- A. Posterior digastric complex
 - Stapedius m
 - Posterior belly of digastric m (posterior digastric m)
 - Stylohyoid m
 - Digastric tendon

¹A definite premuscle mass from the second branchial arch was not evident for the muscles with a question mark. However, each of these muscles probably develops from the precursor indicated.

more numerous in the area lateral to the otic vesicle. No discrete condensations are present in the arch. The cells that will develop into muscle are in an early pre-myoblast state. Deep to the branchial grooves the mesenchyme is continuous with that of the adjacent arches. This is also true for the sparse mesenchyme dorsal to the arch.

The first mesenchymal condensation in the second arch is observed in an 8.0 mm embryo and represents the primordium of the second branchial (Reichert's) cartilage. It is located medial to the facial nerve, just dorsal to the origin of the chorda tympani nerve. At 9.5–10.5 mm the primordium enlarges and is slightly rostral to the facial nerve. It extends ventrally and medially to an area which is rostral to the caudalmost part of the pharynx and is circular to oval in transverse sections.

Superficial. A superficial condensation appears in the caudolateral part of the arch by 10.5 mm. Its border is not well defined but is roughly fusiform to oval on transverse section. Ventrally it blends with the dense mesenchyme in the arch. By 10.6–14.0 mm the condensation is developing extensions into the region caudal to the second arch (fig. 2). This caudal extension is most prominent at its dorsal and ventral extremes. The dorsal part spreads into the future occipital and posterior auricular regions and is designated the *occipital lamina*. It is more apparent in 18.0 mm embryos but is less dense than the mesenchyme within the arch (figs. 4, 13). The posterior auricular branch of the facial nerve is developing deep to the lamina. The ventral part of the caudal extension that is present at 14.0 mm (fig. 2) grows into the rostralateral aspect of the upper cervical region and is designated the *cervical lamina*. A collection of mesenchymal cells also extends rostrally into the mandibular arch region and is designated the *mandibular lamina*. It is not well defined at 14.0 mm, but becomes more apparent at 15.0 and 16.0 mm, and at 18.0 mm it is continuous with the *cervical lamina* (figs. 4, 14). In 14.0 mm embryos, the mesenchyme in the dorsal part of the arch is slightly more cellular than the loose mesenchyme dorsal to the arch. At 18.0 mm, this more cellular mesenchyme appears as another extension from the second arch and spreads in a dorsal direction as a *temporal lamina* (figs. 4, 12).

Deep. The most discrete second arch premuscle condensation in 10.5–14.0 mm embryos is located caudal and medial to the facial nerve in the deep part of the

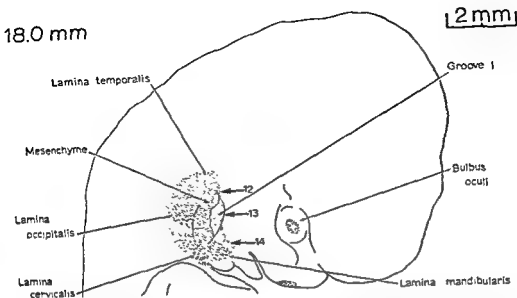


Fig. 4 The superficial facial muscle masses of an 18.0 mm embryo, 8.5 weeks, Bodian's protargol stain. Taken from a graphic reconstruction. Mesenchymal cells and premyoblasts are shown as stipple; myoblasts are shown as interrupted lines with the direction of the lines indicating the myoblasts' orientation. See plate 1, figures 12, 13 and 14 for explanation of numbered arrows.

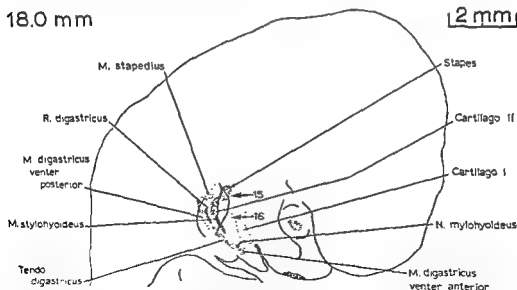


Fig. 5 The deep facial muscle masses of the same 18.0 mm embryo as in figure 4. See plate 1, figures 15 and 16 for explanation of numbered arrows.

are early myoblasts and the most mature premuscle cells in the second arch area are located in the occipital lamina and in the dorsal part of the posterior digastric complex. The cells in both of these re-

gions are closely related to branches of the facial nerve. By 18–20 mm the myoblasts increase in number and are more mature; some have become middle myoblasts. Since the myoblasts are numerous,

arch and is designated the *posterior digastric complex* (fig. 3). At 14 mm it is continuous laterally with the deep aspect of the *cervical lamina*. The complex increases in size as it courses ventrally and then becomes slightly constricted as it proceeds into the mandibular arch where it is continuous with another densely cellular concentration, the *mylohyoid complex*. The *posterior digastric complex* receives a series of small, diffuse branches from the caudal aspect of the facial nerve. These branches can be traced ventrally within the complex to the region of the first branchial groove. They could not be traced beyond the constricted part of the condensation in any of the embryos examined. The most dorsal part of the *mylohyoid complex* receives a small, single branch from the mandibular division of the trigeminal nerve. This continuous group of condensations represents the first appearance of the digastric, stylohyoid and mylohyoid muscles. By 18 mm the dorsal part is dividing into the posterior belly of the digastric (*posterior digastric*) and stylohyoid muscles (figs. 5, 16). The ventral part is dividing into the anterior belly of the digastric (*anterior digastric*) and mylohyoid muscles. The intermediate region becomes more constricted and is developing into the digastric tendon. The

stylohyoid muscle develops from the rostral part of the *posterior digastric complex* immediately caudal to the second arch cartilage.

The dorsal extent of the *posterior digastric complex* is continuous on the medial side of the facial nerve with the dorsal part of the second branchial cartilage. In this region will develop the stapedius muscle and the stapes of the middle ear. At 18.0 mm the stapes is forming in an area adjacent to the dorsal end of the second arch cartilage (fig. 5). The stapes at this time is a ring-like condensation with the stapedia artery coursing through it. A small collection of late premyoblasts is located caudal to the dorsal tip of the second arch cartilage in 14.0 mm embryos (fig. 3) and is the first appearance of the stapedius muscle. These premyoblasts are adjacent to the medial side of the facial nerve and course rostrally to the vicinity of the second arch cartilage. At 18–20 mm the stapedius muscle is better defined (figs. 5, 15) and is composed mostly of early myoblasts which join the cells connecting the stapes and the second arch cartilage.

Histogenesis. Most of the premuscle cells in 14–16 mm embryos are late premyoblasts. None of the cells are mature myoblasts. By 18 mm many of the cells

14.0 mm

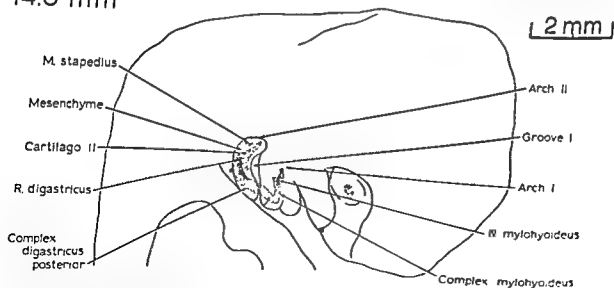


Fig. 3 The deep part of the second branchial arch of the same 14.0 mm embryo as in figure 2. All mesenchymal condensations in the deep part of the second arch and one of the condensations in the first arch are shown as stipple.

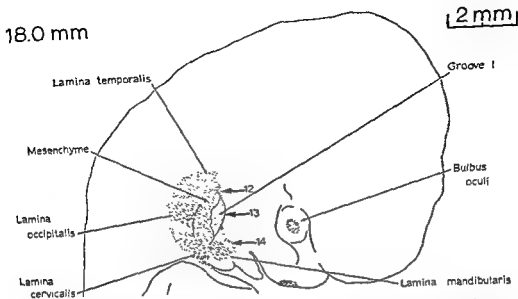


Fig. 4 The superficial facial muscle masses of an 18.0 mm embryo, 8.5 weeks, Bodian's protargol stain. Taken from a graphic reconstruction. Mesenchymal cells and premyoblasts are shown as stipple; myoblasts are shown as interrupted lines with the direction of the lines indicating the myoblasts' orientation. See plate 1, figures 12, 13 and 14 for explanation of numbered arrows.

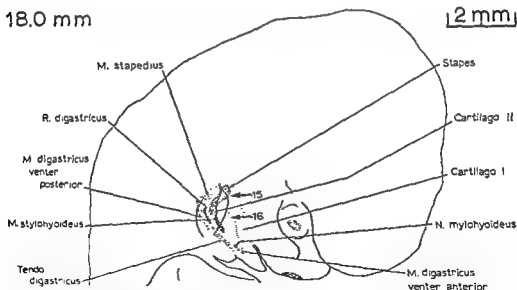


Fig. 5 The deep facial muscle masses of the same 18.0 mm embryo as in figure 4. See plate 1, figures 15 and 16 for explanation of numbered arrows.

are early myoblasts and the most mature premuscle cells in the second arch area are located in the *occipital lamina* and in the dorsal part of the posterior digastric complex. The cells in both of these re-

gions are closely related to branches of the facial nerve. By 18–20 mm the myoblasts increase in number and are more mature; some have become middle myoblasts. Since the myoblasts are numerous,

arch and is designated the *posterior digastric complex* (fig. 3). At 14 mm it is continuous laterally with the deep aspect of the *cervical lamina*. The complex increases in size as it courses ventrally and then becomes slightly constricted as it proceeds into the mandibular arch where it is continuous with another densely cellular concentration, the *mylohyoid complex*. The *posterior digastric complex* receives a series of small, diffuse branches from the caudal aspect of the facial nerve. These branches can be traced ventrally within the complex to the region of the first branchial groove. They could not be traced beyond the constricted part of the condensation in any of the embryos examined. The most dorsal part of the *mylohyoid complex* receives a small, single branch from the mandibular division of the trigeminal nerve. This continuous group of condensations represents the first appearance of the digastric, stylohyoid and mylohyoid muscles. By 18 mm the dorsal part is dividing into the posterior belly of the digastric (posterior digastric) and stylohyoid muscles (figs. 5, 16). The ventral part is dividing into the anterior belly of the digastric (anterior digastric) and mylohyoid muscles. The intermediate region becomes more constricted and is developing into the digastric tendon. The

stylohyoid muscle develops from the rostral part of the *posterior digastric complex* immediately caudal to the second arch cartilage.

The dorsal extent of the *posterior digastric complex* is continuous on the medial side of the facial nerve with the dorsal part of the second branchial cartilage. In this region will develop the stapedius muscle and the stapes of the middle ear. At 18.0 mm the stapes is forming in an area adjacent to the dorsal end of the second arch cartilage (fig. 5). The stapes at this time is a ring-like condensation with the stapedia artery coursing through it. A small collection of late premyoblasts is located caudal to the dorsal tip of the second arch cartilage in 14.0 mm embryos (fig. 3) and is the first appearance of the stapedius muscle. These premyoblasts are adjacent to the medial side of the facial nerve and course rostrally to the vicinity of the second arch cartilage. At 18–20 mm the stapedius muscle is better defined (figs. 5, 15) and is composed mostly of early myoblasts which join the cells connecting the stapes and the second arch cartilage.

Histogenesis. Most of the premuscle cells in 14–16 mm embryos are late premyoblasts. None of the cells are mature myoblasts. By 18 mm many of the cells

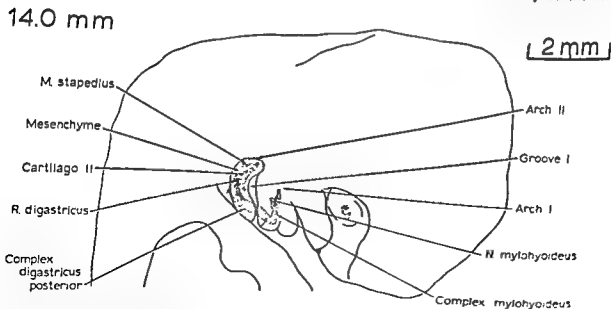


Fig. 3 The deep part of the second branchial arch of the same 14.0 mm embryo as in figure 2. All mesenchymal condensations in the deep part of the second arch and one of the condensations in the first arch are shown as stipple.

22.2 mm

3 mm

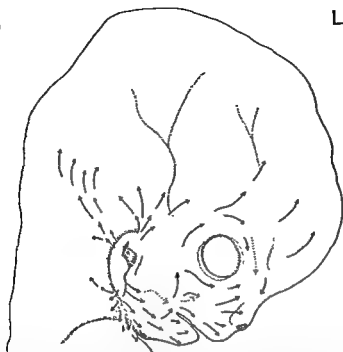


Fig. 7 Groups of arrows superimposed on the same embryo as in figure 6 indicate the future location and apparent direction of growth of the superficial laminae. The stippled arrows in the supraorbital, infraorbital and buccal regions indicate the regions where the corrugator supercilli, levator anguli oris and buccinator muscles respectively, appear to form by delamination from the deep surface of the more superficial layer of muscle.

differentiated of any of the premuscle cells in the superficial muscles at this time.

In 20-23 mm specimens a small band of late premyoblasts and early myoblasts, the occipital *platysma*, courses dorsally from the caudal part of the developing auricle and represents the precursor of the occipital part of the *platysma*. By 26 mm it is a narrow band that blends with the dorsal border of the *cervical lamina*. It is composed of several narrow bundles of myoblasts in 37-45 mm which course into the occipital region. They are superficial to the sternomastoid muscle and in some fetuses are continuous with the ventral border of the trapezius muscle.

Ventral to the first branchial groove at 20-23 mm the *cervical* and *mandibular laminae* are united in a continuous thick layer of middle myoblasts and many premyoblasts. The layer of cells extends into the ventral part of the upper cervical region (*cervical lamina*) and also into the

mandibular arch (*mandibular lamina*). Most of the myoblasts in the mandibular part are directed rostrally and ventrally; those in the cervical part are directed caudally. The myoblasts in the junction region are essentially horizontal in their orientation. Most of the superficial myoblasts in 24-26 mm specimens are concentrated in united *cervical* and *mandibular laminae*. The entire *cervical lamina* develops into the cervical part of the *platysma* and much of the *mandibular lamina* forms its mandibular extension. The premyoblasts are gradually replaced by myoblasts. The premuscle cells are continuous with dense collections of mesenchymal cells in the auricular region. The *mandibular lamina* extends almost to the angle of the mouth. By 27-40 mm the *platysma* is thinner and slightly broader as it extends to the shoulder region. At its caudal border the myoblasts are gradually replaced with premyoblasts or mes-

the laminae and deeper muscle masses are easier to outline, trace and identify.

Stage III: facial muscle differentiation
(20.0 to 45.0 mm)

Superficial Muscles. The superficial laminae present in earlier embryos are well developed in 20-23 mm specimens and two additional structures, the *infra-orbital lamina* and the *occipital platysma* appear (fig. 6). The directions of development of each of the laminae present at 22.2 mm are illustrated in figure 7 by groups of arrows. At 24-26 mm the laminae extend farther from the second arch region where the auricle is forming (fig. 8) and by 27-45 mm they subdivide into individual muscles at variable distances from the auricle (fig. 9).

The *temporal lamina* is composed of loosely arranged late premyoblasts at 20-23 mm. It is better developed by 26 mm where it courses rostrally and cranially and is composed of many premyoblasts and some early myoblasts. In 27-40 mm

fetuses the lamina is a thin layer of myoblasts which has spread into the temporal region forming the *auricularis superior muscle* (fig. 9). As the lamina courses cranially it is gradually replaced by premyoblasts or active fibroblasts. The *auricularis anterior muscle* is present at 40-45 mm as a small collection of cells immediately rostral to the auricle. It does not develop from the *temporal lamina* but from mesenchyme adjacent to the first branchial groove.

The *occipital lamina* contains occasional early myoblasts at 20-23 mm and courses dorsally toward the occipital region. The number of myoblasts increases by 26 mm. The major part of the lamina forms the occipital belly of the *occipitofrontalis* (occipitalis) muscle but both bellies of the *auricularis posterior* muscle also apparently develop from it between 27 and 40 mm (fig. 9). In one specimen the two muscles were continuous. Many of the cells of the *occipitalis* muscle in 40-45 mm fetuses are myotubes and are the best

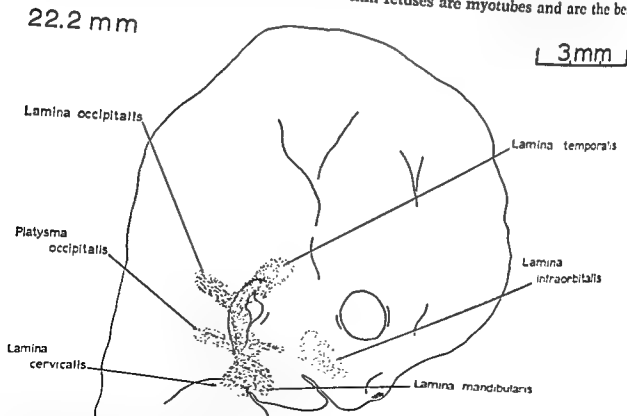


Fig. 6 The superficial facial muscle masses of a 22.2 mm embryo, nine weeks, Bodian's protargol stain. Taken from a wax reconstruction. Mesenchymal cells and premyoblasts are shown as stipple;

enchymal cells which can be traced to the level of the developing clavicle. At 40-45 mm the platysma extends to the midline in the mental and submental regions, but not in the cervical region.

A triangular group of myoblasts is located at the rostral termination of the *mandibular lamina* at 26 mm which extends to the angle of the mouth. It is on a plane superficial in the *mandibular lamina* and represents the first appearance of the depressor anguli oris muscle. The direction of the myoblasts differs from those in the *mandibular lamina* by 90°. The myoblasts are more closely packed as they approach the angle of the mouth. The muscle is well defined between 27 and 45 mm and is superficial to the platysma.

The orbicularis oris muscle has begun to develop by 37 mm where it is a loose collection of middle myoblasts which is thicker in the upper than in the lower lip. The myoblasts are sparse in the midline. By 40-45 mm the muscle is made up of late myoblasts and completely encircles the mouth.

In 20-23 mm specimens the *mandibular lamina* is continuous with a loose collection of mesenchymal cells in the infraorbital region, the *infraorbital lamina*. The region of continuity is narrow and is limited to the area immediately rostral to the ventral part of the first branchial groove. Since the *infraorbital lamina* is highly vascular, it is difficult to determine if its component cells are forming facial muscles or blood vessels. Considerable changes take place by 24-26 mm. In the most lateral aspect of the infraorbital region, a discrete band of myoblasts has formed. It is round to oval in transverse section and represents the first appearance of the zygomaticus major muscle. The muscle courses from the region of the developing zygoma to the angle of the mouth where it is continuous with the depressor anguli oris muscle. Medial to the zygomaticus major muscle, the *infraorbital lamina* is composed of premyoblasts and myoblasts which are superficial to the infraorbital plexus of nerves. The lamina extends laterally and dorsally into the area immediately above the zygomaticus major muscle. In 27-45 mm fetuses, the zygomaticus major muscle is a very prominent

band that is continuous along its medial border with the zygomaticus and orbicularis oculi muscles. The zygomaticus minor muscle is continuous medially with a sheet of myoblasts that courses into the upper lip and lateral aspect of the nose. No definite levator labial or nasal muscles are identifiable.

At 37 mm, the orbicularis oculi muscle is developing around the eye, but does not yet completely encircle it. The muscle is thickest laterally and thins as it spreads dorsally. The *infraorbital* portion is partly superficial to the zygomaticus muscles and *infraorbital lamina*. It courses medially and disappears at the side of the nose. Mesenchymal cells, probably premyoblasts, are arranged in a layer in the superior palpebrum and in the medial part of the orbital region. Only the most medial portion of the orbital part of the orbicularis oculi muscle is deficient in 40-45 mm fetuses. Myoblasts are present in most of the orbital part, but the palpebral part remains in a premyoblastic state.

The frontal belly of the occipitofrontalis (frontalis) muscle begins to develop in 27-45 mm fetuses, but is not well defined. Its premuscle cells are mainly premyoblasts which show little orientation. The majority of the cells cranial to the frontal, temporal and occipital regions are premyoblasts or active fibroblasts which form a thin layer superficial to the developing calvarium. In 40-45 mm specimens, this layer extends to the vertex of the head, but thins in the midline in the frontoparietal and occipitoparietal regions. As development proceeds, the cells become oriented mainly in a rostradorsal direction and form the galea aponeurotica. Myoblasts connecting the frontalis and occipitalis muscles were not observed in any of the specimens.

The buccinator muscle first appears at 26 mm, but is difficult to outline since it is primarily composed of premyoblasts and early myoblasts. Its dorsal boundary is especially difficult to define since it gradually blends with the mesenchymal cells lateral to the pharynx. The buccinator mass becomes superficial as it approaches the angle of the mouth where it joins the deep aspect of the more superficial muscle masses in the region. A nerve supply to

26.0 mm

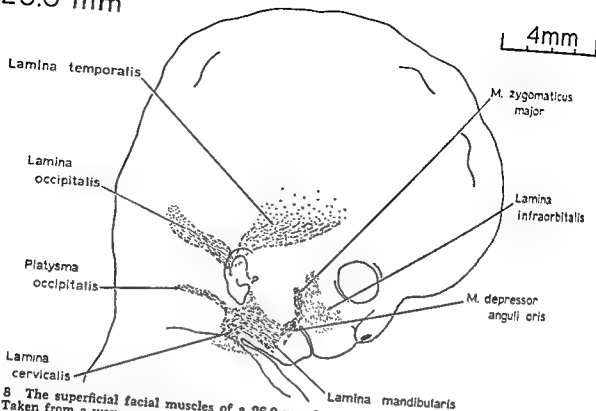


Fig. 8 The superficial facial muscles of a 26.0 mm fetus, ten weeks, erythrosin and toluidin blue stain. Taken from a wax reconstruction. Mesenchymal cells and premyoblasts are shown as stipple; myoblasts are shown as interrupted lines.

37.0 mm

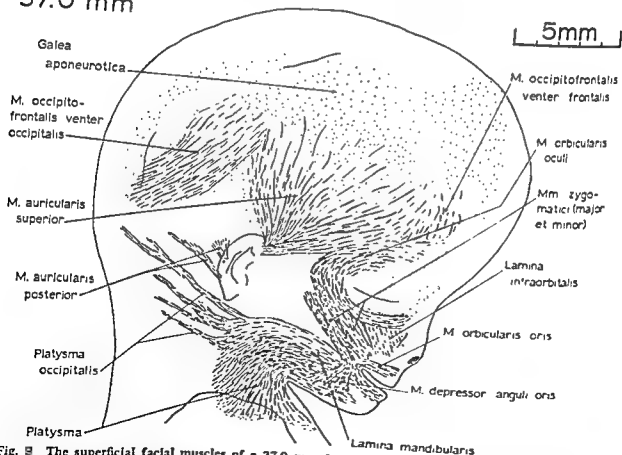


Fig. 9 The superficial facial muscles of a 37.0 mm fetus, 11 weeks, Bodian's protargol and erythrosin stain. Taken from a wax reconstruction. Fibroblasts and premyoblasts are shown as stipple; myoblasts are shown as interrupted lines. The closeness of the lines is proportional to the relative concentration of premuscle cells.

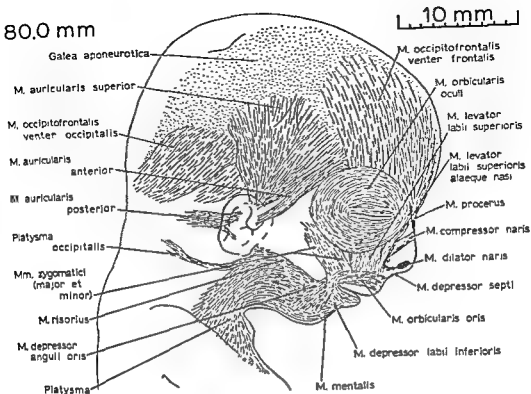


Fig. 10 The superficial facial muscles of an 80.0 mm fetus, 14.5 weeks, quadruple stain. Taken from a wax reconstruction. Fibroblasts (galea aponeurotica) are shown as stipple; myotubes are shown as lines.

The zygomaticus major and minor muscles are sometimes separate between 50 and 58 mm, but become more difficult to separate from each other by 80–142 mm. The levator labii superioris muscle is identifiable in the infraorbital region of 50–58 mm fetuses and is often separated by blood vessels into superficial and deep parts. The superficial part is continuous cranially with the orbicularis oculi muscle and the deep part attaches to the maxillary bone immediately caudal to the orbit. Both parts unite as they pass into the upper lip and are superficial to the infraorbital plexus of nerves. A sheet of myoblasts in the lateral nasal area is also separated into two parts by blood vessels. The myoblasts course caudally toward the upper lip and form, by 80 mm, the levator labii superioris alaeque nasi muscle. At this time, the compressor naris muscle is present on the lateral aspect of the nose. It courses from the bridge of the nose,

passing deep to the levator labii superioris alaeque nasi muscle, and ending adjacent to the maxillary bone. The dilator naris muscle is evident at the lower, lateral part of the nose. It is obliquely situated and blends with the deeper part of the orbicularis oris muscle. The depressor septi muscle is caudal to the nasal septum and courses in a vertical direction. At 142 mm, it courses from the naris into the upper lip where the fibers pass deep to the orbicularis oris muscle to attach to the maxillary bone.

The orbital part of the orbicularis oculi muscle is easily defined at 50–58 mm, but the palpebral part remains poorly developed. The myoblasts disappear at the periphery of the eyelids and are most numerous laterally and cranio-medially. The cranio-medial part joins with the frontalis muscle and both extend onto the bridge of the nose as the procerus muscle. The

the muscle was not observed until 37 mm. At this time, the muscle is more apparent and is divided in its dorsal half into a large caudal and a small cranial portion with the parotid duct coursing between them. The caudal portion extends farther dorsally, and between 37 and 45 mm, it blends with the superior constrictor of the pharynx. At this age, the muscle is completely pierced by the buccal branch of the mandibular nerve.

By 37 mm, the levator anguli oris muscle has formed deep to the caudal and lateral part of the infraorbital plexus. It begins cranially adjacent to the developing maxillary bone and courses caudally and laterally to join with the zygomaticus and buccinator muscles at the angle of the mouth. Caudal to the angle of the mouth, the muscle is sometimes continuous with the mandibular part of the platysma and the depressor anguli oris muscle.

Deep muscles. All of the deep facial muscles are recognizable in the previous stage but in the present stage they become more distinct and increase in size. Between 20 and 26 mm, the cranial end of the posterior digastric muscle is immediately caudal to the dorsal end of the stapedius muscle. As development proceeds, this distance becomes greater. The stapedius muscle remains close to the medial aspect of the facial nerve, sometimes receiving a short, but obvious, branch from the nerve. It is made up of early and middle myoblasts which terminate medial to the hyostapedial connection between the stapes and cranial end of the second arch cartilage.

The stylohyoid muscle is rostral to the caudal half of the posterior digastric muscle and dorsal to the second arch cartilage. As it proceeds caudally, it is sometimes lateral to the posterior digastric muscle and sometimes surrounds it before terminating in mesenchyme of the hyoid region. The digastric tendon is a dense collection of darkly staining cells that courses into the depths of both the posterior and anterior parts of the digastric muscle.

Stage IV: definitive location of the facial muscles (50 to 146 mm)

Superficial Muscles. Additional superficial muscles can be identified between

50 and 58 mm and all of these muscles can be recognized and outlined at 80 mm in their definitive position (fig. 10).

At 58 mm, the auricularis anterior muscle is a short band of myoblasts coursing cranially from the rostral aspect of the auricle, and at 80 mm it is adjacent to the rostral border of the auricularis superior muscle. No separation could be seen between these two muscles at 142 mm. Dorsal to the auricularis posterior muscle a thin and small sheet of muscle is occasionally present in the lower occipital or upper cervical region. Its muscle cells are mostly directed transversely and compose the transversus nuchae muscle.

Between 58 and 80 mm, the occipital platysma is a single, discrete band which takes a variable path from the platysma into the occipital region. This muscle could not be identified in the grossly dissected, 142 mm fetus. At 58 mm, the mandibular part of the platysma extends into the mental region where it is continuous with vertically directed muscle cells that extend into the lower lip and represent the depressor labii inferioris muscle. This arrangement is observed better at 80 mm where the mentalis muscle is defined for the first time. The risorius muscle develops as a thickening along the cranial border of the platysma. Its state of development is variable.

At 58 mm, the buccinator muscle extends farther dorsally, and by 80 mm it extends to the region of the lateral pterygoid plate (fig. 11). Between 101 and 146 mm, it unites dorsally with the superior pharyngeal constrictor muscle. A decussation of its muscle cells at the angle of the mouth is apparent at 80 mm. By 142 mm, a large fat pad has developed superficial to the buccinator but deep to the risorius and platysma muscles. The levator anguli oris muscle grows considerably in thickness and length deep to the infraorbital plexus of nerves.

In 58-80 mm fetuses, the orbicularis oris muscle is well developed, completely encircles the mouth, but is difficult to divide into superficial and deep parts. It has become thicker and is continuous with the perioral muscles. Its medial part in the upper lip lags in development.

Stage V: facial muscles in dissected late fetuses (210, 270 and 360 mm)

The muscles increase in size and extent as the head and neck regions become larger and, in most cases, the boundaries between individual muscles become more prominent. Since the muscles reach their definitive location as early as 58 mm, only gradual changes occur between 146 mm and term.

Superficial muscles. The transversus nuchae muscle is present in the 210 and 270 mm fetuses and is almost continuous with the auricularis posterior muscle. The latter muscle is composed of two bellies in all three specimens. The occipital platysma muscle could not be identified. In the term infant, the platysma extends caudally to the level of the nipple. A distinct, thickened risorius muscle is not always present. The boundary between the zygomaticus muscles is difficult to define, but there is usually a small gap between the zygomaticus minor and levator labii superioris muscles. All of the superficial muscles are delicate and most are deep to a layer of subcutaneous fat, but superficial to their nerve supply. Most of the bony attachments are established, but are not firmly anchored.

Deep muscles. The stylohyoid muscle is smaller and its fibers are less tightly bound together than those of the digastric muscle. All of the deep muscles are attached to bone or cartilage and their attachments are generally more firmly anchored than are the superficial muscles.

DISCUSSION

1. Muscles of expression

Futamura ('06) stated that by 31 to 34 days (9-13 mm)* the superficial muscle blastema becomes voluminous and spreads out dorsally, ventrally and orally. These early, superficial extensions have been designated the *occipital* (dorsally), *cervical* (ventrally) and *mandibular* (orally) laminae. As the neck develops and increases in length, the *cervical lamina* expands to produce the platysma. This manner of development is similar to that described by Rahl (1887) and Futamura ('06). According to Bryce ('23) bundles of fibers sometimes are found in the defini-

tive state extending from the dorsal border of the platysma to the cervical fascia over the sternomastoid and trapezius muscles, and even to the mastoid process. This inconsistent strip of muscle, the *occipital platysma*, appears very early in development (22.2 mm), but diminishes in size as development progresses and could not be found in late fetuses. Huber ('31) stated that it is a vestige of the nuchal portion of the platysma which reflects our primate ancestry.

At 6 weeks (18-24 mm), Futamura ('06) described two layers of pre-muscle tissue; a deep layer that he identified with the sphincter colli of lower vertebrates and a superficial layer which he looked upon as the platysma (colli) of lower forms. In the present study, no attempt is made to describe the ontogeny of the facial muscles on the basis of their phylogeny. The muscles are divided into groups according to their manner of development and definitive location. Futamura ('06) described the deep layer as giving origin to primitive sphincter arrangements around the eye, nose, mouth and ear, and except in the case of the mouth, these early sphincters disappear and are replaced by new formations from the superficial layer. The present study did not reveal sphincters at 18-24 mm in any of these regions (figs. 4, 6). Sphincters completely encircling the nose and auricle were never observed and the orbicularis oris and oculi muscles do not become complete sphincters until approximately 40-45 mm.

Popowsky (1895) found no superficial muscles at 28 mm except the cervical portion of the platysma (*cervical lamina*). Huber ('31) demonstrated the presence of an additional muscle (auricularis posterior) which is identified in the present work as the *occipital lamina*. The present technique revealed additional regions of muscle development, the temporal and *infraorbital laminae* and the *occipital platysma*, as early as 18-22 mm (figs. 4, 6).

Futamura ('06) observed the anlage of the quadratus labii superioris muscle at 6 weeks (18-24 mm) which is similar to

*Futamura ('06) gave an estimated age in days or weeks for his specimens. The millimeter measurements in parentheses are the approximate crown-rump lengths of his specimens calculated from Mall's ('10) graph.

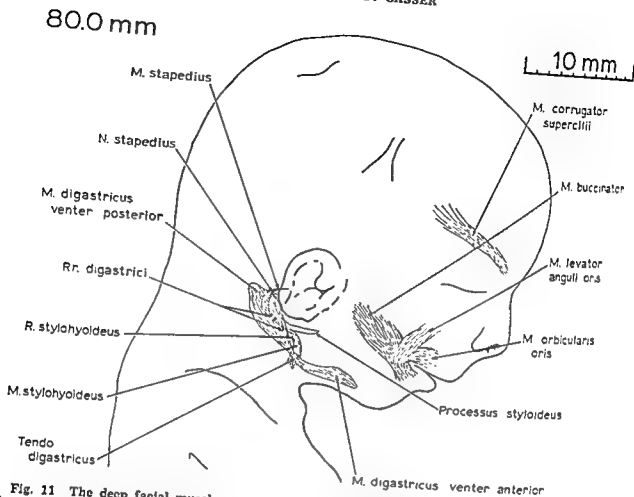


Fig. 11 The deep facial muscles and the deeper superficial facial muscles in the same 80.0 mm fetus as in figure 10. The outline of the stapedius muscle and styloid process deep to the posterior digastric muscle is shown as stipple.

corrugator supercilii muscle appears deep to the supraorbital part of the orbicularis oculi muscle. It becomes larger by 80 mm and extends as a thick band into the lateral aspect of the supraorbital region (fig. 11). At this same time, the medial part of the orbicularis oculi muscle surrounds the lacrimal sac and canaliculi, and the palpebral part is present throughout the major portion of the eyelids.

Between 50 and 58 mm, the frontalis muscle is a thin sheet of myoblasts covering the major part of the frontal region, but is not continuous across the midline until 80 mm. The muscle is thin as it approaches the vertex of the head and the myoblasts are gradually replaced by active fibroblasts. At the vertex, the galea aponeurotica is represented as a layer of fibroblasts. The layer is not only continuous peripherally with the frontalis, but also

with the occipitalis and auricularis superior muscles.

Deep muscles. The stapedius muscle is very large at 58 and 80 mm in comparison with the middle ear region and is oriented in an almost vertical plane (fig. 11). No significant changes occur in the posterior digastric and stylohyoid muscles. In 60 and 146 mm fetuses, the posterior digastric muscle is large, while the stylohyoid muscle is correspondingly small.

The cells of the facial muscles at 50-58 mm are late myoblasts and myotubes. By 80 mm, they are primarily myotubes, and by 146 mm, they are early muscle fibers. The bony or cartilaginous attachments of the muscles are not very apparent. Occasionally, connective tissue fibers are present which partially anchor the muscle cells to the periosteum of developing bone.

muscle develops along with the mylohyoid muscle in the ventral part of the first arch.

Ruge ('10) and Bryce ('23) pointed out the rare occurrence of a definitive muscular connection between the occipital fascia and the posterior digastric muscle. This connection probably represents a retention of an earlier connection (14 mm) between the posterior digastric complex and the cervical lamina.

The time and manner of development of the stapedius muscle agrees with Futamura's ('06) and Schimert's ('33) descriptions, but disagrees with Broman (1898) who believed the muscle develops from the connection between the stapes and the second arch (Reichert's) cartilage. No explanation can be given for the variability in the size and orientation of this muscle during development.

4. Histogenesis and pattern of differentiation

In his studies on the labial muscles, Futamura ('06) saw no transverse striations at 22 weeks (170 mm), faint striations at 26 weeks (220 mm) and distinct striations at 30 weeks (250 mm). The present work reveals transverse striations in myotubes (e.g., orbicularis oris muscle) at 58 mm which become very apparent at 80 mm. Early muscle fibers are present at 146 mm.

Contrary to the statements of Popowsky (1895) the superficial musculature at the end of the third month (58 mm) is already differentiated. This is substantiated by Huber ('31) who produced contractions of the muscles in a living 55 mm fetus through electrical stimulation. In their studies on the appearance of human fetal reflexes, Hooker ('52, '58) and Humphrey ('64, '65) observed, at 37-47 mm, a squint type reflex produced by contraction of the orbicularis oculi muscle. The orbital part of the muscle almost completely surrounds the eye at 41 mm and is composed of late myoblasts. At 47-49 mm, these investigators produced a scowl type reflex by contraction of the corrugator supercilii muscle. This muscle is well differentiated by 58 mm when it is composed of late myoblasts and occasional myotubes. By 60-64 mm, Hooker ('52, '58) and Humphrey ('64, '65) produced momentary lip closure and

at 74-79 mm, lip closure was maintained. At 58 mm, the orbicularis oris muscle is well developed, completely encircles the mouth and is composed mostly of late myoblasts with some myotubes. They observed a sneer type reflex produced by an elevation of the angle of the mouth and ala of the nose at 74 to 88 mm. All of the facial muscles, including the infraorbital ones, have differentiated by 80 mm and are made up of myotubes. Comparison of the degree of histogenetic development of the premuscle cells with the age at which reflexes can be elicited lends support to the view that late myoblasts, with unstriated fibrils in their cytoplasm, are not only able to contract, but that their contractions are influenced to some degree by nerve impulses.

A definite pattern of differentiation is evident in the formation of the facial muscles. The present investigation supports Futamura's ('06) findings that differentiation of the muscles begins earlier in the deep than in the superficial regions and earlier in the lower lateral than in the upper medial regions. In addition, studies show that the muscles in the occipital region (e.g., occipitalis) differentiate and become striated earlier than the lateral facial muscles (e.g., zygomaticus and depressor anguli oris) which in turn differentiate before the muscles close to the midline of the face.

Superficial muscle masses spread from the region of the second arch in all directions except one, that is directly rostrally (fig. 7). The most likely reason for this is the presence of the external auditory meatus which is replacing the first branchial groove. The deep meatus probably causes cells from the second arch to migrate around it so that cell groups must extend first cranially or caudally before they can course rostrally.

In most of the specimens studied, the development of the peripheral branches of the facial nerve follow *pari passu* the development of the facial muscle masses (Gasser, '67). A close relationship exists between the muscles and the nerve throughout development and each appears to influence the histogenesis and morphogenesis of the other. As the muscle masses form, the nerve supply to them differentiates.

what is identified here as the *infraorbital lamina*. A small connection exists between the *infraorbital lamina* and the second arch region at 22 mm (fig. 6), which is less evident at 26 mm (fig. 8) when the lamina is more prominent. The origin of the premuscle cells in the lamina and exactly which muscles on the face develop from the lamina is questionable (table 1). The cells of the *infraorbital lamina* could be descendants of cells in the second branchial arch, their migration taking place at an earlier time when they could not be recognized as premuscle cells and did not form a discrete condensation. The *infraorbital lamina* gives origin to all of the muscles in the *infraorbital* region and probably contributes to the formation of the muscles of the nose, most of the *orbicularis oculi* and some of the *orbicularis oris* muscles.

By 8 to 9 weeks (32–36 mm), Futamura ('06) reported the facial muscles to be well differentiated for the most part. Huber ('31) pointed out that the critical period of development is between the second and third months of prenatal life. There is a sudden surge in facial muscle differentiation between 26 and 37 mm, but deficiencies are present in the palpebral part of the *orbicularis oculi* and in all of the muscles close to the middle of the face. The present findings agree with Zuckermann-Zicha's ('25) report that the palpebral part of the *orbicularis oculi* muscle differentiates between 55 and 80 mm.

The origin of the premuscle cells of the buccinator muscle is questionable. They probably migrated from the deep aspect of the *mandibular lamina* at an earlier age. The cells of the levator anguli oris muscle most likely have the same origin as those in the buccinator muscle.

2. Occipitofrontalis and auricularis superior muscles

Although both bellies of the occipitofrontalis muscles are described definitively as components of a single muscle, they develop separately. At 37 mm (fig. 9), the occipital belly and the auricularis posterior muscle have replaced the *occipital lamina*. Bryce ('23) mentioned that these two muscles are sometimes united in the definitive condition. The frontal belly

differentiates later in the frontal region and its origin is difficult to establish. The corrugator supercilii muscle probably originates from its deep surface. The auricularis superior muscle develops from the *temporal lamina*. The muscles of the scalp gradually thin as they approach the vertex of the head and become continuous with a layer of fibroblasts from which the galea aponeurotica develops. According to Bryce ('23), some authors regard the aponeurosis as representing the degenerated portion of a primitive fronto-occipital sheet. A continuous layer of myoblasts connecting the frontal and occipital areas was not observed in any of the specimens. It is difficult to consider the fibroblasts as dedifferentiated myoblasts; they probably differentiated directly from mesenchymal cells.

3. Deep muscles

A concept of the *posterior digastric complex* from which the posterior digastric, stylohyoid and stapedius muscles develop was presented by Rahl in 1887. Futamura ('06) reported seeing twigs from the facial nerve coursing to the complex at 35–36 days (13–15 mm). At this early age, some of the fibers course into the most ventral and slightly constricted part of the complex to the caudal aspect of the *mandibular arch*. No fibers continue into the *mylohyoid complex* since it already receives an innervation from a poorly developed inferior dental nerve. These findings indicate a dual origin for the digastric muscle, the posterior belly from the *posterior digastric complex* of the second arch and the anterior belly from the *mylohyoid complex* of the first arch. However, each complex is always continuous with one another deep to the first branchial groove. Gegenbaur (1890) and Futamura ('06) believed that the digastric muscle develops from two independent parts. Some investigators consider the muscle to develop as a separation from the sternomastoid muscle. A union with this latter muscle was not observed in any of the specimens. Consideration of past and present data suggests that the posterior digastric muscle as well as the digastric tendon develop from the second arch, and the anterior digastric

muscle develops along with the mylohyoid muscle in the ventral part of the first arch.

Ruge ('10) and Bryce ('23) pointed out the rare occurrence of a definitive muscular connection between the occipital fascia and the posterior digastric muscle. This connection probably represents a retention of an earlier connection (14 mm) between the posterior digastric complex and the cervical lamina.

The time and manner of development of the stapedius muscle agrees with Futamura's ('06) and Schimert's ('33) descriptions, but disagrees with Broman (1898) who believed the muscle develops from the connection between the stapes and the second arch (Reichert's) cartilage. No explanation can be given for the variability in the size and orientation of this muscle during development.

4. Histogenesis and pattern of differentiation

In his studies on the labial muscles, Futamura ('06) saw no transverse striations at 22 weeks (170 mm), faint striations at 26 weeks (220 mm) and distinct striations at 30 weeks (250 mm). The present work reveals transverse striations in myotubes (e.g., orbicularis oris muscle) at 58 mm which become very apparent at 80 mm. Early muscle fibers are present at 146 mm.

Contrary to the statements of Popowsky (1895) the superficial musculature at the end of the third month (58 mm) is already differentiated. This is substantiated by Huber ('31) who produced contractions of the muscles in a living 55 mm fetus through electrical stimulation. In their studies on the appearance of human fetal reflexes, Hooker ('52, '58) and Humphrey ('64, '65) observed, at 37-47 mm, a squint type reflex produced by contraction of the orbicularis oculi muscle. The orbital part of the muscle almost completely surrounds the eye at 41 mm and is composed of late myoblasts. At 47-49 mm, these investigators produced a scowl type reflex by contraction of the corrugator supercilli muscle. This muscle is well differentiated by 58 mm when it is composed of late myoblasts and occasional myotubes. By 60-64 mm, Hooker ('52, '58) and Humphrey ('64, '65) produced momentary lip closure and

at 74-79 mm, lip closure was maintained. At 58 mm, the orbicularis oris muscle is well developed, completely encircles the mouth and is composed mostly of late myoblasts with some myotubes. They observed a sneer type reflex produced by an elevation of the angle of the mouth and ala of the nose at 74 to 88 mm. All of the facial muscles, including the infraorbital ones, have differentiated by 80 mm and are made up of myotubes. Comparison of the degree of histogenetic development of the premuscle cells with the age at which reflexes can be elicited lends support to the view that late myoblasts, with unstriated fibrils in their cytoplasm, are not only able to contract, but that their contractions are influenced to some degree by nerve impulses.

A definite pattern of differentiation is evident in the formation of the facial muscles. The present investigation supports Futamura's ('06) findings that differentiation of the muscles begins earlier in the deep than in the superficial regions and earlier in the lower lateral than in the upper medial regions. In addition, studies show that the muscles in the occipital region (e.g., occipitalis) differentiate and become striated earlier than the lateral facial muscles (e.g., zygomaticus and depressor anguli oris) which in turn differentiate before the muscles close to the midline of the face.

Superficial muscle masses spread from the region of the second arch in all directions except one, that is directly rostrally (fig. 7). The most likely reason for this is the presence of the external auditory meatus which is replacing the first branchial groove. The deep meatus probably causes cells from the second arch to migrate around it so that cell groups must extend first cranially or caudally before they can course rostrally.

In most of the specimens studied, the development of the peripheral branches of the facial nerve follow *pari passu* the development of the facial muscle masses (Gasser, '67). A close relationship exists between the muscles and the nerve throughout development and each appears to influence the histogenesis and morphogenesis of the other. As the muscle masses form, the nerve supply to them differentiates.

what is identified here as the *infraorbital lamina*. A small connection exists between the *infraorbital lamina* and the second arch region at 22 mm (fig. 6), which is less evident at 26 mm (fig. 8) when the lamina is more prominent. The origin of the premuscle cells in the lamina and exactly which muscles on the face develop from the lamina is questionable (table 1). The cells of the *infraorbital lamina* could be descendants of cells in the second branchial arch, their migration taking place at an earlier time when they could not be recognized as premuscle cells and did not form a discrete condensation. The *infraorbital lamina* gives origin to all of the muscles in the *infraorbital* region and probably contributes to the formation of the muscles of the nose, most of the orbicularis oculi and some of the orbicularis oris muscles.

By 8 to 11 weeks (32–36 mm), Futamura ('06) reported the facial muscles to be well differentiated for the most part. Huber ('31) pointed out that the critical period of development is between the second and third months of prenatal life. There is a sudden surge in facial muscle differentiation between 26 and 37 mm, but deficiencies are present in the palpebral part of the orbicularis oculi and in all of the muscles close to the middle of the face. The present findings agree with Zuckermann-Zicha's ('25) report that the palpebral part of the orbicularis oculi muscle differentiates between 55 and 80 mm.

The origin of the premuscle cells of the buccinator muscle is questionable. They probably migrated from the deep aspect of the *mandibular lamina* at an earlier age. The cells of the levator anguli oris muscle most likely have the same origin as those in the buccinator muscle.

2. Occipitofrontalis and auricularis superior muscles

Although both bellies of the occipitofrontalis muscles are described definitively as components of a single muscle, they develop separately. At 37 mm (fig. 9), the occipital belly and the auricularis posterior muscle have replaced the *occipital lamina*. Bryce ('23) mentioned that these two muscles are sometimes united in the definitive condition. The frontal belly

differentiates later in the frontal region and its origin is difficult to establish. The corrugator supercilii muscle probably originates from its deep surface. The auricularis superior muscle develops from the *temporal lamina*. The muscles of the scalp gradually thin as they approach the vertex of the head and become continuous with a layer of fibroblasts from which the galea aponeurotica develops. According to Bryce ('23), some authors regard the aponeurosis as representing the degenerated portion of a primitive fronto-occipital sheet. A continuous layer of myoblasts connecting the frontal and occipital areas was not observed in any of the specimens. It is difficult to consider the fibroblasts as dedifferentiated myoblasts; they probably differentiated directly from mesenchymal cells.

3. Deep muscles

A concept of the *posterior digastric complex* from which the posterior digastric, stylohyoid and stapedius muscles develop was presented by Rahl in 1887. Futamura ('06) reported seeing twigs from the facial nerve coursing to the complex at 35–36 days (13–15 mm). At this early age, some of the fibers course into the most ventral and slightly constricted part of the complex to the caudal aspect of the *mandibular arch*. No fibers continue into the *mylohyoid complex* since it already receives an innervation from a poorly developed inferior dental nerve. These findings indicate a dual origin for the digastric muscle, the posterior belly from the *posterior digastric complex* of the second arch and the anterior belly from the *mylohyoid complex* of the first arch. However, each complex is always continuous with one another deep to the first branchial groove. Gegenbaur (1890) and Futamura ('06) believed that the digastric muscle develops from two independent parts. Some investigators consider the muscle to develop as a separation from the sternomastoid muscle. A union with this latter muscle was not observed in any of the specimens. Consideration of past and present data suggests that the posterior digastric muscle as well as the digastric tendon develop from the second arch, and the anterior digastric

muscle develops along with the mylohyoid muscle in the ventral part of the first arch.

Ruge ('10) and Bryce ('23) pointed out the rare occurrence of a definitive muscular connection between the occipital fascia and the posterior digastric muscle. This connection probably represents a retention of an earlier connection (14 mm) between the posterior digastric complex and the cervical lamina.

The time and manner of development of the stapedius muscle agrees with Futamura's ('06) and Schimert's ('33) descriptions, but disagrees with Broman (1898) who believed the muscle develops from the connection between the stapes and the second arch (Reichert's) cartilage. No explanation can be given for the variability in the size and orientation of this muscle during development.

4. Histogenesis and pattern of differentiation

In his studies on the labial muscles, Futamura ('06) saw no transverse striations at 22 weeks (170 mm), faint striations at 26 weeks (220 mm) and distinct striations at 30 weeks (250 mm). The present work reveals transverse striations in myotubes (e.g., orbicularis oris muscle) at 58 mm which become very apparent at 60 mm. Early muscle fibers are present at 146 mm.

Contrary to the statements of Popowsky (1895) the superficial musculature at the end of the third month (58 mm) is already differentiated. This is substantiated by Huber ('31) who produced contractions of the muscles in a living 55 mm fetus through electrical stimulation. In their studies on the appearance of human fetal reflexes, Hooker ('52, '58) and Humphrey ('64, '65) observed, at 37-47 mm, a squint type reflex produced by contraction of the orbicularis oculi muscle. The orbital part of the muscle almost completely surrounds the eye at 41 mm and is composed of late myoblasts. At 47-49 mm, these investigators produced a scowl type reflex by contraction of the corrugator supercilii muscle. This muscle is well differentiated by 58 mm when it is composed of late myoblasts and occasional myotubes. By 60-64 mm, Hooker ('52, '58) and Humphrey ('64, '65) produced momentary lip closure and

at 74-79 mm, lip closure was maintained. At 58 mm, the orbicularis oris muscle is well developed, completely encircles the mouth and is composed mostly of late myoblasts with some myotubes. They observed a sneer type reflex produced by an elevation of the angle of the mouth and ala of the nose at 74 to 88 mm. All of the facial muscles, including the infraorbital ones, have differentiated by 80 mm and are made up of myotubes. Comparison of the degree of histogenetic development of the premuscle cells with the age at which reflexes can be elicited lends support to the view that late myoblasts, with unstriated fibrils in their cytoplasm, are not only able to contract, but that their contractions are influenced to some degree by nerve impulses.

A definite pattern of differentiation is evident in the formation of the facial muscles. The present investigation supports Futamura's ('06) findings that differentiation of the muscles begins earlier in the deep than in the superficial regions and earlier in the lower lateral than in the upper medial regions. In addition, studies show that the muscles in the occipital region (e.g., occipitalis) differentiate and become striated earlier than the lateral facial muscles (e.g., zygomaticus and depressor anguli oris) which in turn differentiate before the muscles close to the midline of the face.

Superficial muscle masses spread from the region of the second arch in all directions except one, that is directly rostrally (fig. 7). The most likely reason for this is the presence of the external auditory meatus which is replacing the first branchial groove. The deep meatus probably causes cells from the second arch to migrate around it so that cell groups must extend first cranially or caudally before they can course rostrally.

In most of the specimens studied, the development of the peripheral branches of the facial nerve follow *pari passu* the development of the facial muscle masses (Gasser, '67). A close relationship exists between the muscles and the nerve throughout development and each appears to influence the histogenesis and morphogenesis of the other. As the muscle masses form, the nerve supply to them differentiates.

The premuscle cells in the vicinity of the nerve fibers are further differentiated than those more distant from the nerve fibers.

ACKNOWLEDGMENTS

Appreciation is expressed to Dr. Tryphena Humphrey, Dr. E. C. Sensenig and to the late Dr. Davenport Hooker for making their collections of human embryonic material available during this investigation.

LITERATURE CITED

- Born, G. 1883 Die Plattenmodellirmethode. Arch. f. Micr. Anat., 22: 584-589.
 ——— 1888 Noch einmal die Plattenmodellirmethode. Z. Wiss. Mikr., 5: 433-455.
 Boyd, J. D. 1960 Development of striated muscle. Structure and Function of Muscle. Vol. 1. Ed. by G. H. Bourne. Academic Press, New York. Chap. III, 63-85.
 Broman, I. 1898 Ueber Entwicklungsgeschichte der Gehörknöchelchen beim Menschen. Anat. Hefte, 11: 509-661.
 Bryce, T. H. 1923 Myology. Quain's Elements of Anatomy, 11th ed. Vol. 4, part 2. Ed. by E. S. Schafer, J. Symington and T. H. Bryce. Longmans, Green Co., London 31-74.
 Futamura, R. 1906 Über die Entwicklung der Facialis-muskulatur des Menschen. Anat. Hefte, 30: 433-516.
 Gasser, R. F. 1967 The development of the facial nerve in man. Ann. Otol., in press.
 Gegenbaur, C. 1890 Lehrbuch der Anatomie des Menschen. 4 Aufl., Band 2, Wilhelm Engelmann, Leipzig, 448-449.
 Hooker, D. 1952 The Prenatal Origin of Behavior. 18th Porter Lecture. University of Kansas Press, Lawrence, Chap. II, 54-86.
 ——— 1958 Evidence of prenatal function of the central nervous system in man. James Arthur Lecture on The evolution of the human brain, 1957. The American Museum of Natural History, New York.
 Huber, E. 1931 Evolution of Facial Musculature and Facial Expression. The Johns Hopkins Press, Baltimore 1-184.
 Humphrey, T. 1964 Some correlations between the appearance of human fetal reflexes and the development of the nervous system. Prog. Brain Res., 4: 93-135.
 ——— 1965 Personal communication.
 Mall, F. P. 1910 Manual of Human Embryology. Vol. 1. Ed. by F. Keibel and F. P. Mall. J. B. Lippincott Co., Philadelphia. Chap. VIII, 180-201.
 ——— 1918 On the age of human embryo. Am. J. Anat., 23: 397-422.
 Popowsky, I. 1895 Zur Entwicklungsgeschichte des N. facialis beim Menschen. Morph. Jahrb., 23: 329-374.
 Rabl, K. 1887 Über das Gebiet des Nervus facialis. Anat. Anz., 2: 219-227.
 Ruge, G. 1910 Verbindungen des Platysma mit der tiefen Muskulatur des Halses beim Menschen. Morph. Jahrb., 41: 708-724.
 Schimert, J. 1933 Zur Entwicklungsgeschichte des Musculus stapedius beim Menschen. Anat. Anz., 76: 317-332.
 Streeter, G. L. 1920 Weight, sitting height, head size, foot length and mensural age of the human embryo. Contr. Embryol. Carneg. Instn., 11: 143-170.
 Zuckermann-Zicha, M. 1925 Sur le développement de la musculature des paupières chez l'homme. Arch. de Biol., 35: 313-323.

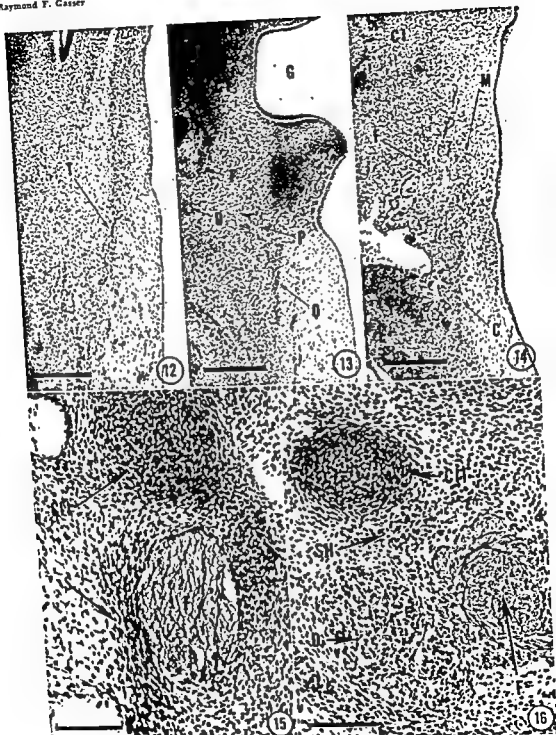
PLATE 1

EXPLANATION OF FIGURES

- 12 A section through the temporal lamina (T) of the same 18.0 mm as in figure 4, 8.5 weeks, Bodian's protargol stain, 10 μ . Scale = 300 μ . Arrow 12 in figure 4 indicates level and plane of section.
- 13 A section through the occipital lamina (O) of the same embryo as in figure 4. Scale = 300 μ . Arrow 13 in figure 4 indicates level and plane of section. CT, chorda tympani nerve; D, posterior digastric muscle; F, facial nerve; G, first branchial groove; P, posterior auricular nerve.
- 14 A section through the cervical (C) and mandibular (M) laminae of the same embryo as in figure 4. Scale = 300 μ . Arrow 14 in figure 4 indicates level and plane of section. Cl, first branchial (Meckel's) cartilage; F, terminal branches of facial nerve.
- 15 A section through the stapedius muscle (S) of the same embryo as in figure 5. Scale = 100 μ . Arrow 15 in figure 5 indicates level and plane of section. CII, second branchial (Reichert's) cartilage; F, facial nerve.
- 16 A section through the posterior digastric muscle (D) of the same embryo as in figure 5. Scale = 100 μ . Arrow 16 in figure 5 indicates level and plane of section. CIII, second branchial (Reichert's) cartilage; F, facial nerve; SH, stylohyoid muscle.

FACIAL MUSCLE DEVELOPMENT

Raymond F. Gasser



The premuscle cells in the vicinity of the nerve fibers are further differentiated than those more distant from the nerve fibers.

ACKNOWLEDGMENTS

Appreciation is expressed to Dr. Tryphena Humphrey, Dr. E. C. Sensenig and to the late Dr. Davenport Hooker for making their collections of human embryonic material available during this investigation.

LITERATURE CITED

- Born, G. 1883 *Die Plattenmodellirmethode*. Arch. f. Micr. Anat., 22: 584-589.
- 1888 *Noch einmal die Plattenmodellirmethode*. Z. Wiss. Mikr., 5: 433-455.
- Boyd, J. D. 1960 *Development of striated muscle. Structure and Function of Muscle*. Vol. 1. Ed. by G. H. Bourne. Academic Press, New York. Chap. III, 63-85.
- Broman, I. 1898 *Ueber Entwicklungsgeschichte der Gehörknöchelchen beim Menschen*. Anat. Hefte, 11: 509-601.
- Bryce, T. H. 1923 *Myology. Quain's Elements of Anatomy*. 11th ed. Vol. 4, part 2. Ed. by E. S. Schafer, J. Symington and T. H. Bryce. Longmans, Green Co., London 31-74.
- Futamura, R. 1906 *Über die Entwicklung der Facialismuskulatur des Menschen*. Anat. Hefte, 30: 433-516.
- Gasser, R. F. 1967 *The development of the facial nerve in man*. Ann. Otol., in press.
- Gegenbaur, C. 1890 *Lehrbuch der Anatomie des Menschen*. 4 Aufl., Band 2, Wilhelm Engelmann, Leipzig, 448-449.
- Hooker, D. 1952 *The Prenatal Origin of Behavior*. 18th Porter Lecture. University of Kansas Press, Lawrence, Chap. II, 54-86.
- 1958 *Evidence of prenatal function of the central nervous system in man*. James Arthur Lecture on The evolution of the human brain, 1957. The American Museum of Natural History, New York.
- Huber, E. 1931 *Evolution of Facial Musculature and Facial Expression*. The Johns Hopkins Press, Baltimore 1-184.
- Humphrey, T. 1964 *Some correlations between the appearance of human fetal reflexes and the development of the nervous system*. Prog. Brain Res., 4: 93-135.
- 1965 *Personal communication*.
- Mall, F. P. 1910 *Manual of Human Embryology*. Vol. 1. Ed. by F. Keibel and F. P. Mall. J. B. Lippincott Co., Philadelphia. Chap. VIII, 180-201.
- 1918 *On the age of human embryos*. Am. J. Anat., 23: 397-422.
- Popowsky, I. 1895 *Zur Entwicklungsgeschichte des N. facialis beim Menschen*. Morph. Jahrb., 23: 329-374.
- Rabl, K. 1887 *Über das Gebiet des Nervus facialis*. Anat. Anz., 2: 219-227.
- Ruge, G. 1910 *Verbindungen des Platysma mit der tiefen Musculatur des Halses beim Menschen*. Morph. Jahrb., 41: 708-724.
- Schimert, J. 1933 *Zur Entwicklungsgeschichte des Musculus stapedius beim Menschen*. Anat. Anz., 76: 317-332.
- Streeter, G. L. 1920 *Weight, sitting height, head size, foot length and menstrual age of the human embryo*. Contr. Embryol. Carneg. Instn., 11: 143-170.
- Zuckermann-Zicha, M. 1925 *Sur le développement de la musculature des paupières chez l'homme*. Arch. de Biol., 35: 313-323.

PLATE 1

EXPLANATION OF FIGURES

- 12 A section through the temporal lamina (T) of the same 18.0 mm as in figure 4, 8.5 weeks, Bodian's protargol stain, 10 μ . Scale = 300 μ . Arrow 12 in figure 4 indicates level and plane of section.
- 13 A section through the occipital lamina (O) of the same embryo as in figure 4. Scale = 300 μ . Arrow 13 in figure 4 indicates level and plane of section. CT, chorda tympani nerve; D, posterior digastric muscle; F, facial nerve; G, first branchial groove; P, posterior auricular nerve.
- 14 A section through the cervical (C) and mandibular (M) laminae of the same embryo as in figure 4. Scale = 300 μ . Arrow 14 in figure 4 indicates level and plane of section. CI, first branchial (Meckel's) cartilage; F, terminal branches of facial nerve.
- 15 A section through the stapedius muscle (S) of the same embryo as in figure 5. Scale = 100 μ . Arrow 15 in figure 5 indicates level and plane of section. CII, second branchial (Reichert's) cartilage; F, facial nerve.
- 16 A section through the posterior digastric muscle (D) of the same embryo as in figure 5. Scale = 100 μ . Arrow 16 in figure 5 indicates level and plane of section. CIII, second branchial (Reichert's) cartilage; F, facial nerve; SH, stylohyoid muscle.

Localization of Uptake of Tritiated Norepinephrine by Rat Brain In Vivo and In Vitro Using Electron Microscopic Autoradiography¹

NICHOLAS J. LENN²

Laboratory of Neuroanatomical Sciences, National Institute of Neurological Diseases and Blindness, National Institutes of Health, Bethesda, Maryland

ABSTRACT Previous studies have identified granular vesicles in peripheral adrenergic axons, and larger granular vesicles in various brain regions which seem to be correlated with the presence of norepinephrine. In the present study, electron microscopic autoradiography was used to localize ³H-norepinephrine taken up by brain slices in vitro and by brain in vivo after injection via the lateral ventricle. In both preparations, the label was found predominantly in relation to small, unmyelinated axons and nerve endings. Many of these contained granular vesicles in axons which were located in regions of the brain known to contain norepinephrine. It is suggested on the basis of this study and previous work, that exogenous norepinephrine is accumulated by brain axons and nerve endings which contain endogenous norepinephrine, and that the presence of granular vesicles is a common feature of such structures.

In peripheral adrenergic axons, electron microscopy has revealed the presence of granular and agranular synaptic vesicles averaging 500 Å in diameter in the nerve endings (Richardson, '62). The proportion of granular vesicles is decreased following reserpine (Pellegrino de Iraldi and De Robertis, '63), or metaraminol (Bondareff, '66) administration, and increased with monoamine oxidase inhibition (Pellegrino de Iraldi and De Robertis, '63), norepinephrine administration (Bondareff, '66), or with potassium permanganate fixation (Richardson, '66a). Electron microscopic autoradiography has revealed that intravenously administered norepinephrine is localized to the regions of adrenergic axons containing mixed granular and agranular synaptic vesicles (Wolfe et al., '62; Wolfe and Potter, '63). On the basis of these various lines of evidence, it appears probable that at least a portion of the norepinephrine in peripheral adrenergic nerve terminals resides in vesicles, with the amount of amine in particular vesicles determining whether or not they appear with a dense core, or granule (Richardson, '66b).

Many studies of brain fine structure have revealed a correlation between the presence of norepinephrine and the occur-

rence of small numbers of larger granular vesicles (average diameter 1000 Å). Pellegrino de Iraldi et al. ('63), Bloom et al. ('66) and Fuxe et al. ('65) have demonstrated such granular vesicles in nerve endings within portions of the brain which have been shown to contain varicose adrenergic axons by fluorescence histochemistry (Fuxe, '65). Ishii et al. ('65) found a good correlation between the number of granular vesicles and the content of norepinephrine when medial and lateral portions of the hypothalamus were compared. De Robertis et al. ('65) found a correlation between norepinephrine content and the number of granular vesicles in subcellular fractions from hypothalamus and from whole brain. As in the peripheral sympathetic nerves, the proportion of granular vesicles in the hypothalamus can be decreased by reserpine (Shimizu and Ishii, '64), oxypertin (Matsuoka et al., '65) administration, and increased by administration of a norepinephrine precursor, dihydroxyphenylalanine (Hashimoto et al., '65). Wood ('66) using an electron

¹This work formed part of a thesis submitted in partial fulfillment of the requirements for the Ph.D. degree to the Department of Anatomy, University of Chicago.

²Present address: Department of Pediatrics, University of Chicago, Chicago, Illinois.

micrographs and the location of the 500 silver grains was tabulated. The method of scoring silver grain location that seemed to give the most meaningful results involved placing a circle of 0.25 μ radius over each silver grain and assigning it to the single structure which occupied the greatest area of the circle. With this method it was found that 45% of the silver grains were in relation to nerve endings (figs. 1-8), of which approximately one half were seen to contain at least one granular vesicle. Another 25% of the silver grains were in relation to small unmyelinated axons (figs. 11-13), many of which also contained granular vesicles. Many, if not all, of these small axons represented telodendrons or preterminal segments, often being seen in direct continuity with the nerve endings. The nerve endings included profiles larger than small axons containing synaptic vesicles. Thus the total localization to preterminal and terminal portions of axons in this region was 70%.

Of the remaining 30% of silver grains, approximately 18% were in relation to dendrites (fig. 9), and 7%, to the cytoplasm of neuronal perikarya (fig. 10). Since neuronal perikarya and dendrites in the lateral septum do not contain endogenous norepinephrine (Dahlström and Fuxe, '64), the significance of this localization was not clear. That these elements, particularly the dendrites, have a large surface area may mean that a relatively minor, non-specific uptake could account for this localization. It is interesting, in relation to the fine structure of perikarya in the locus coeruleus known to contain endogenous norepinephrine (Lenn, '65), that here, too, norepinephrine in perikarya and dendrites was not seen to be localized either to granular or agranular vesicles. If any cytoplasmic localization was present, it was rather to the endoplasmic reticulum, including the perinuclear cistern (fig. 10).

The remaining 5% of the silver grains were localized to neuronal nuclei, astrocytes and an endothelial cell. Since this percentage is well below the 10% background level, the grains in these locations were considered to represent background.

Of the specimens from the brain slices, that from the preoptic area was found to

show a positive autoradiographic response after two months' exposure. The number of developed silver grains over the tissue sections was five times that over the bare Parlodion, as estimated by total counts of 71 unselected windows on duplicate grids. Since, as would be expected, the fine structure was less elegantly preserved in incubated brain slices, quantitative analysis could not be performed with great accuracy. In 160 electronmicrographs taken from unselected windows the localization of the tritium label was again characterized as being in relation to one or more cytological elements of the tissue. Thus the probable localization of most of the tritium disintegrations (225 silver grains) was in relation to myelinated (10%), and particularly small unmyelinated (40%) axons (figs. 14, 15), and nerve endings (30%) (figs. 16-18). It is possible that the remaining grains represented only the 20% background, but it seems more likely that some of the norepinephrine was localized in dendrites, neuronal perikarya and perhaps other tissue elements.

In both of the present experiments, the above results, in conjunction with other lines of evidence to be discussed below, suggested that norepinephrine was accumulated by structures which contain endogenous norepinephrine. The following is a description of the structures which were labeled. This description depends primarily on the well-fixed material from the *in vivo* experiment, but as far as can be judged there was no difference between the two experiments, except for the near absence of myelinated axons from the *in vivo* specimen. The myelinated axons contained neurofilaments, neurotubules, mitochondria and smooth surfaced endoplasmic reticulum, with only occasional vesicles of various sizes. The unmyelinated axons (figs. 8, 11-15), 0.1 to 0.6 μ in diameter, were arranged in groups, and were frequently seen to end by enlarging into a nerve ending. Several examples of an axon connecting two nerve endings were seen (fig. 8). The axons contained neurotubules, small numbers of vesicles some of which contained granules, mitochondria and smooth surfaced endoplasmic reticulum. The nerve endings (figs. 1-8, 16-18) were quite variable in size, due

microscopic histochemical method which does not distinguish norepinephrine from dihydroxyphenylalanine and 5-hydroxytryptamine, found the reaction product in the form of granules. With post-osmication granular vesicles were seen as apparently the only site of reaction. These studies all favor the interpretation that nerve endings in the brain which contain norepinephrine are characterized by the presence of granular vesicles. However, such interpretations all depend upon correlation rather than direct identification of norepinephrine containing axons and their endings.

In the present study, electron microscopic autoradiography was used to localize the uptake of tritiated norepinephrine by brain *in vivo* and *in vitro* in order to directly identify structures capable of accumulating this amine. With such preparations, the cytology of structures having this capacity for uptake may be described without depending upon correlations with histochemical studies or with drug effects. For the *in vitro* study brain slices from normal rats were incubated in a solution containing norepinephrine. The *in vivo* study used normal rats injected with norepinephrine via the lateral ventricle. Aghajanian and Bloom ('66a) have used this *in vivo* technique to study uptake of tritiated norepinephrine in the hypothalamus. Although they allowed much shorter survival after injection, the results were similar to those of the present study. The present report will show that the norepinephrine was accumulated predominantly in axons and their endings, and will describe the electron microscopic appearance of these structures.

MATERIALS AND METHODS

Normal adult Sprague-Dawley rats weighing approximately 200 gm were used. Free-hand coronal slices were taken from animals anesthetized by cervical dislocation. These were incubated at 37°C for 30 minutes in 20 ml of Krebs-Ringer solution containing dl-7-³H-norepinephrine (25 μ gm/ml; 6.87 c/mM), rinsed once in fresh ice-cold Krebs-Ringer solution, and kept for two hours over ice. Portions selected from the caudate nucleus and hypothalamus were transferred to iced 2%

OsO₄ in phosphate buffer, pH 7.0 (Milonig, '64; without glucose).

Another rat was anesthetized with pentobarbital and a fine glass cannula introduced stereotactically to the coordinates of the lateral ventricle. A return of cerebrospinal fluid was seen in the cannula. Thirty μ l of dl-7-³H-norepinephrine (30 μ Ci; 6 μ gm) was injected through the cannula. After 15 hours, during which time it recovered from the anesthesia and showed no obvious effect of the procedure, the animal was anesthetized with chloral hydrate, and perfused via the aorta with saline (McEwen, '56) followed by the same osmium solution. Selected regions of the brain were obtained by dissection. The lateral ventricle on the side of the injection was noted to be slightly enlarged.

All tissue was dehydrated in methanol and embedded in Araldite. One-micron sections on glass slides and thin sections (silver to gold interference colors) on copper grids bearing a Parlodion membrane were coated with Ilford L-4 emulsion (Caro and van Tubergen, '62; first method). Regions showing a positive autoradiographic response on the thicker sections examined with phase contrast optics were selected for thin sectioning. The latter specimens were exposed in boxes containing desiccant at 4°C for approximately two months. They were developed in Kodak Microdol for five minutes, and stained for 30 seconds with lead citrate (Venable and Coggeshall, '65). Duplicate grids were studied from each specimen reported here. The successful production of closely packed monolayers of silver halide grains was confirmed by examining undeveloped grids of the same batches.

RESULTS

The specimen from the lateral septal nucleus was the only one from the brain of the animal injected via the lateral ventricle that showed a concentration of silver grains which was significantly above background after two months' exposure. On the grids from this region, the number of silver grains over unselected portions of the positive tissue region was approximately ten times the background level over windows covered only by Parlodion. The grains were counted on 200 unselected electron-

out that a significant part of the tritium in the brain at all time intervals studied was in the form of metabolites of norepinephrine, especially normetanephrine. Snyder et al. ('65) found this compound to be mostly in the supernatant fluid with only about one-fourth of it in the nerve endings. The action of reserpine and amphetamine on exogenous norepinephrine injected into the lateral ventricle was the same as their action on endogenous norepinephrine (Glowinski and Axelrod, '65; Glowinski et al., '66). These data taken together strongly suggest that when the brain is exposed *in vivo* to exogenous norepinephrine, the amine is taken up so as to mix with the endogenous norepinephrine already *in situ*. The subsequent fate of the exogenous amine would then be the same as the fate of endogenous norepinephrine. This conclusion is also supported by other experiments. Aghajanian and Bloom ('66b) found the same localization of tritium after ³H-dihydroxyphenylalanine administration as after ³H-norepinephrine administration, but both were different from that obtained after ³H-5-hydroxytryptamine administration (Aghajanian and Bloom, '66c). Hamberger and Hamberger ('66) have shown by fluorescence histochemistry that intravenously injected norepinephrine is localized by typical varicose axons if the blood-brain barrier is previously damaged. In the absence of such damage, Fuxe and Hillarp ('64) using fluorescence histochemistry and Samaražski and Marks ('62) using light microscope autoradiography have found similar uptake in norepinephrine containing regions which have a less efficient barrier such as the median eminence.

In the case of brain slices exposed to exogenous norepinephrine *in vitro*, there is also evidence indicating that the uptake is into norepinephrine containing structures, and that such uptake is of physiological significance. Dengler et al. ('61) showed that norepinephrine was concentrated by brain tissue incubated *in vitro*. Ross and Renyi ('66) have shown similar uptake of norepinephrine and metaraminol, and deduced from regional differences in amount of uptake, and from the effects of drugs, that the uptake was into adrenergic structures. Hamberger and Masuoka

('65) have studied the uptake of norepinephrine by brain slices with the fluorescence histochemical method for monoamines. They found the exogenous norepinephrine localized to typical varicose axons, indistinguishable from those which contain endogenous norepinephrine, and to non-varicose, more proximal portions of axons. Baldessarini and Kopin ('66) have found that brain slices, identical to those studied here, release norepinephrine at a sharply increased rate following mild electrical stimulation or increased concentration of potassium, both of which are known to depolarize neurons in such slices (Hillman and McIlwain, '61). Tritiated norepinephrine, endogenously formed from labeled dihydroxyphenylethylamine by brain slices *in vitro*, was also released by electrical stimulation, suggesting that the exogenous norepinephrine was released from a site of physiological storage (Baldessarini and Kopin, personal communication). All of these results suggest that exogenous norepinephrine is highly localized to adrenergic structures in brain slices.

An experiment which attempts to localize a small molecule by autoradiography is subject to the possibility of movement of the molecule during the preparation of the tissue. Lacking any direct measure of the effect of the various steps on the location of the norepinephrine, we can consider two lines of evidence. In brain slices such as those used here, the loss of radioactivity was measured. Of 92% of the label recovered, one-half was in the osmium solution and methanol, and one-half in the fixed tissue (averages of six experiments, unpublished observations). Since so much norepinephrine is lost from the tissue, it seems quite possible that all of the norepinephrine that is displaced by the solutions is removed completely from the tissue. The more firmly bound norepinephrine would then remain in its pre-fixation position where it is demonstrated by autoradiography. This reasoning is supported by the observations of the various authors cited above, all showing consistent localization of norepinephrine, regardless of whether the tissue was prepared by freeze-drying, with little chance of dis-

in part to varying planes of section, approaching 2μ in greatest dimension. Many were seen in synaptic contact, usually with dendrites (figs. 1, 7, 17) or occasionally with perikarya. The few examples of two nerve endings connected by a segment of axon did not show synaptic contacts. Therefore, the relation between the varicosities described in light microscope histochemistry as being typical of norepinephrine containing preterminal axons, and preterminal and terminal nerve endings seen with the electron microscope, which would have been clarified by such an observation, remains unsettled. Thus, the term nerve ending was used here in the general sense of enlarged portions of axons containing synaptic vesicles, whether or not a synaptic contact was seen. The synaptic contacts were typical of synapses in the mammalian central nervous system (Palay, '58). Pre- and post-synaptic membranes were increased in density, with the synaptic cleft widened to approximately 250 \AA in the region of increased density, and containing a dense lamina (fig. 1). The cytoplasm of the post-synaptic member contained a variable accumulation of dense material subjacent to the segment of increased density. Synaptic vesicles tended to cluster presynaptically. The great majority of the vesicles in most endings were agranular, approximately $300\text{--}600\text{ \AA}$ in diameter. About one-half of the endings contained one or a few vesicles averaging approximately 1000 \AA in diameter, with a dense core separated from the surrounding membrane by a lucid zone. These are the typical granular vesicles of the central nervous system following osmium tetroxide or glutaraldehyde fixation which usually appear to be scattered indiscriminately within the endings. Since such endings contained so few granular vesicles, it is possible that many or all of the labeled endings lacking granular vesicles actually did contain some at levels outside of the plane of section. Some sparsely vesiculated endings actually contained more vesicles, relatively and absolutely, of the granular kind.

DISCUSSION

The present results, together with previous findings, suggest that tritiated nor-

epinephrine is accumulated by structures in the brain which contain endogenous norepinephrine. The experiments of Glowinski et al. ('65) show that norepinephrine injected into the lateral ventricle of the rat is lost from the brain, largely as metabolites, in a multiphasic manner. This multiphasic exponential loss, which is similar to that of norepinephrine formed endogenously from ^3H -dihydroxyphenylalanine (Burack and Drackóczy, '64), is associated with at least two pools of norepinephrine. Within 12 hours after injection the half-life of ^3H -norepinephrine in the brain is three hours. After 12 hours, this half-life changes to 17 hours (Glowinski et al., '65). The autoradiographic study of Aghajanian and Bloom ('66a) used survival times of one to four hours after injection, and therefore demonstrated the localization of the rapidly turning over pool. In the present study, the slowly turning over pool was localized by allowing the animal to survive injection by 15 hours, a time at which only 3% of the administered tritium remained in the brain (Glowinski et al., '65). It is very interesting that the results of these two autoradiographic studies are essentially the same in spite of this difference in survival time, as well as the different brain regions involved. This similarity in results is consistent with the suggestion of Musacchio et al. ('65) that differences in binding rather than anatomical localization account for the existence of more than one pool of norepinephrine.

Further evidence that exogenous norepinephrine injected into the lateral ventricle mixes with endogenous norepinephrine is available. Gross autoradiography has shown that the exogenous norepinephrine administered by this route is localized to regions of high endogenous norepinephrine content (Reivich and Glowinski, '65; cited in Glowinski et al., '66). Snyder et al. ('65) found that the exogenous norepinephrine was highly localized to nerve endings in homogenized brain, as is endogenous norepinephrine (Potter and Axelrod, '63). However, appreciable amounts of the amine were found in the other subcellular fractions, perhaps corresponding in part to the other sites of localization found in the present study. It should also be pointed

ut that a significant part of the tritium in the brain at all time intervals studied was in the form of metabolites of norepinephrine, especially normetanephrine. Snyder et al. ('65) found this compound to be mostly in the supernatant fluid with only about one-fourth of it in the nerve endings. The action of reserpine and amphetamine on exogenous norepinephrine injected into the lateral ventricle was the same as their action on endogenous norepinephrine (Glowinski and Axelrod, '65; Glowinski et al., '66). These data taken together strongly suggest that when the brain is exposed *in vivo* to exogenous norepinephrine, the amine is taken up so as to mix with the endogenous norepinephrine already *in situ*. The subsequent fate of the exogenous amine would then be the same as the fate of endogenous norepinephrine. This conclusion is also supported by other experiments. Aghajanian and Bloom ('66b) found the same localization of tritium after ³H-dihydroxyphenylalanine administration as after ³H-norepinephrine administration, but both were different from that obtained after ³H-5-hydroxytryptamine administration (Aghajanian and Bloom, '66c). Hamberger and Hamberger ('66) have shown by fluorescence histochemistry that intravenously injected norepinephrine is localized by typical varicose axons if the blood-brain barrier is previously damaged. In the absence of such damage, Fuxe and Hillarp ('64) using fluorescence histochemistry and Samrajski and Marks ('62) using light microscope autoradiography have found similar uptake in norepinephrine containing regions which have a less efficient barrier such as the median eminence.

In the case of brain slices exposed to exogenous norepinephrine *in vitro*, there is also evidence indicating that the uptake is into norepinephrine containing structures, and that such uptake is of physiological significance. Dengler et al. ('61) showed that norepinephrine was concentrated by brain tissue incubated *in vitro*. Ross and Renyi ('66) have shown similar uptake of norepinephrine and metaraminol, and deduced from regional differences in amount of uptake, and from the effects of drugs, that the uptake was into adrenergic structures. Hamberger and Masuoka

('65) have studied the uptake of norepinephrine by brain slices with the fluorescence histochemical method for monoamines. They found the exogenous norepinephrine localized to typical varicose axons, indistinguishable from those which contain endogenous norepinephrine, and to non-varicose, more proximal portions of axons. Baldessarini and Kopin ('66) have found that brain slices, identical to those studied here, release norepinephrine at a sharply increased rate following mild electrical stimulation or increased concentration of potassium, both of which are known to depolarize neurons in such slices (Hillman and McIlwain, '61). Tritiated norepinephrine, endogenously formed from labeled dihydroxyphenylethylamine by brain slices *in vitro*, was also released by electrical stimulation, suggesting that the exogenous norepinephrine was released from a site of physiological storage (Baldessarini and Kopin, personal communication). All of these results suggest that exogenous norepinephrine is highly localized to adrenergic structures in brain slices.

An experiment which attempts to localize a small molecule by autoradiography is subject to the possibility of movement of the molecule during the preparation of the tissue. Lacking any direct measure of the effect of the various steps on the location of the norepinephrine, we can consider two lines of evidence. In brain slices such as those used here, the loss of radioactivity was measured. Of 92% of the label recovered, one-half was in the osmium solution and methanol, and one-half in the fixed tissue (averages of six experiments, unpublished observations). Since so much norepinephrine is lost from the tissue, it seems quite possible that all of the norepinephrine that is displaced by the solutions is removed completely from the tissue. The more firmly bound norepinephrine would then remain in its pre-fixation position where it is demonstrated by autoradiography. This reasoning is supported by the observations of the various authors cited above, all showing consistent localization of norepinephrine, regardless of whether the tissue was prepared by freeze-drying, with little chance of dis-

placement, or by treatment in aqueous solutions.

With its half-life of twelve and one-half years, 1% of tritium atoms disintegrate in a two-month period, which was the length of exposure in the present experiment. Moreover, autoradiography as used here detects less than 25% of disintegrations (Caro and Schnös, '65), perhaps as few as 10%. Thus, only about 0.1% of the tritium present was revealed as silver grains, and so it is highly probable that many of the structures which contained exogenous norepinephrine did not bear silver grains in the autoradiographs. By not comparing labeled to unlabeled structures, and not considering the proportion of a tissue element labeled, we avoid any misinterpretation due to the fact that the exposure time was long enough only to allow a very small proportion of disintegrations to occur.

Caro ('62) gives figures as low as 0.1μ for the resolution of autoradiographic localization in preparations similar to those used here. However, in scoring "hits" in a tightly packed tissue like brain, the opposite issue becomes important. That is, how far a silver grain can appear from the site of the tritium disintegration. Caro and Schnös ('65) showed that the upper limit is about 0.25μ , and Caro ('62) estimates that at least 90% fall within this distance. Hence, a circle 0.25μ in radius was used in the present analysis to identify the possible sites of the disintegration responsible for each silver grain observed. A silver grain was considered to be located at the mid-point of the line connecting its two ends, if the ends were visible (Caro and van Tubergen, '62). If not, the center of the mass of silver was taken to be the location of the grain (Caro, '62).

It might seem important to measure the relative volumes of the elements of the tissue under study, and to compare the results to the relative distribution of silver grains over these elements. However, since this type of analysis can only reveal large differences, it is only applicable when the tissue elements of interest make up a relatively small fraction of the total tissue. In the present material inspection showed that this condition was not met. Indeed, it was expected that in order to obtain

levels of radioactivity above background, regions would have to be studied that were rich in norepinephrine containing nerve endings, as both areas studied in the present experiments are known to be (Fuxe, '65). Several reasons may be suggested to explain why, of many such areas in the rat brain, the preoptic area in the brain slices and lateral septal nucleus in the *in vivo* experiment were the only ones to give positive autoradiographic results. In the case of the brain slices, one reason may be that only regions lying near the surface of the free-hand coronal slices were examined. In the case of the *in vivo* experiment, one important factor was undoubtedly that the region of the lateral septum studied was immediately subependymal, and subjacent to the lateral ventricle, not very far from the site of injection. Kopin et al. ('65) showed that uptake of norepinephrine by tissue is dependent on the dose to which the tissue is exposed and upon the richness of the adrenergic innervation. The product of these two factors might well have been maximal in the lateral septal nucleus. It is clear from the thick sections that the overlying ependyma was not damaged, and that the injection of norepinephrine was not directed into the tissue examined.

In conclusion, the identification and description of brain structures which concentrate exogenous norepinephrine is made possible by autoradiography, and is reinforced by the bulk of previous evidence. It is quite clear that the presence of granular vesicles in such structures is an important feature of their fine structure. Whether the presence of a granular vesicle, in a structure seen by routine electron microscopy in central axons and endings, can be equated with the presence of endogenous norepinephrine remains to be seen, but this seems more likely in the light of the present results. In light of the difference in size of granular vesicles in central and peripheral norepinephrine containing structures (1000 and 500 Å, respectively) and of the relatively small number of granular vesicles in central endings, the question whether the central granular vesicles are the major site of norepinephrine storage must also be left open. It must be remembered that fixation of

peripheral adrenergic structures with solutions of permanganate causes an increase in the proportion of small synaptic vesicles with dense cores, as well as the appearance of such vesicles in sites where osmium fixation reveals only agranular vesicles (Richardson, '66b). Whether in the central nervous system the small synaptic vesicles, which did not have dense cores after osmium fixation, would have such after some other form of preparation, and whether this would be a better criterion for recognizing norepinephrine containing structures also remains to be seen. Unfortunately, permanganate fixed material is unsatisfactory for autoradiography due to the bleaching action of the photographic solutions. Observation of permanganate fixed brain by routine methods has so far failed to reveal small granular vesicles (unpublished observations).

ACKNOWLEDGMENTS

K. C. Richardson, in whose laboratory these experiments were performed, unfailingly provided counsel on many details of technique and interpretation throughout the course of the work. The author is deeply indebted to Drs. I. J. Kopin and R. J. Baldessarini for preparing the animals and brain slices studied.

LITERATURE CITED

- Aghajanian, G. K., and F. E. Bloom 1966a Electron microscopic autoradiography of rat hypothalamus after intraventricular ³H-norepinephrine. *Science*, in press.
- 1966b Electron-microscopic autoradiography of rat brain following ³H-DOPA. *Fed. Proc.*, 25: 383.
- 1966c Electron-microscopic autoradiography of rat brain following ³H-serotonin. *Biochem. Pharmacol.*, in press.
- Baldessarini, R. J., and I. J. Kopin 1966 Norepinephrine-³H release from brain slices by electrical stimulation. *Science*, in press.
- Bloom, F. E., G. A. Aghajanian and R. J. Barnett 1966 Regional brain amines and the fine structural identification of norepinephrine. *Anat. Rec.*, 154: 318-319.
- Bondareff, W. 1966 Submicroscopic localization of norepinephrine in sympathetic nerves of rat pineal. *Anat. Rec.*, 154: 498-499.
- Burack, W. R., and P. R. Drackoczy 1964 The turnover of endogenously labeled catecholamine in several regions of the sympathetic nervous system. *J. Pharmacol.*, 144: 66-75.
- Caro, L. G. 1962 High-resolution autoradiography. II. The problem of resolution. *J. Cell Biol.*, 15: 189-199.
- Caro, L. G., and M. Schnös 1965 Tritium and phosphorus-32 in high-resolution autoradiography. *Science*, 149: 60-62.
- Caro, L. G., and R. P. van Tubergen 1962 High-resolution autoradiography. I. Methods. *J. Cell Biol.*, 15: 173-188.
- Dahlström, A., and K. Fuxe 1964 Evidence for the existence of monoamine-containing neurons in the central nervous system. I. Demonstration of monoamines in the cell bodies of brain stem neurons. *Acta Physiol. Scand.*, 62: Suppl. 232.
- Dengler, H. J., H. E. Spiegel and E. O. Titus 1961 Uptake of tritium-labeled norepinephrine in brain and other tissues of cat *in vitro*. *Science*, 133: 1072-1073.
- De Robertis, E., A. Pellegrino de Iraldi, G. Rodriguez de Lores Arnaiz and L. M. Zieher 1965 Synaptic vesicles from the rat hypothalamus. Isolation and norepinephrine content. *Life Sci.*, 4: 193-201.
- Fuxe, K. 1965 Evidence for the existence of monoamine neurons in the central nervous system. IV. Distribution of monoamine nerve terminals in the central nervous system. *Acta Physiol. Scand.*, 64: Suppl. 247, 37-85.
- Fuxe, K., and N.-A. Hillarp 1964 Uptake of l-dopa and noradrenaline by central catecholamine neurons. *Life Sci.*, 3: 1403-1406.
- Fuxe, K., T. Hökfelt and O. Nilsson 1965 A fluorescence and electronmicroscopic study on certain brain regions rich in monoamine terminals. *Am. J. Anat.*, 117: 33-46.
- Glowinski, J., and J. Axelrod 1965 Effect of drugs on the uptake, release, and metabolism of ³H-norepinephrine in the rat brain. *J. Pharmacol.*, 149: 43-49.
- Glowinski, J., L. L. Iversen and J. Axelrod 1966 Storage and synthesis of norepinephrine in the reserpine-treated rat brain. *J. Pharmacol.*, 151: 385-399.
- Glowinski, J., I. J. Kopin and J. Axelrod 1965 Metabolism of ³H-norepinephrine in the rat brain. *J. Neurochem.*, 12: 25-30.
- Hamberger, A., and B. Hamberger 1966 Uptake of catecholamines and penetration of trypan blue after blood-brain barrier lesions. *Z. Zellforsch.*, 70: 386-392.
- Hamberger, B., and D. Masuoka 1965 Localization of catecholamine uptake in rat brain slices. *Acta Pharmacol. Toxicol.*, 22: 363-368.
- Hashimoto, Y., S. Ishii, Y. Ohi, N. Shimizu and R. Imajumi 1965 Effect of dopa on the norepinephrine and dopamine contents and on the granulated vesicles of the hypothalamus of reserpine-treated rabbits. *Jap. J. Pharmacol.*, 15: 395-400.
- Hillman, H., and H. M. McIlwain 1961 Membrane potentials in mammalian cerebral tissues *in vitro*: dependence on ionic environment. *J. Physiol.*, 157: 263-278.
- Ishii, S., N. Shimizu, M. Masuoka and R. Imajumi 1965 Correlation between catecholamine content and numbers of granulated vesicles in rabbit hypothalamus. *Biochem. Pharmacol.*, 14: 183-184.
- Kopin, I. J., E. K. Gordon and W. D. Horst 1965 Studies on uptake of l-norepinephrine-¹⁴C. *Biochem. Pharmacol.*, 14: 753-759.

placement, or by treatment in aqueous solutions.

With its half-life of twelve and one-half years, 1% of tritium atoms disintegrate in a two-month period, which was the length of exposure in the present experiment. Moreover, autoradiography as used here detects less than 25% of disintegrations (Caro and Schnös, '65), perhaps as few as 10%. Thus, only about 0.1% of the tritium present was revealed as silver grains, and so it is highly probable that many of the structures which contained exogenous norepinephrine did not bear silver grains in the autoradiographs. By not comparing labeled to unlabeled structures, and not considering the proportion of a tissue element labeled, we avoid any misinterpretation due to the fact that the exposure time was long enough only to allow a very small proportion of disintegrations to occur.

Caro ('62) gives figures as low as 0.1μ for the resolution of autoradiographic localization in preparations similar to those used here. However, in scoring "hits" in a tightly packed tissue like brain, the opposite issue becomes important. That is, how far a silver grain can appear from the site of the tritium disintegration. Caro and Schnös ('65) showed that the upper limit is about 0.25μ , and Caro ('62) estimates that at least 90% fall within this distance. Hence, a circle 0.25μ in radius was used in the present analysis to identify the possible sites of the disintegration responsible for each silver grain observed. A silver grain was considered to be located at the mid-point of the line connecting its two ends, if the ends were visible (Caro and van Tubergen, '62). If not, the center of the mass of silver was taken to be the location of the grain (Caro, '62).

It might seem important to measure the relative volumes of the elements of the tissue under study, and to compare the results to the relative distribution of silver grains over these elements. However, since this type of analysis can only reveal large differences, it is only applicable when the tissue elements of interest make up a relatively small fraction of the total tissue. In the present material inspection showed that this condition was not met. Indeed, it was expected that in order to obtain

levels of radioactivity above background, regions would have to be studied that were rich in norepinephrine containing nerve endings, as both areas studied in the present experiments are known to be (Fuxe, '65). Several reasons may be suggested to explain why, of many such areas in the rat brain, the preoptic area in the brain slices and lateral septal nucleus in the *in vivo* experiment were the only ones to give positive autoradiographic results. In the case of the brain slices, one reason may be that only regions lying near the surface of the free-hand coronal slices were examined. In the case of the *in vivo* experiment, one important factor was undoubtedly that the region of the lateral septum studied was immediately subependymal, and subjacent to the lateral ventricle, not very far from the site of injection. Kopin et al. ('65) showed that uptake of norepinephrine by tissue is dependent on the dose to which the tissue is exposed and upon the richness of the adrenergic innervation. The product of these two factors might well have been maximal in the lateral septal nucleus. It is clear from the thick sections that the overlying ependyma was not damaged, and that the injection of norepinephrine was not directly into the tissue examined.

In conclusion, the identification and description of brain structures which concentrate exogenous norepinephrine is made possible by autoradiography, and is reinforced by the bulk of previous evidence. It is quite clear that the presence of granular vesicles in such structures is an important feature of their fine structure. Whether the presence of a granular vesicle, in a structure seen by routine electron microscopy in central axons and endings, can be equated with the presence of endogenous norepinephrine remains to be seen, but this seems more likely in the light of the present results. In light of the difference in size of granular vesicles in central and peripheral norepinephrine containing structures (1000 and 500 Å, respectively) and of the relatively small number of granular vesicles in central endings, the question whether the central granular vesicles are the major site of norepinephrine storage must also be left open. It must be remembered that fixation of

peripheral adrenergic structures with solutions of permanganate causes an increase in the proportion of small synaptic vesicles with dense cores, as well as the appearance of such vesicles in sites where osmium fixation reveals only agranular vesicles (Richardson, '66b). Whether in the central nervous system the small synaptic vesicles, which did not have dense cores after osmium fixation, would have such after some other form of preparation, and whether this would be a better criterion for recognizing norepinephrine-containing structures also remains to be seen. Unfortunately, permanganate fixed material is unsatisfactory for autoradiography due to the bleaching action of the photographic solutions. Observation of permanganate fixed brain by routine methods has so far failed to reveal small granular vesicles (unpublished observations).

ACKNOWLEDGMENTS

K. C. Richardson, in whose laboratory these experiments were performed, unflinchingly provided counsel on many details of technique and interpretation throughout the course of the work. The author is deeply indebted to Drs. I. J. Kopin and R. J. Baldessarini for preparing the animals and brain slices studied.

LITERATURE CITED

- Aghajanian, G. K., and F. E. Bloom 1966a Electron microscopic autoradiography of rat hypothalamus after intraventricular ³H-norepinephrine. *Science*, in press.
- 1966b Electron-microscopic autoradiography of rat brain following ³H-DOPA. *Fed. Proc.*, 25: 383.
- 1966c Electron-microscopic autoradiography of rat brain following ³H-serotonin. *Biochem. Pharmacol.*, in press.
- Baldessarini, R. J., and I. J. Kopin 1966 Norepinephrine-H³ release from brain slices by electrical stimulation. *Science*, in press.
- Bloom, F. E., G. A. Aghajanian and R. J. Barnett 1966 Regional brain amines and the fine structural identification of norepinephrine. *Anat. Rec.*, 154: 318-319.
- Bondareff, W. 1966 Submicroscopic localization of norepinephrine in sympathetic nerves of rat pineal. *Anat. Rec.*, 154: 498-499.
- Buzack, W. R., and P. R. Drackocy 1964 The turnover of endogenously labeled catecholamine in several regions of the sympathetic nervous system. *J. Pharmacol.*, 144: 66-75.
- Caro, L. G. 1962 High-resolution autoradiography. II. The problem of resolution. *J. Cell Biol.*, 15: 189-199.
- Caro, L. G., and M. Schnöds 1965 Tritium and phosphorus-32 in high-resolution autoradiography. *Science*, 149: 60-62.
- Caro, L. G., and R. P. van Tubergen 1962 High-resolution autoradiography. I. Methods. *J. Cell Biol.*, 15: 173-188.
- Dahlström, A., and K. Fuxe 1964 Evidence for the existence of monoamine-containing neurons in the central nervous system. I. Demonstration of monoamines in the cell bodies of brain stem neurons. *Acta Physiol. Scand.*, 62: Suppl. 232.
- Dengler, H. J., H. E. Spiegel and E. O. Titus 1961 Uptake of tritium-labeled norepinephrine in brain and other tissues of cat *in vitro*. *Science*, 133: 1072-1073.
- De Robertis, E., A. Fellegrino de Iraldi, G. Rodriguez de Lores Arnaiz and L. M. Zieher 1965 Synaptic vesicles from the rat hypothalamus. Isolation and norepinephrine content. *Life Sci.*, 4: 193-201.
- Fuxe, K. 1965 Evidence for the existence of monoamine neurons in the central nervous system. IV. Distribution of monoamine nerve terminals in the central nervous system. *Acta Physiol. Scand.*, 64: Suppl. 247, 37-85.
- Fuxe, K., and N.-A. Hillarp 1964 Uptake of l-dopa and noradrenaline by central catecholamine neurons. *Life Sci.*, 3: 1403-1406.
- Fuxe, K., T. Hökfelt and O. Nilsson 1965 A fluorescence and electronmicroscopic study on certain brain regions rich in monoamine terminals. *Am. J. Anat.*, 117: 33-46.
- Glowinski, J., and J. Axelrod 1965 Effect of drugs on the uptake, release, and metabolism of ³H-norepinephrine in the rat brain. *J. Pharmacol.*, 149: 43-49.
- Glowinski, J., L. L. Iversen and J. Axelrod 1966 Storage and synthesis of norepinephrine in the reserpine-treated rat brain. *J. Pharmacol.*, 151: 385-399.
- Glowinski, J., I. J. Kopin and J. Axelrod 1965 Metabolism of ³H-norepinephrine in the rat brain. *J. Neurochem.*, 12: 25-30.
- Hamberger, A., and B. Hamberger 1966 Uptake of catecholamines and penetration of trypan blue after blood-brain barrier lesions. *Z. Zellforsch.*, 70: 386-392.
- Hamberger, B., and D. Masuoka 1965 Localization of catecholamine uptake in rat brain slices. *Acta Pharmacol. Toxicol.*, 22: 363-368.
- Hashimoto, Y., S. Ishii, Y. Ohi, N. Shimizu and R. Imazumi 1965 Effect of dopa on the norepinephrine and dopamine contents and on the granulated vesicles of the hypothalamus of reserpinized rabbits. *Jap. J. Pharmacol.*, 15: 395-400.
- Hillman, H., and H. M. McIlwain 1961 Membrane potentials in mammalian cerebral tissues *in vitro*: dependence on ionic environment. *J. Physiol.*, 157: 263-278.
- Ishii, S., N. Shimizu, M. Masuoka and R. Imazumi 1965 Correlation between catecholamine content and numbers of granulated vesicles in rabbit hypothalamus. *Biochem. Pharmacol.*, 14: 183-184.
- Kopin, I. J., E. K. Gordon and W. D. Horst 1965 Studies on uptake of l-norepinephrine-¹⁴C. *Biochem. Pharmacol.*, 14: 753-759.

- Lenn, N. J. 1965 Electron microscopic observations on monoamine-containing brain stem neurons in normal and drug-treated rats. *Anat. Rec.*, 153: 399-406.
- Matsuoka, M., S. Ishii, N. Shimizu and R. Imazumi 1965 Effect of Win 18501-2 on the content of catecholamines and the number of catecholamine-containing granules in the rabbit hypothalamus. *Experientia*, 21: 121-125.
- McEwen, L. M. 1956 The effect on the isolated rabbit heart of vagal stimulation and its modification by cocaine, hexamethonium and ouabain. *J. Physiol.*, 131: 678-689.
- Millonig, G. 1962 Further observation on a phosphate buffer for osmium solutions in fixation. Fifth Intern. Congr. Electron Microscopy, S. S. Bresse, Jr., ed., Academic Press, New York, vol 2. P8.
- Musacchio, J. M., I. J. Kopin and V. K. Weise 1965 Subcellular distribution of some sympathomimetic amines and their β -hydroxylated derivatives in the rat heart. *J. Pharmacol.*, 148: 22-28.
- Palay, S. L. 1958 The morphology of synapses in the central nervous system. *Exptl. Cell Res.*, Suppl. 5: 275-293.
- Pellegrino de Iraldi, A., and E. De Robertis 1963 Action of reserpine, iproniazid and pyrogallol on nerve endings of the pineal gland. *Intern. J. Neuropharmacol.*, 2: 231-239.
- Pellegrino de Iraldi, A., H. F. Duggan and E. De Robertis 1963 Adrenergic synaptic vesicles in the anterior hypothalamus of the rat. *Anat. Rec.*, 145: 521-531.
- Potter, L. T., and J. Axelrod 1963 Subcellular localization of catecholamines in tissues of the rat. *J. Pharmacol.*, 142: 291-298.
- Richardson, K. C. 1962 The fine structure of autonomic nerve endings in smooth muscle of the rat vas deferens. *J. Anat.*, 96: 427-442.
- 1966a Electron microscopic identification of autonomic nerve endings. *Nature*, 210: 756.
- 1966b Electron microscopic identification of adrenergic nerve endings. *Anat. Rec.*, 154: 484.
- Ross, S. B., and A. L. Renyi 1966 Active uptake of tritiated metaraminol by mouse brain slices *in vitro*. *Life Sci.*, 5: 639-647.
- Samorajski, T., and B. H. Marks 1962 Localization of tritiated norepinephrine in mouse brain. *J. Histochem. Cytochem.*, 10: 392-399.
- Shimizu, N., and S. Ishii 1964 Electron microscopic observation of catecholamine-containing granules in the hypothalamus and area postrema and their changes following reserpine injection. *Arch. Histol. Jap.*, 24: 489-497.
- Snyder, S. H., J. Glowinski and J. Axelrod 1965 The storage of norepinephrine and some of its derivatives in brain synaptosomes. *Life Sci.*, 4: 797-807.
- Venable, J. H., and R. Coggeshall 1965 A simplified lead citrate stain for use in electron microscopy. *J. Cell Biol.*, 25: 407-408.
- Wolfe, D. E., and L. T. Potter 1963 Localization of norepinephrine in the atrial myocardium. *Anat. Rec.*, 145: 301.
- Wolfe, D. E., L. T. Potter, K. C. Richardson and J. Axelrod 1962 Localizing tritiated norepinephrine in sympathetic axons by electron microscopic autoradiography. *Science*, 138: 440-442.
- Wood, J. G. 1966 Electron microscopic localization of amines in central nervous tissue. *Nature*, 209: 1131-1133.

PLATE 1

EXPLANATION OF FIGURES

- 1-13 Autoradiographs of the nucleus septi lateralis from the rat injected with ^3H -norepinephrine via the lateral ventricle. Arrows indicate silver grains. $\times 40,000$.
- 1 A nerve ending is seen labeled with a silver grain. Note the synaptic contact which the nerve ending makes with a dendrite.
- 2-6 Nerve endings are seen labeled with silver grains. They have a varying content of granular and agranular vesicles.

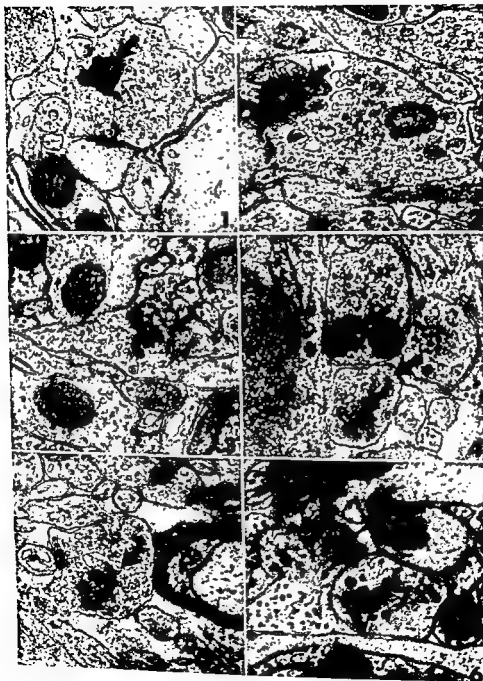


PLATE 2

EXPLANATION OF FIGURES

- 7 A nerve ending is seen labeled with a silver grain. Note the synaptic contact which the nerve ending makes with a dendrite.
- 8 Two nerve endings are seen connected by a segment of axon (star). One of these nerve endings is labeled with a silver grain.
- 9 A dendrite is seen labeled with a silver grain.
- 10 A portion of a neuronal perikaryon is seen labeled with a silver grain over the endoplasmic reticulum near the perinuclear cistern.

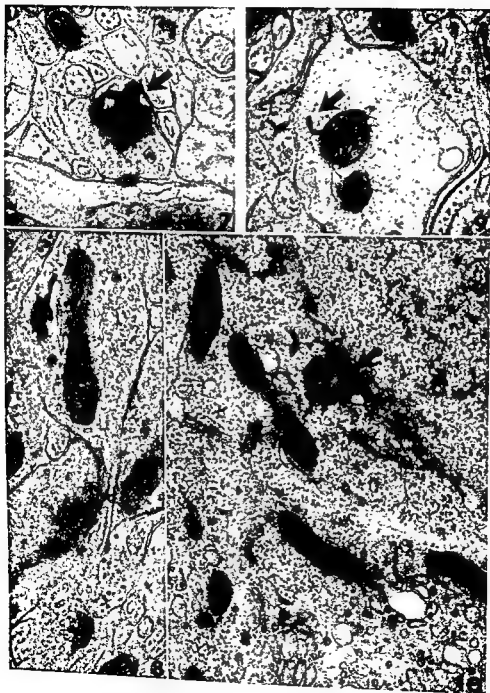


PLATE 2

EXPLANATION OF FIGURES

- 7 A nerve ending is seen labeled with a silver grain. Note the synaptic contact which the nerve ending makes with a dendrite.
- 8 Two nerve endings are seen connected by a segment of axon (star). One of these nerve endings is labeled with a silver grain.
- 9 A dendrite is seen labeled with a silver grain.
- 10 A portion of a neuronal perikaryon is seen labeled with a silver grain over the endoplasmic reticulum near the perinuclear cistern.

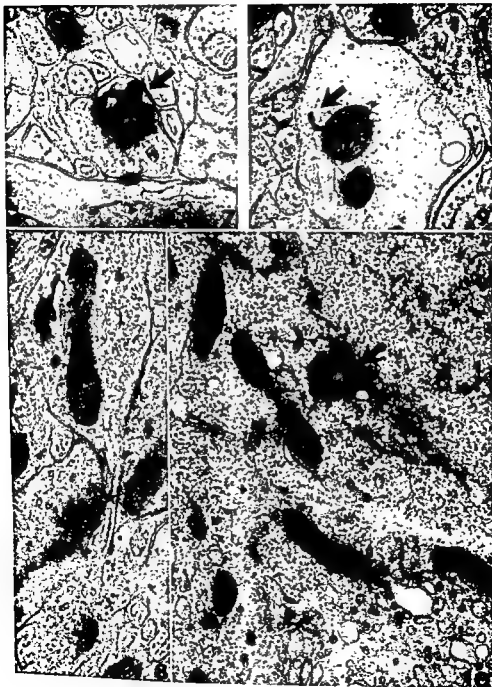
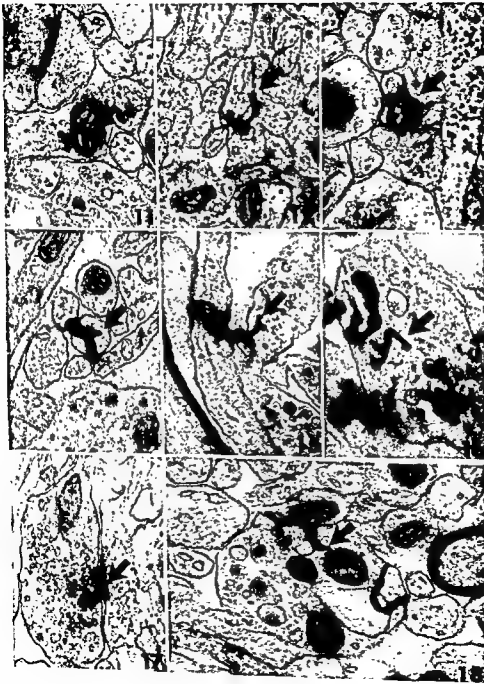


PLATE 3

EXPLANATION OF FIGURES

- 11-13 Groups of preterminal axons are seen labeled with silver grains.
- 14-18 Autoradiographs of the preoptic area from a brain slice incubated in ^3H -norepinephrine *in vitro*. Arrows indicate silver grains. $\times 40,000$.
- 14 A group of preterminal axons is seen labeled with a silver grain.
- 15 An equivocally located silver grain is seen in relation to a preterminal axon and two vesicle containing nerve endings, one of which contains a number of granular vesicles.
- 16-18 Nerve endings, containing mixed granular and agranular vesicles, are seen labeled with one or more silver grains. Note the synaptic contact between the nerve ending and dendrite in figure 17.



Effects of Pinealectomy in the Newborn Female Rat¹

LAURENCE E. WRAGG

Department of Anatomy, Northwestern University, Chicago, Illinois

ABSTRACT That pinealectomy in the rat is followed by ovarian hypertrophy is an assumption which is rather widely accepted and which is fundamental to much contemporary pineal research. Nevertheless an analysis of the alleged supporting literature shows it to be surprisingly weak and limited to animals operated at three to four weeks of age. In several mammals young pineals have been shown to equal or exceed older pineals in certain metabolic activities, but the effect of pineal ablation in the newborn rat is unknown. This report is based on Holtzman female rats pinealectomized at three days, and sacrificed at 60 days of age. The animals comprise a littermate series of eight normal, eight sham operated and eight pinealectomized; and a non littermate series of 18 normal, 17 sham operated, and ten pinealectomized rats. Pinealectomy was proved complete by microscopy of serial sections. Pinealectomized animals in both series did not differ from normals in the weight of the body, ovary, uterus, adrenal, or hypophysis; nor was there a difference in time of vaginal opening, estrous cycle, or 24 hour urinary sodium and potassium output.

Since the turn of the century there has been a sustained controversy whether the pineal body in the mammal inhibits gonadal activity. In the present decade a number of authors have assumed that it does, and interest has been demonstrated in the mechanism by which it acts. (Milcou and Pavel, '60; Meyer et al., '61; Thieblot and Blaise, '63; Chu et al., '64; Moszkowska, '63, '64, '65; Reiter and Hester, '66).

This assumption however is based on weak evidence. The weakest, sometimes involving only two or three experimental animals, has only rarely been mentioned since the monograph of Kitay and Altschule appeared in 1954, and since 1954 it is probably this monograph which has been the most frequently used reference on pineal function.² These authors have summarized the world literature on pineal physiology, but have avoided abstracts and reviews — which they claim are often incomplete, misleading, or inaccurate — and have studied original papers to present a critical analysis of available data, with emphasis on its statistical significance.

This valuable reference work has apparently been widely accepted, for I have yet to see it criticised. Nevertheless it is my opinion that the review of Kitay and Altschule is subject to the same criticism these authors have of other reviews — it may be misleading. For example they point out that pineal inhibition of gonadal de-

velopment is suggested by several lines of evidence; chiefly, that pinealectomy is followed by gonadal hypertrophy and that pineal extract injection is followed by gonadal atrophy.

More specifically, the best evidence available today (including the review of Kitay and Altschule) supports the thesis that pinealectomy induces ovarian hypertrophy in the rat. Indeed, one author (Roth, '65) recently stated that he elected to work on pinealectomy in the male rat because results in females were consistent and adequately documented.

In their monograph, Kitay and Altschule cite 18 references purporting to demonstrate gonadal hypertrophy following pinealectomy, and eight others which report no change. In these 26 papers, they claim that ovarian hypertrophy was demonstrated with statistical significance by three authors, but they discard the remaining work on pinealectomy and rat ovary, including all negative results.

Let us now consider the papers of these three authors: Izawa ('26c), Simonnet et al. ('51b,c), and Kitay ('54).

Kitay and Altschule note that the first author, Izawa ('26c) used only Wistar rats, used littermate controls, had ten

¹ This paper appeared in abstract form in *Anat. Rec.*, 151: 435-436, 1965.

² Another monograph (Thieblot and Le Bars, '55) is longer in text and wider in scope, but it is less critical and less often quoted.

pinealectomized and ten control animals, operated on all rats at 20 da, sacrificed them at 85 da, and proved completeness of operation by histological study of serial sections. Operated animals had reproductive organ weights significantly heavier than controls. This is certainly a persuasive presentation, but Kitay and Altschule omitted the following important aspects of Izawa's work.

The experiment was reported twice: once as a series of articles in *Tr. Soc. Path. Jap.* ('26a,b,c,d) and again in the *Am. J. Physiol.* ('26e) when a few additional organs were also compared. It is unusual that in both papers he refers to his other work on pinealectomy but in neither of these two papers is a reference made to the other.

Despite there being no comparable tables of data in the papers it is almost certain that they are based on the same animals. The work for both reports was done at the Wistar Institute of Anatomy and Biology; both papers were published the same year; the number of animals in each group, age at operation and at sacrifice, average body weight of operated females are all identical; and the following year (*Tr. Soc. Path. Jap.*, '27), in discussing his previous work on pinealectomy in rats, Izawa referred only to the *Am. J. Physiol.* ('26e).

This 1926e report has been criticized and the conclusions considered weak by Andersen and Wolf ('34). They pointed out that: (1) Izawa's operated animals were slightly heavier at operation than the controls and this difference would increase normally up to the age of about 100 da. (2) Normal rats (males) aged 85 days varied in weight from the amazingly low figure of 76.1 gm to 176 gm but no explanation is given (normal females varied from 116.5 to 156 gm). (3) Although Izawa stated that operated animals were heavier (by 17.7% in females and 24.2% in males), so great was the variability in body weight that statistical analyses showed no significance to the differences as calculated by Andersen and Wolf. (4) Since it is doubtful that heavier body weights were the result of operation, it must be doubted that heavier reproductive organs were related to the operation.

Had Andersen and Wolf also read the report in the Japanese journal their doubt would have deepened. In neither paper is the reader provided with complete data. In the Japanese report mean organ weights of operated and normal rats are compared, certain differences are stated to occur, but the significance is not calculated. In the American journal no data whatsoever are given for organ weights, and it is merely stated that differences are or are not of statistical significance. The method of calculating organ weight differences is given but it was based on tables of data of another author and should be read in the original.

"Using the table for the organ in question as it appears in *The Rat* (Donaldson, '24) the percentage increase in the weight of the organ from the body weight of the controls (here, for males, 136 gm) to the body weight of the tests (here, for males, 168.7 gm) is calculated. For the brain to take that as an example, this is found to be (loc. cit. table 144) 3.2%. The observed brain weight (1.680 gm) in the controls is therefore raised by this percentage (3.2%). This gives 1.7338 gm as the brain weight of the controls when the body weight is increased from 136 gm, the observed value, to 168.7 gm, the value for the tests. . . ."

By this process Izawa reworked the data. He is consistent about ovarian and uterine weight differences, but reversed his conclusions about other organs. For example, in the Japanese journal he states that pinealectomy induces accelerated growth of hypophysis, adrenal, pancreas, and thyroid, but in the American journal and from the same data, he states that all these organs weigh less in the pinealectomized rat, but not significantly so.

Although no organ weights are given in the American journal, body measurements are tabulated both as individual and as average values—the only such table in either paper. Averages for operated females (final body length, initial and final body weight) agree to the decimal in both papers, but for control females, and all males, average values differ by 0.2 to 10.7 gm, and 1.1 to 5.4 mm.

There is a subtle suggestion of statistical respectability in the Japanese journal

for each average measurement is accompanied by standard deviation, probable error of mean, and coefficient of variability. Nevertheless certain stated differences are not statistically significant.

In the Japanese report Izawa states that after discarding data of incomplete pinealectomies his final numbers for 20 remaining animals were ten operated and ten littermate controls. It is only upon studying tables in the American paper that the reader becomes impressed by the fact that per litter he had as many as three operated animals but never more than one control. Thus data from one control animal were repeated for each operated animal of the litter. In the tables for both males and females, the control animal whose statistics are repeated three times, has the lowest body weight in the entire table.

In the second source of information (Simmonet et al., '51b,c) 22-day-old female Wistar rats were operated on, and sacrificed at around 50 days. According to Kitay and Altschule, there were three experiments in which ovaries of pinealectomized animals were significantly heavier than controls, and one in which there was no difference. On studying the original data, it is discouraging to find that the average body weight of one group of control animals at sacrifice was within the authors' stated range of body weights at the initiation of the experiment, whereas operated animals weighed 55% more than controls.

Ovarian weights are surprising. They were reported to vary from one series in which those of operated animals were 5.8% lighter, to another similar experiment where they were 111% heavier than controls.

In still another paper published the same year (Simmonet and Thieblot, '51a) the same senior author reported no increase in ovarian weight of six operated animals.

The third author (Kitay, '54) is said to have added evidence that pinealectomy induces ovarian hypertrophy. If he did so he also cast doubt on the work he was confirming — for twice he repeated a pinealectomy series similar to Simmonet et al., and twice failed to find ovarian hypertrophy. Kitay then operated at a later age

of 26 and of 30 days and showed ovarian hypertrophy in these animals when sacrificed at 50 days of age.

Confusion is heightened by the three different histological descriptions of the ovary given by these three sources of authority. They state that: (1) Ovaries in pinealectomized rats have many well-developed follicles; the controls, none (Izawa et al., '27). (2) There is massive luteinization in operated animals, with no such change in controls (Simmonet et al., '51b). (3) There is no difference in follicular appearance between operated and control (Kitay, '54).

Similarly Izawa states that the uterus increases in weight in pinealectomized rats, but Kitay found no change.

The lack of consistency within and between papers of these three authors, and the wide range of ovarian and body weights, cast doubt on the reported significance of pinealectomy. Nevertheless they have been cited specifically by authors such as Kitay, '54; Wurtman, Axelrod, and Chu, '63; Kitay and Altschule, '54; and these citing authors have subsequently been quoted (e.g. Wurtman, Altschule and Holmgren, '59) to show that pinealectomy induces ovarian hypertrophy in the rat.

Kitay and Altschule are frequently guarded and conservative in their summaries. They admit that Izawa's work is not conclusive — not because of any of the criticisms noted above, but because controls were not sham operated, and organ weights were not adjusted to body weight.³ Data for male rats are even less convincing than for females but Kitay and Altschule state:

"Pinealectomy . . . in the rat consistently stimulates the genital system; it causes gonadal hypertrophy . . ."

and their review has been cited as the authority for similar statements, e.g. Kapfers, '62 and Reiss et al., '63.

Since 1954, Wurtman et al. ('59) have confirmed the work of Kitay. Their report appears convincing — indeed it has been termed "a significant advance" since 1954

³These criticisms are difficult to defend because Kitay himself ('54) had already shown that sham operation has no effect on ovarian weight; and the conversion based on body weight was calculated in the American journal report and the ovarian weight difference reasserted by Izawa.

in our understanding of pineal function (Meyer et al., '61).⁴

The effect of pinealectomy throughout early growth and development of the rat merits further study because the pineal has been shown to be active at a very early age. Owman showed evidence for rat pineal activity in utero both histologically ('61) and functionally ('63). At two weeks of age mitotic activity ceases (Quay and Levine, '57) and adult levels of serotonin are present (Quay and Halevy, '62). Turning to other species, the one to three month old goat pineal has a higher respiratory quotient and rate of amino acid formation than that of older animals (Hellman and Larsson, '61); and assays of three enzymes (hydroxyindole-O-methyl transferase, monoamine oxidase, histamine-N-methyl transferase) in human pineals show similar levels from childhood, through adolescence to old age (Wurtman et al., '64). After studying tumors of the human pineal, David et al. ('63) stated that absence of the pineal prior to puberty is pathologic and leads to precocious puberty.

It is frequently postulated that the pineal inhibits gonadal development by inhibiting pituitary gonadotrophins (e.g. Milcou et al., '60; Thieblot and Blaise, '63; Moszkowska, '63, '64, '65; and many others).

In this light, the effect of pinealectomy throughout the entire developmental period is of particular interest. Nevertheless the effect of pinealectomy in the newborn rat is unknown. In one attempt at its demonstration (Andersen and Wolf, '34) operative mortalities and infections of survivors were so numerous that too few animals were left for convincing statistical analysis. These authors concluded however that pinealectomy in the newborn rat has no effect on developing endocrine organs.

The effects of pinealectomy on growth rate, uterine weight, vaginal opening, estrous cycle, pituitary weight, and on adrenal weight and electrolyte balance are even less well documented than are the effects on the ovary.

Clearly there is need for a well-controlled, convincing study of the effects of pinealectomy in the newborn female rat. Thus the present study was undertaken.

MATERIALS AND METHODS

Animals and care

Variables were reduced to a minimum. Holtzman rats only were used. They were maintained under natural diurnal lighting conditions with free access to Rockland mouse and rat diet and water. The experimental period extended from July to January. The animals were raised in the laboratory of the author and were tended and handled by him alone. In one series termed "littermate series" pinealectomized, sham-operated, and normal animals were selected from each litter. Each unit of three animals was raised under identical environmental conditions — and sacrificed on the same day. In other litters, not all three categories were represented, but all animals were treated as nearly identically as possible.

Animals were identified by code number, except when grouped in threes by category for urine collections.

Operation

At the age of three days, animals were weighed and "normals" were returned to the nest. Animals to be operated on were placed in the freezing unit of a refrigerator until motionless. The operative site and instruments were cleaned with alcohol. Then, under a dissecting microscope the usual midline incision through skin, and transverse incision through occipital bone and dura were made. Short incisions were directed anteriorly from the ends of the transverse incision in the occipital bone and the small flap so formed was lifted with iris forceps and torn anteriorly to the level of the confluence of sinuses. The dura was then grasped and torn anteriorly, but not through, the transverse sinuses. On looking obliquely, the pineal body was visible beneath the intact confluence of

⁴After this brief review of the best evidence that pinealectomy induces ovarian hypertrophy, a discussion of negative results would be superfluous. Two recent reports however are of interest. (1) Gittes and Chu ('65) found no effect on ovarian weights when rats were pinealectomized at eight weeks of age, and kept in predominant darkness for the six to eight weeks prior to sacrifice at six to seven and one-half months. (2) Kitay and Altschule consider Shellabarger's work on chicks ('52) operated at two days of age, as among the best positive data available on pinealectomy effects. Recently Stalsberg ('65) did an extensive study on chicks pinealectomized at six-day embryos. Although pineal fragments were found at sacrifice, the results are interpreted as differing from those of Shellabarger.

sinuses. With a second pair of curved iris forceps the dural attachment of the body was grasped and the pineal tissue lifted out. Dural and bone flaps were replaced. The skin was closed with one or two interrupted sutures of 5-0 silk, then painted with dilute collodion to discourage the mother from opening the wound and killing the neonate. Animals were then earmarked, warmed, and returned to the nest.

Pinealectomy is often considered a difficult operation (discussed in Thieblot and Le Bars, '55) and modifications for its performance are still being described (Bruinvels et al., '64; Roth, '65; Hoffman and Reiter, '65a). The ease of operating on a young animal has apparently only rarely been appreciated (e.g. Einhorn and Rowntree, '39; D'Amour and D'Amour, '37), but the procedure here described must be the simplest, safest, and most rapid of all methods. No special equipment is required. In young animals the occipital bone is very easily cut. The major cause of death in older animals does not occur since there are no diploic veins to bleed, and dural sinuses are not opened. Hypothermia as the anesthetic agent helps minimize bleeding, and except for one occasion when three animals were inadvertently forgotten in the freezer, there were no anesthesia deaths. The pineal is readily visualized for removal although it can be removed blindly as well. Animals recover in a few minutes. The method requires about two minutes from the opening incision to the rewarming phase and has been learned successfully by technicians in half a day. Beginners may require a cold operating table (ice in towelling) to prolong anesthesia.

Whereas many investigators have difficulty accumulating operated animals (Andersen and Wolf, '34; Kitay and Altschule, '54; Thieblot and Blaise, '63) there were no mortalities at operation in this series. By the end of the experiment (60 days) the following animals had died: 4 of 47 pinealectomies, 5 of 30 sham operated, 3 of 29 normals.

Since validity of results depended on absolute assurance that pinealectomy had been complete, the operative area of the brain was embedded post mortem, serially sectioned, stained with hematoxylin and eosin and studied histologically.

Only 18 of 43 operated animals were totally free of pineal tissue. Frequently the remnant was in the base or stalk area and sometimes only 8-10 cells in diameter. Incidence of total extirpation by this method did not increase when the pineal was removed after elongation of the stalk (8 to 10 days—Kappers, '60). Electrocautery or cryosurgery might be a more effective method of ablating the organ.

Animal weight

Since daily weighings before and after surgery excite the mother and endanger the young, animals were weighed only at operation (day 3) and at weekly intervals thereafter. Only three weights are given in this paper—the weight at 3, 14, and 60 days.

Organ weights

At 60 \pm one-half days, between 9:00 A.M. and 6:00 P.M., animals were sacrificed with ether. Fresh organs were removed, and trimmed on moist blotting paper under a binocular microscope. In the case of the uterus; mesometrium, tubes and vagina were removed and the organ was opened to blot away free fluid. The ovary was cleaned by opening the bursa and cutting structures at the hilus. All weighing was done on a Roller Smith balance by one person.

Vaginal opening and smear

After age 30 days animals were examined daily for vaginal opening. Between the ages of 45 and 60 days vaginal smears were made at 12 \pm 1 hour intervals. Tap water was used and cells were examined fresh, unstained, under low power.

Urine electrolytes

Twenty-four-hour urine samples were collected on two or on three occasions from littermates totalling six in each category of pinealectomized, sham-operated, and normal animals. Metabolism cages and glassware were distilled-water rinsed; diuresis was promoted by feeding only 5% glucose in distilled water; and analysis for sodium and potassium was done on a Baird flame photometer.

TABLE 1
Weight in grams of normal (N), sham operated (Sh), and pinealectomized (P) female rats

	Day 3 (operated)	Day 14	Day 60
Littermates			
N (8) ¹	8.4 ± 0.18		
Sh (8)	8.4 ± 0.18	29.2 ± 2.1	183.5 ± 8.1
P (8)	8.4 ± 0.18	26.9 ± 2.4	177.1 ± 8.7
		27.2 ± 2.2	183.9 ± 5.6
Non littermates			
N (18)	8.0 ± 0.26		
Sh (17)	7.8 ± 0.25	30.0 ± 1.54	176.2 ± 5.20
P (10)	8.2 ± 0.24	26.6 ± 1.30	165.8 ± 5.92
		28.1 ± 1.27	168.7 ± 6.04

¹ Number of animals.

OBSERVATIONS AND DISCUSSIONS

1. *Rate of growth.* Table 1 shows that female rats pinealectomized at three days of age grow at the same rate as do sham-operated and normal animals.

Accelerated bodily growth and development in pinealectomized animals has been reported frequently but supporting statistically significant data are few (Kitay and Altschule, '54). Malm et al. ('59) have claimed that pinealectomy in male rats induces postoperative growth acceleration, lasting up to the fifteenth week but with no significant difference thereafter.

No difference in operated female rats was found when large numbers were used (Kitay, '54), or when controls consisted of both sham-operated and normal littermates (Andersen and Wolf, '34; Davis and Martin, '40). Our observations agree with these findings by showing that weights of female rats pinealectomized at birth do not differ from controls during the first two months of life.

2. *Ovarian and uterine weights.* Table 2 shows that ovarian and uterine weights of female rats which had been pinealectomized at three days of age do not differ at 60 days of age from those of sham-operated and normal controls.

The paucity of statistically significant data to support the widely held theory that pinealectomy induces ovarian hypertrophy has been discussed in the introduction.

For many years some of the experimental evidence was based on one, two, or three experimental animals — some of which is still cited (Thieblot and Blaise, '63). In the two most convincing demonstrations that ovarian hypertrophy follows

pinealectomy, the operation was performed at 26 or 30 days and the animals sacrificed at 50 or 54 days (Kitay, '54; Wurtman et al., '59). The present series shows that absence of the pineal throughout the period of postnatal growth and maturation has no effect on the weight of reproductive organs in the female rat.

3. *Vaginal opening and estrous cycle.* There is no difference from normals in the time of vaginal opening (table 2) or in the estrous cycle (table 3) of rats pinealectomized neonatally.

There is little information available concerning the effect of pinealectomy on vaginal opening and estrous cycle. Mesaki ('39) claims that two pinealectomized rats had onset of estrus 12 days before three sham operated littermates; and three others, 18 days before littermate controls.

Kitay and Altschule make note of the following reports: (1) At 53 days a patent vaginal canal appeared in 18 of 28 pinealectomized but only three of 15 control rats (Simonnet et al., '51b). Note that mean and range were not given. (2) There was no difference in time of vaginal opening or in estrous cycle (no details given) in a group of six rats pinealectomized at birth, compared with four sham operated and seven intact controls (Anderson and Wolf, '34). (3) There was no difference among six pinealectomized and four controls (del Castillo, '28).

The belief that estrus is prolonged appears to be based on one statistically significant paper (Katagiri, '43) in which 20 operated and 20 control mice were used; however, delay was reported in cats (Davis

TABLE 2
Body weight, ovarian weight, uterine weight, and day of vaginal opening in normal, sham operated, and pinealectomized rats¹

Litter	Body wt in gm			Ovarian wt in mg			Uterine wt in mg			Day of vaginal opening		
	N	Sh	P	N	Sh	P	N	Sh	P	N	Sh	P
Littermate series												
A	272	211	201	75.4	82.8	61.0	304.2	337.2	312.4	40	40	41
B	196	200	199	56.4	59.4	52.8	249.0	280.4	421.0	44	40	44
C	170	146	183	51.4	45.2	47.2	214.8	401.0	147.2	41	45	45
D	204	188	205	61.0	67.4	71.6	381.4	415.4	271.0	40	39	38
E	184	189	173	52.8	55.3	54.0	205.3	421.0	247.0	39	40	45
F	177	177	168	50.0	58.5	52.4	374.2	313.0	246.4	44	42	42
G	161	143	163	56.0	53.6	50.4	354.0	341.6	196.4	41	38	41
H	154	161	177	52.0	48.8	54.0	418.0	402.0	423.6	37	41	36
Mean	183.5	177.1	183.9	56.0	59.1	56.2	312.6	363.9	293.1	40.7	40.8	41.5
	±8.1	±6.7	±5.6	±2.9	±4.1	±2.6	±28.8	±21.3	±34.9	±0.84	±0.75	±1.15
Non littermate series ²												
Mean	176.2	165.8	168.7	55.1	47.6	50.8	311.2	284.4	307.4	40.7	42.8	37.8
	±5.20	±5.92	±6.04	±2.66	±2.42	±2.10	±20.51	±20.92	±25.27	±1.17	±1.47	±1.08

¹ Rats operated on at three days and sacrificed at 60 days of age.² Number of animals per group: N, 16; Sh, 17; P, 10.

and Martin, '40) but no change in rats (Andersen and Wolf, '34).

It is strange that on the basis of these papers, Kitay and Altschule state,

"The observed effects of pinealectomy on the vaginal membrane (acceleration of opening) and on the estrus cycle (prolongation of the estral phase) are uniform, and the data cited are statistically significant."

They later state,

"... not enough evidence is available to permit final conclusions."

nevertheless this reference has been cited — even by Altschule — to show that pinealectomy hastens vaginal opening (Meyer, Wurtman, Altschule and Lazo-Wasem, '61; Thieblot and Blaise, '63).

More recently a significant increase in duration of estrus in rats pinealectomized at four and at eight weeks has been reported. This occurred in diurnal lighting (Chu, '64) as well as in constant light and in predominant darkness (Glittes and Chu, '65).

The present series shows clearly that rats pinealectomized at three days of age do not differ from normal animals in time of vaginal opening or in the first few estrous cycles.

4. Adrenal weight and urinary electrolytes. Pinealectomy in the neonatal rat does not induce a change in adrenal weight, (table 4) nor is there alteration in urinary sodium and potassium output (table 5). There is however a uniform tendency for increased sodium and potassium preservation in all groups as they grow from 30 to 50 days of age. This undoubtedly reflects the development of a more efficient kidney during this period of immaturity. Interestingly enough, the change is similar in operated and in normal animals.

When Farrell ('59) showed glomerulotropic activity of beef pineal extract in dogs, there was revived interest in the effect of the pineal on the adrenal gland.

Both prior and subsequent papers have claimed that the adrenal of various species hypertrophies after pinealectomy. In a review of 16 such papers, Kitay and Altschule ('54) find that none demonstrates a difference of statistical significance. Since that time, Wurtman et al. ('59) pinealectomized female rats at 26 days and sacri-

TABLE 3
Estrous cycle in normal, sham operated, and pinealectomized rats¹

Experimental animal	No. of animals	Proestrus		Estrus		Metestrus		Diestrus	
		Duration ²	Obs. ³	Duration	Obs.	Duration	Obs.	Duration	Obs.
Normal	12	14(0-24)	25	39(24-60)	24	7(0-12)	30	62(48-132)	25
Sham operated	10	11(0-24)	25	42(24-72)	26	9(0-12)	28	51(24-84)	26
Pinealectomized	9	13(0-24)	19	41(24-72)	20	9(0-24)	21	65(36-120)	18

¹ Animals operated at three days of age; smears taken at 12 hour intervals from age 45-60 da.
² Duration: average duration (to closest hour) with range in parentheses.
³ Obs.: number of completed phases observed.

TABLE 4
Adrenal weight (in mg) in normal, sham operated, and pinealectomized female rats

	Normal	Sham operated	Pinealectomized
Littermate series	53.5 ± 2.2 (8)	51.9 ± 2.3 (8)	51.9 ± 2.5 (8)
Non littermate series	49.3 ± 1.36(18)	48.2 ± 1.79(17)	47.8 ± 1.48(10)

TABLE 5
Sodium and potassium excretion in normal, sham operated, and pinealectomized female rats

Age in days	No. of animals per group	Urinary excretion in M Eq/Kg/24 hours						24 hour urine		
		Na			K			Na:K ratio		
		N	Sh	P	N	Sh	P	N	Sh	P
30	3 (Series A) ¹	4.58	5.53	4.87	6.3	6.4	7.1	0.73	0.86	0.68
40	3 (Series A) ¹	1.80	3.70	3.50	5.6	6.0	6.2	0.32	0.62	0.56
40	3 (Series B)	2.60	3.30	3.50	5.4	6.9	6.4	0.48	0.47	0.55
50	3 (Series A) ¹	1.52	0.73	2.06	4.7	4.4	5.3	0.32	0.17	0.39
50	3 (Series B)	2.58	2.53	2.10	4.9	5.9	4.7	0.52	0.43	0.40
Mean value		2.62	3.16	3.21	5.4	5.9	5.9	0.47	0.51	0.52

¹ A small pineal fragment was present in one of the animals of the pinealectomized group.

TABLE 6
Pituitary weight (in mg) in normal, sham operated, and pinealectomized female rats

	Normal	Sham operated	Pinealectomized
Littermate series	9.4 ± 0.53(8)	9.1 ± 0.45(8)	8.7 ± 0.24(8)
Non littermate series	8.8 ± 0.33(18)	8.3 ± 0.34(17)	7.9 ± 0.46(10)

ficed them at 54 days of age and found a significant increase in adrenal weight over sham operated and normal controls. They suggest that the pineal inhibits adrenal growth. However in 1960 Wurtman et al. were unable to demonstrate a significant effect of pinealectomy on the zona glomerulosa of the adrenal, nor on aldosterone production as measured indirectly by urinary potassium excretion in four operated and four normal female rats.

There have been many studies which either supported or denied the concept of pineal adrenoglomerulotropin. However, Farrell himself ('60), using dogs, soon

found that pinealectomy did not permanently alter aldosterone secretion, and he has proposed the concept of a mid-brain-epiphyseal complex with both inhibitory and stimulatory elements for steroid output.

The present study denies adrenal hypertrophy or change in urinary electrolytes in rats pinealectomized at birth.

5. *Pituitary weight.* Table 6 shows no effect of pinealectomy on pituitary weight. After tabulating pinealectomy effects in various species Kitay and Altschule found 17 reports of pituitary hypertrophy and

seven of no change, but none of the reports was convincing to these reviewers.

In 1956 Holmes was unable to find any difference in cell counts of the pituitaries of normal and pinealectomized rats. Similarly, this report shows no effect on pituitary weight following pinealectomy at three days of age.

Presentation of data and statistical analysis

Data are presented separately for littermates and for non littermates except in table 3 (estrous cycle) where animals were few, and in table 5 (urine electrolytes) where only littermates were used.

Organ weights were not adjusted to body weight because in each series one control group is almost identical in body weight to the operated group. In addition, analysis of variance of the littermate series obviates the necessity for such a conversion.

Means with standard deviation are presented, but for those values most disputed, i.e. ovarian and uterine weight and day of vaginal opening, individual data for littermates are tabulated along with pertinent body weights (table 2).

Inspection alone shows that pinealectomy induced no deviation from normal in any of the eight measurements taken. Nevertheless, the littermate series was subjected to analysis of variance, and non littermates to the *t* test (table 7). The data of table 5 (urine electrolytes) were not analysed since they probably do not merit statistical treatment.

Analysis of variance shows a difference between litters ($P < 0.005$ to < 0.1) except for uterine weight ($P > 0.25$). *P* values for treatments were all far below the 0.05 level.

Similarly for non littermates none of the *F* values which might show that pinealectomized animals differ from normal animals approached the 0.05 level of confidence. The day of vaginal opening of pinealectomized animals was advanced relative to sham operated animals at a low level of confidence. Since they varied in the opposite direction in the littermate series the difference must be attributed to chance. The diestrous phase in sham operated animals appeared to be shorter than in the other two groups ($P < 0.02$).

CONCLUSIONS

There is widespread belief that pinealectomy in the rat induces gonadal hypertrophy, but considering the existing literature, supporting experimental evidence is surprisingly scarce and variable. The embarrassment of negative studies is reflected in the many theories to explain such discrepancies. Some of the theories have been in the literature for years (discussed by Thieblot and Le Bars, '55) and they are still being repeated and added to—for examples: there are differences in age, strain, or environment (Kitay and Altschule, '54; Thieblot and Blaise, '63); numbers were too few; operation might be incomplete (Reiter and Hester, '66), might damage significant brain nuclei, or damage vasculature (Reiss, '63); the pineal contains both inhibitory and stimulatory principles (Reiss, '63); pinealectomy effects are subtle in the normal photoperiod and require other influences for augmentation (Hoffman and Reiter, '65); other tissue may assume certain pineal functions (Quay, '65); and pineal influence may be circadian in rhythm rather than continuously prolonged (Quay, '63).

Other lines of investigation relating to pineal and gonads are also controversial, but the recurrence of this theme from varied studies tends to be cumulatively persuasive toward the belief in such a relationship.

It seems clear from the present study (and from Anderson and Wolf, '34) that pinealectomy in newborn rats has no effect on the weights of the body, ovary, uterus, adrenal, or pituitary; on the onset of puberty, the estrous cycle, or urinary electrolytes.

In old rats too it is believed that pinealectomy has no effect on the reproductive system (Kitay and Altschule, '54; Thieblot and Le Bars, '55; Gittes and Chu, '65; and others).

Only within a restricted age range is there reasonable evidence that pinealectomy induces ovarian hypertrophy (i.e. operated at 26 to 30 days and sacrificed at 50 to 54 days).

If the pineal modifies gonadal development it must be during a narrow phase of growth, and by a mechanism which can be

TABLE 7
Summary of statistical analysis

t-test		Analysis of variance						
N-P	Sh-P	N-Sh	Source of variance	d/f	Mean square	F ratio	P	
Body wt day 3	> 0.4	> 0.2	Body wt day 60	litter	7	1145.4285	10.18	
day 14	> 0.5	> 0.2		treat	2	115.1250	1.02	
day 60	> 0.1	> 0.2		error	14	112.5536	< 0.005	
Ovarian wt	> 0.2	> 0.2	Ovarian wt.	litter	7	207.2121	8.008	
		> 0.1		treat	2	19.0067	0.7346	
				error	14	25.8743	< 0.005	
Uterine wt	> 0.5	> 0.5	Uterine wt	litter	7	6848.8879	1.11	
		> 0.4		treat	2	13383.6430	> 0.25	
				error	14	6179.5622	< 0.1	
Vaginal Op.	> 0.1	< 0.05	Vaginal Op.	litter	7	11.6607	2.58	
		> 0.2		treat	2	1.7917	0.39	
				error	14	4.5536	< 0.1	
Proestrus	> 0.5		Adrenal wt.					
Estrus	> 0.4							
Metestrus	> 0.5	> 0.3						
Diestrus		< 0.02						
Adrenal wt	> 0.4	> 0.5	Adrenal wt.	litter	7	95.7637	4.99	
				treat	2	9.2830	0.48	
				error	14	19.1763	< 0.01	
Pituitary wt.	> 0.5	> 0.5	Pituitary wt.	litter	7	3.1837	5.22	
				treat	2	0.8600	1.40	
				error	14	0.6100	< 0.005	

compensated for or by-passed when the pineal is extirpated early in life.

Certainly the statement that pinealectomy in itself induces ovarian hypertrophy is inadequately supported by existing reports. If an effect exists a more specific definition of its cause and incidence is needed.

ACKNOWLEDGMENTS

I am grateful to Drs. C. R. S. Machado and S. Harris for doing the statistical analysis of the data.

This study was supported in part by NIH grant 1S-01-FR-0531101.

LITERATURE CITED

- Andersen, D. H., and A. Wolf 1934 Pinealectomy in rats, with a critical survey of the literature. *J. Physiol.*, 81: 49-62.
- Bruinvels, J., J. C. Houten and J. Van Noordwijk 1964 Influence of pinealectomy and hypophysectomy on the renin content of rat kidneys. *Quart. Jour. Exptl. Physiol.*, 49: 95-102.
- del Castillo, E. B. 1928 Action de la splenectomie et de l'epiphysectomie sur le cycle oestral du rat blanc. *C. Rend. Soc. Biol.*, 99: 1404-1405.
- Chu, E. W., R. J. Wurtman and J. Axelrod 1964 An inhibitory effect of melatonin on the estrous phase of the estrous cycle of the rodent. *Endocrinology*, 75: 238-242.
- D'Amour, M. C., and F. E. D'Amour 1937 Effects of pinealectomy over several generations. *Proc. Soc. Exptl. Biol. Med.*, 37: 244-246.
- David, M., E. Bernard-Weil and D. Dilenge 1963 Les tumeurs de la glande pineale, 24: 287-330.
- Einhorn, N. H., and L. O. Rowntree 1939 Experimental phases of the pineal problem. *Endocrinology*, 24: 221-229.
- Farrell, G. 1959 Glomerulotropic activity of an actions extract of pineal tissue. *Endocrinology*, 65: 239-241.
- 1960 Adrenoglomerulotropin. *Circulation*, 21: 1009-1015.
- Gitter, R. F., and E. W. Chu 1965 Reversal of the effect of pinealectomy in female rats by multiple isogenic pineal transplants. *Endocrinology*, 77: 1061-1067.
- Hellman, B., and S. Larsson 1961 Metabolism of tagged glucose by the pineal gland. *Nutrition Reviews*, 30: 115-116.
- Hoffman, R. A., and R. J. Reiter 1965 Pineal Gland: Influence on gonads of male hamsters. *Sci.*, 148: 1609-1610.
- 1965a Rapid pinealectomy in hamsters and other small rodents. *Anat. Rec.*, 153: 19-22.
- Holmes, R. L. 1956 Effect of pinealectomy on the rat pituitary. *Nature*, 177: 791.
- Izawa, Y. 1926a The effects of pinealectomy at 20 days of age on the growth in body length, body weight and tail length of male and female albino rats. *Tr. Soc. Path. Jap.*, 16: 60-69.
- 1926b The effect of pinealectomy at 20 days of age on the growth of the brain and spinal cord of the male and female albino rats. *Tr. Soc. Path. Jap.*, 16: 69-72.
- 1926c The effect of pinealectomy at 20 days of age on the growth of the reproductive system of the male and female albino rats. *Tr. Soc. Path. Jap.*, 16: 72-78.
- 1926d The effects of pinealectomy at 20 days of age on the growth of the glands of internal secretion of male and female albino rats. *Tr. Soc. Path. Jap.*, 16: 78-86.
- 1926e On some anatomical changes which follow removal of the pineal body from both sexes of the immature albino rat. *Am. J. Physiol.*, 77: 126-139.
- Izawa, Y., and S. Akiyama 1927 On some anatomical changes which follow pinealectomy at 20 days of age in both sexes of the albino rat. *Tr. Soc. Path. Jap.*, 17: 320-324.
- Kappers, J. A. 1960 The development, topographical relations and innervation of the epiphysis cerebri in the albino rat. *Z. Zellforsch.*, 52: 163-215.
- 1962 Melatonin, a pineal compound. Preliminary investigations on its function in the rat. *Gen. Comp. Endocr.*, 2: 610-611.
- Katagiri, E. 1943 Studies on the pineal gland; pinealectomy and the sexual cycle. *Osaka igak-kai zasshi*, 42: 935-938. (Quoted from Kitay and Altschule, '54.)
- Kitay, J. I. 1954 Effects of pinealectomy on ovary weight in immature rats. *Endocrinology*, 54: 114-116.
- Kitay, J. I., and M. D. Altschule 1954 The pineal gland. Harvard Univ. Press, Cambridge, Mass., 280 pp.
- Malm, O. J., O. E. Skaug and P. Lingjorde 1959 The effect of pinealectomy on bodily growth, survival rate, and P^{32} uptake in the rat. *Acta endocr. (Kbh.)*, 30: 22-28.
- Mesaki, T. 1939 An experimental study on the effect of the pineal function on the sexual cycle and sexual hormones. *Jap. J. Obstet.*, 22: 26-30.
- Meyer, C. J., R. J. Wurtman, M. D. Altschule and E. A. Lazo-Wasem 1961 The arrest of prolonged estrus in "middle-aged" rats by pineal gland extract. *Endocrinology*, 68: 795-800.
- Milcrou, S. M., and S. Pavel 1960 Antigonadotropic function of the pineal gland and the oxytocin of the neurosecretory hypothalamic system. *Nature*, 187: 950-951.
- Moszkowska, A. 1963 L'antagonisme epiphysio-hypophysaire. *Ann. Endocr.*, 24: 215-226.
- 1964 Quelques arguments en faveur de la specificite zoologique de l'activite antagonadotrope de l'epiphyse. *Ann. Endocr.* 25 (5 Suppl.), 79-85.
- 1965 Contribution a l'etude du mecanisme de l'antagonisme epiphysio-hypophysaire. *Prog. in Brain Res.*, Vol. X: 564-575.
- Owman, C. 1961 Secretory activity of the fetal pineal gland of the rat. *Acta Morph. Neerl. Scand.*, 3: 367-394.
- 1963 Evidence for a functional significance of the fetal pineal gland of the rat. *Gen. Comp. Endocr.*, 3: 723-724.

- Quay, W. B. 1963 Circadian rhythms in rat pineal serotonin and its modifications by estrous cycle and photoperiod. *Gen. Comp. Endocr.*, 3: 473-479.
- 1965 Retinal and pineal hydroxyindole-O-methyl transferase activity in vertebrates. *Life Sciences*, 4: 983-991.
- Quay, W. B., and A. Halevy 1962 Experimental modification of the rat pineal's content of serotonin and related indole amines. *Physiol. Zool.*, 35: 1-7.
- Quay, W. B., and B. E. Levine 1957 Pineal growth and mitotic activity in the rat: The effects of colchicine and sex hormones. *Anat. Rec.*, 129: 65-77.
- Reiss, M., F. E. Badrick and J. H. Halkerston 1963 Action of pineal extracts on the gonads and their function. *J. Endocr.*, 27: 107-118.
- Reiter, R. J., and R. J. Hester 1966 Metabolic regulation of physiological activity: III. Neuroendocrinological interrelationships. Research Laboratories, Edgewood Arsenal, Maryland.
- Roth, W. D. 1965 Metabolic and morphologic studies on the rat pineal organ during puberty. *Prog. in Brain Res.*, Vol. X: 552-562.
- Roth, W. D., R. J. Wurtman and M. D. Altschule 1962 Morphologic changes in the pineal parenchyma cells of rats exposed to continuous light or darkness. *Endocrinology*, 71: 888-892.
- Shellabarger, C. J. 1952 Studies on the pineal body in the white leghorn cockerel. Ph.D. Thesis, Department of Zoology, Indiana University.
- Simonnet, H., and L. Thieblot 1951a Recherches experimentales sur la physiologie de la glande pineale. *Acta Endocr. (Copenhagen)*, 7: 306-320.
- Simonnet, H., L. Thieblot and T. Melik 1951b Influence de l'epiphyse sur l'ovaire de la jeune rate. *Ann. Endocr.*, 12: 202-205.
- Simonnet, H., L. Thieblot, V. Segal and T. Melik 1951c Modifications du tractus genitale femelle consecutives a l'epiphysectomie. *J. Physiol. (Paris)*, 43: 864-866.
- Stalsberg, H. 1965 Effects of extirpation of the epiphysis cerebri in 6-day chick embryo. *Acta endocrinologica, Suppl.*, 97: 1-119.
- Thieblot, L., et H. Le Bars 1955 La glande pineale ou epiphyse. Librairie Maloine S. A., Paris. 203 pp.
- Thieblot, L., and S. Blaise 1963 Influence de la glande pineale sur les gonades. *Ann. Endocr.*, 24: 270-286.
- Wurtman, R. J., M. D. Altschule and U. Holmgren 1959 Effects of pinealectomy and of a bovine pineal extract in rats. *Am. J. Physiol.*, 197: 108-110.
- Wurtman, R. J., M. D. Altschule, R. O. Greep, J. L. Falk and G. Grave 1960 The pineal gland and aldosterone. *Am. J. Physiol.*, 199: 1109-1111.
- Wurtman, R. J., W. Roth, M. D. Altschule and J. J. Wurtman 1961 Interactions of the pineal and exposure to continuous light on organ weights of female rats. *Acta Endocr. (Copenhagen)*, 36: 617-624.
- Wurtman, R. J., J. Axelrod and E. W. Chu 1963 Melatonin, a pineal substance: Effect on rat ovary. *Sci.*, 141: 277-278.
- Wurtman, R. J., J. Axelrod and J. D. Barchas 1964 Age and enzyme activity in the human pineal. *Jour. Clin. End. and Metab.*, 24: 299-301.

Light and Electron Microscopic Observations on the Inner Plexiform Layer of the Rabbit Retina¹

GIUSEPPINA RAVIOLA AND ELIO RAVIOLA

*Institute of Human Anatomy, University of Pavia, Pavia, Italy, and
Department of Anatomy, Harvard Medical School,
Boston, Massachusetts*

ABSTRACT By comparison of electron micrographs with light microscopical specimens impregnated with the Golgi technique, the large endings of the rod bipolar cells have been identified in the innermost region of the inner plexiform layer of the rabbit retina.

The rod bipolar endings contain ribbons and synaptic vesicles, do not synapse with the perikaryon of the ganglion cells, are presynaptic to ganglion cell dendrites and to nerve processes which contain synaptic vesicles but lack ribbons. In these synaptic contacts a ribbon is closely associated with the presynaptic membrane and a dense web of fuzzy material is adherent to the cytoplasmic aspect of the postsynaptic membrane. Commonly, one of these synaptic contacts involves a rod bipolar ending and two postsynaptic processes. The postsynaptic process which is provided with synaptic vesicles is often, in turn, presynaptic to the same rod bipolar ending. This synaptic contact is characterized by the presence of a cluster of vesicles closely related to the presynaptic membrane, whereas the postsynaptic membrane lacks a definite subsynaptic web.

In the intermediate and scleral regions of the inner plexiform layer endings containing ribbons and synaptic vesicles show with neighboring nerve processes a synaptic pattern similar to the rod bipolar endings. Nerve processes containing synaptic vesicles but lacking ribbons are presynaptic to the perikaryon and dendrites of the ganglion cells; the synaptic contact shows a cluster of vesicles adherent to the presynaptic membrane. Bipolar cells are proposed as the source of the ribbon containing processes while amacrine cells are proposed as the source of the processes devoid of ribbons and presynaptic to both bipolar endings and ganglion cell dendrites and perikarya.

The inner plexiform layer of the vertebrate retina is the region of synaptic interplay of the bipolar, ganglion and amacrine cells. It has been generally accepted since Cajal's studies (1893, '11, '33) that rod bipolar cells synapse with the bodies and the ascending dendrites of the ganglion cells, while cone bipolar cells synapse with finer dendritic twigs of the ganglion cells.

The connections of the amacrine cells have been poorly understood with light microscopy. Since Cajal's statement (1893) that amacrine cells might influence in some way both ganglion and bipolar cells, no further knowledge has been gained about the significance of these enigmatic elements which lack an axon.

With the electron microscope nerve endings containing synaptic ribbons have been reported (Missotten, '60; Fine, '62; Villegas, '64) in the inner plexiform layer and have been claimed to belong to the bipolar cells (Missotten, '60; Missotten et al., '64; Allen, as cited by Sjöstrand and

Nilsson, '64). Kidd ('62) has described the fine structure of the synaptic contacts in the layer and has proposed that amacrine cell processes might contribute to the composition of the complex groups of nerve endings which serially synapse with each other.

Recently Dowling and Boycott ('65) have reported that in the retina of primates, nerve endings probably belonging to the bipolar cells contain synaptic vesicles and ribbons. The ribbons are located near presumed points of synaptic contact. The bipolar cell endings are presynaptic at the ribbon contacts to a pair of postsynaptic processes, one of which is identified as a ganglion cell dendrite, while the other is assumed to be an amacrine cell process. This amacrine cell process is, in turn, presynaptic to the same bipolar cell ending at a synaptic contact that displays a cluster

¹Supported in part by United States Public Health Service research grant, GM 10182 and training grant, GS4-406.

- Quay, W. B. 1963 Circadian rhythm in rat pineal serotonin and its modifications by estrous cycle and photoperiod. *Gen. Comp. Endocr.*, 3: 473-479.
- 1965 Retinal and pineal hydroxyindole-O-methyl transferase activity in vertebrates. *Life Sciences*, 4: 983-991.
- Quay, W. B., and A. Halevy 1962 Experimental modification of the rat pineal's content of serotonin and related indole amines. *Physiol. Zool.*, 35: 1-7.
- Quay, W. B., and B. E. Levine 1957 Pineal growth and mitotic activity in the rat: The effects of colchicine and sex hormones. *Anat. Rec.*, 129: 65-77.
- Reiss, M., F. E. Badrick and J. H. Halkerston 1963 Action of pineal extracts on the gonads and their function. *J. Endocr.*, 27: 107-118.
- Reiter, R. J., and R. J. Hester 1966 Metabolic regulation of physiological activity: III. Neuroendocrinological interrelationships. Research Laboratories, Edgewood Arsenal, Maryland.
- Roth, W. D. 1965 Metabolic and morphologic studies on the rat pineal organ during puberty. *Prog. in Brain Res.*, Vol. X: 552-562.
- Roth, W. D., R. J. Wurtman and M. D. Altschule 1962 Morphologic changes in the pineal parenchyma cells of rats exposed to continuous light or darkness. *Endocrinology*, 71: 888-892.
- Shellabarger, C. J. 1952 Studies on the pineal body in the white leghorn cockerel. Ph.D. Thesis, Department of Zoology, Indiana University.
- Simonnet, H., and L. Thieblot 1951a Recherches experimentales sur la physiologie de la glande pineale. *Acta Endocr. (Copenhagen)*, 7: 306-320.
- Simonnet, H., L. Thieblot and T. Melik 1951b Influence de l'epiphyse sur l'ovaire de la jeune rate. *Ann. Endocr.*, 12: 202-205.
- Simonnet, H., L. Thieblot, V. Segal and T. Melik 1951c Modifications du tractus genitale femelle consecutives a l'epiphysectomie. *J. Physiol. (Paris)*, 43: 864-866.
- Stalsberg, H. 1965 Effects of extirpation of the epiphysis cerebri in 8-day chick embryos. *Acta endocrinologica, Suppl.*, 97: 1-119.
- Thieblot, L., et H. Le Bars 1955 La glande pineale ou epiphyse. *Librairie Maloine S. A.*, Paris. 203 pp.
- Thieblot, L., and S. Blaise 1963 Influence de la glande pineale sur les gonades. *Ann. Endocr.*, 24: 270-286.
- Wurtman, R. J., M. D. Altschule and U. Holmgren 1959 Effects of pinealectomy and of a bovine pineal extract in rats. *Am. J. Physiol.*, 197: 108-110.
- Wurtman, R. J., M. D. Altschule, R. O. Greep, J. L. Falk and G. Grave 1960 The pineal gland and aldosterone. *Am. J. Physiol.*, 199: 1109-1111.
- Wurtman, R. J., W. Roth, M. D. Altschule and J. J. Wurtman 1961 Interactions of the pineal and exposure to continuous light on organ weights of female rats. *Acta Endocr. (Copenhagen)*, 36: 617-624.
- Wurtman, R. J., J. Axelrod and E. W. Chu 1963 Melatonin, a pineal substance: Effect on rat ovary. *Sci.*, 141: 277-278.
- Wurtman, R. J., J. Axelrod and J. D. Barchas 1964 Age and enzyme activity in the human pineal. *Jour. Clin. End. and Metab.*, 24: 299-301.

of cone bipolar expansions (fig. 6). The diffuse amacrine cells have a short thick process which soon ramifies into many branches spread throughout the whole width of the inner plexiform layer (fig. 7). The processes of both kinds of amacrine cells may reach the vitreal boundary of the inner plexiform layer and, along their course, display small varicosities not exceeding 2.5μ in diameter.

The dendrites of the ganglion cells run a long tangential course in the inner plexiform layer. The thick, main pillars of the Müller cells are radially oriented and supply the layer with thin tangentially oriented filiform expansions.

Electron microscopy

In electron micrographs of perpendicular sections of the retina, the inner plexiform layer is $15-25 \mu$ in thickness and consists of a tangle of intertwined, tightly packed and often synapsing nerve processes. A relatively small number of Müller cell processes, containing glycogen granules and tubular or vesicular elements of the smooth-surfaced endoplasmic reticulum are interspersed among groups of nerve processes. The main pillars of the Müller cells are radially oriented and are rich in glycogen granules, bundles of filaments $50-60 \text{ \AA}$ in thickness, and branching and anastomosing tubules of the smooth-surfaced endoplasmic reticulum (figs. 8, 9). A few myelinated nerve fibers are also present.

At the boundary with the inner nuclear layer, radially oriented nerve processes which are $0.4-0.8 \mu$ in diameter and contain microtubules enter the inner plexiform layer and soon pass out of the plane of section. These processes seem to originate from cell bodies located in the inner nuclear layer and they may well represent the vitreal processes of bipolar and amacrine cells. Cell bodies that are situated in the innermost row of the inner nuclear layer and have their Golgi complex and centrioles located on the vitreal side of the nucleus have been assumed to belong to amacrine cells. At the vitreal limit of the inner plexiform layer, the main dendritic trunks of the ganglion cells are frequently found connected with their perikarya. These dendrites contain mitochondria, a few

vesicular profiles of the smooth-surfaced endoplasmic reticulum, free ribosomes, and cisternae of the rough-surfaced endoplasmic reticulum that are occasionally clustered as small Nissl bodies. Dendrites, too, may be followed in a single section for short distances.

A prominent feature of the inner plexiform layer is a row of nerve endings, $2-4 \mu$ in diameter, lying near the boundary between the inner plexiform layer and the ganglion cell layer (figs. 8, 9). These endings are sometimes continuous with the processes that contain microtubules and have a radial or oblique course through the inner plexiform layer (fig. 10). Because of a close correspondence with respect to size and location in electron and light microscopical specimens, these endings are identified as the terminal expansions of the vitreal processes of the rod bipolars.

The rod bipolar endings contain ribbons, vesicles, and mitochondria. The ribbons are $400-600 \text{ \AA}$ thick, $0.1-1 \mu$ long, of undetermined width, and they display a high electron density. Most ribbons appear closely related to the plasma membrane. Some of them have been found randomly scattered in the neuroplasm of the endings either singly dispersed or piled in stacks of three to four elements lying roughly parallel to each other (fig. 11). Many vesicles, $350-500 \text{ \AA}$ in diameter, are distributed throughout the whole rod bipolar ending and around the ribbons they are more closely clustered. Where the ribbons are in stacks, rows of vesicles regularly occupy the interstices between adjacent ribbons. In the rod bipolar endings the mitochondria are scarce.

Two types of morphological specializations occur at the contact region between the rod bipolar ending and the adjacent nerve processes. One type is similar to synaptic contacts which have been described in the central nervous system (Palay, '56, '58). The synaptic cleft is $130-180 \text{ \AA}$ in width and is occupied by a moderately dense material of indistinct submicroscopical organization. The rod bipolar ending does not show any ribbon or obvious cluster of vesicles near the synaptic junction, while the adjacent nerve process displays a cluster of vesicles $350-500 \text{ \AA}$ in diameter, closely

of vesicles adjacent to the presynaptic membrane, but lacks ribbons. Outside the central area, tight junctions appear to connect bipolar cell endings to ganglion cell perikarya. These authors also mention synaptic contacts between amacrine cell processes and ganglion cell dendrites and perikarya, amacrine-to-amacrine synapses and one synaptic contact between adjacent bipolar cell endings.

In this paper the fine structure of the inner plexiform layer of the rabbit retina is reported. In electron micrographs rod bipolar endings have been recognized by comparison with light microscopical specimens impregnated by the Golgi method. Cone bipolar endings and amacrine cell processes also have been tentatively identified. Finally, some suggestions are presented about the synaptic connections involving bipolar, ganglion and amacrine cells.

MATERIALS AND METHODS

Adult male and female rabbits were used. For light microscopy, the retina was detached from the pigment layer, rolled up, coated with celloidin and doubly impregnated by the Golgi method with the procedure of Cajal (1893). For electron microscopy, phosphate buffered 2% OsO_4 was injected into the vitreous cavity of anaesthetized animals after removal of the vitreous body. Specimens were embedded in Epon or Araldite. Sections were stained with uranyl acetate followed either by lead cacodylate (Karnovsky, '61, meth. B) or by lead citrate (Venable and Coggeshall, '65). Electron micrographs were taken with a Siemens Elmiskop 1 or with an RCA EMU 3F microscope.

All specimens were taken from the retinal regions adjacent to the medullary rays.

OBSERVATIONS

Light microscopy

Specific investigations with the Golgi technique on the inner plexiform layer of the rabbit retina are lacking. However, our light microscopical findings did not differ noticeably from those reported by Cajal as representative of mammalian retina. Therefore a short account is given only of those observations which have been useful in interpreting the electron micrographs.

In the rabbit retina two different kinds of bipolar cells have been impregnated. In the first variety, a dense bush of short dendrites fans out from the cell body through the whole extent of the outer plexiform layer while an unbranched vitreal process extends to the innermost portion of the inner plexiform layer. There it ends in a very simple conical arborization, consisting of a few large terminal expansions. These endings are typically 3-5 μ in diameter and appear to lie closely contiguous to the bodies of the ganglion cells (figs. 2, 3). This kind of bipolar cell closely resembles the rod bipolar cells of Cajal's classification. The dendrites of the second kind of bipolar cell spread out from the cell body at an obtuse angle and at the vitreal limit of the outer plexiform layer acquire a tangential course while in the inner plexiform layer their vitreal processes give origin to many tortuous branches, all lying in a single tangential plane. Each branch is provided with many small varicosities, less than 2.5 μ in diameter (figs. 4, 5). These flattened arborizations spread at different levels but they have never been observed in the innermost portion of the inner plexiform layer. This kind of bipolar cell closely resembles Cajal's cone bipolars.

We have used Cajal's terminology to designate the two kinds of bipolar cells that we have stained in rabbit retina because of the substantial similarity between these cells and the morphological varieties illustrated by Cajal in other non-primate mammals. Although the rod bipolars of the rabbit retina resemble Polyak's ('41) "mop" variety and the cone bipolars resemble Polyak's "flat top" variety in the primate retina, an exact evaluation of the extent of this homology will require further study. "Midget" bipolar cells, which have been described by Polyak in primate retina, have not been impregnated in our specimens.

Both unistratified and diffuse amacrine cells have been impregnated and each of these cells has a round cell body lying in the most vitreal row of the inner nuclear layer. The processes of the unistratified amacrine cells end in the inner plexiform layer with a scanty conical arborization flattened in a tangential direction, but this stratification is never so regular as that

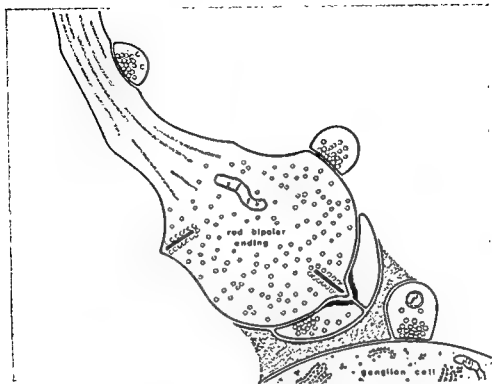


Fig. 1. Synaptic connections of a rod bipolar ending.

In order to complete the picture of the synaptic relationships of the rod bipolar endings additional nerve processes should be mentioned that are presynaptic to the rod bipolar endings without being, in turn, postsynaptic to them. These processes consistently lack a ribbon; a cluster of synaptic vesicles is found near the presynaptic membrane. Similar synaptic contacts have also been observed along the course of the vitreal process of a rod bipolar cell where the process has been identified by its continuity with an expanded ending (fig. 10).

The rod bipolar endings are rarely found in contact with the ganglion cell body, being separated from it by glial or neural processes whose thickness is often beyond the limit of resolution of the light microscope. They have never been found in synaptic contact. In places, small endings have been observed to make synaptic contact on the scleral aspect of the perikarya of the ganglion cells. No ribbons have been found in these endings and the postsyn-

naptic membrane lacks an obvious subsynaptic web (fig. 15).

In the intermediate and scleral regions of the inner plexiform layer where the tortuous branches of the vitreal processes of cone bipolars are found, many nerve processes, not exceeding 2.5μ in diameter and containing ribbons and synaptic vesicles, display a synaptic pattern which closely resembles that of the rod bipolar endings in the innermost portion of the layer.

Some additional synaptic patterns have been observed.

Large dendrites of the ganglion cells are often postsynaptic to ribbon-containing endings as well as to other nerve processes which lack ribbons (fig. 12). Occasionally the peculiar arrangement of synapsing nerve processes has been observed which is illustrated in figure 13; an ending makes a ribbon synaptic contact on both a ganglion cell dendrite and another nerve process that contains synaptic vesicles,

associated with the plasma membrane (fig. 18). By analogy with the central nervous system, the cluster of vesicles adhering to the plasma membrane is assumed to label the presynaptic element. The rod bipolar ending would be the postsynaptic element.

The other type of morphological specialization is characterized by the presence of a ribbon surrounded by a cluster of vesicles in the rod bipolar ending. The ribbon is closely related and often perpendicular to the plasma membrane. In this area the intercellular cleft is increased up to 130–210 Å and is occupied by a moderately dense material. Finally, a band of dense, fuzzy material, 200–500 Å thick, is found adhering to the cytoplasmic side of the cell membrane of the contacted nerve processes (fig. 17). An analogous dense material has been reported as an integral constituent of several synaptic contacts in the central nervous system and has been called a subsynaptic web (De Robertis, '62) or postsynaptic thickening (Gray and Guillery, '66).

The complex of ribbon, vesicles, enlarged intercellular cleft and layer of fuzzy material may be regarded as a significant morphological unit, although ribbons surrounded by a cluster of vesicles are also found scattered in the neuropil without any obvious relationships with the plasma membrane.

Contacts provided with a ribbon surrounded by a cluster of vesicles have never been observed in places where synaptic transmission has been demonstrated physiologically. However, the rod bipolar endings always appear as the postsynaptic element at the synaptic contacts that lack a ribbon or a definite subsynaptic web. Thus the complex of ribbon, vesicles, intercellular cleft, and layer of fuzzy material, remains the only possible candidate as the active site for a synaptic output from the rod bipolar endings. We assume that these endings behave as presynaptic elements also by analogy with the outer plexiform layer, where the ribbon is located on the presynaptic side of the photoreceptor-bipolar synapse. For the sake of brevity then, the complex of ribbon, vesicles, and synaptic junction will be referred to as a ribbon synaptic contact.

The rod bipolar endings and the adjacent nerve processes display a complex pattern of multiple, reciprocal synaptic connections. These have been schematically represented in text figure 1.

The rod bipolar endings have a wavy outline owing to the presence of superficial depressions in which lodge adjacent nerve processes. Often a wedge-shaped projection of a rod bipolar ending, containing a ribbon oriented along the long axis, penetrates a short distance into the cleft between a pair of neighboring nerve processes. A subsynaptic web is present on the cytoplasmic aspect of the plasmalemma of both the nerve processes that lie beside the presynaptic wedge, so that there appears to be two postsynaptic processes associated at a single synaptic contact (fig. 9). The two postsynaptic processes may be similar or different. Occasionally one of them can be identified as a dendrite of a ganglion cell because of its relatively large dimensions, absence of synaptic vesicles and its content of a few free ribosomes. The other postsynaptic process, or in places, both postsynaptic processes may contain synaptic vesicles and a few mitochondria. They have never been observed to contain synaptic ribbons.

In many instances, one of the two processes that are postsynaptic to a bipolar ending at a single ribbon synaptic contact, is, in turn, presynaptic to the same rod bipolar ending. This second synaptic contact is characterized by vesicles clustered near the presynaptic membrane but no definite subsynaptic web is associated with the postsynaptic membrane. These endings therefore display two synaptic contacts with opposite morphological polarities and the individual synaptic contacts are separated by a few tenths of a micron (fig. 9).

Some variants of this basic pattern have been found which possibly result from unfavorable planes of section through the synaptic complexes described above. Examples are ribbon synaptic contacts involving a single postsynaptic process, or synaptic contacts consisting of a subsynaptic web on the inner aspect of the plasmalemma of a nerve process adjacent to a rod bipolar ending but lacking any ribbon or cluster of vesicles associated with the presynaptic membrane (fig. 9).

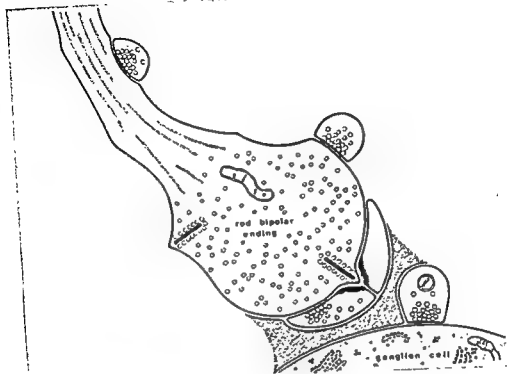


Fig. 1 Synaptic connections of a rod bipolar ending.

In order to complete the picture of the synaptic relationships of the rod bipolar endings additional nerve processes should be mentioned that are presynaptic to the rod bipolar endings without being, in turn, postsynaptic to them. These processes consistently lack a ribbon; a cluster of synaptic vesicles is found near the presynaptic membrane. Similar synaptic contacts have also been observed along the course of the vitreal process of a rod bipolar cell where the process has been identified by its continuity with an expanded ending (fig. 10).

The rod bipolar endings are rarely found in contact with the ganglion cell body, being separated from it by glial or neural processes whose thickness is often beyond the limit of resolution of the light microscope. They have never been found in synaptic contact. In places, small endings have been observed to make synaptic contact on the scleral aspect of the perikarya of the ganglion cells. No ribbons have been found in these endings and the postsynaptic

naptic membrane lacks an obvious subsynaptic web (fig. 15).

In the intermediate and scleral regions of the inner plexiform layer where the tortuous branches of the vitreal processes of cone bipolars are found, many nerve processes, not exceeding 2.5μ in diameter and containing ribbons and synaptic vesicles, display a synaptic pattern which closely resembles that of the rod bipolar endings in the innermost portion of the layer.

Some additional synaptic patterns have been observed.

Large dendrites of the ganglion cells are often postsynaptic to ribbon-containing endings as well as to other nerve processes which lack ribbons (fig. 12). Occasionally the peculiar arrangement of synapsing nerve processes has been observed which is illustrated in figure 13; an ending makes a ribbon synaptic contact on both a ganglion cell dendrite and another nerve process that contains synaptic vesicles,

but lacks a ribbon. This latter process in turn makes synaptic contact on the same dendrite. Therefore two synaptic contacts lie a few tenths of a micron apart on the surface of the same ganglion cell dendrite. While their polarities are the same, they are morphologically different.

Rows of up to four nerve processes all in synaptic contact with each other are not uncommon in the inner plexiform layer. The first presynaptic process of the sequence makes a ribbon synaptic contact with a second process containing synaptic vesicles. The vesicles are clumped near another synaptic junction lacking a subsynaptic web and involving a third nerve process. The third process of the sequence establishes in turn a ribbon synaptic contact with a fourth nerve process (fig. 16).

Finally a few examples have been found of endings, which are presynaptic to the process of an amacrine cell. These synaptic contacts lie at a short distance from the cell body and are the type that lack a ribbon and a definite subsynaptic web (fig. 14).

In the inner plexiform layer the plasma membranes of adjacent nerve processes have occasionally been seen to fuse, obliterating the intercellular cleft; therefore, in the area of membrane fusion, the nerve processes appear connected by a quintuple layered or tight junction (fig. 19). In other places a segment of the plasma membranes of adjacent nerve processes appears triple layered and asymmetric, with an inner leaflet denser and thicker than the outer one; the intercellular space is 120–130 Å in width and is filled with a moderately dense material. Moreover, a dense web of fuzzy material is present adhering to the inner leaflet of the plasma membrane of both adjacent nerve processes (fig. 20). These specialized junctions resemble the desmosome-like junctions described in the cerebellum by Gray ('61). However, they appear to be more similar to the intermediate junctions (zonulae adherentes) connecting adjacent epithelial cells.

Intermediate junctions contiguous to or situated between tight junctions were occasionally found in the outer plexiform layer connecting adjacent processes presumably belonging to the horizontal cells

(fig. 21). On the contrary, tight junctions and intermediate junctions in the inner plexiform layer never appeared to be combined in a single junctional complex. However, this dissociation in the occurrence of the two types of junctions may perhaps be related to the plane of section.

A few nerve processes have also been found which are provided with spherical in-pocketings of the plasmalemma, 800–900 Å in diameter. The wall of the crypt is coated on both sides with a thin layer of moderately dense, fuzzy material and its cavity is occupied by a minute protrusion of the neighboring nerve or glial process (fig. 22). Similar features have been reported by Westrum and Blackstad ('62) in nerve processes of the hippocampal cortex. They may represent a peculiar kind of coated vesicle.

DISCUSSION

Bipolar cell endings, ganglion cell dendrites and amacrine cell processes are the principal neural components of the inner plexiform layer. Degenerating fibers or endings seem to be lacking in the inner plexiform layer of the rabbit retina after the optic nerve is crushed (Cragg, '62), but a few are found in the retina of monkeys and cats after the optic tract or nerve is sectioned (Brooke et al., '65). Moreover, in the avian retina, the centrifugal fibers end in the inner nuclear layer where they synapse with amacrine and displaced ganglion cells (Cajal, '11, Maturana and Frenk, '65).

The synaptic contacts between nerve processes of the inner plexiform layer can be classified into two varieties: one with a ribbon in the presynaptic ending and a subsynaptic web adhering to the postsynaptic membrane and another which lacks both of these features. Both kinds of synaptic contacts have been described by Kidd ('62) in cat and pigeon retinas and have been equated with the type 1 and 2 synapses found by Gray ('59) in the cerebral cortex. One obvious difference between Gray's type 1 and the ribbon synaptic contact is the presence of a ribbon in addition to the synaptic vesicles. Another difference is that synaptic vesicles seem to be preferentially clustered around the ribbon rather than near the presynaptic

membrane. Finally, in our specimens, the synaptic cleft is 130-210 Å instead of 300 Å.

According to Kidd, the synaptic contacts that lack ribbons or a definite subsynaptic web are quite similar to Gray's type 2 synapses. A subtle difference found in our specimens is that the synaptic cleft is smaller, being only 130-180 Å in width, but still containing a moderately dense material.

The large nerve endings that lie in a row at the boundary between the inner plexiform layer and the ganglion cell layer could be identified as the vitreal endings of the rod bipolar cells because of the close correspondence of their size, shape and location in electron micrographs and in specimens stained by the Golgi technique. It is these rod bipolar endings that contain synaptic ribbons and synaptic vesicles. Missotten *et al.* ('64) have made the same identification of similar endings found in human retina.

A constant feature of the rod bipolar endings is that they are only presynaptic at contacts provided with a synaptic ribbon and a subsynaptic web whereas they are postsynaptic at synaptic contacts lacking both a ribbon and a definite subsynaptic web.

Besides the rod bipolar endings and the ganglion cell dendrites, nerve processes are commonly found in the innermost region of the layer, which lack ribbons and are presynaptic to the rod bipolar endings. By a process of elimination they may be identified as amacrine cell processes because light microscopical studies have consistently shown that rod bipolar endings, ganglion cell dendrites, and amacrine cell processes are the only neural components of the innermost region of the inner plexiform layer.

In contrast to the traditional schema based upon light microscopical observations rod bipolar endings have never been found synapsing on the perikarya of ganglion cells but rather appear to be typically presynaptic to a pair of postsynaptic processes at a single specialized contact. One of these may sometimes be identified as a ganglion cell dendrite, while the other one, being in turn presynaptic to the same

rod bipolar ending, may be identified as an amacrine cell process.

One might also suppose that the small nerve endings, that make synaptic contacts on the perikarya of the ganglion cells belong to amacrine cells. However, their identification by comparison with light microscopical findings is much less obvious, mainly on account of their smaller number.

Throughout the remainder of the inner plexiform layer, ribbon containing processes are found which display a synaptic pattern similar to that of rod bipolar endings. It can therefore be supposed that these endings are the branches of the vitreal processes of cone bipolar cells. This identification leaves the amacrine cell processes to be accounted for and therefore leads to the suggestion that the amacrine cell processes are those which lack synaptic ribbons and are postsynaptic to ribbon synaptic contacts and presynaptic to ribbon-containing endings and ganglion cell dendrites. The identification of these processes as amacrine is merely presumptive and is based on the assumptions, (1) that all bipolar cell endings display the same synaptic pattern, (2) that ganglion cell dendrites are constantly postsynaptic, and (3) that centrifugal fibers represent but a small component of the inner plexiform layer. Still unknown are the specific connections of the different varieties of amacrine and ganglion cells and the nature of the nerve processes which lack ribbons and synapse with the amacrine cell processes.

The synaptic relationships of the bipolar, ganglion and amacrine cells in the inner plexiform layer of the rabbit retina closely parallel those reported in the primate retina (Dowling and Boycott, '65). However, we have seen neither tight junctions between the rod bipolar endings and the ganglion cell perikarya nor bipolar-to-bipolar synaptic contacts. The origin of the nerve processes of the inner plexiform layer of the rabbit retina, which are connected by tight junctions, is unknown. We have also been unable to identify with certainty, in our specimens, amacrine-to-amacrine synaptic contacts.

We have studied in the rabbit the retinal regions adjacent to the medullary rays,

where cones are scarce and "midget" bipolar cells seem to be lacking. Dowling and Boycott have studied the primate central area, which is rich in cones and "midget" bipolar cells. In both cases, however, ■ bipolar ending, ■ ganglion cell dendrite and an amacrine cell process are arranged in a similar highly characteristic synaptic pattern. This pattern is thus the same, even when different varieties of bipolar cells are involved.

Therefore, three different morphological features are superimposed in the architecture of the inner plexiform layer: the distribution of the nerve processes within the layer, the precise arrangement of the terminals at the synapse, and the different kinds of synaptic contacts. The distribution of the nerve processes within the layer determines the specificity of the interneuronal connections. The arrangement of the terminals at the synapse might represent a device for local control of the signal transmission and for integration of the influences from the surrounding retinal regions. The variety of synaptic contacts is possibly correlated with different chemical transmitters.

An increasing number of fascinating coincidences between morphological and physiological data has supported the suggestion that excitation and inhibition in the central nervous system are mediated by different morphological specializations at the synaptic contacts between nerve elements. For example, synaptic contacts of Gray's type 2, that are found on the bodies of the pyramidal cells of the hippocampal cortex (Blackstad and Flood, '63) have been thought to account for the inhibitory postsynaptic potential evoked in these cells by commissural, septal and local stimulation (Andersen et al., '63). On the other hand, Gray's type 1 synaptic contacts found on the dendritic spines of these cells have been assumed to be excitatory in nature (Eccles, '64). Also in the olfactory bulb the presumably excitatory contacts of mitral dendrites on granule dendrites consistently have a subsynaptic web, whereas the granule-to-mitral contacts which are presumably inhibitory, lack one (Rall et al., '66). In other regions of the central nervous system, excitatory and inhibitory influences have been assumed to be medi-

ated by synaptic contacts that are associated with synaptic vesicles of different shape (Uchizono, '65; Bodian, '66) or size (Lenn and Reese, '66).

In the inner plexiform layer of the rabbit retina, bipolar endings and amacrine cell processes are mutually pre- and postsynaptic at synaptic contacts which are morphologically different and display opposite morphological polarities. Moreover, bipolar endings and amacrine cell processes seem to be presynaptic to the same ganglion cell dendrite at synaptic contacts which are morphologically different. It is likely that in such synaptic arrangements, morphologically different synaptic contacts would have different physiological activities, even if an excitatory or inhibitory function cannot yet be inferred exclusively on morphological grounds.

Indeed, it has long been thought that amacrine cells might be inhibitory interneurons (Graham and Granit, '31). More recently Barlow and Levick ('65) have reported in the rabbit retina a class of ganglion cells selectively responding to the movement of the stimulus in one direction and they have suggested that this directional selectivity is mediated by interneurons of the inner nuclear layer that are first excited by the photoreceptors and then selectively inhibit bipolar cells ordered in an appropriate direction. These inhibitory interneurons have been thought to be horizontal cells but the alternative of a presynaptic inhibition acting upon bipolar cell endings has not been excluded. The amacrine cells were thought to mediate the lateral inhibition that acts upon a ganglion cell from the retinal region surrounding the receptive field. However, Barlow and Levick's schema is only concerned with a single type of inhibitory mechanism acting upon a particular group of retinal units. Other classes of ganglion cells have been reported in the rabbit retina (Barlow et al., '64) and the functional interplay in the inner plexiform layer which allows them to integrate synaptic influences converging from the excitatory and inhibitory areas of their receptive field is still poorly understood.

While specific physiological evidence on retina is not available, a suggestive morphological parallel exists between retinal

amacrine cells and the granule cells of the olfactory bulb (Rall et al., '66). Both are axonless interneurons. Moreover, the dendrite-like processes of the granule cells are joined to a single mitral cell secondary dendrite by two kinds of synaptic contacts with opposite morphological polarities recalling the amacrine-bipolar relationships.

A further analogy may be provided from the cuneate nucleus of the cat (Walberg, '65), where it has been proposed that the same inhibitory interneurons contact both the presynaptic axonal ending and the postsynaptic dendrites and perikaryon. This synaptic pattern recalls the relationships of the amacrine cells with both bipolar and ganglion cells.

Therefore, the hypothesis that emerges from this study of the fine structure of the synaptic pattern in the inner plexiform layer is that bipolar cells might excite both ganglion and amacrine cells and that amacrine cells, perhaps two varieties of them, inhibit both bipolar and ganglion cells.

ACKNOWLEDGMENTS

The authors are very grateful to Dr. T. S. Reese for the valuable discussions and criticism during the preparation of the English manuscript.

LITERATURE CITED

- Andersen, P., J. C. Eccles and Y. L  yning 1963 Recurrent inhibition in the hippocampus with identification of the inhibitory cell and its synapses. *Nature*, 198: 541-542.
- Barlow, H. B., R. M. Hill and W. R. Levick 1964 Retinal ganglion cells responding selectively to direction and speed of image motion in the rabbit. *J. Physiol.*, 173: 377-407.
- Barlow, H. B., and W. R. Levick 1965 The mechanism of directionally selective units in rabbit's retina. *J. Physiol.*, 168: 477-504.
- Blackstad, T. W., and P. R. Flood 1963 Ultrastructure of hippocampal axo-somatic synapses. *Nature*, 198: 542-543.
- Bodian, D. 1966 Electron microscopy: two major synaptic types on spinal motoneurons. *Science*, 151: 1093-1094.
- Brooke, R. N. L., J. deC. Downer and T. P. S. Powell 1965 Centrifugal fibres to the retina in the monkey and cat. *Nature*, 207: 1365-1367.
- Cragg, B. G. 1962 Centrifugal fibers to the retina and olfactory bulb and composition of the supraoptic commissures in the rabbit. *Exptl. Neurol.*, 5: 406-427.
- De Robertis, E. D. 1962 Fine structure of synapses in the CNS. *Proc. 4th Intern. Congr. Neuropathol.*, Munich 1961. Ed. by H. Jacob, Thieme, Stuttgart, Vol. II, 35-38.
- Dowling, J. E., and B. B. Boycott 1965 Neural connections of the retina: fine structure of the inner plexiform layer. *Cold Spring Harbor Symposia on Quantitative Biology. Sensory Receptors*, XXX: 393-402.
- Eccles, J. C. 1964 The physiology of synapses. Springer, Berlin.
- Fine, B. S. 1962 Synaptic lamellas in the human retina: an electron microscopic study. *J. Neuropathol. Exp. Neurol.*, 22: 253-261.
- Graham, J., and R. Granit 1931 Comparative studies on the peripheral and central retina. VI. Inhibition, summation and synchronization of impulses in the retina. *Am. J. Physiol.*, 98: 664-673.
- Gray, E. G. 1959 Axo-somatic and axo-dendritic synapses of the cerebral cortex: an electron microscope study. *J. Anat.*, 93: 420-433.
- 1961 The granule cells, mossy synapses and Purkinje spine synapses of the cerebellum: light and electron microscope observations. *J. Anat.*, 95: 345-356.
- Gray, E. G., and R. W. Guillery 1966 Synaptic morphology in the normal and degenerating nervous system. *Int. Rev. Cytol.*, 19: 111-173.
- Karnovsky, M. J. 1961 Simple method for "staining with lead" at high pH in electron microscopy. *J. Biophys. Biochem. Cytol.*, 11: 729-732.
- Kidd, M. 1962 Electron microscopy of the inner plexiform layer of the retina in the cat and in the pigeon. *J. Anat.*, 96: 179-187.
- Lenn, N. J., and T. S. Reese 1966 The fine structure of nerve endings in the nucleus of the trapezoid body and the ventral cochlear nucleus. *Am. J. Anat.*, 118: 375-390.
- Maturana, H. R., and S. Frenk 1965 Synaptic connections of the centrifugal fibers in the pigeon retina. *Science*, 150: 359-361.
- Missotten, L. 1960 Etude des synapses de la r  tine humaine au microscope   lectronique. *Proc. Europ. Reg. Conf. Electr. Micr. Delft 1960*. Ed. by A. L. Houwink and B. J. Spit, Vol. II, 818-821.
- Missotten, L., E. De Hauwere et A. Guzik 1964 L'ultrastructure de la r  tine humaine. A propos des cellules bipolaires et de leurs synapses. *Bull. Soc. Belge Ophthal.*, 137: 277-293.
- Palay, S. L. 1956 Synapses in the central nervous system. *J. Biophys. Biochem. Cytol.*, Suppl. 2: 193-202.
- 1958 The morphology of synapses in the central nervous system. *Exp. Cell Res.*, Suppl. 5: 275-293.
- Polyak, S. L. 1941 The retina. The University of Chicago Press, Chicago.
- Rall, W., G. M. Shepherd, T. S. Reese and M. W. Brightman 1966 Dendrodendritic synaptic pathway for inhibition in the olfactory bulb. *Exptl. Neurol.*, 14: 44-56.
- Ramon y Cajal, S. 1893 La r  tine des vert  br  s. *La Cellule*, 9: 119-258.
- 1911 Histologie du syst  me nerveux de l'homme et des vert  br  s. A. Maloine, Paris, Vol. II.
- 1933 La r  tine des vert  br  s. *Trab. Lab. Invest. Biol. Univ. Madrid*, 28: Appendix.

- Sjöstrand, F. S., and S. E. Nilsson 1964 The structure of the rabbit retina as revealed by electron microscopy. In: *The rabbit in eye research*. Ed. by J. H. Prince, Thomas, Springfield, 448-513.
- Uchizono, K. 1965 Characteristics of excitatory and inhibitory synapses in the central nervous system of the cat. *Nature*, 207: 642-643.
- Venable, J. H., and R. Coggeshall 1965 A simplified lead citrate stain for use in electron microscopy. *J. Cell Biol.*, 25: 407-408.
- Villegas, G. M. 1964 Ultrastructure of the human retina. *J. Anat.*, 98: 501-513.
- Walberg, F. 1965 Axoaxonic contacts in the cuneate nucleus, probable basis for presynaptic depolarization. *Exptl. Neurol.*, 13: 218-231.
- Westrum, L. E., and T. W. Blackstad 1962 An electron microscopic study of the stratum radiatum of the rat hippocampus (regio superior CA 1) with particular emphasis on synaptology. *J. Comp. Neur.*, 119: 281-310.

PLATE 1

EXPLANATION OF FIGURES

- 2,3 Rod bipolar cells of the rabbit retina. The vitreal process gives origin to a few large terminal expansions, that lie at the vitreal boundary region of the inner plexiform layer, and are closely contiguous to the bodies of the ganglion cells. The approximate extent of the inner plexiform layer is indicated by the arrow and the boundary between the inner plexiform layer and ganglion cell layer is always towards the bottom of the page. 670 \times .
- 4 Cone bipolar cells. Their vitreal processes branch in the scleral and intermediate regions of the inner plexiform layer. The flattened arborization consists of thin tortuous branches that run a tangential course confined to a single level of the inner plexiform layer. 750 \times .
- 5 The branches of the vitreal process of a cone bipolar cell are provided with many small varicosities that appear much smaller in diameter than the endings of the vitreal process of the rod bipolar cells. In the background, out of focus, the vitreal process of a rod bipolar cell reaches the vitreal boundary of the inner plexiform layer. 750 \times .
- 6,7 Two amacrine cells, one of the stratified (fig. 5) and another of the diffuse (fig. 6) variety. The varicosities found along the processes of the amacrine cells are also smaller in size than the endings of the vitreal processes of the rod bipolar cells. 670 \times .

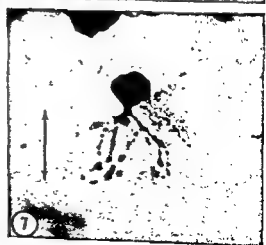
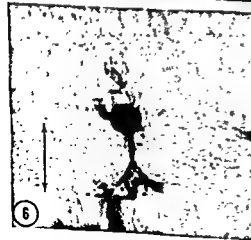
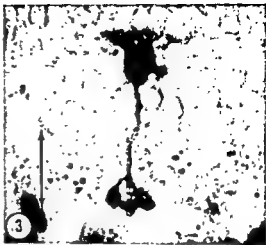
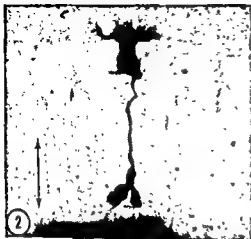


PLATE 2

EXPLANATION OF FIGURE

- 8 Survey electron micrograph of the inner plexiform layer of the rabbit retina. Near the vitreal boundary of the layer, at the bottom of the picture, a large ending (RBE) is seen containing synaptic vesicles and ribbons. With respect to size and location it corresponds to a terminal expansion of the vitreal process of a rod bipolar cell. Above, the perikaryon of a cell of the inner nuclear layer (IN). On right, the radially oriented main pillar of a Müller cell (MÜ) crosses the inner plexiform layer and gives origin to a branch (asterisk) that runs laterally through the neuropil. At D is the dendrite of a ganglion cell. 12,800 \times .

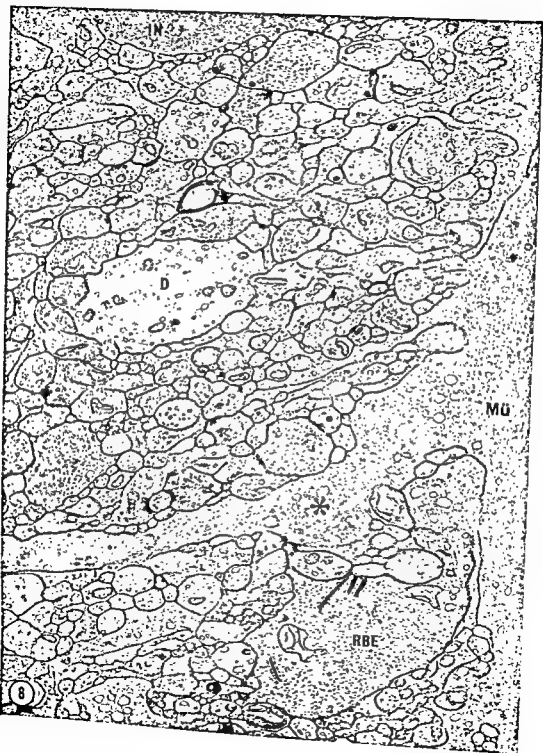


PLATE 3

EXPLANATION OF FIGURE

- 9 Boundary region between inner plexiform and ganglion cell layer. A rod bipolar ending (RBE) is in synaptic contact with four adjacent nerve processes (1-4). Distinguishing features of the synaptic contact of the rod bipolar ending with nerve processes 1 and 2 are the ribbon adjacent to the presynaptic membrane and the band of dense material (arrows) adhering to the cytoplasmic aspect of the plasmalemma of both postsynaptic processes. The nerve processes labeled 2 and 4 are presynaptic to the rod bipolar ending. These synaptic contacts show a cluster of synaptic vesicles closely related to the presynaptic membrane. The specialized contact of the rod bipolar ending with the nerve process 3 (arrow) may represent a grazing section through a synaptic complex like that at 1 and 2.

Below, the vitreal end of a Müller cell (Mü) contains glycogen particles and tubules of the smooth-surfaced endoplasmic reticulum. 31,900 \times .

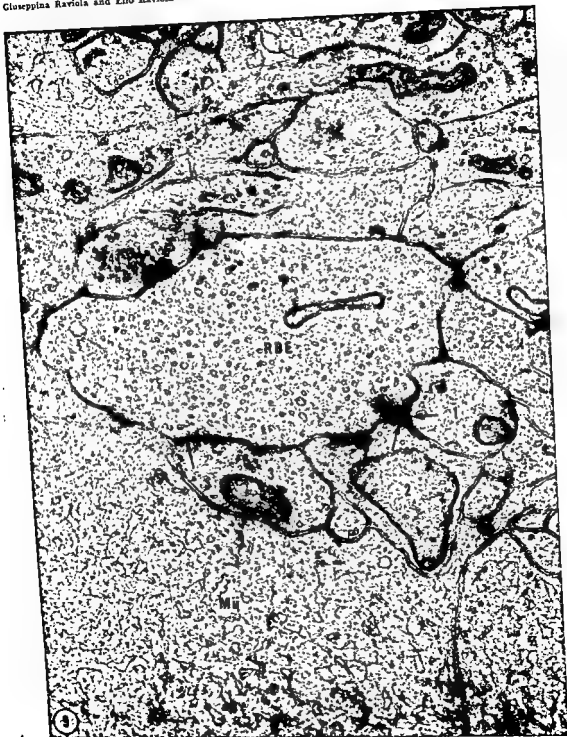
INNER PLEXIFORM LAYER OF THE RETINA
Giuseppina Raviola and Elio Raviola

PLATE 4

EXPLANATION OF FIGURES

- 10 A branch of the vitreal process of a rod bipolar cell is identified by its continuity with the large bipolar ending (RBE) that lies near the inner boundary of the inner plexiform layer. A small nerve process makes synaptic contact (arrow) with the bipolar process at some distance from the ending. 22,800 \times .
- 11 Bipolar ending containing four ribbons. The interstices between adjacent ribbons are occupied by rows of vesicles. 33,600 \times .
- 12 Intermediate region of the inner plexiform layer. A ganglion cell dendrite (D) runs from left to right progressively tapering. A nerve ending (BE) makes a ribbon synaptic contact with the dendrite. A second smaller process that lacks a ribbon makes another synaptic contact with the same dendrite (arrow). 32,800 \times .

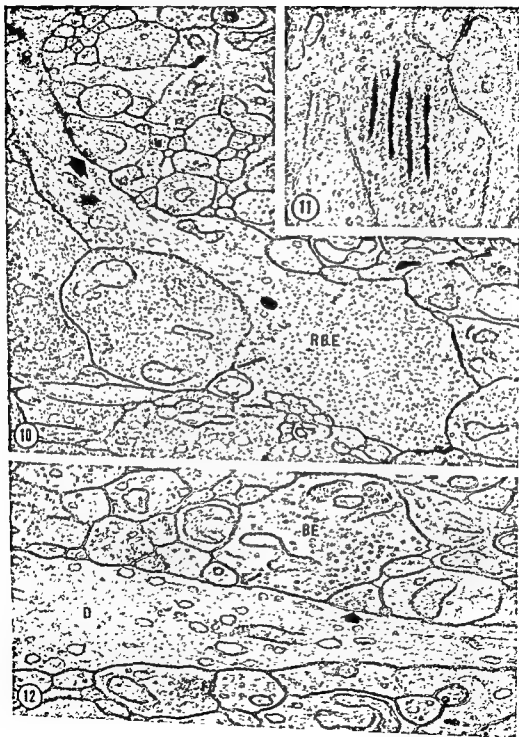


PLATE 5

EXPLANATION OF FIGURES

- 13 Intermediate region of the inner plexiform layer. A nerve ending (BE) contacts both a ganglion cell dendrite (D) and another nerve process (star) at a single ribbon synaptic contact. The nerve process that is labeled by the star is, in turn, presynaptic to the same dendrite. This second synaptic contact lacks a ribbon but shows a clustering of synaptic vesicles near the presynaptic membrane. 30,400 X.
- 14 The body of an amacrine cell is recognized because elements of the Golgi complex (g) are located on the vitreal side of the nucleus (n). The process of the amacrine cell is contacted (arrow) by a nerve process that lacks a synaptic ribbon. This presynaptic ending contains a cluster of synaptic vesicles near the presynaptic membrane. 17,500 X.
- 15 A nerve process makes a synaptic contact (arrow) on the perikaryon of a ganglion cell (GC). A cluster of synaptic vesicles is closely related to the presynaptic membrane and no definite subsynaptic web is adherent to the ganglion cell membrane. Fl: flagellum. 34,900 X.

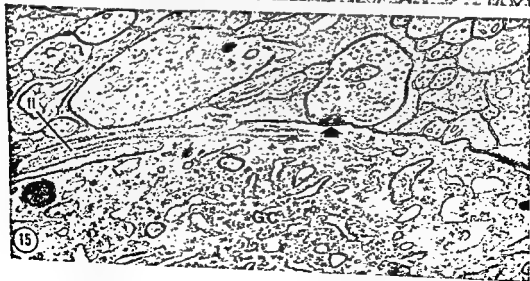


PLATE 6

EXPLANATION OF FIGURES

- 16 Four nerve processes serially synapsing with each other. 140,000 \times .
- 17 Synaptic contact between a bipolar ending (BE) and a ganglion cell dendrite (D). The ribbon has been cut obliquely. A moderately dense material is present in the synaptic cleft and seems to be more concentrated near the postsynaptic membrane (Insert). A web of fuzzy material (ssw) is adherent to the inner aspect of the postsynaptic membrane (psm); prm: presynaptic membrane. 240,000 \times . Insert, 400,000 \times .
- 18 Synaptic contact on a bipolar ending (BE). A cluster of synaptic vesicles is closely related to the presynaptic membrane (prm). Moderately dense material is present in the synaptic cleft. No subsynaptic web is found on the cytoplasmic aspect of the postsynaptic membrane (psm). 245,000 \times .

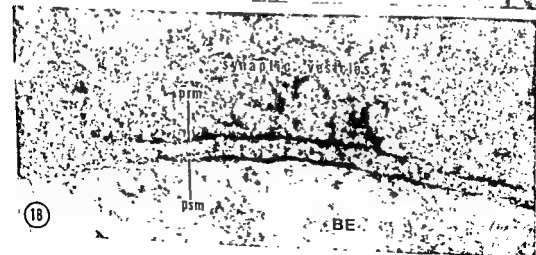
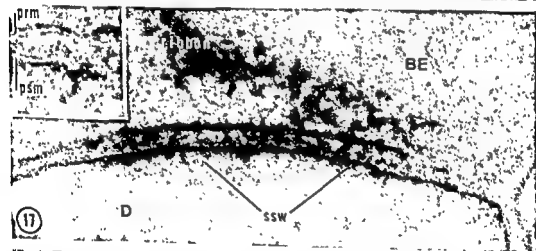


PLATE 6

EXPLANATION OF FIGURES

- 16 Four nerve processes serially synapsing with each other. 140,000 X.
- 17 Synaptic contact between a bipolar ending (BE) and a ganglion cell dendrite (D). The ribbon has been cut obliquely. A moderately dense material is present in the synaptic cleft and seems to be more concentrated near the postsynaptic membrane (insert). A web of fuzzy material (ssw) is adherent to the inner aspect of the postsynaptic membrane (psm); prm: presynaptic membrane. 240,000 X. Insert, 400,000 X.
- 18 Synaptic contact on a bipolar ending (BE). A cluster of synaptic vesicles is closely related to the presynaptic membrane (prm). Moderately dense material is present in the synaptic cleft. No subsynaptic web is found on the cytoplasmic aspect of the postsynaptic membrane (psm). 245,000 X.

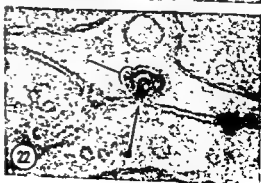
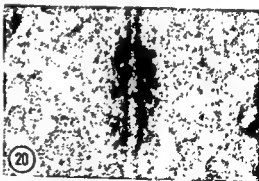
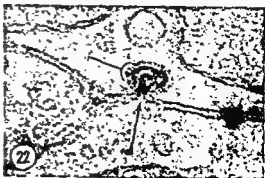
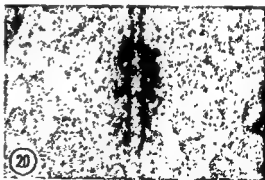


PLATE 7

EXPLANATION OF FIGURES

- 19 Tight junction between adjacent nerve processes in the inner plexiform layer. The arrows point to the fusion line. 175,000 \times .
- 20 Intermediate junction between adjacent nerve processes in the inner plexiform layer. 152,000 \times .
- 21 Outer plexiform layer of the rabbit retina. A junctional complex between adjacent processes that probably belong to horizontal cells. An intermediate junction (ij) is inserted between two tight junctions (tj). 152,000 \times .
- 22 Coated inpocketing of the plasma membrane of a nerve process. A minute evagination (arrow) of the plasma membrane of the adjacent process penetrates the concavity of the invagination. The bristle-like coat is indicated. 104,000 \times .



A Light and Electron Microscopic Study of the Pecten of the Pigeon Eye¹

ELIO RAVIOLA AND GIUSEPPINA RAVIOLA*

Department of Anatomy, Harvard Medical School, Boston, Massachusetts

ABSTRACT The pecten in the pigeon is a pleated lamina that consists of blood vessels and interstitial pigment cells. Arterioles with thin, unspecialized endothelium give origin to an exceedingly dense capillary network. The endothelial cells of the capillaries are provided on both the luminal and basal surfaces with thin lamellar processes, constricted at their origins from the cell body. Luminal lamellae are long, erect and have a prevailing longitudinal orientation. Basal lamellae are shorter, more irregularly oriented and more closely compressed. Besides the usual complement of cytoplasmic organelles, a moderate number of coated vesicles and of coated and uncoated in-pocketings of the plasmalemma is present in the endothelial cells. A labyrinthine system of interstices surrounds the stalks of the basal lamellae and contains a material that resembles the substance of the basement lamina in density and texture. A similar material is found on the outer surface of the basal lamellae and imperceptibly merges with the ground substance of an unusually thick adventitial layer that is permeated by numerous unit fibrils of collagen. The capillary network is drained by venules, whose wall resembles the capillary wall. The pigment cells contain melanin granules, large mitochondria and many bundles of filaments. They are sandwiched between two basement laminae and separate the blood vessels from the vitreous body. The bridge of the pecten consists of pigment cells with a few interspersed capillaries.

The pecten of the avian eye is a pigmented organ, projecting from the optic disc into the vitreous body. In neognathous birds, it consists of a thin, pleated lamina composed of blood vessels and interstitial pigment cells.

Unusual features in the wall of the blood vessels of the pecten had already been noticed by numerous light microscopists. Kajikawa ('23) observed that the endothelial cells appear finely striated and thus resemble, to some extent, the brush border region of cells of the proximal convoluted tubules of the kidney. Because of this similarity, he suggested that the endothelial cells might be involved in secretory activity. Successive, less detailed descriptions (Mann, '24a, b; Menner, '38; Kauth and Sommer, '53) mainly pointed out the uncommon thickness of the endothelial cells.

A prominent, highly refractile coat was seen investing the endothelium (Mihalovics, 1873; Mann, '24a, b) and was claimed to consist of hyaline connective tissue (Bachsch and Cellert, '35). A PAS-positive basement membrane, intervening between the endothelium and the connective tissue coat, was more recently reported (ORahilly and Meyer, '61).

With the electron microscope, the endothelial cells of the capillaries of the pecten display luminal and basal specializations that appear to be unique in the vertebrate vascular system. Discrepancies, however, exist in the literature about the precise configuration of these unusual endothelial cells. A. Tanaka ('60) observed luminal microvilli and basal membrane infoldings, whereas Semba ('62) expressed the opinion that both luminal and basal specializations are pleat-like extensions. Seaman ('62) and Seaman and Storm ('63) at first reported membrane infoldings on both the luminal and the basal surfaces of the endothelial cells and this observation was confirmed by Fischlschweiger and ORahilly ('64). More recently they mention a luminal brush border (Seaman and Storm, '66).

In all published micrographs an impressive number of rows of vesicles are seen in the luminal region of the endothelial cells. These have been interpreted either as evidence of a high micropinocytotic activity (A. Tanaka, '60; Semba, '62; Seaman and

¹Supported by research grant RG-6729 and training grant GM-00406 from the Institute of General Medical Sciences, National Institutes of Health.

*Both authors are on leave of absence from the Institute of Human Anatomy of the University of Pavia, Pavia, Italy.

Storm, '63) or as representing sections of tortuous canaliculi of the smooth surfaced endoplasmic reticulum (Seaman and Storm, '63). An increase in number of vesicles and changes in complexity of the membrane infoldings were claimed to follow the administration of acetazolamide (Seaman and Himelfarb, '63) and the vesicles were also reported to transport ferritin across the endothelium (Seaman and Storm, '66).

The observations reported heretofore have been based upon study of material fixed with osmium tetroxide, which is known to be inadequate for preservation of some membranous structures (Tormey, '64; Franzini-Armstrong and Porter, '64). Extensive distortion and reorganization during fixation of a labyrinthine system of membrane limited processes, so that they appear as rows of vesicles or as fenestrated cisternae, might account for some of the previous discrepant descriptions of the endothelium of the vessels in the pecten.

The main purpose of this study is to illustrate the fine structure of the capillaries of the pecten in the pigeon after fixation with aldehydes. In addition, a complete light and electron microscopic description of the vascular tree and of the pigmented interstitial tissue of this organ is provided.

MATERIALS AND METHODS

One to fifteen year old pigeons of both sexes were used.

In order to visualize the vascular network of the pecten a mixture of carbon and gelatin (Majno et al., '61) was injected through the carotid artery. After formaldehyde fixation, the pecten was isolated, bleached with peracetic acid to eliminate melanin, unfolded and prepared as a whole-mount.

Histochemical tests for melanin (Pearse, '61) were carried out on paraffin sections of Carnoy fixed material.

For light microscopy the pecten was fixed in veronal-acetate buffered osmium tetroxide (Caulfield, '57) and embedded in methacrylate. Sections 1 μ thick were stained with toluidine blue (Richardson et al., '60) or the PAS reaction.

For electron microscopy, a variety of fixative fluids were employed, containing either

osmium tetroxide or glutaraldehyde in different buffers. Most satisfactory results were obtained with the 0.1 M phosphate buffered formaldehyde-glutaraldehyde mixture of Karnovsky ('65), containing about 2% formaldehyde and 2.5% glutaraldehyde. The fixative fluid was injected into the vitreous cavity of the anaesthetized animal after partial removal of the vitreous body and it was continuously renewed for one-half hour. The eyeball was then removed, opened and placed into fresh fixative for two hours. The pecten was subsequently dissected, postfixed in phosphate buffered osmium tetroxide (Millonig, '61), dehydrated in methanol and embedded in araldite. In some pigeons the eye was fixed by vascular perfusion through the carotid artery. Occasional specimens were stained in block with aqueous uranyl acetate after the osmium postfixation, according to a modification of Farquhar and Palade's ('65) procedure (Karnovsky, personal communication). Thin sections were stained with uranyl acetate followed by lead citrate (Venable and Coggeshall, '65). Micrographs were taken with the electron microscopes RCA 3F and Siemens Elmiskop 1.

OBSERVATIONS

Light microscopy

The pecten of the pigeon is trapezoidal in shape and is black or brown in color. The base of the trapezoid inserts upon the head and the cauda of the optic nerve and the rest projects into the vitreous body. It consists of a pleated lamina, 25 to 120 μ in thickness, whose sinuous course is fixed distally by its attachment to a compact cord of pigmented tissue, "the bridge," running like a handrail along the free margin of the organ. The number of pleats varies between 15 and 18, one or two of which do not reach the distal edge and merge with the dorso-temporal side of the trapezoid.

In specimens injected with carbon (fig. 1) sizeable vessels run a straight, parallel course from the base to the bridge. Usually they are spaced individually at regular intervals along the lamina; less commonly they run in pairs. It is impossible to dis-

*We mean by "pleat" or "fold" the repeat sinusoid of the plicated lamina.

tinguish which large vessel is afferent and which is efferent on the basis of the vascular injections alone. Collateral and terminal branches of smaller caliber originate from or merge with the large vessels at various angles and give rise to an exceedingly dense capillary network, which spans the intervals between neighboring large vessels. The capillaries are arranged almost everywhere in two layers, but anastomoses between capillaries of the two layers are common. The irregular meshes of the capillary network are elongated in the direction parallel to the proximo-distal axis of the pecten.

In transverse sections (fig. 2), the sinusoidal lamina is seen to consist of blood vessels and interstitial cells containing pigment granules. Two types of vessels can be recognized: a few with thin endothelium and many with unusually thick endothelium.

The first type ranges from 25 to 50 μ in diameter, with endothelium less than 0.5 μ in thickness. The endothelium is invested by a discontinuous layer of flattened cells. An exceptionally thick layer of PAS-positive material splits to enclose each of these cells. Outside of this layer is a prominent fibrillar coat, in which other flattened cells are occasionally embedded. Two to four of such vessels with thin endothelium are irregularly distributed in each fold of the pecten but they are never found at the edges of the folds. Serial sections through the base of the pecten and the underlying cauda of the optic nerve (fig. 5) demonstrate that these vessels arise from the basal artery of the pecten. They must therefore be regarded as afferent vessels.

The second type of vessel ranges from 5 to 80 μ in diameter and is provided with an endothelium 2 to 3 μ thick (fig. 3). Capillaries 20 μ or less in diameter are preponderant, while large vessels with thick endothelium number only 2 or 3 in each fold, and are usually located at its edges. Serial sections through the base of the pecten and the underlying ocular tunics (figs. 5, 6) show that the largest vessels of the pecten, which have a thick endothelium in the lamina, acquire a thin endothelial lining at the base of the pecten, then pass through the bundles of the optic nerve fibers and finally join a large vein situated

in the choroid, immediately beneath and parallel to the cauda of the optic nerve. Therefore, the large vessels with thick endothelium are efferent.

With the light microscope the walls of the capillaries and the efferent vessels appear similar. The endothelium on both the luminal and basal surfaces is provided with a radially striated border. External to the basal striated border the endothelium is invested by a fibrillar coat, 0.5 μ in thickness. In some places it appears uniformly stained by the PAS reaction, while in other places it displays the three-layered appearance described by O'Rahilly and Meyer ('61), with an inner positive layer, an intermediate weakly-stained layer and an external positive layer adhering to the interstitial pigment cells. Fusiform or crescentic cells are often closely applied to the outer surface of the endothelium (fig. 3). These were identified by Kajikawa ('23) as Rouget cells.

The interstitial pigment cells contain brown granules that are intensely argentaffin, are bleached by oxidizing agents and are PAS-negative. On the basis of these histochemical properties they are considered to be a melanin pigment, as previously claimed by Bachsich and Gellert ('35).

A thin PAS-positive line follows the sinusous contour of the pecten and separates the vitreous body from both the pigment cells and the wall of the vessels. This lamina may correspond to the external limiting membrane of O'Rahilly and Meyer ('61); it is continuous at the base of the pecten with the inner limiting membrane of the retina. Therefore it is distinct from and is covered by the hyaloid membrane, which corresponds to the cortical tissue layer of the vitreous body (Balazs et al., '64).

The bridge is crescent-shaped in vertical sections of the pecten (fig. 4). Its surface is often provided with narrow depressions, occasionally deep and tortuous, that afford attachment for fibers of the vitreous body. The bridge consists mainly of a network of anastomosing cords of pigment cells. The meshes of the network are occupied by capillaries, some of which have a thick, other a thin endothelial lining. The endothelium is surrounded by a PAS-positive lamina which is, in turn, invested by a

prominent fibrillar coat. A PAS-positive boundary layer of irregular thickness separates the cords of the pigment cells from the vessel walls. A similar, but thicker layer extends over the entire surface of the bridge and separates the pigment cells from the vitreous body. In many places strands of PAS-positive material, continuous with the perivascular and boundary layers, penetrate deeply into the pigment cell cords.

In most of the animals the pigment cells of the bridge contain, in addition to melanin granules, round or oval cytoplasmic bodies, 2 to 6 μ in diameter, which are stained lilac with toluidine blue and remain unstained with the PAS reaction.

Although the basic organization of the pecten in neognathous birds is the same, the present description of the vascular tree of this organ in the pigeon differs in many details from the previous reports on other species. A main vein at the base of the pecten running parallel to and near the basal artery, was described both in the sparrow (Slonaker, '18) and the domestic fowl (Mann, '24a,b) and confirmed in other species by Menner ('38). Moreover, a supplying artery was described along the middle of each fold and a draining vein was found along the edges of the lamina. No such artery has been noticed by A. Tanaka ('60) in *Uroloncha striata domestica* and *Passer montanus*. As noted by H. Tanaka ('38), however, the distribution of the blood vessels in the pecten differs for each species of bird. This no doubt explains some of the discrepancies between the present and the previous reports.

Electron microscopy

Capillaries. The endothelial cells of the pecten capillaries are provided on both the luminal and basal surfaces with radially oriented, slender processes (figs. 7, 8). The cell body, interposed between the luminal and basal processes, is a continuous strip of cytoplasm usually about 0.3 μ in thickness, but attenuated in some places to as little as 500 Å. The nucleus occupies a lenticular thickening of the cell body.

In transverse sections of the capillary, the luminal processes, at some distance from the nuclear bulge, are about 1 μ long,

550 to 750 Å thick and slightly constricted at their insertion upon the cell body. In some areas, they are erect, parallel and closely compressed; elsewhere they are flexed and irregularly oriented. Most of them are unbranched, but some bifurcate and in a few instances the branches that originate from the bifurcation fuse again forming a circular eyelet. Adjacent luminal processes often are found alternately connected to and disconnected from the underlying cell body (fig. 10). In grazing sections of the surface of the endothelial cells (fig. 9) most luminal processes appear as elongated profiles with a prevailing longitudinal orientation with respect to the vessel axis. Finally, longitudinal sections of the capillaries show that luminal processes are not microvilli but are leaflets or lamellae variable in shape and broader towards the lumen than at their base. This last feature explains why many luminal processes appear in cross section disconnected from the cell body.

The lamelliform processes are shorter, fewer in number and more disordered in the vicinity of the nuclear bulge than elsewhere on the luminal surface (fig. 8). Occasionally they are recurving and have fused with the cell body at their distal end.

The unit membrane limiting the luminal processes does not have an obvious external fuzzy coat (figs. 11, 14). Although patches of filamentous material are occasionally observed near the outer aspect of the membrane, similar material is also present far away from it in the vessel lumen and may well represent a component of the blood plasma precipitated by the fixative.

The basal processes of the endothellum, like the luminal ones, are pedunculated lamellae (fig. 13). However, they are shorter than the adluminal processes, more frequently branched and often more closely compressed (fig. 11). In places they are aligned in orderly array and form a fairly regular border 0.8 μ in thickness at the cell base. In other areas they bend at an acute angle, becoming oriented parallel to the cell body and stacked one upon the other. At the nuclear bulge they are fewer, shorter and more disordered than elsewhere.

Sections of larger processes are occasionally found interspersed among the pro-

files of the basal lamellae. These may contain cytoplasmic organelles but are never found in continuity with the endothelial cell body and are believed to belong to pericytes.

The basal lamellae appear disconnected from the cell body more often than the luminal processes (fig. 11) possibly because their stalks are narrower and less often included in the plane of section. A cleft, 300 to 1300 Å in thickness, frequently intervenes between the proximal edge of these disconnected basal lamellae and the outer surface of the cell body. On the other hand the lateral surfaces of adjacent basal lamellae are almost everywhere closely adjoined, with an intervening space of 35 to 170 Å in thickness. Thus, a labyrinthine system of narrow interstices surrounds the stalks of the basal lamellae between their closely packed, expanded portions and the endothelial cell body. This system of interstices contains an amorphous or finely filamentous material, that resembles the substance of the basement lamina in density and texture. The identification of this material with the basement lamina is also substantiated by the presence of small densities, which may be regarded as rudimentary half-desmosomes, on the adjacent plasmalemma of the endothelial cell body. Basement lamina-like material is also irregularly condensed on the outer surface of the basal processes, imperceptibly merging with the thick pericapillary adventitia. When occasional gaps are found between adjacent basal lamellae, the inner and outer condensations of basement lamina-like material appear continuous with each other (fig. 7).

The nucleus of the endothelial cells is unremarkable. One or two centrioles are found beside the nucleus (fig. 10). The Golgi apparatus is somewhat larger than in the endothelial cells of the usual capillaries and occurs on either the luminal or the basal side of the centrioles. Sometimes it is circular in shape and completely surrounds the centrioles. A small number of mitochondria 0.1 to 0.6 µ in diameter, are scattered throughout the cell body; they display a moderate number of cristae and a dense matrix. Free ribosomes are fairly abundant, while elements of the rough surfaced endoplasmic reticulum are scarce.

Near the origin from the cell body of both the luminal and basal processes small invaginations of the cell membrane are found that are coated on both the inner and outer surfaces with a nap of short filaments or spines. Uncoated invaginations of the cell membrane are seen at the bottom of the grooves between adjacent processes (fig. 14). Coated and uncoated vesicles are scattered in moderate number throughout the cytoplasm of the endothelial cell.

A few very dense, membrane-bounded granules (figs. 10, 11) and rods are also found. The granules are 75 to 125 mµ in diameter, the rods 120 by 650 mµ. The granules may perhaps represent the cross sectional profiles of the rods. These structures may correspond to the rod-shaped bodies that were reported in the endothelium of arteries and in the endocardium of rat and man (Weibel and Palade, '64), although distinct inner tubular structures were not observed in our material.

Filaments, 55 to 65 Å in thickness, microtubules, occasional dense and multivesicular bodies complete the list of cytoplasmic organelles.

At least two endothelial cells and often three or more, encircle the vessel lumen (fig. 8). Intercellular junctions are established only between adjacent cell bodies and involve neither the luminal nor the basal processes. At the junction (fig. 15) the opposing plasma membranes are 35 to 190 Å apart except at one or two points where they either fuse or appear very closely apposed. These points are located at a variable distance from the vessel lumen. The cytoplasmic matrix is more dense near the junction than elsewhere in the cell body. The basal lamellae of the neighboring endothelial cells sometimes interdigitate beneath the intercellular junction.

Near the endothelium the adventitia of the capillary consists of fibrils, 70 to 100 Å in diameter, that lack striations and are embedded in a basement lamina-like material. As one moves outward from the endothelium, the fibrils increase in thickness, and the interfibrillar material becomes no longer perceptible. The outermost fibrils are about 400 Å in diameter and occasionally display a cross striation with a periodicity about the same as that typical

prominent fibrillar coat. A PAS-positive boundary layer of irregular thickness separates the cords of the pigment cells from the vessel walls. A similar, but thicker layer extends over the entire surface of the bridge and separates the pigment cells from the vitreous body. In many places strands of PAS-positive material, continuous with the perivascular and boundary layers, penetrate deeply into the pigment cell cords.

In most of the animals the pigment cells of the bridge contain, in addition to melanin granules, round or oval cytoplasmic bodies, 2 to 6 μ in diameter, which are stained lilac with toluidine blue and remain unstained with the PAS reaction.

Although the basic organization of the pecten in neognathous birds is the same, the present description of the vascular tree of this organ in the pigeon differs in many details from the previous reports on other species. A main vein at the base of the pecten running parallel to and near the basal artery, was described both in the sparrow (Slonaker, '18) and the domestic fowl (Mann, '24a,b) and confirmed in other species by Menner ('38). Moreover, a supplying artery was described along the middle of each fold and a draining vein was found along the edges of the lamina. No such artery has been noticed by A. Tanaka ('60) in *Uroloncha striata domestica* and *Passer montanus*. As noted by H. Tanaka ('38), however, the distribution of the blood vessels in the pecten differs for each species of bird. This no doubt explains some of the discrepancies between the present and the previous reports.

Electron microscopy

Capillaries. The endothelial cells of the pecten capillaries are provided on both the luminal and basal surfaces with radially oriented, slender processes (figs. 7, 8). The cell body, interposed between the luminal and basal processes, is a continuous strip of cytoplasm usually about 0.3 μ in thickness, but attenuated in some places to as little as 500 Å. The nucleus occupies a lenticular thickening of the cell body.

In transverse sections of the capillary, the luminal processes, at some distance from the nuclear bulge, are about 1 μ long,

550 to 750 Å thick and slightly constricted at their insertion upon the cell body. In some areas, they are erect, parallel and closely compressed; elsewhere they are flexed and irregularly oriented. Most of them are unbranched, but some bifurcate and in a few instances the branches that originate from the bifurcation fuse again forming a circular eyelet. Adjacent luminal processes often are found alternately connected to and disconnected from the underlying cell body (fig. 10). In grazing sections of the surface of the endothelial cells (fig. 9) most luminal processes appear as elongated profiles with a prevailing longitudinal orientation with respect to the vessel axis. Finally, longitudinal sections of the capillaries show that luminal processes are not microvilli but are leaflets or lamellae variable in shape and broader towards the lumen than at their base. This last feature explains why many luminal processes appear in cross section disconnected from the cell body.

The lamelliform processes are shorter, fewer in number and more disordered in the vicinity of the nuclear bulge than elsewhere on the luminal surface (fig. 8). Occasionally they are recurring and have fused with the cell body at their distal end.

The unit membrane limiting the luminal processes does not have an obvious external fuzzy coat (figs. 11, 14). Although patches of filamentous material are occasionally observed near the outer aspect of the membrane, similar material is also present far away from it in the vessel lumen and may well represent a component of the blood plasma precipitated by the fixative.

The basal processes of the endothellum, like the luminal ones, are pedunculated lamellae (fig. 13). However, they are shorter than the adluminal processes, more frequently branched and often more closely compressed (fig. 11). In places they are aligned in orderly array and form a fairly regular border 0.8 μ in thickness at the cell base. In other areas they bend at an acute angle, becoming oriented parallel to the cell body and stacked one upon the other. At the nuclear bulge they are fewer, shorter and more disordered than elsewhere.

Sections of larger processes are occasionally found interspersed among the pro-

whose thickness varies between 230 Å and 0.6μ (fig. 7). One is interposed between the pigment cells and the vascular adventitia, the other separates the pigment cells from the vitreous body (fig. 18). The two basement laminae form a continuous barrier between the vessels and the vitreous body and delimit a compartment that is incompletely filled by the pigment cells. Interruptions of the investment of pigment cells often occur along that segment of the vessel wall which protrudes farthest into the vitreous body. Here only the two basement laminae intervene between the vascular adventitia and the vitreous body, in some places separated from one another by a thin, clear interspace, and in other places, fused.

Empty irregular spaces or channels occur among neighboring bodies or processes of the pigment cells (figs. 7, 20). Many finger-like projections of the pigment cells protrude into these spaces. Similar projections are also present in smaller numbers on the remaining surface of the pigment cells and penetrate the adjacent basement laminae. Small maculae occludentes may be found connecting adjacent processes of the pigment cells.

The cytoplasm of the pigment cells contains round, very dense melanin granules, up to 2μ in diameter (figs. 7, 20). Premelanosomes (Fitzpatrick et al., '66) similar to those reported in epidermal (Drochmans, '60) or hair bulb (Birbeck, '63) melanocytes were not observed. Mitochondria are fairly numerous and extremely variable in their dimensions. Some of them reach 2.8μ in diameter and display sparse lamellar cristae and a plentiful, moderately dense matrix (fig. 20). Dilated intracristal spaces of a few mitochondria contain bundles of helicoidal filaments (fig. 21). These filaments resemble those reported in mitochondria of glial cells of the corpus striatum in the rat (Mugnaini, '64).

Bundles of filaments, 60 to 120 Å in thickness, are widely scattered throughout the pigment cell body and processes. In a juxtanuclear situation, one or two centrioles are found, surrounded by a well developed Golgi apparatus (fig. 20). Often one centriole of the pair constitutes the basal body of an abortive flagellum,

that projects into a narrow cylindrical channel (fig. 22), whose opening at the cell surface is only rarely encountered. Near the Golgi elements are found membrane-bounded granules, 120 to 270 m μ in diameter, that contain a moderately dense material. Free ribosomes are numerous, while the elements of the rough surfaced endoplasmic reticulum are scarce. Microtubules are commonly found. Coated invaginations of the plasma membrane are present in small numbers along the whole surface of the pigment cells. A few coated vesicles are also scattered throughout the cytoplasm.

Bridge. The vessels of the bridge are capillaries. Some are very similar to the capillaries of the lamina of the pecten except that they possess an exceedingly thick adventitial coat. Others are provided with a thin, unspecialized endothelium.

The cords of pigment cells are separated both from the vascular adventitia and the vitreous body by thick basement laminae. Moreover strands of basement lamina-like material penetrate deeply into the pigment cell cords in a tortuous course. From the peripheral basement lamina, collagen fibrils radiate into the vitreous body.

The pigment cells (fig. 23) are irregular in shape and tightly packed. Peripheral microvilli and large intercellular channels are lacking. Neighboring cells are occasionally connected by tight and intermediate junctions, either isolated or combined in a single junctional complex.

The main difference between the pigment cells of the bridge and those of the lamina of the pecten resides in the presence in the former of large, non-membrane-bounded areas of cytoplasm which contain a flocculent material of low electron density evidently corresponding to the large PAS-negative bodies observed with the light microscope. The chemical nature and significance of this material is obscure.

DISCUSSION

After aldehyde fixation, the luminal and basal surface specializations of the endothelial cells of the capillaries and venules of the pecten consist of lamellar processes of irregular shape and somewhat constricted at their origin from the cell body. After primary fixation in osmium tetroxide

of collagen fibrils. The orientation of the adventitial fibrils with respect to the vessel axis is quite inconstant (figs. 7, 8).

The fusiform or crescentic cells that are applied to the outer surface of the endothelium have a nucleus with a slightly coarser chromatin pattern than the endothelial cell nucleus. Their scanty cytoplasm contains one or two centrioles, a small Golgi apparatus, sparse mitochondria, occasional microtubules, some coated vesicles and a few enlarged sacks of the rough surfaced endoplasmic reticulum which are filled with a moderately dense material. Although a few of these cells appear completely embedded in the capillary adventitia (fig. 7), many exhibit noteworthy relationships with the endothelial cells. Some course parallel to the endothelial cell at a certain distance from it, but are provided with thin processes, that curve through the adventitia and reach the outer surface of the endothelium where they intermingle with the basal lamellae. Other cells of this type are closely applied to the outside of the endothelium (fig. 16) or are even inserted into a niche in the outer surface of the endothelium. In some instances they are separated from the endothelium by a faint condensation of basement lamina-like material while in other places they make direct contact and show a small number of processes that interdigitate with the basal lamellae.

These cells, in spite of their lack of a complete investment of a basement lamina, may be regarded as pericytes on account of their intimate connections with the endothelium. Furthermore, areas of direct contact between pericytes and endothelial cells have also been reported in other tissues (Macher and Vogell, '62; Kuwabara and Cogan, '63).

Afferent vessels. The largest afferent vessels within the lamina of the pecten may be identified as arterioles (figs. 17, 19). The luminal and basal surfaces of the endothelial cells are smooth, with the exception of the usual marginal folds at the cell junctions (Fawcett, '63). In addition to the usual complement of cytoplasmic organelles these endothelial cells contain dense granules and rodlets similar to those seen in the capillary endothelial cells. A few coated and uncoated vesicles and

invaginations of the plasmalemma are also found.

The endothelium is invested by a single, occasionally discontinuous layer of flattened smooth muscle cells. A faint basement lamina is commonly interposed between the endothelium and the muscle cells, but areas of close contiguity are also found.

The prominent adventitia, 1.5 to 2.5 μ in thickness, consists of inner and outer layers, which gradually merge into each other. The inner layer is composed of concentric sheaths of material, resembling the substance of the basement lamina, and is permeated by thin unit fibrils of collagen. The outer layer consists only of collagen fibrils, that increase progressively in diameter in a centrifugal direction and finally acquire a distinct cross striation. Flattened connective tissue cells are commonly found embedded in the adventitia.

As the distance increases from the base of the pecten, the muscle coat of the arterioles becomes largely discontinuous and finally disappears and the adventitia becomes thinner and less clearly stratified. Sporadic lamellae begin to appear on either the luminal or the basal surface of the endothelial cells. The arteriole thus undergoes a gradual transition into an afferent capillary (fig. 18).

Efferent vessels. The wall of the large efferent vessels of the pecten is very similar to the wall of the capillaries (fig. 12). However, the luminal lamellae of the endothelial cells are less erect and less closely packed while the basal lamellae are often more compactly arranged. The adventitial coat is thicker. Pericytes are commonly observed. Because of the large diameter and the lack of a muscular investment, the efferent vessels of the pecten may be identified as postcapillary venules.

Pigment cells. The pigment cells (figs. 7, 20) are stellate elements, whose bodies occupy the grooves between the vessels and thus smooth out the surface of the lamina of the pecten. Processes radiate from the cell bodies and embrace the blood vessels, intervening between them and the vitreous body and penetrating deeply into the interstices between adjacent vessels.

The pigment cells are everywhere sandwiched between two basement laminae,

whose thickness varies between 230 Å and 0.6 μ (fig. 7). One is interposed between the pigment cells and the vascular adventitia, the other separates the pigment cells from the vitreous body (fig. 18). The two basement laminae form a continuous barrier between the vessels and the vitreous body and delimit a compartment that is incompletely filled by the pigment cells. Interruptions of the investment of pigment cells often occur along that segment of the vessel wall which protrudes farthest into the vitreous body. Here only the two basement laminae intervene between the vascular adventitia and the vitreous body, in some places separated from one another by a thin, clear interspace, and in other places, fused.

Empty irregular spaces or channels occur among neighboring bodies or processes of the pigment cells (figs. 7, 20). Many finger-like projections of the pigment cells protrude into these spaces. Similar projections are also present in smaller numbers on the remaining surface of the pigment cells and penetrate the adjacent basement laminae. Small maculae occludentes may be found connecting adjacent processes of the pigment cells.

The cytoplasm of the pigment cells contains round, very dense melanin granules, up to 2 μ in diameter (figs. 7, 20). Premelanosomes (Fitzpatrick et al., '66) similar to those reported in epidermal (Drochmans, '60) or hair bulb (Birbeck, '63) melanocytes were not observed. Mitochondria are fairly numerous and extremely variable in their dimensions. Some of them reach 2.8 μ in diameter and display sparse lamellar cristae and a plentiful, moderately dense matrix (fig. 20). Dilated intracristal spaces of a few mitochondria contain bundles of helical filaments (fig. 21). These filaments resemble those reported in mitochondria of glial cells of the corpus striatum in the rat (Mugnaini, '64).

Bundles of filaments, 60 to 120 Å in thickness, are widely scattered throughout the pigment cell body and processes. In a juxtanuclear situation, one or two centrioles are found, surrounded by a well developed Golgi apparatus (fig. 20). Often one centriole of the pair constitutes the basal body of an abortive flagellum,

that projects into a narrow cylindrical channel (fig. 22), whose opening at the cell surface is only rarely encountered. Near the Golgi elements are found membrane-bounded granules, 120 to 270 m μ in diameter, that contain a moderately dense material. Free ribosomes are numerous, while the elements of the rough surfaced endoplasmic reticulum are scarce. Microtubules are commonly found. Coated invaginations of the plasma membrane are present in small numbers along the whole surface of the pigment cells. A few coated vesicles are also scattered throughout the cytoplasm.

Bridge. The vessels of the bridge are capillaries. Some are very similar to the capillaries of the lamina of the pecten except that they possess an exceedingly thick adventitial coat. Others are provided with a thin, unspecialized endothelium.

The cords of pigment cells are separated both from the vascular adventitia and the vitreous body by thick basement laminae. Moreover strands of basement lamina-like material penetrate deeply into the pigment cell cords in a tortuous course. From the peripheral basement lamina, collagen fibrils radiate into the vitreous body.

The pigment cells (fig. 23) are irregular in shape and tightly packed. Peripheral microvilli and large intercellular channels are lacking. Neighboring cells are occasionally connected by tight and intermediate junctions, either isolated or combined in a single junctional complex.

The main difference between the pigment cells of the bridge and those of the lamina of the pecten resides in the presence in the former of large, non-membrane-bounded areas of cytoplasm which contain a flocculent material of low electron density evidently corresponding to the large PAS-negative bodies observed with the light microscope. The chemical nature and significance of this material is obscure.

DISCUSSION

After aldehyde fixation, the luminal and basal surface specializations of the endothelial cells of the capillaries and venules of the pecten consist of lamellar processes of irregular shape and somewhat constricted at their origin from the cell body. After primary fixation in osmium tetroxide

we constantly observed an extensive rearrangement of the limiting membranes of adjacent luminal lamellae resulting in rows of vesicles. Also Dalton's fluid, followed by formalin postfixation, a technique which preserves the tubular form of the smooth surfaced endoplasmic reticulum in steroid secreting cells (Christensen and Fawcett, '61) did not completely prevent vesiculation of membranes even when perfused intravascularly.

Thus, some discrepancies in previous descriptions of the endothelial cell specializations of these vessels actually reflect the multifarious aspects of a fixation artifact. Our results confirm the inference of Semba ('62) with respect to the laminar shape of both the luminal and basal processes, based upon a reconstruction with serial sections of the basal labyrinth of the endothelial cells.

Adjacent luminal and basal lamelliform processes are indubitably separated by a fold of the plasma membrane, but to designate the endothelial specializations as luminal and basal infoldings of the plasma membrane (Seaman and Storm, '63; Fischlschweiger and O'Rahilly, '64) gives an inadequate representation of their tridimensional configuration. Most of the basal epithelial cell specializations, formerly interpreted as membrane infoldings, have since been found to represent the limiting membranes of interdigitating processes, that belong to the same or to neighboring epithelial cells (Rhodin, '58; Parks, '61; Tandler, '63; Bulger, '63; Tormey, '63; Bulger, '65). In the capillaries and venules of the pecten an interdigitation of basal lamellae of adjacent endothelial cells, with an intermingling of a small number of processes of pericytes, contributes but little to the composition of the basal labyrinth of the endothelial cells. In fact, the surface area of the endothelial cell is so great in relation to the small width of the basal lamellae, that the elaborate configuration of the basal labyrinth is better explained as resulting from the interdigitation of pedunculated and branched lamellae of a single cell.

In our specimens there is no evidence for the existence of a mucopolysaccharide coat on the luminal side of the endothelial cells, as reported by Seaman and Storm

('66). The endothelium is not stained by the PAS reaction at the light microscope level and in the electron micrographs no definite fuzzy coat seems to be attached to the outer surface of the luminal limiting membrane.

With optimal fixation vesicles do not seem exceedingly abundant in the endothelium of the vessels of the pecten and certainly they are much fewer in number than in the capillary endothelium of both mammalian skeletal and cardiac muscle (Palade, '61). Furthermore rows of vesicles are completely lacking. Coated vesicles and both coated and uncoated invaginations of the plasmalemma are present in the same endothelial cell. The coexistence of both kinds of structures which have been related with the micropinocytosis (Palade, '60; Roth and Porter, '64) constitutes a further argument in favour of the idea (Fawcett, '66) that a certain degree of specificity may exist in their respective roles in transport into or through the cell.

With the exception of the coated vesicles and the microtubules, the endothelial cells of the capillaries and venules of the pecten display a complement of cytoplasmic organelles similar to that of the endothelial cells of the "muscle type" (Fawcett, '63) or "continuous" (Majno, '65) capillaries. Coated vesicles and microtubules, however, are particularly well preserved by the aldehyde fixation and thus far no specific study of their occurrence after aldehyde fixation in the capillary endothelium of organs other than the pecten is available for comparison.

No definite intercellular boundaries were recognized in the endothelium of the capillaries of the pecten by Seaman ('62) and Seaman and Storm ('63). Terminal bars have been described by Semba ('62) and Fischlschweiger and O'Rahilly ('64). In our specimens the intercellular junctions do not differ from those connecting endothelial cells in the capillaries of other organs (cf. Muir and Peters, '62; Karnovsky and Cotran, '66).

Both the basement lamina and the adventitia of the vessels of the pecten have uncommon features. In the arterioles the inner layer of the thick adventitia is unusually rich in a moderately dense mate-

rial, that is similar in submicroscopical organization to the substance of the basement lamina. Vessels resembling the arterioles of the pecten were found at the corneal limbus (Jakus, '64) and in the human retina (Hogan and Feeney, '63), but the significance of the uncommon morphology of the adventitia is unknown.

In the capillaries and venules it is not clear whether the discontinuous layer of moderately dense material interposed between the endothelial cell body and the expanded portions of the basal lamellae is to be regarded as the basement lamina, or the irregular condensation of similar material at the inner margin of the adventitia. In PAS-stained specimens, only the inner adventitia is strongly positive, while the former layer is so thin and so largely discontinuous, that it may not be resolved by the light microscope. The significance of such an unusual distribution of basement lamina-like material is obscure.

The thick adventitia of the capillaries and venules of the pecten is very rich in unstriated fibrils. These are assumed to be collagen because they exhibit a progressive increase in thickness as one proceeds towards the periphery of the adventitia, where typical collagen fibrils are found. Thin, unstriated collagen fibrils are reported in Bowman's layer of the human cornea (Jakus, '61) and in the vitreous body (Olsen, '65), while a hexagonal array of nodes and filaments is found in Descemet's membrane, which is known to be a collagenous structure (Jakus, '56). It is perhaps more than a coincidence that unusual patterns of polymerization of tropocollagen occur in many places in the vertebrate eye.

The nature of the pigment cells in the pecten was long debated. They were assumed to be ectodermal in origin by Mann ('24a, b) and glial in nature by Blochmann and von Husen ('11), Kajikawa ('23) and Kauth and Sommer ('53). Bachsich and Gellert ('35) regarded them as connective tissue cells, and no glial cells were found in the pecten by Seaman and Storm ('63). Melanocytes containing bundles of filaments and separated from the connective tissue by a basement lamina can hardly be regarded as connective tissue cells. They are, however, cytologically different from the

glial cells of the central nervous system and have no relationships with nerve fibers which are few or lacking in the pecten (Blochmann and von Husen, '11; Kajikawa, '23; Bachsich and Gellert, '35; Menner, '38; Seaman and Storm, '63). Thus, it seems inappropriate to regard them as glial cells.

Two continuous basement laminae with an intervening discontinuous layer of pigment cells are interposed between the vessels of the pecten and the vitreous body. Such an investment should have some influences in limiting the exchanges between vessels and vitreous body. The basement lamina, at least in the blood vessels, seems to be impermeable to some large colloidal particles (Majno, '65). On the other hand the free diffusion of small-sized particles may be restricted to the large spaces between neighboring pigment cells, as suggested by A. Tanaka ('60) and Semba ('62). However, we do not know whether the patency of these channels is actively controlled by the pigment cells or merely reflects a fixation artifact.

In contrast to the findings of Semba ('62) no hyalocytes were observed adhering to the surface of the pecten in the pigeon.

It is more than a century that the function of the pecten has challenged the imagination of investigators. An extensive discussion of opinions expressed prior to 1942, is reported by Walls. On the basis of comparative anatomical arguments, Walls arrived at a conclusion consonant with the conception of Denissenko (1881), Slonaker ('18) and Mann ('24a, b) that the pecten is mainly concerned with the nourishment of the avascular avian retina. A few biochemical and physiological contributions have been added. An unusually high carbonic anhydrase activity was reported by Leiner ('40) and confirmed by Kauth and Sommer ('53). Crozier and Wolf ('44) reintroduced Menner's idea ('38) that the shadow of the pecten upon the retina may act as a grating in improving the perception of small moving objects, while Griffin ('52) speculated about a role of the pecten in avian navigation. A re-examination of the question as to whether or not the pecten casts a shadow

upon the retina, is beyond the scope of this study.

When specific physiological evidence is lacking, descriptive investigations may contribute but little to understanding the function of an organ, unless they reveal incontrovertible structural analogies with other organs whose function is well known. An analogy insistently recurrent in the ophthalmological literature relates the pecten functionally to other highly vascular organs of the vertebrate eye, such as the choroid rete (Prince, '56; François and Neetens, '62), the processus falciformis in fishes, and the ectodermal conus papillaris in lizards (Walls, '42; Duke-Elder, '58). The choroid rete is a countercurrent system of capillaries with an unspecialized endothelial lining (Fawcett, '63) which seems to be responsible for maintenance of high oxygen tension in the vitreous body (Wittenberg and Wittenberg, '61). On the contrary, a regular arrangement and packing of afferent and efferent capillaries is lacking in the vascular network of the pecten in the pigeon, as well as in that of other birds (H. Tanaka, '38). Furthermore, collateral capillaries shunt the blood from the afferent to the efferent vessels along the whole extent of the organ. Thus, the vascular network of the pecten cannot be regarded as a countercurrent system.

The endothelial cells of the capillaries of the conus papillaris in *Anolis carolinensis* (unpublished observations) are provided with sparse, blunt, luminal microvilli and a few short and irregular basal projections, both somewhat reminiscent of the more complex specializations of the endothelial cells of the capillaries in the pecten. But, the function of the conus papillaris is likewise unknown.

Previous submicroscopical descriptions, which attributed to the endothelial cells of the capillaries of the pecten a luminal brush border and basal membrane infoldings, seemed to provide a satisfactory morphological analogy with the epithelial cells of the proximal convoluted tubules of the kidney. On this basis, the endothelial cells were assumed to be engaged in active transport (A. Tanaka, '60; Semba, '62; Seaman and Storm, '63, '66). The morphological similarities are less obvious in our material but it is nonetheless true that

like epithelial cells engaged in active transport, the endothelial cells of the vessels of the pecten have a very large surface, bounding a system of narrow extracellular spaces. A significant difference, however, is that actively transporting epithelial cells have a definite morphological polarity and are connected by junctional complexes which are claimed to seal the intercellular spaces (Farquhar and Palade, '63). No clear morphological polarity is seen in the endothelial cells of the vessels of the pecten and the impermeability of the intercellular junctions in capillary endothelium has recently been questioned, at least in muscle (Karnovsky and Cotran, '66).

A role in active transport still remains the only reasonable inference to be drawn from the specializations of the endothelial cells of the vessels of the pecten. The paucity of mitochondria in these cells does not appear a cogent objection. Active transport, large area of the membrane specializations and number of mitochondria do not seem to be invariably correlated. Actively transporting cells do not necessarily contain either a membranous labyrinth, as already pointed out (Bulger, '65), or an unusual complement of mitochondria. Finally, it appears impossible to estimate the cellular oxidative capacity solely on the basis of the mitochondrial morphology. Thus, one cannot exclude the possibility that active transport in the pecten might be supported by anaerobic glycolysis as in the nephron of poikilothermic animals (Himmelhoeh and Karnovsky, '61; Karnovsky, '63).

The high carbonic anhydrase activity, relates the pecten to other organs actively transporting solutes. This enzyme is present in the mammalian ciliary body (Wistrand, '51), where it seems to be involved with the production of the aqueous humor, either directly by providing ions to be secreted or indirectly in maintaining the intracellular buffering (Berliner and Orloff, '56; Becker, '59; Langham, '58). However, it should be pointed out that the relationships between carbonic anhydrase and active transport are not yet perfectly understood (Kinsey and Reddy, '64), and the enzyme distribution is not always coincident with obvious morphological specializations of the plasma membrane. In

the eye, the lens and the retina also have a high carbonic anhydrase activity (Bakker, '39; Leiner, '40).

Indeed, a parallel exists between the pecten and the ciliary body, both displaying specialized cells that are intercalated between the blood stream and the ocular environment. The pecten might represent, as suggested by Walls ('42), a subsidiary vascular supply for the endocular tissues and its specialized endothelial cells might well introduce some corrections in the composition of the fluids that diffuse from the blood stream into the vitreous body. Such a picture, however, is probably oversimplified, and may merely reflect the fact that we still do not know very much about the significance of the pecten.

ACKNOWLEDGMENTS

The authors are greatly indebted to Dr. Don W. Fawcett and Dr. Susumu Ito for their continuous interest and advice during the course of the study and the revision of the manuscript.

The kindness of Dr. Richard E. Coggeshall and Dr. Donald Feldman in reading the English text is also gratefully acknowledged.

LITERATURE CITED

- Bachsch, P., und A. Gellert 1935 Beiträge zur Kenntnis der Struktur und Funktion des Pecten im Vogelaugen. A. von Graefes Archiv Ophthalm., 133: 448-460.
- Bakker, A. 1939 Über Kohlensäureanhydrase in normalen und kataraktösen Linsen. A. von Graefes Archiv Ophthalm., 140: 543-552.
- Balazs, E. A., L. Z. J. Toth, E. A. Eckel and A. P. Mitchell 1964 Studies on the structure of the vitreous body. XII Cytological and histochemical studies on the corneal tissue layer. Exp. Eye Res., 3: 57-71.
- Becker, B. 1939 Carbonic anhydrase and the formation of aqueous humor. Am. J. Ophthalm., 47, Part II: 342-361.
- Berliner, R. W., and J. Orloff 1956 Carbonic anhydrase inhibitors. Pharmac. Rev., 8: 137-174.
- Birbeck, M. S. C. 1963 Electron microscopy of melanocytes: the fine structure of hair-bulb premelanosomes. Ann. N. Y. Acad. Sci., 100: 540-547.
- Blochmann, F., und E. von Hussen 1911 Ist der Pecten des Vogelauges ein Sinnesorgan? Biol. Zbl., 31: 150-156.
- Bulger, R. E. 1963 Fine structure of the rectal (salt secreting) gland in the spiny dogfish, *Squalus acanthias*. Anat. Rec., 147: 95-127.
- 1965 The fine structure of the glomerular nephron of the toadfish, *Opsanus tau*. Am. J. Anat., 117: 171-192.
- Caulfield, J. B. 1957 Effects of varying the vehicle for OsO_4 in tissue fixation. J. Biophys. Biochem. Cytol., 3: 827-830.
- Christensen, A. K., and D. W. Fawcett 1961 The normal fine structure of opossum testicular interstitial cells. J. Biophys. Biochem. Cytol., 9: 653-670.
- Crozier, W. J., and E. Wolf 1944 Theory and measurement of visual mechanisms. X Modifications of the flicker response contour, and the significance of the avian pecten. J. Gen. Physiol., 27: 287-313.
- Denissenko, G. 1881 Ueber den Bau und die Funktion des Kammes (Pecten) im Auge der Vögel. Arch. mikr. Anat., 19: 733-741.
- Drochmans, P. 1960 Electron microscope studies of epidermal melanocytes, and the fine structure of melanin granules. J. Biophys. Biochem. Cytol., 8: 165-180.
- Duke-Elder, S. 1958 The eye in evolution. In: System of Ophthalmology. Ed. by S. Duke-Elder, Kimpton, London, Vol. 1.
- Farquhar, M. G., and G. E. Palade 1963 Junctional complexes in various epithelia. J. Cell Biol., 17: 375-412.
- 1965 Cell junctions in amphibian skin. J. Cell Biol., 26: 263-291.
- Fawcett, D. W. 1963 Comparative observations on the fine structure of blood capillaries. In: The Peripheral Blood Vessels. Ed. by J. L. Orbison and D. Smith, Williams and Wilkins, Baltimore, 17-44.
- 1966 The Cell, Its Organelles and Inclusions. Saunders, Philadelphia, 358.
- Fischlschweiger, W., and R. O'Rahilly 1964 The ultrastructure of the pecten oculi. Anat. Rec. (abs.), 148: 282.
- Fitzpatrick, T. B., W. C. Quevedo, Jr., A. L. Levene, V. J. McGovern, Y. Mishima and A. G. Oetle 1966 Terminology of vertebrate melanin-containing cells: 1965. Science, 152: 88-89.
- François, J., and A. Neetens 1962 Comparative anatomy of the vascular supply of the eye in vertebrates. In: The Eye. Ed. by H. Davson, Academic Press, New York, Vol. 1, 369-416.
- Franzini-Armstrong, C., and K. R. Porter 1964 Sarcoplasmic invaginations constituting the T-system in fish muscle fibers. J. Cell Biol., 22: 675-696.
- Griffin, D. R. 1962 Bird navigation. Biol. Rev., 27: 359-393.
- Himmelhoch, S. R., and M. J. Karnovsky 1961 Oxidative and hydrolytic enzymes in the nephron of *Necturus maculosus*. J. Biophys. Biochem. Cytol., 9: 893-908.
- Hogan, M. J., and L. Feeney 1963 The ultrastructure of the retinal vessels. II. The small vessels. J. Ultrastruct. Res., 9: 29-46.
- Jakus, M. A. 1956 Studies on the cornea. II. The fine structure of Descemet's membrane. J. Biophys. Biochem. Cytol., 2, Suppl.: 243-252.
- 1961 The fine structure of the human cornea. In: The Structure of the Eye. Ed. by G. K. Smelser, Academic Press, New York, 343-366.

upon the retina, is beyond the scope of this study.

When specific physiological evidence is lacking, descriptive investigations may contribute but little to understanding the function of an organ, unless they reveal incontrovertible structural analogies with other organs whose function is well known. An analogy insistently recurrent in the ophthalmological literature relates the pecten functionally to other highly vascular organs of the vertebrate eye, such as the choroid rete (Prince, '56; François and Neetens, '62), the processus falciformis in fishes, and the ectodermal conus papillaris in lizards (Walls, '42; Duke-Elder, '58). The choroid rete is a countercurrent system of capillaries with an unspecialized endothelial lining (Fawcett, '63) which seems to be responsible for maintenance of high oxygen tension in the vitreous body (Wittenberg and Wittenberg, '61). On the contrary, a regular arrangement and packing of afferent and efferent capillaries is lacking in the vascular network of the pecten in the pigeon, as well as in that of other birds (H. Tanaka, '38). Furthermore, collateral capillaries shunt the blood from the afferent to the efferent vessels along the whole extent of the organ. Thus, the vascular network of the pecten cannot be regarded as a countercurrent system.

The endothelial cells of the capillaries of the conus papillaris in *Anolis carolinensis* (unpublished observations) are provided with sparse, blunt, luminal microvilli and a few short and irregular basal projections, both somewhat reminiscent of the more complex specializations of the endothelial cells of the capillaries in the pecten. But, the function of the conus papillaris is likewise unknown.

Previous submicroscopical descriptions, which attributed to the endothelial cells of the capillaries of the pecten a luminal brush border and basal membrane infoldings, seemed to provide a satisfactory morphological analogy with the epithelial cells of the proximal convoluted tubules of the kidney. On this basis, the endothelial cells were assumed to be engaged in active transport (A. Tanaka, '60; Semba, '62; Seaman and Storm, '63, '66). The morphological similarities are less obvious in our material but it is nonetheless true that

like epithelial cells engaged in active transport, the endothelial cells of the vessels of the pecten have a very large surface, bounding a system of narrow extracellular spaces. A significant difference, however, is that actively transporting epithelial cells have a definite morphological polarity and are connected by junctional complexes which are claimed to seal the intercellular spaces (Farquhar and Palade, '63). No clear morphological polarity is seen in the endothelial cells of the vessels of the pecten and the impermeability of the intercellular junctions in capillary endothelium has recently been questioned, at least in muscle (Karnovsky and Cotran, '66).

A role in active transport still remains the only reasonable inference to be drawn from the specializations of the endothelial cells of the vessels of the pecten. The paucity of mitochondria in these cells does not appear a cogent objection. Active transport, large area of the membrane specializations and number of mitochondria do not seem to be invariably correlated. Actively transporting cells do not necessarily contain either a membranous labyrinth, as already pointed out (Bulger, '65), or an unusual complement of mitochondria. Finally, it appears impossible to estimate the cellular oxidative capacity solely on the basis of the mitochondrial morphology. Thus, one cannot exclude the possibility that active transport in the pecten might be supported by anaerobic glycolysis as in the nephron of poikilothermic animals (Himmelhoeh and Karnovsky, '61; Karnovsky, '63).

The high carbonic anhydrase activity, relates the pecten to other organs actively transporting solutes. This enzyme is present in the mammalian ciliary body (Wistrand, '51), where it seems to be involved with the production of the aqueous humor, either directly by providing ions to be secreted or indirectly in maintaining the intracellular buffering (Berliner and Orloff, '56; Becker, '59; Langham, '58). However, it should be pointed out that the relationships between carbonic anhydrase and active transport are not yet perfectly understood (Kinsey and Reddy, '64), and the enzyme distribution is not always coincident with obvious morphological specializations of the plasma membrane. In

the eye, the lens and the retina also have a high carbonic anhydrase activity (Bakker, '39; Leiner, '40).

Indeed, a parallel exists between the pecten and the ciliary body, both displaying specialized cells that are intercalated between the blood stream and the ocular environment. The pecten might represent, as suggested by Walls ('42), a subsidiary vascular supply for the endocular tissues and its specialized endothelial cells might well introduce some corrections in the composition of the fluids that diffuse from the blood stream into the vitreous body. Such a picture, however, is probably oversimplified, and may merely reflect the fact that we still do not know very much about the significance of the pecten.

ACKNOWLEDGMENTS

The authors are greatly indebted to Dr. Don W. Fawcett and Dr. Susumu Ito for their continuous interest and advice during the course of the study and the revision of the manuscript.

The kindness of Dr. Richard E. Coggeshall and Dr. Donald Feldman in reading the English text is also gratefully acknowledged.

LITERATURE CITED

- Bachsch, P., und A. Gellert 1935 Beiträge zur Kenntnis der Struktur und Funktion des Pecten im Vogelaug. A. von Graefes Archiv Ophthalm., 133: 448-460.
- Bakker, A. 1939 Über Kohlensäureanhydrase in normalen und kataraktösen Linsen. A. von Graefes Archiv Ophthalm., 140: 543-552.
- Balazs, E. A., L. Z. J. Toth, E. A. Eckel and A. P. Mitchell 1964 Studies on the structure of the vitreous body. XII Cytological and histochemical studies on the cortical tissue layer. Exp. Eye Res., 3: 57-71.
- Becker, B. 1959 Carbonic anhydrase and the formation of aqueous humor. Am. J. Ophthalm., 47, Part II: 342-361.
- Beslmet, R. W., and J. Orloff 1956 Carbonic anhydrase inhibitors. Pharmac. Rev., 8: 137-174.
- Birbeck, M. S. C. 1963 Electron microscopy of melanocytes: the fine structure of hair-bulb premelanosomes. Ann. N. Y. Acad. Sci., 100: 540-547.
- Blochmann, F., und E. von Husen 1911 Ist der Pecten des Vogelauges ein Sinnesorgan? Biol. Zbl., 31: 150-156.
- Bulger, R. E. 1963 Fine structure of the rectal (salt secreting) gland in the spiny dogfish, *Squalus acanthias*. Anat. Rec., 147: 95-127.
- 1965 The fine structure of the aglomerular nephron of the toadfish, *Opsanus tau*. Am. J. Anat., 117: 171-192.
- Caulfield, J. B. 1957 Effects of varying the vehicle for OsO_4 in tissue fixation. J. Biophys. Biochem. Cytol., 3: 827-830.
- Christensen, A. K., and D. W. Fawcett 1961 The normal fine structure of opossum testicular interstitial cells. J. Biophys. Biochem. Cytol., 9: 653-670.
- Crozier, W. J., and E. Wolf 1944 Theory and measurement of visual mechanisms. X Modifications of the flicker response contour, and the significance of the avian pecten. J. Gen. Physiol., 27: 287-313.
- Denissenko, G. 1881 Ueber den Bau und die Function des Kammes (Pecten) im Auge der Vögel. Arch. mikr. Anat., 19: 733-741.
- Drochmans, P. 1960 Electron microscope studies of epidermal melanocytes, and the fine structure of melanin granules. J. Biophys. Biochem. Cytol., 8: 165-180.
- Duke-Elder, S. 1958 The eye in evolution. In: System of Ophthalmology, Ed. by S. Duke-Elder, Kimpton, London, Vol. 1.
- Farquhar, M. G., and G. E. Palade 1963 Junctional complexes in various epithelia. J. Cell Biol., 17: 375-412.
- 1965 Cell junctions in amphibian skin. J. Cell Biol., 26: 263-291.
- Fawcett, D. W. 1963 Comparative observations on the fine structure of blood capillaries. In: The Peripheral Blood Vessels. Ed. by J. L. Orbison and D. Smith, Williams and Wilkins, Baltimore, 17-44.
- 1966 The Cell. Its Organelles and Inclusions. Saunders, Philadelphia, 358.
- Fischlschweiger, W., and R. O'Rahilly 1964 The ultrastructure of the pecten oculi. Anat. Rec. (abs.), 148: 282.
- Fitzpatrick, T. B., W. C. Quevedo, Jr., A. L. Levene, V. J. McGovern, Y. Mishima and A. G. Oettle 1966 Terminology of vertebrate melanin-containing cells: 1965. Science, 152: 88-89.
- François, J., and A. Neetens 1962 Comparative anatomy of the vascular supply of the eye in vertebrates. In: The Eye. Ed. by H. Dawson, Academic Press, New York, Vol. 1, 369-416.
- Franzini-Armstrong, C., and K. R. Porter 1964 Sarcolemmal invaginations constituting the T-system in fish muscle fibers. J. Cell Biol., 22: 675-696.
- Griffin, D. R. 1962 Bird navigation. Biol. Rev., 27: 359-393.
- Himmelfoch, S. R., and M. J. Karnovsky 1961 Oxidative and hydrolytic enzymes in the nephron of *Necturus maculosus*. J. Biophys. Biochem. Cytol., 9: 893-908.
- Hogan, M. J., and L. Feeney 1963 The ultrastructure of the retinal vessels. II. The small vessels. J. Ultrastr. Res., 9: 29-46.
- Jakus, M. A. 1956 Studies on the cornea. II. The fine structure of Descemet's membrane. J. Biophys. Biochem. Cytol., 2, Suppl.: 243-252.
- 1961 The fine structure of the human cornea. In: The Structure of the Eye. Ed. by C. K. Smelser, Academic Press, New York, 343-366.

upon the retina, is beyond the scope of this study.

When specific physiological evidence is lacking, descriptive investigations may contribute but little to understanding the function of an organ, unless they reveal incontrovertible structural analogies with other organs whose function is well known. An analogy insistently recurrent in the ophthalmological literature relates the pecten functionally to other highly vascular organs of the vertebrate eye, such as the choroid rete (Prince, '56; François and Neetens, '62), the processus falciformis in fishes, and the ectodermal conus papillaris in lizards (Walls, '42; Duke-Elder, '58). The choroid rete is a countercurrent system of capillaries with an unspecialized endothelial lining (Fawcett, '63) which seems to be responsible for maintenance of high oxygen tension in the vitreous body (Wittenberg and Wittenberg, '61). On the contrary, a regular arrangement and packing of afferent and efferent capillaries is lacking in the vascular network of the pecten in the pigeon, as well as in that of other birds (H. Tanaka, '38). Furthermore, collateral capillaries shunt the blood from the afferent to the efferent vessels along the whole extent of the organ. Thus, the vascular network of the pecten cannot be regarded as a countercurrent system.

The endothelial cells of the capillaries of the conus papillaris in *Anolis carolinensis* (unpublished observations) are provided with sparse, blunt, luminal microvilli and a few short and irregular basal projections, both somewhat reminiscent of the more complex specializations of the endothelial cells of the capillaries in the pecten. But, the function of the conus papillaris is likewise unknown.

Previous submicroscopical descriptions, which attributed to the endothelial cells of the capillaries of the pecten a luminal brush border and basal membrane infoldings, seemed to provide a satisfactory morphological analogy with the epithelial cells of the proximal convoluted tubules of the kidney. On this basis, the endothelial cells were assumed to be engaged in active transport (A. Tanaka, '60; Semba, '62; Seaman and Storm, '63, '66). The morphological similarities are less obvious in our material but it is nonetheless true that

like epithelial cells engaged in active transport, the endothelial cells of the vessels of the pecten have a very large surface, bounding a system of narrow extracellular spaces. A significant difference, however, is that actively transporting epithelial cells have a definite morphological polarity and are connected by junctional complexes which are claimed to seal the intercellular spaces (Farquhar and Palade, '63). No clear morphological polarity is seen in the endothelial cells of the vessels of the pecten and the impermeability of the intercellular junctions in capillary endothelium has recently been questioned, at least in muscle (Karnovsky and Cotran, '66).

A role in active transport still remains the only reasonable inference to be drawn from the specializations of the endothelial cells of the vessels of the pecten. The paucity of mitochondria in these cells does not appear a cogent objection. Active transport, large area of the membrane specializations and number of mitochondria do not seem to be invariably correlated. Actively transporting cells do not necessarily contain either a membranous labyrinth, as already pointed out (Bulger, '65), or an unusual complement of mitochondria. Finally, it appears impossible to estimate the cellular oxidative capacity solely on the basis of the mitochondrial morphology. Thus, one cannot exclude the possibility that active transport in the pecten might be supported by anaerobic glycolysis as in the nephron of poikilothermic animals (Himmelhoeh and Karnovsky, '61; Karnovsky, '63).

The high carbonic anhydrase activity, relates the pecten to other organs actively transporting solutes. This enzyme is present in the mammalian ciliary body (Wistrand, '51), where it seems to be involved with the production of the aqueous humor, either directly by providing ions to be secreted or indirectly in maintaining the intracellular buffering (Berliner and Orloff, '56; Becker, '59; Langham, '58). However, it should be pointed out that the relationships between carbonic anhydrase and active transport are not yet perfectly understood (Kinsey and Reddy, '64), and the enzyme distribution is not always coincident with obvious morphological specializations of the plasma membrane. In

- Torrey, J. McD. 1963 Fine structure of the ciliary epithelium of the rabbit, with particular reference to "infolded membranes," "vesicles," and the effects of diamox. *J. Cell Biol.*, 17: 641-659.
- 1964 Differences in membrane configuration between osmium tetroxide-fixed and glutaraldehyde-fixed ciliary epithelium. *J. Cell Biol.*, 23: 658-664.
- Venable, J. H., and R. Coggeshall 1965 A simplified lead citrate stain for use in electron microscopy. *J. Cell Biol.*, 25: 407-408.

- Walls, G. L. 1942 *The Vertebrate Eye and its Adaptive Radiation*. Hafner, New York.
- Welbel, E. R., and G. E. Palade 1964 New cytoplasmic components in arterial endothelia. *J. Cell Biol.*, 23: 101-112.
- Wistrand, P. J. 1951 Carbonic anhydrase in the anterior uvea of the rabbit. *Acta Physiol. Scandinav.*, 24: 144-148.
- Wittenberg, J. B., and B. A. Wittenberg 1961 Active transport of oxygen into the eye of fish. *Biol. Bull.*, 121: 379.

- 1964 Ocular Fine Structure. Churchill, London.
- Kajikawa, J. 1923 Beiträge zur Anatomie und Physiologie des Vogelauges. A. von Graefes Archiv Ophthalm., 112: 260-346.
- Karnovsky, M. J. 1963 The fine structure of mitochondria in the frog nephron correlated with cytochrome oxidase activity. Exptl. Molec. Pathol., 2: 347-366.
- 1965 A formaldehyde-glutaraldehyde fixative of high osmolality for use in electron microscopy. J. Cell Biol., 27: 137-138A.
- Karnovsky, M. J., and R. S. Cotran 1966 The intercellular passage of exogenous peroxidase across endothelium and mesothelium. Anat. Rec. (abs.), 154: 365.
- Kauth, H., and H. Sommer 1953 Das Ferment Kohlensäureanhydratase im Tierkörper. IV. Über die Funktion des Pektin im Vogelaugo. Biol. Zbl., 72: 196-209.
- Kinsey, V. E., and D. V. N. Reddy 1964 Chemistry and dynamics of aqueous humor. In: The Rabbit in Eye Research. Ed. by Y. H. Prince, Thomas, Springfield, 218-319.
- Kuwabara, T., and D. G. Cogan 1963 Retinal vascular patterns. VI. Mural cells of the retinal capillaries. Arch. Ophthalm., 69: 492-502.
- Langham, M. E. 1958 Aqueous humor and control of intra-ocular pressure. Physiol. Rev., 38: 215-242.
- Leiner, M. 1940 Das Atmungsferment Kohlensäureanhydrase im Tierkörper. Naturwiss., 28: 165-171.
- Macher, E., and W. Vogell 1962 Elektronenmikroskopische Untersuchungen an Hautkapillaren. Dermatologica, 124: 110-128.
- Majno, G. 1965 Ultrastructure of the vascular membrane. In: Handbook of Physiology. Section 2: Circulation. Vol. III, Chapter 64, 2293-2375.
- Majno, G., G. E. Palade and G. I. Schoeff 1961 Studies on inflammation. II. The site of action of histamine and serotonin along the vascular tree: a topographic study. J. Biophys. Biochem. Cytol., 11: 607-626.
- Mann, I. C. 1924a The pecten of *Gallus domesticus*. Quart. J. Microscop. Sci., 68: 413-442.
- 1924b The function of the pecten. Brit. J. Ophthalm., 8: 209-226.
- Menner, E. 1938 Die Bedeutung des Pecten im Auge des Vogels für die Wahrnehmung von Bewegungen, nebst Bemerkungen über seine Ontogenie und Histologie. Zool. Jhb. Abt. Zool. und Physiol., 58: 481-538.
- Mihalkovics, V. 1973 Untersuchungen über den Kamm des Vogelauges. Arch. mikr. Anat., 9: 591-597.
- Millonig, G. 1961 Advantages of a phosphate buffer for OsO_4 solutions in fixation. J. Appl. Physics, 32: 1637.
- Mugnaini, E. 1964 Helical filaments in astrocytic mitochondria of the corpus striatum in the rat. J. Cell Biol., 23: 173-182.
- Muir, A. R., and A. Peters 1962 Quintuple-layered membrane junctions at terminal bars between endothelial cells. J. Cell Biol., 12: 443-448.
- Olsen, B. R. 1965 Electron microscope studies on collagen. IV. Structure of vitrosin fibrils and interaction properties of vitrosin molecules. J. Ultrast. Res., 13: 172-191.
- O'Rahilly, R., and D. B. Meyer 1961 The development and histochemistry of the pecten oculi. In: The Structure of the Eye. Ed. by G. K. Smelser, Academic Press, New York, 207-219.
- Palade, G. E. 1960 Transport in quanta across the endothelium of blood capillaries. Anat. Rec. (abs.), 136: 254.
- 1961 Blood capillaries of the heart and other organs. Circulation, 24: 368-384.
- Parks, H. F. 1961 On the fine structure of the parotid gland of mouse and rat. Am. J. Anat., 108: 303-329.
- Pearse, A. G. E. 1961 Histochemistry Theoretical and Applied. Little Brown Co., Boston.
- Prince, J. H. 1956 Comparative Anatomy of the Eye. Thomas, Springfield.
- Rhodin, J. 1958 Anatomy of kidney tubules. Int. Rev. Cytol., 7: 485-534.
- Richardson, K. C., L. Jarett and E. H. Finke 1960 Embedding in epoxy resins for ultrathin sectioning in electron microscopy. Stain Technol., 35: 313-323.
- Roth, T. F., and K. R. Porter 1964 Yolk protein uptake in the oocyte of the mosquito *Aedes aegypti* L. J. Cell Biol., 20: 313-332.
- Seaman, A. R. 1962 A correlated light and electron microscope study of the pecten oculi in the adult chicken (*Gallus domesticus*). Anat. Rec. (abs.), 142: 277-278.
- Seaman, A. R., and T. M. Himelfarb 1963 Correlated ultrafine structural changes of the avian pecten oculi and ciliary body of *Gallus domesticus*. Preliminary observations on the physiology. I. Effects of decreased intraocular pressure induced by intravenous injection of acetazolamide (Diamox). Am. J. Ophthalmol., 56: 278-296.
- Seaman, A. R., and H. Storm 1963 A correlated light and electron microscope study on the pecten oculi of the domestic fowl (*Gallus domesticus*). Exp. Eye Res., 2: 163-172.
- 1966 The uptake and transport of colloidal particles in the capillaries of the "pecten oculi" of the domestic fowl (*Gallus domesticus*). Anat. Rec. (abs.), 154: 488.
- Semba, T. 1962 The fine structure of the pecten studied with the electron microscope. I. Chick pecten. Kyushu J. Med. Sci., 13: 217-232.
- Slonaker, J. R. 1918 A physiological study of the anatomy of the eye and its accessory parts of the English sparrow (*Passer domesticus*). J. Morph., 31: 351-459.
- Tanaka, A. 1960 Electron microscopic study on the avian pectines. I. Dobutsugaku Zasshi, 69: 314-317.
- Tanaka, H. 1938 The blood-vessel distribution and pigmentation in pectens of Japanese birds. Jap. J. Med. Sci., 7: 133-151.
- Tandler, B. 1963 Ultrastructure of the human submaxillary gland. II. The base of the striated duct cells. J. Ultrast. Res., 9: 65-75.



PLATE 1

EXPLANATION OF FIGURE

- 1 Face view of a segment of the pecten lamina after vascular injection with carbon. The large vessels on left and right run a parallel, straight course from the basal to the apical edge of the organ. A dense capillary network spans the intervals between the large vessels. Anastomoses between the capillaries, are present, but they are not as frequent as apparent in this picture, in which vessels running in two different planes are superimposed. Magnification 225 X.

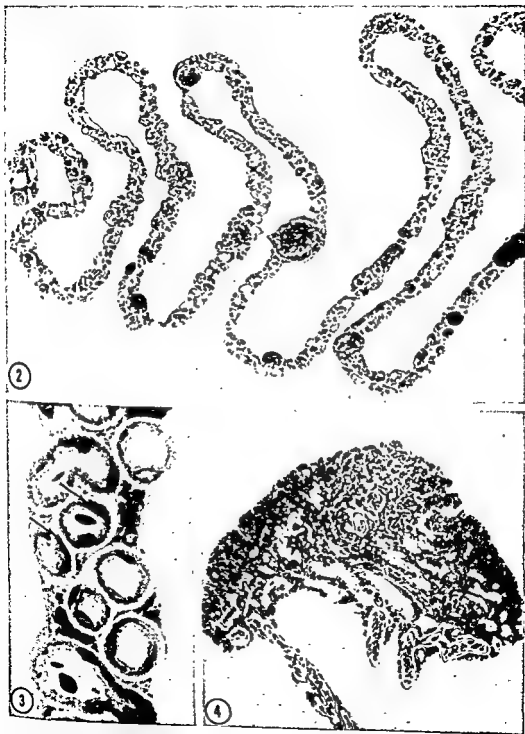


PLATE 2

EXPLANATION OF FIGURES

- 2 In transverse section the pecten appears as a thin, pleated lamina. Capillaries are generally arranged in two layers. Sizeable vessels lie both at the middle and the edges of the folds. Only the ventro-nasal portion of the transverse section of the pecten is included in the micrograph. Toluidine blue. Magnification 145 \times .
- 3 The capillaries are provided with a thick endothelium and a prominent adventitial coat. Pericytes (arrows) are closely applied to the outer surface of the endothelial cells. Cells containing granules of melanin occupy the grooves between the vessels, and thus smooth out the surface of the lamina. Toluidine blue. Magnification 1,350 \times .
- 4 At the distal edge the pecten merges into the bridge, a compact mass of pigment cells with a few, interspersed blood vessels. Toluidine blue. Magnification 175 \times .

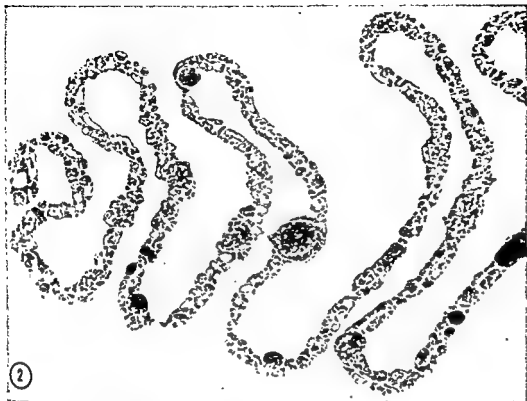


PLATE 3

EXPLANATION OF FIGURES

- 5 Oblique section through the insertion of the pecten upon the optic nerve cauda (ONC). A venule (ve) is present at the edge of a fold in the pecten. A basal artery (A) is lodged in a groove on the vitreal surface of the mass of optic nerve fibers and gives off two arterioles. Below the optic nerve cauda is a large choroidal vein (V). The arrows point to Bruch's membrane. RE: retina. PAS-hematoxylin. Magnification 235 \times .
- Serial section of the same specimen of figure 5. The venule (ve) has now reached the base of the pecten and merges with the deep choroidal vein (V). A: basal artery; ONC: optic nerve cauda; RE: retina. Toluidine blue. Magnification 235 \times .

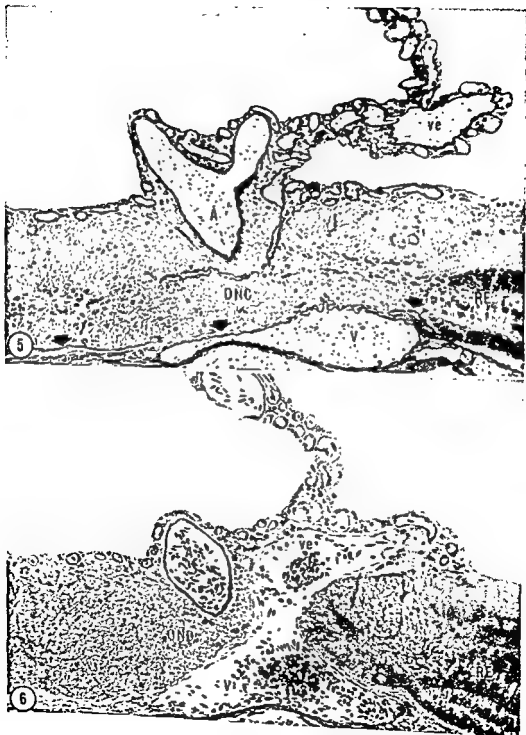


PLATE 4

EXPLANATION OF FIGURE

- 7 In this electron micrograph, the walls of two capillaries are shown, with a pigment cell in between. The lumen of the capillary above contains a heterophil leucocyte. On both the luminal and basal sides, the endothelial cells are provided with slender processes, which sometimes branch. The endothelial cell body is a continuous strip of cytoplasm intervening between the luminal and basal processes. Basal processes are tangentially cut in the vessel above and can be seen to better advantage on the lower right. The adventitia (adv) of the vessels are thick. At the center-right a flattened pericyte parallels, at some distance, the endothelial outline. A basement lamina (bl) is interposed between the adventitia of the capillaries and the pigment cells. The latter contain melanin granules, have irregular outlines and are provided with many finger-like projections. Tortuous empty spaces intervene between neighboring processes of the pigment cells. At the arrow, basement lamina-like material of the adventitia penetrates a gap between adjacent basal processes and reaches the outer surface of the endothelial cell body. Magnification 18,700 \times .



PLATE 5

EXPLANATION OF FIGURE

- The walls of two capillaries are shown, above and below. In the vessel above, three endothelial cells encircle the lumen; the arrows point to intercellular junctions. The luminal processes, at some distance from the nucleus, are longer and arranged in more regular fashion than those at the nuclear bulge. In the cytoplasm of the endothelial cells, mitochondria are scarce. Basal processes are shorter than the luminal ones. On left and right, the adventitia of the two capillaries are separated from each other by the basement laminae (bl) of the pigment cells, but fuse in the middle of the picture. Numerous fibrils of collagen permeate the adventitia. In the upper left corner, a single, thick basement lamina separates the adventitia of the capillary from the vitreous body (VB). Magnification 17,800 \times .



PLATE 6

EXPLANATION OF FIGURES

- 9 Although circular profiles are occasionally found, a grazing section of the luminal surface of the endothelial cell shows that the majority of the apical processes are lamellar in shape. The arrow points to a coated invagination of the limiting membrane of a luminal process. Magnification 23,500 \times .
- 10 The endothelial cells of the capillaries display the usual complement of cytoplasmic organelles. Two centrioles and the Golgi complex are located near the nucleus. A few mitochondria are scattered throughout the cytoplasm. A dense granule is also present (arrow). Notice that some luminal and basal processes appear disconnected from the cell body. Magnification 26,500 \times .

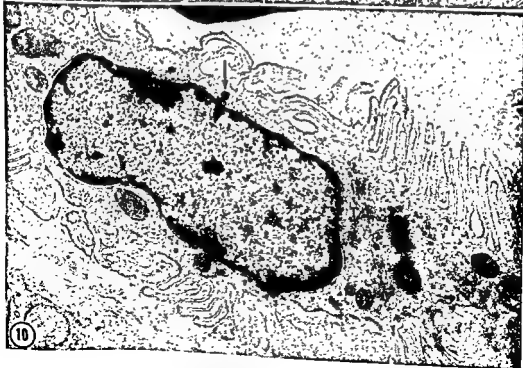


PLATE 7

EXPLANATION OF FIGURES

- 11 Two basal processes (bp) originate from the body of an endothelial cell of a capillary by a common short stalk. In this plane of section many basal processes appear disconnected from the cell body, separated from it by a large cleft filled with a moderately dense material (arrows). A similar material is irregularly condensed on the outer surface of the basal processes. A dense granule is contained in the cytoplasm of the endothelial cell. Magnification 40,000 \times .
- 12 The endothelial cells of the venules do not differ noticeably from the endothelial cells of the capillaries. Again, most basal processes appear detached from the cell body. Some are separated from it by a narrow interstice (arrows), others by a large cleft, filled with a moderately dense material. Magnification 45,000 \times .
- 13 In tangential section a basal process appears to be a pedunculated lamella with a narrow stalk (arrows). Uncoated invaginations of the plasma membrane and uncoated vesicles are indicated (v). Magnification 63,000 \times .



PLATE 8

EXPLANATION OF FIGURES

- 14 A coated invagination of the plasmalemma of a luminal lamella (star). An uncoated invagination of the plasmalemma (asterisk) originates at the base of the same lamella. End: endothelial cell body. Magnification 100,000 \times .
- 15 Junction between two endothelial cells (end) of a capillary. Two fusions or close appositions of the adjoining cell membranes are indicated by the arrows. Lp: luminal process; bp: basal process. Magnification 140,000 \times .
- 16 A pericyte is closely applied to the outer surface of the endothelium (end) of a capillary and, in places, directly contacts the basal processes of the endothelial cell (arrows). Magnification 23,500 \times .

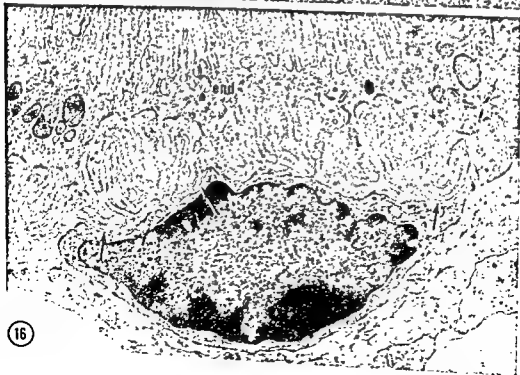
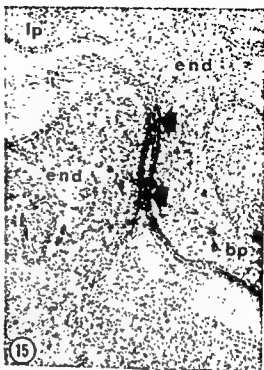


PLATE 8

EXPLANATION OF FIGURES

- 14 A coated invagination of the plasmalemma of a luminal lamella (star). An uncoated invagination of the plasmalemma (asterisk) originates at the base of the same lamella. End: endothelial cell body. Magnification 100,000 \times .
- 15 Junction between two endothelial cells (end) of a capillary. Two fusions or close appositions of the adjoining cell membranes are indicated by the arrows. Lp: luminal process; bp: basal process. Magnification 140,000 \times .
- 16 A pericyte is closely applied to the outer surface of the endothelium (end) of a capillary and, in places, directly contacts the basal processes of the endothelial cell (arrows). Magnification 23,500 \times .

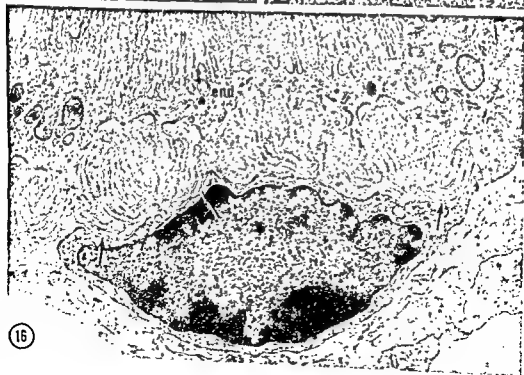
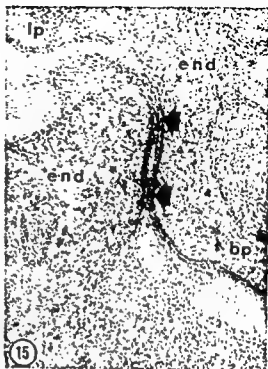


PLATE 8

EXPLANATION OF FIGURES

- 14 A coated invagination of the plasmalemma of a luminal lamella (star). An uncoated invagination of the plasmalemma (asterisk) originates at the base of the same lamella. End: endothelial cell body. Magnification 100,000 \times .
- 15 Junction between two endothelial cells (end) of a capillary. Two fusions or close appositions of the adjoining cell membranes are indicated by the arrows. Lp: luminal process; bp: basal process. Magnification 140,000 \times .
- 16 A pericyte is closely applied to the outer surface of the endothelium (end) of a capillary and, in places, directly contacts the basal processes of the endothelial cell (arrows). Magnification 23,500 \times .

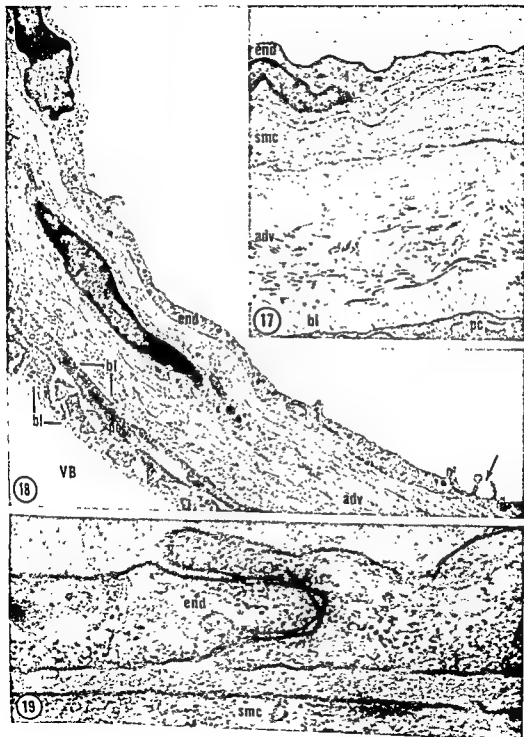


PLATE 9

EXPLANATION OF FIGURES

- 17 The wall of the arterioles of the pecten is composed of unspecialized endothelial cells (end), a single sheath of smooth muscle cells (smc) and a thick adventitia (adv). The inner region of the adventitia mainly consists of layers of basement lamina-like material, while the outer region is rich in collagen fibrils. Below, a basement lamina (bl) intervenes between the adventitia of the vessel and a pigment cell (pc). Magnification 22,200 \times .
- 18 Afferent capillaries are very large in diameter. Marginal folds are present at the endothelial cell junctions and sparse luminal processes (arrow) begin to appear. The cytoplasm of the endothelial cell contains many dense granules. A pericyte is embedded in the adventitia (adv). Processes of the pigment cells (pc) sandwiched between two basement laminae (bl) separate the adventitia of the vessel from the vitreous body (VB). End: endothelium. Magnification 16,000 \times .
- 19 In the wall of the arterioles the endothelial cells (end) are separated from the smooth muscle cells (smc) by a faint basement lamina. The junctions between adjacent endothelial cells closely parallel in morphology those seen in the wall of the capillaries. Magnification 80,000 \times .



PLATE 10

EXPLANATION OF FIGURE

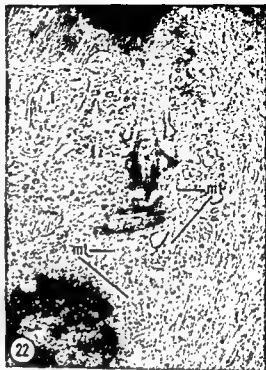
- 20 The pigment cells contain melanin granules, large mitochondria, and many bundles of filaments (f). A centriole, surrounded by the Golgi complex, is present in the cell at the center. Tortuous channels intervene between the bodies of adjacent pigment cells. Finger-like projections protrude into these spaces and also penetrate the adjacent basement lamina (bl). Magnification 26,000 X.



PLATE 11

EXPLANATION OF FIGURES

- 21 A bundle of filaments (arrow) is contained in the dilated intracristal space of a mitochondrion in a pigment cell. The filaments are obliquely cut, and their helicoidal shape is not clearly appreciated. Magnification 57,500 \times .
- 22 One of the two centrioles of a pigment cell constitutes the basal body of a flagellum. It is provided with a prominent satellite upon which a microtubule is inserted. Mt: microtubules; f: filaments. Magnification 33,000 \times .
- 23 Free in the cytoplasm of the pigment cells of the bridge are large masses of flocculent material of moderate electron density. Neighboring pigment cells are connected by tight junctions (arrows). On upper left and upper right, strands of basement lamina-like material (asterisks) are seen, which deeply penetrate between the pigment cells. Magnification 22,900 \times .



The Fine Structure of the Zona Glomerulosa and the Zona Fasciculata of the Adrenal Cortex of the Opossum¹

JOHN A. LONG AND ALBERT L. JONES

Department of Anatomy, Harvard Medical School,
Boston, Massachusetts

ABSTRACT The normal fine structure of the zona glomerulosa and the zona fasciculata of the opossum is described, with emphasis on the structure of the smooth surfaced endoplasmic reticulum (SER) and mitochondria. The cells of the zona glomerulosa are characterized by the presence of numerous rod-shaped mitochondria with shelf-like cristae, small amounts of tubular SER and moderate amounts of rough surfaced endoplasmic reticulum. The cells of the zona fasciculata possess large quantities of SER, spherical mitochondria with tubular cristae and a few profiles of rough surfaced reticulum. A Golgi apparatus is present in cells of both zones as are coated vesicles, coated invaginations of the plasmalemma, lysosomes and lipid droplets. It is concluded that the tubular SER seen in electron micrographs corresponds closely to the form of this membrane system found in the living cell. The functional significance of the associations observed among lipid droplets, mitochondria and SER are discussed.

The role of the adrenal gland in metabolism and homeostasis has been investigated for over a century. The contributions to our current understanding of this organ by investigators using the light microscope have been substantial, and it was anticipated that the electron microscope would provide further insight into the remaining problems. This expectation has not been realized. Study of the ultrastructure of the adrenal cortex has lagged behind similar investigations of other mammalian organs, largely because of the difficulty of achieving adequate preservation of the cell organelles, especially the smooth surfaced endoplasmic reticulum. In studies on the interstitial tissue of the testis, Christensen and Fawcett ('61) succeeded in preserving this organelle in the form of a continuous canalicular system and predicted that a tubular configuration of the smooth reticulum would be observed in suitably fixed specimens of other steroid secreting organs. This expectation is borne out in the present paper, which records the results of a reinvestigation of the fine structure of the adrenal cortex utilizing improved methods of fixation and embedding. Special emphasis is laid on the morphology of the endoplasmic reticulum and the mitochondria because of their major role in steroid biosynthesis. It is hoped that these

observations will correct some of the misconceptions engendered by earlier studies and will serve as a baseline for future work correlating alterations in adrenal activity with ultrastructural changes.

MATERIALS AND METHODS

Under intraperitoneal pentobarbital anesthesia, adrenal glands were removed from young adult opossums, *Didelphis virginiana*, of both sexes. Pentobarbital was employed as an anesthetic because this substance, although not a true neuroendocrine blocking agent (Munson, '63), does block stressful sensory stimuli which might cause the release of ACTH and thereby alter the morphology of the adrenal gland (Royce and Sayers, '58). The animals were killed between 8:00 A.M. and 9:00 A.M. to avoid the possibility of variations due to a diurnal rhythm in adrenal activity. The adrenals were removed quickly and cut into narrow strips that included not only the cortex but also a portion of capsule and medulla as an aid in subsequent tissue orientation. Initial fixation was carried out at 0-4°C for one hour in either Dalton's ('55) dichromate buffered osmium tetroxide or in Karnov-

¹Supported by grant GM 406-06 and grant GM 06729-06 from the Institute of General Medical Sciences, National Institutes of Health, U.S. Public Health Service.

sky's ('65) glutaraldehyde-paraformaldehyde mixture. Post-fixation of the osmium-fixed material was carried out for an additional hour in 10% neutral formalcalcium. The aldehyde-fixed material was post-fixed in Millonig's ('61) phosphate buffered osmium tetroxide. The tissues were rapidly dehydrated with increasing concentrations of cold ethanol and embedded in epon according to the technique of Luft ('61). Thick sections (1 μ) stained with toluidine blue were examined with the light microscope in order to identify and select areas for more detailed study. Thin sections were stained with lead citrate (Venable and Coggeshall, '65) and were examined in an RCA EMU 3F or 3G electron microscope. The images obtained by use of the two types of fixatives (osmium and aldehyde) are distinguishable but are similar enough to permit a single description.

OBSERVATIONS

When viewed with the light microscope, the opossum adrenal presents the familiar mammalian pattern of organization with a cortex surrounding a medulla. The cortex is clearly divisible into a zona glomerulosa, zona fasciculata and zona reticularis. The columnar cells of the zona glomerulosa are arranged in arcades while the cells of the zona fasciculata form nearly straight cords which are one cell thick and separated from adjacent cords by vascular spaces. The zona reticularis is a relatively thin zone adjacent to the medulla and is composed of an irregular array of darker staining cells. Lipid droplets are found in all of the cortical cells but are most abundant in the outermost cells of the fasciculata.

Zona glomerulosa

Electron micrographs of low magnification reveal to advantage the form of the cells in the zona glomerulosa and the number and disposition of their organelles (fig. 1). The endoplasmic reticulum comprises both the agranular and granular form of this organelle. The smooth surfaced endoplasmic reticulum is not as prevalent as in the zona fasciculata (compare figs. 4, 11) but is represented by tubular elements of considerable length (figs.

4, 7) and not by vesicles as has been so commonly reported in the literature. The tubules have a cross-sectional diameter of approximately 500A and freely anastomose with one another. The rough surfaced or granular form of the reticulum is relatively more abundant than in the cells of the fasciculata. It is not aggregated in parallel cisternae but is, for the most part, tubular in form and distributed throughout the cytoplasm. In many places there are clear communications between the two categories of reticulum (arrow, figs. 4, 7). In addition to the ribosomes associated with the reticulum, many clusters of ribosomes are found free in the cytoplasmic matrix.

Numerous short, rod-like mitochondria are present. For the most part, the inner membrane is thrown into flat lamelliform cristae but occasional cristae are encountered that have the angular appearance described for mitochondria of certain other cell types by Revel et al. ('63) (fig. 4). Several small dense granules are usually seen in the matrix of each mitochondrion.

The well developed Golgi apparatus is situated close to the nucleus but seemingly in no special orientation with respect to the vascular pole of the cell (figs. 1, 14, 15). There is, however, a tendency for the fenestrated outermost Golgi cisterna to be oriented toward the cell surface (fig. 14). A large number of small vesicles, some of which have the appearance of coated vesicles, are associated with the cisternae of the Golgi complex (arrow, fig. 15). One or two centrioles are commonly found in the Golgi region. In several instances a rudimentary cilium was observed developing from a centriole, but a fully formed typical cilium has not been seen. Multivesicular bodies are also observed from time to time in close proximity to the Golgi apparatus.

Dense, membrane-limited structures, presumed to be lysosomes, are frequent in cells of the zona glomerulosa (figs. 4, 7). Similar granules, noted in the rat adrenal cortex by Belt ('58), were referred to as microbodies by that author. However, Penney and Barnett ('65), working with rat and hamster adrenal have identified similar granules as lysosomes by their his-

tochemically demonstrable acid phosphatase activity.

Most glomerulosa cells have from one to several lipid droplets included within each plane of section. The droplets are in the matrix of the cytoplasm, not bounded by a membrane and show a wide variation in size. Some droplets are spherical whereas others have irregular outlines (fig. 2). Mitochondria and profiles of smooth reticulum are occasionally found in close association with their surface.

The nucleus is irregular in outline and may be somewhat eccentrically placed in the cell. As usual, the pores in the nuclear envelope are closed by a thin dense septum or diaphragm (fig. 7). The nucleolus is relatively large and is often at the periphery of the nucleus (figs. 1, 17). It is composed of fine filamentous material in which are suspended granules somewhat smaller than cytoplasmic ribosomes.

The limiting membrane of the glomerulosa cell is smooth over most of its surface but shows irregularly oriented microvilli on lateral surfaces where several cells meet and on surfaces bordering on the subendothelial space. Coated invaginations of the plasmalemma are regularly observed (figs. 4, 7), which may be related to the coated vesicles seen in the Golgi region. A few poorly differentiated desmosomes are seen along the boundary between adjacent parenchymal cells. At such sites, the membranes of the two cells are slightly closer together and there is a local increase in the electron density of the membranes and of the immediately adjacent cytoplasm (fig. 15). The basement lamina is seen only at surfaces next to the perivascular space (fig. 4).

Zona fasciculata

The cells of the zona fasciculata make up most of the thickness of the cortex and have relatively more cytoplasm than the cells of the zona glomerulosa. A low power electron micrograph is presented in figure 8.

The most striking feature of the cytology of this zone is the elaborate development of the smooth surfaced cytoplasmic membranes (figs. 8, 11, 12, 13, 16), which form an anastomosing system of tubular elements that seem to fill most of the cell.

Its tubular appearance and plexiform configuration are in marked contrast to the discontinuous vesicular nature of this organelle as described heretofore. The diameter of the tubules ranges from 500–1000A. They seem to have a content of appreciable density (figs. 12, 13) but this appearance is in part attributable to the fact that the full thickness of many of the slender tubules is included within the section and the membranes on both their upper and lower surfaces scatter electrons and thereby contribute to the density observed. When seen in cross section, the interior of tubules shows little density (arrow, fig. 13). On rare occasions, we have observed round dense particles approximately 500A in diameter within the lumen of the smooth endoplasmic reticulum (arrows, figs. 5, 6). The chemical nature of these particles is unknown.

Rough surfaced membranes of the endoplasmic reticulum are rare but many ribosomes are free in the ground cytoplasm. Short profiles of the granular reticulum are occasionally observed in continuity with the agranular membranes (arrow, fig. 8).

Mitochondria in the zona fasciculata are larger and more pleomorphic than those of the glomerulosa. In addition, their inner membranes are in the form of tubules of varying length in contrast to the predominately lamellar cristae seen in mitochondria of the glomerulosa (compare figs. 4, 11).

The Golgi region is occupied by arrays of parallel cisternae with numerous associated vesicles (fig. 16). Some of the vesicles appear to be of the coated variety. When the Golgi sacs are seen *en face*, they present a fenestrated appearance (arrow, fig. 16). Occasionally, one or two centrioles are seen in the Golgi region (figs. 9, 10). An inclusion of unknown significance is sometimes encountered near the Golgi apparatus (inset, fig. 11). In section, it appears about 0.2 to 0.4 μ in diameter and comprises two concentric membranous elements about 250–300A apart. Between the two membranes are what appear to be radial striations with a hint of a central line midway between the two membranes. In the center of the structure are other

components which may be part of the ground cytoplasm.

Lipid droplets are not abundant in this zone except in its outermost part, but they are larger than those in the zona glomerulosa (fig. 2, compare with fig. 3). As in the glomerulosa, the variations in their appearance may reflect variations in physiological state or chemical composition of the lipid. Mitochondria and elements of the smooth endoplasmic reticulum are occasionally seen in close association with the lipid droplets. We have found no evidence to support Belt's thesis ('58) that lipid droplets may arise from "microbodies" (here interpreted as lysosomes).

The nucleus of cells in the fasciculata is spherical and is bounded by a typical nuclear envelope. The nucleolus is less compact than in the cells of the zona glomerulosa and it appears to be made up of a granular component of approximately the same dimensions as cytoplasmic ribosomes and a filamentous component.

The plasma membranes of adjacent parenchymal cells are smooth and closely apposed. In certain areas there are thickenings and increased density of small portions of adjacent limiting membranes which are thought to represent attachment zones. Microvilli adjacent to the subendothelial space are more prominent in this cell type than in the cells of the glomerulosa. Coated invaginations are also seen at the surfaces of the cells of this zone but less frequently than in the cells of the glomerulosa. A basement lamina covers those surfaces of the cell bordering on the subendothelial space.

The endothelium of the vascular channels is of the fenestrated type—attenuated regions in the endothelium are penetrated by pores which are closed only by a very thin diaphragm (arrow, fig. 18). The cells lining the sinusoids of the adrenal cortex are often assumed to belong to the reticuloendothelial system, but no evidence of phagocytosis was seen in endothelial cells in this study.

Small fibers exhibiting the periodicity typical of collagen are found in the subendothelial space and are interpreted as corresponding to the reticular fibers demonstrated in this location by light microscopists. Cells in the subendothelial space

are of two types. One appears to be a fibroblast (fig. 18) and is the probable source of the reticular fibers. The other type is a rather large, rounded cell with few signs of cytoplasmic differentiation. These may correspond to the hematopoietic cells referred to by Deane ('62, p. 23).

An interesting negative observation is that we have seen no evidence of glycogen in the cortical cells of this species although our preliminary chemical determinations by the Somogyi-Nelson method indicate the presence of up to 0.4 mg glycogen per 100 gm cortical tissue. It is possible that the glycogen may be present in the beta form and not readily distinguishable from ribosomes in thin sections (Revel, '64).

DISCUSSION

Over the past decade, numerous ultrastructural investigations have been carried out on the normal and experimentally altered adrenal cortex. Much of the early work utilized tissue that was inadequately fixed according to present-day standards. Nonetheless, far reaching functional interpretations were based on this poorly preserved material. Some of these conclusions must now be re-examined in the light of improved techniques of fixation and embedding.

In earlier studies, the smooth endoplasmic reticulum of the adrenal cortex was described as a population of closed vesicles of varying diameter. Exceptions are the work of Ross et al. ('58), Volk and Scarpelli ('64) and Penney and his co-workers ('63) who have illustrated a tubular configuration of the smooth endoplasmic reticulum similar in morphology to that reported in this paper. The tubular nature of this membrane system has also been demonstrated in other cell types known to be secreting steroid hormones, such as the corpus luteum (Enders, '62; Enders and Lyons, '64) and the interstitial cells of the testis (Christensen, '65; Christensen and Fawcett, '61; '66). That this configuration of the agranular reticulum is the form more likely to be found in the living cell can be supported by three arguments. (1) In the living cell, a continuous input of energy would be required to maintain the tubular form whereas the vesicular form is the configuration of minimum free en-

ergy. Rapid fixation would be expected to maintain the *in vivo* form of this membrane system but fixation itself would not be expected to convert vesicles to tubules since this would involve a change to a higher energy state. (2) Two different types of primary fixatives, namely osmium tetroxide and glutaraldehyde, preserve the tubular form of the SER. This suggests that this form is not due to some vagary of a particular fixative. (3) Tubular agranular reticulum is observed in the outer portions of a block of tissue where the other organelles are well fixed by currently accepted standards, whereas the vesicular form is seen in the more central regions of the block where damaged mitochondria and other evidences of inadequate tissue preservation abound.

The biochemical pathways leading to the formation of adrenal steroids and the subcellular localization of the enzymes involved form the background against which the morphology of the adrenal cortex must be interpreted. Acetate is converted to cholesterol through a long series of intermediates and the enzymes responsible for this sequence are localized in the soluble, mitochondrial and microsomal fractions of cell homogenates (Popják and Cornforth, '60; Olson, '65). The cholesterol thus formed may be attacked by pregnenolone synthetase, found in mitochondria (Halkerston et al., '61), which leads to scission of the sidechain and the formation of pregnenolone and isocaproic aldehyde. Pregnenolone then undergoes an irreversible dehydrogenation and shift of the double bond from C5-6 to C4-5 catalyzed by a microsomal enzyme system yielding progesterone as the product (Beyer and Samuels, '56). This key intermediate is then hydroxylated at various positions to yield the steroid hormones of the adrenal cortex. The 21 hydroxylase and the 17 α hydroxylase are both microsomal enzymes and require NADPH, and molecular oxygen for activity (Hofmann, '60; Ryan and Engel, '57), while 11 β hydroxylase activity is found in mitochondrial fractions (Sharma et al., '62; Hayano and Dorfman, '62).

The purity of the fractions used by those approaching the problem with biochemical methods have not been checked by observation with the electron microscope. The

microsomal fraction of adrenal cell homogenates is no doubt largely derived from the smooth endoplasmic reticulum since morphological studies show that this is by far the most abundant of the membrane systems of the cell.

From the above information, it is possible to predict certain topographic relationships among the lipid droplets, mitochondria and smooth endoplasmic reticulum of the adrenocortical cell which may be morphological correlates of the biosynthetic pathway outlined above.

Much of the cholesterol and cholesterol ester is revealed to be in the lipid droplets by the Schultz reaction, a histochemical modification of the Liebermann-Burchardt color reaction (see Deane, '62, for many references). Since microsomal enzymes are responsible for some of the final steps in the synthesis of cholesterol, the frequently observed association of smooth endoplasmic reticulum with lipid droplets becomes meaningful. On the other hand, Armstrong et al. ('64) working with *Corpora lutea*, have obtained evidence that newly synthesized cholesterol does not equilibrate rapidly with the total cellular cholesterol and that the newly synthesized fraction is preferentially utilized for progesterone formation. Fawcett ('63) has suggested that a function of the SER could be the storage of cholesterol as a component of the membrane with the implication that this cholesterol would be more readily available for hormone synthesis than that stored in lipid droplets.

Since pregnenolone synthetase, the enzyme responsible for side chain cleavage and the formation of pregnenolone is found in mitochondria, a close association between the site of storage (lipid droplets, SER) or synthesis (membranes of SER) of cholesterol and the localization of this enzyme would be expected. Christensen and Fawcett ('66) have described close associations between smooth membranes and mitochondria in mouse interstitial cells and Lindner ('66) has briefly reported similar findings in cells of the juxtamedullary region of the hedgehog adrenal. Penney ('66) reports depletion of lipid droplets and closer juxtaposition of mitochondria to the droplets in the adrenal cortex of cold stressed guinea pigs. We

have seen indications of these relationships in normal opossum adrenal cells. Acute stimulation with ACTH might make them more prominent.

Certain of the hydroxylases catalyzing the formation of corticosteroids from progesterone are found in the microsomal fraction which in the intact adrenocortical cell is almost certainly represented by the abundant smooth endoplasmic reticulum. In the case of long term functional demand for hormone production, an hypertrophy of the agranular reticulum is to be expected. An analogous situation occurs in hepatocytes when phenobarbital is administered to hamsters and other mammals (review, Jones and Fawcett, '66). The hydroxylases responsible for the detoxification of this compound are localized in the SER and in response to increased functional demand, this system of membranes is increased in quantity.

Other authors have attempted to relate their ultrastructural findings to the information concerning the pathways of steroid hormone biosynthesis and the subcellular localization of enzymatic activity. Discontinuities in mitochondrial membranes or the formation of blebs from the outer membrane in adrenals of normal animals have been reported (Lever, '56; Luse, '61; Nishikawa et al., '63; Sabatini and deRobertis, '61; Sabatini et al., '62; and Schwartz et al., '62). The frequency of this appearance is said to be increased after ACTH injection or stress. In a study of cellular changes in the zona glomerulosa of rats after stimulation of this zone by sodium deprivation, Giacomelli et al. ('65) report the presence of mitochondria which appear to be open to the surrounding cytoplasm. Certain of the authors making such claims (Sabatini and deRobertis, '61; Sabatini et al., '62; Schwartz et al., '62; Giacomelli et al., '65) propose that the openings in the mitochondrial membrane and the vesicles apparently pinched off from mitochondria are a morphological expression of the pathway that steroid hormone precursors take from the mitochondria to the surrounding cytoplasm where further enzymatic changes take place. These phenomena have not been observed in our material. Neither did Yates ('65) report discontinuous outer mitochondrial

membranes in the zona reticularis of the Syrian hamster after ACTH administration. We believe these appearances can be explained as due either to inadequate preservation of the mitochondria or as consequences of tangential sectioning of the ends of mitochondria giving a spurious appearance of continuity between mitochondrial matrix and ground cytoplasm.

Golgi material and secretion

A large amount of information has accumulated concerning protein secreting cells as a result of the combined efforts of morphologists and biochemists utilizing the techniques of cell fractionation, electron microscopy and autoradiography (Palade et al., '62; Revel and Hay, '63). These investigations have established that the protein secretion accumulates in the Golgi region and is discharged from the cell when the membrane surrounding the secretion granule fuses with the plasma-lemma.

On the other hand, the process whereby steroid hormones are secreted is poorly understood. No visible accumulation of secretory product occurs and no evidence is seen of hormone release from the surface of the cells. This may be explained in part by the fact that steroid hormones are effective in low concentrations and large quantities of hormone are not present in the cells at a given moment.

The participation of Golgi material in the secretion of lipids has not been extensively investigated. Palay ('58) has observed that the Golgi complex plays a role in the production of the secretory product of Meibomian glands and Ellis and Henrikson ('63) suggest that sebum is segregated in cisternae of the Golgi material in partially mature cells of human sebaceous glands.

Reese and Moon ('38) observed that hypophysectomy of the rat produces shrinkage of the Golgi of fasciculata cells while injection of ACTH induces marked hypertrophy of this organelle. These observations suggest that the Golgi material may play some part in the secretion of steroid hormones from adrenocortical cells. Electron microscopic studies have not been notably successful in elucidating this aspect of adrenal cytology. Penney ('65) has

noted that in cold-stressed rats, the Golgi apparatus has a normal appearance and other investigators (Sabatini et al., '62; Yates, '65) studying adrenals in various animals after hypophysectomy and injection of ACTH report no changes in the Golgi material.

The Golgi apparatus is also involved in sulfation of mucopolysaccharides in goblet cells (Lane et al., '64) and in the chondrocyte (Godman and Lane, '64) and possibly in the synthesis or segregation of complex polysaccharides in the acrosome of spermatis (Fawcett, '59) and in Brunner's glands in mice (Friend, '65).

With the above facts in mind, we may speculate on the role played by the Golgi apparatus in adrenocortical cells. The Golgi apparatus in this cell type is large and appears to be active by currently accepted cytological criteria. The inactive Golgi is characterized by the presence of flattened cisternae while an active organelle is more dispersed and the cisternae appear shorter and often distended (Friend, '65; Fawcett, '66). This is consistent with the previously mentioned light microscopical results. Recent biochemical investigations have emphasized the importance of steroid conjugates, particularly sulfates, in biosynthetic reactions (Calvin et al., '63). It is possible that conjugation of steroid hormones occurs in the Golgi apparatus of adrenocortical cells and that the product is secreted as the more water-soluble sulfate or glucuronide. The presence of coated vesicles in the Golgi region and the similarity of these vesicles to the coated invaginations noted at the cell surface suggest the possibility that these specialized membranous elements may be a pathway for the secretion of hormonal steroids.

Belt et al. ('65) have reported electron dense granules bounded by a smooth membrane within the cytoplasm of pelican adrenal cells. Granules of similar dimensions and electron density but without the membrane were observed between adjacent parenchymal cells and in the subendothelial space. Occasional small invaginations of the plasmalemma were also noted. Belt et al. suggest that the dense bodies are hormone synthesized within the smooth membranes, carried to the cell surface and secreted by a process of reverse pinocytosis.

The plasmalemmal invaginations illustrated by these authors appear to be similar to the coated invaginations seen in the opossum adrenal and we have noted dense granules within the lumen of the endoplasmic reticulum which may correspond to the granules observed by Belt and his co-workers. Autoradiography utilizing labelled cholesterol as a hormonal precursor may help clarify the secretory pathway in these cells.

Endothelium

The final barriers interposed between the secreted hormone and the vascular space are the basement lamina and the endothelium. The basement lamina is a continuous structure over the surface of the parenchymal cells adjacent to the vascular space. The endothelium is of the fenestrated type with but a thin diaphragm closing the fenestrae. Whether either of these structures is an impediment to the passage of steroid hormones is not known.

Most authors agree in calling the vascular channels of the adrenal cortex sinusoids but in some cases for the wrong reasons. Sinusoids were originally defined by Minot ('00) as irregular endothelial lined vascular spaces, usually of large and variable caliber, in close association with the parenchyma. This particular relationship develops embryologically by an ingrowth of the parenchyma into a large vascular space. This is in contrast to the development of typical capillaries where vasoformative cells are added to the ends of previously formed vessels producing dichotomous growth. Some time after Minot's definition of sinusoids, the capacity for phagocytosis by the endothelial cells was added as a characteristic. This is an attribute of the cells lining liver sinusoids and was formerly thought to be characteristic of the sinusoidal vascular network of endocrine organs as well. In the adrenal cortex it is now thought (Greep, '61) that the endothelial cells are non-phagocytic and that the deposits of vital dye observed by many earlier microscopists are simply adsorbed to the surfaces of the lining cells or are taken up by subendothelial macrophages. We have seen no evidences of phagocytosis on the part of the endothelial cells but, based on the ontogenetic criteria

have seen indications of these relationships in normal opossum adrenal cells. Acute stimulation with ACTH might make them more prominent.

Certain of the hydroxylases catalyzing the formation of corticosteroids from progesterone are found in the microsomal fraction which in the intact adrenocortical cell is almost certainly represented by the abundant smooth endoplasmic reticulum. In the case of long term functional demand for hormone production, an hypertrophy of the agranular reticulum is to be expected. An analogous situation occurs in hepatocytes when phenobarbital is administered to hamsters and other mammals (review, Jones and Fawcett, '66). The hydroxylases responsible for the detoxification of this compound are localized in the SER and in response to increased functional demand, this system of membranes is increased in quantity.

Other authors have attempted to relate their ultrastructural findings to the information concerning the pathways of steroid hormone biosynthesis and the subcellular localization of enzymatic activity. Discontinuities in mitochondrial membranes or the formation of blebs from the outer membrane in adrenals of normal animals have been reported (Lever, '56; Luse, '61; Nishikawa et al., '63; Sabatini and deRobertis, '61; Sabatini et al., '62; and Schwartz et al., '62). The frequency of this appearance is said to be increased after ACTH injection or stress. In a study of cellular changes in the zona glomerulosa of rats after stimulation of this zone by sodium deprivation, Giacomelli et al. ('65) report the presence of mitochondria which appear to be open to the surrounding cytoplasm. Certain of the authors making such claims (Sabatini and deRobertis, '61; Sabatini et al., '62; Schwartz et al., '62; Giacomelli et al., '65) propose that the openings in the mitochondrial membrane and the vesicles apparently pinched off from mitochondria are a morphological expression of the pathway that steroid hormone precursors take from the mitochondria to the surrounding cytoplasm where further enzymatic changes take place. These phenomena have not been observed in our material. Neither did Yates ('65) report discontinuous outer mitochondrial

membranes in the zona reticularis of the Syrian hamster after ACTH administration. We believe these appearances can be explained as due either to inadequate preservation of the mitochondria or as consequences of tangential sectioning of the ends of mitochondria giving a spurious appearance of continuity between mitochondrial matrix and ground cytoplasm.

Golgi material and secretion

A large amount of information has accumulated concerning protein secreting cells as a result of the combined efforts of morphologists and biochemists utilizing the techniques of cell fractionation, electron microscopy and autoradiography (Palade et al., '62; Revel and Hay, '63). These investigations have established that the protein secretion accumulates in the Golgi region and is discharged from the cell when the membrane surrounding the secretion granule fuses with the plasma-lemma.

On the other hand, the process whereby steroid hormones are secreted is poorly understood. No visible accumulation of secretory product occurs and no evidence is seen of hormone release from the surface of the cells. This may be explained in part by the fact that steroid hormones are effective in low concentrations and large quantities of hormone are not present in the cells at a given moment.

The participation of Golgi material in the secretion of lipids has not been extensively investigated. Palay ('58) has observed that the Golgi complex plays a role in the production of the secretory product of Meibomian glands and Ellis and Henrikson ('63) suggest that sebum is segregated in cisternae of the Golgi material in partially mature cells of human sebaceous glands.

Reese and Moon ('38) observed that hypophysectomy of the rat produces shrinkage of the Golgi of fasciculata cells while injection of ACTH induces marked hypertrophy of this organelle. These observations suggest that the Golgi material may play some part in the secretion of steroid hormones from adrenocortical cells. Electron microscopic studies have not been notably successful in elucidating this aspect of adrenal cytology. Penney ('65) has

- the organs of Vertebrata. *Proc. Boston Soc. Nat. Hist.*, 29: 185-215.
- Munson, P. L. 1963 Pharmacology of neuroendocrine blocking agents. In: *Advances in Neuroendocrinology*. (A. V. Nalbandov, ed.) University of Illinois Press, Urbana, Illinois. pp. 427-444.
- Nishikawa, M., I. Murone and T. Sato 1963 Electron microscopic investigations of the adrenal cortex. *Endocrinol.*, 72: 197-209.
- Olson, J. A. 1965 The biosynthesis of cholesterol. *Ergh. Physiol.*, 56: 173-215.
- Palade, G. E., P. Siekevitz and L. G. Caro 1962 Structure, chemistry and function of the pancreatic exocrine cell. In: *The Exocrine Pancreas*. (A. V. S. DeReuck and M. Cameron, eds.) Ciba Foundation Symposium. Little, Brown and Co., Boston. pp. 23-48.
- Palay, S. L. 1958 The morphology of secretion. In: *Frontiers in Cytology*. (S. L. Palay, ed.) Yale University Press, New Haven. pp. 305-342.
- Penney, D. P. 1965 Some fine structural changes in the rat adrenal cortex following short term exposure to cold. *Anat. Rec.*, 151: 469.
- 1966 Fine structural localization of esterase in the guinea pig adrenal cortex. *Anat. Rec.*, 154: 481.
- Penney, D. P., and R. J. Barneff 1965 The fine structural localization and selective inhibition of nucleoside phosphatases in the rat adrenal cortex. *Anat. Rec.*, 152: 265-278.
- Penney, D. P., D. I. Patt and W. C. Dixon, Jr. 1963 The fine structure of regenerating adrenocortical autotransplants in the rat. *Anat. Rec.*, 146: 319-335.
- Popják, G., and J. W. Cornforth 1960 The biosynthesis of cholesterol. *Adv. Enzymol.*, 22: 281-335. Interscience Publishers, Inc., New York.
- Reese, J. D., and H. D. Moon 1938 The Golgi apparatus of the cells of the adrenal cortex after hypophysectomy and on the administration of the adrenocorticotrophic hormone. *Anat. Rec.*, 70: 543-558.
- Revel, J. P. 1964 Electron microscopy of glycogen. *J. Histochem. Cytochem.*, 12: 104-114.
- Revel, J. P., D. W. Fawcett and C. W. Philpott 1963 Observations on mitochondrial structure. Angular configurations of the cristae. *J. Cell Biol.*, 16: 187-195.
- Revel, J. P., and E. D. Hay 1963 An autoradiographic and electron microscopic study of collagen synthesis in differentiating cartilage. *Zeit. Zellforsch.*, 61: 110-144.
- Ross, M. H., G. D. Pappas, J. T. Lanman and J. Lind 1958 Electron microscope observations on the endoplasmic reticulum in the human fetal adrenal. *J. Biophys. Biochem. Cytol.*, 4: 659-662.
- Royce, P. C., and G. Sayers 1958 Blood ACTH: Effects of ether, pentobarbital, epinephrine and pain. *Endocrinol.*, 63: 794-800.
- Ryan, K. J., and L. L. Engel 1957 Hydroxylation of steroids at C-21. *J. Biol. Chem.*, 225: 103-114.
- Sabatini, D. D., and E. D. P. deRobertis 1961 Ultrastructural zonation of adrenocortex in the rat. *J. Biophys. Biochem. Cytol.*, 9: 105-119.
- Sabatini, D. D., E. D. P. deRobertis and H. B. Bleicher 1962 Submicroscopic study of the pituitary action on the adrenocortex of the rat. *Endocrinol.*, 70: 390-406.
- Schwartz, W., H. J. Merker and G. Suchowsky 1962 Elektronenmikroskopische Untersuchungen über die Wirkungen von ACTH und Stress auf die Nebennierenrinde der Ratte. *Virchows Arch. Path. Anat.*, 335: 165-179.
- Sharma, D. C., E. Forchielli and R. I. Dorfman 1962 Preparation and properties of a soluble steroid 11 β -hydroxylase from bovine adrenal cortex. *J. Biol. Chem.*, 237: 1495-1499.
- Venable, J. H., and R. Coggeshall 1965 A simplified lead citrate stain for use in electron microscopy. *J. Cell Biol.*, 25: 407-408.
- Volk, T. L., and D. G. Scarpelli 1964 Alterations of fine structure of the rat adrenal cortex after administration of triparanol. *Lab. Invest.*, 13: 1205-1214.
- Yates, R. D. 1965 Fine structural observations on untreated and ACTH treated adrenocortical cells of the zona reticularis of Syrian hamsters. *Zeit. Zellforsch.*, 66: 384-395.

Note Added in Proof

In a recent study of the adrenal cortex of the Rhesus monkey, R. M. Brenner (*Am. J. Anat.*, 119: 429-454, 1966) has also demonstrated the tubular nature of the SER in cells of this gland.

of Minot ('00), the vascular channels can still be classified as sinusoids.

ACKNOWLEDGMENTS

The authors wish to thank Drs. D. W. Fawcett and E. D. Hay for their critical reading of the manuscript and Miss Gabrielle Rouiller for her technical assistance.

LITERATURE CITED

- Armstrong, D. T., J. O'Brien and R. O. Greep 1964 Effects of luteinizing hormone on prostest biosynthesis in the luteinized rat ovary. *Endocrinol.*, 75: 488-500.
- Belt, W. D. 1958 The origin of adrenal cortical mitochondria and liposomes: a preliminary report. *J. Biophys. Biochem. Cytol.*, 4: 337-340.
- Belt, W. D., M. N. Sheridan, R. A. Knouff and F. A. Hartman 1965 Fine structural study of a possible mechanism of secretion by the interrenal cells of the brown pelican. *Zeit. Zellforsch.*, 68: 864-873.
- Beyer, K. F., and L. T. Samuels 1956 Distribution of steroid-3 β -ol-dehydrogenase in cellular structures of the adrenal gland. *J. Biol. Chem.*, 219: 69-76.
- Calvin, H. I., R. L. VandeWiele and S. Lieberman 1963 Evidence that steroid sulfates serve as biosynthetic intermediates: *in vivo* conversion of pregnenolone-sulfate-S³⁵ to dehydroisoandrosterone-sulfate-S³⁵. *Biochem.*, 2: 648-653.
- Christensen, A. K., and D. W. Fawcett 1961 The normal fine structure of opossum testicular interstitial cells. *J. Biophys. Biochem. Cytol.*, 9: 653-670.
- Christensen, A. K. 1965 The fine structure of testicular interstitial cells in guinea pigs. *J. Cell Biol.*, 26: 911-935.
- Christensen, A. K., and D. W. Fawcett 1966 The fine structure of testicular interstitial cells in mice. *Am. J. Anat.*, 118: 551-571.
- Dalton, A. J. 1955 A chrome-osmium fixation for electron microscopy. *Anat. Rec.*, 121: 281.
- Deane, H. W. 1962 The anatomy, chemistry and physiology of adrenocortical tissue. In: *Handbuch der Experimentellen Pharmacologie*. (O. Eichler and A. Farah, eds.) Vol. 14, Part 1, pp. 1-185. Springer-Verlag, Berlin.
- Ellis, R. A., and R. L. Henrikson 1963 The ultrastructure of the sebaceous glands of man. *Adv. Biol. Skin*, 4: 94-109. Macmillan Co., New York.
- Enders, A. C. 1962 Observations on the fine structure of lutein cells. *J. Cell Biol.*, 12: 101-113.
- Enders, A. C., and N. R. Lyons 1964 Observations on the fine structure of lutein cells. II. The effects of hypophysectomy and mammothrophic hormone in the rat. *J. Cell Biol.*, 22: 127-141.
- Fawcett, D. W. 1959 Changes in the fine structure of the cytoplasmic organelles during differentiation. In: *Developmental Cytology* (D. Rudnick, ed.) 16th Symposium of the Society for the Study of Development and Growth. The Ronald Press Co., New York. pp. 161-189.
- 1963 Structural and functional variations in the membranes of the cytoplasm. In: *Intracellular Membranous Structure* (S. Seno and E. V. Cowdry, eds.) Symposia of the Society for Cellular Chemistry, Vol. 14. Okayama, Japan. pp. 15-40.
- 1966 An Atlas of Fine Structure. The Cell. Its Organelles and Inclusions. W. B. Saunders Co., Philadelphia, pp. vii-448.
- Friend, D. S. 1965 The fine structure of Brunner's glands in the mouse. *J. Cell Biol.*, 25: 563-576.
- Glacemelli, F., J. Wiener and D. Spiro 1965 Cytological alterations related to stimulation of the zona glomerulosa of the adrenal gland. *J. Cell Biol.*, 26: 499-521.
- Godman, G. C., and N. Lane 1964 On the site of sulfation in the chondrocyte. *J. Cell Biol.*, 21: 353-366.
- Greep, R. O. 1961 The structure of the adrenal cortex. In: *The Adrenal Cortex* (H. D. Moon, ed.) Paul B. Hoeber, Inc., New York. pp. 23-45.
- Halkerston, I. D. K., J. Eickhorn and O. Hechter 1961 A requirement for reduced triphosphopyridine nucleotide for cholesterol side-chain cleavage by mitochondrial fractions of bovine adrenal cortex. *J. Biol. Chem.*, 236: 374-380.
- Hayano, M., and R. I. Dorfman 1962 Enzymes of steroid hydroxylation. In: *Methods in Enzymology* (S. P. Colowick and N. O. Kaplan, eds.) Academic Press, New York. pp. 503-512.
- Hofmann, F. G. 1960 Steroid C-17 hydroxylation in guinea-pig-adrenal homogenates. *Biochim. Biophys. Acta*, 37: 566-567.
- Jones, A. L., and D. W. Fawcett 1966 Hypertrophy of the agranular endoplasmic reticulum in hamster liver induced by phenobarbital (with a review of the functions of this organelle in liver). *J. Histochem. Cytochem.*, 14: 215-232.
- Karnovsky, M. J. 1965 A formaldehyde-glutaraldehyde fixative of high osmolarity for use in electron microscopy. *J. Cell Biol.*, 27: 137A-138A.
- Lane, N., L. Caro, L. R. Otero-Villardebó and G. C. Godman 1964 On the site of sulfation in colonic goblet cells. *J. Cell Biol.*, 21: 339-351.
- Lever, J. D. 1956 Physiologically induced changes in adrenocortical mitochondria. *J. Biophys. Biochem. Cytol.*, 2 (Suppl.): 313-318.
- Lindner, E. 1966 Mitochondrien mit Vesikeln in dichter Kugelpackung und ihre Bedeutung für die Funktion der juxtamedullären Zone der Nebennierenrinde vom Igel (*Eriacus europaeus* L.). *Naturwissenschaften*, 53: 43-44.
- Luft, J. H. 1961 Improvements in epoxy resin embedding methods. *J. Biophys. Biochem. Cytol.*, 9: 409-414.
- Luse, S. 1961 Electron microscopic observations on the adrenal gland. In: *The Adrenal Cortex* (H. D. Moon, ed.) Paul B. Hoeber, Inc., New York. pp. 46-69.
- Millonig, G. 1961 Advantages of a phosphate buffer for OsO₄ solutions in fixation. *J. Appl. Phys.*, 32: 1637.
- Minot, C. S. 1900 On a hitherto unrecognized form of blood circulation without capillaries in



PLATE 1

EXPLANATION OF FIGURE

- 1 Low power electron micrograph of several cells of the opossum zona glomerulosa. The nuclei are large in relation to the overall cell size and contain one or two prominent nucleoli. A cross section of an invagination of the nuclear envelope is seen at the arrow. Rod-shaped mitochondria are abundant and distributed evenly throughout the cytoplasm except for a small peripheral zone. Golgi material (G) and electron dense granules (lysosome, ly) are in evidence. Dalton's fixative. 8,100 X.

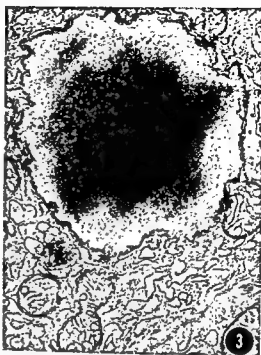


PLATE 2

EXPLANATION OF FIGURES

- 2, 3 Lipid droplets in the zona glomerulosa (fig. 2) are considerably smaller than those of the zona fasciculata (fig. 3). The significance, if any, of the differences in density of the droplets, is unknown. Elements of the smooth surfaced endoplasmic reticulum are closely applied to the droplets (arrow) suggestive of a functional relationship. Dalton's fixative. 32,000 \times .
- 4 Portions of several cells of the zona glomerulosa. Some of the mitochondria possess angular cristae and intramitochondrial dense granules. The endoplasmic reticulum is moderately well developed and is composed of both smooth and rough surfaced membranes which occasionally are interconnected (arrow). The long tubular profiles of the smooth endoplasmic reticulum are frequently applied to the surfaces of mitochondria. A coated invagination (ci) is present at the surface of one cell and coated vesicles of variable size are present within the cytoplasm. A basement lamina (bl) covers the surface of the parenchymal cells adjacent to the subendothelial space. Dalton's fixative. 19,000 \times .



PLATE 2

EXPLANATION OF FIGURES

- 2, 3 Lipid droplets in the zona glomerulosa (fig. 2) are considerably smaller than those of the zona fasciculata (fig. 3). The significance, if any, of the differences in density of the droplets, is unknown. Elements of the smooth surfaced endoplasmic reticulum are closely applied to the droplets (arrow) suggestive of a functional relationship. Dalton's fixative. 32,000 \times .
- 4 Portions of several cells of the zona glomerulosa. Some of the mitochondria possess angular cristae and intramitochondrial dense granules. The endoplasmic reticulum is moderately well developed and is composed of both smooth and rough surfaced membranes which occasionally are interconnected (arrow). The long tubular profiles of the smooth endoplasmic reticulum are frequently applied to the surfaces of mitochondria. A coated invagination (ci) is present at the surface of one cell and coated vesicles of variable size are present within the cytoplasm. A basement lamina (bl) covers the surface of the parenchymal cells adjacent to the subendothelial space. Dalton's fixative. 19,000 \times .

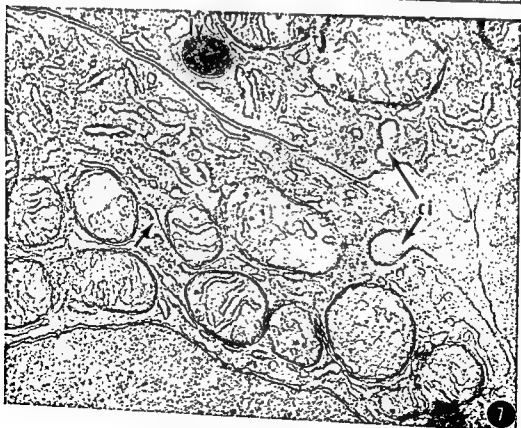


PLATE 3

EXPLANATION OF FIGURES

- 5, 6 Two examples of small (500 Å) dense bodies found within the lumen of the endoplasmic reticulum in both the zona glomerulosa (fig. 5) and zona fasciculata (fig. 6). The nature of these bodies is unknown. The tubular shape of the smooth endoplasmic reticulum is seen to good advantage at this magnification. Continuity between smooth and rough intracytoplasmic membranes is observed near the arrow in figure 6. Free ribosomes are observed in the ground cytoplasm. Dalton's fixative. 44,500 \times .
- 7 The smooth surfaced endoplasmic reticulum is less well developed in the glomerulosa cell, shown here, than in the cells of the fasciculata whereas the rough endoplasmic reticulum is more prevalent in the cells of the glomerulosa (compare with figs. 8, 11, 12, 13, 16). A lysosome (ly) and two coated invaginations (ci) are illustrated. Dalton's fixative. 37,000 \times .

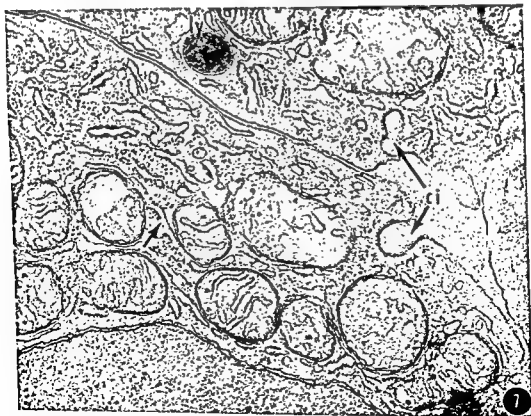


PLATE 3

EXPLANATION OF FIGURES

- 5, 6 Two examples of small (500 Å) dense bodies found within the lumen of the endoplasmic reticulum in both the zona glomerulosa (fig. 5) and zona fasciculata (fig. 6). The nature of these bodies is unknown. The tubular shape of the smooth endoplasmic reticulum is seen to good advantage at this magnification. Continuity between smooth and rough intracytoplasmic membranes is observed near the arrow in figure 6. Free ribosomes are observed in the ground cytoplasm. Dalton's fixative. 44,500 ×.
- 7 The smooth surfaced endoplasmic reticulum is less well developed in the glomerulosa cell, shown here, than in the cells of the fasciculata whereas the rough endoplasmic reticulum is more prevalent in the cells of the glomerulosa (compare with figs. 8, 11, 12, 13, 16). A lysosome (ly) and two coated invaginations (ci) are illustrated. Dalton's fixative. 37,000 ×.

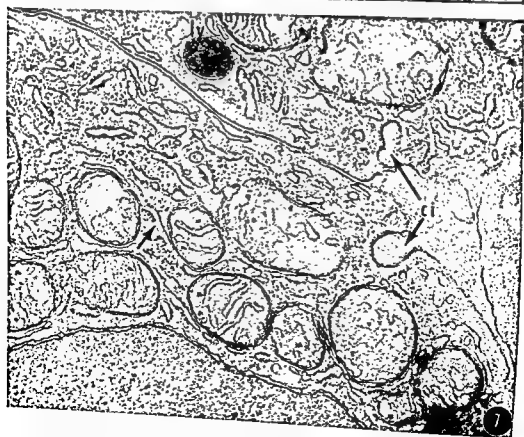


PLATE 4

EXPLANATION OF FIGURE

- 8 The cells of the zona fasciculata are larger than those of the zona glomerulosa and are characterized by large, variably shaped mitochondria with tubular cristae and an abundance of smooth endoplasmic reticulum. A few profiles of ribosome-studded membranes can be observed although most ribosomes appear to be free within the cytoplasm. Karnovsky's fixative. 20,000 \times .



PLATE 4

EXPLANATION OF FIGURE

- 8 The cells of the zona fasciculata are larger than those of the zona glomerulosa and are characterized by large, variably shaped mitochondria with tubular cristae and an abundance of smooth endoplasmic reticulum. A few profiles of ribosome-studded membranes can be observed although most ribosomes appear to be free within the cytoplasm. Karnovsky's fixative. 20,000 \times .



PLATE 5

EXPLANATION OF FIGURES

- 9, 10 These electron micrographs illustrate the juxtannuclear position of centrioles ($500\text{ m}\mu \times 160\text{ m}\mu$) within cells of the zona fasciculata. Karnovsky's fixative. 37,000 \times .
- 11 A portion of a cell from the zona fasciculata demonstrating the abundance of the tubular form of agranular reticulum, spherical mitochondria with villiform cristae and free ribosomes. Karnovsky's fixative. 30,000 \times . Inset: A relatively high magnification electron micrograph of an inclusion of unknown significance found in association with Golgi material in a zona glomerulosa cell. Dalton's fixative. 66,500 \times .

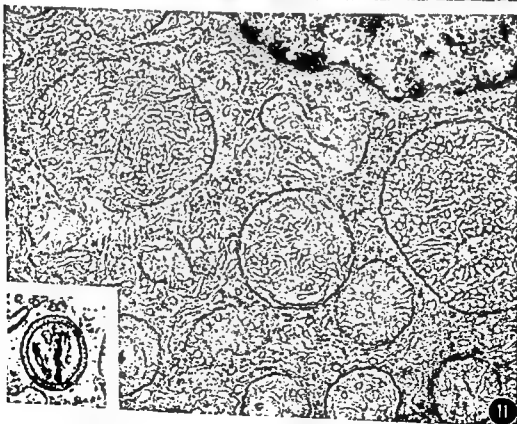


PLATE ■

EXPLANATION OF FIGURES

- 12, 13 The extraordinarily well developed smooth surfaced endoplasmic reticulum of the zona fasciculata cells appears in the form of freely anastomosing interwoven tubules. These membranes, because of their abundance are thought to make up the microsomal fraction of adrenal cortical homogenates and are therefore implicated in certain steps of steroidogenesis. Superimposition of the upper and lower membranes contributes to the increase in electron density of tubules seen in longitudinal section. Cross sections (arrow) of these tubules reveals no such inner opacity. Karnovsky's fixative. 53,000 X.

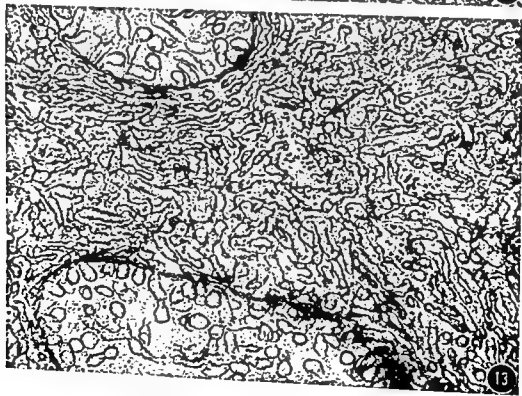
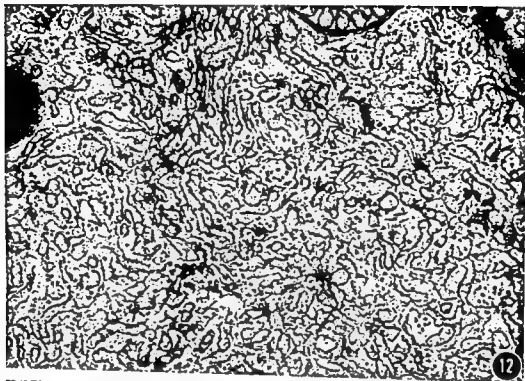


PLATE 7

EXPLANATION OF FIGURES

- 14, 15 Golgi apparatus in cells of the zona glomerulosa. In figure 14 the cisterna of the Golgi closest to the plasma membrane appears to be fenestrated. A coated vesicle is seen at the arrow in figure 15. Local increases in electron density of the plasma membrane may represent areas of cell adhesions (A). Dalton's fixative. 30,000 \times .
- 16 This portion of a cell from the zona fasciculata shows multiple areas of Golgi material adjacent to the nucleus. A Golgi cisterna when seen en face (arrow) appears fenestrated. Again, note the prominence of the tubular agranular reticulum. Karnovsky's fixative. 27,000 \times .

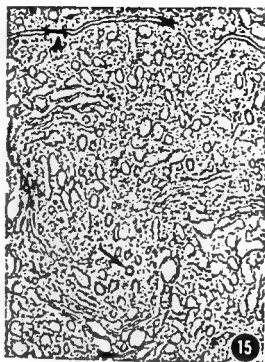
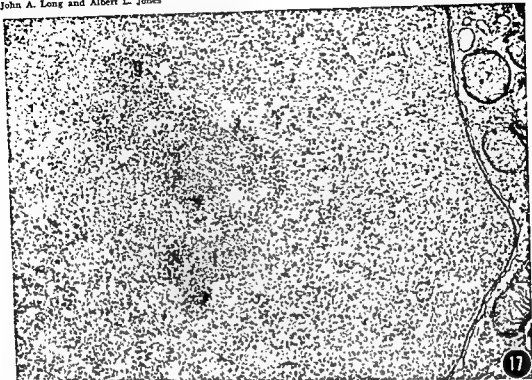


PLATE 8

EXPLANATION OF FIGURES

- 17 The nucleolus of a glomerulosa cell is seen here at high magnification. It is composed of granules (g) similar in size to cytoplasmic ribosomes embedded in a network of filaments (f). Dalton's fixative. 27,000 \times .
- 18 The endothelium of the opossum adrenal cortex is continuous and possesses multiple fenestrae 700–1000 \AA in diameter which are closed by a thin diaphragm (arrow). Processes of fibroblasts (fb) are observed in the subendothelial space. Dalton's fixative. 35,000 \times .



Changes in Cells, Matrix and Water of Calcifying Turkey Leg Tendons¹

MILTON B. ENGEL AND EUGENIO ZERLOTTI

Departments of Orthodontics and Histology, University of Illinois,
College of Dentistry at the Medical Center, Chicago

ABSTRACT Alterations in morphology and composition of ossifying turkey leg tendons were followed using biophysical and histochemical procedures in combination with improved methods of tissue preparation. The principal biophysical changes accompanying calcification were loss of water, increase in shrinkage temperature, shifts in form birefringence curves and increased resistance to the disrupting effects of potassium iodide. Fibroblasts of the tendon were modified to cuboidal cells; at the same time, intracellular lipid increased and presumptive secretion of glycoproteins and lipids into the contiguous matrix was observed. As the bony tendon matured, osteocytes appeared and the stainability of the matrix with the periodic acid-Schiff reagent and dinitrofluorobenzene was markedly diminished. The matrix changes were interpreted as representing increased cross-linking of a negatively charged biological polyelectrolyte. Concurrently, diminished binding of calcium, the formation of hydrophobic lipid-containing phases and the lowering of dielectric constant favor the precipitation of bone salts. During calcification, barriers to diffusion, including low vascularity, tend to create a closed, or partially closed, system in the tissue. Then, the mineral phases form with minimal transfer of electrolytes to the circulation. According to the phase rule, the formation of insoluble bone salts stabilizes the heterogeneous biological structure.

The morphological changes in cells and matrix occurring during the direct conversion of a soft connective tissue to bone can be observed at a simple level in the ossification of tendon. This process, as it occurs in the limb tendons of many birds, has been described in detail at least since the middle of the last century. The papers of Lieberkühn (1860, 1863) and of Ranvier (1889a, b) are especially complete. Certain aspects of the cellular changes including the accumulation of lipid and the presence of cartilaginous or chondroid elements were further discussed by Renault (1871-72).

In this century, histologic changes during ossification in turkey tendons were described by Retterer and Lelièvre ('11). Some of the earlier work is summarized by Weidenreich in Von Mollendorff's Handbook ('30). Our interest in this metaplasia, as it occurs in the turkey (*Meleagris*), was aroused by the series of papers published by Johnson ('60), Nylen et al ('60), and Likins et al. ('60). These authors considered certain of the histological, histochemical and chemical features in the transformation. Also, they studied submicroscopic changes and presented

chemical evidence with respect to mineral components and the amino acids, lysine and hydroxylysine.

Between the twelfth and sixteenth week, tendons of the turkey thigh and leg undergo a distinct metaplasia. With the exception of those parts which pass through joints such as the tibio-tarsal, the collagenous tissues are transformed to a type of bone. This change is accompanied by an increased infiltration or appearance of lipid in cells and in portions of the extracellular matrix.

In earlier electrochemical studies (Engel et al., '62), it was shown that the tendon behaves as an amphoteric colloid which is negatively charged at physiologic pH. This biological polyelectrolyte has the capacity to bind calcium. The degree of calcium binding appeared to diminish with the onset of ossification. These results stimulated further studies employing histochemical and biophysical methods.

The following account is based on a study of changes in the tendons in a se-

¹This work was supported by grants from the United States Public Health Service, DE 01849, General Research Support Grant and Career Development Award 1-E3-DE-32,729-01 (E. Z.) and from the Graduate College Research Board.

ries of animals ranging in age from 4 to 40 weeks. The methods of tissue preparation are substantially different from those followed by previous workers. Most of the material which is described here was cut in a cryostat at very low temperature and then dried in the frozen state. In this way, denaturation of most tissue constituents was avoided and shifts in diffusible substances and in lipids were prevented. Procedures for fixation of various components in order to immobilize them were introduced when necessary, and under well defined conditions. More precise cytological localization of tissue constituents was assured. The new methods increased the validity of quantitative studies done by polarization microscopy and of observations at high magnification employing interference microscopy and microradiography. Corollary evidence was also obtained from studies of shrinkage temperature and water content of tendons at various ages.

The results of these combined studies lead us to conclude that as the leg tendons mature, the extracellular matrix of the connective tissue loses water, becoming more highly aggregated and crosslinked, simultaneously altering in chemical composition. These changes suggest that the dielectric properties of the matrix are modified in a major way, affecting the distribution and solubility of all ions, including calcium and various forms of phosphate. The change in the morphologic and physico-chemical properties of the extracellular colloids would then favor the precipitation of bone salts.

MATERIAL

The Beltsville white turkey was used in this study. Birds whose ages ranged from 4 to 40 weeks were obtained from two suppliers in a neighboring area. A total of over 65 birds were used. Animals of various intermediate stages were studied; most observations were concentrated on ages 4, 8, 10, 12, 13, 15, 16, 18, 20, 30 and 40 weeks. In any one age group, there were at least four animals.

The animals were sacrificed by decapitation, and the leg tendons were dissected immediately. The gastrocnemius tendon was used for determinations of water

content and for morphological and histochemical studies. This tendon is bifurcated, (fig. 1) forming a Y shape. The distal part of the Y was not calcified, even in the oldest group. For histology, the upper portions of the Y (proximal part) were examined. Water determinations were made on both proximal and distal arms; measurements of shrinkage temperatures were done on various flexor tendons of the lower limb.

METHODS

Fixation for microscopic study

Initially, a number of tissues were fixed by the freeze-drying method of Gersh (32), embedded in paraffin (M.P. 60-62°C) and sectioned. The sections were deparaffined in xylene or petroleum ether before staining. This method minimizes the loss or dislocation of soluble tissue components accompanying the use of liquid fixatives, but it does not prevent the denaturation and lipid extraction which can occur during embedding in waxes or plastics. In order to avoid these artifacts, a refined procedure was employed in the preparation of most of the tissues.

Small pieces of the gastrocnemius tendon approximately 2×2 mm were rapidly removed and placed on small brass blocks using a drop of blood as the adhesive. The block and tissue were then rapidly immersed in isopentane, chilled in liquid nitrogen to about -150°C and subsequently transferred directly to liquid nitrogen. The blocks were then mounted on a Jung microtome in a Dittes cryostat where the temperature was maintained at -50°C to -60°C . Sections were cut at 6 and 10 μ . These were transferred to a vacuum chamber in the cryostat and dehydrated at temperatures around -40°C for 24 hours. Although sections prepared in this manner are not uniformly good, some suffering from ice crystals and cutting imperfections, many excellent sections were obtained. These were usually stored at -15°C in airtight tubes in an atmosphere of nitrogen or maintained at -40°C in a vacuum.

Histochemical methods

Dinitrofluorobenzene reactions. Reactive amino groups of lysine-hydroxylysine

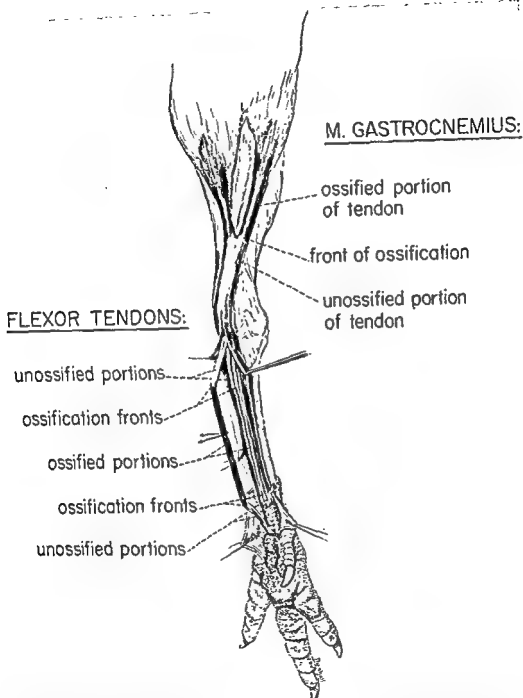


Fig. 1 Dissection of posterior aspect of leg of 20 week turkey. At this time, the larger part of all leg tendons is ossified. The characteristic Y formed by the bifurcation of the more superficial gastrocnemius tendon is illustrated. A tarsal tendon is retracted to show relations of ossified and unossified portions and the ossification fronts or "junctions."

ries of animals ranging in age from 4 to 40 weeks. The methods of tissue preparation are substantially different from those followed by previous workers. Most of the material which is described here was cut in a cryostat at very low temperature and then dried in the frozen state. In this way, denaturation of most tissue constituents was avoided and shifts in diffusible substances and in lipids were prevented. Procedures for fixation of various components in order to immobilize them were introduced when necessary, and under well defined conditions. More precise cytological localization of tissue constituents was assured. The new methods increased the validity of quantitative studies done by polarization microscopy and of observations at high magnification employing interference microscopy and microradiography. Corollary evidence was also obtained from studies of shrinkage temperature and water content of tendons at various ages.

The results of these combined studies lead us to conclude that as the leg tendons mature, the extracellular matrix of the connective tissue loses water, becoming more highly aggregated and crosslinked, simultaneously altering in chemical composition. These changes suggest that the dielectric properties of the matrix are modified in a major way, affecting the distribution and solubility of all ions, including calcium and various forms of phosphate. The change in the morphologic and physico-chemical properties of the extracellular colloids would then favor the precipitation of bone salts.

MATERIAL

The Beltsville white turkey was used in this study. Birds whose ages ranged from 4 to 40 weeks were obtained from two suppliers in a neighboring area. A total of over 65 birds were used. Animals of various intermediate stages were studied; most observations were concentrated on ages 4, 8, 10, 12, 13, 15, 16, 18, 20, 30 and 40 weeks. In any one age group, there were at least four animals.

The animals were sacrificed by decapitation, and the leg tendons were dissected immediately. The gastrocnemius tendon was used for determinations of water

content and for morphological and histochemical studies. This tendon is bifurcated, (fig. 1) forming a Y shape. The distal part of the Y was not calcified, even in the oldest group. For histology, the upper portions of the Y (proximal part) were examined. Water determinations were made on both proximal and distal arms; measurements of shrinkage temperatures were done on various flexor tendons of the lower limb.

METHODS

Fixation for microscopic study

Initially, a number of tissues were fixed by the freeze-drying method of Gersh ("32), embedded in paraffin (M.P. 60–62°C) and sectioned. The sections were deparaffined in xylene or petroleum ether before staining. This method minimizes the loss or dislocation of soluble tissue components accompanying the use of liquid fixatives, but it does not prevent the denaturation and lipid extraction which can occur during embedding in waxes or plastics. In order to avoid these artifacts, a refined procedure was employed in the preparation of most of the tissues.

Small pieces of the gastrocnemius tendon approximately 2×2 mm were rapidly removed and placed on small brass blocks using a drop of blood as the adhesive. The block and tissue were then rapidly immersed in isopentane, chilled in liquid nitrogen to about -150°C and subsequently transferred directly to liquid nitrogen. The blocks were then mounted on a Jung microtome in a Dittes cryostat where the temperature was maintained at -50°C to -60°C . Sections were cut at 6 and 10 μ . These were transferred to a vacuum chamber in the cryostat and dehydrated at temperatures around -40°C for 24 hours. Although sections prepared in this manner are not uniformly good, some suffering from ice crystals and cutting imperfections, many excellent sections were obtained. These were usually stored at -15°C in airtight tubes in an atmosphere of nitrogen or maintained at -40°C in a vacuum.

Histochemical methods

Dinitrofluorobenzene reactions. Reactive amino groups of lysine-hydroxylysine

areas. The study was not further pursued at the time; a complete report of this and additional work is deferred for a future publication.

Microradiography

Microradiographs of 6 μ sections of turkeys aged 16, 20, and 40 weeks were taken with a Phillips CMR II X-ray apparatus. The undecalcified freeze-dried sections were mounted directly on the emulsion side of Kodak High Resolution plates which had been cut into small squares (0.8×0.8 cm) and placed into the film holder. In order to improve contrast and to avoid x-ray scattering, air was removed from the radiographic camera with a vacuum pump. For such a material, the best results were achieved using a voltage of 2.5 Kv and 2.0 mA at an exposure of 2-3 minutes.

Under these conditions, the radiation has a wave length of maximum intensity at approximately 7.3 Å. This lies beyond the calcium K-absorption edge (3.06 Å), but the ratio between the mass absorption coefficients of calcium and organic components at this wave length is sufficiently high to permit good contrast between mineralized and unmineralized structures.

The plates were developed with Gavaert G209H or Kodak D19 developers for four minutes at exactly 20°C, fixed, washed, dehydrated and mounted in Permount. The sections were removed from the plates before processing, mounted on slides and stained with PAS or DNFB to permit direct comparison with the same fields in the microradiographs.

Interference microscopy

Six micron tissue sections from 16 and 40 week old birds were imbibed in turkey serum and examined with a Leitz interference microscope. The tissues were first examined with polychromatic light with the fringes in the field and the optical path differences roughly estimated. More precise measurements of the retardations were made in monochromatic light at 546 m μ using an Arago wedge compensator. The contrast between the mineral and organic phases is very high due to the difference in their refractive indices (n) and specific densities (δ) (for apatite: $\delta = 3.13$ and $n = 1.640$, for collagen, $\delta = 1.27$ and $n =$

1.530) (Davies and Engstrom, '54; Hale, '58). Quantitative determinations of dry or wet mass were not made at this time.

Polarization microscopy

Sections of the gastrocnemius tendons, cut at 10 μ were dehydrated as described above and mounted in imbibing media of refractive indices varying from 1.400 to 1.700.^a The optical path differences were measured with a Leitz polarizing microscope, using a Brace-Koehler compensator with $\lambda/10$ retardation. Six micron sections were used to study the pericellular areas in calcified tissues and in the these instances, a compensator with $\lambda/30$ retardation was used. Monochromatic light with a wave length of 550 m μ was obtained with a mercury lamp and a Zeiss interference wedge. The retardations of the tissues were calculated using the Fresnel intensity equation as modified by Köhler ('21).

Form birefringence curves were obtained by plotting the retardations of the tissue sections as a function of the refractive indices of the imbibing media. The birefringence is expected to be higher when the difference between the refractive indices of the two components ($n_1 - n_2$) is greater. When $n_1 = n_2$, the form birefringence is nil and if a path difference can still be measured, it is due to the intrinsic birefringence of the components. The shapes of the curves are not only dependent upon the difference $n_1 - n_2$, but also on the relative volumes of the two components. Assuming that rodlets have a preferential orientation in the medium of different refractive index, Wiener ('13) proposed the following equation for an ideal case:

$$n_s^2 - n_a^2 = \frac{\delta_1 \delta_2 (n_1^2 - n_2^2)^2}{(1 + \delta_1) n_1^2 + \delta_1 n_2^2}$$

Where: $n_s^2 - n_a^2$ is equivalent to the dielectric constant for the given frequency and; δ_1 and δ_2 refer to the relative volumes of the components. This equation, or its modification proposed by Bear et al. ('37) must be used guardedly, since more than two components are certainly involved in biological systems. Other limiting factors may be changes in the relative volumes,

^a The imbibing media were supplied by R. D. Car-gille Laboratories, and the refractive indices were confirmed with a Leitz Jolly refractometer. Measurements of retardations were made after 24-48 hours to permit complete imbibition of the media by the tissues.

and terminal amino groups* were visualized with dinitrofluorobenzene (DNFB) according to the method of Zerlotti and Engel ('62). Some sections were treated with citrate buffer (0.1 M) or 0.01 M HCl for 24 hours before reacting with the DNFB reagent, in order to expose masked or unreactive amino groups. Undoubtedly, some soluble protein was also lost. The sections were examined with monochromatic light at 410 m μ , using a mercury HBO 200 lamp and a Zeiss interference wedge.

Periodic acid-schiff reaction. Certain carbohydrate-protein complexes were visualized with the periodic acid-Schiff reagent (PAS). Presumably these are glycoproteins containing free 1, 2 glycol groups. Sections were denatured usually in 95% ethanol before reacting; others were treated with paraformaldehyde vapor for four hours at 45°C in vacuo. Unreacted paraformaldehyde was removed by immersing sections in ethanol. Also effective for denaturation or crosslinking were 95% ethanol-formalin 1:1 (V/V), 0.093 M 1, 5, difluoro-2,4-dinitrobenzene (DNFFB) in acetone-bicarbonate solution (Goland et al., '65; Zahn, '55), or as a vapor in vacuo at 62°C. In the latter, unreacted DNFFB was removed by further evacuation after the reagent was removed from the chamber. Use of these reagents did not appear to diminish the reactivity of the tissues with the PAS method. Treatment with ethanol alone does not prevent the swelling which occurs in tissues from young animals exposed to periodic acid. Therefore, it must be presumed that some components of the tissue are displaced or dissolved by the oxidizing solution when this type of denaturation was used. Minimal swelling was observed following the use of DNFFB. To distinguish glycogen from glycoprotein, some sections were treated for 30 minutes with α -amylase (1 mg/ml) at pH 7.0 in Sorenson's phosphate buffer. Extraction with the buffer solution was used as a control.

Lipids

In order to avoid or minimize solution and shifts in distribution of the lipids, sections were transferred, while cold, to a container saturated with the vapor of fresh

osmium tetroxide at +5°C for 2-5 minutes. Sections were then stained with Oil Red O, Oil Blue or Sudan Black. The dyes were made up as saturated solutions in 60% or 100% propanol. The solutions were allowed to stand for at least 24 hours after preparation and filtered before use. Staining time ranged from 30 minutes to two hours. Excess stain was removed by brief rinses in 60% propanol followed by water, and sections were mounted in glycerol gel. Some sections were exposed to chloroform-methanol 4:1 (V/V) at 60°C for 1 to 24 hours before staining, in order to remove most lipids. This control was used for tissues fixed with osmium vapor, as well as with unfixed tissues. No stainable lipid was observed in the unfixed sections. Osmium fixation led to some retention of stainable material. This method probably does not reveal the more strongly bound lipid fraction described by Irving ('63) which is unmasked and stained only after decalcification.

The reaction for plasmalogens was carried out according to the method of Hack ('52). This involves oxidation for five minutes in 0.026 M HgCl₂ followed by treatment with the leucofuchsin reagent. Tissues carried through this procedure were not pretreated with osmium and it is probable that some diffusion of lipids did occur. For control purposes, some sections were extracted with chloroform-methanol (4:1). Others were placed directly in the leucofuchsin reagent in order to reveal preformed aldehydes.

Metachromasia

Some sections were stained with 0.5% solutions of toluidine blue, pH 7.0, mounted in water and examined immediately. Newly calcified areas were highly metachromatic and the staining could not be abolished by prior treatments with testicular hyaluronidase or sialidase. Decalcification with EDTA or 5% formic acid removed the metachromatic substances. The metachromatic areas also showed dichroism when observed with polarized light and the dichroic ratios seemed to vary sharply in uncalcified and mineralized

* These occur in negligible concentration in native collagens where the solid phase predominates (Bowes and Moss, '51; Solomons and Irving, '58).

areas. The study was not further pursued at the time; a complete report of this and additional work is deferred for a future publication.

Microradiography

Microradiographs of 6 μ sections of turkeys aged 16, 20, and 40 weeks were taken with a Phillips CMR 5 X-ray apparatus. The undecalcified freeze-dried sections were mounted directly on the emulsion side of Kodak High Resolution plates which had been cut into small squares (0.8×0.8 cm) and placed into the film holder. In order to improve contrast and to avoid x-ray scattering, air was removed from the radiographic camera with a vacuum pump. For such a material, the best results were achieved using a voltage of 2.5 Kv and 2.0 mA at an exposure of 2-3 minutes.

Under these conditions, the radiation has a wave length of maximum intensity at approximately 7.3 Å. This lies beyond the calcium K-absorption edge (3.06 Å), but the ratio between the mass absorption coefficients of calcium and organic components at this wave length is sufficiently high to permit good contrast between mineralized and unmineralized structures.

The plates were developed with Gavaert G209H or Kodak D19 developers for four minutes at exactly 20°C, fixed, washed, dehydrated and mounted in Permount. The sections were removed from the plates before processing, mounted on slides and stained with PAS or DNFB to permit direct comparison with the same fields in the microradiographs.

Interference microscopy

Six micron tissue sections from 16 and 40 week old birds were imbibed in turkey serum and examined with a Leitz interference microscope. The tissues were first examined with polychromatic light with the fringes in the field and the optical path differences roughly estimated. More precise measurements of the retardations were made in monochromatic light at 546 m μ using an Arago wedge compensator. The contrast between the mineral and organic phases is very high due to the difference in their refractive indices (n) and specific densities (δ) (for apatite: $\delta = 3.13$ and $n = 1.640$, for collagen, $\delta \approx 1.27$ and $n \approx$

1.530) (Davies and Engstrom, '54; Hale, '58). Quantitative determinations of dry or wet mass were not made at this time.

Polarization microscopy

Sections of the gastrocnemius tendons, cut at 10 μ were dehydrated as described above and mounted in imbibing media of refractive indices varying from 1.400 to 1.700.² The optical path differences were measured with a Leitz polarizing microscope, using a Brace-Kochler compensator with $\lambda/10$ retardation. Six micron sections were used to study the pericellular areas in calcified tissues and in the these instances, a compensator with $\lambda/30$ retardation was used. Monochromatic light with a wave length of 550 m μ was obtained with a mercury lamp and a Zeiss interference wedge. The retardations of the tissues were calculated using the Fresnel intensity equation as modified by Köhler ('21).

Form birefringence curves were obtained by plotting the retardations of the tissue sections as a function of the refractive indices of the imbibing media. The birefringence is expected to be higher when the difference between the refractive indices of the two components ($n_1 - n_2$) is greater. When $n_1 = n_2$, the form birefringence is nil and if a path difference can still be measured, it is due to the intrinsic birefringence of the components. The shapes of the curves are not only dependent upon the difference $n_1 - n_2$, but also on the relative volumes of the two components. Assuming that rodlets have a preferential orientation in the medium of different refractive index, Wiener ('13) proposed the following equation for an ideal case:

$$n^2 - n_0^2 = \frac{\delta_1 \delta_2 (n_1^2 - n_2^2)^2}{(1 + \delta_1) n_1^3 + \delta_2 n_2^3}$$

Where: $n^2 - n_0^2$ is equivalent to the dielectric constant for the given frequency and: δ_1 and δ_2 refer to the relative volumes of the components. This equation, or its modification proposed by Bear et al. ('37) must be used guardedly, since more than two components are certainly involved in biological systems. Other limiting factors may be changes in the relative volumes,

² The imbibing media were supplied by R. D. Car-gille Laboratories, and the refractive indices were confirmed with a Leitz Jell refractometer. Measurements of retardations were made after 24-48 hours to permit complete imbibition of the media by the tissues.

due to differential shrinkage or swelling, and interaction of reactive groups of the tissues with those of the imbibing media (Frey-Wyssling, '40). However, Wiener's equation remains of great value in the qualitative interpretation of form birefringence curves (Schmitt, '44 and Bennett, '50).

The intrinsic birefringence is taken at the minimum retardation of the imbibing curve, and it is expressed as an absolute value. This value was calculated from the equation $\Pi = \frac{\Gamma}{t}$, where Π is the birefringence, Γ the retardation and t the thickness. This treatment is considered to be semi-quantitative because errors due to unevenness of sections and other unknown factors could prevail. All these studies were confined to birds of ages 4 to 16 weeks, since in calcified tissues, the negative birefringence of the apatite crystals is superimposed on the positive form and intrinsic birefringencies of the collagen. At the present time, this creates unsurmountable barriers to quantitative analysis of the system.

Contraction of tendons with potassium iodide solutions

Collagen fibers, when treated at 23° to 25°C with concentrated solution of KI, contract markedly and lose their anisotropy (Banga et al., '56). This has been interpreted as due to the weakening and breaking of inter and/or intramolecular bonds causing disruption of the protein macromolecules. Also, the salt is thought to alter the state of the water associated with non-polar groups (Verzar et al., '65). A minimum of 20 sections of tissues from 4, 10 and 16 week old turkeys were treated with 0.3, 0.6, 1.2, 1.5, 1.8 and 2.4 M solutions of KI for ten minutes at room temperature, washed in 75% alcohol, dehydrated, cleared and mounted in Permount. The refractive index of Permount was determined, and depending on the amount of toluene added, it varied from 1.520 to 1.530 (final value of the solid medium). In this range of the curve, the retardation is at a minimum and it would be due mainly to the intrinsic birefringence of the preparation. Optical path differences were measured as described above.

Shrinkage temperature measurements

Collagenous tissue, when heated in a moist environment, shrinks markedly. The temperature at which this dimensional change begins is called the shrinkage temperature (T_s) (Gustavson, '56).

Pieces of uncalcified tendon 4-6 cm in length, and 2-3 mm in width, from the distal part of the leg, were excised in order to determine shrinkage temperatures. Measurements were made with a Grass force-displacement transducer (FT-10) connected to an Offner Type R Dynograph. Uncalcified tendons from turkeys 4, 6, 10, 13 and 16 weeks old were used to record shrinkage temperatures. The tendons of the lower limb calcify at approximately 16 weeks, therefore, in older turkeys, the uncalcified portions which go through the tibio-tarsal articulation were used.

One end of the tendon was fixed to the bottom of a brass tube with fine stainless steel wire, and the other extremity was connected to the transducer. The tube was lined with wet filter paper to maintain a humid environment, and the temperature was raised 6-7°C/minute by a heating tape which surrounded the tube. The temperature was determined with a thermometer placed inside the tube and every degree of rise indicated on the recording paper by means of the manual marking lever. Six to fourteen measurements were made on each age group. This humidified chamber was chosen in order to prevent the loss of soluble components which takes place when the tissues are immersed in water (Verzar, '64). The (T_s) was considered to be the temperature at which the first deflection of the recording pen occurred. No quantitative measurements of force displacement were made. The tension applied to the tendons during their connection to the apparatus varied from 1.5 to 3.5 g. Considering that part of this value was due to the weight of the tissues and that the cross sectional areas of the tendons were very large (1.5 - 4 mm²) as compared to those reported by other authors (Verzar, '56, '63), it is reasonable to assume that the variable tension did not affect our results in any significant way. The lower shrinkage temperature obtained for young tendons with somewhat smaller

cross sectional areas substantiated this assumption.

Water determination

The measurements of water content were made on the gastrocnemius tendons of turkeys ranging from 4 to 35 weeks of age. Small pieces (50-200 mg) were rapidly excised from the proximal and distal portions of the tendon in the region of the bifurcation, weighed, and then dried in a constant weight "in vacuo" at 21-23°C over phosphorus pentoxide. The specimens were dehydrated after 24 hours. In young birds (4-6 weeks), where the tendons were finer, the specimens were removed in a humidified chamber to avoid loss of water prior to weighing.

RESULTS

Morphology as shown with hematoxylin and eosin

Tendons of 4-week old turkeys were very cellular with the fibroblasts localized in rows between the bundles (fig. 4). Some cells, probably very young fibroblasts, were larger and fusiform, with round or oval nuclei, and abundant basophilic cytoplasm. In tissues of 6 and 10-week old birds, the number of cells decreased and the collagen bundles were of larger diameter (fig. 5).

In scattered areas of 13-week old tendons, cuboidal cells with round nuclei and basophilic cytoplasm were observed. A lightly stained, pericellular matrix was seen around some of these cells. Most fibroblasts were elongated, containing an inconspicuous cytoplasm. In some areas, the bundles were irregularly stained with eosin (fig. 6).

At 16 weeks, regions of calcification, verified by microradiography, were identified by light blue staining of the extracellular components. The cuboidal cells, arranged in rows and resembling chondrocytes, had basophilic cytoplasm (figs. 7, 8). The boundary between calcified and uncalcified areas (which will be termed the junction) was not well defined with this stain. In areas where calcification had proceeded further, the tendons were not as basophilic as in regions of beginning calcification. The cells were separated from each other by matrix substance

which formed intercellular septae. This matrix was lightly stained with eosin in the uncalcified areas and at the junction, but was slightly basophilic in more mature calcified zones. In cross sections, the fiber bundles were separated by a prominent eosinophilic sheath. The bundles themselves were colored light blue.

At 20 weeks, the cells near the junction had the same characteristics as those observed at 16 weeks. Those of more mature calcified tissues were smaller and had lost the cytoplasmic basophilia. The intercellular septae were larger, the cells being farther apart.

After 30 weeks, the junction was sharper and some young osteons could be observed. The osteoid borders were lightly stained and the boundary between the osteoid and the calcified tissue was generally identified by a basophilic line. In some calcified areas, the cells took an elongated form with intensely stained nuclei, resembling osteocytes. Near the junction and in a few scattered places, the cells still retained their cuboidal shape, but most resembled osteocytes (fig. 10). In cross section, the bundles were surrounded by an uncalcified or poorly calcified matrix, which was more abundant than that of 16 week old tissues. The bundles also seemed to be subdivided into smaller sub-units than those of younger birds. Some isolated areas resembled cartilage, containing cuboidal cells embedded in a basophilic matrix (fig. 9). The osteons were more numerous, showing weakly eosinophilic osteoid borders. The lamellar structure of the Haversian systems could be visualized in some sections. This was more clearly identified by the polarizing microscope, since the long axis of the collagen of some lamellae was approximately perpendicular to that of the collagen bundles of the tendon.

Dinitrofluorobenzene reactivity

At four and six weeks, the extracellular components were very reactive to DNFB and the fibers seemed to stain more intensely than the interfibrillar ground substance. It was not possible to determine if this high reactivity was due to free ϵ -amino groups (lysine-hydroxylysine) of the collagen or of an extrafibrillar component closely associated with the fibers. Between

the bundles, there were large, fusiform fibroblasts with round nuclei, containing one or two nucleoli. The chromatin was loosely arranged and reactive to DNFB. The nucleoli were more intensely stained than the rest of the cellular structures. The cytoplasm of these cells was stained and contained small reactive granules which were barely resolvable (fig. 12).

In the 10-week old birds, the extracellular organization and reactivity of the tendons were very similar to those of younger animals. The cells, however, were elongated, with very reactive nuclei and barely visible cytoplasm (fig. 11). No marked changes in reactivity were detected in the extracellular substance at 13 weeks, but the round cells of some localized areas had very reactive nuclei. No particular changes were found in the pericellular matrix. The fibroblasts were faintly stained.

At 16 weeks, the uncalcified bundles seemed to be as reactive to DNFB as those of younger tendons, but the calcified areas showed a marked decrease in reactivity and a coarse granular appearance (fig. 13). The fibers could not be seen as distinctly as before, and their low reactivity contrasted with the intensely stained uncalcified bundles (figs. 14, 15) and borders of osteoid (figs. 18, 19). Cross sections showed that the bundles were ensheathed by a very thin layer of DNFB-positive extracellular substance. The granular appearance of the calcified areas was very distinct in these sections (fig. 20).

The large cuboidal cells in the uncalcified tendon near the junction had round, reactive nuclei; small, highly DNFB-positive granules were noted in the cytoplasm. The matrix around these cells was less intensely stained than the remainder of the uncalcified matrix (fig. 16).

In regions where calcification was beginning, the pericellular matrix formed septae which were more reactive than the contiguous mineralized matrix. In some mature areas where the calcification process had proceeded for a longer time, the reactivity of these septae diminished and was usually indistinguishable from that of the adjacent matrix (fig. 17). In a few instances, the matrix adjoining the cell retained its high reactivity.

In the uncalcified areas of 20-week old turkeys, and in the zones near the junction, the picture was similar to the one described for the 16 week birds. The calcified matrix was more homogeneous and showed lower reactivity. Far from the junction, the septae between the cells were large and generally as reactive as the rest of the extracellular matrix. The cells were smaller and the nuclei were more reactive. The cytoplasm was barely stained (fig. 21).

The most marked difference between the 30-week group and the preceding one was the increase in diameter of the intercellular septae and the appearance of some small, fusiform cells, resembling osteocytes (fig. 23). In these cells, the nuclei were elongated and more reactive than those of the other cells.

The matrix had extremely low reactivity at 40 weeks. The junction was very sharp in contrast to those of younger tissues, where calcified and uncalcified tissues interpenetrated (fig. 22). Near the junction, the cuboidal cells were small and had intensely stained nuclei. Most of the cells were flattened, appearing as thin slits. The immediate surrounding areas had the same reactivity as the rest of the matrix. In cross section, areas around the bundles which were less highly calcified were slightly more reactive to DNFB than the bundles themselves.

Calcified tendons reacted intensely with DNFB after treatment with acid citrate buffer or 0.01N HCl (fig. 24). These results show that the ϵ -amino groups of lysine-hydroxylysine are probably masked in the native state and are rendered free to react with DNFB after treatment with citrate or acid.

Periodic acid-Schiff reaction

In young tendons (4-10 weeks), the collagen fibers were embedded in a faintly stained matrix, indicating the presence of carbohydrate-protein complexes. The cells, aligned in almost longitudinal continuity, appeared to form the outlines of the collagen bundle and their cytoplasm was more reactive than the extracellular components (fig. 25). This intracellular PAS-positive material, more evident in sections of 4-6-week old turkeys, had a fine granular appearance, but the size of the granules was

almost at the limit of resolution of the microscope. In cross section, the bundles were bounded by a thin sheath of a more intensely stained extracellular material (fig. 26).

At 13 weeks, most of the extracellular matrix had the same reactivity as that of younger birds, but the cytoplasm of fibroblasts was barely visible. However, in some regions where the first cuboidal cells were noticed, the surrounding tissue was more intensely stained. The cytoplasm of these cuboidal cells contained highly reactive, coarse granules, which resisted amylase digestion. Some of these cells were surrounded by a thin layer of PAS-positive matrix.

In a large number of sections of 15-16-week old birds, the stained tissues were compared with their own microradiographs; in this way, the areas of ossification could be accurately localized and studied. Uncalcified matrix close to the areas of mineralization and matrix of newly calcified zones stained intensely, in contrast to the light staining of more radiopaque regions. The cuboidal cells in uncalcified areas and those embedded in newly mineralized matrix contained a large number of PAS-positive granules (figs. 28, 29, 30). The pericellular matrix was very reactive. Cells of regions where mineralization had progressed further had less PAS-positive material in their cytoplasm and they were separated from each other by septae showing varying degrees of reactivity (figs. 34, 35). Usually, the more mineralized septae were less intensely stained. In cross section, the interbundle material was more abundant in areas of ossification and stained more intensely than the bundles themselves (fig. 27). The microradiographs showed that this material was less calcified.

At 20 weeks, the intensity of the staining of the cellular and extracellular components decreased, with the exception of the cells at the junction which still contained highly reactive cytoplasmic granules and were surrounded by a PAS-positive pericellular matrix.

In older animals (30-40 weeks), the fibrous structure of the matrix was masked and the PAS reaction was very weak. The cells resembled osteocytes and rarely con-

tained any stained material in their cytoplasm (fig. 33). The pericellular matrix could not be differentiated from the surrounding calcified tissues, but thin lines of PAS-positive material outlined the bundles. In cross sections, the interbundle sheaths were clearly seen and stained more intensely than the bundles (fig. 31). Microradiographs proved them to be less densely calcified (fig. 32).

Distribution of lipids

The following description is based largely on the staining reaction with Oil Red O. Extraction of sections with chloroform-methanol 4:1 (v/v) at 60°C for 1-4 hours removed virtually all stainable material from extracellular and cellular sites. This is reasonable evidence that the stainable material contained lipids. If the sections were first treated with osmium tetroxide vapor, slight residual staining was occasionally observed. This reinforces the notion that osmium vapor fixation modifies the solubility of some tissue lipids.

In young animals (4-10 weeks), moderate amounts of intracellular lipids were demonstrated in the cytoplasm and nuclei of the fibroblasts (figs. 36, 37). The staining was not entirely generalized; granules or droplets were present in some cells. Also, there was considerable variability in the degree of staining of the heterogeneous cell population. Some cells contained small amounts of material, others were intensely colored. In general, nuclei were less deeply stained than cytoplasmic or extracellular substance. Only small amounts of extracellular lipid were observed in young tendons.

In animals aged around 16 weeks, somewhat increased amounts of stainable material were present in the cells and in the extracellular matrix. Mineralized matrix which appears around this time in young bone was barely colored. Cytoplasm of the young bone cells was filled with Oil Red O stainable material; the nuclei were virtually unstained. In cross section, the sheaths which surrounded the larger bundles of collagen fibrils were stained rather deeply and they appeared prominent in relation to the bundle.

As the calcification of the tendon proceeded (16–22 weeks) striking changes occurred in certain apparently randomly distributed tendon fibers contiguous to regions of mineralization. The fibers stained deeply with Oil Red O (fig. 44). Interfibrillar material, especially as viewed in cross section, was not as deeply colored. The distribution of intracellular lipid in the young osteocytes is illustrated in figure 39.

More extensive calcification was exhibited in tendons from birds aged 22–30 weeks. General lipid staining was observed in the fibrous matrices of periosteal regions and in the zone contiguous to the junction with the mineralized part (fig. 41). Fibroblasts immediately adjacent to calcifying areas were intensely stained. Bone cells occasionally were noted to contain discrete lipid droplets (fig. 40), as well as diffusely distributed lipid. In the calcified parts, some regions of pericellular matrix contained considerable quantities of lipid (fig. 38). In general, however, the calcified matrix, with the exception of the interbundle sheaths (Cf. fig. 46) was only weakly stained in an irregular fashion. Cells at the periphery of small marrow spaces, adjacent to the new bone matrix, contained large amounts of lipid. In cross sections, the collagen bundles of mineralized tendon were outlined by the deeply stained connective tissue cells and their process (fig. 45).

In the 30–40 week group, no remarkable differences were observed except where circumscribed regions occasionally appeared with morphological characteristics similar to cartilage. The matrix of these regions stained with moderate intensity and the large cells contained large inclusions of lipid (fig. 42). More mature regions of mineralized tendon were barely colored, except for the bundle sheaths (fig. 46). The included cells and their processes viewed in longitudinal or cross sections contained high concentrations of lipids (fig. 43).

Plasmal reaction

In animals of all age groups, plasmalogenes could be demonstrated in the cells. Precise localization in the cytoplasm could not be made because of the probability of diffusion artifacts. Small amounts of pre-

formed aldehydes, which could be extracted with methanol-chloroform, were also present. After HgCl_2 oxidation, the cells were stained more intensely. In some cells, the reactive material was demonstrated as granules of variable size (about 1–3 μ). In animals where calcification had begun, an interesting finding was made after sections were exposed to air for several hours: the cells and contiguous extracellular substance reacted fairly intensely with the Schiff reagent without prior treatment with periodic acid. This reaction was prevented if the sections were first treated with lipid solvents. Evidently, the abundant lipids present were labile and underwent oxidative change which yielded aldehyde groups.

Interference microscopy and microradiography

The optical path difference or retardation of the mineral phase of calcified tissues, as observed with the interference microscope, is much higher than that of the organic matrix. This is due to the differences in refractive index and specific density between the two components. Mineralized areas are more radiopaque than uncalcified matrix because at the wave length generally used, calcium has a higher mass absorption coefficient than the organic part. Observations were limited to 16 and 40-week old turkeys.

Sixteen weeks. In newly calcified tissues examined with the interference microscope, granules were visualized with higher optical path differences than in the uncalcified areas (fig. 48). The granules, observed to be very small in the junction, seemed to coalesce and to form clusters of varying sizes in the deeper zones of the calcified areas. In the microradiographs, these granules could not be observed, possibly because of the lower resolution of the radiographic plates and also because of overlay effects. A narrow area of transition was observed between uncalcified and calcified tissues. This area showed higher opacity than the uncalcified tendon, but absorbed less radiation than the mineralized tissue (fig. 14). In cross sections observed with the interference microscope, a heavier accumulation of calcified granules was noted in the periphery of the

bundles at the junction (fig. 49). The more completely calcified bundles were more homogeneous, although coarsely granular. The calcified bundles were surrounded by a thin sheath of extracellular substance with smaller retardation and lower radiopacity than the bundles themselves. Viewed with the interference microscope, this region contained granules of high retardation. Most sheaths were usually more radiopaque than the uncalcified tissues. Some intercellular septae at the junction had approximately the same optical path difference and radiopacity as the uncalcified tissue. Deeper in the calcified area, these septae had approximately the same optical path difference and radiopacity as the adjacent calcified bundles.

Forty weeks. In these older birds, most of the calcified tendons had a more uniform appearance with a few small areas showing granules or aggregates of granules. The junction did not show a transition zone and the limit between calcified and uncalcified tissues was distinct and abrupt. The borders of osteoid were less radiopaque than the calcified matrix. The extracellular components had a higher optical path difference than the 16-week old tissues and most of the cells were very similar to osteocytes. The areas around these cells did not show any difference in retardation or radiopacity from the surrounding calcified matrix. In a few areas, there was a small number of cuboidal cells which resembled those seen in young birds; they were separated by septae in varying stages of mineralization. In cross section, the bundles seemed to be subdivided into smaller bundles. The sheaths around the bundles were less calcified as revealed by the lower retardation and radiopacity (figs. 32, 47).

In these tissues, differences in degree of mineralization between the lamellae of osteons were detected in some Haversian systems by interferometry and microradiographs. When the same osteons were examined with the polarizing microscope, the more highly calcified areas of the osteons corresponded exactly to the more birefringent lamellae seen by polarization microscopy.

Polarization microscopy

Turkey tendons showed the characteristic positive intrinsic and form birefringence of collagen fibers, with the slow axis of transmission parallel to their long axis (Schmidt, '24) (figs. 50, 51).

In longitudinal sections from young birds, the collagen bundles were separated by areas of apparent isotropy⁴ occupied by the cells. Around 16 weeks, the septae between the cuboidal cells were weakly birefringent and their slow axis of transmission formed an angle of approximately 90° with that of the collagen bundles (fig. 52). This could be observed in calcified areas and also in uncalcified regions near the junction.

When viewed in cross section, the bundles themselves did not show birefringence, since the light path was parallel to the optical axis of the fibers. In calcified tendons, the bundles were surrounded by a birefringent sheath (fig. 53), which retained its anisotropy even after decalcification. When a first order red plate was used or the sign of birefringence was determined with the Köhler compensator, these sheaths showed a negative birefringence which is a characteristic of lamellar structures.

The form birefringence curves of tendons of birds aged 4, 6 and 10 weeks were very similar and presented a minimum retardation corresponding to the refractive index 1.530 (fig. 2). There was a marked change in the curve of tissues from 13-week old animals. The retardations in the range of refractive indices 1.400 to 1.452 were similar, as were those for 1.600, 1.650 and 1.700. This produced a much steeper curve with the minimum at the same refractive index as in curves of younger birds.

In the 16 week old tendons, the form birefringence curve of the junction was characterized by a shift in the refractive index of the minimum retardation to 1.640. The curve was flat in the region between 1.450 and 1.550. This finding suggests the presence of elongated crystallites, probably apatite ($n = 1.640$, Davies and Eng-

⁴ The term "apparent isotropy" is used here because, although there is evidence of the weak anisotropic nature of some intracellular structures (Schmidt, '44), its detection and measurement require special modifications in optics not available to us.

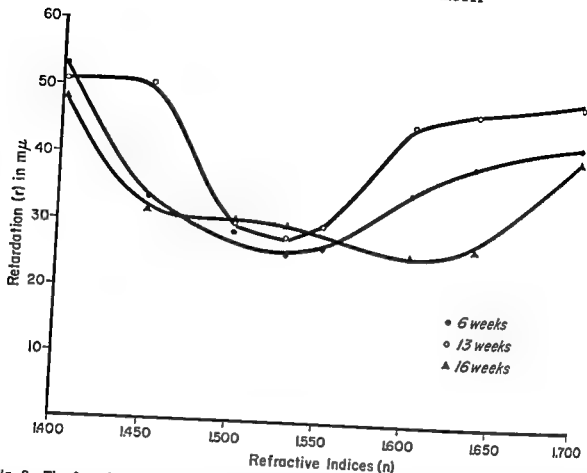


Fig. 2 The form birefringence curves of 4, 6 and 10 week old tendons are similar and are represented in the figure by the curve given by the 6 weeks group. The minimum retardation observed at $n = 1.530$ corresponds to the intrinsic birefringence of the tendon. The curve obtained for 13-week old tissues shows minimum retardation at the same refractive index, but it is steeper, due to change in the relative volumes of the two components (collagen and ground substance). At 16 weeks, the minimum retardation is observed at $n = 1.640$, probably due to the mineral crystallites oriented parallel to the long axis of the collagen.

ström, '54) oriented parallel to the long axis of the collagen. This result is in agreement with previous studies using electron microscopy (Nylen et al., '60) and x-ray diffraction (Myers and Engström, '65). In uncalcified areas, at some distance (approximately 200μ) from the junction, the curves resemble those obtained for tendons of 10-week old birds with a minimum retardation at 1.530. The intercellular septae at the junction showed form birefringence curves with shapes similar to those of calcifying collagen bundles, but with lower optical path differences.

The intrinsic birefringence was unchanged from 4 to 10 weeks (0.0025), but slightly higher in tissues 13 and 16 weeks old (0.0030 and 0.0035 respectively). It is difficult, however, to determine the exact significance of these values, since there

were concurrent changes in the partial volumes and in the nature of the tissue components.

Contraction of the tendons with potassium iodide solutions

Solutions of KI produced a decrease in the birefringence of the tendons of all age groups studied (figs. 54, 55). Complete loss of anisotropy was observed in tendons of 4-week old birds after treatment with 1.5 M KI. In 10-week old tendons treated with 1.5 M KI, some areas were isotropic and other regions showed a loss of 61.5% of the original birefringence. Tissue of 16-week turkeys immersed in solutions at this concentration lost 45% of their birefringence and isotropy was only observed when the KI concentration was increased to 1.8 M. The changes in

TABLE 1
Changes in retardation and percentage loss of birefringence of uncalcified tendons treated with KI solutions

Concentration KI (M)	4 Weeks		10 Weeks		16 Weeks	
	(ms)	Loss of I ¹	(ms)	Loss of I ¹	(ms)	Loss of I ¹
		%		%		%
Control	38	—	39	—	40	—
0.3	25	34.3	32	18	34	15
0.6	23	39.5	32	18	32	20
1.2	17	55.3	21	47.8	26	35
1.5	0	100	15 ¹	61.5 ¹	23	45
1.8	0	100	0	100	0	100
2.4	0	100	0	100	—	100

¹ Some areas showed complete loss of birefringence.

retardation and the percentage loss of birefringence are given in table 1.

Shrinkage temperature (Ts)

Shrinkage temperatures were determined only on tissues which were not calcified. The shrinkage temperature rose from 62°C at four weeks, to 66.8°C at 16 weeks, with a range of 61–62°C and 65–67°C respectively. No difference was noted between 10 and 13-week groups.

In older birds, the tendons which go through the tibio-tarsal joint and do not ordinarily calcify showed a shrinkage temperature similar to the tissues of young turkeys, which calcify at 16 weeks. There was no change between 20 and 30 weeks, but the 35 and 40 week old tissues showed an increased shrinkage temperature presumably associated with further maturation.

Water determination

Water content of calcifying and non-calcifying tendon, expressed as per cent of fresh weight, declined with age. In the noncalcifying distal part of the gastrocnemius, water fell from 80.6% at four weeks to 57.3% at 35 weeks. Somewhat lower initial values were observed in the proximal portion of the tendon which was destined to calcify. At four weeks, water concentration was 75%; this dropped to 59.1% at 13 weeks. At the onset of calcification of this tendon (16 weeks), 39.3% water was found. In the noncalcifying part during the same period, the water decrease was insignificant, from 61.7 to 60.3%. Lowest values for calcified tendon were attained by 30 weeks, 24.4%,

TABLE 2
Shrinkage temperatures of uncalcified tendons

Age	Ts (mean) °C	Ts (range) °C	± S.D.
4 Weeks (8) ¹	62.0	61–63	0.2
6 Weeks (9)	63.5	62–64	0.2
10 Weeks (9)	65.0	64–66	1.0
13 Weeks (9)	64.3	63–65	0.2
16 Weeks (14)	66.8	65–67	0.2
20 Weeks (6)	64.1	63–65	0.1
30 Weeks (6)	64.2	63–66	0.8
35 Weeks (6)	68.2	65–67	0.4
40 Weeks (9)	66.1	65–67	0.2

¹ Number of measurements.

² Tendons passing through the tibio-tarsal articulation.

and no further decline was observed during the remaining period which was studied (fig. 3).

DISCUSSION

Calcification of connective tissues involves changes in morphology, composition and micellar organization. In the ossification of avian tendon, these processes are somewhat less complicated because the original cellular and extracellular structures are fairly well defined and less heterogeneous, and their transformation appears to be relatively direct. The direction of our work and the interpretation of the observations were strongly influenced by earlier morphological, histochemical and physiochemical studies of connective tissues in varying physiological states (Catchpole et al., '66; Engel et al., '54; Gersh and Catchpole, '49, '60; Joseph et al., '52, '54, '59, '65). Certain generalizations emerging from those studies and bearing on the current work are briefly mentioned.

The extracellular matrix of connective tissues consists of fibrillar parts, mainly

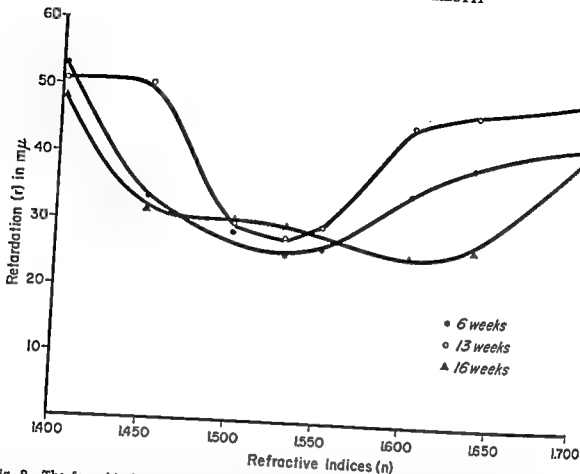


Fig. 2 The form birefringence curves of 4, 6 and 10 week old tendons are similar and are represented in the figure by the curve given by the 6 weeks group. The minimum retardation observed at $n = 1.530$ corresponds to the intrinsic birefringence of the tendon. The curve obtained for 13-week old tissues shows minimum retardation at the same refractive index, but it is steeper, due to change in the relative volumes of the two components (collagen and ground substance). At 16 weeks, the minimum retardation is observed at $n = 1.640$, probably due to the mineral crystallites oriented parallel to the long axis of the collagen.

ström, '54) oriented parallel to the long axis of the collagen. This result is in agreement with previous studies using electron microscopy (Nylon et al., '60) and x-ray diffraction (Myers and Engström, '65). In uncalcified areas, at some distance (approximately 200μ) from the junction, the curves resemble those obtained for tendons of 10-week old birds with a minimum retardation at 1.530. The intercellular septae at the junction showed form birefringence curves with shapes similar to those of calcifying collagen bundles, but with lower optical path differences.

The intrinsic birefringence was unchanged from 4 to 10 weeks (0.0025), but slightly higher in tissues 13 and 16 weeks old (0.0030 and 0.0035 respectively). It is difficult, however, to determine the exact significance of these values, since there

were concurrent changes in the partial volumes and in the nature of the tissue components.

Contraction of the tendons with potassium iodide solutions

Solutions of KI produced a decrease in the birefringence of the tendons of all age groups studied (figs. 54, 55). Complete loss of anisotropy was observed in tendons of 4-week old birds after treatment with 1.5 M KI. In 10-week old tendons treated with 1.5 M KI, some areas were isotropic and other regions showed a loss of 61.5% of the original birefringence. Tissue of 16-week turkeys immersed in solutions at this concentration lost 45% of their birefringence and isotropy was only observed when the KI concentration was increased to 1.8 M. The changes in

TABLE 1
Changes in retardation and percentage loss of birefringence of uncalcified tendons treated with KI solutions

Concentration KI (M)	4 Weeks		10 Weeks		18 Weeks	
	(mμ)	Loss of I ¹	(mμ)	Loss of I ¹	(mμ)	Loss of I ¹
		%		%		%
Control	38	—	39	—	40	—
0.3	25	34.3	32	18	34	15
0.6	23	39.5	32	18	32	20
1.2	17	55.3	21	47.8	26	35
1.5	0	100	15 ¹	61.5 ¹	22	45
1.8	0	100	0	100	0	100
2.4	0	100	0	100	0	100

¹ Some areas showed complete loss of birefringence.

retardation and the percentage loss of birefringence are given in table 1.

Shrinkage temperature (Ts)

Shrinkage temperatures were determined only on tissues which were not calcified. The shrinkage temperature rose from 62°C at four weeks, to 66.8°C at 16 weeks, with a range of 61–62°C and 65–67°C respectively. No difference was noted between 10 and 13-week groups.

In older birds, the tendons which go through the tibio-tarsal joint and do not ordinarily calcify showed a shrinkage temperature similar to the tissues of young turkeys, which calcify at 16 weeks. There was no change between 20 and 30 weeks, but the 35 and 40 week old tissues showed an increased shrinkage temperature presumably associated with further maturation.

Water determination

Water content of calcifying and non-calcifying tendon, expressed as per cent of fresh weight, declined with age. In the noncalcifying distal part of the gastrocnemius, water fell from 80.6% at four weeks to 57.3% at 35 weeks. Somewhat lower initial values were observed in the proximal portion of the tendon which was destined to calcify. At four weeks, water concentration was 75%; this dropped to 59.1% at 13 weeks. At the onset of calcification of this tendon (16 weeks), 39.3% water was found. In the noncalcifying part during the same period, the water decrease was insignificant, from 61.7 to 60.3%. Lowest values for calcified tendon were attained by 30 weeks, 24.4%,

TABLE 2
Shrinkage temperatures of uncalcified tendons

Age	Ts (mean) °C	Ts (range) °C	± S.D.
4 Weeks (6) ¹	62.0	61–63	0.2
6 Weeks (9)	63.5	62–64	0.2
10 Weeks (9)	65.0	64–66	1.0
13 Weeks (9)	64.3	63–65	0.2
16 Weeks (14)	66.8	65–67	0.2
20 Weeks ¹ (6)	64.1	63–65	0.1
30 Weeks ¹ (6)	64.2	63–66	0.8
35 Weeks ¹ (6)	66.2	65–67	0.4
40 Weeks ¹ (9)	66.1	65–67	0.2

¹ Number of measurements.

² Tendons passing through the tibio-tarsal articulation.

and no further decline was observed during the remaining period which was studied (fig. 3).

DISCUSSION

Calcification of connective tissues involves changes in morphology, composition and micellar organization. In the ossification of avian tendon, these processes are somewhat less complicated because the original cellular and extracellular structures are fairly well defined and less heterogeneous, and their transformation appears to be relatively direct. The direction of our work and the interpretation of the observations were strongly influenced by earlier morphological, histochemical and physiochemical studies of connective tissues in varying physiological states (Catchpole et al., '66; Engel et al., '54; Gersh and Catchpole, '49, '60; Joseph et al., '52, '54, '59, '65). Certain generalizations emerging from those studies and bearing on the current work are briefly mentioned.

The extracellular matrix of connective tissues consists of fibrillar parts, mainly

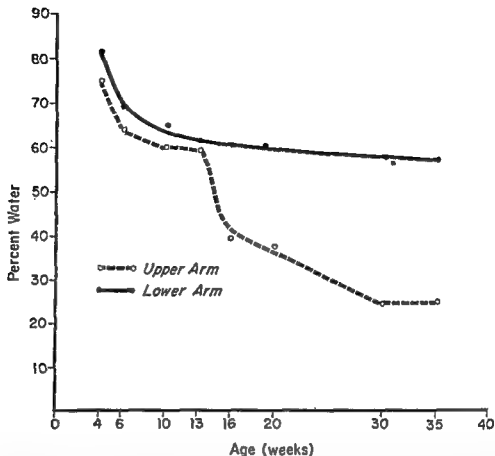


Fig. 3 The solid line represents the changes in water content in a portion of the gastrocnemius tendon which does not calcify. The per cent water drops rapidly during the first weeks but decreases only slightly after 16 weeks. Tendons represented by the dashed line calcify around 16 weeks, when a sharp drop in water concentration is observed. After 30 weeks, the water remains constant.

collagen, with some reticular and elastic fibers, and a non-fibrillar ground substance containing various carbohydrate-protein complexes, lipids, water, electrolytes and other unidentified components. These vary in different tissues. It is believed that collagen and ground substance together form complex coacervates which include colloid-rich and water-rich phases coexisting in equilibrium. Because of the predominance of anionic groups, such as carboxylate and sulfate, the tissues have a net negative charge at physiologic pH. Using an electrochemical method, *in vivo* titration curves of tissue colloids have been determined. These differ to some extent depending upon chemical composition and physicochemical state. From the curves, certain general inferences have been made with respect to the behavior of proton-binding groups and the existence of cross-

linking low energy bonds. These probably include hydrogen bonds and electrostatic bonds between oppositely charged groups. In essence, connective tissues act as amphoteric polyelectrolytes with isoelectric points between pH 2 and 2.5.

The negative charge of the colloidal matrix is neutralized by the physiological cations. The concentration of free calcium ions is considerably higher than that in blood plasma. In addition, there is a large fraction which is bound to the connective tissue colloids through electrostatic forces or by chelation (Engel et al., '54, Joseph et al., '65).

Titration curves of turkey tendons have been determined *in vivo*; at physiologic pH, the net negative charge was in the neighborhood of 0.060 Eq/kgm tissue water. The negative charge density was not appreciably affected by maturation, but

preliminary experiments suggested that calcification of the tendon was preceded by a diminished calcium binding capacity. These earlier results imply that changes in physicochemical state or in composition accompanied ossification.

Changes in the state of aggregation

The rise of shrinkage temperature* of maturing and aging tendon, together with loss of water and resistance to change of birefringence on exposure to KI, indicates an increased stability in conformation and internal structure. This may be due to crosslinking of the structural proteins which is generally assumed to occur in aging. This view was first proposed by Bjorksten in 1941, and considered by Gustavson ('56) in connection with the aging of collagen. Gustavson emphasized reactions of collagen with biologic aldehydes. Similar ideas have been developed by Verzar ('56, '63, '64), Zinsser et al. ('57, '63), Joseph and Bose ('62), Milch ('63) and Sinex ('64). The study of various types of crosslinks in purified collagen is now evoking much interest (Gallop, '64; Glimcher, '65; Piez et al., '60, '61; Veis, '64; Veis et al., '64, '65). However, it is premature to extrapolate the conclusions reached with pure collagen to the complex native coacervates of collagen and ground substance which exist in all connective tissues.

As the process of calcification proceeds and the matrix matures, the staining of the tendon with dinitrofluorobenzene is diminished or disappears. Presumably, this reflects either a change in concentration or reactivity of ϵ -amino groups of lysine-hydroxylysine. Pretreatment of mineralized tissues with dilute acid (0.01M HCl) or with citrate buffer, pH 3.5, or prolonged treatment with DNFB reagent (over 12 hours) will again elicit the reaction. These results suggest that the amino groups are masked through coulombic interactions or some other type of relatively weak crosslinking. The ϵ -amino groups of lysine-hydroxylysine are known to be involved in inter and intramolecular linkages, playing an important role in stabilizing the tertiary structure of macromolecules. Their availability to DNFB has been shown to change during denatura-

tion (Porter, '48), aging (Joseph and Bose, '62), and calcification (Solomons and Irving, '58; Zerlotti and Engel, '62). An additional explanation may involve the arrangement of water around these groups in an ice-like state (Klotz, '65), thereby modifying their reactivity.

Changes in composition

From the histochemical evidence presented in this paper and that reported by Johnson ('60) it is clear that changes in cellular morphology and secretory activity accompany the physical changes. Granules and aggregates of protein, glycoprotein and lipid are observed in the cells; presumably these are precursors of the modified extracellular matrix. Carbohydrate containing substances and lipids are demonstrated in greater amounts in the matrix concurrently with the physicochemical events which precede and accompany mineralization.

At later stages in calcification, the periodic acid-Schiff reaction of the matrix is very weak. This was already noted as characteristic of maturing bone by Heller-Steinberg ('51), Engel ('52), and Cobb ('53). However, a strong reaction can be elicited by preliminary exposure to acid or citrate buffer. Perhaps 1,2-glycol groups participate in forming some type of internal bond which contributes to the aggregation of the structure. Biochemical studies have shown that various carbohydrate fractions are linked to collagen through weak and strong bonds and these seem to play an important role in the stabilization of the collagen molecule (Gallop, '64; Grassman et al., '57; Mathews, '65; and Schneider, '49). Unfortunately, the interactions between collagen and ground substance in the native state are not actually revealed in studies of this kind because most of the extra-fibrillar components are extracted during the preparation of the tissues. On the other hand, valuable information concerning some aspects of these interactions is obtained by studying

*The rise in shrinkage temperature observed in aging (Brown and Cosden, '58; Radhakrishnan et al., '62) appears to imply increased aggregation by crosslinkage of macromolecules. When collagen was treated *in vitro* with crosslinking agents, like glutaric dialdehyde, the shrinkage temperature was raised from 62.5 to 81°C. At the same time, the dielectric constant of the dried specimens dropped from approximately 8 to 3 (Milch et al., '61).

with the polarization microscope carefully prepared tissue sections which are close to the native state.

When longitudinal sections of tendon mounted in a series of media of increasing refractive index are examined with polarized light, the retardation curves go through a minimum. The notable change in the form birefringence curve at 13 weeks also supports the notion that the nature and relative volume of the ground substance is significantly changed at this point. The curves appear to follow the Wiener mixed body equation, and they indicate that the structural orientation is due only in part to an intrinsic or textural component, collagen. The partial volume of the matrix in which the fibers are embedded contributes to the shape and height of the curve above its minimum. The ground substance appears to interact with collagen to form an oriented structure. The studies of Vidal ('63, '65) on the effects of hyaluronidase on the retardation of polarized light and on the dichroism of toluidine blue as demonstrated in guinea pig tendon, provides further evidence of this organizing role of the extrafibrillar matrix. Mismahl and Strohmaler ('64), making quantitative evaluations of the phenol reaction of Von Ebner, were also able to show the preferential orientation of the ground substance in human skin.

At the time when ossification of the tendon begins, there is an influx of chloroform-methanol extractable lipids. Using analytical methods on calcifying cartilage and bone, Wuthier and Shapiro ('66a, '66b) found a large fraction of neutral lipid. Further confirmation comes from the microscopic study of bone by Enlow et al. ('65). The former workers also reported that an acidic lipid was strongly bound to cartilage and bone and was only extracted by acid solvents after decalcification. This fraction seems to correspond to the material staining with Sudan Black which was found in calcifying areas of bone by Irving ('63).

Perhaps the loss of water can be regarded as a central event in the calcification process; the influx of lipids would be favored under these conditions, representing the formation of hydrophobic phases. From theoretical considerations, the remaining

water might be expected to be highly organized, especially around non-polar groups, forming clathrates (Klotz, '65). Also, hydrophobic bonding in the matrix structures would be favored (Nemethy and Scheraga, '60; Scheraga, '65; Bernal, '65). Under these conditions, changes in the dielectric properties of the heterogeneous medium would be expected (Witnauer, '61).

The lipids were given special significance in pathologic calcification by Wells ('06) and many pathologists consider them as the essential components in the pathogenesis of atherosclerosis. In recent years, some of the views expressed by Wells have been revived in a modified form and chemical binding of calcium by various lipid or lipoprotein complexes has been considered (Fels, '61; Kanabrocki et al., '60). If the changes in ossification of avian tendon can be considered as having some relevance to processes in pathologic calcification, perhaps a different role could be assigned to the lipid: as signalling the formation of hydrophobic phases.

Earlier physicochemical studies and the current biophysical and histochemical observations lead to some tentative and partial explanations of the transformation of the turkey tendon to a bony tissue.

During maturation, the various components of the negatively charged tendon matrix undergo progressive crosslinking through increased interactions between molecules due to Van der Waals forces, electrostatic and hydrogen bonds, ester linkages and covalent bonds. The change is initiated when the cells secrete new substances which alter the chemical reactivity of their environs. Simultaneously, water is lost (Cf. Gersh, '60), its state of organization is modified and the concentrations of ionic and bound cations, including calcium, shift. According to thermodynamics, this represents changes in the standard chemical potentials of water and electrolytes in the colloid-rich and water-rich phases of the tendon. The influx of lipids may contribute in a major way to changes of standard chemical potential and ion distribution.

The modified matrix, relatively rich in lipids and poor in water, has undergone a highly significant alteration in composi-

tion and in the organization of its constituents. This would be consonant with a lowering of the average dielectric constant of the structure. In this new physicochemical environment, the solubility constants of the various species of calcium salts found in bone would be modified.² Calcium ions released from their protein bound state or present in aqueous phases would tend to precipitate at lower ionic concentrations of calcium and phosphate than in an ideal solution where the water is in a less organized state.

During calcification, barriers to diffusion, including low vascularity, tend to create a closed, or partially closed, system in the tissue. Then the mineral phases form with minimal transfer of electrolytes to the circulation. According to the phase rule, the formation of insoluble bone salts stabilizes the heterogeneous biological structure.

ACKNOWLEDGMENTS

We thank Mr. William Winn, biological photographer, and Mr. Robert Parshall, medical illustrator, for their assistance with the illustrations.

LITERATURE CITED

- Bangs, I. J., Baló and D. Szabó 1956 Sub-microscopic structure of collagen fibers: their contraction and relaxation. *Acta Morphol Acad. Sci. Hung.*, 6: 391-403.
- Bear, R. S., F. O. Schmitt and J. Z. Young 1937 The ultrastructure of nerve axoplasm. *Proc. Roy. Soc. Lond., Series B*, 123: 505-519.
- Bennett, H. S. 1950 The microscopical investigation of biological materials with polarized light. In: *McClung Handbook of Microscopical Techniques*. R. McClung Ed., 3rd ed., P. B. Hoeber, Inc., New York, pp. 591-677.
- Bernal, J. D. 1965 The structure of water and its biological implications. *Soc. Exp. Biol. Symp.*, 19: 17-32.
- Bjorksten, J. 1941 Recent developments in protein chemistry. *Chem. Industries*, 48: 746-751.
- 1942 Chemistry of duplication. *Chem. Industries*, 50: 68-72.
- Born, M. 1920 Volumes and heats of hydration of ions. *Physik. Z.*, 1: 45-48.
- Bowes, J. H., and J. A. Moss 1951 Free amino groups of collagen. *Nature*, 168: 514-515.
- Brown, P. C., and R. Consden 1958 Variation with age of shrinkage temperature of human collagen. *Nature*, 181: 349-350.
- Catchpole, H. R., N. R. Joseph and M. B. Engel 1966 Thermodynamic relations of polyelectrolytes and inorganic ions of connective tissue. *Fed. Proc.*, 25: 1124-1126.
- Cobb, J. D. 1953 Relation of glycogen, phosphorylase and ground substance to calcification of bone. *A.M.A. Arch. Pathol.*, 55: 496-502.
- Davies, H. C., and A. Engström 1954 Interferometric and x-ray absorption studies of bone tissue. *Exp. Cell Res.*, 7: 243-255.
- Debye, P. 1945 Polar molecules. Dover Publ., New York.
- Engel, M. B. 1952 Mobilization of mucoprotein by parathyroid extract. *A.M.A. Arch. Pathol.*, 53: 339-351.
- Engel, M. B., N. R. Joseph and H. R. Catchpole 1954 Homeostasis of connective tissues. Calcium-sodium equilibrium. *A.M.A. Arch. Pathol.*, 58: 26-39.
- Engel, M. B., N. R. Joseph and D. M. Laskin 1962 Morphologic and physicochemical events in calcification of turkey tendon. Preprinted abstracts of the 40th General Meeting of the Int. Assn. Dent. Res., p. 29.
- Enlow, D. H., J. L. Conklin and S. Bang 1963 Observations on the occurrence and the distribution of lipids in compact bone. *Clin. Orthopaedics*, 38: 157-169.
- Fels, I. G. 1961 Binding of calcium ions by the aorta. *Nature*, 190: 1012-1013.
- Frey-Wissling, A. 1940 Analyse der Formdoppelbrechungskurven. *Kolloid Zeitsch.*, 80: 33-40.
- Gallop, P. M. 1964 Concerning some special features of the collagen molecule. *Biophys. J.*, 4: 79-92.
- Gersh, I. 1932 The Altman technique for fixation by drying while freezing. *Anat. Rec.*, 53: 309-337.
- 1960 Ground substance and calcification. In: *Bone as a Tissue*, K. Rodahl, J. T. Nicholson and E. M. Brown (Eds.), McGraw-Hill Book Co., New York, pp. 128-143.
- Gersh, I., and H. R. Catchpole 1949 The organization of ground substance and basement membrane and its significance in tissue injury, disease and growth. *Am. J. Anat.*, 85: 457-521.
- 1960 The nature of ground substance of connective tissue. *Persp. Biol. Med.*, 3: 282-319.
- Glimcher, M. J., and E. Katz 1965 The organization of collagen in bone: the role of non-covalent bonds in the relative insolubility of bone collagen. *J. Ultrastr. Res.*, 12: 705-729.
- Goland, P., E. Scheiman-Tager and M. B. Engel 1965 Enamel preservation during decalcification following fixation by some reactive halogen compounds. *J. Dent. Res.*, 44: 342-349.
- Grassman, W., U. Hofmann, K. Kühn, H. Hörmann, H. Endres and K. Wolf 1957 Electron microscope and chemical studies of the carbohydrate groups of collagen. In: *Connective Tissue*. R. E. Tunbridge, Ed., Thomas, Springfield, Illinois, pp. 157-171.
- Gustavson, K. H. 1956 The chemistry and reactivity of collagen. Academic Press, New York.
- *The solubility of any salt is determined by its standard chemical potential in any medium. The standard chemical potential is proportional to the square of the ionic charge and inversely proportional to the ionic radius and to the dielectric constant of the solvent (Born, 20; Debye, 45; Joseph, 66).

- Hack, M. H. 1952 A new histochemical technique for lipides applied to plasmal. *Anat. Rec.*, 112: 275-301.
- Hale, A. J. 1958 The interference microscope in biological research. E. S. Livingstone Ltd., London.
- Heller-Steinberg, M. 1951 Ground substance, bone salts, and cellular activity in bone formation and destruction. *Am. J. Anat.*, 89: 347-379.
- Irving, J. T. 1963 The sudanophil material at sites of calcification. *Arch. Oral Biol.*, 8: 735-745.
- Johnson, L. C. 1960 Mineralization of turkey leg tendon. I — Histology and Histochemistry of mineralization. In: *Calcification in Biological Systems*. R. Sognnaes Ed., Amer. Assoc. Adv. Sci., pp. 117-149.
- Joseph, K. T., and S. M. Bose 1962 Influence of biological ageing on the stability of skin collagen in albino rats. In: *Collagen*. N. Ramanathan Ed., Interscience Publ., New York, pp. 371-393.
- Joseph, N. R. 1966 Intracellular hydration of ions in relation to age. *Gerontologia*, 12: 155-173.
- Joseph, N. R., M. B. Engel and H. R. Catchpole 1952 Interaction of ions and connective tissue. *Biochim. Biophys. Acta*, 8: 575-587.
- 1954 Homeostasis of connective tissues. II. Potassium-sodium equilibrium. *A.M.A. Arch. Pathol.*, 58: 40-58.
- 1965 Distribution of ions in biological systems. *Nature*, 206: 8-10.
- Joseph, N. R., H. R. Catchpole, D. M. Laskin and M. B. Engel 1959 Titration curves of colloidal surfaces. II. Connective tissues. *Arch. Biochem. Biophys.*, 84: 224-242.
- Kanabrocki, E. L., I. G. Fels and E. Kaplan 1960 Calcium, cholesterol and collagen levels in human aortas. *J. Gerontol.*, 15: 383-387.
- Klotz, I. M. 1965 Role of water structure in macromolecules. *Fed. Proc.*, 24 Suppl., 15: S-24-S-33.
- Köhler, A. 1921 Ein Glimmerplättchen Grau. I. Ordnung zur Untersuchung sehr schwach doppel brechender Präparate. *Zeitsch. Wissen. Mikr.*, 38: 29-42.
- Lewis, M. S., and K. A. Piez 1964 Sedimentation-equilibrium studies of the molecular weight of single and double chains from rat-skin collagen. *Biochem.*, 3: 1126-1131.
- Lieberkühn, N. 1860 Ueber die Ossification. Die Ossification des Sehngewebes. *Arch. Anat. Physiol. Wissen. Med.*, pp. 824-846.
- 1863 Weitere Beiträge zur Lehre von der Ossification. *Arch. Anat. Physiol. Wissen. Med.*, pp. 614.
- Likins, R. C., K. A. Piez and M. L. Kunde 1960 Mineralization of turkey leg tendon. III. Chemical nature of the protein and mineral phases. In: *Calcification in Biological Systems*. R. Sognnaes, Ed., Amer. Assoc. Adv. Sci., pp. 143-149.
- Mathews, M. B. 1965 The interaction of collagen and acid mucopolysaccharides. *Biochem. J.*, 96: 710-716.
- Milch, R. A. 1963 Studies of collagen tissue ageing: Interaction of certain intermediary metabolites with collagen. *Gerontologia*, 7: 129-152.
- Milch, R. A., L. J. Frisco and E. A. Szymkowiak 1965 Solid-state dielectric properties of aldehyde-treated goatskin collagen. *Biorheology*, 3: 9-20.
- Missahl, H. P., and B. Strohmaier 1961 Anlagerung von Teilstücken der Grundsubstanz an kollagen Fasern. *Zschft. Ges. Exp. Med.*, 138: 452-460.
- Myers, H. M., and A. Engström 1965 A note on the organization of hydroxyapatite in calcified tendons. *Exp. Cell Res.*, 40: 182-185.
- Nemethy, G., and H. A. Scheraga 1962 The structure of water and hydrophobic bonding in proteins. III. The thermodynamic properties of hydrophobic bonds in proteins. *J. Phys. Chem.*, 66: 1773-1789.
- Nylen, M. U., D. B. Scott and V. M. Mosley 1960 Mineralization of turkey leg tendon. II. Collagen-mineral relations revealed by electron and x-ray microscopy. In: *Calcification in Biological Systems*. R. Sognnaes, Ed., Amer. Assoc. Adv. Sci., pp. 129-142.
- Piez, K. A., E. Weiss and M. S. Lewis 1960 The separation and characterization of the α and β components of calf skin collagen. *J. Biol. Chem.*, 235: 1987-1991.
- Piez, K. A., M. S. Lewis, G. Martin and J. Gross 1961 Subunits of the collagen molecule. *Biochim. Biophys. Acta*, 53: 596-598.
- Porter, R. R. 1948 The unreactive amino groups of proteins. *Biochim. Biophys. Acta*, 2: 105-112.
- Radhakrishnan, V. M., N. Ramanathan and Y. Nayudamma 1964 A note on the effect of age and sex on the shrinkage temperature of tendon collagen. *Leather Sci.*, 11: 102-104.
- Ranvier, L. 1889a Des plaques chondroïdes des tendons des oiseaux. *Compt. Rend. Soc. Acad. Sci.*, 108: 433-435.
- 1889b Traité technique d'histologie. 2ème ed., Librairie F. Savy, Paris.
- Renaud, J. 1871-72 Recherches sur la transformation vésiculeuse des éléments cellulaires des tendons. *Arch. Physiol. Norm. Pathol.*, 4: 271-292.
- Retterer, E. et A. Lellèvre 1911 Phénomènes cytologiques des tendons des oiseaux en voie d'ossification. *Compt. Rend. Sci. Mem. Soc. Biol.*, 71: 596-599.
- Scheraga, H. A. 1965 The effects of solutes on the structure of water and its implications for protein structure. *Ann. N. Y. Acad. Sci.*, 125: 253-276.
- Schmidt, W. J. 1924 Die Bausteine des Tierkörpers im polarisierten Licht. F. Cohen, Bonn.
- Schmitt, F. O. 1944 Structural proteins of cells and tissues. *Adv. Prot. Chem.*, 1: 25-68.
- Schneider, F. 1949 Über die Bedeutung des Zuckers in Kollagen. *Angew. Chem.*, 61: 259-260.
- Sinex, F. M. 1964 Cross-linkage and aging. *Adv. Gerontol. Res.*, 1: 165-180.
- Solomons, C. C., and J. T. Irving 1958 The reaction of some hard and soft tissues collagen

- with 1-fluoro-2:4-dinitrobenzene. *Biochem. J.*, 70: 179-182.
- Veis, A. 1964 The macromolecular chemistry of gelatin. Academic Press, New York.
- Veis, A., and J. Anesey 1965 Modes of intermolecular cross-linking in mature insoluble collagen. *J. Biol. Chem.*, 240: 3899-3908.
- Veis, A., J. Anesey and J. Cohen 1960 The depolymerization of collagen fibers. *J. Am. Leather Chem. Assoc.*, 10: 548-560.
- Verzar, F. 1956 Das Altern des Kollagens. *Helv. Physiol. Acta*, 14: 207-220.
- 1963 Lectures on experimental gerontology. Thomas, Springfield, Illinois.
- 1964 Aging of the collagen fiber. *Int. Rev. Connect. Tissue Res.*, 2: 243-300.
- Verzar, F., H. Spichtin and W. Gashe 1965 Renaturation of collagen fibers after different methods of denaturation. *Gerontologia*, 11: 226-234.
- Vidal, B. C. 1963 Pleochroism in tendon and its bearing to acid mucopolysaccharides. *Protoplasma*, 56: 529-536.
- 1965 The part played by the mucopolysaccharides in the form birefringence of the collagen. *Protoplasma*, 59: 472-479.
- Weidenreich, F. 1930 Das Knochengewebe. Die Gewebe. In: *Handbuch der Mikroskopischen Anatomie des Menschen*. W. v. Möllendorff, Verlag, Berlin, pp. 391-520.
- Wells, H. G. 1906 Pathological calcification. *J. Med. Res.*, 14: 491-525.
- Wiener, O. 1913 Die Theorie des Mischkörpers für das Feld der stationären Strömung. *Akad. der Wissen. Math. Nat. Kl.*, 32: 507-604.
- Witmaner, L. P. 1961 Dynamic electrical behavior of untanned hide containing sorbed water. *J. Amer. Leather Chem. Assoc.*, 56: 343-356.
- Wuthier, R. E., and L. M. Shapiro 1966a Discovery of two unidentified lipids associated with the mineral phase of calcified tissues. Preprinted Abstracts, 44th General Meeting, Int. Assoc. Dent. Res., pp. 40.
- 1966b Comparison of lipids from calcifying and non-calcifying tissues. Preprinted Abstracts, 44th General Meeting, Int. Assoc. Dent. Res., pp. 40.
- Zahn, H. 1955 Cross-linking reactions with amino acids and fibrous proteins. *Proc. Int. Wool Text. Res. Conf., Australia*, pp. 425-450.
- Zerlotti, E., and M. B. Engel 1962 The reactivity of proteins of some connective tissues and epithelial structures with 2,4-dinitrofluorobenzene. *J. Histochem. Cytochem.*, 10: 537-546.
- Zinsser, H. H., E. M. Butt and J. Leonard 1957 Metal content correlation in aging aorta. *J. Amer. Ger. Soc.*, 5: 20-26.
- Zinsser, H. H., J. Bjorksten, F. A. Andrews and I. S. Light 1963 Changes in collagen structure induced by naturally cross linking agents. Abstracts, Annual Meeting, Gerontological Soc. *The Gerontologist*, 3: 13 (Sept., Part II).

PLATE 1

EXPLANATION OF FIGURES

All sections were stained with hematoxylin and eosin. A wratten filter no. 58 was employed for photomicrography.

- 4 Tendon from 4-week turkey showing bundles of collagenous fibers separated by linear arrays of large fibroblasts. 700 \times .
- 5 At 10 weeks, the collagen bundles appear more compact and the cells are less numerous and smaller. 700 \times .
- 6 The tendons of 13 week old turkeys presented some areas, as this one shown here, where the staining was uneven with regions of intense eosinophilia. In the center, a large number of cells, probably proliferating connective cells, are seen. 700 \times .
- 7 Cells in 16 week tendons are transformed to cuboidal form. Fibrillar components of matrix are not so distinctly visualized. 700 \times .
- 8 Cuboidal cells with deeply stained basophilic nuclei in 16 week newly calcified tendon. The matrix is deeply stained with hematoxylin. 700 \times .
- 9 Calcified region of 20 week tendon. A group of chondroid cells are embedded in a portion of the basophilic, calcified matrix. 700 \times .
- 10 Tendon at 30 weeks. Nuclei of cuboidal cells are intensely stained. Basophilia of the matrix is reduced. 700 \times .

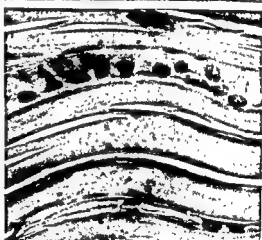
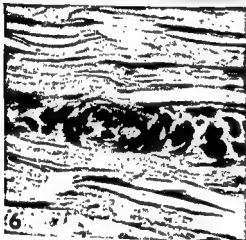
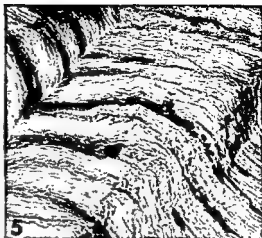
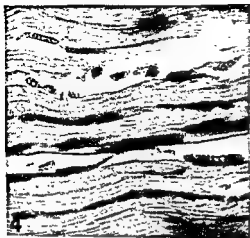


PLATE 1

EXPLANATION OF FIGURES

All sections were stained with hematoxylin and eosin. A wratten filter no. 58 was employed for photomicrography.

- 4 Tendon from 4-week turkey showing bundles of collagenous fibers separated by linear arrays of large fibroblasts. 700 X.
- 5 At 10 weeks, the collagen bundles appear more compact and the cells are less numerous and smaller. 700 X.
- 6 The tendons of 13 week old turkeys presented some areas, as this one shown here, where the staining was uneven with regions of intense eosinophilia. In the center, a large number of cells, probably proliferating connective cells, are seen. 700 X.
- 7 Cells in 16 week tendons are transformed to cuboidal form. Fibrillar components of matrix are not so distinctly visualized. 700 X.
- 8 Cuboidal cells with deeply stained basophilic nuclei in 16 week newly calcified tendon. The matrix is deeply stained with hematoxylin. 700 X.
- 9 Calcified region of 20 week tendon. A group of chondroid cells are embedded in a portion of the basophilic, calcified matrix. 700 X.
- 10 Tendon at 30 weeks. Nuclei of cuboidal cells are intensely stained. Basophilia of the matrix is reduced. 700 X.

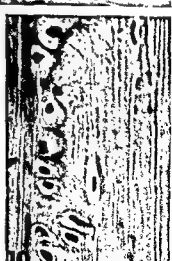
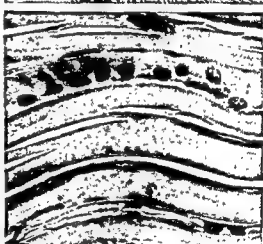
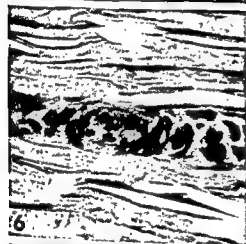
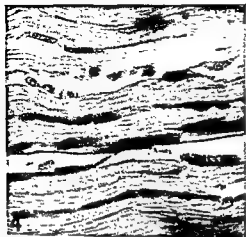


PLATE 2

EXPLANATION OF FIGURES

Sections shown in figures 11-24 were stained with dinitrofluorobenzene (DNFB).

- 11 At ten weeks, the collagen fibers stained with DNFB and the nuclei of fibroblasts are highly reactive. The cytoplasm is barely visible. 700 \times .
- 12 At four weeks, the tendon is highly reactive. The cytoplasm of large, young fibroblasts is also DNFB-positive (arrows). 1480 \times .
- 13 Tendon of 16-week bird. The young bone matrix (m) reacts with DNFB to some degree, but its staining intensity is considerably weaker than interbundle sheaths which are less mineralized (s) and these correspond to structures seen in cross section of the unmineralized tissue. Both nucleus and cytoplasm of cells are well stained. 700 \times .
- 14-15 Microradiograph and DNFB stain of the same section respectively.
- 14 Region of junction in tendon of 16 week bird. Calcified part appears white (m); radiolucent holes correspond to cells or lacunae. Imperfection in section due to fold (a). Mass absorption coefficient of unmineralized matrix (u) is low in relation to mineralized areas. 700 \times .
- 15 Radiopaque regions of matrix in figure 14 are unreactive with DNFB (m), while the stained areas appear as radiolucent structures (u) in figure 14. Artefact (a). 700 \times .
- 16 Sixteen week tendon stained with DNFB. Cuboidal cells are surrounded by the new matrix (arrow), which stains less intensely than the uncalcified fibrous bundles (u). 1500 \times .
- 17 The calcified tendon (m) shows low reactivity to DNFB, but the unmineralized tissue (u) is intensely stained. Seventeen week old turkey. 700 \times .

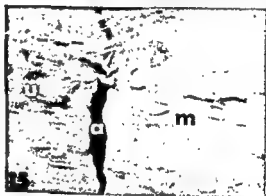


PLATE 2

EXPLANATION OF FIGURES

Sections shown in figures 11-24 were stained with dinitrofluorobenzene (DNFB).

- 11 At ten weeks, the collagen fibers stained with DNFB and the nuclei of fibroblasts are highly reactive. The cytoplasm is barely visible. 700 X.
- 12 At four weeks, the tendon is highly reactive. The cytoplasm of large, young fibroblasts is also DNFB-positive (arrows). 1480 X.
- 13 Tendon of 16-week bird. The young bone matrix (m) reacts with DNFB to some degree, but its staining intensity is considerably weaker than interbundle sheaths which are less mineralized (s) and these correspond to structures seen in cross section of the unmineralized tissue. Both nucleus and cytoplasm of cells are well stained. 700 X.
- 14-15 Microradiograph and DNFB stain of the same section respectively.
- 14 Region of junction in tendon of 16 week bird. Calcified part appears white (m); radiolucent holes correspond to cells or lacunae. Imperfection in section due to fold (a). Mass absorption coefficient of unmineralized matrix (u) is low in relation to mineralized areas. 700 X.
- 15 Radiopaque regions of matrix in figure 14 are unreactive with DNFB (m), while the stained areas appear as radiolucent structures (u) in figure 14. Artifact (a). 700 X.
- 16 Sixteen week tendon stained with DNFB. Cuboidal cells are surrounded by the new matrix (arrow), which stains less intensely than the uncalcified fibrous bundles (u). 1500 X.
- 17 The calcified tendon (m) shows low reactivity to DNFB, but the unmineralized tissue (u) is intensely stained. Seventeen week old turkey. 700 X.

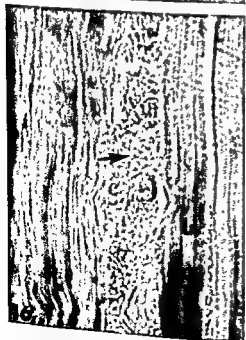
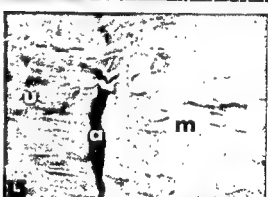
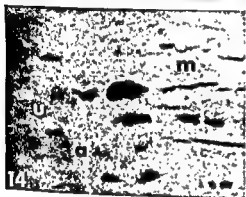


PLATE 3

EXPLANATION OF FIGURES

Figures 18 and 19 Microradiograph and DNFB stain respectively of calcified tendon.

- 18 Osteoid borders are radiolucent. 700 \times .
- 19 The less calcified osteoid is highly reactive to DNFB. The more highly mineralized contiguous matrix barely reacts. 700 \times .
- 20 Cross section of a calcifying tendon stained with DNFB. Note the cytoplasmic reactivity of the cuboidal cells (arrow) and the irregular distribution of stained areas in the bundles. 1500 \times .
- 21 Tendon of an 18-week old bird stained with DNFB. The calcified tissue has a granular appearance and the cuboidal cells are smaller and have highly reactive nuclei. 700 \times .

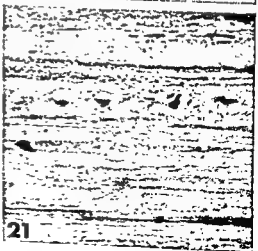
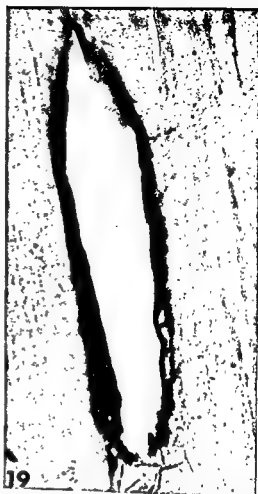


PLATE 3

EXPLANATION OF FIGURES

Figures 18 and 19 Microradiograph and DNFB stain respectively of calcified tendon.

- 18 Osteoid borders are radiolucent. 700 \times .
- 19 The less calcified osteoid is highly reactive to DNFB. The more highly mineralized contiguous matrix barely reacts. 700 \times .
- 20 Cross section of a calcifying tendon stained with DNFB. Note the cytoplasmic reactivity of the cuboidal cells (arrow) and the irregular distribution of stained areas in the bundles. 1500 \times .
- 21 Tendon of an 18-week old bird stained with DNFB. The calcified tissue has a granular appearance and the cuboidal cells are smaller and have highly reactive nuclei. 700 \times .

CALCIFICATION OF TURKEY LEG TENDON

Milton B. Engel and Eugenio Zerlotti

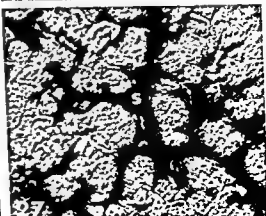
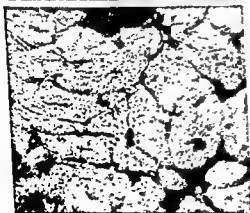
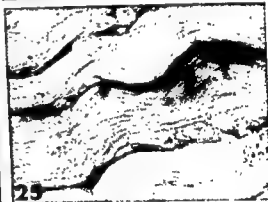


PLATE 4

EXPLANATION OF FIGURES

- 22 At 40 weeks, the junction is sharp, with the calcified areas (m) unstained with DNFB. Some cuboidal cells resembling those observed in earlier stages are still seen. Uncalcified tendon (u). 700 X.
- 23 Osteocytes (arrows) of 40-week old turkey tendons. The nuclei are DNFB positive, but the calcified tendon is unreactive. 1480 X.
- 24 Calcified tendon of 30-week old turkey. The tissue shows disruptive effect of exposure to citrate buffer before staining. The buffer elicited DNFB reactivity in normally unreactive sites. 700 X.
- 25 Tendon of young turkey, six weeks; elongated fibroblasts with processes and cytoplasm containing glycoprotein appear to form sheaths of the collagen bundles. The fibrils stain due either to their intrinsic glycoprotein content or to coating by ground substance. The section shows signs of swelling after exposure to periodic acid. 700 X.
- 26 Cross section of 13-week tendon shows enhanced reactivity of incomplete sheath structures (s) surrounding tendon bundles. 700 X.
- 27 Cross section of calcified turkey tendon from a 20 week bird, stained with PAS. The interbundle sheath (s) is intensely stained. 700 X.

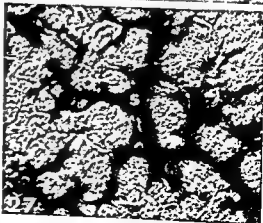
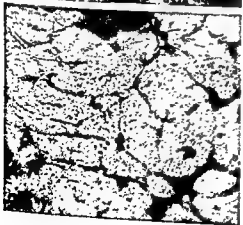
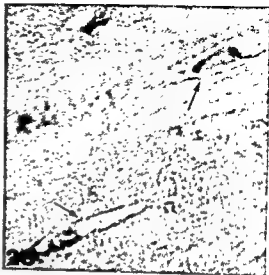


PLATE 5

EXPLANATION OF FIGURES

- 28 Longitudinal section of tendon in which bundles are outlined by reactive sheaths. Fibrillar components of the tendon are barely discerned. Some cells contain aggregates or granules of glycoprotein. 1500 \times .
- 29 Stage of early mineralization at 18 weeks. Enlarged tendon cells are outlined by intensely PAS positive substance. 700 \times .
- 30 Stage of early mineralization at 16 weeks. The enlarged cells are outlined by intensely reactive PAS positive material. Individual cells are separated by septae which are usually homogeneously deeply stained, or at least, very reactive at the cell surface. 700 \times .

Figures 31 and 32 Cross section of calcified tendon of 35-week old turkey. PAS stained and microradiograph of the same section, respectively. A coinciding area in both sections is outlined. 600 \times .

- 31 The interbundle sheaths are stained with PAS in contrast with the bundles which are unreactive.
- 32 The radiopaque bundles are surrounded by the less mineralized sheaths.
- 33 Mature bone of 40-week tendon. The matrix reacts only weakly with the PAS reagents. Cells displaced during sectioning indicated by slits (arrow) in the matrix texture. 700 \times .

Figures 34 and 35 PAS stain and microradiograph, respectively, of 16 week tendon. 600 \times .

- 34 The intercellular septae are deeply stained at the cell borders. The central part is less reactive (arrows).
- 35 Microradiograph of same section as figure 34, showing the partly calcified septae (arrows).



PLATE 6

EXPLANATION OF FIGURES

Sections shown in figures 36-46 were fixed with osmium tetroxide vapors at 5°C for 2-5 minutes and then stained with Oil Red O.

- 36 Cells of 6-week turkey laden with lipid. 700 ×
- 37 Aggregate of large young fibroblasts in ten-week turkey tendon, showing lipid staining of cellular organelles. 1500 ×.
- 38 Lipid aggregates in cells and pericellular matrix of ossified 22-week tendon. 700 ×.
- 39 Cuboidal cells of 20-week tendon containing lipid. Extracellular matrix is lightly stained. 700 ×.

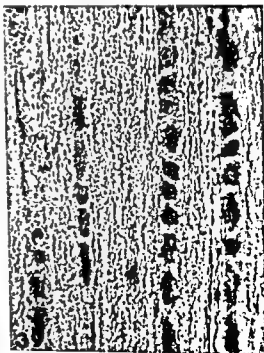
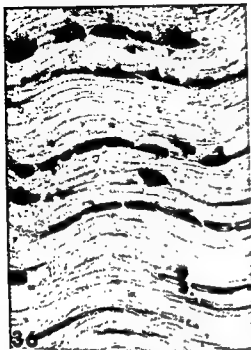


PLATE 7

EXPLANATION OF FIGURES

- 40 Large lipid aggregates or droplets in a cell of ossified tendon at 26 weeks. 1500 X.
- 41 Junction of ossified (m) and uncalcified (u) portion of tendon at 26 weeks. Cells in both areas contain considerable lipid. The most striking difference lies in the heavy deposition of extracellular lipid in the tissue contiguous to the ossified tendon. 700 X.
- 42 Heavily stained cells in a region which resembles cartilage at 30 weeks. 700 X.
- 43 Deeply stained osteocytes and processes in ossified tendon at 40 weeks. 700 X.
- 44 Lipid distribution in uncalcified tendon fibrils at 22 weeks. The interfibrillar substance in some regions seems to be free of lipid. 700 X.

CALCIFICATION OF TURKEY LEG TENDON
Milton B. Engel and Eugenio Zerlotti



PLATE 8

EXPLANATION OF FIGURES

- 45 Stained lipid of cells and their processes outline ossified tendon bundles at 22 weeks. 1500 X.
- 46 High concentrations of lipid in sheaths (s) surrounding more highly mineralized bundles of 35-week tendon. 700 X.

Figures 47-49 Photomicrographs made through the Leitz interference microscope.

- 47 Cross section of a 35-week old tendon photographed with white light and with the interference fringes in the field. The optical path difference given by the tissue is approximately two orders as shown by the dislocation of fringe (f). The less calcified sheaths around the bundles have lower retardations (arrows). 1150 X.
- 48 The junction is clearly visible in this section of a 16 week old turkey tendon. The mineral (m) has a high retardation and appears dark. Granules are observed at the junction. 600 X.
- 49 Cross section of a 16-week old turkey tendon. The mineral (m) first appears as granules at the periphery of the bundles (arrows). 600 X.

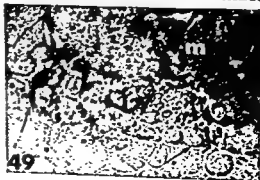
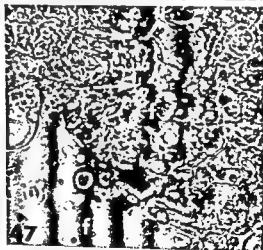
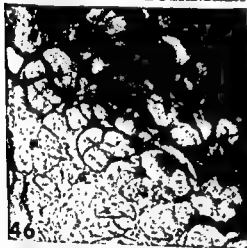
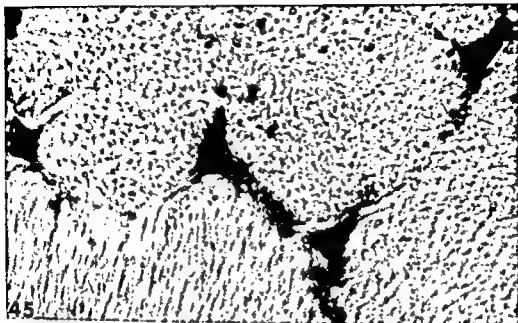


PLATE II

EXPLANATION OF FIGURES

- 45 Stained lipid of cells and their processes outline ossified tendon bundles at 22 weeks. 1500 X.
- 46 High concentrations of lipid in sheaths (s) surrounding more highly mineralized bundles of 35-week tendon. 700 X.

Figures 47-49 Photomicrographs made through the Lertz interference microscope.

- 47 Cross section of a 35-week old tendon photographed with white light and with the interference fringes in the field. The optical path difference given by the tissue is approximately two orders as shown by the dislocation of fringe (f). The less calcified sheaths around the bundles have lower retardations (arrows). 1150 X.
- 48 The junction is clearly visible in this section of a 16 week old turkey tendon. The mineral (m) has a high retardation and appears dark. Granules are observed at the junction. 600 X.
- 49 Cross section of a 16-week old turkey tendon. The mineral (m) first appears as granules at the periphery of the bundles (arrows). 600 X.

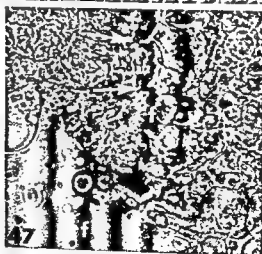
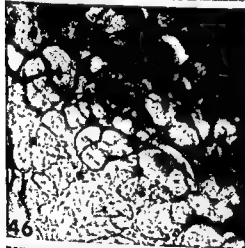
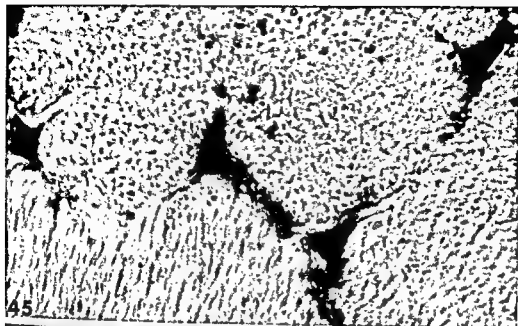
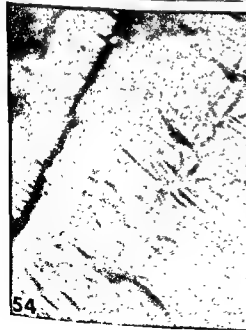
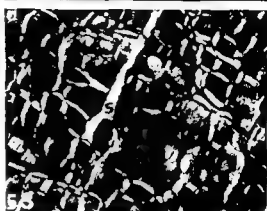
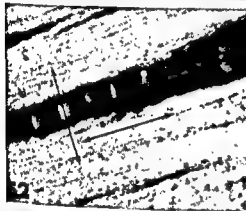
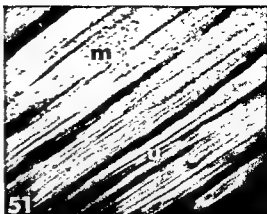
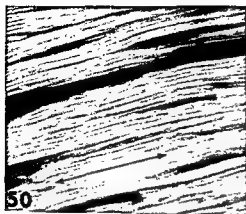


PLATE 9

EXPLANATION OF FIGURES

All sections were unstained, imbibed in Permout and photographed in the polarizing microscope with monochromatic light ($\lambda = 546 \text{ m}\mu$).

- 50 Section of uncalcified leg tendon of a ten-week old turkey. The collagen fibers are positively birefringent. The slow axis of transmission is indicated by the arrow. 650 \times .
- 51 The birefringence of the mineralized area (m) is only slightly higher than that of the uncalcified tissue (u). Sixteen week old. 650 \times .
- 52 The longitudinal section shows the low birefringence of the intercellular septae as compared to the calcified 16-week old tendon. The slow axis of transmission of the septae forms a 90° angle with that of the bundles, as indicated by the arrows. 1150 \times .
- 53 Cross section of a leg tendon of a 35-week old turkey, showing the highly birefringent sheaths (s) surrounding the calcified bundles. These appear dark because the light path of the microscope is parallel to their optical axis. 650 \times .
- 54 Longitudinal section of a tendon of a 4-week old turkey treated with 1.2M KI. The birefringence is very low and the bundles are wrinkled due to shrinkage. 650 \times .
- 55 The uncalcified tendon of a 16-week old treated with 1.2M KI shows decreased birefringence, but the effects are less marked than those observed in young birds (fig. 54). 650 \times .



An Electron- and Light-Microscope Study of Sinus Structure in Perfused Rabbit and Dog Spleens¹

CAROLYN EYSTER THOMAS
Department of Anatomy, Northwestern University Medical School,
Chicago, Illinois²

ABSTRACT The removal of blood cells by low-pressure perfusion produced well-delineated views of the sinus wall in rabbit and dog spleens. The sinus wall contained three elements: an inner layer of sinus cells, an intermediate layer of basement membrane, and an outer layer of cord-limiting cells. Sinus and cord-limiting cells, apparently similar to each other in cytoplasmic detail, appeared to be reticular cells that possessed only a limited capacity for phagocytosis of gold particles. Apertures in the sinus wall enabled blood cells to pass through the wall. Many apertures in perfused spleen contained no cells and yet remained patent. Sinus cells often were contiguous and commonly did not alternate with apertures. However, sinus-cell interdigitation was slight, and evidence for tight junctions and desmosomes between sinus cells was inconclusive.

Attempts to characterize the architecture of the splenic red pulp have been numerous; nevertheless, conclusive evidence pertaining to several controversial features still has not appeared. Important unresolved questions concern the structure of the sinus wall, the possibility of the existence of permanent openings between the sinus cells, the characteristics of these suspected openings, and the nature of the blood circulation in the sinuses and cord spaces. Twenty years ago the sinus wall seemed to most investigators to contain only two elements, the sinus cells and the encircling reticular fibers. Opinion regarding sinus-wall apertures ranged from one extreme to the other: some authors held that there were no openings in the sinus wall; some held that there were potential openings covered by thin extracellular membranes; some held that the sinus cells were in loose apposition and that blood cells could force their way through the wall; and still others believed that permanent openings lay between the sinus cells. Though some authors did maintain that the apertures were long slits that extended from one end of a sinus to the other, structural details of splenic circulation, including the open, the closed, and combined concepts, found adherents. Björkman's ('47) imposing review of the literature from 1686 through 1946 relates the evolution of the divergent viewpoints on these several questions.

Since 1946 investigators have undertaken additional significant studies. Snook ('50), using silver-impregnated sections, compared the spleens of 14 mammals and classified them into two categories, sinusal and non-sinusal; he believed that much of the confusion regarding splenic structure resulted from the comparison of spleens from different species. Snook ('58) studied the rabbit spleen with standard histologic techniques; he suggested that subsequent comparative studies on the spleen of this same species with transillumination and electron-microscope techniques would likely be particularly informative. Lewis ('56) observed the development of spleens in prene casts to investigate splenic circulation in mature specimens (Lewis, '57). Peck and Hoerr ('51a,b) and Parpart, Whipple and Chang ('55) investigated the mouse spleen with transillumination techniques, but the conclusions of the two groups conflicted sharply. Williams ('50) studied splenic autografts in transparent ear chambers in the rabbit. Most of the reformed characteristic splenic structure, surviving the six-month study period, In recent years the electron microscope has made possible more detailed descriptions of the splenic red pulp. Roberts and Latta ('64) described three forms of retic-

¹ USPHS Grant AM-06998 and USPHS General Research Support Grant 1-GS-70 furnished the financial support for this research.
² Present address: Department of Anatomy, Chicago Medical School, Chicago, Illinois.

ular cells that occurred randomly in the sinus walls and cords. Moore, Mumaw and Schoenberg ('64) observed in the rabbit that blood cells crossing the sinus wall "passed through" the basement membrane and pushed adjacent sinus cells apart. Movat and Fernando ('64) presented cytologic details of several cell forms that they had identified in the splenic red pulp. Weiss ('57, '62, '63) has been an important contributor to recent advances in interpretation of splenic red-pulp architecture. He described three layers in the sinus wall and presented a number of new cytologic details.

During the last 20 years the points of contention have remained essentially the same. Investigators still have not firmly established the structure of the sinus wall. Recent workers have generally observed cells migrating across the wall, but they have not agreed upon the manner by which this penetration of the wall occurs. Though modern authors often shun the terminology of the open and closed circulation theories, the controversy over the nature of splenic circulation persists.

This paper reports the results of an electron- and light-microscope study of the splenic sinus in rabbits and dogs. Preliminary preparation of the tissue entailed removal of much of the blood by low-pressure perfusion. The subjects of investigation were the general architecture of the sinus wall, the cytology of sinus and cord-limiting cells, the structure and relations of basement membrane, sinus-wall apertures, and phagocytosis by sinus and cord cells.

MATERIALS AND METHODS

Splenic tissue for this study came from five albino rabbits that weighed between 4 and 5 kg and from 12 mongrel dogs that weighed between 5 and 12 kg. All animals received pentobarbital sodium. In the rabbit ligation of major gastrosplenic arteries preceded the insertion of a 25-gauge needle into a branch of the splenic artery. A ligature secured the needle in the artery, and polyethylene tubing joined a syringe to the needle. In the dog omission of gastrosplenic ligation resulted in less splenic manipulation; the perfusion setup was like that utilized in the rabbit except for the substitution of an 18-gauge needle.

Three of the rabbits received 2 cm³ colloidal gold peripherally through an ear vein, and ten of the dogs received 2 cm³ colloidal gold centrally through the perfusion setup. Gold infusion preceded perfusion by about five minutes in all animals. The perfusion fluid was 6.5% glutaraldehyde, buffered with 0.1 M sodium cacodylate and adjusted to a pH of 7.2 (Sabatini, Bensch and Barnett, '63). Five to 20 cm³ of this solution flowed continuously for five to ten minutes through the rabbit spleens. Twenty to 60 cm³ of glutaraldehyde required 2.5 to seven minutes to pass smoothly through the dog spleens. A light even pressure, associated with a rotary movement, advanced the plunger of the syringe slowly; individually calculated mean rates ranged from 0.5 to 3 cm³/min. in the rabbit and from 5 to 10 cm³/min. in the dog. Increased resistance to the advance of the plunger, an event that generally just preceded or followed cessation of the heartbeat, resulted in immediate termination of the perfusion; thus some spleens received more fluid than others.

Simplicity of the experimental equipment, by expediting the procedure, helped to prevent overexposure of the spleen and unnecessary delay in perfusion. Manometric tests of the experimental technique did not include the animal preparation; however, they did indicate that the pressures at the hub of the needle probably ranged from 5 to 10 mm Hg. Since glutaraldehyde always entered through a branch of the splenic artery, the perfusion fluid passed through less than half of each spleen. This circumstance provided a control by permitting constant visual comparison of perfused to non-perfused portions of the spleen. Perfused areas did not swell nor become distorted, though they did blanch and become firmer. Two spleens shrank during perfusion and did not provide well-fixed tissue.

Small blocks of the perfused spleens underwent additional fixation by an immersion in buffered glutaraldehyde at about 4°C. Rabbit spleens remained in the solution for 45 minutes; dog spleens, for two hours. Washing of the tissues either in water or in 0.05 M sodium cacodylate followed. The rabbit tissue received only a brief rinsing; the dog tissue, a more thorough ablation that lasted four to six hours.

ular cells that occurred randomly in the sinus walls and cords. Moore, Mumaw and Schoenberg ('64) observed in the rabbit that blood cells crossing the sinus wall "passed through" the basement membrane and pushed adjacent sinus cells apart. Movat and Fernando ('64) presented cytologic details of several cell forms that they had identified in the splenic red pulp. Weiss ('57, '62, '63) has been an important contributor to recent advances in interpretation of splenic red-pulp architecture. He described three layers in the sinus wall and presented a number of new cytologic details.

During the last 20 years the points of contention have remained essentially the same. Investigators still have not firmly established the structure of the sinus wall. Recent workers have generally observed cells migrating across the wall, but they have not agreed upon the manner by which this penetration of the wall occurs. Though modern authors often shun the terminology of the open and closed circulation theories, the controversy over the nature of splenic circulation persists.

This paper reports the results of an electron- and light-microscope study of the splenic sinus in rabbits and dogs. Preliminary preparation of the tissue entailed removal of much of the blood by low-pressure perfusion. The subjects of investigation were the general architecture of the sinus wall, the cytology of sinus and cord-limiting cells, the structure and relations of basement membrane, sinus-wall apertures, and phagocytosis by sinus and cord cells.

MATERIALS AND METHODS

Splenic tissue for this study came from five albino rabbits that weighed between 4 and 5 kg and from 12 mongrel dogs that weighed between 8 and 12 kg. All animals received pentobarbital sodium. In the rabbit ligation of major gastrosplenic arteries preceded the insertion of a 25-gauge needle into a branch of the splenic artery. A ligature secured the needle in the artery, and polyethylene tubing joined a syringe to the needle. In the dog omission of gastrosplenic ligation resulted in less splenic manipulation; the perfusion setup was like that utilized in the rabbit except for the substitution of an 18-gauge needle.

Three of the rabbits received 2 cm³ colloidal gold peripherally through an ear vein, and ten of the dogs received 2 cm³ colloidal gold centrally through the perfusion setup. Gold infusion preceded perfusion by about five minutes in all animals. The perfusion fluid was 6.5% glutaraldehyde, buffered with 0.1 M sodium cacodylate and adjusted to a pH of 7.2 (Sabatini, Bensch and Barnett, '63). Five to 20 cm³ of this solution flowed continuously for five to ten minutes through the rabbit spleens. Twenty to 60 cm³ of glutaraldehyde required 2.5 to seven minutes to pass smoothly through the dog spleens. A light even pressure, associated with a rotary movement, advanced the plunger of the syringe slowly; individually calculated mean rates ranged from 0.5 to 3 cm³/min. in the rabbit and from 5 to 10 cm³/min. in the dog. Increased resistance to the advance of the plunger, an event that generally just preceded or followed cessation of the heartbeat, resulted in immediate termination of the perfusion; thus some spleens received more fluid than others.

Simplicity of the experimental equipment, by expediting the procedure, helped to prevent overexposure of the spleen and unnecessary delay in perfusion. Manometric tests of the experimental technique did not include the animal preparation; however, they did indicate that the pressures at the hub of the needle probably ranged from 5 to 10 mm Hg. Since glutaraldehyde always entered through a branch of the splenic artery, the perfusion fluid passed through less than half of each spleen. This circumstance provided a control by permitting constant visual comparison of perfused to non-perfused portions of the spleen. Perfused areas did not swell nor become distorted, though they did blanch and become firmer. Two spleens shrank during perfusion and did not provide well-fixed tissue.

Small blocks of the perfused spleens underwent additional fixation by an immersion in buffered glutaraldehyde at about 4°C. Rabbit spleens remained in the solution for 45 minutes; dog spleens, for two hours. Washing of the tissues either in water or in 0.05 M sodium cacodylate followed. The rabbit tissue received only a brief rinsing; the dog tissue, a more thorough ablation that lasted four to six hours.

Sections of sinus cells generally contained large and small vacuoles, numerous mitochondria, some endoplasmic reticulum, some ribosomes, and an occasional lipid inclusion. Pinocytotic vesicles were particularly abundant in the dog, lay along luminal, lateral, and basal surfaces, and contributed to surface unevenness. Cord-cell cytoplasm resembled sinus-cell cytoplasm. Two forms of indeterminate cytoplasmic concentration (Weiss, '57, '63) appeared in both sinus and cord cells (fig. 6). A narrow band of dense cytoplasm frequently bordered the basement membrane; occasionally the band extended along the lateral portions of the cell membranes. Various shaped islands of dense cytoplasm also occurred at the basal end of the cell. The basement membrane was not always present with this form of concentration, and the islands usually did not immediately border the cell surface. All concentrations were granular, and in the dog the granules within the islands often lay in a lattice-like pattern. Both forms of concentration stained more heavily with osmium than the basement membrane did (fig. 7).

Sinus-wall apertures varied in frequency. Lengthy stretches of unperforated sinus wall occurred (fig. 5), but sometimes apertures nearly alternated with sinus cells (fig. 9). In sections most apertures measured 2 μ or less in diameter, but some measured up to 5 or 6 μ . The rim of the aperture contained either all three wall elements or the sinus cell alone; both formations sometimes occurred in the same aperture. The sinus cell often extended a lip over the end of the basement membrane; but at times the lip was absent, and the end of the basement membrane was exposed. Ruptured basement or cell membranes, distorted sinus or cord-limiting cells, or other evidence suggesting that the apertures were artifacts did not appear.

Erythrocytes, leucocytes, platelets, and free macrophages frequently occupied the apertures and appeared to be in transit through the sinus wall. Many cells lay partly in the cord space, partly in the aperture, and partly in the sinus. Cells occupied the apertures in varying degrees. A cell might completely fill an aperture; sometimes a cell, bulging on each side of the wall, appeared to be squeezing through an

aperture, which perhaps enlarged temporarily to accommodate the cell. On the other hand, a cell might partially occupy an aperture with fluid separating the cell from the aperture rim (fig. 8).

Some cells occupied apertures in unusual ways. Figure nine shows a free macrophage which lay mostly in a cord space but which had extensions through three neighboring apertures into the sinus. Distorted erythrocytes appeared in a few of the apertures (fig. 11). Each of these cells consisted of two masses connected by a narrow U-shaped bridge. The bridge lay on the cord side of the wall and extended through two neighboring apertures into the sinus; the masses lay in the sinus. There were no examples of the reverse situations, wherein the body of a free macrophage or the bridge of a distorted erythrocyte lay in the sinus with the cell extensions directed through apertures toward the cord spaces.

Apertures that contained no cells were also common (right aperture in figs. 8, 10). Apparently the presence of formed blood elements was not essential for the maintenance of aperture patency. Cell-free apertures occurred even in areas where less thorough perfusion had left behind much plasma.

Compared to free macrophages, sinus and cord-limiting cells possessed only a limited capacity for phagocytosis. Sinus and cord-limiting cells occasionally contained dense clumps of material that they had phagocytosed under normal conditions. In gold-injected animals some sinus and cord-limiting cells contained a few gold particles that lay without surrounding membrane in the cytoplasm; in contrast nearby free macrophages contained gold particles in high concentration (figs. 10, 13). The basement membrane remained nearly devoid of gold.

DISCUSSION

The primary purpose in perfusing the spleen was to remove blood cells and thus to clarify views of the red pulp. The procedure appears to have been largely successful in this purpose: by alleviating cell crowding, reduction in blood-cell content allowed easy differentiation of fixed splenic cells from free cells; consequently, good delineation of basic structural features of

permanently were apparent, many cell-free apertures, nevertheless, appeared to remain patent in perfused spleen. Perfusion, however, evidently is not essential for demonstrating cell-free apertures. Weiss ('57) published an electron micrograph that revealed a cell-free aperture in a non-perfused spleen. Section thinness prevented complete evaluation of the size and shape of apertures and sinus cells; the absence of slit-like apertures and rod-shaped sinus cells in the sections of the present study does not by itself refute their existence. Speculation concerning aperture characteristics thus continues. The number, size, shape, patency, and location of apertures may be variable. If the actual situation involves intermittent aperture patency, structural features may limit apertures to specific locations. Conceivably, the separation of contiguous sinus cells would be relatively simple where interdigitation, tight junctions, desmosomes, cord-cell extensions, and basement membrane did not complicate the junction. However, cord-cell extensions and basement membrane bridged many of the sinus-cell junctions in this study. One supposition is that even these junctions may separate intermittently. The fineness of the cord-cell extensions and the apparent lack of high structural organization in the basement membrane prompt the conjecture that increased pressure from blood cells and plasma may result in attenuation of junction-bridging structures. The presence of an uncovered basement-membrane termination in an aperture rim (see Observations) would perhaps indicate the recent opening of the aperture.

4. The configuration of a few free macrophages and erythrocytes suggested that at least in local areas perfusion fluid flowed from cord spaces into sinuses (see Observations). The applicability of this observation to the circulatory schema of normal living spleen is problematic.

Since structural relationships may possibly vary with large changes in perfusion pressure, comparison of high- to low-pressure studies would perhaps assist in the resolution of some of these questions.

ACKNOWLEDGMENTS

The author gratefully acknowledges the general guidance of Dr. James C. Hampton

and the surgical assistance of Dr. Howard C. Hopps.

LITERATURE CITED

- Bell, G. H., J. N. Davidson and H. Scarborough 1965 *Textbook of Physiology and Biochemistry*. Williams and Wilkins Co., Baltimore. Chap. 29, 534-543.
- Björkman, S. E. 1947 The splenic circulation. With special reference to the function of the spleen sinus wall. *Acta Med. Scand.*, 123 (Supplement 191): 1-89.
- Grim, E. 1963 *Handbook of Physiology*, Section 2: Circulation. Ed. by W. F. Hamilton and P. Dow. American Physiological Society, Washington, D.C. Vol. II, Chap. 42, 1439-1456.
- Landis, E. M., and J. R. Pappenheimer 1963 *Handbook of Physiology*, Section 2: Circulation. Ed. by W. F. Hamilton and P. Dow. American Physiological Society, Washington, D.C. Vol. II, Chap. 29, 961-1034.
- Lewis, O. J. 1956 The development of the circulation in the spleen of the foetal rabbit. *J. Anat. (London)*, 90: 282-289.
- 1957 The blood vessels of the adult mammalian spleen. *J. Anat. (London)*, 91: 245-250.
- Luft, J. H. 1961 Improvements in epoxy resin embedding methods. *J. Biophys. and Biochem. Cytol.*, 9: 409-414.
- Moore, R. D., V. R. Mumaw and M. D. Schoenberg 1964 The structure of the spleen and its functional implications. *Exp. and Molecular Path.*, 3: 31-50.
- Movat, H. Z., and N. V. P. Fernando 1964 The fine structure of lymphoid tissue. *Exp. and Molecular Path.*, 3: 546-568.
- Palade, G. E. 1952 A study of fixation for electron microscopy. *J. Exp. Med.*, 95: 285-298.
- Parpart, A. K., A. O. Whipple and J. Chang 1955 The microcirculation of the spleen of the mouse. *Angiology*, 6: 350-362.
- Peck, H. M., and N. L. Hoerr 1951a The intermediary circulation in the red pulp of the mouse spleen. *Anat. Rec.*, 109: 447-477.
- 1951b The effect of environmental temperature changes on the circulation of the mouse spleen. *Anat. Rec.*, 109: 479-493.
- Reynolds, E. S. 1963 The use of lead citrate at high pH as an electron-opaque stain in electron microscopy. *J. Cell Biol.*, 17: 208-213.
- Richardson, K. C., L. Jarrett and E. H. Finke 1960 Embedding in epoxy resins for ultrathin sectioning in electron microscopy. *Stain Tech.*, 35: 313-323.
- Roberts, D. K., and J. S. Latta 1964 Electron microscopic studies on the red pulp of the rabbit spleen. *Anat. Rec.*, 148: 81-101.
- Sabatini, D. D., K. Bensch and R. J. Barnett 1963 Cytochemistry and electron microscopy: the preservation of cellular ultrastructure and enzymatic activity by aldehyde fixation. *J. Cell Biol.*, 17: 19-58.
- Sherlock, S. 1958 *Circulation: Proceedings of the Harvey Tercentenary Congress*. Ed. by J. McMichael. Blackwell Scientific Publications Ltd., Oxford. 366-378.



Abbreviations

B, basement membrane	L, lipid inclusion
C, cord-limiting cell	M, free macrophage
CS, cord space	P, phagocytosed material
G, gold particles	S, sinus cell
K, cytoplasmic concentration in sinus or cord-limiting cell	SL, sinus lumen
	W, leucocyte

PLATE 1

EXPLANATION OF FIGURES

- 1 Rabbit. Photomicrograph. The sinus abundance produces a locally cavernous spleen. Although perfusion has nearly cleared most of the sinuses, many blood cells remain in a few of them. Mallory's azure II-methylene blue. $\times 180$.
- 2 Dog. Photomicrograph. The cord areas predominate. Several sinuses, which are nearly clear of blood cells, are present. Mallory's azure II-methylene blue. $\times 360$.

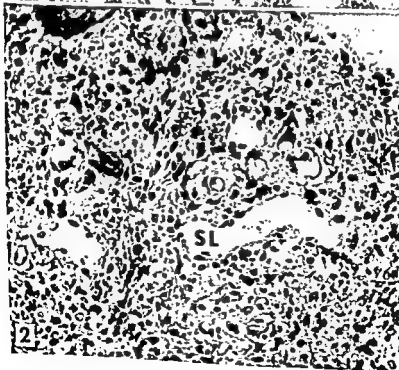


PLATE 2

EXPLANATION OF FIGURE

- 3 Rabbit. This electron-micrograph montage reveals the general architecture of the splenic red pulp. The cord area in the upper left corner diminishes to a narrow strip between two sinuses and then expands to occupy much of the lower half of the field. Above the center of the field an erythrocyte is present in an aperture between a cord space and a sinus. To distinguish the three elements of the sinus wall at this magnification is difficult. Uranyl acetate. $\times 3,000$.

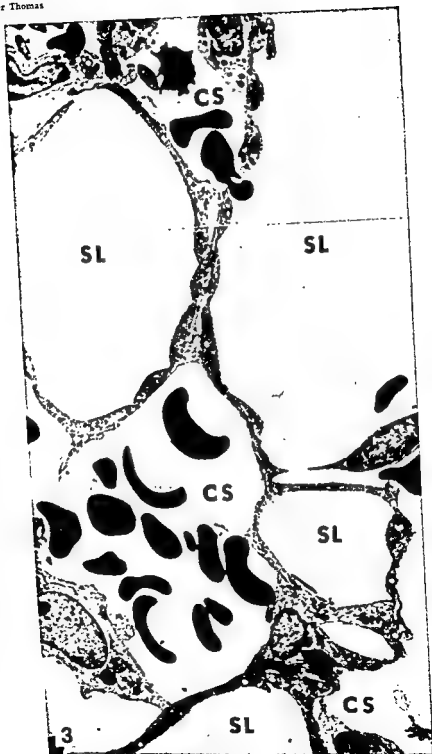
SINUS STRUCTURE IN PERFUSED SPLEEN
Carolyn Hyster Thomas

PLATE 2

EXPLANATION OF FIGURE

- 3 Rabbit. This electron-micrograph montage reveals the general architecture of the splenic red pulp. The cord area in the upper left corner diminishes to a narrow strip between two sinuses and then expands to occupy much of the lower half of the field. Above the center of the field an erythrocyte is present in an aperture between a cord space and a sinus. To distinguish the three elements of the sinus wall at this magnification is difficult. Uranyl acetate. $\times 3,000$.

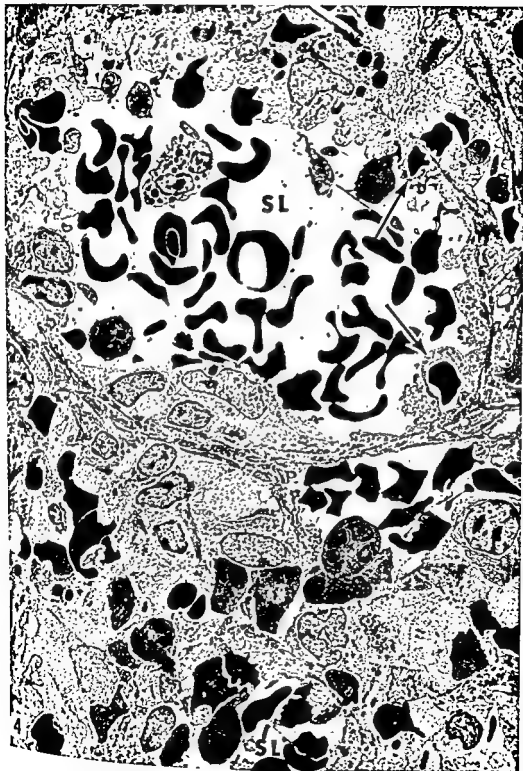


PLATE 3

EXPLANATION OF FIGURE

- 4 Dog. The general architecture of the splenic red pulp is evident in this electron-micrograph montage. Two sinuses are present, and the remainder of the field is cord. At two locations in the right portion of the upper sinus (arrows) a ring of sinus-cell cytoplasm surrounds an erythrocyte. One of these cytoplasmic rings appears in figure 13. The apertures and the three elements of the sinus wall are difficult to see at this magnification. Uranyl acetate. $\times 2,500$.

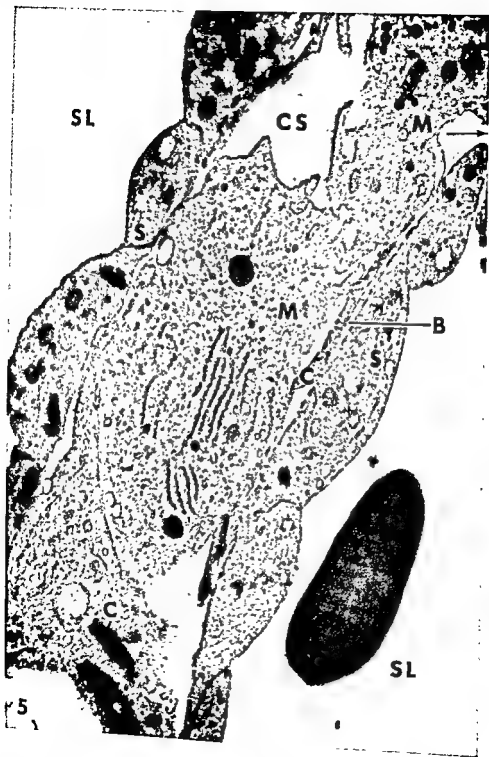


PLATE 4

EXPLANATION OF FIGURE

- 5 Rabbit. A narrow strip of cord separates two sinuses. All three elements are present in the upper portion of the right sinus wall: an inner layer of sinus cells, an intermediate layer of basement membrane, and an outer layer of cord-limiting cells. Some of the other areas of the wall consist of sinus cell alone. In the lowest part of the cord a cell, which a more inclusive micrograph revealed to be a cord-limiting cell, stretches across the cord from one sinus to the other. The free macrophages contain gold particles which at this magnification are barely discernible. One of the macrophages is located partly within a sinus-wall aperture (arrow). Uranyl acetate. $\times 18,000$.

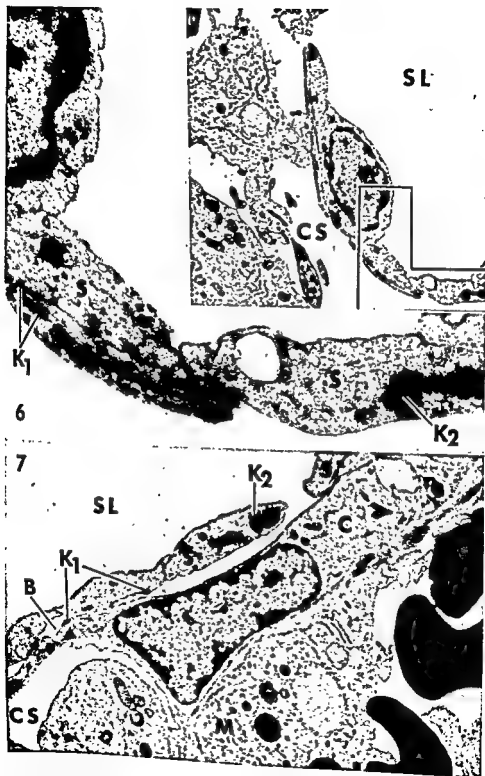


PLATE 5

EXPLANATION OF FIGURES

- Rabbit. The inset indicates that the lower portion of the large micrograph is cord, that the upper portion is sinus, and that sinus wall separates these two portions. In the large micrograph all three elements form the left half of the wall; a sinus cell alone, the right half. Two forms of cytoplasmic concentration appear. In the cord cell and two of the sinus cells narrow bands of dense cytoplasm (K_1) border the basement membrane. In the right sinus cell an island of dense cytoplasm (K_2) appears over the part of the basal surface where no basement membrane is present. An aperture appears in the upper portion of the inset. Uranyl acetate. $\times 8,000$; $\times 27,000$.
- 7 Rabbit. A fortunate section in the center of the field reveals the body of a cord-limiting cell with its nucleus and processes. A space separates the cell body from the sinus wall, but the cell processes attach to the wall and participate in its formation. The free macrophage in the cord contains gold particles. Careful inspection reveals that some of the sinus and cord-limiting cells contain a few isolated gold particles. (Compare figure 13 for identification of gold particles.) The omission of post-staining has caused the basement membrane to appear paler but has left the opacity of the cytoplasmic concentrations (K_1 and K_2) nearly unaltered. $\times 8,000$.

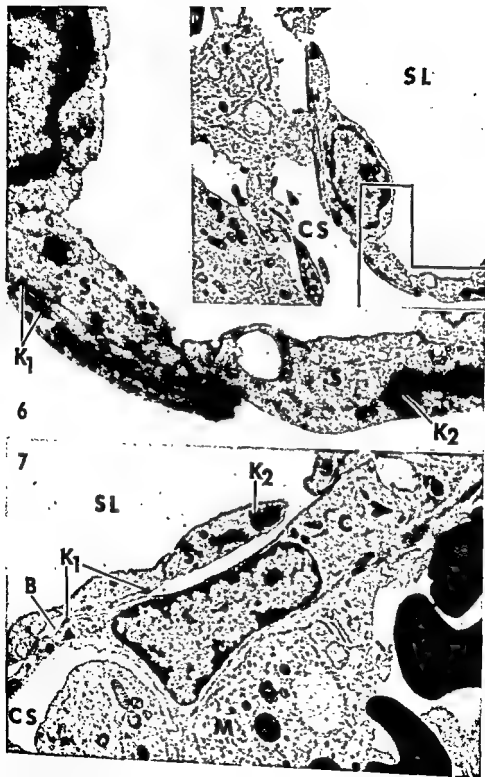


PLATE 6

EXPLANATION OF FIGURES

- 8 Dog. Two apertures (arrows) appear in the sinus wall. The right aperture contains no cells. A leucocyte projects into the left aperture without touching its rim. The presence of plasma in the apertures and the surrounding area suggests that perfusion was less thorough in this particular region. Uranyl acetate and lead citrate. $\times 14,500$.
- 9 Rabbit. A free macrophage lies mostly in a cord space but has extensions through three neighboring apertures (arrows) into the sinus lumen. In the middle aperture the macrophage appears to be continuous with a sinus cell; a later section from the same block, however, revealed cell membranes between these cells. Oblique sectioning of the cell membranes possibly accounts for their apparent absence. The cytoplasm of the macrophage contains more gold and is less dense than the cytoplasm of the sinus cell. (Compare figure 13 for identification of gold particles.) Uranyl acetate. $\times 16,000$.

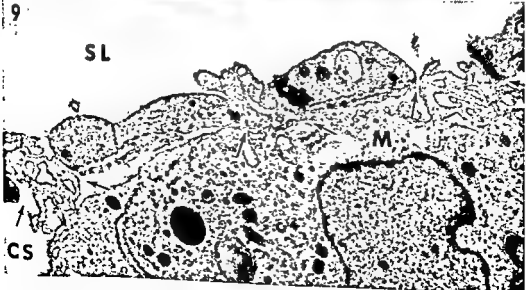
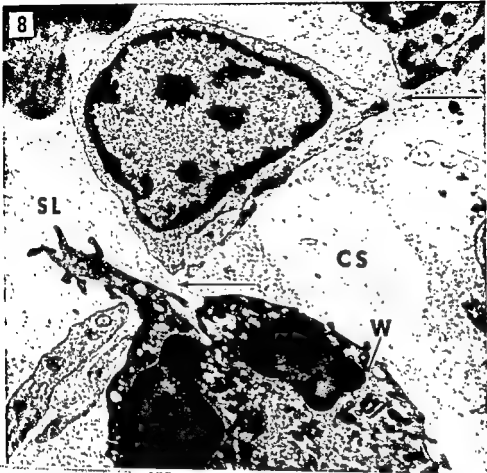


PLATE 6

EXPLANATION OF FIGURES

- 8 Dog. Two apertures (arrows) appear in the sinus wall. The right aperture contains no cells. A leucocyte projects into the left aperture without touching its rim. The presence of plasma in the apertures and the surrounding area suggests that perfusion was less thorough in this particular region. Uranyl acetate and lead citrate. $\times 14,500$.
- 9 Rabbit. A free macrophage lies mostly in a cord space but has extensions through three neighboring apertures (arrows) into the sinus lumen. In the middle aperture the macrophage appears to be continuous with a sinus cell; a later section from the same block, however, revealed cell membranes between these cells. Oblique sectioning of the cell membranes possibly accounts for their apparent absence. The cytoplasm of the macrophage contains more gold and is less dense than the cytoplasm of the sinus cell. (Compare figure 13 for identification of gold particles.) Uranyl acetate. $\times 16,000$.

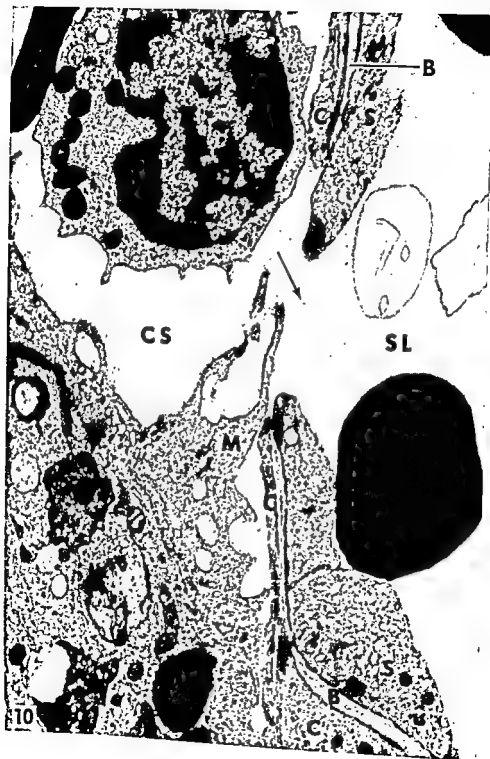


PLATE 7

EXPLANATION OF FIGURE

- 10 Rabbit. The sinus wall contains an aperture (arrow) that is devoid of cells and plasma; the delicate extension of a free macrophage lies nearby. The macrophage contains many gold particles; the sinus and cord cells contain much less gold. Lead citrate. \times 19,500.

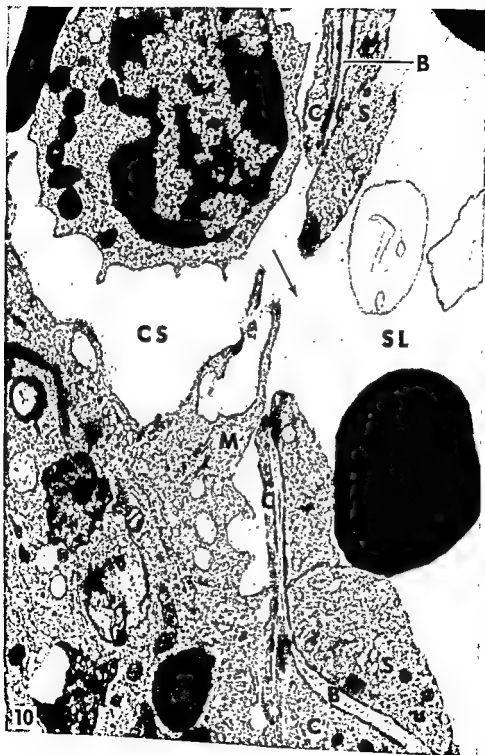


PLATE 8

EXPLANATION OF FIGURE

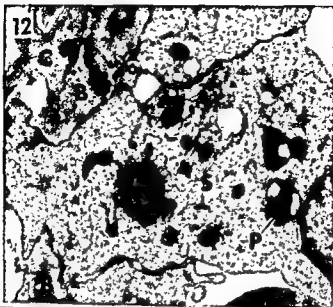
- 11 Dog. In the upper left corner an erythrocyte occupies a space between two sinus cells. A cord cell appears to occlude this potential aperture. A diagonal section through an aperture may have produced this appearance. The lowest erythrocyte consists of two masses connected by a narrow U-shaped bridge. The bridge lies on the cord side of the wall and extends through two neighboring apertures (arrows) into the sinus; the masses lie in the sinus. In addition to the divided erythrocyte the lower aperture contains part of another cell as well. Above the divided erythrocyte another erythrocyte occupies an aperture which may actually be continuous with the aperture just below. Uranyl acetate and lead citrate. $\times 22,000$.



PLATE 9

EXPLANATION OF FIGURES

- 12 Dog. The appearance of the upper sinus-cell junction suggests the possibility of a tight junction. A tangential section through twisted cell membranes would be a likely alternative interpretation. The intercellular space in the lower sinus-cell junction probably extends the entire distance from the basement membrane to the sinus lumen. Pinocytotic vesicles and cytoplasmic concentrations lie along the lower junction. The sinus cell contains a lipid inclusion; interestingly, the inclusion somewhat resembles basement membrane. Two large masses of granular material in the sinus cell may represent phagocytosed material, possibly residue from degenerating erythrocytes. A few scattered gold particles appear in the cytoplasm. Uranyl acetate. $\times 17,500$.
- 13 Dog. Near the upper right corner a small patch of plasma contains some gold particles. Along the right margin of the micrograph portions of free macrophages contain large quantities of gold particles. In sharp contrast the sinus cells contain only a few gold particles. The particles appear to lie free in the cytoplasm. This micrograph is an enlarged area from figure 4. Uranyl acetate. $\times 18,500$.



The Ultrastructure of Myofibers in a Reptilian Heart: The boa constrictor¹

LEE VIRN LEAK

Department of Surgery, Harvard Medical School and the
General Surgical Services, Massachusetts General Hospital,
Boston, Massachusetts

ABSTRACT Electron microscopic observation of cardiac myofibers from the boa constrictor depict several features that differ from other vertebrate cardiac and striated muscle cells. The indentations in the sarcolemma do not penetrate into the deep sarcoplasmic matrix to form a transverse tubular system, instead the regular indentations extend the circumference of the myofiber at the regions of the M line and are continuous with the latter via a dense homogeneous material that occurs at regular intervals along the subsarcolemmal surface. This dense material provides a direct contact between the sarcolemma and the contractile system.

A complex sarcoplasmic reticulum was not observed around the myofibrils or in the sarcoplasmic matrix, instead there were small vesicles dispersed about the sarcoplasm. These myofibers are compared with the slow or tonic muscle fiber (Felderstruktur) which also lacks a transverse tubular system and contains an irregular sarcoplasmic reticulum.

Deep invaginations of the cell membrane that were continuous with the transverse tubular system and penetrated deep within the interior of the myofiber of cardiac muscle were first reported by Linder ('57) in the canine myocardium. A similar relationship between the sarcolemma and the transverse tubules within the sarcoplasm of different mammalian cardiac muscles was also demonstrated by Simpson and Oertel ('61, '62), Nelson and Benson ('63) and Simpson ('65). In addition a similar condition was noted in two invertebrate heart muscles, i.e. the cockroach myocardium by Edwards and Challice ('60) and the myocardium of the snail by North ('62). Recent investigations on several types of striated muscles in both invertebrates (Smith, '61; Hagopian, '66) and vertebrates (Franzini-Armstrong and Porter, '64a; Simpson, '65) have demonstrated that the transverse tubules communicate with the intracellular space in addition to providing morphological data in support of the hypothesis that the tubules of the sarcoplasmic reticulum are responsible for the intracellular transmission of the activating impulse in striated muscles (Ruska et al., '58; Peachey and Porter, '59).

In their ultrastructural studies on the turtle atrium Fawcett and Selby ('58) ob-

served a close relationship between the dense accumulations in the regions of the desmosomes and the Z disc, and noted the absence of a complex sarcoplasmic reticulum in the sarcoplasmic matrix. Instead, they observed many small vesicles dispersed in the sarcoplasmic matrix. However, similar detailed ultrastructural studies for other reptilian myocardial cells have not been reported. As part of a comparative study of the distribution of myofibrils, transverse tubules and sarcoplasmic reticulum in the myocardial cells from representative groups of the evolutionary scale, i.e. representative species from each class of animals, the fine structure of the myocardium of the *boa constrictor* has been examined. The present communication is concerned with the intimate association of the sarcolemma with the contractile system at the Z band region, and the form and distribution of the myofibrils within the myocardial cells of the *boa constrictor*.

MATERIALS AND METHODS

Samples of heart muscle were obtained from the ventricles of seven *boa constrictors* ranging from one to six feet in length. The tissue was fixed in phosphate buffered

¹This work was supported by USPHS grant HE-0664 (HEP).

formalin (Pease, '62), washed and post-fixed in phosphate buffered osmium tetroxide (Millonig, '61) or prefixed in 4% glutaraldehyde (Sabatini et al., '63), washed and postfixed in phosphate buffered osmium tetroxide, or fixed in phosphate buffered osmium tetroxide without prefixation. After osmium tetroxide fixation some of the tissue was treated with 0.5% uranyl acetate in Michaelis buffer at pH5 (Farquhar and Palade, '65). After dehydration in a graded series of alcohols followed by propylene oxide, the tissue was embedded in epon (Luft, '61). Sections were cut on a Porter-Blum MT-2 ultramicrotome with DuPont diamond knives and double stained with uranyl acetate (Watson, '58) and lead citrate (Venable and Coggeshall, '65), and thereafter examined with a Philips EM 200 electron microscope.

OBSERVATIONS

The cardiac muscle fibers of the boa constrictor are elongated with centrally located nuclei (fig. 1). The undulating sarcolemma that surrounds the muscle fiber is more deeply invaginated at the Z band than other regions of the sarcomere. This situation is more pronounced in the contracted myofibers than cells in the relaxed state. In the contracted myofiber there are numerous small projections and slight invaginations that are produced along the lateral surface of the myofiber which interdigitate with the apposing contracted cell so that the lateral surfaces of the two adjacent myocardial cells are held in intimate association during contraction (fig. 2). The slight invaginations occur with some regularity along the lateral sarcolemma, and longitudinal sections that are cut tangential to the surface of the myofibers indicate that these indentations extend the circumference of the myofiber (figs. 3, 7). None of the invaginations were observed to make deep penetration into the sarcoplasm to connect to, or form a transverse tubular system as observed in the myocardial and skeletal muscle cells of other vertebrates. Instead, the slight invaginations along the plasma membrane terminate at the Z bands to which they are structurally connected by an electron dense material, that provides continuity with the plasma membrane and the dense

Z band that extends the width of the contractile system (figs. 1, 4, 5). The intimate association of the slight indentations along the plasma membrane with the Z band, can best be demonstrated in longitudinal sections that are cut near the periphery of the cell as shown in figure 7. In cross sections the plane of the section is not perfectly transverse over the entire myofiber, however, there are regions in which portions of the Z band can be traced across the width of the cell. Frequently the dense material appears to form a lining that is intimately associated with the inner surface of the sarcolemma for varying distances as if to form a "subsarcolemmal coating" or "lining." This dense material does not form a continuous lining underneath the sarcolemma, however, in a number of situations the dense substance can be followed along the inner surface of the sarcolemma for the length of several sarcomeres (figs. 1, 4). The width of the "subsarcolemmal coat" is about 60 m μ , however, the thickness of this dense material is increased to 90 m μ near the A-I junction before it becomes continuous with the Z band proper (fig. 4). The dense material connecting the sarcolemma to the Z band region is similar in opacity and structure to the very electron dense cytoplasmic accumulations that occur at various regions along the sarcolemma that comprise the intercalated disc. It is also similar to the dense regions or plaques of desmosomes (macula adherens). Infrequently dense regions are also observed at various intervals along the inner surface of the transverse sarcolemma.

In areas where adjacent myocardial cells are not closely apposed to each other, there is a basal lamina around the cell which also takes on the wavy or scalloped appearance of the sarcolemma (figs. 1, 3, 5).

The nerve endings appear as several units as shown in figure 5, and in some sections they seem to follow a course that is perpendicular to the long axis of the myofiber, and are usually observed between the blood capillary and the myofiber.

In the myocardium of the boa constrictor the shape of the myofibers range from irregular to cylindrical forms with the myofibrils being orientated parallel to the long axis of the cell. The myofilaments are

arranged in a circumferential fashion, so that in transverse sections through the central parts of the cell the myofibrils appear fused with each other and form a continuous bundle that is arranged around the centrally located nucleus and mitochondria (fig. 6). The average width of the myofibrils is ca. 1.5μ . The thin actin filaments are orientated in a trigonal position with respect to the thick myosin filaments while the thick myosin filaments are hexagonally arranged (figs. 6, 12) as noted in other vertebrate myocardial and striated muscle cells (Huxley and Hanson, '60; Stenger and Spiro, '61). In the semi-contracted state the various cross bands of the myofibril can be identified. However, in the relaxed myofiber the boundary of each region is well defined (figs. 8, 9). The sarcomere length of the relaxed myofiber is 1.7μ , and measures up to μ in glycerinated myofibers (fig. 10), while in the contracted myofibril it may be as short as 0.5μ (fig. 2). In tissue that is stained with uranyl acetate after osmium tetroxide fixation, the margins for each of the bands that comprise the sarcomere are clearly delineated (fig. 8). Most of the H band region is occupied by the dense M band (figs. 8, 9). In the relaxed state an irregular dense band is observed across the central region of the I band and is similar to the N band described by other investigators (figs. 8, 9, 10). The zig-zag pattern that is characteristic for the Z line is also demonstrated in the cardiac myofibrils of the boa constrictor. In the thicker sections the Z line appears as an irregular dense band that is composed of a homogeneous granular material (fig. 13), while in the thinner sections filaments that are thicker than the I filaments cross the Z line (figs. 14, 15). The organization of the filaments that comprise the Z line is similar to that described by Knappeis and Carlson ('62) and Franzini-Armstrong and Porter ('64b) in striated muscle, and by Garamvölgyi ('65) in insect flight muscle.

As observed in other vertebrate and invertebrate muscle cells the thick myosin filaments extend the entire length of the A band proper, while the thin actin filaments extend from the dense Z line to the H zone. Lateral cross-bridges are apparent in both the longitudinal and transverse

sections of the thick myofilaments (figs. 9, 12). Occasionally thick and thin filaments that are arranged perpendicular to the long axis of the myofiber occur in the subsarcolemmal region (fig. 11).

The mitochondria are numerous and occur in large clusters in the central portion of the myofiber, they fill the central sarcoplasmic core between the nucleus and the transverse plasma membrane so that the inner boundaries of the contractile system that extend between the nucleus and the transverse plasmalemma remain in intimate association with the mitochondria (figs. 1, 2, 20). The topographical association of the mitochondria with the contractile components can best be seen in transverse sections as shown in figure 6. Occasionally they appear aligned along the long axis of the nucleus (fig. 1) and frequently occur in the peripheral sarcoplasm between the myofibrils and the sarcolemma. In addition they are also observed within bundles of the myofibrils (fig. 5). The diameter of the mitochondria varies according to the state of contraction of the myofibrils. Similarly the length of the mitochondria may vary from very short in the contracted myofibril, or the length of one mitochondrion may extend the length of several sarcomeres in the relaxed myofibril (fig. 23). In the contracted myofiber the mitochondria appear clumped in the sarcoplasmic core near the two nuclear poles as shown in figure 2.

The sarcoplasmic reticulum and transverse tubular systems are conspicuously absent from the sarcoplasmic matrix in the myocardial cells of the boa constrictor. Observations of longitudinal and transverse sections of ventricular tissue from seven animals that were prefixed in buffered formalin, or glutaraldehyde and postfixed in osmium tetroxide, or fixed in osmium tetroxide alone have failed to demonstrate a continuous system of interconnecting tubules around the myofibrils or a transverse tubular system similar to that reported for mammalian cardiac or striated muscle cells. Small vesicles occur in the subsarcolemmal sarcoplasm and the perinuclear sarcoplasmic matrix. On close examination the vesicles seem to be single units which may occur in small groups, and are similar

formalin (Pease, '62), washed and post-fixed in phosphate buffered osmium tetroxide (Millonig, '61) or prefixed in 4% glutaraldehyde (Sabatini et al., '63), washed and postfixed in phosphate buffered osmium tetroxide, or fixed in phosphate buffered osmium tetroxide without prefixation. After osmium tetroxide fixation some of the tissue was treated with 0.5% uranyl acetate in Michaelis buffer at pH5 (Farquhar and Palade, '65). After dehydration in a graded series of alcohols followed by propylene oxide, the tissue was embedded in epon (Luft, '61). Sections were cut on a Porter-Blum MT-2 ultramicrotome with DuPont diamond knives and double stained with uranyl acetate (Watson, '58) and lead citrate (Venable and Coggeshall, '65), and thereafter examined with a Phillips EM 200 electron microscope.

OBSERVATIONS

The cardiac muscle fibers of the boa constrictor are elongated with centrally located nuclei (fig. 1). The undulating sarcolemma that surrounds the muscle fiber is more deeply invaginated at the Z band than other regions of the sarcomere. This situation is more pronounced in the contracted myofibers than cells in the relaxed state. In the contracted myofiber there are numerous small projections and slight invaginations that are produced along the lateral surface of the myofiber which interdigitate with the apposing contracted cell so that the lateral surfaces of the two adjacent myocardial cells are held in intimate association during contraction (fig. 2). The slight invaginations occur with some regularity along the lateral sarcolemma, and longitudinal sections that are cut tangential to the surface of the myofibers indicate that these indentations extend the circumference of the myofiber (figs. 3, 7). None of the invaginations were observed to make deep penetration into the sarcoplasm to connect to, or form a transverse tubular system as observed in the myocardial and skeletal muscle cells of other vertebrates. Instead, the slight invaginations along the plasma membrane terminate at the Z bands to which they are structurally connected by an electron dense material, that provides continuity with the plasma membrane and the dense

Z band that extends the width of the contractile system (figs. 1, 4, 5). The intimate association of the slight indentations along the plasma membrane with the Z band, can best be demonstrated in longitudinal sections that are cut near the periphery of the cell as shown in figure 7. In cross sections the plane of the section is not perfectly transverse over the entire myofiber, however, there are regions in which portions of the Z band can be traced across the width of the cell. Frequently the dense material appears to form a lining that is intimately associated with the inner surface of the sarcolemma for varying distances as if to form a "subsarcolemmal coating" or "lining." This dense material does not form a continuous lining underneath the sarcolemma, however, in a number of situations the dense substance can be followed along the inner surface of the sarcolemma for the length of several sarcomeres (figs. 1, 4). The width of the "subsarcolemmal coat" is about 60 m μ , however, the thickness of this dense material is increased to 90 m μ near the A-I junction before it becomes continuous with the Z band proper (fig. 4). The dense material connecting the sarcolemma to the Z band region is similar in opacity and structure to the very electron dense cytoplasmic accumulations that occur at various regions along the sarcolemma that comprise the intercalated disc. It is also similar to the dense regions or plaques of desmosomes (macula adherens). Infrequently dense regions are also observed at various intervals along the inner surface of the transverse sarcolemma.

In areas where adjacent myocardial cells are not closely apposed to each other, there is a basal lamina around the cell which also takes on the wavy or scalloped appearance of the sarcolemma (figs. 1, 3, 5).

The nerve endings appear as several units as shown in figure 5, and in some sections they seem to follow a course that is perpendicular to the long axis of the myofiber, and are usually observed between the blood capillary and the myofiber.

In the myocardium of the boa constrictor the shape of the myofibers range from irregular to cylindrical forms with the myofibrils being orientated parallel to the long axis of the cell. The myofilaments are

arranged in a circumferential fashion, so that in transverse sections through the central parts of the cell the myofibrils appear fused with each other and form a continuous bundle that is arranged around the centrally located nucleus and mitochondria (fig. 6). The average width of the myofibrils is ca. 1.5μ . The thin actin filaments are orientated in a trigonal position with respect to the thick myosin filaments while the thick myosin filaments are hexagonally arranged (figs. 6, 12) as noted in other vertebrate myocardial and striated muscle cells (Huxley and Hanson, '60; Stenger and Spiro, '61). In the semi-contracted state the various cross bands of the myofibril can be identified. However, in the relaxed myofiber the boundary of each region is well defined (figs. 8, 9). The sarcomere length of the relaxed myofiber is 1.7μ , and measures up to 2μ in glycerinated myofibers (fig. 10), while in the contracted myofibril it may be as short as 0.5μ (fig. 2). In tissue that is stained with uranyl acetate after osmium tetroxide fixation, the margins for each of the bands that comprise the sarcomere are clearly delineated (fig. 8). Most of the H band region is occupied by the dense M band (figs. 8, 9). In the relaxed state an irregular dense band is observed across the central region of the I band and is similar to the N band described by other investigators (figs. 8, 9, 10). The zig-zag pattern that is characteristic for the Z line is also demonstrated in the cardiac myofibrils of the boa constrictor. In the thicker sections the Z line appears as an irregular dense band that is composed of a homogeneous granular material (fig. 13), while in the thinner sections filaments that are thicker than the I filaments cross the Z line (figs. 14, 15). The organization of the filaments that comprise the Z line is similar to that described by Knappeis and Carlson ('62) and Franzini-Armstrong and Porter ('64b) in striated muscle, and by Garavito ('65) in insect flight muscle.

As observed in other vertebrate and invertebrate muscle cells the thick myosin filaments extend the entire length of the A band proper, while the thin actin filaments extend from the dense Z line to the H zone. Lateral cross-bridges are apparent in both the longitudinal and transverse

sections of the thick myofilaments (figs. 9, 12). Occasionally thick and thin filaments that are arranged perpendicular to the long axis of the myofiber occur in the subsarcolemmal region (fig. 11).

The mitochondria are numerous and occur in large clusters in the central portion of the myofiber, they fill the central sarcoplasmic core between the nucleus and the transverse plasma membrane so that the inner boundaries of the contractile system that extend between the nucleus and the transverse plasmalemma remain in intimate association with the mitochondria (figs. 1, 2, 20). The topographical association of the mitochondria with the contractile components can best be seen in transverse sections as shown in figure 6. Occasionally they appear aligned along the long axis of the nucleus (fig. 1) and frequently occur in the peripheral sarcoplasm between the myofibrils and the sarcolemma. In addition they are also observed within bundles of the myofibrils (fig. 5). The diameter of the mitochondria varies according to the state of contraction of the myofibrils. Similarly the length of the mitochondria may vary from very short in the contracted myofibril, or the length of one mitochondrion may extend the length of several sarcomeres in the relaxed myofibril (fig. 23). In the contracted myofiber the mitochondria appear clumped in the sarcoplasmic core near the two nuclear poles as shown in figure 2.

The sarcoplasmic reticulum and transverse tubular systems are conspicuously absent from the sarcoplasmic matrix in the myocardial cells of the boa constrictor. Observations of longitudinal and transverse sections of ventricular tissue from seven animals that were prefixed in buffered formalin, or glutaraldehyde and postfixied in osmium tetroxide, or fixed in osmium tetroxide alone have failed to demonstrate a continuous system of interconnecting tubules around the myofibrils or a transverse tubular system similar to that reported for mammalian cardiac or striated muscle cells. Small vesicles occur in the subsarcolemmal sarcoplasm and the perinuclear sarcoplasmic matrix. On close examination the vesicles seem to be single units which may occur in small groups, and are similar

to the small vesicles that are associated with the Golgi apparatus (figs. 1, 3, 20, 22).

In addition to the many small vesicles in the peripheral sarcoplasmic matrix, there are numerous small dense granules ca 250A in diameter with slightly irregular outlines that are similar to the glycogen granules reported in other vertebrate myocardial cells as well as a number of different cell types (figs. 4, 7). The Golgi apparatus occupies a position adjacent to the nucleus and also in the central sarcoplasmic core between the mitochondria that occur in this region. It is composed of crescent shaped cisternae that form lamellar stacks with numerous vesicles closely associated with its peripheral regions (figs. 1, 20, 22). Small vesicles 500 to 1,000A in diameter also appear in the juxtannuclear region in close association with the Golgi apparatus and between the mitochondria that are situated in the perinuclear regions of the cell (figs. 1, 17, 20). In addition to the small vesicles dense granules ranging from 0.1 μ to 0.5 μ in diameter appear in the sarcoplasmic matrix adjacent to the nuclear poles (figs. 17, 20, 21). These granules are bound by a limiting membrane and the content varies from an electron-opaque material to a dense granular substance (fig. 21). Occasionally the granules contain an irregular array of membranes as shown in figure 21 (see insert). These dense granules are intimately associated with the Golgi complex and are similar to the specific atrial granules described by Jamieson and Palade ('64) in several mammals including man. Lipid vacuoles appear in the peripheral sarcoplasm and also between the mitochondria in various parts of the myocardial cell (figs. 1, 3). Paired centrioles are often observed in the perinuclear sarcoplasm with the long axis of one being perpendicular to the long axis of the other. The composition of nine evenly spaced triplet hollow fibrils that is characteristic for other cell types, is also apparent in the cardiac muscle cells of the boa constrictor (fig. 17).

The distal ends of adjacent myofibers are held in intimate contact by the intercalated discs which occur along the transverse surfaces of apposing plasma membranes. The characteristic wavy appearance within the intercalated disc noted

for other vertebrate myocardial cells is also evident in the myofibers of boa constrictor myocardium (figs. 16, 18, 19). The terminating myofibrils are inserted into the specialized dense regions of the transverse plasma membrane and are held in close apposition to a similar region of the apposing cell, with which it interdigitates.

DISCUSSION

The above description of the myocardial cells of the boa constrictor depicts several important features that differ from other vertebrate cardiac and striated muscle cells. Transverse tubular invaginations of the sarcolemma which penetrate deep into the sarcoplasmic matrix are not observed. Neither is there an organized sarcotubular system investing the myofibrils or pervading the sarcoplasmic matrix after the use of improved fixation and embedding methods that have been used to demonstrate these structures in other myocardial cells (Porter and Palade, '57; Lindner, '57; Stenger and Spiro, '61; Simpson and Oertel, '61, '62; Nelson and Benson, '63; Simpson, '65) and striated muscle cells (Franzini-Armstrong and Porter, '64a; Huxley, '64; Peachey, '65).

The typical appearance of the myofibers in the cardiac muscle of the boa constrictor is summarized in the diagram shown in figure 24. The undulating sarcolemma is in direct contact with the contractile system through regular indentations that extend the circumference of the cell at the Z line and is connected to the latter via a dense homogeneous material that occurs at various regions along the inner surface of the sarcolemma ("subsarcolemmal coat"). In an earlier study on reptilian skeletal muscle, Robertson ('56) observed that the Z band was attached to the sarcolemma (surface membrane complex) by the accumulation of a dense amorphous material which had a greater density than the surrounding sarcoplasm, and suggested that this attachment of sarcolemma to the Z line produced the scalloped effect that had been described previously in rat cardiac muscle (Hodge et al., '54).

It is of interest to note that even in the relaxed and the glycerinated myofibers, the slight indentations still persist along the sarcolemma and in most cases the con-

tinuity with the Z line is maintained via the dense homogeneous material along the inner surface of the sarcolemma. However, similar studies on other vertebrate cardiac myofibers have demonstrated that the sarcolemmal invaginations are continuous with a transverse tubular system (Porter and Palade, '57; Lindner, '57; Simpson and Oertels, '61; Nelson and Benson, '63; Simpson, '65) which may represent the element that could act as a pathway for the spread of the activating impulse into the interior of the muscle fiber (Huxley and Taylor, '58; Bennett, '60; Huxley, '59). Similarly, the sarcoplasmic reticulum which surrounds the myofibrils and pervades the sarcoplasmic matrix in other vertebrate and invertebrate muscle cells, may also play a role as an intracellular conducting system (Porter and Palade, '57; Huxley and Taylor, '58; Peachey and Porter, '59; Porter, '61; Revel, '62; Smith, '61; Franzini-Armstrong, '64; Franzini-Armstrong and Porter, '64; Peachey, '65).

The absence of the transverse tubular system and the occurrence of an irregular sarcoplasmic reticulum have been suggested as being characteristic features for the slow or tonic muscle fibers (i.e. Felderstruktur) in certain striated muscle of the snake (Hess, '65), in the cat (Hess and Pilar, '63), in the chicken (Hess, '61), in the frog (Hess, '60; Peachey and Huxley, '62) and in the guinea pig (Hess, '61). Physiological studies on the slow muscles have demonstrated that these muscle fibers undergo a sustained contracture instead of a contraction or a twitch when the nerve to them is stimulated; on the other hand the twitch fibers show propagated impulse activity and non-graded contractile activity when they are stimulated (Kuffler and Vaughn Williams, '53; Hess and Pilar, '63). The studies of Clarke and Marx ('60) on the heart rates of several snakes suggest that these animals have a slow heart rate, and that the average heart beat for a constrictor is 15 beats per minute. That the amount and development of the sarcoplasmic reticulum and transverse tubular system are related to the speed of the muscle or the rate of contraction was suggested from comparing the contracture speed of striated and smooth muscle cells (Peachey and Porter, '59), from studies on the fast

acting swim bladder muscle by Fawcett and Revel ('61) and the cricothyroid muscle in the bat by Revel ('62, '64). In comparing the amount and distribution of the sarcoplasmic reticulum in animals with various heart rates, Slaughterback ('63) observed that with a reduction in the heart rates of turtles there was a corresponding decrease in the amount and also the complexity of the sarcoplasmic reticulum.

The failure to find a transverse tubular system and a sarcoplasmic reticulum in the cardiac myofibers of the boa constrictor after using various improved preparation methods that have been successfully used to demonstrate both the tubular and reticular systems in a number of other vertebrate cardiac and striated muscle cells, strongly suggest that these systems are non-existent or that they are poorly developed in the cardiac myofibers of this animal. Preliminary observations on the cardiac myofibers of the iguana indicate that the tubular and reticular systems are also absent. However, similar methods of preparation, when used on the intercostal muscles from both the boa constrictor and the iguana, demonstrated a well developed tubular and reticular system for these striated muscle cells.

If the transverse tubular system serves as a pathway for spreading the activating impulse into the interior of the myofiber and if the sarcoplasmic reticulum acts as an intracellular conducting system for other vertebrate and invertebrate striated and cardiac muscle cells, then what are the observable morphological features in the cardiac myofiber of the boa constrictor that could perform similar activities? The intimate association of the sarcolemma to the contractile system at the Z band suggests this region as a likely site for spreading the activating impulse into the interior of the myofiber. Since the myofibrils form a continuous bundle and are arranged circumferentially, each sarcolemmal indentation would represent a connection of the plasma membrane to the contractile system via the Z band. If the complexity of the transverse tubular and reticular systems are directly related to the speed of contraction for the muscle cell (Peachey and Porter, '59; Peachey and Huxley, '62; Revel, '64; Slaughterback, '63; Hess, '65)

to the small vesicles that are associated with the Golgi apparatus (figs. 1, 3, 20, 22).

In addition to the many small vesicles in the peripheral sarcoplasmic matrix, there are numerous small dense granules ca 250A in diameter with slightly irregular outlines that are similar to the glycogen granules reported in other vertebrate myocardial cells as well as a number of different cell types (figs. 4, 7). The Golgi apparatus occupies a position adjacent to the nucleus and also in the central sarcoplasmic core between the mitochondria that occur in this region. It is composed of crescent shaped cisternae that form lamellar stacks with numerous vesicles closely associated with its peripheral regions (figs. 1, 20, 22). Small vesicles 500 to 1,000A in diameter also appear in the juxtanuclear region in close association with the Golgi apparatus and between the mitochondria that are situated in the perinuclear regions of the cell (figs. 1, 17, 20). In addition to the small vesicles dense granules ranging from 0.1 μ to 0.5 μ in diameter appear in the sarcoplasmic matrix adjacent to the nuclear poles (figs. 17, 20, 21). These granules are bound by a limiting membrane and the content varies from an electron-opaque material to a dense granular substance (fig. 21). Occasionally the granules contain an irregular array of membranes as shown in figure 21 (see insert). These dense granules are intimately associated with the Golgi complex and are similar to the specific atrial granules described by Jamieson and Palade ('64) in several mammals including man. Lipid vacuoles appear in the peripheral sarcoplasm and also between the mitochondria in various parts of the myocardial cell (figs. 1, 3). Paired centrioles are often observed in the perinuclear sarcoplasm with the long axis of one being perpendicular to the long axis of the other. The composition of nine evenly spaced triplet hollow fibrils that is characteristic for other cell types, is also apparent in the cardiac muscle cells of the boa constrictor (fig. 17).

The distal ends of adjacent myofibers are held in intimate contact by the intercalated discs which occur along the transverse surfaces of apposing plasma membranes. The characteristic wavy appearance within the intercalated disc noted

for other vertebrate myocardial cells is also evident in the myofibers of boa constrictor myocardium (figs. 16, 18, 19). The terminating myofibrils are inserted into the specialized dense regions of the transverse plasma membrane and are held in close apposition to a similar region of the apposing cell, with which it interdigitates.

DISCUSSION

The above description of the myocardial cells of the boa constrictor depicts several important features that differ from other vertebrate cardiac and striated muscle cells. Transverse tubular invaginations of the sarcolemma which penetrate deep into the sarcoplasmic matrix are not observed. Neither is there an organized sarcotubular system investing the myofibrils or pervading the sarcoplasmic matrix after the use of improved fixation and embedding methods that have been used to demonstrate these structures in other myocardial cells (Porter and Palade, '57; Lindner, '57; Stenger and Spiro, '61; Simpson and Oertels, '61, '62; Nelson and Benson, '63; Simpson, '65) and striated muscle cells (Franzini-Armstrong and Porter, '64a; Huxley, '64; Peachey, '65).

The typical appearance of the myofibers in the cardiac muscle of the boa constrictor is summarized in the diagram shown in figure 24. The undulating sarcolemma is in direct contact with the contractile system through regular indentations that extend the circumference of the cell at the Z line and is connected to the latter via a dense homogeneous material that occurs at various regions along the inner surface of the sarcolemma ("subsarcolemmal coat"). In an earlier study on reptilian skeletal muscle, Robertson ('56) observed that the Z band was attached to the sarcolemma (surface membrane complex) by the accumulation of a dense amorphous material which had a greater density than the surrounding sarcoplasm, and suggested that this attachment of sarcolemma to the Z line produced the scalloped effect that had been described previously in rat cardiac muscle (Hodge et al., '54).

It is of interest to note that even in the relaxed and the glycerinated myofibers, the slight indentations still persist along the sarcolemma and in most cases the con-

tinuity with the Z line is maintained via the dense homogeneous material along the inner surface of the sarcolemma. However, similar studies on other vertebrate cardiac myofibers have demonstrated that the sarcolemmal invaginations are continuous with a transverse tubular system (Porter and Palade, '57; Lindner, '57; Simpson and Oertels, '61; Nelson and Benson, '63; Simpson, '65) which may represent the element that could act as a pathway for the spread of the activating impulse into the interior of the muscle fiber (Huxley and Taylor, '58; Bennett, '60; Huxley, '59). Similarly, the sarcoplasmic reticulum which surrounds the myofibrils and pervades the sarcoplasmic matrix in other vertebrate and invertebrate muscle cells, may also play a role as an intracellular conducting system (Porter and Palade, '57; Huxley and Taylor, '58; Peachey and Porter, '59; Porter, '61; Revel, '62; Smith, '61; Franzini-Armstrong, '64; Franzini-Armstrong and Porter, '64; Peachey, '65).

The absence of the transverse tubular system and the occurrence of an irregular sarcoplasmic reticulum have been suggested as being characteristic features for the slow or tonic muscle fibers (i.e. Felderstruktur) in certain striated muscle of the snake (Hess, '65), in the cat (Hess and Pilar, '63), in the chicken (Hess, '61), in the frog (Hess, '60; Peachey and Huxley, '62) and in the guinea pig (Hess, '61). Physiological studies on the slow muscles have demonstrated that these muscle fibers undergo a sustained contracture instead of a contraction or a twitch when the nerve to them is stimulated; on the other hand the twitch fibers show propagated impulse activity and non-graded contractile activity when they are stimulated (Kuffler and Vaughn Williams, '53; Hess and Pilar, '63). The studies of Clarke and Marx ('60) on the heart rates of several snakes suggest that these animals have a slow heart rate, and that the average heart beat for a constrictor is 15 beats per minute. That the amount and development of the sarcoplasmic reticulum and transverse tubular system are related to the speed of the muscle or the rate of contraction was suggested from comparing the contracture speed of striated and smooth muscle cells (Peachey and Porter, '59), from studies on the fast

acting swim bladder muscle by Fawcett and Revel ('61) and the cricothyroid muscle in the bat by Revel ('62, '64). In comparing the amount and distribution of the sarcoplasmic reticulum in animals with various heart rates, Slaughterback ('63) observed that with a reduction in the heart rates of turtles there was a corresponding decrease in the amount and also the complexity of the sarcoplasmic reticulum.

The failure to find a transverse tubular system and a sarcoplasmic reticulum in the cardiac myofibers of the boa constrictor after using various improved preparation methods that have been successfully used to demonstrate both the tubular and reticular systems in a number of other vertebrate cardiac and striated muscle cells, strongly suggest that these systems are non-existent or that they are poorly developed in the cardiac myofibers of this animal. Preliminary observations on the cardiac myofibers of the iguana indicate that the tubular and reticular systems are also absent. However, similar methods of preparation, when used on the intercostal muscles from both the boa constrictor and the iguana, demonstrated a well developed tubular and reticular system for these striated muscle cells.

If the transverse tubular system serves as a pathway for spreading the activating impulse into the interior of the myofiber and if the sarcoplasmic reticulum acts as an intracellular conducting system for other vertebrate and invertebrate striated and cardiac muscle cells, then what are the observable morphological features in the cardiac myofiber of the boa constrictor that could perform similar activities? The intimate association of the sarcolemma to the contractile system at the Z band suggests this region as a likely site for spreading the activating impulse into the interior of the myofiber. Since the myofibrils form a continuous bundle and are arranged circumferentially, each sarcolemmal indentation would represent a connection of the plasma membrane to the contractile system via the Z band. If the complexity of the transverse tubular and reticular systems are directly related to the speed of contraction for the muscle cell (Peachey and Porter, '59; Peachey and Huxley, '62; Revel, '64; Slaughterback, '63; Hess, '65)

then the observations of Clarke and Marx ('60) would suggest that the cardiac muscle fibers of the boa constrictor are of the slow type and presumably would not require a fast acting or contracting myofiber. The slow heart rate in this animal may be related to the absence of a transverse tubular system or a complex sarcoplasmic reticulum in the cardiac myofibers of the boa constrictor. The application of the local activation experiments of Huxley and Taylor ('58) on cardiac myofibers of this and other vertebrates should provide physiological information which will shed additional light on this problem.

ACKNOWLEDGMENT

Appreciation is expressed to Mrs. Heldie Seiler for her able technical assistance. Indebtedness is acknowledged to Mrs. G. Clayton for typing the manuscript.

LITERATURE CITED

- Bennett, H. S. 1960 The structure of striated muscle as seen by the electron microscope. In: *Structure and Function of Muscle*. I. (G. H. Bourne, ed.) New York Academic Press, Inc., I: 137-181.
- Clarke, G. K., and T. I. Marx 1960 Heart rates of unanesthetized snakes by electrocardiography. *Copeia* No. 3, 236-238.
- Edwards, G. A., and C. E. Challice 1961 The ultrastructure of the heart of the cockroach. *Blattella germanica*, *Ann. Entomol. Soc. Amer.*, 53: 369-383.
- Farquhar, M. G., and G. E. Palade 1965 Cell junctions in Amphibian Skin. *J. Cell Biol.*, 26: 263-291.
- Fawcett, D. W., and J. P. Revel 1961 The sarcoplasmic reticulum of a fast acting fish muscle. *J. Biophysic. Biochem. Cytol.*, 10: (suppl.) 89-108.
- Fawcett, D. W., and C. C. Selby 1958 Observations of the fine structure of the turtle atrium. *J. Biophysic. Biochem. Cytol.*, 4: 63-72.
- Franzini-Armstrong, C. 1964 Fine structure of sarcoplasmic reticulum and transverse tubular system in muscle fibers. *Fed. Proc.*, 23: 887-895.
- Franzini-Armstrong, C., and K. R. Porter 1964a Sarcoplasmic invaginations constituting the T system in fish muscle fibers. *J. Cell Biol.*, 22: 675-696.
- 1964b The Z disc of skeletal muscle fibrils. *Z. Zellforsch.*, 61: 661-672.
- Garamvölgyi, M. 1965 The arrangement of the myofilaments in the insect flight muscle. I. *J. Ultrastr. Res.*, 13: 409-424.
- Hagopian, M. 1966 The myofilament arrangement in the femoral muscle of the cockroach. *Leucophaea Maderae Fabricius*, *J. Cell Biol.*, 28: 545-562.
- Hess, A. 1960 The structure of extrafusal muscle fibers in the frog and their innervation studied by the Cholinesterase technique. *Am. J. Anat.*, 107: 129-152.
- 1961 The structure of slow and fast extrafusal muscle fibers in the extraocular muscles and their nerve endings in guinea pigs. *J. Cell. and Comp. Physiol.* 58: 63-79.
- 1965 The sarcoplasmic reticulum, the T system, and the motor terminals of slow and twitch muscle fibers in the garter snake. *J. Cell Biol.*, 26: 467-476.
- Hess, A., and G. Pilar 1963 Slow fibers in the extraocular muscles of the cat. *J. Physiol.*, 169: 780-798.
- Hodge, A. J., H. E. Huxley and D. Spiro 1954 Electron microscope studies on ultrathin sections of muscle. *J. Exp. Med.*, 99: 201-206.
- Huxley, A. F. 1959 Local activation of muscle. *Ann. N. Y. Acad. Sci.*, 81: 446-452.
- Huxley, A. F., and R. E. Taylor 1958 Local activation of striated muscle fibers. *J. Physiol.*, 144: 426-441.
- Huxley, H. E. 1964 Evidence for continuity between the central elements of the triads and extracellular space in frog sartorius muscle. *Nature*, 202: 1067-1071.
- Huxley, H. E., and J. Hanson 1960 The Molecular basis of Contraction in Cross-striated Muscles. In: *The Structure and Function of Muscle*. I. (G. H. Bourne, ed.) New York, Academic Press, Inc., I: 183-227.
- Jamieson, J. D., and G. E. Palade 1964 Specific granules in atrial muscle cells. *J. Cell Biol.*, 23: 151-172.
- Knappeis, G. G., and F. Carlsen 1962 The ultrastructure of the Z disc in skeletal muscle. *J. Cell Biol.*, 13: 223-235.
- Kuffler, S. W., and E. M. Vaughan Williams 1953 Properties of the "slow" skeletal muscle fibers of the frog. *J. Physiol.*, 121: 318-340.
- Lindner E. 1957 Die submikroskopische morphologie des herzmuskels. *Z. Zellforsch.*, 45: 702-746.
- Luft, J. H. 1961 Improvements in epoxy resin embedding methods. *J. Biophys. Biochem. Cytol.*, 9: 409-414.
- Millonig, G. 1961 Advantages of a phosphate buffer for OsO_4 solutions in fixation. *Proc. E.M.S.A.* (abstract).
- Nelson, D. A., and E. S. Benson 1963 On the structural continuities of the transverse tubular system of rabbit and human myocardial cells. *J. Cell Biol.*, 16: 297-313.
- North, R. J. 1963 The fine structure of the myofiber in the heart of the snail, *Helix aspersa*. *J. Ultrastr. Res.*, 8: 206-218.
- Peachey, L. D. 1965 The sarcoplasmic reticulum and transverse tubules of the frog's sartorius. *J. Cell Biol.*, 25: 209-231.
- Peachey, L. D., and A. F. Huxley 1962 Structural identification of twitch and slow striated muscle fibers of the frog. *J. Cell Biol.*, 13: 177-180.
- Peachey, L. D., and K. R. Porter 1959 Intracellular impulse conduction in muscle cells. *Science*, 129: 721-722.

- Fease, D. C. 1962 Buffered formaldehyde as a killing agent and primary fixative for electron microscopy. *Anat. Rec.*, 142: 342 (abstract).
- Porter, K. R. 1961 The sarcoplasmic reticulum. Its recent history and present status. *J. Biophys. Biochem. Cytol.*, 10: (suppl.) 219-226.
- Porter, K. R., and G. E. Palade 1957 Studies on the endoplasmic reticulum, its form and distribution in striated muscle cells. *J. Biophys. Biochem. Cytol.*, 3: 269-300.
- Revel, J. P. 1962 The sarcoplasmic reticulum of the cat cricothyroid muscle. *J. Cell Biol.*, 12: 571-588.
- Revel, J. P. 1964 The sarcoplasmic reticulum of fast-acting muscle. In: *Biochemistry of Muscle Contracture*. (J. Gergely, ed.) Little Brown and Co., Boston, pp. 232.
- Robertson, J. D. 1956 Some features of the ultrastructure of reptilian skeletal muscle. *J. Biophys. Biochem. Cytol.*, 2: 369-380.
- Ruska, H., G. A. Edwards and R. Caesar 1958 A concept of intracellular transmission of excitation by means of the endoplasmic reticulum. *Experientia*, 14: 117-120.
- Sabatini, D. D., K. Bensch and R. J. Barnett 1963 Cytochemistry and electron microscopy. The preservation of cellular ultrastructure and enzymatic activity by aldehyde fixation. *J. Cell Biol.*, 17: 19-58.
- Simpson, F. O. 1965 The transverse tubular system in mammalian myocardial cells. *Am. J. Anat.*, 117: 1-8.
- Simpson, F. O., and S. J. Oertels 1961 Relationship of the sarcoplasmic reticulum to sarcolemma in sheep cardiac muscle. *Nature*, 189: 758-759.
- 1962 The fine structure of sheep myocardial cells: sarcolemmal invaginations and the transverse tubular system. *J. Cell Biol.*, 12: 91-100.
- Slautterback, D. 1963 The sarcoplasmic reticulum in a turtle heart. *J. Cell Biol.*, 19: 66A.
- Smith, D. S. 1961 The structure of insect fibrillar flight muscle. *J. Biophys. Biochem. Cytol.*, 10: (suppl.) 123-158.
- Stenger, R. J., and D. Spiro 1961 The ultrastructure of mammalian cardiac muscle. *J. Biophys. Biochem. Cytol.*, 9: 325-351.
- Venable, J. H., and R. Coggeshall 1965 A simplified lead citrate stain for use in electron microscopy. *J. Cell Biol.*, 25: 407-408.
- Watson, M. L. 1958 Staining of tissue sections for electron microscopy with heavy metals. *J. Biophys. Biochem. Cytol.*, 4: 475-478.

PLATE 1

EXPLANATION OF FIGURE

- 1 Longitudinal section through the central part of myofiber, which demonstrates the indentations of the sarcolemma (arrow) at the Z band region (Z). The nucleus (n) which contains a nucleolus (nu) is centrally located with mitochondria (m) in the perinuclear region, adjacent to the nucleus, and also in the peripheral sarcoplasm. Lipid vacuoles (L) appear in the periphery and also the sarcoplasmic core. The Golgi (G) complex appears in the juxtannuclear position. Note the intimate association of the sarcolemma (SL) with the Z band (double arrows). A basal lamina (bl) surrounds the myofiber and takes on the scalloped appearance of the sarcolemma. Collagen fibers (CF) occur in the connective tissue area. $\times 18,000$.



PLATE 2

EXPLANATION OF FIGURES

- 2 In the contracted myofiber projections and indentations occur along the lateral surface of the myofiber which interdigitates so that adjacent myocardial cells are held in close apposition (arrows). Mitochondria (m) are clumped at nuclear (n) pole. $\times 16,000$.
- 3 This micrograph shows a grazing section through periphery of myofiber which demonstrates the shallow indentations (*) which terminate at the Z line (arrows). Golgi complex (G), vesicles (v), and extracted lipid vacuoles (L) are shown in cell at bottom. Numerous pinocytotic vesicles (v) occur in subsarcolemmal sarcoplasmic region. $\times 20,000$.

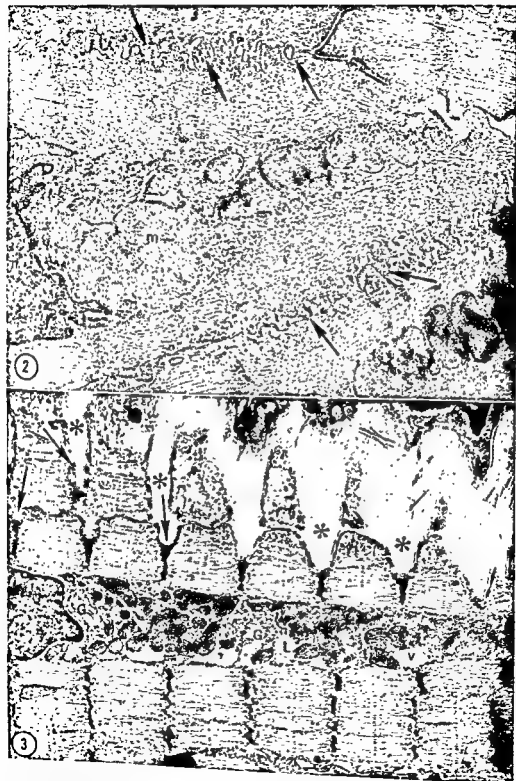


PLATE 3

EXPLANATION OF FIGURE

- 4 This micrograph shows the intimate relationship between the sarcolemma (SL) and the Z band via dense homogeneous substance (arrows). The dense substance forms a coat along the inner surface of the sarcolemma. Dense glycogen granules (g) also occur in the subsarcolemmal sarcoplasm. Basal lamina (bl) surrounds the myofiber. $\times 107,000$.

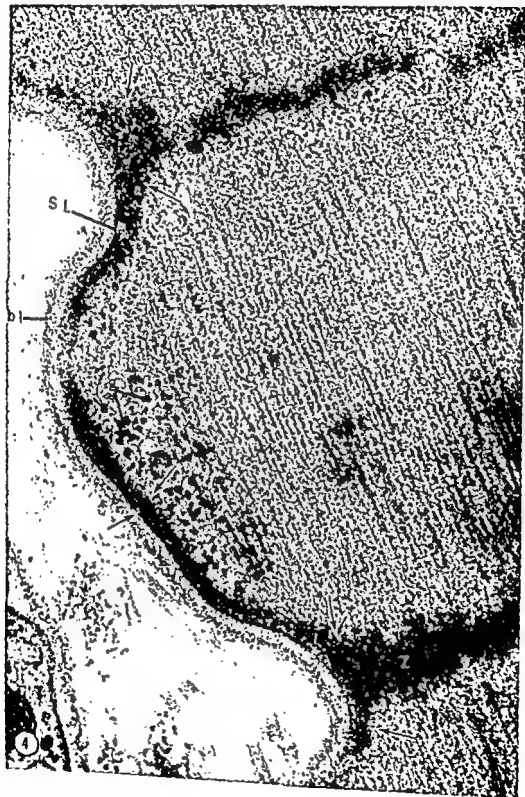


PLATE 4

EXPLANATION OF FIGURES

- 5 The nerve ending (arrows) occurs between blood capillary (BC) and myofiber. $\times 29,000$.
- 6 Transverse section which demonstrates the continuous bundle of myofibrils with the mitochondria (m) located in the center of the myofiber. Dense accumulations (arrows) occur along the inner surface of the sarcolemma and are similar to the dense plaques of the desmosome (D). $\times 38,500$.

CARDIAC MYOFIBERS OF THE BOA CONSTRICTOR

Lee Vinn Leak

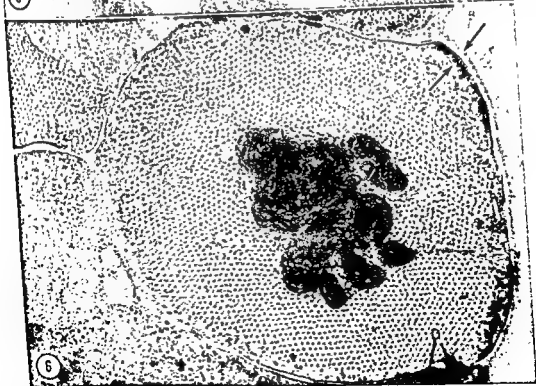
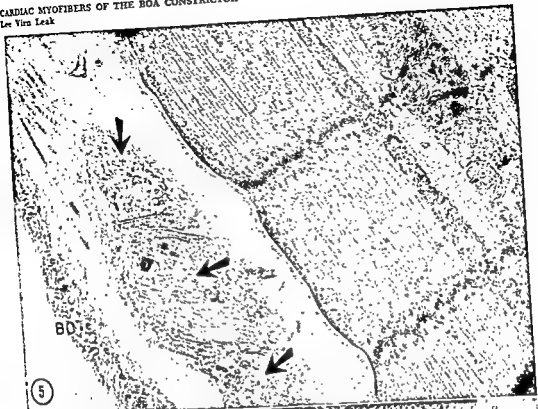


PLATE 5

EXPLANATION OF FIGURES

- 7 Longitudinal section cut near periphery of cell which shows the extent of the Z line across the myofiber (arrows). Vesicles (v), granules (g) and part of Z band are shown in portion where section grazed the surface of the myofiber. $\times 23,000$.
- 8 This micrograph shows the close association of adjacent cells at the Z band region (arrow). The M band (M), H zone (H), A band (A) and I band with a central dense line, the N band (N) are clearly shown. Intercalated disc (ID) is shown in lower part of micrograph. Mitochondria (m) and vesicles (v) occur in the peripheral sarcoplasm. $\times 29,000$.



PLATE 6

EXPLANATION OF FIGURES

- 9 Lateral cross bridges are apparent along the thick myosin filaments (arrows). The boundary of each region is well delineated. $\times 47,600$.
- 10 Longitudinal section from glycerinated myofiber. The sarcolemma (SL) is connected to the contractile system via the Z band (arrow). $\times 29,000$.
- 11 Myofibrils in the subsarcolemmal sarcoplasm that are perpendicular (arrows) to the long axis of the myofiber. $\times 39,000$.
- 12 Enlarged micrograph which shows the arrangement of thick and thin filaments. Lateral cross-bridges are apparent between the thick and thin filaments (arrows). The arrangement of thin filaments around the thick filaments are shown in circle. $\times 45,000$.

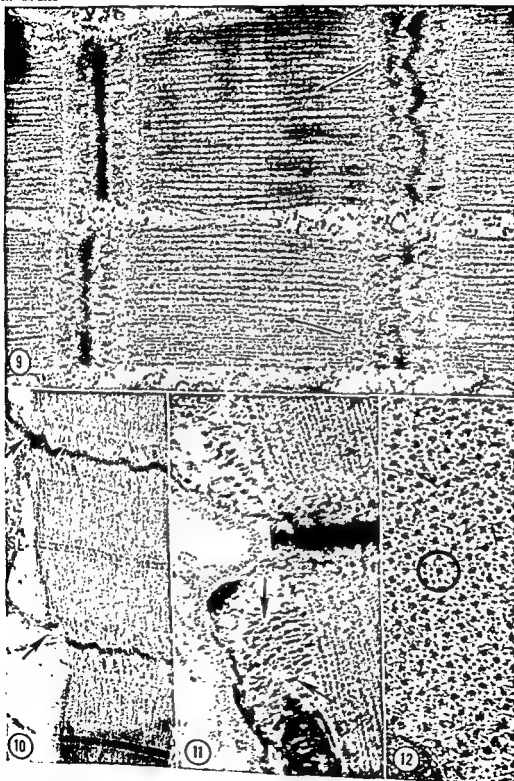


PLATE 7

EXPLANATION OF FIGURES

- 13 This enlarged micrograph shows the close association of Z band to the sarcolemma (arrow). $\times 70,000$.
- 14 The dense filaments which make up the N band (N) of the I region are similar to the dense filaments in the Z band. The zig-zag pattern is apparent at the arrows, where the actin filament (I filament) seems to branch into two dense lines in both the N band and Z band regions. $\times 102,500$.
- 15 Enlarged micrograph showing longitudinal section through Z band, which demonstrates the connection of I filaments to the very dense Z line (arrows). $\times 123,000$.



PLATE 7

EXPLANATION OF FIGURES

- 13 This enlarged micrograph shows the close association of Z band to the sarcolemma (arrow). $\times 70,000$.
- 14 The dense filaments which make up the N band (N) of the I region are similar to the dense filaments in the Z band. The zig-zag pattern is apparent at the arrows, where the actin filament (I filament) seems to branch into two dense lines in both the N band and Z band regions. $\times 102,500$.
- 15 Enlarged micrograph showing longitudinal section through Z band, which demonstrates the connection of I filaments to the very dense Z line (arrows). $\times 123,000$.

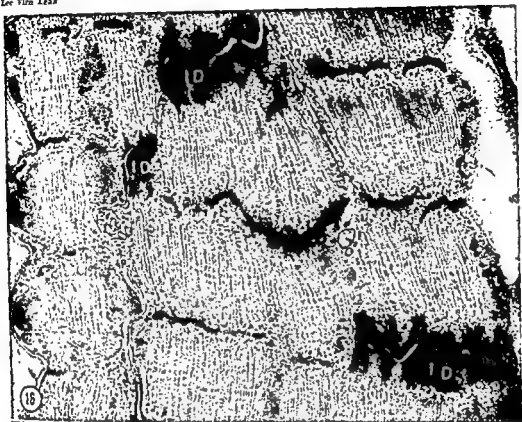


PLATE 8

EXPLANATION OF FIGURES

- 16 Apposing myofibers are held in close apposition by intercalated disc (ID). $\times 19,250$.
- 17 Dense granules (dg) of varying size, centrioles (Ce), vesicles (v), and membranes of the Golgi apparatus and mitochondria (m) appear in the sarcoplasmic core. A desmosome (D) occurs at left. $\times 53,750$.

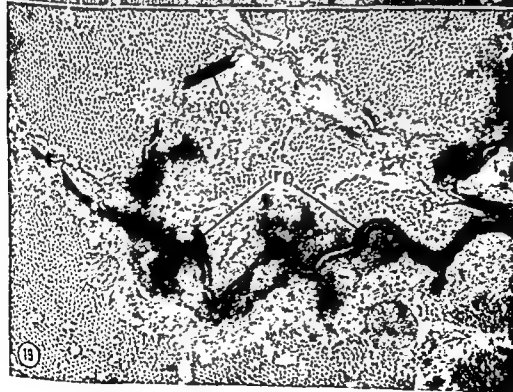


PLATE 9

EXPLANATION OF FIGURES

- 18** Longitudinal section of myofiber which demonstrates the wavy appearance of the intercalated disc (arrows). $\times 20,000$.
- 19** Transverse section through myofibers that passes through the intercalated disc (ID). Desmosomes (D) are apparent at other regions of the sarcolemma. $\times 37,000$.



PLATE 10

EXPLANATION OF FIGURES

- 20 Numerous small vesicles (v) with and without a dense core are closely associated with the Golgi (G). One of the large dense granules (dg) contains very small particles and membranes (arrows). $\times 16,000$.
- 21 This micrograph is from a section cut through the perinuclear region of the myofiber. Numerous mitochondria (m) occur in the sarcoplasmic core between the contractile units. The large dense granule (dg) contains membranes in its very dense matrix (see insert). $\times 27,500$; Insert $\times 125,000$.
- 22 Longitudinal section of myofiber in which the Golgi complex (g) occurs near the transverse sarcolemma (SL). The basal lamina (bl), mitochondria (m) and a portion of the nucleus (n) are shown. $\times 18,000$.
- 23 This peripherally located mitochondrion (m) extends the length of three sarcomeres. $\times 16,000$.

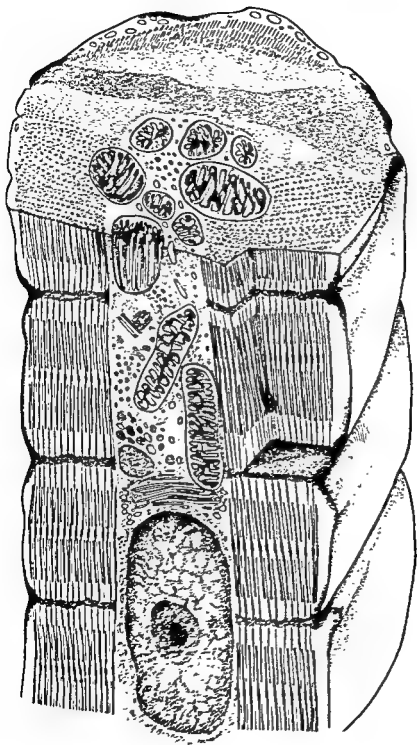


PLATE 11

EXPLANATION OF FIGURE

- 24 This diagram was constructed from collated electron micrographs and summarizes observations made on cardiac myofibers of the boa constrictor. The slight indentations along the sarcolemma are continuous with the Z band by a dense material along the inner surface of the sarcolemma. The myofibers form a continuous bundle and are arranged circumferentially so that the nucleus occupies the central regions of the myofiber with most of the mitochondria being located in the perinuclear sarcoplasmic core between the nucleus and transverse sarcolemma. Occasionally they occur in the subsarcoplasmic region and also between the myofibrils. A transverse tubular system and a complex sarcoplasmic reticulum are not apparent; instead many small vesicles occur throughout the peripheral and central sarcoplasmic matrix.

A Light and Electron Microscopical Study of Neurofibrils and Neurofilaments at Neuro-Neuronal Junctions in the Dorsal Lateral Geniculate Nucleus of the Cat¹

R. W. GUILLERY

Anatomy Department, The University of Wisconsin, Madison, Wisconsin

ABSTRACT Neurofibrillar rings and spheres one-half to 2 μ in diameter occur throughout the dorsal lateral geniculate nucleus of the cat. Counts confirm that they occur predominantly in laminae A and A1, and only rarely in lamina B and the central interlaminar nucleus. The rings lie in zones of lightly argyrophilic tissue between perikarya and rarely contact cell bodies. The argyrophilic zones are 5–20 μ wide, forming a continuous reticulum throughout laminae A and A1.

Electron micrographs show rings and nests of neurofilaments that match the neurofibrillar structures in size and distribution. These filaments are not found in axons, but occur in spheroid dendritic appendages, which have previously been described on Golgi preparations. The appendages lie in synaptic zones which are 5–20 μ wide and encapsulated by glial lamellae. Within the zones two major types of specialized contact are recognizable. "Regular" contacts (axo-dendritic and axo-axonal) resemble synaptic contacts in other parts of the CNS. "Filamentous" contacts (axo-dendritic and dendro-dendritic) show neurofilaments in the dendritic cytoplasm and show no concentration of vesicles on the axonal side. Within the appendages filaments from adjacent filamentous contacts join to form a nest around a group of mitochondria.

Comparison with previous studies suggests that these dendritic appendages, which receive regular and filamentous contacts, form a major receptive site for the retinal afferents.

Neurofibrillar stains, such as the meth-ods of Cajal ('03), Bielschowsky ('04) or Glees ('46), show small, annular, reticular or spherical structures in many parts of the nervous system. At most sites these are clearly recognizable as axonal "boutons"², either terminal or *en passage*. The structure of these boutons, their relationship to cell bodies and dendrites and their behavior during degeneration has been fully described and discussed (e.g. Cajal, '54; Hoff, '32a,b; Schimert, '38).

In the normal dorsal lateral geniculate nucleus of the monkey such boutons are extremely rare, although many large dense boutons appear in the nucleus 5–7 days after cutting the optic nerve (Glees and Le Gros Clark, '41; Glees, '61). In the cat, however, the normal lateral geniculate nucleus contains a great many small annular or spherical structures which resemble the classical boutons in many respects (Glees, '41; Hayhow, '59; Szentágothai, '63; Smith et al., '64). Hayhow and Glees have treated these as axonal boutons and have studied them in normal material and after optic

nerve section (see also Smith et al., '64). Hayhow found an evaluation of the changes that occur in these "boutons" difficult and based his interpretation of degenerative changes mainly on the axonal debris that occurs in the nucleus following optic nerve section. Szentágothai ('63) has argued that these neurofibrillar structures differ from classical boutons since they are predominantly axo-dendritic rather than axo-somatic. However, he did regard them as axon terminals, specifically as the claw shaped terminals of the optic nerve fibers that he described on Golgi preparations.

The present study was undertaken to investigate the difference between neurofibrillar preparations of normal cat and normal monkey lateral geniculate nucleus, to relate the neurofibrillar "boutons" of the

¹This project received support from a General Research Support Grant to the University of Wisconsin Medical School from the National Institutes of Health, Division of Research Facilities and Resources, and from grant NB-05907 from the National Institute of Neurological Diseases and Blindness, United States Public Health Service. The patient technical assistance given by Mrs. Elaine Lanzer at all stages of the project is gratefully acknowledged.

²See Gray and Guillery ('66) for a discussion of the use of this term.

hyde:paraformaldehyde mixture in a cacodylate buffer (Karnovsky, '65). The blocks from these animals were post-fixed in 1.3% osmium tetroxide in a 0.067M s-collidine buffer.

Some of the blocks were dehydrated in ethanol and embedded in Araldite, some were stained with 1% phosphotungstic acid in absolute ethanol before embedding and some were dehydrated in acetone, stained with 1% uranyl acetate in acetone and then embedded (Westrum, '65). The sections from the unstained blocks and some of the sections from the blocks stained with uranyl acetate were stained with lead citrate (Reynolds, '63).

Counts of neurofibrillar knots (see below) were done on the sections prepared by the Nauta method. The knots were counted under an oil immersion objective, with an eyepiece grid that outlined an area of section $75 \mu \times 75 \mu$. The grid divided this area into 400 squares and all the knots that could be seen in the area at all depths of focus were counted. The fields to be counted were selected at $\times 25$ magnification. At this magnification the larger vessels could be avoided, the individual laminae of the lateral geniculate nucleus were readily identifiable, but the knots could not be seen. On each section about ten fields were selected from each lamina and these fields were spaced evenly through the whole of each clearly recognizable lamina.

The terminology used for the dorsal lateral geniculate nucleus follows Hayhow's description (Hayhow, '58).

RESULTS

(1) Neurofibrillar stains

All of the neurofibrillar methods that have been used show small, discreet, dark, round or oval profiles scattered between the perikarya (figs. 1-4). These profiles vary in size from one-half to 2μ across. Many have a translucent center, while others appear completely opaque (see figs. 2, 3, 4). These are neurofibrillar structures and they resemble the boutons that are found in other parts of the nervous system. However, since the evidence that is to be presented suggests that they are not axonal structures the term "bouton" is inappropriate. Instead they will be called fibrillar knots.

The knots show no continuity with the surrounding fiber plexus. That is, they show no "tails" which could lead one to regard them as fiber terminals. Where, rarely, a knot does appear to be continuous with a fiber (as in figs. 2, 4 at the arrows), careful study usually shows that the two structures are in proximity but not in continuity.

In view of the small size of the knots it is difficult to determine their three dimensional structure with the light microscope. They may be spherical or ring shaped, or both forms may be present. Occasionally it is possible to see a larger knot which is clearly a ring since it lies oblique to the plane of the section and one part can be brought into focus while another part is out of focus. However, such appearances are rare and it is probable that the majority of the knots are spherical.

The impregnation obtained with the block Cajal methods shows the knots in each of the 12 blocks. The quality of the impregnation varies from one block to another and also shows some variation in different parts of the same block. This irregularity of the stain makes it impossible to determine whether or not the material from the three month old kitten contains fewer knots than does the material from the adult cats (see below).

In some regions of the Cajal blocks the knots are preferentially stained and the surrounding tissues are poorly stained or not stained at all (figs. 2, 3). In such regions it is possible to see that the knots lie predominantly in narrow, $5-20 \mu$ wide, zones or bands in which the background is slightly darkened. These dark bands (fig. 3), separated from each other by lighter zones, appear to form a three dimensional reticulum around the cells of the lateral geniculate nucleus. The knots usually lie in small clusters at some distance from the perikarya and it is rare to see a knot which appears to contact a cell body.

The knots occur frequently in laminae A and A1. They are seen rarely in lamina B or, where this can be clearly identified, in the central interlaminar nucleus (fig. 1).

The paraffin Nauta sections show a more regular impregnation throughout the whole of a series. The general fiber plexus

cat lateral geniculate nucleus to the structures that have previously been described on Golgi preparations (Szentágothai, '63; Guillery, '66) and to compare the morphology and the distribution of these "boutons" with filamentous structures identifiable by electron microscopy.

In many parts of the nervous system where neurofibrillar boutons are seen with the light microscope, electron micrographs show bundles of neurofilaments in axon terminals. The morphology and distribution of these filamentous bundles in both normal and degenerating material is such that one must regard the neurofilaments, or their immediate environment, as argyrophilic and as forming a basis for the neurofibrillar structures (Boycott et al., '61; Gray and Guillery, '61, '66). In view of this evidence it was thought that electron micrographs would show neurofilamentous rings and spheres in axon terminals of the normal lateral geniculate nucleus of the cat, and that these would correspond to the neurofibrillar rings and spheres seen with the light microscope. Since neurofilaments are rarely seen in normal axon terminals in the lateral geniculate nucleus of the monkey (Colonnier and Guillery, '64), where neurofibrillar boutons are rare, such a finding would have given useful information for further comparisons between the cat and the monkey, especially for a comparison of the changes that occur in the lateral geniculate nucleus following optic nerve section (see Cook et al., '51; Glees, '41, '61; Hayhow, '59; Matthews et al., '60).

The results to be reported below show that axon terminals in the lateral geniculate nuclei of the cat and monkey do not differ in filamentous contents. It is rare to see bundles of neurofilaments in the axon terminals of either. However, both show an unusual type of neuro-neuronal contact, which is characterized by an irregular membrane thickening and a concentration of filaments on the dendritic side of the contact (see Colonnier and Guillery, '64; Pappas et al., '66). In the monkey these dendritic filaments form a thin lamina which would be beyond the resolving power of the light microscope. In the cat the filaments often form complex annular or spherical nests of a size that would be

readily recognizable with the light microscope. The nests occur in spherical or grape-like dendritic appendages, which appear to be a major receptive specialization for the incoming optic nerve fibers (Szentágothai, '63; Guillery, '66).

MATERIALS AND METHODS

Three adult cats of unknown age (weight from 2.8 to 3.8 kg) and one nine month old cat (weight 1.25 kg) were perfused under sodium pentobarbital anesthesia with saline followed by formol saline. Blocks containing the lateral geniculate nuclei were embedded in paraffin, cut at 10-15 μ in frontal or parasagittal planes, and two series were prepared from each block. One was stained with thionin and the other with the Nauta method (Nauta and Gyax, '51; see Guillery et al., '61).

Three cats were used for block Cajal stains. Each lateral geniculate nucleus was hemisected and from each animal two blocks were prepared according to Cajal's formula 5 and two according to Cajal's formula 3 (see Romeis, '48). One of these cats (adult, 2.85 kg) was decapitated under pentobarbital anesthesia and the tissues fixed by immersion. A second adult cat (2.75 kg) and a three month old kitten (0.85 kg) were perfused with formol saline and the tissues subsequently treated according to the Cajal formulae.

Eight cats were used for electron microscopy. Six cats were perfused with a buffered Ringer's solution followed by 3-5% glutaraldehyde in a phosphate buffer. Blocks were taken from the lateral geniculate nucleus, rinsed either in buffer or in the buffered Ringer's solution and transferred to 1% osmium tetroxide in either a veronal or a phosphate buffer. All solutions were adjusted to pH 7.4. In two of these six animals the skull was opened prior to perfusion. While cold Ringer's solution was being perfused a part of one lateral geniculate nucleus was rapidly removed and transferred to buffered 1% osmium tetroxide. The animal was then perfused with glutaraldehyde and the other lateral geniculate nucleus treated as above.

Two cats were perfused with buffered Ringer's solution followed by a glutaralde-

hyde:paraformaldehyde mixture in a cacodylate buffer (Karnovsky, '65). The blocks from these animals were post-fixed in 1.3% osmium tetroxide in a 0.067M s-collidine buffer.

Some of the blocks were dehydrated in ethanol and embedded in Araldite, some were stained with 1% phosphotungstic acid in absolute ethanol before embedding and some were dehydrated in acetone, stained with 1% uranyl acetate in acetone and then embedded (Westrum, '65). The sections from the unstained blocks and some of the sections from the blocks stained with uranyl acetate were stained with lead citrate (Reynolds, '63).

Counts of neurofibrillar knots (see below) were done on the sections prepared by the Nauta method. The knots were counted under an oil immersion objective, with an eyepiece grid that outlined an area of section $75\mu \times 75\mu$. The grid divided this area into 400 squares and all the knots that could be seen in the area at all depths of focus were counted. The fields to be counted were selected at $\times 25$ magnification. At this magnification the larger vesicles could be avoided, the individual laminae of the lateral geniculate nucleus were readily identifiable, but the knots could not be seen. On each section about ten fields were selected from each lamina and these fields were spaced evenly through the whole of each clearly recognizable lamina.

The terminology used for the dorsal lateral geniculate nucleus follows Hayhow's description (Hayhow, '58).

RESULTS

(1) Neurofibrillar stains

All of the neurofibrillar methods that have been used show small, discreet, dark, round or oval profiles scattered between the perikarya (figs. 1-4). These profiles vary in size from one-half to 2μ across. Many have a translucent center, while others appear completely opaque (see figs. 2, 3, 4). These are neurofibrillar structures and they resemble the boutons that are found in other parts of the nervous system. However, since the evidence that is to be presented suggests that they are not axonal structures the term "bouton" is inappropriate. Instead they will be called fibrillar knots.

The knots show no continuity with the surrounding fiber plexus. That is, they show no "tails" which could lead one to regard them as fiber terminals. Where, rarely, a knot does appear to be continuous with a fiber (as in figs. 2, 4 at the arrows), careful study usually shows that the two structures are in proximity but not in continuity.

In view of the small size of the knots it is difficult to determine their three dimensional structure with the light microscope. They may be spherical or ring shaped, or both forms may be present. Occasionally it is possible to see a larger knot which is clearly a ring since it lies oblique to the plane of the section and one part can be brought into focus while another part is out of focus. However, such appearances are rare and it is probable that the majority of the knots are spherical.

The impregnation obtained with the block Cajal methods shows the knots in each of the 12 blocks. The quality of the impregnation varies from one block to another and also shows some variation in different parts of the same block. This irregularity of the stain makes it impossible to determine whether or not the material from the three month old kitten contains fewer knots than does the material from the adult cats (see below).

In some regions of the Cajal blocks the knots are preferentially stained and the surrounding tissues are poorly stained or not stained at all (figs. 2, 3). In such regions it is possible to see that the knots lie predominantly in narrow, $5-20\mu$ wide, zones or bands in which the background is slightly darkened. These dark bands (fig. 3), separated from each other by lighter zones, appear to form a three dimensional reticulum around the cells of the lateral geniculate nucleus. The knots usually lie in small clusters at some distance from the perikarya and it is rare to see a knot which appears to contact a cell body.

The knots occur frequently in laminae A and A1. They are seen rarely in lamina B or, where this can be clearly identified, in the central interlamina nucleus (fig. 1).

The paraffin Nauta sections show a more regular impregnation throughout the whole of a series. The general fiber plexus

in the lateral geniculate nucleus is well shown and the knots are clearly recognizable (fig. 4). The relatively heavy fiber stain makes it more difficult to obtain photographs of the knots, but the even quality of the neurofibrillar stain allows a more detailed study of their distribution. The knots again occur predominantly in zones 5-20 μ wide. These zones are separated from each other by areas relatively free of knots in which the perikarya and a rich fiber plexus can be seen. Preliminary plots of the distribution of the knots were made on seven sections taken from three different animals. Each of these plots showed that there are relatively few knots in lamina B and indicated that the central interlaminar nucleus contains fewer knots than do laminae A and A1.

Counts of the number of knots per unit area confirm these conclusions (table 1). The results for cat W12 (9 month old cat) are given as the number of knots per unit field $75 \mu \times 75 \mu$. The results for cat W14 (adult cat) have been adjusted to allow a comparison between the two animals. This was necessary since the sections of W12 were cut at 10 μ while those of W14 were cut at 12 μ . Sample measurements of section thickness with a graduated fine focusing adjustment confirm the microtome readings. Since the average diameter of the knots is approximately 1.5 μ the original counts from W14 have been corrected by a factor of 11.5/13.5. In spite of this correction the counts for laminae A and

A1 are significantly higher in W14 than in W12 (t test; 0.01 probability level).

Comparison of counts from different laminae in a single animal shows that there is no significant difference between laminae A and A1 but that these laminae gave significantly higher counts than the other laminae (t test; 0.01 probability level). Further, the counts show significantly more knots in the central interlaminar nucleus than in lamina B. However, since the central interlaminar nucleus is narrow and its borders are wavy the counts for this nucleus often included some tissue that belonged to the adjacent A or A1 laminae. The error introduced by this factor may well account for the higher counts obtained for the central interlaminar nucleus. The error was not corrected since the primary aim was to determine whether or not there was a difference between the A and A1 laminae and the central interlaminar nucleus.

(2) Electron microscopical observations

A. General organization of synaptic contacts. The organization of synaptic contacts in the lateral geniculate nucleus will not be dealt with in detail here. Since the aim of the present study was to determine whether electron micrographs could give further information about the structure and relationships of the neurofibrillar knots, only the features relevant to these will be described.

Within laminae A and A1 it is common to see neuronal profiles which are closely related to each other and which form small synaptic zones that are partially or completely separated from surrounding tissues by thin glial lamellae (G, see figs. 7, 14, 15). These synaptic zones correspond to the "glomeruli" that Szentágothai ('63) and Pappas et al. ('66) described in the lateral geniculate nucleus of the cat and are similar to the synaptic "islands" described in the monkey by Colonnier and Guillery ('64). For reasons given on p. 592 they will be called encapsulated synaptic zones in the present account.

Within these zones the synaptic processes of axons and dendrites can generally be recognized on the basis of criteria that have been discussed previously (see Colonnier and Guillery, '64; Gray and Guillery,

TABLE 1

Number of neurofibrillar knots per unit area of section, $75 \mu \times 75 \mu$, in the lateral geniculate nucleus

Lamina	Number of fields in sample	Mean number of knots per field	S.E. of mean
Cat W12			
A	40	23.0	1.36
A1	40	24.5	1.51
NIC	40	5.9	0.68
B	40	2.9	0.37
Cat W14			
A	29	38.6 ¹	2.30
A1	25	33.0 ¹	2.00
NIC	32	7.6 ¹	0.81
B	25	3.0 ¹	0.68

¹ The individual counts for W14 were adjusted to allow for the difference in section thickness (see text).

'66). The largest axon terminals or synaptic knobs, up to 3μ or more in diameter, are generally found within the encapsulated synaptic zones (A, figs. 6, 14, 15). However, since these synaptic knobs often have an irregular outline, interdigitating freely with each other and with adjacent neuronal profiles it is usual to see axonal profiles that vary greatly in size (see figs. 5, 14, 15). For the present account all of the synaptic knobs within the encapsulated zones will be treated as a single population, although the possibility that there is more than one type of axon present in the zones cannot be excluded (compare Stentégothai, '63, '65; Colonnier and Guillery, '64; Guillery, '66).

B. Neurofilaments in neuronal profiles. It is rare to see neurofilaments in any of the profiles that contain synaptic vesicles, either in the large synaptic knobs that occur in the encapsulated zones or in the smaller knobs that are seen in the adjacent lateral geniculate tissues. Occasionally a large bag contains a small bundle of filaments (fig. 6, N), but these bundles have never been seen to form a pattern that could readily be interpreted as a section of a filamentous ring or sphere. In this the lateral geniculate nucleus of the cat is similar to that of the monkey (Colonnier and Guillery, '64). Sometimes it is possible to recognize fine granular or filamentous material between the synaptic vesicles in the synaptic knobs (figs. 8, 9, 10). However, this material is generally distinguishable from the neurofilaments, especially on the thicker sections, in which filaments stand out clearly.

In some of the neuronal profiles that lie within the encapsulated synaptic zones neurofilaments can be seen. These filaments sometimes form dense networks (figs. 5, 7, 9), sometimes appear as oblique sections through a ring (figs. 12, 13) and sometimes form two groups of dots such as would be expected from a radial section through a ring (figs. 6, 9). These nests or rings of neurofilaments vary in diameter from one-half to 2μ . The filaments always pass close to the membrane of the neuronal profile and are usually arranged around a group of mitochondria. On the basis of the contacts that they form and the continuities that they show the profiles

that contain these filaments are regarded as dendritic appendages (see below).

C. The dendritic appendages. The dendritic appendages that contain the filaments generally have an oval or round outline. It is unusual to see one of them continuous with a profile that can be readily interpreted as a dendritic branch. Sometimes, however, such continuity can be traced through a short narrow stalk, either on a single section or on serial sections. On figures 12 and 13 such a stalk is shown. The stalk is sharply curved and the filaments lie in a dendritic appendage that is closely applied to its parent dendrite.

It is clear that one cannot expect to see the continuity between the appendage and the dendritic branch often if the appendages are usually supported by fine curved stalks similar to that shown in figures 12 and 13. Since the most common picture of the dendritic appendages is that shown in figures 7 and 9 it may be concluded that many appendages do in fact have extremely fine, probably somewhat curved stalks. The region marked S in the upper left part of figure 9 may represent one end of such a stalk.

A few appendages show a different relationship. Thus figure 5 shows an appendage (DA) which has a broad base continuous with a dendritic profile (D), and figure 15 (?DA) may represent a section of a similar structure. Such relationships are not seen often.

The dendritic appendages that contain nests or rings of filaments very commonly occur in groups of two or three on a section (see e.g. fig. 9). If one appendage is seen, close search of nearby tissue often reveals one or two more. These appendages have been seen frequently in laminae A and A1. It would be misleading to claim any precision for statements regarding the frequency with which particular structures are found in the present material. However, as a general indication about the material that has been examined it can be said that within a single grid square ($75\mu \times 75\mu$) that was mainly or completely covered by reasonably well preserved tissue from lamina A or A1, a careful search has shown up to ten clearly identifiable sections of filamentous rings and nests ranging from one-half to 2μ in diameter.

in the lateral geniculate nucleus is well shown and the knots are clearly recognizable (fig. 4). The relatively heavy fiber stain makes it more difficult to obtain photographs of the knots, but the even quality of the neurofibrillar stain allows a more detailed study of their distribution. The knots again occur predominantly in zones 5–20 μ wide. These zones are separated from each other by areas relatively free of knots in which the perikarya and a rich fiber plexus can be seen. Preliminary plots of the distribution of the knots were made on seven sections taken from three different animals. Each of these plots showed that there are relatively few knots in lamina II and indicated that the central interlaminar nucleus contains fewer knots than do laminae A and A1.

Counts of the number of knots per unit area confirm these conclusions (table 1). The results for cat W12 (9 month old cat) are given as the number of knots per unit field $75 \mu \times 75 \mu$. The results for cat W14 (adult cat) have been adjusted to allow a comparison between the two animals. This was necessary since the sections of W12 were cut at 10 μ while those of W14 were cut at 12 μ . Sample measurements of section thickness with a graduated fine focusing adjustment confirm the microtome readings. Since the average diameter of the knots is approximately 1.5 μ the original counts from W14 have been corrected by a factor of 11.5/13.5. In spite of this correction the counts for laminae A and

A1 are significantly higher in W14 than in W12 (*t* test; 0.01 probability level).

Comparison of counts from different laminae in a single animal shows that there is no significant difference between laminae A and A1 but that these laminae gave significantly higher counts than the other laminae (*t* test; 0.01 probability level). Further, the counts show significantly more knots in the central interlaminar nucleus than in lamina B. However, since the central interlaminar nucleus is narrow and its borders are wavy the counts for this nucleus often included some tissue that belonged to the adjacent A or A1 laminae. The error introduced by this factor may well account for the higher counts obtained for the central interlaminar nucleus. The error was not corrected since the primary aim was to determine whether or not there was a difference between the A and A1 laminae and the central interlaminar nucleus.

(2) Electron microscopical observations

A. *General organization of synaptic contacts.* The organization of synaptic contacts in the lateral geniculate nucleus will not be dealt with in detail here. Since the aim of the present study was to determine whether electron micrographs could give further information about the structure and relationships of the neurofibrillar knots, only the features relevant to these will be described.

Within laminae A and A1 it is common to see neuronal profiles which are closely related to each other and which form small synaptic zones that are partially or completely separated from surrounding tissues by thin glial lamellae (G, see figs. 7, 14, 15). These synaptic zones correspond to the "glomeruli" that Szentágothai ('63) and Pappas et al. ('66) described in the lateral geniculate nucleus of the cat and are similar to the synaptic "islands" described in the monkey by Colonnier and Guillery ('64). For reasons given on p. 592 they will be called encapsulated synaptic zones in the present account.

Within these zones the synaptic processes of axons and dendrites can generally be recognized on the basis of criteria that have been discussed previously (see Colonnier and Guillery, '64; Gray and Guillery,

TABLE 1

Number of neurofibrillar knots per unit area of section, $75 \mu \times 75 \mu$, in the lateral geniculate nucleus

Lamina	Number of fields in sample	Mean number of knots per field	S.E. of mean
Cat W12			
A	40	23.0	1.36
A1	40	24.5	1.51
NIC	40	5.9	0.68
II	40	2.9	0.37
Cat W14			
A	29	38.6 ¹	2.30
A1	25	33.0 ¹	2.00
NIC	32	7.6 ¹	0.81
B	25	3.0 ¹	0.68

¹ The individual counts for W14 were adjusted to allow for the difference in section thickness (see text).

cytoplasmic surface of both membranes, so that one can easily gain the impression that short bands of electron dense material are passing across the extracellular cleft, from one neuronal profile to the other.

Regular and asymmetrical filamentous contacts occur adjacent to each other on a single pair of apposed membranes (e.g. fig. 10), but whereas the regular contacts occur throughout the tissues of the lateral geniculate nucleus the filamentous contacts occur predominantly in the encapsulated synaptic zones, and there commonly involve one of the dendritic appendages that contain a ring or nest of neurofilaments. It is unusual to see a profile of one of these dendritic appendages that does not have a filamentous contact upon it. Filamentous contacts also occasionally occur on dendritic branches, and there they are associated with a small zone of filaments that lies subjacent to the contact.

The relationships described above have been seen consistently in all of the material used in the present study. The filaments and the structure of the filamentous contacts were shown most clearly when PTA was used as a block stain. The sections that were stained with lead citrate did not show these features as clearly (see figs. 14, 15), and these sections were not used to study the distribution of the filaments (see above). The clearest pictures were obtained from the blocks that were not fixed in aldehydes, and most of the illustrations are taken from this material (see MATERIALS AND METHODS).

DISCUSSION

Neurofibrillar rings and spheres, the neurofibrillar knots of the present account, can be seen with the light microscope in the dorsal lateral geniculate nucleus of the cat. These knots occur predominantly in laminae A and A1 and are rare in lamina B and in the central interlaminar nucleus.

The knots have been previously described (Glees, '41; Hayhow, '58; Szentágothai, '63; Smith et al., '64) and have been treated as axonal structures, similar to the "boutons" that are seen in other parts of the nervous system. Hayhow ('58) described them in all the laminae of the lateral geniculate nucleus. However, since his was not a quantitative study there is

no need to assume that his material differed significantly from that used here.

Neurofibrillar methods generally show more boutons on tissues taken from old animals than on tissues taken from young animals (for references see Gray and Guillery, '66). Since the maximum change appears to occur between birth and three months (Windle, '30; Davenport, '33), the present material, obtained from cats three months and older does not add significantly to this problem. The difference that was observed between cat W12 (aged 8 months) and cat W14 (adult, age unknown) may perhaps be related to a continuing slow change that has been reported during adult life (Minckler, '42), or it may be that such differences occur between adult cats irrespective of age. More extensive quantitative studies are required to demonstrate whether age related changes occur in the neurofibrillar knots.

The neurofibrillar knots that are found in the dorsal lateral geniculate nucleus have also been studied with the electron microscope. No structures corresponding to the knots can be seen in axon terminals. Instead the knots have been identified as nests and rings of neurofilaments that lie in spherical or ovoid dendritic appendages. This identification is important because it raises the question whether neurofibrillar rings and spheres that occur in some other parts of the nervous system may not also be dendritic, rather than axonal as has been generally assumed. Further, it explains why the interpretation of axonal degeneration in the lateral geniculate nucleus of the cat has proved so difficult when neurofibrillar methods were used (e.g. Hayhow, '58, '59).

The interpretation of the neurofibrillar knots as dendritic rather than axonal structures depends upon several arguments. One is that the neurofibrils visible with the light microscope correspond to groups of neurofilaments that can be seen on electron micrographs, another concerns the identification of dendritic profiles on electron micrographs, and a third deals with the morphology of dendritic appendages in the lateral geniculate nucleus of the cat. Each will be considered below.

The arguments in favor of considering that neurofibrils are seen on silver prep-

In some grid squares it was not possible to find any, most commonly between two and six have been seen. Material obtained from lamina II usually shows no such structures. Occasionally a single filamentous nest or ring has been found there. No separate study of the central interlaminar nucleus has been made.

D. Specialized neuro-neuronal contacts. It is possible to recognize two distinct types of neuro-neuronal contact within the lateral geniculate nucleus. They correspond to the "regular" and "filamentous" contacts described by Colonnier and Guillery ('64). The regular contacts (R, figs. 8, 9, 10) are, in general, similar to synaptic contacts that are seen in many parts of the nervous system. They show a group of synaptic vesicles close to the presynaptic membrane, they commonly show a thin band of extracellular material in the synaptic cleft and there is an electron dense thickening closely applied to the postsynaptic membrane. Usually sections of regular contacts are not longer than about $1/4 \mu$. The presynaptic component of a regular contact always shows the characteristics of a synaptic knob. The postsynaptic component often has the characteristics of a dendrite, sometimes appears to be another synaptic knob (figs. 6, 8) and sometimes cannot be clearly recognized as either. Occasional axo-somatic contacts also occur.

Where one of the neuronal profiles that contains a nest or ring of filaments makes a regular contact, the asymmetry of the contact is always such that these neuronal profiles must be regarded as postsynaptic. Although a great many of these neuronal profiles have been seen, and regular contacts occur on them commonly, it has not been possible to find an exception to this statement.

Filamentous contacts (F, figs. 8-11) may be either symmetrical or asymmetrical. The former occur between two dendritic profiles and the latter occur between a synaptic knob and a dendritic profile. Filamentous contacts that involve the perikaryon are rare in the present material (compare Colonnier and Guillery, '64; Pappas et al., '66). The filamentous contacts are larger than the regular contacts and sections commonly show lengths of

one-half to 1μ (figs. 7-11). There is an indication that the apposed neuronal membranes at the filamentous contacts are relatively undulated (figs. 6, 8, 10, 15), whereas they are straight at the regular contacts. This undulation may well be produced during fixation, but it is a feature that has been encountered frequently and generally distinguishes regular from filamentous contacts. More strikingly, synaptic vesicles do not crowd close to the axonal membrane of the asymmetrical filamentous contacts and the only structures that can be seen close to the membrane on the axonal side are small irregular patches of granular or filamentous material (see especially figs. 8-11). On the dendritic side of both types of filamentous contacts neurofilaments always pass relatively close to the membrane, but are separated from the membrane by an intermediate region, which contains electron dense granular or filamentous material (figs. 8-11 marked I on fig. 8). Occasionally some scattered vesicles also occur in or close to the intermediate region, but most commonly they lie within a membranous sac, forming a multivesicular body (fig. 14, M; fig. 13).

The structure of the granular intermediate region is not clear on the present material, nor can the precise relationship of the filaments to this region be defined. The filaments always lie close to the intermediate region (figs. 8-11), and sometimes appear to enter it (fig. 10). The intermediate region is not everywhere closely applied to the dendritic membrane. Zones of pale cytoplasm lie between the membrane and parts of the intermediate region. This partial separation between the intermediate region and the neuronal membrane shows considerable variation, and the possibility that the granular material moves during fixation cannot be excluded. Granular material, however, is commonly seen closely applied to some parts of the dendritic membrane (figs. 8-11), and opposite these regions of close apposition it is often possible to see some material between the two neuronal membranes (figs. 8, 11, at unlabeled arrows). At the places marked in these figures the extracellular material is in close register with electron dense material applied to the

tacts, which are characteristically formed upon these profiles are also to be seen on dendritic branches (see Pappas et al., '66, and fig. 15). At such sites the filaments always lie on the dendritic, not the axonal side.

A comparison between cat and monkey is of some relevance to the above arguments. In the monkey Colonnier and Guillery ('64) found asymmetrical filamentous contacts upon dendrites and perikarya. In addition they described symmetrical dendro-dendritic and soma-somatic filamentous contacts. The filamentous contacts that are seen in the cat are similar to those found in the monkey, and it is not unreasonable to assume that both represent a similar functional specialization. In the monkey axo-somatic and soma-somatic contacts appear to be more common than in the cat (O'Leary et al., '65; Colonnier and Guillery, '64) and the axo- and dendro-dendritic contacts often involve larger dendritic profiles which are more readily identifiable. It is concluded that in both species the filaments that lie close to filamentous contacts occur in either dendrites or perikarya, not in axons.

In the lateral geniculate nucleus of the monkey these filaments generally form a small flattened nest parallel to the neuronal membrane. It has been possible to see them extend for a considerable distance beyond the membrane of the filamentous contact in only one instance, where they formed a filamentous ring (see Gray and Guillery, '66, fig. 35). In the cat the filaments generally extend well beyond the membrane and commonly form rings or nests in the dendritic cytoplasm. This difference between the two species is closely related to the difference that is seen when the lateral geniculate nucleus is examined by neurofibrillar methods. Whereas the cat shows a great many neurofibrillar knots, the monkey shows relatively few.

The distribution of the filaments throughout the cytoplasm of the dendritic appendages in the cat is often so extensive that no particular relationship between the filamentous contacts and the filaments is apparent (see e.g. figs. 7, 9). The association between the two is seen most clearly where there are relatively few filaments.

Thus it is seen clearly at most filamentous contacts in the monkey and at filamentous contacts that involve dendritic branches in the cat.

The dendritic appendages that contain the neurofibrillar knots also merit consideration. Szentágothai ('63, '65) described rounded dendritic appendages in the lateral geniculate nucleus of the cat on Golgi preparations and on electron micrographs. He considered that these appendages were the primary receptor surface for the retinal afferents. He showed that the appendages contain mitochondria, but he did not show the neurofilaments (see p. 590). Guillery ('66), working with Golgi preparations from the lateral geniculate nucleus of the cat also showed these appendages. Occasionally it is possible to see an appendage with an extremely fine stalk, but generally the stalks cannot be resolved on the thick Golgi sections. The majority of the appendages occur in clusters close to the branching points of the dendrites of "class 2" cells (see Guillery, '66). The class 2 cells are only found in laminae A and A1, and their dendrites only rarely cross laminar borders. When such a dendrite does cross a laminar border, the part of the dendrite that crosses the border does not carry clusters of appendages. That is, the clusters occur in laminae A and A1, they do not occur in lamina B, nor do they occur on dendrites that cross between major laminae through the central interlaminar nucleus. The shape, size and laminar distribution of these dendritic appendages corresponds closely to the shape, size and distribution of the neurofibrillar knots. It is probable that only a proportion of the dendritic appendages of class 2 cells contain filamentous nests that can be identified on silver preparations. However, it can be concluded that the same dendritic appendages can be studied with silver methods, Golgi methods, and on electron micrographs.

The dendritic appendages usually have a thin stalk, they commonly contain several mitochondria and a variable number of filaments grouped around the mitochondria. They make filamentous contacts with adjacent axons and with each other. Golgi preparations show that the appendages tend to occur in clusters and a similar

arations where silver is deposited on or around neurofilaments have been fully reviewed recently (Guillery, '65; Gray and Guillery, '66). The evidence is based upon electron microscopical examinations of tissues which show neurofibrillar specializations. Wherever such specializations are seen in the normal, degenerating, regenerating or developing nervous system it is possible to see neurofilamentous bundles or tangles that match the neurofibrillar structures closely in shape, size and distribution. Direct electron microscopical examination of tissues stained with silver methods provides additional evidence (Gray and Guillery, '61; Lund and Westrum, '66). Although this interpretation has been questioned (Walberg, '64), no alternative explanation of the characteristic morphology of neurofibrillar structures has been offered.

On the present material the neurofilaments were most difficult to see on sections stained with lead citrate only, and were most easily seen when phosphotungstic acid was used as a block stain. Since Walberg's ('64) entirely negative findings were based on material stained with lead compounds only, it is difficult to regard these as a strong argument against the interpretation being considered here. The difference between the present results and those of Szentágothai ('63, '65), who described no neurofilamentous bundles in either axons or dendrites in the lateral geniculate nucleus of the cat, may also be due to the different methods of preparation that were used. The "non-synaptic junctions" of Pappas et al. ('66) clearly correspond to the filamentous contacts. Pappas et al. show the electron dense material of the intermediate region and also show the filaments subjacent to this, lying in dendritic cytoplasm. They do not show the filamentous rings or nests, since they illustrate filamentous contacts upon dendritic stems or branches, not upon appendages.

It has been shown that bundles of neurofilaments occur in neuronal profiles in the lateral geniculate nucleus, and that the shape, size and laminar distribution of these neurofilamentous bundles is what would be expected from a study of the neurofibrillar knots. It is difficult to deter-

mine whether the matching is equally good in terms of numbers. However, if one assumes that there are approximately 30 knots to be seen in a $75 \mu \times 75 \mu$ area of a 10μ thick section (table 1), and if one takes 1.5μ as the average diameter of the knots, then one would expect to find about 4.7 knots per $75 \mu \times 75 \mu$ area on a 600 \AA thick section

$$\frac{30 \times 0.06}{10.0} \times \left[\frac{1.5}{0.06} + 1 \right]$$

This figure only represents a very approximate estimate. It takes no account of the Abercrombie ('46) correction for the light microscopical results, ignores the different degrees of shrinkage that tissues suffer when prepared for light or electron microscopy, and is based on an approximation of the section thickness used for electron microscopy. It is given here because it does indicate the sort of reduction in numbers that can be expected when structures of this size are examined by light and electron microscopical methods, and because it suggests that the number of neurofilamentous rings and nests that was found was approximately equal to the expected number.

The neuronal profiles within which the filamentous bundles were found have been identified as dendritic appendages. This identification is based primarily on two features. The first is that the profiles were never seen to contain groups of relatively uniform vesicles which could be regarded as synaptic vesicles. The second is that the profiles were never seen to make a synaptic contact the asymmetry of which would lead one to regard these profiles as presynaptic to another structure. Insofar as this asymmetry of synaptic contacts (see Gray and Guillery, '66) depends upon synaptic vesicles being present on the presynaptic side, the second feature is no different from the first. However, the asymmetry also depends upon the local membrane thickenings and upon the presynaptic dense projections (Gray, '63), and these were clearly identifiable in many synaptic junctions of the present material.

Two further features also argue in favor of regarding these profiles as dendritic. One is that occasionally it was possible to trace such a profile into a dendritic branch. The second is that the filamentous con-

tacts, which are characteristically formed upon these profiles are also to be seen on dendritic branches (see Pappas et al., '66, and fig. 15). At such sites the filaments always lie on the dendritic, not the axonal side.

A comparison between cat and monkey is of some relevance to the above arguments. In the monkey Colonnier and Guillery ('64) found asymmetrical filamentous contacts upon dendrites and perikarya. In addition they described symmetrical dendro-dendritic and soma-somatic filamentous contacts. The filamentous contacts that are seen in the cat are similar to those found in the monkey, and it is not unreasonable to assume that both represent a similar functional specialization. In the monkey axo-somatic and soma-somatic contacts appear to be more common than in the cat (O'Leary et al., '65; Colonnier and Guillery, '64) and the axo- and dendro-dendritic contacts often involve larger dendritic profiles which are more readily identifiable. It is concluded that in both species the filaments that lie close to filamentous contacts occur in either dendrites or perikarya, not in axons.

In the lateral geniculate nucleus of the monkey these filaments generally form a small flattened nest parallel to the neuronal membrane. It has been possible to see them extend for a considerable distance beyond the membrane of the filamentous contact in only one instance, where they formed a filamentous ring (see Gray and Guillery, '66, fig. 35). In the cat the filaments generally extend well beyond the membrane and commonly form rings or nests in the dendritic cytoplasm. This difference between the two species is closely related to the difference that is seen when the lateral geniculate nucleus is examined by neurofibrillar methods. Whereas the cat shows a great many neurofibrillar knots, the monkey shows relatively few.

The distribution of the filaments throughout the cytoplasm of the dendritic appendages in the cat is often so extensive that no particular relationship between the filamentous contacts and the filaments is apparent (see e.g. figs. 7, 9). The association between the two is seen most clearly where there are relatively few filaments.

Thus it is seen clearly at most filamentous contacts in the monkey and at filamentous contacts that involve dendritic branches in the cat.

The dendritic appendages that contain the neurofibrillar knots also merit consideration. Szentágothai ('63, '65) described rounded dendritic appendages in the lateral geniculate nucleus of the cat on Golgi preparations and on electron micrographs. He considered that these appendages were the primary receptor surface for the retinal afferents. He showed that the appendages contain mitochondria, but he did not show the neurofilaments (see p. 590). Guillery ('66), working with Golgi preparations from the lateral geniculate nucleus of the cat also showed these appendages. Occasionally it is possible to see an appendage with an extremely fine stalk, but generally the stalks cannot be resolved on the thick Golgi sections. The majority of the appendages occur in clusters close to the branching points of the dendrites of "class 2" cells (see Guillery, '66). The class 2 cells are only found in laminae A and A1, and their dendrites only rarely cross laminar borders. When such a dendrite does cross a laminar border, the part of the dendrite that crosses the border does not carry clusters of appendages. That is, the clusters occur in laminae A and A1, they do not occur in lamina B, nor do they occur on dendrites that cross between major laminae through the central interlaminar nucleus. The shape, size and laminar distribution of these dendritic appendages corresponds closely to the shape, size and distribution of the neurofibrillar knots. It is probable that only a proportion of the dendritic appendages of class 2 cells contain filamentous nests that can be identified on silver preparations. However, it can be concluded that the same dendritic appendages can be studied with silver methods, Golgi methods, and on electron micrographs.

The dendritic appendages usually have a thin stalk, they commonly contain several mitochondria and a variable number of filaments grouped around the mitochondria. They make filamentous contacts with adjacent axons and with each other. Golgi preparations show that the appendages tend to occur in clusters and a similar

arations where silver is deposited on or around neurofilaments have been fully reviewed recently (Guillery, '65; Gray and Guillery, '66). The evidence is based upon electron microscopical examinations of tissues which show neurofibrillar specializations. Wherever such specializations are seen in the normal, degenerating, regenerating or developing nervous system it is possible to see neurofilamentous bundles or tangles that match the neurofibrillar structures closely in shape, size and distribution. Direct electron microscopical examination of tissues stained with silver methods provides additional evidence (Gray and Guillery, '61; Lund and Westrum, '66). Although this interpretation has been questioned (Walberg, '64), no alternative explanation of the characteristic morphology of neurofibrillar structures has been offered.

On the present material the neurofilaments were most difficult to see on sections stained with lead citrate only, and were most easily seen when phosphotungstic acid was used as a block stain. Since Walberg's ('64) entirely negative findings were based on material stained with lead compounds only, it is difficult to regard these as a strong argument against the interpretation being considered here. The difference between the present results and those of Szentágothai ('63, '65), who described no neurofilamentous bundles in either axons or dendrites in the lateral geniculate nucleus of the cat, may also be due to the different methods of preparation that were used. The "non-synaptic junctions" of Pappas et al. ('66) clearly correspond to the filamentous contacts. Pappas et al. show the electron dense material of the intermediate region and also show the filaments subjacent to this, lying in dendritic cytoplasm. They do not show the filamentous rings or nests, since they illustrate filamentous contacts upon dendritic stems or branches, not upon appendages.

It has been shown that bundles of neurofilaments occur in neuronal profiles in the lateral geniculate nucleus, and that the shape, size and laminar distribution of these neurofilamentous bundles is what would be expected from a study of the neurofibrillar knots. It is difficult to deter-

mine whether the matching is equally good in terms of numbers. However, if one assumes that there are approximately 30 knots to be seen in a $75 \mu \times 75 \mu$ area of a 10μ thick section (table 1), and if one takes 1.5μ as the average diameter of the knots, then one would expect to find about 4.7 knots per $75 \mu \times 75 \mu$ area on a 600 \AA thick section

$$\frac{30 \times 0.06}{10.0} \times \left[\frac{1.5}{0.06} + 1 \right]$$

This figure only represents a very approximate estimate. It takes no account of the Abercrombie ('46) correction for the light microscopical results, ignores the different degrees of shrinkage that tissues suffer when prepared for light or electron microscopy, and is based on an approximation of the section thickness used for electron microscopy. It is given here because it does indicate the sort of reduction in numbers that can be expected when structures of this size are examined by light and electron microscopical methods, and because it suggests that the number of neurofilamentous rings and nests that was found was approximately equal to the expected number.

The neuronal profiles within which the filamentous bundles were found have been identified as dendritic appendages. This identification is based primarily on two features. The first is that the profiles were never seen to contain groups of relatively uniform vesicles which could be regarded as synaptic vesicles. The second is that the profiles were never seen to make a synaptic contact the asymmetry of which would lead one to regard these profiles as presynaptic to another structure. Insofar as this asymmetry of synaptic contacts (see Gray and Guillery, '66) depends upon synaptic vesicles being present on the presynaptic side, the second feature is no different from the first. However, the asymmetry also depends upon the local membrane thickenings and upon the presynaptic dense projections (Gray, '63), and these were clearly identifiable in many synaptic junctions of the present material.

Two further features also argue in favor of regarding these profiles as dendritic. One is that occasionally it was possible to trace such a profile into a dendritic branch. The second is that the filamentous con-

- Guillery, R. W. 1965 Some electron microscopical observations of degenerative changes in central nervous synapses. *Prog. Brain Research*, 14: Degenerative Patterns in the Nervous System, eds. M. Singer and J. P. Schädé, Elsevier, Amsterdam, 57-76.
- 1966 A study of Golgi preparations from the dorsal lateral geniculate nucleus of the adult cat. *J. Comp. Neur.*, 128: 21-50.
- Guillery, R. W., B. Shirra and K. E. Webster 1961 Differential impregnation of degenerating nerve fibers in paraffin-embedded material. *Stain Techn.*, 36: 9-13.
- Hayhow, W. R. 1958 The cytoarchitecture of the lateral geniculate body of the cat in relation to the crossed and uncrossed optic fibers. *J. Comp. Neur.*, 110: 1-64.
- 1959 Experimental degeneration of optic axons in the lateral geniculate body of the cat. *Acta Anat.*, 37: 281-298.
- Hoff, E. C. 1932a Central nerve terminals in the mammalian spinal cord and their examination by experimental degeneration. *Proc. Roy. Soc., B*, 111: 175-188.
- 1932b The distribution of spinal terminals (boutons) of the pyramidal tract determined by experimental degeneration. *Proc. Roy. Soc., B*, 111: 226-237.
- Karnovsky, M. J. 1965 A formaldehyde-glutaraldehyde fixative of high osmolality for use in electron microscopy. *J. Cell Biol.*, 27: 137A-138A.
- Lund, R. D., and L. E. Westrum 1968 Neurofibrils and Nauta method. *Science*, 151: 1397-1399.
- Mathews, M. R., W. M. Cowan and T. P. S. Powell 1960 Transneuronal cell degeneration in the lateral geniculate nucleus of the macaque monkey. *J. Anat. Lond.*, 96: 82-102.
- Münckler, J. 1942 Pathological alterations in surface relationships and morphology at the human synapse. *Amer. J. Pathol.*, 18: 1061-1104.
- Nauta, W. J. H., and P. A. Gygax 1951 Silver impregnation of degenerating axon terminals in the central nervous system. (1) technic (2) chemical notes. *Stain Techn.*, 26: 5-11.
- O'Leary, J. L., J. M. Smith, M. Tidwell and A. B. Harris 1965 Synapses in the lateral geniculate nucleus of the primate. *Neurology*, 15: 548-555.
- Pappas, G. D., E. B. Cohen and D. P. Purpura 1966 Fine structure of synaptic and non-synaptic neuronal relations in the thalamus of the cat. *The Thalamus*, Eds. D. P. Purpura and M. D. Yahr. Columbia University Press, New York, 47-75.
- Reynolds, E. S. 1963 The use of lead citrate at high pH as an electron-opaque stain in electron microscopy. *J. Cell Biol.*, 17: 208-212.
- Romeis, B. 1948 *Mikroskopische Technik*. 15th Edition. Lebniz, Munich.
- Schimert, J. 1938 Die Endigungsweise des Tractus vestibulospinalis. *Z. Anat. Entwickl.-gesch.*, 108: 761-767.
- Smith, J. M., J. L. O'Leary, A. B. Harris and A. J. Gay 1964 Ultrastructural features of the lateral geniculate nucleus of the cat. *J. Comp. Neur.*, 123: 357-378.
- Szentágothai, J. 1963 The structure of the synapse in the lateral geniculate body. *Acta Anat.*, 55: 166-185.
- 1965 The use of degeneration methods in the investigation of short neuronal connections. *Prog. Brain Research*, 14: Degenerative Patterns in the Nervous System, eds. M. Singer and J. P. Schädé, Elsevier, Amsterdam, 1-32.
- Walberg, F. 1964 The early changes in degenerating boutons and the problem of argyrophilia. Light and electron microscopical observations. *J. Comp. Neur.*, 122: 113-137.
- Westrum, L. E. 1965 A combination staining technique for electron microscopy. (1) Nervous tissue. *J. de Microscopie*, 4: 275-278.
- Windle, W. F. 1930 Normal behavioural reactions of kittens correlated with the postnatal development of nerve fiber density in the spinal grey matter. *J. Comp. Neur.*, 50: 479-496.
- Note added in proof:** Several papers that deal with synaptic structures in the lateral geniculate nucleus have appeared recently. The two that deal with the cat are particularly relevant. See:
- Peters, A., and S. L. Palay 1966 The morphology of laminae A and A1 of the dorsal nucleus of the lateral geniculate body of the cat. *J. Anat. Lond.*, 100: 451-486.
- Szentágothai, J., J. Hátori and T. Tömböl 1966 Degeneration and electron microscope analysis of the synaptic glomeruli in the lateral geniculate body. *Exp. Brain Res.*, 2: 283-301.

clustering is seen on neurofibrillar preparations. Electron micrographs show that the appendages occur within the encapsulated synaptic zones and that several may be grouped together in a single zone. It is probable that the synaptic zones are shown in silver preparations as the slightly dark regions within which the knots are particularly concentrated. Since these dark regions appear to form a more or less continuous reticulum through laminae A and A1, and since there is no evidence to demonstrate that the synaptic zones are isolated from each other, the term "synaptic zone" is preferable to "synaptic island" (Colonnier and Guillery, '64) or "glomerulus" (Szentágothai, '63; Pappas et al., '66).

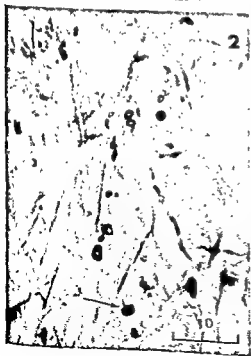
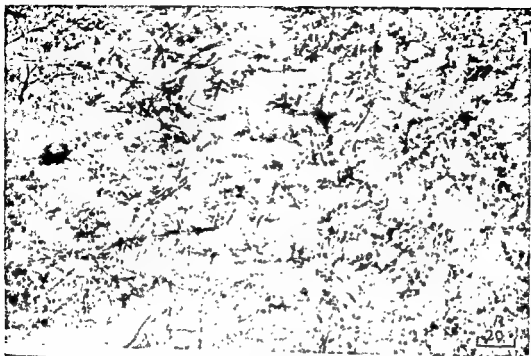
Szentágothai ('63, '65) and Guillery ('66) suggested that the dendritic appendages that were considered above represent a major receptive surface for the incoming retinal afferents. The present material does not give any evidence about the type of contact that these appendages receive in the cat. However, in the monkey Colonnier and Guillery ('64) found that the axons which make filamentous contacts (their LP axons) are retinal afferents, and this would suggest that a similar relationship may be found in the cat.

The possible functional significance of the filamentous contacts was considered by Colonnier and Guillery ('66). The present results again leave this problem unanswered. However, the electron microscopical results do suggest that the filamentous contacts are concerned with processes other than the transmission of nervous impulses. (See also Pappas et al., '66.) Thus, the presence of regular contacts adjacent to filamentous contacts, and the general absence of vesicles close to the axonal membrane of the asymmetrical filamentous contacts suggests that the mechanism of synaptic transmission lies in the regular contacts, not in the filamentous contacts. Further, the occurrence of symmetrical, dendro-dendritic filamentous contacts argues against a role in synaptic transmission. Golgi preparations show that the clusters of dendritic appendages from two separate dendrites often come into intimate relationship with each other and with incoming retinal afferents

(Guillery, '66). The filamentous contacts thus occur between neuronal processes that appear to be forming highly organized and selective interconnections within the synaptic zones. However, the part that the filamentous contacts play in the activity or the development of the zones remains to be determined.

LITERATURE CITED

- Abercrombie, M. 1946 Estimation of nuclear population from microtome sections. *Anat. Rec.*, 94: 239-247.
- Bielschowsky, M. 1904 Die Silberimprägnation der Neurofibrillen. *J. Psychol. Neurol. Leipzig*, 3: 169-189.
- Boycott, B. B., E. G. Gray and R. W. Guillery 1961 Synaptic structure and its alteration with environmental temperature: a study by light and electron microscopy of the central nervous system of lizards. *Proc. Roy. Soc. B.*, 154: 151-172.
- Cajal, S. Ramón Y 1903 Un sencillo método de coloración del retículo protoplásmico. *Trab. Lab. Invest. Biol. Univ. Madrid*, 2: 129-222.
- 1954 *Neuron Theory or Reticular Theory?* Translated by M. U. Purkiss and C. A. Fox. CSIC, Madrid.
- Colonnier, M., and R. W. Guillery 1964 Synaptic organization in the lateral geniculate nucleus of the monkey. *Z. Zellforsch.*, 62: 333-355.
- Cook, W. H., J. H. Walker and M. L. Barr 1951 A cytological study of transneuronal atrophy in the cat and the rabbit. *J. Comp. Neur.*, 94: 267-292.
- Davenport, H. A. 1933 Block staining of nervous tissue with silver. III. Pericellular end bulbs or boutons. *Stain Techn.*, 8: 143-147.
- Glees, P. 1941 The termination of optic fibres in the lateral geniculate body of the cat. *J. Anat. Lond.*, 75: 435-440.
- 1946 Terminal degeneration within the central nervous system as studied by a new silver method. *J. Neuropath. Exp. Neurol.*, 5: 54-59.
- 1961 Terminal degeneration and trans-synaptic atrophy in the lateral geniculate body of the monkey. In: *The Visual System: Neurophysiology and Psychophysics*. Eds., R. Jung and H. Kornhuber. Springer, Berlin.
- Glees, P., and W. E. LeGros Clark 1941 The termination of optic fibers in the lateral geniculate body of the monkey. *J. Anat. Lond.*, 75: 295-308.
- Gray, E. G. 1963 Electron microscopy of pre-synaptic organelles. *J. Anat. Lond.*, 97: 101-106.
- Gray, E. G., and R. W. Guillery 1961 The basis of silver staining of synapses in the mammalian spinal cord: a light and electron microscope study. *J. Physiol. Lond.*, 157: 581-588.
- 1966 Synaptic morphology in the normal and degenerating nervous system. *Int. Rev. Cytol.*, 19: 111-182.



All magnifications are indicated in microns.

PLATE 1

EXPLANATION OF FIGURES

- 1 Low power micrograph of laminae A, A1 and central interlaminar nucleus to show the distribution of the neurofibrillar knots. The central interlaminar nucleus runs vertically through the central part of this figure and is relatively free of knots. The A and A1 laminae lie on either side of this and show the small dark knots which lie in zones of somewhat darkened tissue. Block Cajal, method 5.
- 2 High power micrograph of the neurofibrillar knots from lamina A. Relatively few of the surrounding cells and fibers are stained. The unlabeled arrow indicates a knot that appears to have a fibrous "tail." Careful examination of this section showed that the fiber passed by the knot and did not join it. Block Cajal, method 5.
- 3 Neurofibrillar knots from lamina A. Note that the knots occur predominantly in zones of slightly darkened tissue. Three small zones are seen in the upper left part of the figure and two larger, vertically elongated zones occur in the lower central and lower left parts of the figure. Block Cajal, method 5.

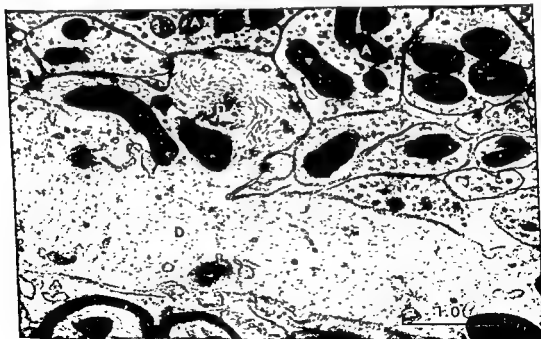


PLATE 2

EXPLANATION OF FIGURES

- 4 Neurofibrillar knots from lamina A1. Paraffin Nauta method. This method shows a more even impregnation of the surrounding fiber plexus than do the block Cajal methods. The unlabeled arrow shows a knot with an apparent tail (see legend for fig. 2).
- 5 A dendrite (D) runs horizontally across the lower part of the figure. To the left of the central part of the figure a dendritic appendage (DA) is shown. It contains a nest of filaments, some scattered vesicles and a central zone of granular material similar to the material of the "intermediate region" (see fig. 8, I). A, axonal synaptic knobs. Note: Figures 5-13 are taken from material fixed in osmium tetroxide and stained with phosphotungstic acid (see Materials and Methods).

LATERAL GENICULATE NUCLEUS OF CAT
R. W. Guillery

PLATE 3

EXPLANATION OF FIGURES

- 6 A large axonal synaptic knob runs vertically through the figure. It makes regular synaptic contacts with other synaptic knobs (A) in the upper left and lower right parts of the figure, and with dendrites in the central left and upper right parts. The axon contains bundles of neurofilaments (N), and some filaments (N) can also be seen in the dendritic profiles. ?F indicates a possible filamentous contact.
- 7 Section of an encapsulated synaptic zone. In the central part of this figure is a neuronal profile (dendritic appendage) that contains a group of mitochondria and a nest of neurofilaments. Two axonal synaptic knobs are labeled (A). The upper makes a regular contact with the dendritic appendage, and the lower makes a filamentous contact. G, glial lamellae.
- 8 Two regular contacts (R1 and R2) and one asymmetrical filamentous contact (F) are shown. R1 is interpreted as axo-axonal, R2 and F as axo-dendritic. Unlabeled arrows indicate regions where electron dense material is closely applied to the membranes and where some extracellular material also occurs between the membranes. I, Intermediate region of the filamentous contact.
- 9 A part of an encapsulated synaptic zone. Three dendritic profiles (D) that contain neurofilaments are shown. The middle one shows two groups of filaments sectioned transversely. The two upper ones are postsynaptic at the regular contacts marked (R). Symmetrical filamentous contacts occur where these dendritic profiles contact each other. In addition, an asymmetrical filamentous contact is present on the upper dendritic profile, adjacent to the regular contact. S, short process which may represent a stalk of a dendritic appendage (see text). See also figure 10.



PLATE 4

EXPLANATION OF FIGURES

- 10 Higher magnification of a part of figure 9. A, Axonal synaptic knob; AF, asymmetrical filamentous contact; D, dendritic profile; F, symmetrical filamentous contact; R, regular contacts. Note that the filaments lie subjacent to the filamentous contacts and not to the regular contacts.
- 11 The figure shows three asymmetrical filamentous contacts (F) upon a dendritic appendage (D). Unlabeled arrows are used as in figure 9. ?R, oblique section through a regular axo-axonal contact.
- 12-13 Two sections (numbers 2 and 4 from a short series) which show a dendritic appendage (DA) that is connected by a short narrow stalk to a dendritic branch (D). Note the bundle of filaments in the dendritic appendage and the asymmetrical filamentous contact in the lower parts of the figures.

LATERAL GENICULATE NUCLEUS OF CAT
R. W. Guillery



PLATE 5

EXPLANATION OF FIGURES

Figures 14 and 15 show material fixed in the same way as the material shown in figures 5-13, but stained with lead citrate instead of phosphotungstic acid.

- 14 A large axonal synaptic bag runs obliquely across the figure. In the central part of the figure two adjacent dendritic profiles are shown which both contain lightly stained filaments. There appears to be an obliquely cut symmetrical filamentous contact between these profiles. A third dendritic profile with filaments is seen in the lower left part of the figure. The regions labeled (F) are interpreted as asymmetrical filamentous contacts. G, glial lamella. R, regular contacts.
- 15 The dendrite (D) receives two regular contacts (R) and a filamentous contact (F). The upper right part of this dendrite may represent a small dendritic appendage (?DA). ?F represents a probable symmetrical filamentous contact. Another is probably also formed on the right side of the dendritic appendage labeled (?DA). Note the undulating membranes at the filamentous contact (F) and note that the filaments and the intermediate regions of the filamentous contacts are only poorly shown on the material stained with lead citrate.

Septal Projections to Nuclei Functioning in Oxytocin Release¹

ERVIN W. POWELL AND DUANE K. RORIE

Department of Anatomy, University of Arkansas, School of Medicine, Little Rock, Arkansas and Department of Anatomy, University of Mississippi, School of Medicine, Jackson, Mississippi

ABSTRACT Terminal degeneration was observed in the paraventricular and supraoptic nuclei of the hypothalamus following lesions in the septum of the squirrel monkey. The degeneration was usually greater in the supraoptic nucleus. A lesion in the posterior dorsal septum resulted in more degeneration in the paraventricular nucleus. Lesions in the dorsal gyrus rectus, genu of the corpus callosum and extreme rostral septum resulted in no identifiable degeneration in the two nuclei. These nuclei have been shown by various investigators to facilitate milk ejection (oxytocin release). Stimulation of the mesencephalic central gray has been shown to influence oxytocin release. Following a lesion in the mid-septal area, degenerating terminals were seen in the mesencephalic central gray. Our results show that the septum is directly connected with the supraoptic and paraventricular nuclei and mesencephalic tectum. Possibly the septum functions in modulating mechanisms having to do not only with lower autonomic responses such as blood pressure, and bladder emptying, but oxytocin release as well.

Stimulation of the mammary gland by suckling or manual manipulation produces impulses which effect oxytocin release. The supraoptic and paraventricular hypothalamic nuclei have been shown to affect oxytocin release (Olivecrona, '57; Nibbelink, '61). As impulses from the mammary gland ascend the neural path, they are analysed and modulated at several levels before reaching the paraventricular and supraoptic nuclei. The brain stem reticular formation plays a role of analysis and integration of the first order (Nauta, '63). It receives a massive influx of fibers from the lemniscal systems conveying general exteroceptive, proprioceptive, and viscerosensitive sensory modalities. Consequently, signals from the midbrain reticular formation could be transmitted to the supraoptic and paraventricular nuclei by way of rostral projections, such as, mamillary peduncle (Cowan, Guillery and Powell, '64), rostral mesencephalic gray matter, and particularly the dorsal longitudinal fasciculus (Morest, '61; Nauta and Kuypers, '58). Stimulation of numerous cerebral areas results in the release of oxytocin (Denamur, '65). Furthermore, a great variety of sensory and emotional stimuli are known to affect its release (Newton, '61; Cross, '61b). There-

fore, other areas are also involved in systems of analysis and integration of oxytocin mechanisms. Stimulation of the mammary gland evokes distinct activation patterns in the hypothalamus, septum, hippocampus, thalamus and cortex (Holland and Cross, '61). This stimulation facilitates the rate of firing of some neurons in the preoptic area and midline thalamic nuclei (Cross and Green, '59). Electrical stimulation of the medial and lateral preoptic areas, septum, dorsal hippocampus, fimbria of fornix and cingulate gyrus results in liberation of oxytocin (Beyer, Anguiano and Mena, '61; Cross, '61a, b; Cross and Silver, '61; Schimizu and Kurotsu, '56). Hence, there is evidence that the limbic system may play a prominent role in oxytocin release. Terminal degeneration was observed in the supraoptic and paraventricular nuclei following lesions in the preoptic region in cats (Nauta, '58). He concluded that these nuclei appear to receive some direct connections from cell groups intercalated in the limbic system-midbrain circuit. The present study pre-

¹This study was supported by USPHS grant NB-06951 from the National Institute of Neurological Diseases and Blindness. Part of this work was done in the Department of Anatomy, University of Mississippi and supported by funds from USPHS grant NB-03585.

one liter of 10% formalin in normal saline. The head, with six square centimeters of calvaria removed, was separated from the body and stored in 10% formalin in the refrigerator. The following day the brain was removed from the skull, placed in fresh 10% formalin, and returned to cold storage. Three weeks later serial frozen sections were made and stained (Nauta and Gyax, '54) to demonstrate degenerating axons and their preterminals (term-

inals). Other sections selected from the series were stained with cresyl violet to assist in the identification of cerebral nuclei.

RESULTS

Following lesions in the septum of the squirrel monkey, degenerating terminals were observed in the paraventricular and supraoptic nuclei of the hypothalamus. A lesion involving the caudate nucleus and

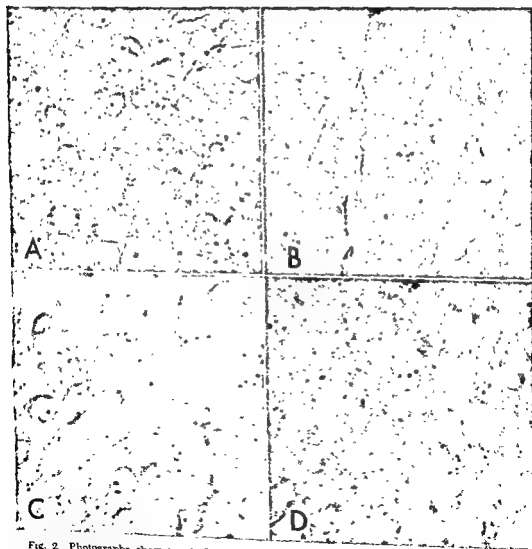


Fig. 2. Photographs show terminal degeneration. A, Supraoptic nucleus following lesion in caudate and lateral septum; B, Paraventricularis nucleus following lesion in caudate and lateral septum. C, Supraoptic nucleus following lesion in posterior dorsal septum; D, Paraventricularis nucleus following lesion in posterior dorsal septum.

sents evidence that the septum is also directly connected with the supraoptic and paraventricular nuclei.

METHODS

The data for this study were obtained from four cases selected from an analysis of ten squirrel monkeys weighing 400 gm or more. The animals were anesthetized with an intraperitoneal injection of 0.2 ml (5 mg/ml) of phencyclidine (Sernylan[®]) per kg of body weight. Xylocaine (0.5%) was used locally where needed. Each monkey was oriented in a Labtronics stereotaxic instrument for the accurate positioning of a monopolar stainless steel electrode. It was 350 μ in diameter and insulated with Epoxylite except at its tip. The electrode

was placed in the septum by inserting it through a small trephine opening made in the skull by means of a dental drill fitted with a small burr. Stereotaxic coordinates ranged between A-11 and A-13, from L $\frac{1}{4}$ to L $\frac{1}{2}$, and H + 7 to H + 5. After the electrode was positioned, the cathode lead of a direct current source was attached to the scalp and the anode lead was attached to the upper free end of the electrode. Small lesions were obtained by passing one milliampere of current through the septal focus for ten seconds. Twenty days post-operatively the animals were anesthetized (Nembutal[®] 0.5 ml of a 50 mg% solution) and perfused with one liter of normal saline containing 0.5 gm of sodium nitrite. The perfusion was continued using

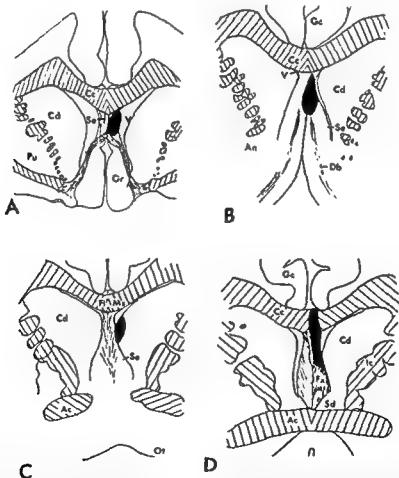


Fig. 1 The blackened areas illustrate the lesion placement in the squirrel monkey septum. A, Rostral septum; B, Mid-septum; C, Caudate and lateral septum; D, Posterior dorsal septum. Abbreviations: Ac, anterior commissure; An, nucleus accumbens; Cc, corpus callosum; Cd, caudate nucleus; Db, diagonal band; Fl, fornix longus; Fx, fornix; Gc, gyrus cinguli; Gr, gyrus rectus; Ic, internal capsule; Ms, medial longitudinal stria; Ot, olfactory tubercle; Pu, putamen; Sd, bed nucleus of the stria terminalis; Se, septum; V, lateral ventricle.

anum and nucleus reuniens in all cases (fig. 3). Of the structures considered in this paper, terminal degeneration was heaviest in the nucleus centromedianum. However, the heavy degeneration to principal target structures such as the mammillary body, hippocampus and anterior thalamic nuclei are not considered in this study.

In three other animals, lesions were placed more rostrally in the most rostral apex of the septum (fig. 1A), in the dorsal gyrus rectus, and in the genu of the corpus callosum. Degenerating terminals were not seen in either the paraventricular or supraoptic nuclei in any one of these.

DISCUSSION

The results show that the septum projects directly to the supraoptic and paraventricular nuclei. Furthermore, direct connections were also shown to exist with the mesencephalic central gray, midline thalamic nuclei, and centromedian intralaminar nucleus. These structures have been shown to influence oxytocin release, except for the centromedian intralaminar nucleus (Cross and Silver, '61; Shimizu and Kurotsu, '56).

The septum is directly connected to the isocortex. The principal connections are made with the gyrus cinguli, orbital frontal cortex, suprasylvian and ectosylvian gyri, (McLardy, '55; Powell, '64; Powell, '66; Pribram, Lennox and Dunsmore, '50). The first two cortical areas have been shown to influence oxytocin release (Beyer, Anguiano and Mena, '61; Cross, '61b). Thus, the septum, a limbic structure having to do with neuroendocrine mechanisms, is structurally connected with the overlying cerebral cortex and lower autonomic nuclei.

Perhaps much of the function ascribed to the septum manifests itself through modulatory mechanisms pertaining to oxytocin release and serves as an 'on-off relay' to the paraventricular and supraoptic nuclei. Stimulation of the septum facilitates oxytocin release (Cross and Silver, '61). Our results show that the fiber projection from the midseptal area is chiefly to the supraoptic nucleus and mainly to the paraventricular nucleus following a lesion placed in the posterior part of the septum. Since this anatomical differential exists in the septum, it would seem that some areas

of this structure might inhibit milk ejection, although no references were encountered which report such a result. Many of the fibers in the dorsal part of the posterior septum are fornix fibers, and as such involve interconnections of the hippocampus. From our results these could be fibers of the hippocampus projecting to the paraventricular nucleus which in turn influences oxytocin release. However, no reference was found where stimulation of the hippocampus inhibited milk ejection. The absence of evidence pertaining to an inhibitory role may indicate that such functions occur at a different cerebral level or pertain to special diffuse inhibitory mechanisms.

LITERATURE CITED

- Beyer, F. C., L. G. Anguiano and J. F. Mena 1961 Oxytocin release in response to stimulation of cingulate gyrus. *Am. J. Physiol.*, 200: 625-627.
- Cowan, W. M., R. W. Gullery and T. P. S. Powell 1964 The origin of the mammillary peduncle and other hypothalamic connections from the midbrain. *J. Anat.*, (London) 98: 345-363.
- Cross, B. A. 1961a Neural control of oxytocin secretion. In: *Oxytocin*, R. Caldeyro-Barcia and H. Heller, eds., Pergamon Press, New York, pp. 24-47.
- 1961b Neural control of lactation. In: *Milk: the mammary gland and its secretions*, Vol. 1. S. K. Kon and A. T. Cowie, eds., Academic Press, New York, pp. 229-277.
- Cross, B. A., and J. D. Green 1959 Activity of single neurons in the hypothalamus: Effect of osmotic and other stimuli. *J. Physiol.*, (London), 148: 554-569.
- Cross, B. A., and I. A. Silver 1961 Neural control oxytocin secretion. (Unpublished experiments.) Cited by B. A. Cross. In: *Oxytocin*, R. Caldeyro-Barcia and H. Heller, eds., Pergamon Press, New York, pp. 24-47.
- Denamur, R. 1965 The hypothalmo-neurohypophyseal system and the milk-ejection reflex. *Dairy Science Abstr.*, 27: 193-224.
- Holland, R. C., and B. A. Cross 1961 Neural control of oxytocin secretion. (Unpublished experiments.) Cited by B. A. Cross. In: *Oxytocin*, R. Caldeyro-Barcia and H. Heller, eds., Pergamon Press, New York, pp. 24-47.
- McLardy, T. 1955 Observations on the fornix of the monkey. II. Fiber studies. *J. Comp. Neur.*, 103: 327-343.
- Morest, D. K. 1961 Connections of the dorsal tegmental nucleus in rat and rabbit. *J. Anat.*, (London) 95: 229-246.
- Nauta, W. J. H. 1958 Hippocampal projections and related neural pathways to the midbrain in the cat. *Brain*, 81: 319-340.
- 1963 Central nervous organization and endocrine motor system. In: *Advances in Neuroendocrinology*, A. V. Nalbandov, ed., University of Illinois Press, Urbana, pp. 5-21.

lateral septum (fig. 1C) resulted in more extensive terminal degeneration in the supraoptic nucleus than in the paraventricular nucleus (fig. 2A,B). Degeneration was slightly more dense in the supraoptic nucleus in all cases except one. In this case, the lesion was located in the posterior dorsal septum (fig. 1D) and resulted in terminal degeneration slightly more heavy in the paraventricular nucleus than in the supraoptic nucleus (fig. 2D,C). Most marked terminal degeneration observed in either

nucleus followed a midseptal lesion involving the medial septal nucleus and diagonal band (fig. 1B). Degenerating terminals were more dense in the supraoptic nucleus than in the paraventricular nucleus. Furthermore, they were distributed more heavily to the lateral part of the supraoptic nucleus.

The midbrain central gray also contained diffuse terminal degeneration in its dorsal and ventral part. Degenerating terminals were observed in the nucleus centromedi-

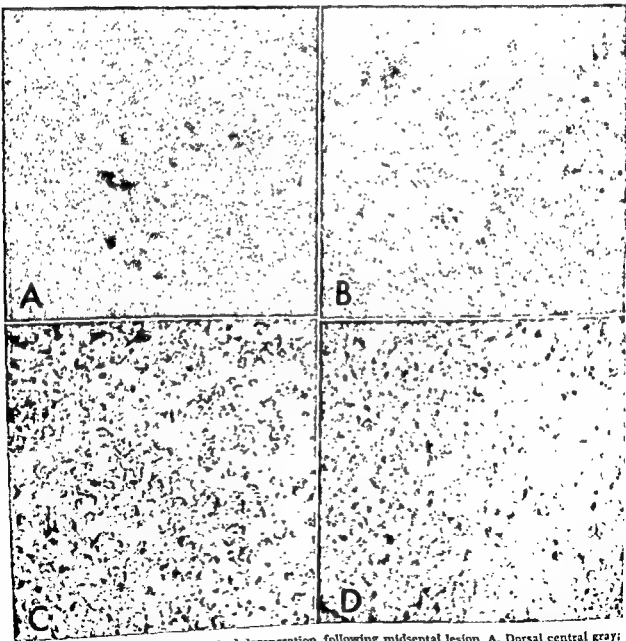


Fig. 3 Photographs show terminal degeneration following midseptal lesion. A, Dorsal central gray; B, Ventral central gray; C, Nucleus centromedianum; D, Nucleus reuniens.

anum and nucleus reuniens in all cases (fig. 3). Of the structures considered in this paper, terminal degeneration was heaviest in the nucleus centromedianum. However, the heavy degeneration to principal target structures such as the mammillary body, hippocampus and anterior thalamic nuclei are not considered in this study.

In three other animals, lesions were placed more rostrally in the most rostral apex of the septum (fig. 1A), in the dorsal gyrus rectus, and in the genu of the corpus callosum. Degenerating terminals were not seen in either the paraventricular or supraoptic nuclei in any one of these.

DISCUSSION

The results show that the septum projects directly to the supraoptic and paraventricular nuclei. Furthermore, direct connections were also shown to exist with the mesencephalic central gray, midline thalamic nuclei, and centromedian intralaminar nucleus. These structures have been shown to influence oxytocin release, except for the centromedian intralaminar nucleus (Cross and Silver, '61; Shimizu and Kurotsu, '56).

The septum is directly connected to the isocortex. The principal connections are made with the gyrus cinguli, orbital frontal cortex, suprasylvian and ectosylvian gyri, (McLardy, '55; Powell, '64; Powell, '66; Pribram, Lennox and Dunsmore, '50). The first two cortical areas have been shown to influence oxytocin release (Beyer, Anguiano and Mena, '61; Cross, '61b). Thus, the septum, a limbic structure having to do with neuroendocrine mechanisms, is structurally connected with the overlying cerebral cortex and lower autonomic nuclei.

Perhaps much of the function ascribed to the septum manifests itself through modulatory mechanisms pertaining to oxytocin release and serves as an 'on-off relay' to the paraventricular and supraoptic nuclei. Stimulation of the septum facilitates oxytocin release (Cross and Silver, '61). Our results show that the fiber projection from the midseptal area is chiefly to the supraoptic nucleus and mainly to the paraventricular nucleus following a lesion placed in the posterior part of the septum. Since this anatomical differential exists in the septum, it would seem that some areas

of this structure might inhibit milk ejection, although no references were encountered which report such a result. Many of the fibers in the dorsal part of the posterior septum are fornix fibers, and as such involve interconnections of the hippocampus. From our results these could be fibers of the hippocampus projecting to the paraventricular nucleus which in turn influences oxytocin release. However, no reference was found where stimulation of the hippocampus inhibited milk ejection. The absence of evidence pertaining to an inhibitory role may indicate that such functions occur at a different cerebral level or pertain to special diffuse inhibitory mechanisms.

LITERATURE CITED

- Beyer, F. C., L. G. Anguiano and J. F. Mena 1961 Oxytocin release in response to stimulation of cingulate gyrus. *Am. J. Physiol.*, 200: 625-627.
- Cowan, W. M., R. W. Gullery and T. P. S. Powell 1964 The origin of the mammillary peduncle and other hypothalamic connexions from the midbrain. *J. Anat.*, (London) 98: 345-363.
- Cross, B. A. 1961a Neural control of oxytocin secretion. In: *Oxytocin*, R. Caldeyro-Barcia and H. Heller, eds., Pergamon Press, New York, pp. 24-47.
- 1961b Neural control of lactation. In: *Milk: the mammary gland and its secretions*, Vol. I. S. K. Kon and A. T. Cowie, eds., Academic Press, New York, pp. 229-277.
- Cross, B. A., and J. D. Green 1959 Activity of single neurons in the hypothalamus: Effect of osmotic and other stimuli. *J. Physiol.*, (London), 148: 554-569.
- Cross, B. A., and I. A. Silver 1961 Neural control oxytocin secretion. (Unpublished experiments.) Cited by B. A. Cross. In: *Oxytocin*, R. Caldeyro-Barcia and H. Heller, eds., Pergamon Press, New York, pp. 24-47.
- Denamur, R. 1965 The hypothalmo-neurohypophyseal system and the milk-ejection reflex. *Dairy Science Abstr.*, 27: 193-224.
- Holland, R. C., and B. A. Cross 1961 Neural control of oxytocin secretion. (Unpublished experiments.) Cited by B. A. Cross. In: *Oxytocin*, R. Caldeyro-Barcia and H. Heller, eds., Pergamon Press, New York, pp. 24-47.
- McLardy, T. 1955 Observations on the fornix of the monkey. II. Fiber studies. *J. Comp. Neur.*, 103: 327-343.
- Morest, D. K. 1961 Connexions of the dorsal tegmental nucleus in rat and rabbit. *J. Anat.*, (London) 95: 229-246.
- Nauta, W. J. H. 1958 Hippocampal projections and related neural pathways to the midbrain in the cat. *Brain*, 81: 319-340.
- 1963 Central nervous organization and endocrine motor system. In: *Advances in Neuroendocrinology*, A. V. Nalbandov, ed., University of Illinois Press, Urbana, pp. 5-21.

- Nauta, W. J. H., and P. A. Gyax 1954 Silver impregnation of degenerating axons in the central nervous system. A modified technique. *Stain Technol.*, 92: 91-93.
- Nauta, W. J. H., and H. G. J. M. Kuypers 1958 Some ascending pathways in the brain stem reticular formation. In: *Reticular Formation of the Brain*. H. H. Jasper, L. D. Proctor, R. S. Knighton, W. C. Noshay, R. T. Costello, eds., Little, Brown and Co., Boston, pp. 3-30.
- Newton, M. 1961 Human Lactation. In: *Milk: the mammary gland and its secretion*. Vol. 1. S. K. Kon and A. T. Cowie, eds., Academic Press, New York, pp. 281-320.
- Nibbelink, D. W. 1961 Paraventricular nuclei, neurohypophysis, and parturition. *Am. J. Physiol.*, 200: 1229-1232.
- Olivecrona, H. 1957 Paraventricular nucleus and pituitary gland. *Acta physiol. scand.*, 40 (suppl. 136) 1-178.
- Powell, E. W. 1964 Corticolimbic interrelations revealed by the evoked potential and degeneration technique. *Exptl. Neurol.*, 10: 463-474.
- 1966 Septal efferents in the cat. *Exptl. Neurol.*, 14: 328-337.
- Pribram, K. H., M. A. Lennox and R. H. Dunsmore 1950 Some connections of the orbitofronto temporal, limbic and hippocampal areas of the *Maccaca mulatta*. *J. Neurophysiol.*, 13: 127-135.
- Schimizu, S., T. Ban and K. Kurotsu 1956 Studies on the milk-ejection induced by the electrical stimulation of the hypothalamus of rabbits. *Med. J. Osaka University*, 7: 79-99.

The Effect of Pregnancy on the Elastic Membranes of Mesometrial Arteries in the Guinea Pig¹

ERNEST N. ALBERT²

Department of Anatomy, Schools of Medicine and Dentistry,
Georgetown University, Washington, D. C.

ABSTRACT Mesometrial arteries were obtained at various stages from adult virgin and primiparous guinea pigs beginning at pregnancy and ending at 40 days post-partum. The tissues were processed routinely and then stained with hematoxylin and eosin, and various elastic tissue stains. Picro-indigo-carmin and Van Gieson were used as counterstains.

It was found that during the early stages of pregnancy the subendothelial cells of mesometrial arteries began to proliferate and the internal elastic membrane showed signs of fragmentation. By term the subendothelial cells formed a several layer thick cushion and the elastic fibers were virtually absent. About 22 days post-partum the subendothelial cells had disappeared and a new internal elastic membrane had formed. These changes are found mainly in the placental mesometrial arteries and to a lesser degree in the peripheral ones. Guinea pigs with unilateral pregnancies exhibited the above changes only on the side of the pregnant horn. It is suggested that the above changes are due to pregnancy and that local hormones elaborated by the placenta may be largely responsible for the alterations in the mesometrial arteries during pregnancy.

The uterus and its blood vessels have been studied by several investigators. The majority of emphasis has been on the morphological and histochemical modifications in the connective tissue and muscle components of the uterus during various stages of the menstrual cycle and pregnancy. In comparison less effort has been devoted to the histological alterations in the uterine blood vessels.

Gardner and Goodall ('06) described some of the changes in post-partum vessels and distinguished these from the atherosclerotic lesions. Goodall ('09), in his work on the involution of the vascular system in parturient uteri described that the uterus renews all its arteries after each pregnancy and that the changes in the walls of the blood vessels of the uterus are closely allied to those around the atrophic corpus luteum. Goodall ('09), and Shaw ('14), and more recently Maher ('59) have described the changes in the elastic components of post-partum uterine vessels. Based upon their observations they suggested that the distribution of elastic tissue could aid in differentiating between the nulliparous and multiparous uteri and that there is an increased amount of elastic tissue around the vessels of parous uteri. Maher ('59) also observed that the elastic tissue of blood ves-

sels loses its normal staining properties for 25-30 days after parturition and that the normal staining reaction is restored 30 days post-partum.

All of the above mentioned investigators studied post-partum uteri. To the best of our knowledge no study has been conducted on the behavior of the elastic tissue of uterine arteries during pregnancy. In the present investigation an attempt has been made to study the changes that take place in the elastic components of the uterine arteries during pregnancy and to speculate on their functional significance. A correlation between these changes and previous findings in the post-partum uterine vessels has been made. We were particularly interested in elucidating mechanisms which might have been responsible for the loss of staining reactions of elastin in post-partum uteri. The present report deals only with primiparous guinea pigs during pregnancy and post-partum. A second report will appear later which will describe further changes that occur in the elastic patterns of uterine arteries with each successive pregnancy.

¹ This study was supported in part by U.S. Public Health Service Grant HD-01394-02 from the National Institute of Child Health and Human Development, National Institutes of Health, Bethesda, Maryland.

² Department of Anatomy, School of Medicine, University of California, Los Angeles, California 90024.

- Nauta, W. J. H., and P. A. Gyax 1954 Silver impregnation of degenerating axons in the central nervous system. A modified technique. *Stain Technol.*, 92: 91-93.
- Nauta, W. J. H., and H. G. J. M. Kuypers 1958 Some ascending pathways in the brain stem reticular formation. In: *Reticular Formation of the Brain*. H. H. Jasper, L. D. Proctor, R. S. Knighton, W. C. Noshay, R. T. Costello, eds., Little, Brown and Co., Boston, pp. 3-30.
- Newton, M. 1961 Human Lactation. In: *Milk: the mammary gland and its secretion*. Vol. 1. S. K. Kon and A. T. Cowie, eds., Academic Press, New York, pp. 281-320.
- Nibbelink, D. W. 1961 Paraventricular nuclei, neurohypophysis, and parturition. *Am. J. Physiol.*, 200: 1229-1232.
- Olivecrona, H. 1957 Paraventricular nucleus and pituitary gland. *Acta physiol. scand.*, 40 (suppl. 136) 1-178.
- Powell, E. W. 1964 Corticolimbic interrelations revealed by the evoked potential and degeneration technique. *Exptl. Neurol.*, 10: 463-474.
- 1966 Septal efferents in the cat. *Exptl. Neurol.*, 14: 328-337.
- Pribram, K. H., M. A. Lennox and R. H. Dunsmore 1950 Some connections of the orbitofronto temporal, limbic and hippocampal areas of the *Macaca mulatta*. *J. Neurophysiol.*, 13: 127-135.
- Schimizu, S., T. Ban and K. Kurotsu 1956 Studies on the milk-ejection induced by the electrical stimulation of the hypothalamus of rabbits. *Med. J. Osaka University*, 7: 79-99.

The Effect of Pregnancy on the Elastic Membranes of Mesometrial Arteries in the Guinea Pig¹

ERNEST N. ALBERT²

Department of Anatomy, Schools of Medicine and Dentistry,
Georgetown University, Washington, D. C.

ABSTRACT Mesometrial arteries were obtained at various stages from adult virgin and primiparous guinea pigs beginning at pregnancy and ending at 40 days post-partum. The tissues were processed routinely and then stained with hematoxylin and eosin, and various elastic tissue stains. Picro-indigo-carmin and Van Gieson were used as counterstains.

It was found that during the early stages of pregnancy the subendothelial cells of mesometrial arteries began to proliferate and the internal elastic membrane showed signs of fragmentation. By term the subendothelial cells formed a several layer thick cushion and the elastic fibers were virtually absent. About 22 days post-partum the subendothelial cells had disappeared and a new internal elastic membrane had formed. These changes are found mainly in the placental mesometrial arteries and to a lesser degree in the peripheral ones. Guinea pigs with unilateral pregnancies exhibited the above changes only on the side of the pregnant horn. It is suggested that the above changes are due to pregnancy and that local hormones elaborated by the placenta may be largely responsible for the alterations in the mesometrial arteries during pregnancy.

The uterus and its blood vessels have been studied by several investigators. The majority of emphasis has been on the morphological and histochemical modifications in the connective tissue and muscle components of the uterus during various stages of the menstrual cycle and pregnancy. In comparison less effort has been devoted to the histological alterations in the uterine blood vessels.

Gardner and Goodall ('06) described some of the changes in post-partum vessels and distinguished these from the atherosclerotic lesions. Goodall ('09), in his work on the involution of the vascular system in parturient uteri described that the uterus renews all its arteries after each pregnancy and that the changes in the walls of the blood vessels of the uterus are closely allied to those around the atrophic corpus luteum. Goodall ('09), and Shaw ('14), and more recently Maher ('59) have described the changes in the elastic components of post-partum uterine vessels. Based upon their observations they suggested that the distribution of elastic tissue could aid in differentiating between the nulliparous and multiparous uteri and that there is an increased amount of elastic tissue around the vessels of parous uteri. Maher ('59) also observed that the elastic tissue of blood ves-

sels loses its normal staining properties for 25-30 days after parturition and that the normal staining reaction is restored 30 days post-partum.

All of the above mentioned investigators studied post-partum uteri. To the best of our knowledge no study has been conducted on the behavior of the elastic tissue of uterine arteries during pregnancy. In the present investigation an attempt has been made to study the changes that take place in the elastic components of the uterine arteries during pregnancy and to speculate on their functional significance. A correlation between these changes and previous findings in the post-partum uterine vessels has been made. We were particularly interested in elucidating mechanisms which might have been responsible for the loss of staining reactions of elastin in post-partum uteri. The present report deals only with primiparous guinea pigs during pregnancy and post-partum. A second report will appear later which will describe further changes that occur in the elastic patterns of uterine arteries with each successive pregnancy.

¹ This study was supported in part by U.S. Public Health Service Grant HD-01394-02 from the National Institute of Child Health and Human Development, National Institutes of Health, Bethesda, Maryland.

² Department of Anatomy, School of Medicine, University of California, Los Angeles, California 90024.

- Nauta, W. J. H., and P. A. Gyax 1954 Silver impregnation of degenerating axons in the central nervous system. A modified technique. *Stain Technol.*, 92: 91-93.
- Nauta, W. J. H., and H. G. J. M. Kuypers 1958 Some ascending pathways in the brain stem reticular formation. In: *Reticular Formation of the Brain*. H. H. Jasper, L. D. Proctor, R. S. Knighton, W. C. Noshay, R. T. Costello, eds., Little, Brown and Co., Boston, pp. 3-30.
- Newton, M. 1961 Human Lactation. In: *Milk: the mammary gland and its secretion*. Vol. 1. S. K. Kon and A. T. Cowie, eds., Academic Press, New York, pp. 281-320.
- Nibbelink, D. W. 1961 Paraventricular nuclei, neurohypophysis, and parturition. *Am. J. Physiol.*, 200: 1229-1232.
- Olivecrona, H. 1957 Paraventricular nucleus and pituitary gland. *Acta physiol. scand.*, 40 (suppl. 136) 1-178.
- Powell, E. W. 1964 Corticolimbic interrelations revealed by the evoked potential and degeneration technique. *Exptl. Neurol.*, 10: 463-474.
- 1966 Septal efferents in the cat. *Exptl. Neurol.*, 14: 328-337.
- Pribram, K. H., M. A. Lennox and R. H. Dunsmore 1950 Some connections of the orbitofronto temporal, limbic and hippocampal areas of the *Maccaca mulatta*. *J. Neurophysiol.*, 13: 127-135.
- Schimizu, S., T. Ban and K. Kurotsu 1936 Studies on the milk-ejection induced by the electrical stimulation of the hypothalamus of rabbits. *Med. J. Osaka University*, 7: 79-99.

occupied by subendothelial cells. The nature and origin of cells between these split lamellae is not yet clear. In some cases the internal elastic membrane showed fragmentation into small pieces rather than splitting into lamellae as described above.

The second stage of gestation. During this stage the subendothelial cells had further proliferated and formed several layer thick cushions which were seen protruded into the lumen of the artery (fig. 5). The endothelial cells seemed to follow the outlines of the cushions formed by proliferated subendothelial cells. However, the endothelial lining did not appear continuous. The elastic lamellae were more fragmented and appeared as small fine strands of fibers scattered throughout the thickness of the arterial cushion. Some of these fibers could also be seen in the media. The external elastic lamina disappears by the sixth week of pregnancy. The number of elastic fibers decreased gradually in the intimal cushions until almost all of them disappeared. At times a few strands remained in the last ten days of gestation (figs. 6-7). The arterial walls showed little orcein, Verhoeff's or Gomori's positive material. The cytoplasm of the inner layer of some intimal cells at this time appeared brownish in orcein stained sections. These intimal cells were large with rounded or oval nuclei possessing cytoplasmic processes and giving the appearance of phagocytic cells. Many of the intimal cells were multinucleated (figs. 8, 9). Small fragments of orcein positive material could be seen within the cytoplasm of these cells (figs. 10-11). These intracytoplasmic fragments have been interpreted as phagocytized pieces of elastic fibers. It is possible that the brown coloration of the cytoplasm is due to the dye released from the phagocytized elastin particles. Thus, by term, the walls of the mesometrial arteries were virtually devoid of any elastic components.

During the second stage the media did not appear well demarcated from the intima and the adventitia. Many cells of the media were also hypertrophied and multinucleated. With Van Gieson and Picro-indigo-carmin these cells stained like muscle cells. The nuclei were large, round or oval and hyperchromatic. Similar cells were also found in the adventitia

which by this time had increased considerably in thickness and cellularity. The elastic tissue was rarely seen in the adventitia of full term mesometrial arteries.

Post-partum changes. The general microscopic organization of the arterial wall of mesometrial arteries taken from 6, 12, and 24 hours post-partum females was similar to those obtained from the full term guinea pigs. However the subendothelial cells, whose cytoplasm stained brownish with orcein during the last few days of pregnancy, now appeared clear. There was also no evidence of any phagocytized elastin particles in the cytoplasm of these cells. The following changes were seen in the mesometrial arteries between the second and fifth days post-partum. The endothelial lining once again appeared continuous. The cells of the intimal cushions under the endothelium showed increased basophilia indicating possible protein synthesis (fig. 12). Sections stained with dyes that specifically stain elastin did not give evidence of any elastic material in these vessels up to about five days after parturition. Occasionally fragments of elastin were seen in the wall of the post-partum arteries. They were thought to be those which had remained from prior to parturition. About six to nine days after delivery further changes in the blood vessels were observed. Gomori's aldehyde fuchsin positive fibrillar material appeared around most of the subendothelial cells (fig. 13). During this period the new fibrous material closely followed the outlines of the cell membranes and appeared continuous with the latter. However the Gomori positive intercellular material could not be stained with other elastic dyes during this time. Later (9-12 days post-partum) the other dyes also gave reactions comparable to those seen with Gomori's elastic stain.

By the sixteenth day post-partum the finer intercellular fibers appeared to organize themselves into thicker and darker staining bands. The lighter staining bands were in the deeper layers of the intima. These coarser bands were observed to occupy the same relative position as that of the original internal elastic membrane (fig. 14) but did not necessarily surround the entire circumference of the vessel during this time. In most cases the entire lumen

MATERIALS AND METHODS

Three month old virgin guinea pigs were bought and kept in the animal house for a period of one week to acclimatize the animals to their new surroundings. Due to the need of accurate records for the time of conception and the length of gestation, vaginal smears were taken daily from the animals for two estrous cycles. All the females except those used as controls were then mated and the time of conception was determined accurately to within 48 hours.

For the purpose of systematic study, the nine week long gestation period of the guinea pig was divided arbitrarily into nine stages of one week each. After parturition, animals were sacrificed at six and 24 hours, 2, 5, 7, 9, 12, 16, 20, 30 and 40 days post-partum. An average of three to five animals were used in each group. Three adult nulliparous female guinea pigs were ovariectomized unilaterally. They were permitted to recover from surgery for one week and then mated. The three unilaterally pregnant female guinea pigs thus obtained, were sacrificed at full term.

The mesometrial arteries which are branches of the main uterine artery and travel through the broad ligament to supply the uterine wall, and representative areas of the uterus were dissected out and fixed in Bouin's solution. Similar specimens were placed in 10% formalin solution for elastase digestion. The tissue were then dehydrated, cleared and embedded in paraffin. Sections were cut at 6 μ thickness and stained with Hematoxylin and Eosin, Taenzer's Orcein, Gomori's aldehyde, and Verhoeff's elastic stains. Picro-indigo-carmin and Van Gieson were used as counter-stains for all the sections except those stained with H and E.

OBSERVATIONS

General observations on mesometrial arteries

The gross and microscopic description of the mesometrial arteries of the adult nulliparous females was similar throughout their lengths to that seen in a typical muscular artery (fig. 1).

During pregnancy the mesometrial arteries become progressively more tortuous and increased in diameter. All mesometrial

arteries however do not exhibit the same amount of tortuosity and increase in diameter. The arteries leading to the placenta (placental arteries) exhibit most pronounced changes and those farther away from the placenta (peripheral arteries) show progressively fewer alterations in accordance with their distance from the placental attachment. The histological changes seen in any given vessel were not uniform throughout its lengths. The first indication of histological alterations was observed in the endometrial arteries and later in myo- and mesometrial vessels. Portions of the arteries which were closest to the uterine horn exhibited maximal changes. Thus, for the sake of consistency, all our observations described below were taken from the part of the mesometrial artery closest to the uterine horn.

The microscopic observations of elastic membranes of mesometrial arteries suggested a cyclic change during pregnancy and post-partum. This was reflected as a breakdown of the elastica interna in early pregnancy, and its disappearance at term. Although these changes were observed in both the peripheral and placental vessels they seemed to be delayed in the former. This process took about 90-100 days. The sequence of changes in placental arteries is outlined below.

The nine week long gestation period was divided into two time intervals, each consisting of approximately 30 days. This enabled us to group our morphological alterations in a more meaningful manner.

The first stage of gestation. During the early part of this stage the endothelium of the mesometrial arteries is formed of flattened cells which form a continuous lining. Later in pregnancy the endothelial lining becomes discontinuous. The subendothelial layer is wider than that seen in the arteries of non pregnant control guinea pigs. Unknown cells are seen scattered in this endothelial space. The internal elastic lamina showed areas of longitudinal splitting. Under higher magnification some subendothelial cells appeared to be surrounded by fine orcein positive elastic material (fig. 3).

Later in the first stage, the splitting of the internal elastic membrane was more clearly defined (fig. 4) and the area was

tures have been reported in arteries of skin, external genitalia, adrenals, fingers and toes (Mollendorf, '26).

In general intimal thickenings are observed in organs that require rapid adjustment of blood flow. The skin responds to external stimuli of temperature changes by constant dilatation and contraction of its arterioles. The genital vessels and glomerular arteriovenous anastomoses also support the hypothesis that organs which respond rapidly and adjust to changes in blood supply, develop intimal cushions. Such an explanation could certainly be entertained in mesometrial vessels of pregnant animals.

The tortuosity and subendothelial (intimal) thickenings in mesometrial arteries may be responsible for buffering the action of the pulsating thrust of blood flow (Markee, '29). It is also possible that near term the intimal cushions may limit the blood supply of the uterus and the fetus by reducing the lumen size and also by active contraction of the muscle cells of the arterial wall. This may constitute one of the factors which initiates parturition. The hypothesis of contracting vessels and decreased blood flow is supported by Markee's ('40) observations on endometrial vessels. This is also in accordance with Knisely's ('34) findings who showed in living uteri of mice that the proximal segment of the placental arteries have an especially contractile segment located near the entrance of the branch into the uterine wall. This segment of the mesometrial arteries was the most affected in our investigation. The contractile property of this segment may be due to the proliferated intimal cells.

The origin and nature of the intimal cells is still open to speculation. It has been suggested that these cells may be of muscular or endothelial origin (Goetz, '36). Trophoblastic origin of these cells has also been suggested on the basis of their similarity in appearance and staining (Van der Horst and Gillman, '46). The first two modes are quite possible, but the last one is less likely since the migration of fetal cells across the placenta may result in antigenic reactions. Trophoblastic origin of subendothelial cells in uterine arteries is further doubted since the cells are in meso-

metrial arteries. These cells should probably be found in veins and not in arteries as the direction of blood flow will favor the former.

Our histochemical studies did not clarify the nature of these cells but tended to associate these cells with muscle cells. It is possible that they originate from multipotential mesenchymal cells found in the subendothelial area. They then become differentiated into cells with phagocytic properties and digest elastin during pregnancy. After labor these cells, presumably acting under a different stimulus, alter their phagocytic function and assume the role of protein (elastin) synthesis. These observations suggest that the same cells may perform different functions under varying stimuli, and that muscle or muscle-like cells are capable of forming elastin. The last view is in accordance with Pease and Paule ('60) who attributed the function of elastin synthesis to aortic muscle cells in newborn rats.

Maher ('59) investigated post-partum uteri only, and reported that elastic membranes of the uterine vessels lose their tinctorial properties for a short time after parturition and regain their staining properties later on. Our studies on mesometrial arteries of pregnant and post-partum guinea pigs showed that the elastic components of blood vessels were fragmented and were removed from the arterial walls during pregnancy. Few days after parturition new elastic fibers were formed and became reorganized as the new internal elastic membrane of the mesometrial arteries. Therefore, it is important that alterations in mesometrial arteries during pregnancy be known before changes due to parturition can be fully understood.

This investigation showed that new elastic fibers first became apparent at about the sixth day after parturition and that not all elastic stains gave a positive reaction at the same stage of development. It is possible that the elastic fibers were formed earlier than the sixth day and could not be identified by histochemical means until they had reached a certain stage of maturity. Hass ('39) reported that newly formed elastic fibers in coronary arteries can only be recognized by their optical properties, and not by their tinc-

became lined by this type of fibrillar material between 16 and 22 days after parturition (figs. 15-16). The morphological orientation and histochemical staining reactions of the newly formed fibrous material in post-partum uterine arteries suggests that it is similar in nature to the elastic tissue demonstrated in blood vessels of non-pregnant and pregnant guinea pigs. On the above basis it is safe for us to assume that the continuous band of fibrillar material under the endothelium is the new internal elastic membrane. There was no evidence of the formation of a new external elastic membrane surrounding the entire media up to 40 days after parturition.

In order to provide additional evidence in support of the elastic nature of this fibrous material cross sections of blood vessels from various post-partum stages were treated with purified elastase. It was found that the elastase specifically digested the orcein, Verhoeff's or Gomori's stained material. The length of time and the concentration of the enzyme needed to digest the "elastic" material varied depending upon whether the "elastin" was from a primiparous young or primiparous old female. The details of these studies will be published later.

DISCUSSION

The alterations and modifications in the mesometrial arteries may be considered to be adaptive to the physiological changes that take place during pregnancy. This hypothesis could be substantiated by the observations that after parturition the mesometrial vessels make an attempt to revert back to their original state before pregnancy. Further evidence in support of the hypothesis is that "vascular alterations may be a direct result of pregnancy" was obtained by experiments involving unilateral pregnancies. Guinea pigs with unilateral pregnancies showed that mesometrial arteries supplying the pregnant horn exhibited fragmentation of the internal and external elastic membranes and increased tortuosity while the arteries on the non pregnant horn remained unaffected.

Localized effects of hormones have been demonstrated previously by Bogdanove and Tarry ('62) who demonstrated a reduction in size of basophilic cells after implanta-

tion of estradiol pellets in the anterior hypophysis of ovariectomized rats. The reduction in size of these cells was observed only in the vicinity of the implanted estrogen pellets. Comparable pellets failed to affect the basophilic cells when placed at some distance from the pituitary. Engle ('53) has shown that the uterus remains much smaller in ectopic pregnancies than in normal intrauterine pregnancy in spite of the fact that the conceptus is in close proximity of the uterus. In our observations arteries going directly to the placenta showed more changes which progressively decreased in arteries away from the placental site. The endometrial vessels were the first to exhibit histological modifications and were followed shortly by myo- and then mesometrial vessels. Our observations along with those of Bogdanove and Tarry ('62) and Engle ('53) suggest that a localized hormonal effect may be responsible for the alterations seen in mesometrial arteries during pregnancy. It is possible that the hormones produced by the placenta may in part be instrumentive in causing changes in blood vessels of the pregnant horn or horns, especially the placental vessels, and modify their structure to accommodate the growing uterus and conceptus.

Danforth et al. ('64) have shown partial breakdown of elastic laminae in the aorta of rabbits with injections of pharmacologic doses of estrogens and progesterones. We have demonstrated local fragmentation and digestion of elastic fibers of mesometrial arteries during pregnancy. These observations suggest a relationship between the breakdown of elastic tissue and circulating hormones. It is possible that the dosage of the hormones was large in Danforth's experiments and thus the effects appeared to be systemic rather than local.

The histological changes observed in mesometrial arteries require consideration both in respect to subendothelial cell proliferation and changes in the elastic components. There are several reports in the literature where intimal proliferations (cushions) have been reported in uterine arteries (Mossman, '37; Wislocki and Streeter, '38). These intimal proliferations have always been considered permanent and metabolically inactive. Similar fea-

torial properties, since no positive staining reactions can be obtained during early stages of development. It is thus possible that the difference in staining properties of elastic tissue may be due to physical, chemical (Pearse, '61) or structural (Dempsey and Lansing, '54) differences. Some support for lack of staining properties of newly formed elastic fibers is obtained from the morphological studies of Dettmer ('52) who showed that elastic fibers are composed of an amorphous matrix with fibrils embedded in it. Hall ('55, '57) confirmed Dettmer's findings and suggested a bi-phasic structure of the elastic fibers. According to Hall the elastic fibers have an inner protein core and an outer mucopolysaccharide coat. Thus, it is possible that the staining of elastic fibers may vary with different stains depending upon the amount and nature of the polysaccharide. Baló, et al. ('54) suggested that there must be different types of mature elastic fibers as they are effected differently by the same elastase preparation.

The fragmentation and removal of elastic tissue from the arterial walls of mesometrial arteries has already been related to the steroids concentration and the phagocytic properties of intimal cells. It is also possible that elastase like enzymes are released in the vicinity of the uterus and thus aid in fragmentation and digestion of the arterial elastin. It has already been shown by Woessner ('62, '63) and Woessner and Brewer ('63) that homogenates of pregnant uteri digest their own collagen. This could well be true for elastin.

LITERATURE CITED

- Baló, J., I. Banga and D. Schuler 1954 Vergleichende Untersuchungen über die Elastolyse der Gefasswand und des lig. nuchae in histologischen Schritten. *Acta morphol. Acad. sci. Hung.*, 4: 141.
- Bogdanove, E., and K. Tarry 1962 Site of estrogen inhibition of the pituitary oophorectomy reaction. Presented at the American Association of Anatomists, 75th Annual Session, Minnetonka, Minnesota, 1962. (Abstract Anatomical Record, vol. 142, P. 218).
- Danforth, D., P. Estrada and J. Buckingham 1964 The effect of pregnancy and enovid on the rabbit vasculature. *Am. Jour. Obstet. and Gynecol.*, 88: 952.
- Dempsey, E., and A. Lansing 1954 Elastic tissue. *Int. Rev. Cytol.*, 3: 437.
- Dettmer, N., I. Neckel and H. Ruska 1951 Elektronen-mikroskopische Befunde an versilberten kollagenen Fibrillen. *Z. Wiss. Mikrosk.*, 60:H.5: 290.
- Engle, E. T. (ed.) 1953 *Pregnancy Wastage*. Charles C Thomas & Co., Springfield, Ill.
- Goetz, R. 1936 Studien zur Placentation der Centetiden. I. Elene Neu-untersuchung der Centetisplacenta. *Z. f. Anat. u. Entwicklungsgesch.*, 106: 315.
- Goodall, J. R. 1909 The involution of puerperal uterus, with special reference to the involution of its circulatory system. *Am. Jour. Obstet. and Diseases of Women and Children*. LX: 921.
- Hall, D. 1961 The chemistry of elastin. In: *The Chemistry of Connective Tissue*. Charles C Thomas, Pub., Springfield, Ill., pp. 45-56.
- 1957 Chemical and enzymatic studies on elastin. In: *Connective Tissue*. R. E. Tunbridge et al., eds. Charles C Thomas, Pub., Springfield, Ill., pp. 238-253.
- Hall, D., M. Keach, R. Reed, H. Saxl, R. Tunbridge and M. Wood 1955 Collagen and elastin in connective tissue. *J. Gerontology*, 10: 388.
- Hass, G. 1939 Elastic tissue. *Arch. Path.*, 27: 334.
- Knisely, M. H. 1934 Microscopic observations on circulatory systems of living transilluminated mammalian spleens and parturient uteri. *Proc. Soc. Exper. Biol. Med.*, 33: 212.
- Maher, J. S. 1959 Morphologic and histochemical changes in post-partum uterine blood vessels. *Arch. Path.*, 67: 175.
- Markee, J. E. 1929 The rhythmic variations in the vascularity of the uterus of the guinea pig during the estrous cycle. *Amer. Jour. Obst. and Gynecol.*, vol. 17, pp. 205-208.
- 1940 Menstruation in intraocular endometrial transplants in the Rhesus monkey. *Contrib. Embryol., Carnegie Inst.*, 28: 221.
- Moellendorff, W. 1926 *Handbuch der mikroskopischen Anatomie des Menschen*. vol. 1.
- Mossman, H. 1937 Comparative morphogenesis of the fetal membranes and accessory uterine structures. *Contrib. embryol., Carnegie Inst.*, 26: 129.
- Pearse, A. G. E. 1961 *Histochemistry, Theoretical and Applied*, 2nd ed., reprinted. Little, Brown and Co., Boston, p. 165.
- Pease, D., and W. Paule 1960 Electron microscopy of elastic arteries: The thoracic aorta of the rat. *Jour. Ultrastruct. Res.*, 3: 469.
- Shaw, W. F. 1914 The subdivisions of Chronic Metritis. *Jour. Obstet. and Gynecol. Brit. Emp.*, 26: 173.
- van der Horst, C., and J. Gillman 1946 The reactions of the uterine blood vessels before, during and after pregnancy in elephantulus. *The South African Journal of Medical Sciences*, 2: No. 1. Biol. Suppl: 103.
- Wislocki, G., and G. Streeter 1938 On the placenta of Macaque from the time of implantation until the formation of the definitive placenta. *Contrib. Embriol. Carnegie Inst.* 27: 1.
- Woessner, J. 1963 Age-related changes of the human uterus and its connective tissue framework. *Jour. Gerontol.*, 18: 220.
- Woessner, J., and T. Brewer 1963 Formation and breakdown of collagen and elastin in the human uterus during pregnancy and postpartum involution. *Biochem. Jour.*, 89: 75.

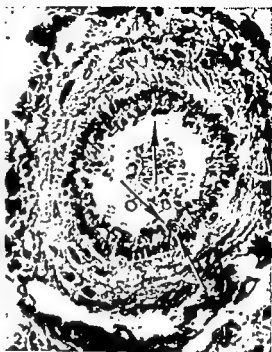


PLATE 1

EXPLANATION OF FIGURES

- 1 Cross section of a mesometrial artery from an adult nulliparous female. Notice the normal distribution of elastic components. Internal (I) and external (E) elastic membranes, $\times 250$.
- 2 Taken from early part of the first stage of pregnancy. Endothelium (E), subendothelial area is wider than in figure 1. Subendothelial cells (C) surrounded by elastic fibers (O), $\times 250$.
- 3 Higher magnification of figure 2. Subendothelial cells are seen to be partially surrounded by elastic fibers (O) which appear to be splitting off from the underlying internal elastic membrane (arrows). Lumen (L), oil immersion.
- 4 Taken from the latter part of the first stage of pregnancy. Subendothelial cells (C) splitting the internal elastic membrane (I). The internal elastic membrane is intact at some points and shows splitting at others, $\times 400$.

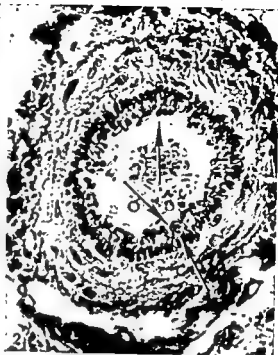


PLATE 2

EXPLANATION OF FIGURES

- 5 Taken from the early part of the second stage of pregnancy. The subendothelial cells form a several layer thick cushion (C). Notice the fragmented elastic fibers (arrows), $\times 250$.
- 6 Taken from full term (9 weeks) pregnant animal. Notice the lack of elastic fibers, $\times 120$.
- 7 Higher magnification of figure 6. Notice the darker staining cytoplasm of the subendothelial cells (C), $\times 250$.
- 8 Notice the multinucleated giant cells (M) seen in the intima, oil immersion.



PLATE 3

EXPLANATION OF FIGURES

- 9 Subendothelial multinucleated cells (M), Lumen (L), $\times 450$.
- 10 Taken from full term pregnant animal. Notice the subendothelial cells with phagocytized elastic particles (arrows) in their cytoplasm, $\times 450$.
- 11 Notice the dark orcein positive granules (G) in the cytoplasm. Nucleus (N), of subendothelial cells taken from 9-week pregnant females, oil immersion.
- 12 Taken from a 5-day post-partum animal. Notice the restored endothelium (E), and the basophilic intimal cells (C), $\times 120$.

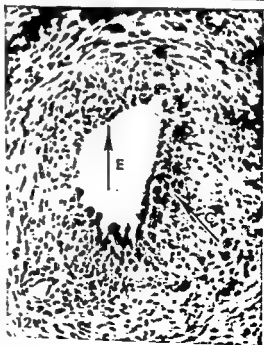
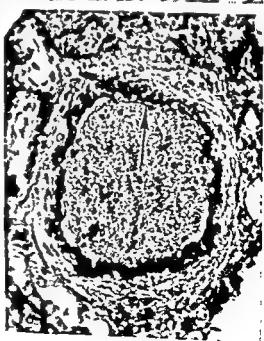
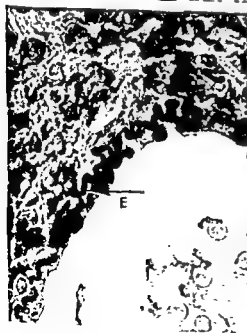


PLATE 4

EXPLANATION OF FIGURES

- 13 Taken from a nine day post-partum animal. The dark fibers (F) are seen surrounding the subendothelial cells. Lumen (L), oil immersion.
- 14 Taken from 12 days post-partum animal. Thicker or darker staining elastic bands (E) appear under the endothelium, oil immersion.
- 15 Taken from 18 days post-partum animals. Notice the thick dark staining corrugated elastic membrane (E) formed under the endothelium, $\times 400$.
- 16 Complete internal elastic membrane (I) seen in 22 days post-partum specimens, $\times 250$.



Circadian Rhythms in Blood Glucose and the Effect of Different Lighting Schedules, Hypophysectomy, Adrenal Medullectomy and Starvation¹

JOHN E. PAULY AND LAWRENCE E. SCHEVING

Departments of Anatomy, Tulane University School of Medicine, New Orleans, Louisiana and The Chicago Medical School, Chicago, Illinois

ABSTRACT With other environmental factors rigidly standardized, normal Sprague-Dawley rats were maintained under the following lighting schedules: (1) LD 12:12, artificial light from 6:00 A.M. to 6:00 P.M. alternating with 12 hours of darkness; (2) DL 12:12, reversal of the first schedule; (3) DD, constant darkness; and (4) LL, constant illumination.

During each lighting regimen, blood glucose levels were determined on separate subgroups of 11 to 18 animals at bi-hourly intervals during a 24-hour period. Significant circadian fluctuations or rhythms under all lighting conditions were found when the mean blood glucose values for each bi-hourly group were plotted as a function of time. Rats maintained under LD 12:12 conditions showed approximately a 25% difference between the maximum and minimum values. When the phasing of the peaks and troughs of blood glucose rhythm in Sprague-Dawley rats was compared with that of a separate colony of Wistar rats, it was noted that they were similar. Starvation of the LD rats for 66 hours did not abolish the characteristic rhythm, although a lower level of blood glucose resulted. The LD 12:12 blood glucose pattern was reversed by reversing the LD cycle 180 degrees. Under LL and DD the troughs and crests seen in the glucose curves were out of phase with those of LD and with each other; this suggested that under LL or DD the rhythm had become free-running because of the absence of the light-dark synchronizer.

Hypophysectomy modified the phasing of the normal LD pattern but did not abolish its fluctuating nature; this suggested that the LD cycle of light no longer was an effective entraining agent. Adrenal medullectomy caused an overall 13% decrease in the 24-hour mean but did not alter the phasing of the LD pattern. The significance of periodicity analysis in relation to bioassay is discussed.

Significant variations have been reported in blood glucose levels during 24-hour periods in a number of mammals. The most frequently cited reference in the literature is that of Pitts ('43) who reported diurnal variations in the blood glucose levels of female rats. His results were based on data obtained from only two hours of sampling, once about noon and again at around midnight; they showed a 10% difference between the means of the two samples. Earlier investigations, Allcroft ('33) in the lactating cow, Jores ('34) in the human and Euler and Holmquist ('34) in the rabbit, all reported diurnal rhythms in blood glucose levels. Other workers Hatlehol ('24), Harding et al. ('32) and Möllerström ('32) reported variations in glucose tolerance during the 24-hour period for man and concluded that henceforth these were predictable for an individual.

In general the practice of sampling at infrequent intervals, once or twice during

the "day" and once or twice during the "night," often with no reference to a defined light-dark cycle, characterized the earlier reports on blood sugar rhythms. This procedure was used frequently by pioneer workers in the field of periodicity who first demonstrated that differences in values of a measured physiological function varied according to the time of sampling. However, in some instances confusing or divergent results emerged because of such infrequent intervals of sampling, and because no overall 24-hour pattern of fluctuation had been established in relation to a defined LD environment. In the first place, it would be fortuitous if one were to select the hours of sampling that showed the true crest or trough of any circadian rhythm ("diurnal" rhythm of earlier workers). Secondly, the true relationships of the rhythmic pattern to an established or

¹This investigation was supported, in part, by Public Health Service Research Grant AM 04659.

controlled light-dark cycle would not be revealed. Zarrow et al. ('52), sampling at only 11:00 A.M. and 11:00 P.M., reported that there was no diurnal rhythm in the blood glucose of sheep. Zarrow's report has been cited in the literature with the inference that sheep differ from other animals in having no diurnal rhythm in their circulating blood sugar. Such an inference is unwarranted with only two sampling times over the 24-hour period.

This investigation was undertaken to study the daily fluctuation that occurs in blood glucose levels of the adult male rat maintained under different but controlled conditions of illumination. The sampling over the 24-hour period in each experiment was done every two hours on different groups of animals. In addition the effects of starvation, hypophysectomy and adrenal medullectomy on blood sugar levels were investigated.

MATERIALS AND METHODS

A colony of 250 male Sprague-Dawley rats, 350 to 400 gm in weight, was housed two to a cage. Rockland rat chow and water were available *ad libitum*. Illumination was exclusively by fluorescent lights controlled by an automatic timing device. The room was entered only three times per week on Monday, Wednesday and Friday at exactly 2:00 P.M. (CST) for the purpose of cleaning the cages and replenishing the food and water supply. Temperature was maintained at $23 \pm 2^\circ\text{C}$.

Using the same colony of animals, four different lighting schedules were employed at different times. The first one was alternating 12-hour periods of light and darkness, the second was the reversal of the first, the third was continuous darkness, and the fourth was continuous illumination (about 650 lux). The abbreviations DD and LL refer to continuous darkness and continuous light; LD x:y refers to a light-dark cycle of x hours of light and y hours of darkness (x was always 12 hours and occurred from 6:00 A.M. to 6:00 P.M.; DL y:x is the designation for the reversed condition (x or light being 12 hours from 6:00 P.M. to 6:00 A.M.). These designations have become customary in the literature and are used in this paper. We refer to the LD animals as "normal" or "controls" be-

cause the LD cycle closely approximates the natural or common laboratory light-dark cycle to which rats are subjected. Consequently, all other conditions are referred to in this paper as experimental. Constant darkness (DD) should be qualified to include the tri-weekly light perturbation of approximately one hour's length when cages were cleaned and food replenished. The light source during this period was the small amount of fluorescent light from the adjacent hallway that diffused into the animal room through the slightly opened door.

After the rat colony had been maintained relatively undisturbed in a particular lighting schedule for at least three weeks, different subgroups of animals (table 1) were removed as gently as possible from the colony every two hours over one 24-hour period. Blood samples were taken in the following manner: (1) about 1 mm of the tip of the tail of the rat was cut off, and the first two drops of blood were discarded; then approximately 0.5 cm³ was collected into a vial containing a few crystals of heparin. (2) Glucose determinations were made on 0.2 cm³ of the heparinized blood by the micro method of Nelson-Somogyi (Somogyi, '45). By setting up an efficient assembly line procedure, it was possible to complete each determination within 55 minutes after collecting the tail blood. In the experiment involving Wistar rats, a Folin and Wu macro method was utilized (Hawk et al., '49). Blood was collected directly from the hearts of animals that just had been sacrificed by cervical dislocation. The experiment involving Wistar rats and the Folin-Wu technique was designated as LD no 1; the experiment utilizing Sprague-Dawley rats and the Nelson-Somogyi technique was designated as LD no. 2. All values in this paper are expressed as mg/100 ml of blood.

After sampling a colony of Sprague-Dawley rats that had been subjected to DD for about one month, the colony was shifted to an LD 12:12 cycle of light. They remained in LD 12:12 for three weeks and then were sampled. Several days after the LD sampling, the colony was deprived of food for about 43 hours; then another sampling period was begun. At the end of this second sampling period the animals

TABLE 1

Bi-hourly means and S.E. over a 24-hour period of blood glucose levels in white male rats under different experimental and lighting regimens; probability values of differences between various compared values. All values are expressed as mg/100 ml of blood

Hour	LD 12:12 no. 1 N = 18*	LD 12:12 no. 2 N = 14	DL 12:12 N = 14	LL no. 1 N = 12	LL no. 2 N = 14	DD N = 14	LD 12:12 starved N = 14	LD 12:12 hypophy- sectomized N = 11	LD 12:12 medul- lectomized N = 12
6:30 A.M.	110 ± 4	99 ± 3	90 ± 2	108 ± 3	99 ± 3	92 ± 4	37 ± 3	98 ± 3	85 ± 2
8:30	115 ± 6	93 ± 3 [†]	93 ± 4	111 ± 3	103 ± 2	89 ± 2	47 ± 8	111 ± 6 [†]	90 ± 2
10:30	108 ± 4	97 ± 2	101 ± 3	102 ± 2	111 ± 2	87 ± 3	46 ± 6	111 ± 4	90 ± 2
12:30 P.M.	104 ± 4	102 ± 2	110 ± 4 [†]	99 ± 3 [†]	116 ± 2 [†]	85 ± 3 [†]	45 ± 4	81 ± 5 [†]	85 ± 2 [†]
2:30	104 ± 3 [†]	100 ± 3	100 ± 3	107 ± 3	107 ± 2	90 ± 2	52 ± 6	96 ± 2	85 ± 2 [†]
4:30	114 ± 5	102 ± 2	102 ± 3	121 ± 4	106 ± 2	96 ± 5	45 ± 2	107 ± 3	85 ± 3 [†]
6:30	110 ± 4	100 ± 3	87 ± 2	122 ± 2 [†]	106 ± 2	107 ± 3	51 ± 2	112 ± 4 [†]	95 ± 3
8:30	119 ± 4	109 ± 3	91 ± 4	118 ± 2	90 ± 2 [†]	112 ± 4	76 ± 4	101 ± 3	97 ± 3 [†]
10:30	132 ± 3 [†]	115 ± 3 [†]	82 ± 4 [†]	98 ± 2 [†]	98 ± 3	106 ± 1	49 ± 3	107 ± 3	97 ± 3 [†]
12:30 A.M.	115 ± 7	110 ± 3	83 ± 2	107 ± 3	93 ± 4	112 ± 4 [†]	33 ± 3	93 ± 6	88 ± 3
2:30	118 ± 4	100 ± 2	84 ± 3	100 ± 2	99 ± 3	95 ± 4	32 ± 4 [†]	101 ± 3	90 ± 4
4:30	115 ± 4	101 ± 2	82 ± 4 [†]	107 ± 7	102 ± 2	95 ± 4	41 ± 3	107 ± 6	89 ± 2
24-hour overall mean	113 ± 1	103 ± 0.9	92 ± 1	108 ± 1	102 ± 0.9	97 ± 2	47 ± 1	102 ± 1.3	90 ± 0.8
High vs. low	< 0.001	< 0.001	< 0.001	< 0.001	< 0.001	< 0.001	< 0.001	< 0.001	< 0.001
24-hour mean vs. high	< 0.1	< 0.001	< 0.02	< 0.001	< 0.001	< 0.001	< 0.001	< 0.001	< 0.001
24-hour mean vs. low	< 0.05	< 0.001	< 0.05	< 0.01	< 0.001	< 0.001	< 0.001	< 0.001	< 0.001

* N = mean number animals at each time point. † indicates peak hour or hours; ‡ indicates lowest hour or hours.

had been without food for about 66 hours; however, water had been continuously available. This experiment was designated as LD-starvation. After a period of recuperation from starvation, the colony was placed into continuous light (LL) (approximately 650 lux). They remained in LL for about one month and were sampled again; this experiment was designated as LL no. 1. The animals were left in LL for another two and one-half months; then another sampling was performed and designated as LL no. 2. Shortly thereafter the colony was returned to LD where they remained several weeks prior to being subjected to DL. To recapitulate, the sequence of sampling was DD, LD, LD-starvation, LL no. 1, LL no. 2 and DL. Before subjecting the colony to a new light condition, it was always adjusted or readjusted to the normal LD 12:12 schedule.

Because of their operated state, the hypophysectomized group of Sprague-Dawley rats living in LD conditions had to be handled differently. Each rat weighed about 100 gm. Ambient temperature was raised to 25°C, and the normal diet was supplemented with milk, lettuce, bread and oranges. The tri-weekly care period was carried out at 10:00 A.M. rather than at 2:00 P.M. The hypophysectomized animals as well as the adrenal medullectomized animals were obtained from the Hormone Assay Laboratories, Chicago, within 48 hours after surgery and were maintained in a LD 12:12 light schedule prior to sampling. No special care was necessary to maintain adrenal medullectomized, animals each of which averaged about 400 gm at sampling.

The times indicated on all figures represent approximate mid-points of the sampling periods which were less than 60 minutes in duration. Statistical analyses were made by calculating the standard error of the difference between the means to be compared and the resulting *t* values. The probability then was determined by referring to standard *t* tables.

RESULTS

LD-12:12 no. 2 (Sprague-Dawley). There was significant fluctuation along the 24-hour time scale (fig. 1; table 1). The highest glucose levels were recorded between 8:30 P.M. and 12:30 A.M. with a

peak of 115 mg/100 ml of blood; the lowest value of 93 mg/100 of blood was recorded at 8:30 A.M. The overall 24-hour mean was 103 mg/100 ml of blood. The statistical significance of this set of data and of other high and low values under all experimental conditions is recorded in table 1 and will not be mentioned again in the section on Results.

DL-12:12. There was an approximate inversion of the rhythmic pattern when the animals were subjected to the reversed light-dark cycle. The maximum value of blood glucose occurred at 12:30 P.M. with a value of 110 mg/100 ml; whereas the minimum value was recorded between 10:30 P.M. and 4:30 A.M. The overall 24-hour mean was 92 mg/100 ml of blood (fig. 1; table 1).

LL no. 1. Blood samples were taken over the 24-hour period after rats had been in LL for one month (LL no. 1) (fig. 2; table 1). The maximum value of 122 mg/100 ml of blood was recorded at 6:30 P.M. There were two low periods, one at 12:30 P.M. and the second at 10:30 P.M.

LL no. 2. Two and one-half months after the LL no. 1 experiment, the same rats were sampled again (continuously in LL). By this time the peak had shifted about six hours and occurred at 12:30 P.M.; the minimum hour was at 8:30 P.M. The overall 24-hour mean in LL no. 1 was 108; whereas the overall 24-hour mean in LL no. 2 was 102 mg/100 ml of blood.

DD. Although the data for this experiment are not shown graphically, the peak level in circulating blood glucose was recorded at 12:30 A.M. with a mean value of 112 mg/100 ml, whereas the minimum (85 mg/100 ml) was recorded at 12:30 P.M. The overall 24-hour mean was 97 mg/100 ml of blood (table 1).

LD-starvation. When blood samples were taken after a period of starvation, there still was significant fluctuation of glucose over the 24-hour time scale. The peak occurred at 8:30 P.M. with a mean value of 76 mg/100 ml; the minimum value occurred at 2:30 A.M. with a value of 32 mg/100 ml of blood. Although absolute bi-hourly mean values were lower, the LD starvation pattern was synchronized very closely with the LD 12:12 pattern (fig. 1; table 1).

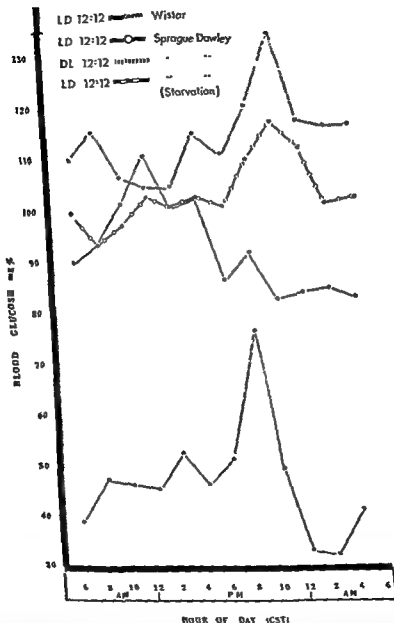


Fig. 1 Reproducibility and the effects of light reversal and starvation. Note the similarity in phasing between Wistar and Sprague-Dawley rats maintained under comparable LD cycles. The values at each point in time in this figure and in all other figures is the mean obtained from separate sub-groups of animals expressed as mg/100 cc blood. The ability of the rhythm to invert subsequent to the inversion of the light-dark cycle 180°, and the persistence of the rhythm during starvation are evident.

had been without food for about 66 hours; however, water had been continuously available. This experiment was designated as LD-starvation. After a period of recuperation from starvation, the colony was placed into continuous light (LL) (approximately 650 lux). They remained in LL for about one month and were sampled again; this experiment was designated as LL no. 1. The animals were left in LL for another two and one-half months; then another sampling was performed and designated as LL no. 2. Shortly thereafter the colony was returned to LD where they remained several weeks prior to being subjected to DL. To recapitulate, the sequence of sampling was DD, LD, LD-starvation, LL no. 1, LL no. 2 and DL. Before subjecting the colony to a new light condition, it was always adjusted or readjusted to the normal LD 12:12 schedule.

Because of their operated state, the hypophysectomized group of Sprague-Dawley rats living in LD conditions had to be handled differently. Each rat weighed about 100 gm. Ambient temperature was raised to 25°C, and the normal diet was supplemented with milk, lettuce, bread and oranges. The tri-weekly care period was carried out at 10:00 A.M. rather than at 2:00 P.M. The hypophysectomized animals as well as the adrenal medullectomized animals were obtained from the Hormone Assay Laboratories, Chicago, within 48 hours after surgery and were maintained in a LD 12:12 light schedule prior to sampling. No special care was necessary to maintain adrenal medullectomized animals each of which averaged about 400 gm at sampling.

The times indicated on all figures represent approximate mid-points of the sampling periods which were less than 60 minutes in duration. Statistical analyses were made by calculating the standard error of the difference between the means to be compared and the resulting *t* values. The probability then was determined by referring to standard *t* tables.

RESULTS

LD-12:12 no. 2 (Sprague-Dawley). There was significant fluctuation along the 24-hour time scale (fig. 1; table 1). The highest glucose levels were recorded between 8:30 P.M. and 12:30 A.M. with a

peak of 115 mg/100 ml of blood; the lowest value of 93 mg/100 of blood was recorded at 8:30 A.M. The overall 24-hour mean was 103 mg/100 ml of blood. The statistical significance of this set of data and of other high and low values under all experimental conditions is recorded in table 1 and will not be mentioned again in the section on Results.

DL-12:12. There was an approximate inversion of the rhythmic pattern when the animals were subjected to the reversed light-dark cycle. The maximum value of blood glucose occurred at 12:30 P.M. with a value of 110 mg/100 ml; whereas the minimum value was recorded between 10:30 P.M. and 4:30 A.M. The overall 24-hour mean was 92 mg/100 ml of blood (fig. 1; table 1).

LL no. 1. Blood samples were taken over the 24-hour period after rats had been in LL for one month (LL no. 1) (fig. 2; table 1). The maximum value of 122 mg/100 ml of blood was recorded at 6:30 P.M. There were two low periods, one at 12:30 P.M. and the second at 10:30 P.M.

LL no. 2. Two and one-half months after the LL no. 1 experiment, the same rats were sampled again (continuously in LL). By this time the peak had shifted about six hours and occurred at 12:30 P.M.; the minimum hour was at 8:30 P.M. The overall 24-hour mean in LL no. 1 was 108; whereas the overall 24-hour mean in LL no. 2 was 102 mg/100 ml of blood.

DD. Although the data for this experiment are not shown graphically, the peak level in circulating blood glucose was recorded at 12:30 A.M. with a mean value of 112 mg/100 ml, whereas the minimum (85 mg/100 ml) was recorded at 12:30 P.M. The overall 24-hour mean was 97 mg/100 ml of blood (table 1).

LD-starvation. When blood samples were taken after a period of starvation, there still was significant fluctuation of glucose over the 24-hour time scale. The peak occurred at 8:30 P.M. with a mean value of 76 mg/100 ml; the minimum value occurred at 2:30 A.M. with a value of 32 mg/100 ml of blood. Although absolute bi-hourly mean values were lower, the LD starvation pattern was synchronized very closely with the LD 12:12 pattern (fig. 1; table 1).

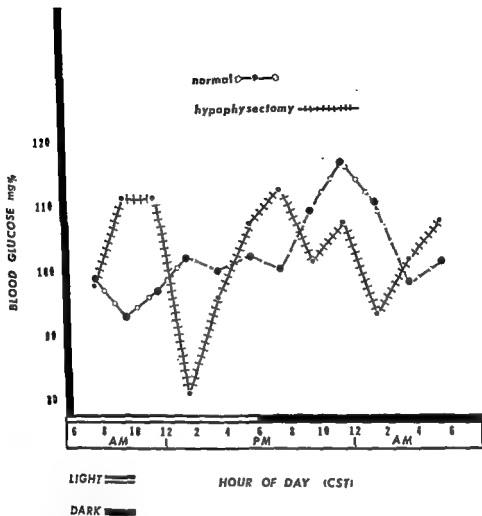


Fig. 3 The difference between the patterns of glucose levels in hypophysectomized and normal animals under LD 12,12.

occur at random, but rather are regulated in time along a 24-hour scale. They are determinable and thereafter predictable and reproducible under comparable, rigidly standardized conditions. The reproducibility in phasing is clearly evident in our experiments. Although not particularly relevant to an analysis of the phasing pattern, a magnitude difference did exist between the two species. Such may be attributable to a species difference; although it is probable that the differences are the results of the methods used to obtain the blood and to measure the glucose. For ex-

ample, in Wistar rats cardiac blood and a Folin and Wu method were employed. The latter technique measures other reducing substances in the blood in addition to glucose and may be responsible for the higher of the two LD peaks seen in figure 1; whereas for Sprague-Dawley rats tail blood and a Nelson-Somogyi method were used. The Nelson-Somogyi technique reflects the "true" glucose, because the nonglucose reducing substances first are precipitated.

Rhythms of this nature frequently are synchronized by the light-dark cycle to which the animals are subjected, and in

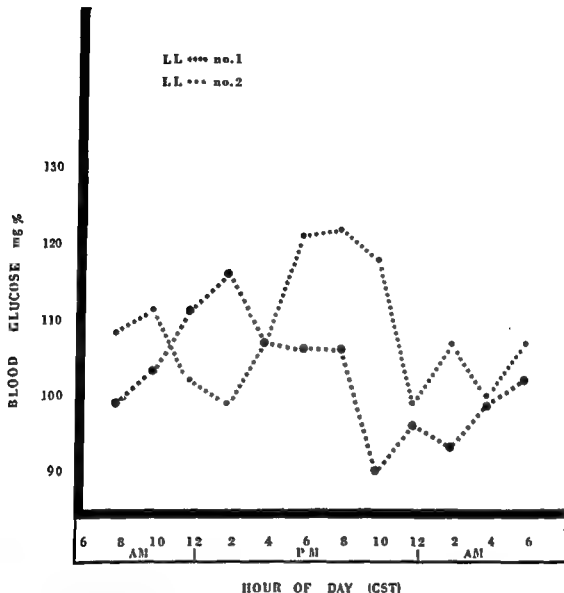


Fig. 2 The drift in peaks and troughs in blood glucose patterns in the absence of the light-dark synchronizer.

LD-hypophysectomized. There were significant fluctuations within the 24-hour period in this experimental group, but the peaks and troughs were not synchronized with the normal LD 12:12 cycle. Two highs occurred, one at 8:30 A.M. with a mean of 111 mg/100 ml of blood and a second at 6:30 P.M. with a mean of 112 mg/100 ml of blood; the lowest blood glucose value (81 mg/100 ml) was recorded at 12:30 P.M. (fig. 3; table 1). There was no temporal relationship to the normal LD 12:12 group.

LD-adrenal medullectomized. The timing in this experimental group was very similar to the normal LD 12:12 group with

maxima occurring between 8:30 and 10:30 P.M. and both hours having identical values (97 mg/100 ml); the minimum occurred between 12:30 and 4:30 P.M. Once again the hours had identical values (97 mg/100 ml).

DISCUSSION

From an examination of figure 1, it is evident that the blood glucose levels in both normal Wistar and Sprague-Dawley rats maintained in a LD 12:12 cycle are rhythmic. By the term "rhythmic" we mean that during a 24-hour period, there is a recurrent sequence of high and low values in a measured function. These values do not

12:12 cycles in this study, the difference between the means in the blood sugar levels at approximately noon and midnight were 8 and 10% respectively. However, our more frequent intervals of sampling permitted a close estimation of the true crests and troughs of these rhythms. The difference between the means of the hours of highest and lowest blood sugar levels in Wistar rats was 27%; whereas in Sprague-Dawley rats it was 24%. We conclude that differences in blood sugar levels of approximately 25% rather than the 10% of Pitts normally can be expected along the 24-hour time scale in rats maintained on a LD 12:12 cycle.

Daily rhythms in a number of physiological functions have been shown to persist when animals are removed from a LD 12:12 cycle and placed into LL or DD. They often persist with a time frequency of slightly more or less than 24 hours; consequently, the phasing of the rhythm will be constantly shifting either forward or backwards in relation to the astronomical clock. When this occurs the rhythm is said to be "free-running." Rhythms having a frequency differing from 24 hours have been called "circadian" (from *circa* and *diem*; Halberg, '60). The blood glucose rhythm appears to be free-running in the absence of a light-dark cycle; this suggests that the rhythm is controlled endogenously. This free-running concept could account for the differences in phasing seen between the rhythm in the glucose levels under LD conditions and the shifted rhythms in LL and DD. The use of biochemical procedures for the determination of the precise frequency of the free-running rhythm are quite difficult and were not attempted in this present investigation.

Some of the early investigators argued that fluctuations in glucose levels were solely a "feeding phenomenon;" therefore, ostensibly to avoid these fluctuations, they employed fasting animals in their studies. It is evident from this investigation that levels of nutrition do affect the absolute values of blood glucose but not the presence or timing of the rhythm (fig. 1). This finding is similar to a report by Chikulas and Scheving ('66) who reported that a liver glycogen rhythm persisted in urodele larvae deprived of food for three weeks.

Figure 3 demonstrates that hypophysectomy does not abolish the fluctuating nature of blood glucose levels. The typical, normal LD pattern is no longer apparent; this suggests that the ability to entrain the rhythm to the LD cycle is dependent on the retino-pituitary axis. These data permit one to point out the desirability of a periodicity analysis in bioassay experiments of this nature. It is obvious that by sampling only once along the 24-hour time scale it would be possible to arrive at different conclusions as to what effect hypophysectomy has on the blood glucose level. If sampling were done at approximately 7:00 A.M., it might appear that hypophysectomy had little effect; at 10:30 A.M., it would appear to have increased the blood sugar; but if sampling were performed during the middle of the dark period, one might conclude that hypophysectomy brought about a decrease in blood sugar. Because of the rhythmic pattern of values from both the normal and experimental animals and because the experimental pattern is so greatly modified, all three conclusions theoretically could be obtained. Obviously the conclusion as to the effect of hypophysectomy is dependent on the time of day chosen for sampling. The increasingly common practice of sampling both controls and experimental animals at the same time of day, presumably to avoid the consequences of rhythms, is not sufficient; for sampling may be done in the trough, on one of the slopes or at the crest of the curve. Because the light-dark cycle of nature is the synchronizing one in many laboratories, biological rhythms will drift as the LD cycle of nature changes from one season to the next; thus sampling at the same clock hour during two seasons of the years may produce different results.

The results of adrenal medullectomy experiments indicate that these glands are not necessary for the timing of the rhythm, but are necessary for the maintenance of the normal levels of blood glucose. Irrespective of the time of day chosen for sampling, the medullectomized rats have a lower blood sugar than the controls. It is quite obvious, however, that when any bioassay is made the time chosen for sampling may have a decided effect on the statistical significance of the results. For example, when the 24-hour means of the normal

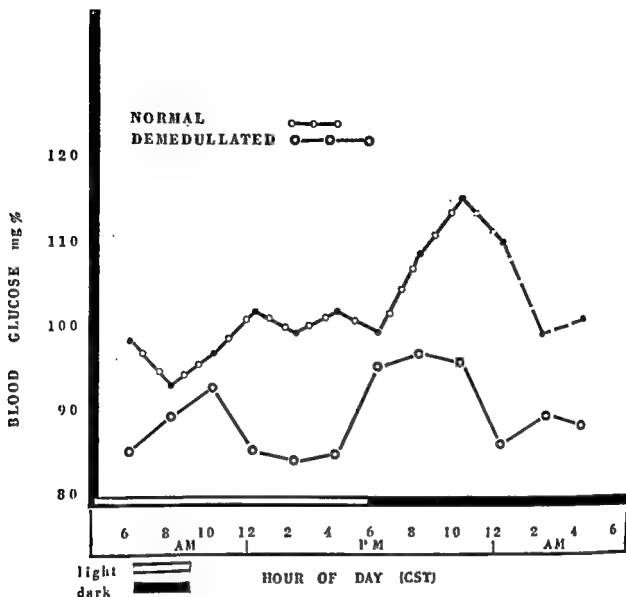


Fig. 4 The effect of adrenal medullectomy on the LD rhythm.

this case the two LD cycles were kept constant. All other parameters in the two studies were controlled carefully, and conditions were identical except that the animals were quartered in different buildings. The dependence of the phasing of the rhythms on the LD cycle also is evident from the fact that the rhythm reversed subsequent to a 180 degree inversion of the environmental LD cycle (fig. 1). The fact that the light-dark cycle is the dominant entraining or synchronizing factor does have a practical application. For example, if an investigator were interested in sampling at a time when the blood sugar was highest and still not lose his sleep, he could artificially

alter the environmental LD cycle of the colony a certain number of degrees, wait an appropriate period for the shift in phasing to occur, and sample at a convenient clock time.

In many laboratories, samples are taken during the morning hours. The results of this study show that such would be a time when blood glucose levels of rats might be expected to be relatively low.

This investigation corroborates the findings of Pitts ('43) who reported a 10% difference between the mean blood glucose levels of rats sampled at approximately noon and midnight. In the Wistar and Sprague-Dawley rats maintained in LD

Index

A

- Actinomycin D administration, an electron microscopic and radioautographic study of the rat parotid gland after 161
- Adrenal cortex of the opossum, the fine structure of the zona glomerulosa and the zona fasciculata of the 463
- Adrenal medullectomy and starvation, circadian rhythms in blood glucose and the effect of different lighting schedules, hypophysectomy 627
- ALBERT, ERNEST N. The effect of pregnancy on the elastic membranes of mesometrial arteries in the guinea pig 611
- Arteries in the guinea pig, the effect of pregnancy on the elastic membranes of mesometrial 611
- Autoradiography, localization of uptake of tritiated norepinephrine by rat brain *in vivo* and *in vitro* using electron microscopic 377
- AVEY, J. K., R. A. MYERS AND L. E. HALE. A study of mineral density surrounding resorption sites in teeth 55

B

- BANG, SEONG. See EVANS, F. GAYNOR 79
- Blood glucose and the effect of different lighting schedules, hypophysectomy, adrenal medullectomy and starvation, circadian rhythms in 627
- Boa constrictor, the ultrastructure of myofibers in a reptilian heart: The 553
- Body segments based on size and weight, properties of 33
- Bone, differences and relationships between the physical properties and the microscopic structure of human femoral, tibial and fibular cortical 79
- Bone fractures produced by high velocity impacts 123
- Bones of the masked shrew, *Sorex cinereus*, microradiographic visualization of structure in 89
- Bones to impact, tolerance of the facial 113
- Brain *in vivo* and *in vitro* using electron microscopic autoradiography, localization of uptake of tritiated norepinephrine by rat 377
- BRODIE, ALLAN G. The interrelation of the digestive and skeletal systems as determinants of tooth position 71
- BURGZ, LYNN J. See HUELKE, DONALD F. 123
- BURDI, ALPHONSE R., AND KATHLEEN FAIST. Morphogenesis of the palate in normal human embryos with special emphasis on the mechanisms involved 149
- BURGOS, M. H., AND R. VITALE-CALPE. The mechanism of spermatid in the toad .. 227

C

- Calcifying turkey leg tendons, changes in cells, matrix and water of 489
- CARPENTER, MALCOLM B. See STEIN, BENNETT M. 281
- Cell, matrix and water of calcifying turkey leg tendons, changes in 489
- Cells of the mouse, an experimental study of microscopic and submicroscopic lipid inclusions in hepatic 253
- Central projections of portions of the vestibular ganglia innervating specific parts of the labyrinth in the rhesus monkey 281
- Changes in cells, matrix and water of calcifying turkey leg tendons 489
- Circadian rhythms in blood glucose and the effect of different lighting schedules, hypophysectomy, adrenal medullectomy and starvation 627
- COHEN, ADOLPH I. An electron microscopic study of the modification by monosodium glutamate of the retinas of normal and "rodless" mice 319
- Continuous attachment of the periodontal membrane 133
- Correlation of types of cortical grain structure with architectural features of the human skull 7
- Cortical grain structure with architectural features of the human skull, correlation of types of 7

D

- DEMPSTER, WILFRED TAYLOR, AND GEORGE R. L. GAUGHAN. Properties of body segments based on size and weight 33
- DEMPSTER, WILFRED T. Correlation of types of cortical grain structure with architectural features of the human skull 7
- Development of the facial muscles in man, the 357
- Differences and relationships between the physical properties and the microscopic structure of the human femoral, tibial and fibular cortical bone 79
- Digestive and skeletal systems as determinants of tooth position, the interrelation of the 71
- Dog spleens, an electron- and light-microscope study of sinus structure in perfused rabbit and 527

E

- Effect of pregnancy on the elastic membranes of mesometrial arteries in the guinea pig, the 611
- Effects of pinealectomy in the newborn female rat 391

and medullectomized animals were compared, they were found to be significantly different; however, several points along the 24-hour time scale were not.

By first knowing the basic rhythm, one can better estimate the best times for administering drugs, performing operative procedures or collecting samples. We agree with Halberg ('60) and others who have suggested that the technique of periodicity analysis should be applied to many studies that attempt to elucidate biological mechanisms.

LITERATURE CITED

- Allcroft, W. M. 1933 Diurnal variations in blood sugar level of the lactating cow. *Biochem. J.*, 27: 1820-1823.
- Chiakulas, J. J., and L. E. Scheving 1966 Periodicity in liver glycogen of urodele larvae. *Comp. Biochem. Physiol.*, 17: 67-91.
- Euler, U. S. von, and A. G. Holmquist 1934 Tagesrhythmik der Adrenalinsekretion und des Kohlenhydratstoffwechsel beim Kaninchen und Igel. *Pfluegers Arch.*, 234: 210-224.
- Halberg, F. 1960 Temporal coordination of physiological function. In: Cold Spring Harbor Symposium on Quantitative Biology, Vol. XXV: 289-310.
- Harding, V. J., D. L. Selby and A. R. Armstrong 1932 Afternoon glycosuria. *Biochem. J.*, 26: 957-962.
- Hatlehol, R. 1924 Blood sugar studies. *Acta Med. Scand., Suppl. 8*: 211-252.
- Hawk, P. B., B. L. Oser and W. H. Summerson 1949 *Practical Physiological Chemistry*, 12th ed. Blakiston Co., Toronto, Chap. XXIII, 520-523.
- Jores, A. 1934 Den 24-Stundenperioden des Menschen. *Med Klin.*, 1: 468-471.
- Möllerström, J. 1932 Periodicity in the carbohydrate metabolism. *Acta Med. Scand. Suppl. 50*: 250-257.
- Pitts, G. C. 1943 A diurnal rhythm in the blood sugar of the white rat. *Amer. J. Physiol.*, 139: 109-116.
- Somogyi, M. 1945 A new reagent for the determination of sugars. *J. Biol. Chem.*, 160: 61-69.
- Zarrow, M. X., M. E. Denison, B. Rosenberg, D. E. Mann, Jr. and G. M. Neher 1952 Effect of insulin and epinephrine on the eosinophil and blood glucose levels in sheep; lack of diurnal rhythm. *Amer. J. Physiol.*, 171: 636-640.

I

- Impacts, bone fractures produced by high velocity 123
- Impact, tolerance of the facial bones to .. 113
- Implantation stages in the rat, a morphological analysis of the early 185
- Interrelation of the digestive and skeletal systems as determinants of tooth position, the 71
- In vitro using electron microscopic autoradiography, localization of uptake of tritiated norepinephrine by rat brain *in vivo* and 377
- In vivo and in vitro using electron microscopic autoradiography, localization of uptake of tritiated norepinephrine by rat brain 377

J

- JONES, ALBERT L. See Long, John A. 463

K

- KRAW, ALLAN G., AND DONALD H. ENLOW. Continuous attachment of the periodontal membrane 133

L

- Labyrinth in the rhesus monkey, central projections of portions of the vestibular ganglia innervating specific parts of the ... 281
- LEAK, LEE VERN. The ultrastructure of myofibers in a reptilian heart: The boa constrictor 553
- Leg tendons, changes in cells, matrix and water of calcifying turkey 449
- LENN, NICHOLAS J. Localization of uptake of tritiated norepinephrine by rat brain *in vivo* and *in vitro* using electron microscopic autoradiography 377
- Light and electron microscopic study of neurofibrils and neurofilaments at neuro-neuronal junctions in the dorsal lateral geniculate nucleus of the cat, a 583
- Light and electron microscopic observations on the inner plexiform layer of the rabbit retina 403
- Light and electron microscopic study of the pecten of the pigeon eye, a 427
- Lighting schedules, hypophysectomy, adrenal medullectomy and starvation, circadian rhythms in blood glucose and the effect of different 627
- Lipid inclusions in hepatic cells of the mouse, an experimental study in microscopical and submicroscopic 253
- Localization of uptake of tritiated norepinephrine by rat brain *in vivo* and *in vitro* using electron microscopic autoradiography 377
- LONG, JOHN A., AND ALBERT L. JONES. The fine structure of the zona glomerulosa and the zona fasciculata of the adrenal cortex of the opossum 463

M

- Man, the development of the facial muscles in 357
- Masked shrew, *Sorex cinereus*, microradiographic visualization of structure in bones of the 69
- Matrix and water of calcifying turkey leg tendons, changes in cells 489
- Mechanism of spermatiation in the toad, the Medullectomy and starvation, circadian rhythms in blood glucose and the effect of different lighting schedules, hypophysectomy, adrenal 227
- Mesometrial arteries in the guinea pig, the effect of pregnancy on the elastic membranes of 627
- MEYERS, R. A. See Avery, J. K. 85
- Mice, an electron microscopic study of the modification by monosodium glutamate of the retinas of normal and "rodless" 319
- Microradiographic visualization of structure in bones of the masked shrew, *Sorex cinereus* 89
- Microscopic and radiosautographic study of the rat parotid gland after acinomyein D administration, an electron 161
- Microscopic and submicroscopic lipid inclusions in hepatic cells of the mouse, an experimental study of 253
- Microscopic structure of human femoral, tibial and fibular cortical bone, differences and relationships between the physical properties and the 79
- Microscopic study of the pecten of the pigeon eye, a light and electron 427
- Mineral density surrounding resorption sites in teeth, a study of 55
- Monkey, central projections of portions of the vestibular ganglia innervating specific parts of the labyrinth in the rhesus 281
- Monosodium glutamate of the retinas of normal and "rodless" mice, an electron microscopic study of the modification by 319
- Morphogenesis of the palate in normal human embryos with special emphasis on the mechanisms involved 149
- Morphological analysis of the early implantation stage in the rat, a 185
- Mouse, an experimental study of microscopical and submicroscopic lipid inclusions in hepatic cells of the 253
- Muscles in man, the development of the facial 357
- Myofibers in a reptilian heart, the ultrastructure of: The boa constrictor 553

N

- Neurofibrils and neurofilaments at neuro-neuronal junctions in the dorsal lateral geniculate nucleus of the cat, a light and electron microscopical study of 583
- Neurofilaments at neuro-neuronal junctions in the dorsal lateral geniculate nucleus of the cat, a light and electron microscopical study of neurofibrils and 583

Elastic membranes of mesometrial arteries in the guinea pig, the effect of pregnancy on the

Electron- and light-microscope study of sinus structure in perfused rabbit and dog spleens, an

Electron microscope study of the modification by monosodium glutamate of the retinas of normal and "rodless" mice, an

Electron microscopic and radioautographic study of the rat parotid gland after actinomycin D administration, on

Electron microscopic observations on the inner plexiform layer of the rabbit retina, light and

Electron microscopic study of the pecten of the pigeon eye, a light and

Embryos with special emphasis on the mechanisms involved, morphogenesis of the palate in normal human

ENDERS, ALLEN C., AND SANDRA SCHILAPKE. A morphological analysis of the early implantation stages in the rat

ENGEL, MILTON B., AND EUGENIO ZERLOTTI. Changes in cells, matrix and water of the calcifying turkey leg tendons

ENLOW, DONALD H. See Kraw, Allan G. ...

EVANS, F. GAYNOR, AND SEONG BANG. Differences and relationships between the physical properties and the microscopic structure of human femoral, tibial and fibular cortical bone

Experimental study of microscopic and sub-microscopic lipid inclusions in hepatic cells of the mouse, an

Eye, a light and electron microscopic study of the pecten of the pigeon

F

Facial bones to impact, tolerance of the ..

FAIST, KATHLEEN. See Burd, Alphonse R. ...

Fasciculata of the adrenal cortex of the opossum, the fine structure of the zona glomerulosa and the zona

FELTS, WILLIAM J. L., AND FRANCIS A. SPURRELL. Microradiographic visualization of structure in bones of the masked shrew, *Sorex cinereus*

Female rat, effects of pinealectomy in the newborn

Femoral, tibial and fibular cortical bone, differences and relationships between the physical properties and the microscopic structure of human

Fibular cortical bone, differences and relationships between the physical properties and the microscopic structure of human femoral, tibial and

Fine structure of the zona glomerulosa and the zona fasciculata of the adrenal cortex of the opossum, the

Fractures produced by high velocity impacts, bone

G

611 Ganglia innervating specific parts of the labyrinth in the rhesus monkey, central projections of portions of the vestibular

527 GASSER, RAYMOND F. The development of the facial muscles in man

319 GAUGHAN, GEORGE R. L. See Dempster, Wilfrid Taylor

Glomerulosa and the zona fasciculata of the adrenal cortex of the opossum, the fine structure of the zona

Glucose and the effect of different lighting schedules, hypophysectomy, adrenal medullectomy and starvation, circadian rhythms in blood

Glutamate of the retinas of normal and "rodless" mice, an electron microscopic study of the modification by monosodium

Grain structure with architectural features of the human skull, correlation of types of cortical

GUILLERY, R. W. A light and electron microscopical study of neurofibrils and neurofilaments at neuro-neuronal junctions in the dorsal lateral geniculate nucleus of the cat

Guinea pig, the effect of pregnancy on the elastic membranes of mesometrial arteries in the

H

HALE, L. E. See Avery, J. K.

HAN, SEONG S. An electron microscopic and radioautographic study of the rat parotid gland after actinomycin D administration

HARGER, JAMES H. See Huelke, Donald F. ...

Heart, the ultrastructure of myofibers in a reptilian: The boa constrictor

Hepatic cells of the mouse, an experimental study of microscopic and submicroscopic lipid inclusions in

HODGSON, VOICR R. Tolerance of the facial bones to impact

HUELKE, DONALD F., LYNN J. BUEGE AND JAMES H. HARGER. Bone fractures produced by high velocity impacts

Human embryos with special emphasis on the mechanisms involved, morphogenesis of the palate in normal

Human femoral, tibial and fibular cortical bone, differences and relationships between the physical properties and the microscopic structure of

Human skull, correlation of types of cortical grain structure with architectural features of the

Hypophysectomy, adrenal medullectomy and starvation, circadian rhythms in blood glucose and the effect of different lighting schedules

- Neuro-neuronal junctions in the dorsal lateral geniculate nucleus of the cat, a light and electron microscopical study of neurofibrils and neurofilaments at 583
- Newborn female rat, effects of pinealectomy in the 391
- Norepinephrine by rat brain *in vivo* and *in vitro* using electron microscopical autoradiography, localization of uptake of tritiated 377
- Nuclei functioning in oxytocin release, septal projections to 605
- Nucleus of the cat, a light and electron microscopical study of neurofibrils and neurofilaments at neuro-neuronal junctions in the dorsal lateral geniculate 583
- O**
- Opossum, the fine structure of the zona glomerulosa and the zona fasciculata of the adrenal cortex of the 463
- Oxytocin release, septal projections to nuclei functioning in 605
- P**
- Palate in normal human embryos with special emphasis on the mechanisms involved, morphogenesis of the 149
- PARKS, HAROLD F. An experimental study of microscopic and submicroscopic lipid inclusions in hepatic cells of the mouse .. 253
- Parotid gland after actinomycin D administration, an electron microscopic and radioautographic study of the rat 161
- PAULY, JOHN E., AND LAWRENCE E. SCHEVING. Circadian rhythms in blood glucose and the effect of different lighting schedules, hypophysectomy, adrenal medullectomy and starvation 627
- Pecten of the pigeon eye, a light and electron microscopic study of the 427
- Peridental membrane, continuous attachment of the 133
- Pigeon eye, a light and electron microscopic study of the pecten of the 427
- Pinealectomy in the newborn female rat, effects of 391
- Plexiform layer of the rabbit retina, light and electron microscopic observations on the inner 403
- POWELL, ERVIN W., AND DUANE K. RORIE. Septal projections to nuclei functioning in oxytocin release 605
- Pregnancy on the elastic membranes of mesometrial arteries in the guinea pig, the effect of 611
- Properties of body segments based on size and weight 33
- R**
- Rabbit and dog spleens, an electron- and light-microscope study of sinus structure in perfused 527
- Rabbit retina, light and electron microscopic observations on the inner plexiform layer of the 403
- Radioautographic study of the rat parotid gland after actinomycin D administration, an electron microscopic and 161
- Rat, a morphological analysis of the early implantation stages in the 185
- Rat brain *in vivo* and *in vitro* using electron microscopic autoradiography, localization of uptake of tritiated norepinephrine by 377
- Rat, effects of pinealectomy in the newborn female 391
- Rat parotid gland after actinomycin D administration, an electron microscopic and radioautographic study of the 161
- RAVIOLA, ELIO, AND GIUSEPPINA RAVIOLA. A light and electron microscope study of the pecten of the pigeon eye 427
- RAVIOLA, ELIO. See Raviola, Giuseppina .. 403
- RAVIOLA, GIUSEPPINA, AND ELIO RAVIOLA. Light and electron microscopic observations on the inner plexiform layer of the rabbit retina 403
- RAVIOLA, GIUSEPPINA. See Raviola, Elio .. 427
- Reptilian heart, the ultrastructure of myofibers in a: The boa constrictor 553
- Resorption sites in teeth, a study of mineral density surrounding 55
- Retina, light and electron microscopic observations on the inner plexiform layer of the rabbit 403
- Retinas of normal and "rodless" mice, an electron microscopic study of the modification by monosodium glutamate of the .. 319
- Rhesus monkey, central projections of portions of the vestibular ganglia innervating specific parts of the labyrinth in the ... 281
- RORIE, DUANE K. See Powell, Ervin W. ... 605
- S**
- SCHEVING, LAWRENCE E. See Pauly, John E. 627
- SCHLAFKE, SANDRA. See Enders, Allen C. .. 185
- Septal projections to nuclei functioning in oxytocin release 605
- Shrew, *Sorex cinereus*, microradiographic visualization of structure in bones of the masked 89
- Sinus structure in perfused rabbit and dog spleens, an electron- and light-microscope study of 527
- Skeletal systems as determinants of tooth position, the interrelation of the digestive and 71
- Skull, correlation of types of cortical grain structure with architectural features of the human 7
- Sorex cinereus*, microradiographic visualization of structure in bones of the masked shrew 89
- Spermiation in the toad, the mechanism of Spleens, an electron- and light-microscope study of sinus structure in perfused rabbit and dog 527
- SPURRELL, FRANCIS A. See Feltz, William J. L. 89
- Starvation, circadian rhythms in blood glucose and the effect of different lighting schedules, hypophysectomy, adrenal medullectomy and 627

- STEIN, BENNETT M., AND MALCOLM B. CARPENTER. Central projections of portions of the vestibular ganglia innervating specific parts of the labyrinth in the rhesus monkey 261
- Study of mineral density surrounding resorption sites in teeth, a 55

T

- Teeth, a study of mineral density surrounding resorption sites in 55
- Tendons, changes in cells, matrix and water of calcifying turkey leg 489
- THOMAS, CAROLYN EYSTER. An electron- and light-microscope study of sinus structure in perfused rabbit and dog spleens 527
- Tibial and fibular cortical bone, differences and relationships between the physical properties and the microscopic structure of the human femoral 79
- Toad, the mechanism of spermiation in the 227
- Tolerance of the facial bones to impact .. 113
- Tooth position, the interrelation of the digestive and skeletal systems as determinants of 71
- Tritiated norepinephrine by rat brain in vivo and in vitro using electron microscopic autoradiography, localization of uptake of 377
- Turkey leg tendons, changes in cells, matrix and water of calcifying 489

U

- Ultrastructure of myofibers in a reptilian heart, the: The boa constrictor 553
- Uptake of tritiated norepinephrine by rat brain in vivo and in vitro using electron microscopic autoradiography, localization of 377

V

- Vestibular ganglia innervating specific parts of the labyrinth in the rhesus monkey, central projections of portions of the ... 281
- VITALI-CALPE, R. See Burgos, M. H. 227

W

- Water of calcifying turkey leg tendons, changes in cells, matrix and 489
- WILFRED TAYLOR DEMPSTER — A biographical sketch 1
- WOODBURN, RUSSELL T. Wilfrid Taylor Dempster — A biographical sketch 1
- WRAIG, LAURENCE E. Effects of pinealectomy in the newborn female rat 391

Z

- ZERLOTTI, EUGENIO. See Engel, Milton B. 489
- Zona glomerulosa and the zona fasciculata of the adrenal cortex of the opossum, the fine structure of the 463

- Neuro-neuronal junctions in the dorsal lateral geniculate nucleus of the cat, a light and electron microscopical study of neurofibrils and neurofilaments at 583
- Newborn female rat, effects of pinealectomy in the 391
- Norepinephrine by rat brain *in vivo* and *in vitro* using electron microscopical autoradiography, localization of uptake of tritiated 377
- Nuclei functioning in oxytocin release, septal projections to 605
- Nucleus of the cat, a light and electron microscopical study of neurofibrils and neurofilaments at neuro-neuronal junctions in the dorsal lateral geniculate 583
- O**
- Opossum, the fine structure of the zona glomerulosa and the zona fasciculata of the adrenal cortex of the 463
- Oxytocin release, septal projections to nuclei functioning in 605
- P**
- Palate in normal human embryos with special emphasis on the mechanisms involved, morphogenesis of the 149
- PARKS, HAROLD F. An experimental study of microscopic and submicroscopic lipid inclusions in hepatic cells of the mouse .. 253
- Parotid gland after actinomycin D administration, an electron microscopic and radioautographic study of the rat 161
- PAULY, JOHN E., AND LAWRENCE E. SCHEVING. Circadian rhythms in blood glucose and the effect of different lighting schedules, hypophysectomy, adrenal medullectomy and starvation 627
- Pecten of the pigeon eye, a light and electron microscopic study of the 427
- Peridontal membrane, continuous attachment of the 133
- Pigeon eye, a light and electron microscopic study of the pecten of the 427
- Pinealectomy in the newborn female rat, effects of 391
- Plexiform layer of the rabbit retina, light and electron microscopic observations on the inner 403
- POWELL, ERVIN W., AND DUANE K. RORIE. Septal projections to nuclei functioning in oxytocin release 605
- Pregnancy on the elastic membranes of mesometrial arteries in the guinea pig, the effect of 611
- Properties of body segments based on size and weight 33
- R**
- Rabbit and dog spleens, an electron- and light-microscope study of sinus structure in perfused 527
- Rabbit retina, light and electron microscopic observations on the inner plexiform layer of the 403
- Radioautographic study of the rat parotid gland after actinomycin D administration, an electron microscopic and 161
- Rat, a morphological analysis of the early implantation stages in the 185
- Rat brain *in vivo* and *in vitro* using electron microscopic autoradiography, localization of uptake of tritiated norepinephrine by 377
- Rat, effects of pinealectomy in the newborn female 391
- Rat parotid gland after actinomycin D administration, an electron microscopic and radioautographic study of the 161
- RAVIOLA, ELIO, AND GIUSEPPINA RAVIOLA. A light and electron microscope study of the pecten of the pigeon eye 427
- RAVIOLA, ELIO. See Raviola, Giuseppina .. 403
- RAVIOLA, GIUSEPPINA, AND ELIO RAVIOLA. Light and electron microscopic observations on the inner plexiform layer of the rabbit retina 403
- RAVIOLA, GIUSEPPINA. See Raviola, Elio .. 427
- Reptilian heart, the ultrastructure of myofibers in a: The boa constrictor 553
- Resorption sites in teeth, a study of mineral density surrounding 55
- Retina, light and electron microscopic observations on the inner plexiform layer of the rabbit 403
- Retinas of normal and "rodless" mice, an electron microscopic study of the modification by monosodium glutamate of the .. 319
- Rhesus monkey, central projections of portions of the vestibular ganglia innervating specific parts of the labyrinth in the ... 281
- RORIE, DUANE K. See Powell, Ervin W. ... 605
- S**
- SCHEVING, LAWRENCE E. See Pauly, John E. 627
- SCHLAFKE, SANDRA. See Enders, Allen C. .. 185
- Septal projections to nuclei functioning in oxytocin release 605
- Shrew, *Sorex cinereus*, microradiographic visualization of structure in bones of the masked 89
- Sinus structure in perfused rabbit and dog spleens, an electron- and light-microscope study of 527
- Skeletal systems as determinants of tooth position, the interrelation of the digestive and 71
- Skull, correlation of types of cortical grain structure with architectural features of the human 71
- Sorex cinereus*, microradiographic visualization of structure in bones of the masked shrew 89
- Spermiation in the toad, the mechanism of Spleens, an electron- and light-microscope study of sinus structure in perfused rabbit and dog 527
- SPURRELL, FRANCIS A. See Felts, William J. L. 89
- Starvation, circadian rhythms in blood glucose and the effect of different lighting schedules, hypophysectomy, adrenal medullectomy and 627

